BINGO
a better future under
CLIMATE CHANGE

BRINGING INNOVATION TO ONGOING
WATER MANAGEMENT

D3.4

Model results for water and land use scenarios completed and analysed

June 2018

www.projectbingo.eu

The BINGO project has received funding from the European Union's Horizon 2020 Research and Innovation programme, under the Grant Agreement number 641739.

Horizon 2020 Societal challenge 5:
Climate action, environment, resource efficiency and raw materials

BINGO

Bringing INnovation to onGOing water management – a better future under climate change

Grant Agreement n° 641739, Research and Innovation Action

Deliverable number:	**D3.4**
Deliverable name:	**Model results for water and land use scenarios completed and analysed**
WP / WP number:	WP3: Integrated analysis of the water cycle
Delivery due date:	Project month 36 (30/06/2018)
Actual date of submission:	29/06/2018
Dissemination level:	Public
Lead beneficiary:	IWW
Responsible scientist/administrator:	Tim aus der Beek (IWW)
Estimated effort (PM):	41.1
Contributor(s):	E. Alves (LNEC), R. Becker (IWW), T. aus der Beek (IWW), A. Bruggeman (CYI), A.B. Fortunato (LNEC), P. Freire (LNEC), A. Gragne (NTNU), M.H.J. van Huijgevoort (KWR), A. Iacovides (IACO), I. Iacovides (IACO), E. Kristvik (NTNU), L. Locatelli (AQUATEC), P.Lorza (WV), M. Mouskoundis (IACO), T. Muthanna (NTNU), M. Nottebohm (IWW), E. Novo (LNEC), M. Oliveira (LNEC), S. Rijpkema (Vitens), M. Rodrigues (LNEC), M. Rodrigues (LNEC), B. Russo (AQUATEC), M. Scheibel (WV), D. Sunyer (AQUATEC), E. Teneketzi (WV), P. Vayanou (IACO), T. Viseu (LNEC), B.R. Voortman (KWR), J.P.M. Witte (KWR)
Estimated effort contributor(s) (PM):	AQUATEC: 3; CYI: 0.1; GLD:1 ; IACO: 4; IWW: 6; KWR: 3; LNEC: 5; NTNU: 6; Vitens: 3, WUPPERVERBAND: 10
Internal reviewer:	See Chapter 9

Changes with respect to the DoA
Not applicable

Dissemination and uptake
This report is public.

Short Summary of results
D3.4 – Model results for water and land use scenarios completed and analysed was developed by IWW, LNEC, NTNU, KWR, AQUALOGY, CYI, IACO, WUPPERVERBAND and all local partners within WP3 - Integrated analysis of the water cycle.

More than 20 hydrological models have been to applied, driven with climatic decadal predictions until 2024. The results will be used by stakeholders, such as water providers and managers, local authorities, and others in order to be prepared for and to cope with near time climate change effects. Furthermore, these model results on future water resources availability and extremes is used by Work Package 4, which will conduct case sensitive risk analysis.
The model results are described in detail in this Deliverable, they focus on multiple water related problems and scales, such as flooding by combined sewer overflows in Badalona, Spain and Bergen, Norway, changes in groundwater recharge for drinking water abstraction in the Veluwe, the Netherlands, altered reservoir management in the Wupper river basin, Germany and in Bergen, Norway, flooding problems in Cyprus, and increasing salinization in Portugal.
The model applications have also shown, that in some cases anticipated land use and water use changes can have large impacts on water resources, especially in combination with climate change effects, such as increases in floods and droughts.
This deliverable also combines different bottom-up approaches on predicting short-term effects until 2024 by pointing out synergies between sites and methods.

Evidence of accomplishment
This report as well as the model output.

TABLE OF CONTENTS

TABLE OF FIGURES

TABLE OF TABLES

1. INTRODUCTION

This document is developed as part of the BINGO (Bringing INnovation to onGOing water management – a better future under climate change) project, which has received funding from the European Union's Horizon 2020 Research and Innovation programme, under the Grant Agreement number 641739. The Project website (www.projectbingo.eu) represents Deliverable 3.4 of Work Package 3 (WP3) – Model results for water and land use scenarios completed and analyzed

2. Model results for water and land use scenarios completed and analysed

In BINGO, WP3 is analyzing and predicting the water cycle at multiple sites in six European countries. Prior to this Deliverable, WP3 has identified the various water and climate related problems at each site (D3.1), developed land-use and water use scenarios (D3.2), and has set-up, calibrated and validated more than 20 models for past conditions (D3.3). Consecutively, D3.4 is applying these models in order to investigate the extent of future water and climate conditions, by applying decadal predictions from WP2. However, as socio-economic changes do also affect the water cycle and can mask its impacts, they are included as land-use and water use scenarios. Finally, the model results are translated into risk assessment in WP4. The figure below depicts the WP3-modelling approach:

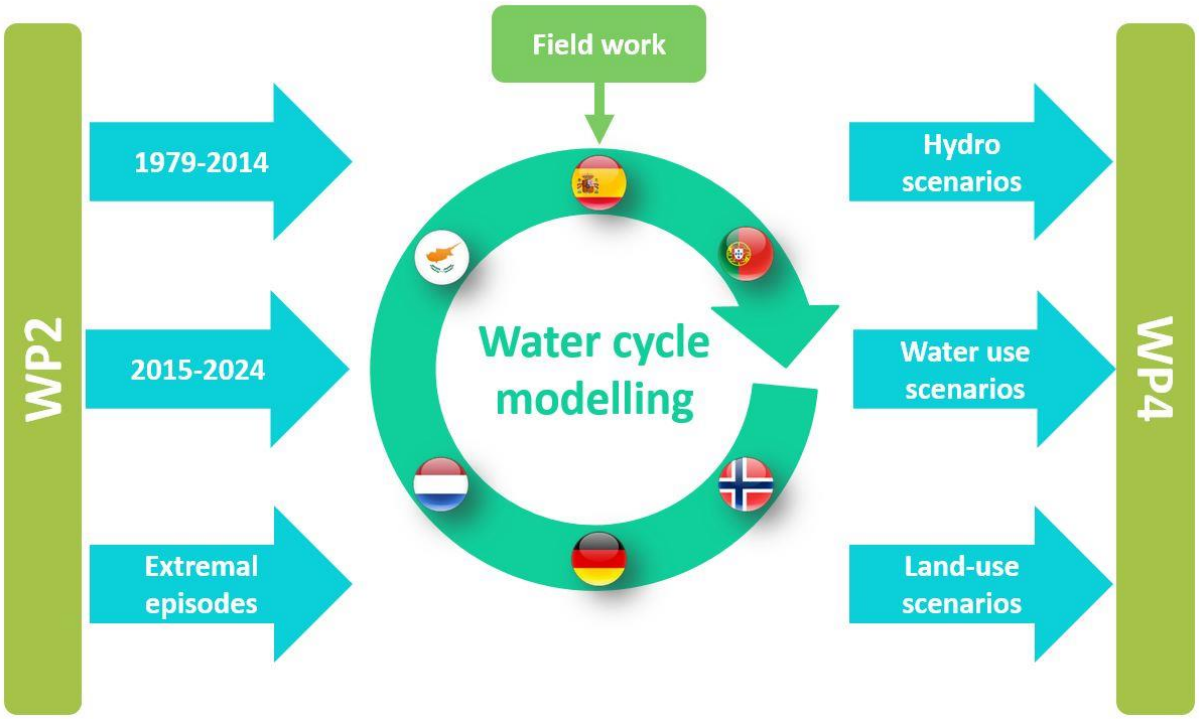

WP3-Modelling approach applied in BINGO

Due to the heterogeneity of the water problems and sites, not all scenarios have been modelled at each site. A summary is provided in the following table:

Overview of model exercises and scenarios at each BINGO site

Country	site/ framework	decadal predictions	land-use changes	water use changes	extremal episodes
Cyprus	Peristerona				
Cyprus	Pedieos		x		x
Germany	Dhünn-TALSIM	x	x	x	
Germany	Dhünn-NASIM	x	x		
Germany	Mirke				x
Germany	Leimbach	x	x		
Netherlands	Veluwe	x	x	x	
Norway	Bergen	x		x	
Norway	Damsgard	x			
Portugal	Estuary	x			
Portugal	Groundwater	x			
Portugal	Floods	x			
Portugal	Surface Water	x			
Spain	Flooding	x	x		
Spain	CSOs	x			

In close collaboration with stakeholders and project partners it was decided that not only short to mid-term predictions are necessary for innovative water management, but also long-term climate impacts on the water cycle need to be considered. Therefore, WP3 will include modelling RCP climate scenarios until 2100 in the final year of BINGO. This has not been planned for in the description of work but has been considered necessary.

3. Cyprus

Model frameworks

For Cyprus, we do not have continuous data for the decadal predictions, only for the extreme events. The Peristerona Watershed is a drought case and we are modeling 30-year RCP runs for the future (extra report). The floods however, have been modelled for the Pedieos Watershed.

3.1. Model objectives in BINGO [Pedieos Watershed]

Pedieos River is the one of the two case studies in Cyprus with the research being focused on the impacts of climate and land use change to the floods. The overall goal of the WP3 for Pedieos case study is the utilization of a calibrated hydrological model, as derived in Task 3.3 (see Deliverable 3.3), in order to enable the assessment and management of single flood events in coping with future climate and land use changes.

The modelling of future climate change scenarios has been carried out, using the derived ensembles for decadal prediction of extremal episodes downscaled to 1 km/1 h for Cyprus research (see Deliverable 2.7).

The land use scenarios modelling have been carried out based on the “Economy” and the “Sustainable” scenarios as developed in Task 3.2 (see Deliverable 3.2).

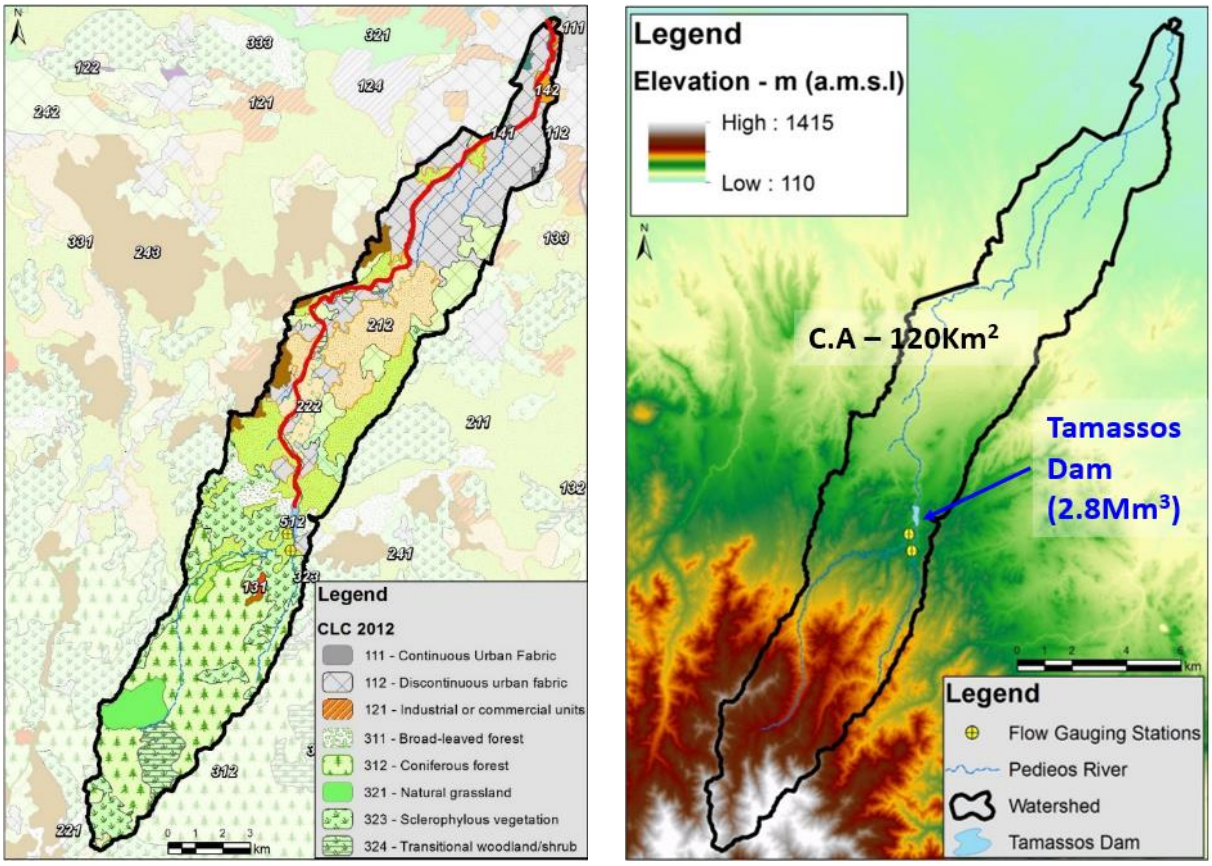

Figure 1: Pedieos Watershed physical characteristics

The Pedieos watershed covers an area of 120 km^2 with the catchment elevation ranging between 1415 m and 110 m over a 35 km of river length. There are two main tributaries which converge to a point just upstream the Tamassos dam of 2.8 Mm^3 capacity, constructed in 2002 to provide flood protection to the downstream residential areas. The

flows of the two tributaries are monitored by two gauging stations. The segment of the river downstream the dam is designated as one of the nineteen (19) areas of potential significant flood risk in Cyprus according to the Flood Directive implementation (WDD 2011). In regards to the land use, the area upstream the dam is mostly covered by *Pinus brutia* forests while in the downstream area the river flows into the greater urban agglomeration of the capital Nicosia (see Figure 1). A more detailed description of the Pedieos watershed can be found in Deliverable 3.1.

3.2. Model application

The model used for the hydrological analysis is the HEC-HMS (W. Scharffenberg 2016) and for the hydraulic simulation and generation of the flood maps, the HEC-RAS and the HEC-GeoRAS models have been employed. The future extreme rainfall events, as derived and provided by WP2 (Deliverable 2.7) within decadal prediction, have been used to simulate and calculate the flood flows and for the generation of the relevant flood maps by an already calibrated model. A brief description of the models together with some graphical information (main screen, user interface, process flowchart) is presented in Deliverable 3.3.

The three ensemble sets (2018, 2022 and 2023) of a total of 15 members (5 precipitation members for each of the three sets) have been simulated and output hydrographs were produced by the hydrologic model. The most extreme member of each ensemble set has been chosen in order to be used for the hydrologic analysis of land-use change scenarios. Therefore, in total 21 hydrologic simulations have been performed for both climate and land use change scenarios. It is noted that the above mentioned simulations were performed assuming that Tamassos Dam is full (Dam capacity 2,875 Mm^3).

The hydraulic model concerns the segment of the river downstream the Tamassos Dam which is populated by rural communities and the dense urban area of Nicosia and its suburb communities. Flood maps with the assumption of the dam being full, were produced as follows:

a) Three flood maps for the three most extreme precipitation members of each ensemble set under climate change conditions.

b) Six maps for the three most extreme precipitation members of each ensemble set under both land use and climate change scenarios (3 extreme events × 2 land use change scenarios).

The above scenarios that were simulated by the hydrologic and hydraulic model are shown in the flow chart below (see Figure 2).

In addition to the above analyses, for better understanding of the effectiveness of Tamassos Dam, additional hydrologic simulations were performed under the following initial dam conditions and scenarios:

- The 2018 most extreme member, considering
  - a) the dam is half full (capacity 1,6Mm^3) and
  - b) almost empty (capacity 0,5Mm^3).

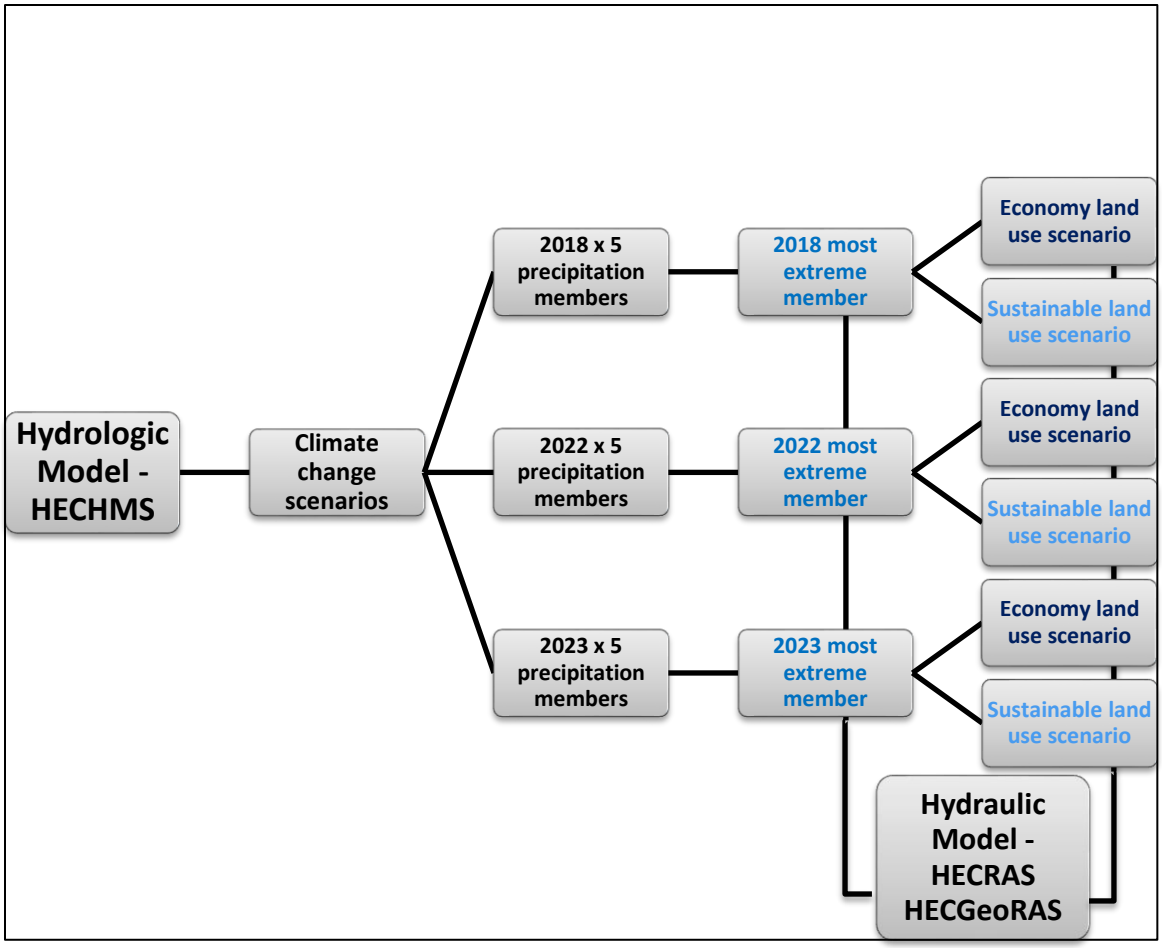

Figure 2: Flow chart of the hydrologic and hydraulic simulations

3.2.1. Data

The main input parameters of the hydrologic model are the following:

→ Sub basin input parameters:
- Sub basin geometric properties
- Losses – "SCS CN" method
- Transformation method – "SCS" unit hydrograph

→ Stream input parameters
- Routing method – "Muskingum-Cunge"

→ Rainfall input data

The model input parameters for the hydrologic model are described in more detail in Deliverable 3.3.

From the above referred parameters of the hydrologic model, the Rainfall input data and Losses (Initial Losses and Curve Number) were modified for the simulation of the climate and land use change scenarios respectively.

The derived hydrographs of the hydrologic model are used as input data for the simulations performed for the hydraulic analysis. These are presented in detail in paragraph 3.2.2.

The data used for the climate change and land use scenarios are described below:

i) Climate change scenarios – Rainfall input data

Three future rainfall scenarios were used as input to the HEC-HMS hydrologic model as derived from Task 2.7 (see Deliverable 2.7). The events, which were selected, among several near-future, within decadal prediction, extreme precipitation episodes, represent the late autumn-early winter rainy season. Total 105 potential future extreme precipitation data were identified by "Miklip" simulations and the three (3) most extreme events were selected and downscaled with the WRF model up to 1km resolution (see Deliverable 2.7).

The following table depicts the selected future extreme rainfall events which were downscaled with the WRF model up to 1 km resolution. Further analysis of the above selected events and the methodology used, is described in Deliverable 2.7 titled "Ensembles for decadal prediction extremal episodes downscaled to1 km/1 h for Cyprus research site".

Table 1: Description of the future extreme precipitation episodes selected for downscaling

(Source: Deliverable 2.7)

Case	Simulation days	Season	Day of Peak	Average of two grid points over Cyprus	Comments
2018	26/11-10/12	Wet	04/Dec	86 mm / 72h	Maximum 3-day rainfall
2022	11/12-25/12	Wet	19/Dec	42 mm / 24 h	Maximum 1-day rainfall
2023	08/11-22/11	Wet	14, 17/Nov	107 mm / 96 h	Maximum 4-day rainfall

Each ensemble set consists of five (5) hourly precipitation members (from this point and onwards referred to as "p16 to p20"). All 15 members were simulated using the HEC- HMS software. It is noted that for each precipitation member, 3 or 4 days including the day of the rainfall peak, were selected for hydrologic simulation purposes. The same parameters, excluding the input rainfall, remain the same as the ones that were used for the simulation of the past event (see Deliverable 3.3).

ii) Land use change scenarios

Two future land use scenarios were developed within the scope of the Task 3.2 for the "Sustainable" and the "Economy" scenarios. The methodology for the development of these scenarios is described in detail in Deliverable 3.2. The produced maps for each scenario are illustrated in Figure 3.

The Pedieos watershed is divided into 43 sub-catchments as depicted in Figure 4. For each sub-catchment, **a new "Curve Number – CN"** was estimated for both scenarios, taking into account the Corine Land Cover (CLC) of 2012 and the soils, according to the methodology followed by the Water Development Department (WDD 2015) for the preparation of the Flood Hazard and Risk Maps for the implementation of the Article 6 of the Floods Directive 70(I)2010.

This methodology was executed for each sub-catchment through an extensive GIS analysis. The main steps of this methodoly are the following:

- Correlation of the soil type to the relevant Hydrological Soil Group-HSG (NEH 2007) according to the correlation of the two parameters that was used in the aforementioned methodology by WDD.
- Correlation of the new land use SCENE categories of both scenarios, Economy and Sustainable with the CLC 2012 categories (see Deliverable 3.2). It is noted that each CLC category is assigned to a CN value based on the HSG and the Antecedent Moisture Condition - AMC (WDD 2015).

- The new CN was estimated for the new land uses for the both scenarios assuming that the “AMC” is at “medium conditions”.
- Finally, each CN was multiplied by the corrector factor as derived from the calibration of the model (see Deliverable 3.2).

Furthermore, the Initial Losses were estimated using the new CNs. This methodology has been chosen, so that this task be comparable and compatible with the existing WDD study.

The following Table 2 summarizes the new estimated CNs and the Initial Losses for the Sustainable and the Economy scenario. Furthermore, it shows the CNs that were used for the simulation of the past conditions (see Deliverable 3.3).

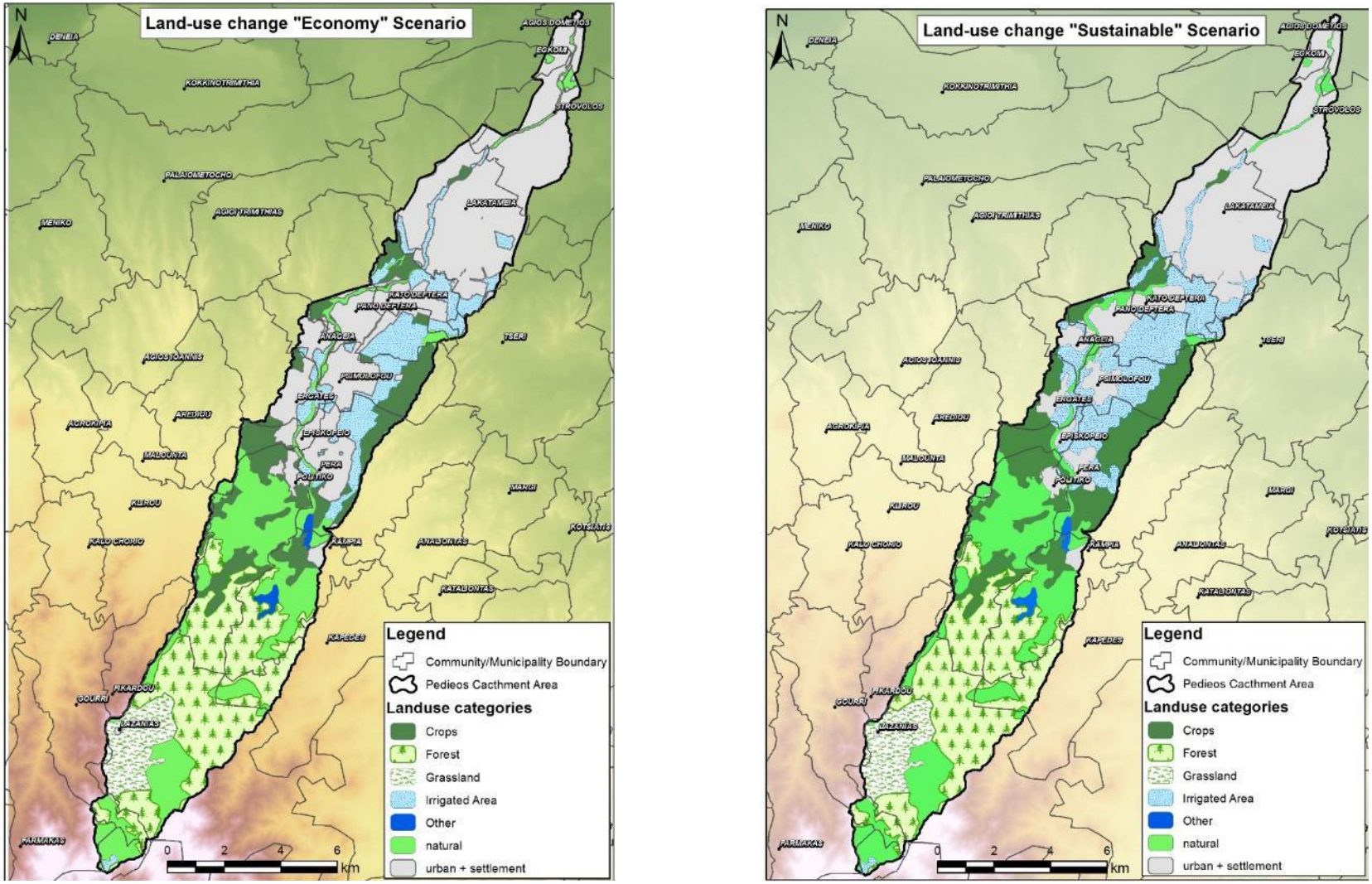

Figure 3: Land use scenarios: a) "Economy scenario (left), b) Sustainable scenario (right) as produced within the Task 3.2

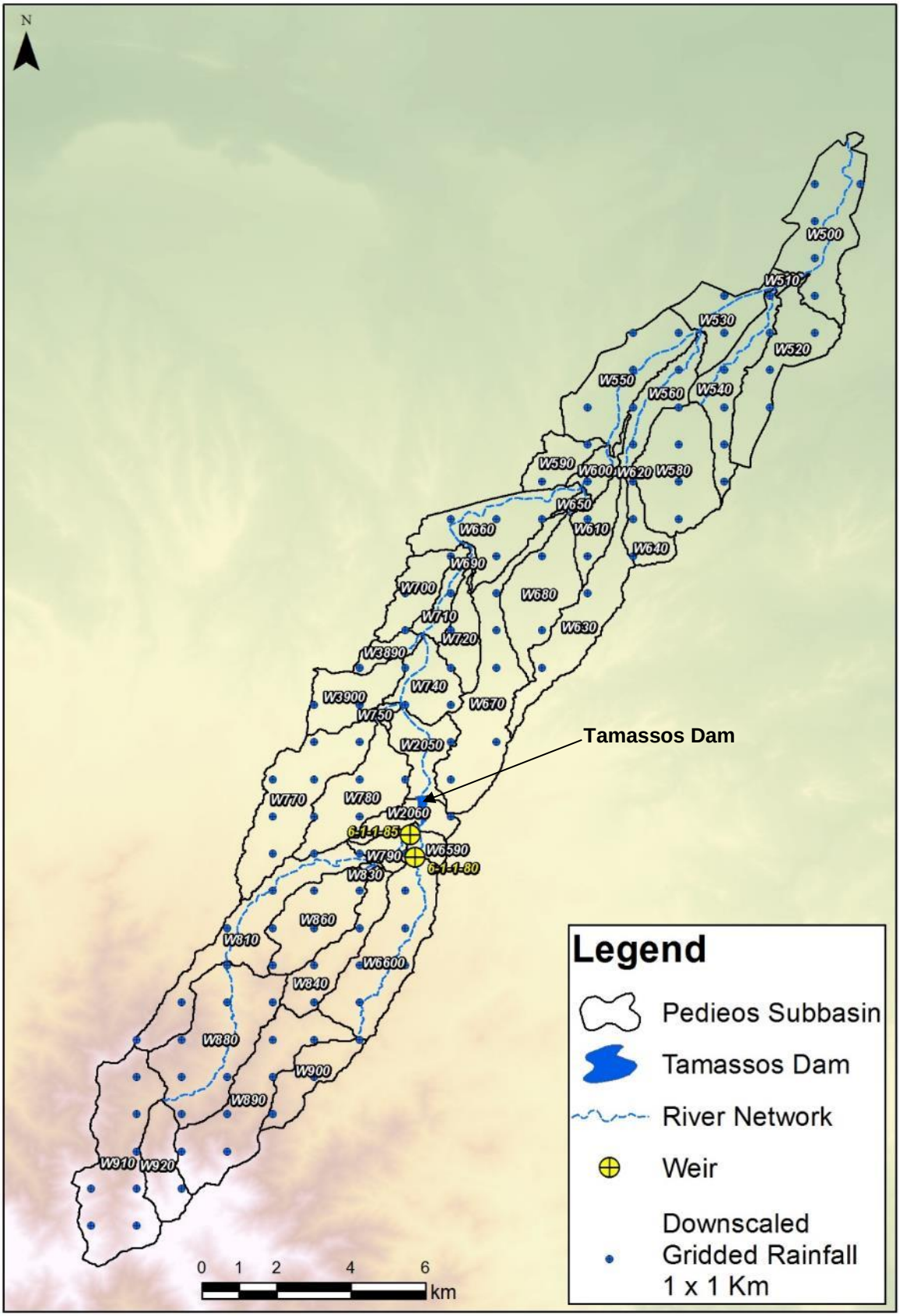

Figure 4: The Pedieos basin, subbasins, weirs location and the grid of downscaled rainfall at 1 × 1 Resolution

Table 2: Curve Number and Initial Losses (mm) for each sub-catchment (as perFigure 4) and land use scenario

Sub-catchment	Current CN	Sustainable scenario		Economy scenario	
		CN	Initial Losses	CN	Initial Losses
W500	87	93	4	94	3
W510	86	95	3	95	3
W520	91	95	3	95	3
W530	89	95	3	95	3
W540	89	92	4	94	3
W550	89	94	3	94	3
W560	91	94	3	94	3
W580	81	93	4	93	4
W590	80	81	12	81	12
W600	79	82	11	88	7
W610	72	82	11	84	10
W620	91	94	3	94	3
W630	81	81	12	83	10
W640	73	80	13	83	10
W650	81	87	8	87	8
W660	78	79	14	84	10
W670	79	80	13	82	11
W680	77	79	14	83	10
W690	71	75	17	83	10
W700	84	85	9	89	6
W710	77	78	14	81	12
W720	77	78	14	82	11
W3890	85	86	8	87	8
W740	73	74	18	79	14
W750	74	74	18	75	17
W2050	79	80	13	81	12
W770	61	61	32	66	26
W780	68	69	23	70	22
W790	72	72	20	72	20
W6590	84	85	9	85	9
W810	62	62	31	62	31
W820	60	60	34	60	34
W830	69	69	23	69	23
W840	60	60	34	60	34
W860	61	61	32	61	32
W880	59	59	35	59	35
W890	56	56	40	56	40
W900	60	60	34	60	34
W910	63	64	29	64	29
W920	64	65	27	65	27
W2060	68	68	24	68	24
W3900	77	78	14	81	12
W6600	56	56	40	56	40

The Curve Number is higher in the Economy scenario due to the fact that the future urban areas are larger compared to the Sustainable scenario.

However, the estimated CN in some sub-catchments is similar for the two scenarios due to the fact that the land use is predicted to remain the same. These sub-catchments, which are covered by the dense urban area of Nicosia and its suburb municipalities, are already residentially saturated. Furthermore, the estimated CNs of the sub-catchments that are covered by the coniferous forest, mainly upstream the Tamassos dam, remain the same for both scenarios as well, because this type of land-use is not anticipated to change in the future.

The predicted future rainfall (climate change) and the new CNs – Initial Losses (land-use change) used as an input data in the hydrologic model for the climate change and land-use change scenarios. The results of the hydrologic model are presented in the paragraph 3.2.2.

3.2.2. Results

- **Hydrologic Model Result**

i) Climate change scenarios

The simulations were performed for 15 precipitation members; 5 for each ensemble set (2018, 2022, and 2023). The derived hydrographs at the outlet of the model for the most extreme future members ("p19" for 2018, "p17" for 2022 and "p16" for 2023) of each examined ensemble set are presented in Figure 5, Figure 6 and Figure 7. As it can be seen the peak discharge for 2018 is 91.8 m^3/s, for 2022 is 48.0 m^3/s and for 2023 is 295.4 m^3/s. The most extreme of all members is the "p.16" of the 2023. As an overall result of the hydrologic analysis of all members of the 2022 ensemble set, this event does not appear so extreme. This is due to fact that the input rainfall is distributed uniformly over time resulting to a smoother pattern of the derived hydrograph.

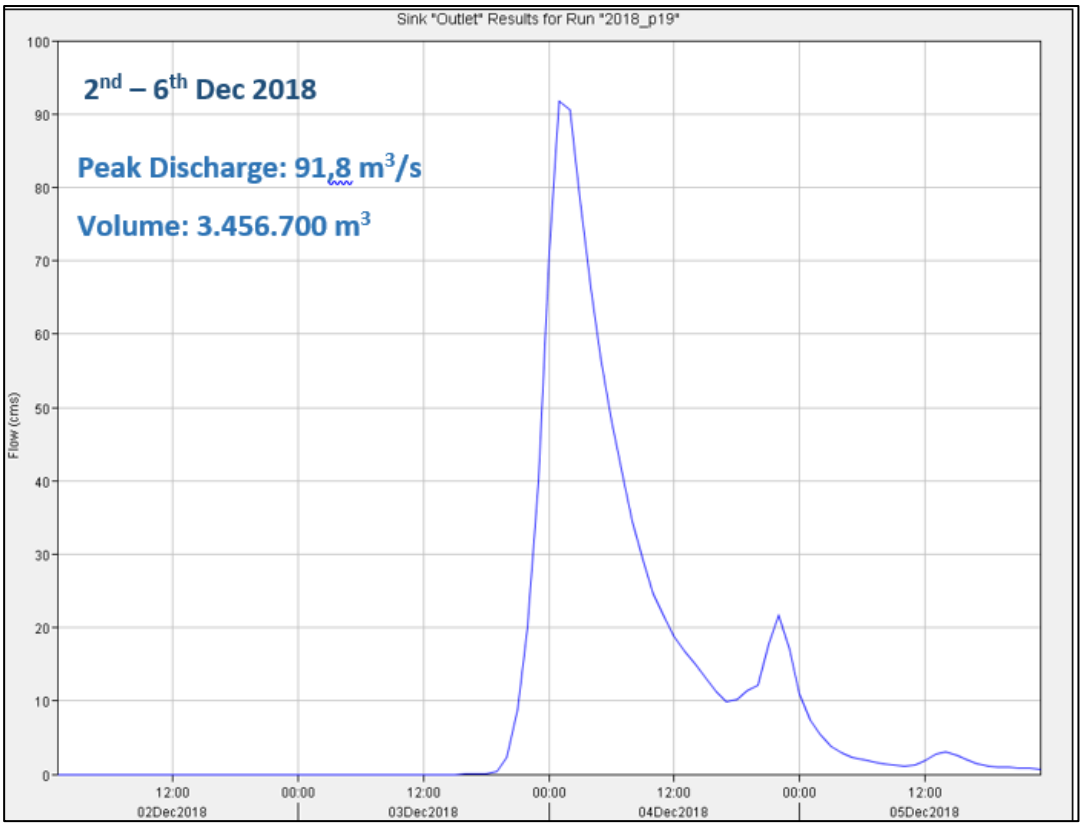

Figure 5: Hydrologic analysis results for 2018 most extreme member ("p19")

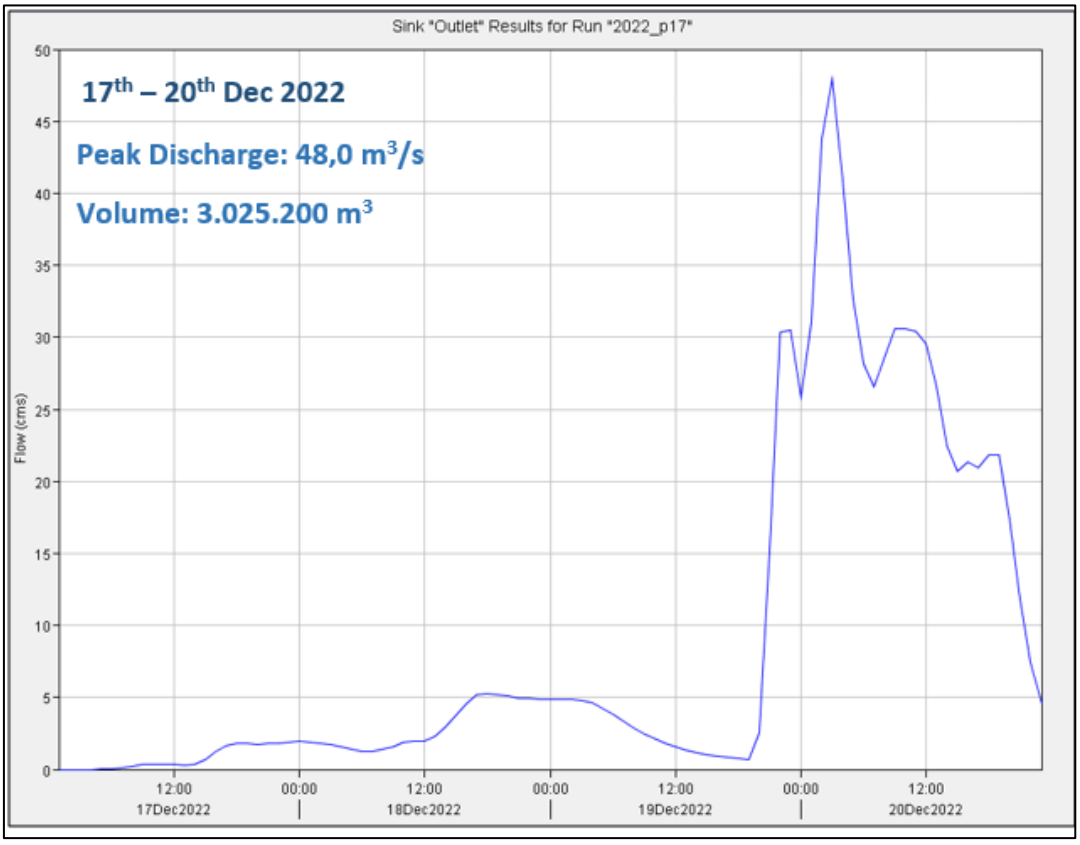

Figure 6: Hydrologic analysis results for 2022 most extreme member ("p17")

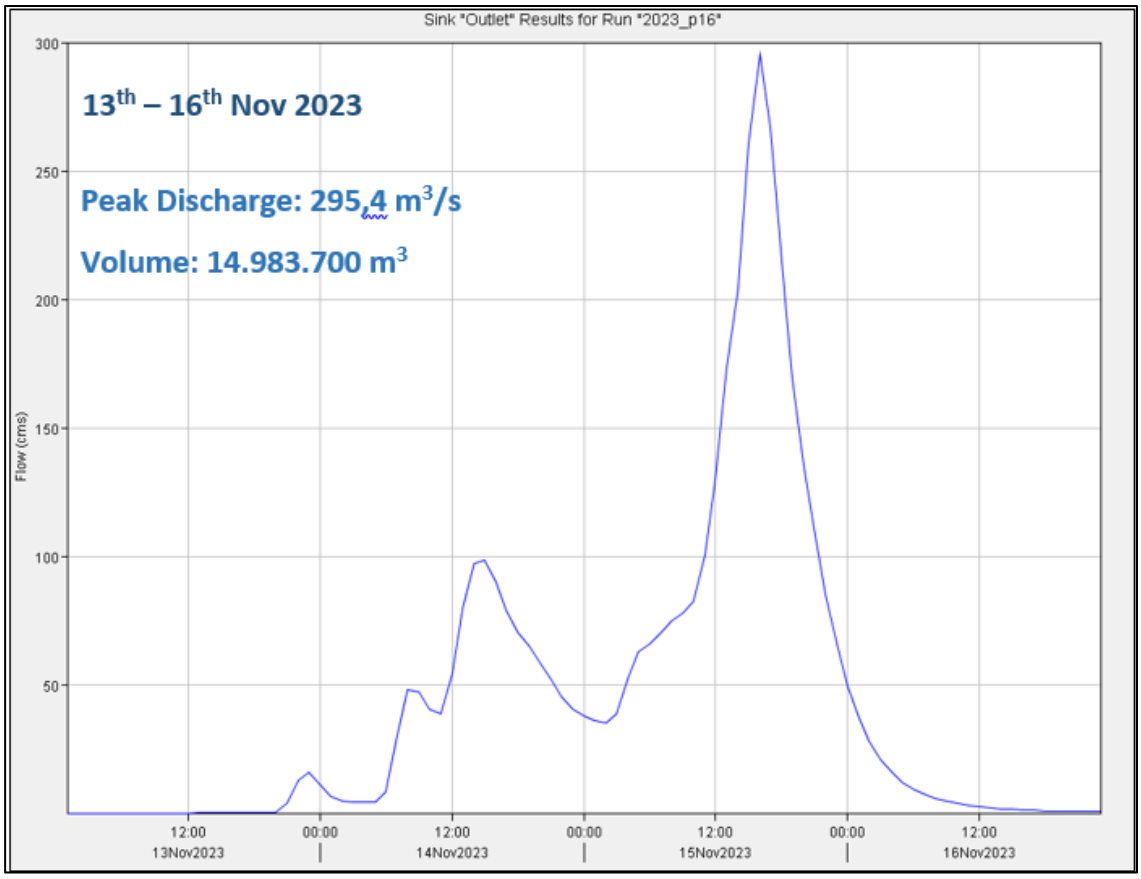

Figure 7: Hydrologic analysis results for 2023 most extreme member ("p16")

A comparison of the future extreme events with the extreme past event of 1989, which is the event that was used for the calibration of the hydrological model (see Deliverable 3.3), has been conducted for a better understanding of the magnitude of each of the future events. Figure 8 shows the hydrograph for "p.19-2018" calculated as derived from the hydrologic analysis at the location of the existing gauging station "6-1-1-85" and the observed hydrograph of 1989 event as recorded from this gauging station. The return period of the 1989 event, based on the statistical analysis of historical annual flows, is about 1 in 50 years, while the most extreme member of 2018 compared to 1989 event is a "1 in 20 years" flood event.

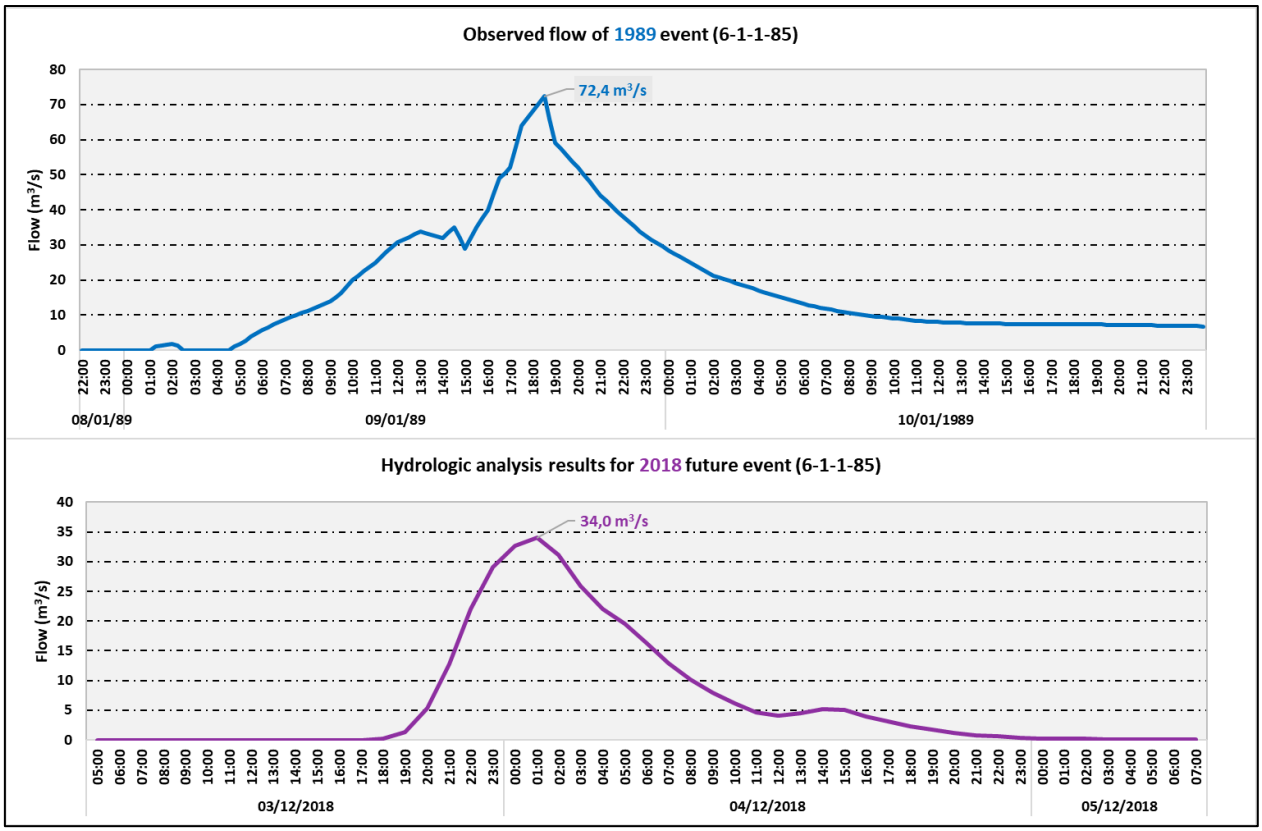

Figure 8: a) Observed flow (m^3/s) of 1989 past extreme event (uppermost graph) and b) Derived hydrograph for "p19-2018" future extreme event at the location of the gauging station "6-1-1-85" (down most graph)

Figure 9 depicts the produced hydrograph, at the location of the gauging station, for the "p.17-2022" most extreme precipitation member. The peak flow (21.2 m^3/s) is much lower than the peak flow of the 1989 event (72.4 m^3/s). The return period of the 2022 event is estimated to be about a "1 in 10 years" flood event.

Figure 10 illustrates the produced hydrograph of the "p16-2023" most extreme member, where the peak flow (95.0 m^3/s) at the flow gauging station is greater than the peak flow of the 1989 observed event (72.4 m^3/s). The return period of the 2023 event is estimated to be "1 in 100 years", which is the most extreme event of all the examined precipitation members.

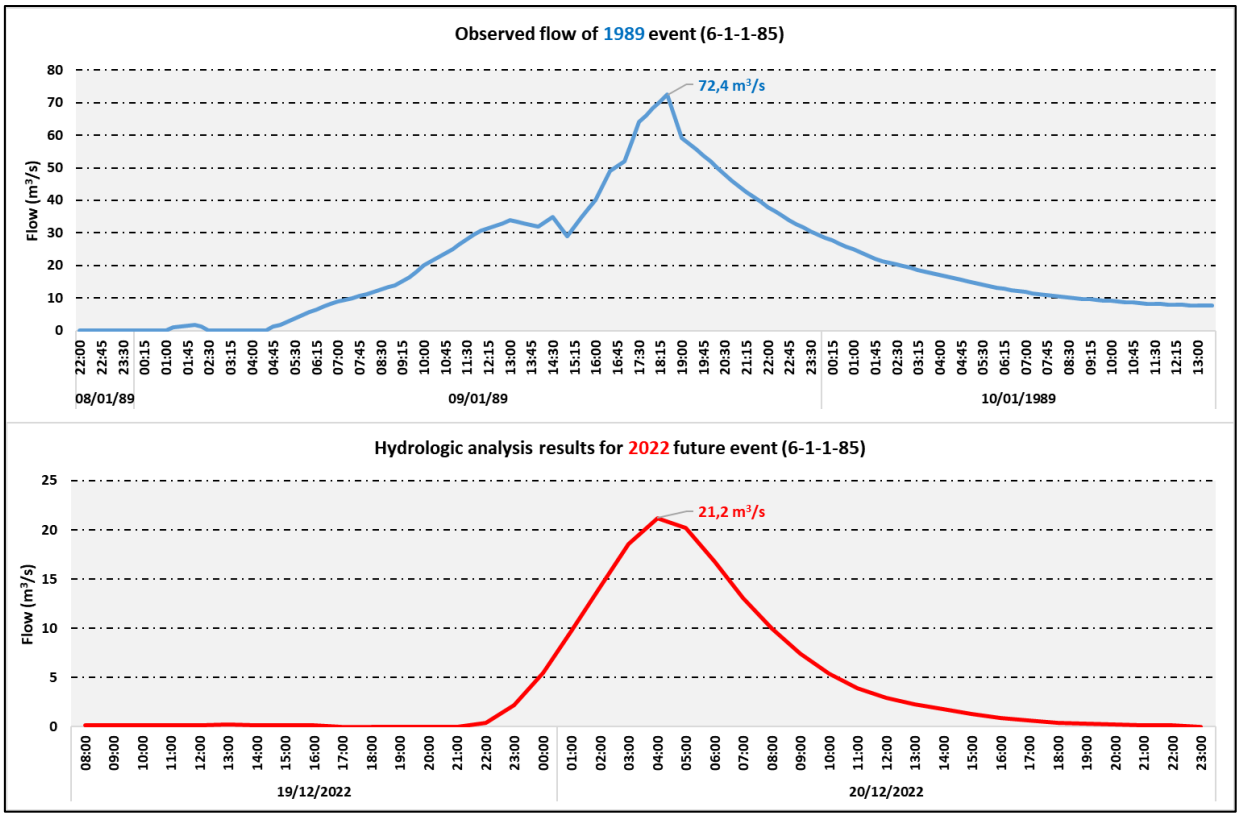

Figure 9: a) Observed flow (m³/s) of 1989 past extreme event (upper graph) and b) Derived hydrograph for "p17-2022" future extreme event at the location of the gauging station "6-1-1-85" (lower graph)

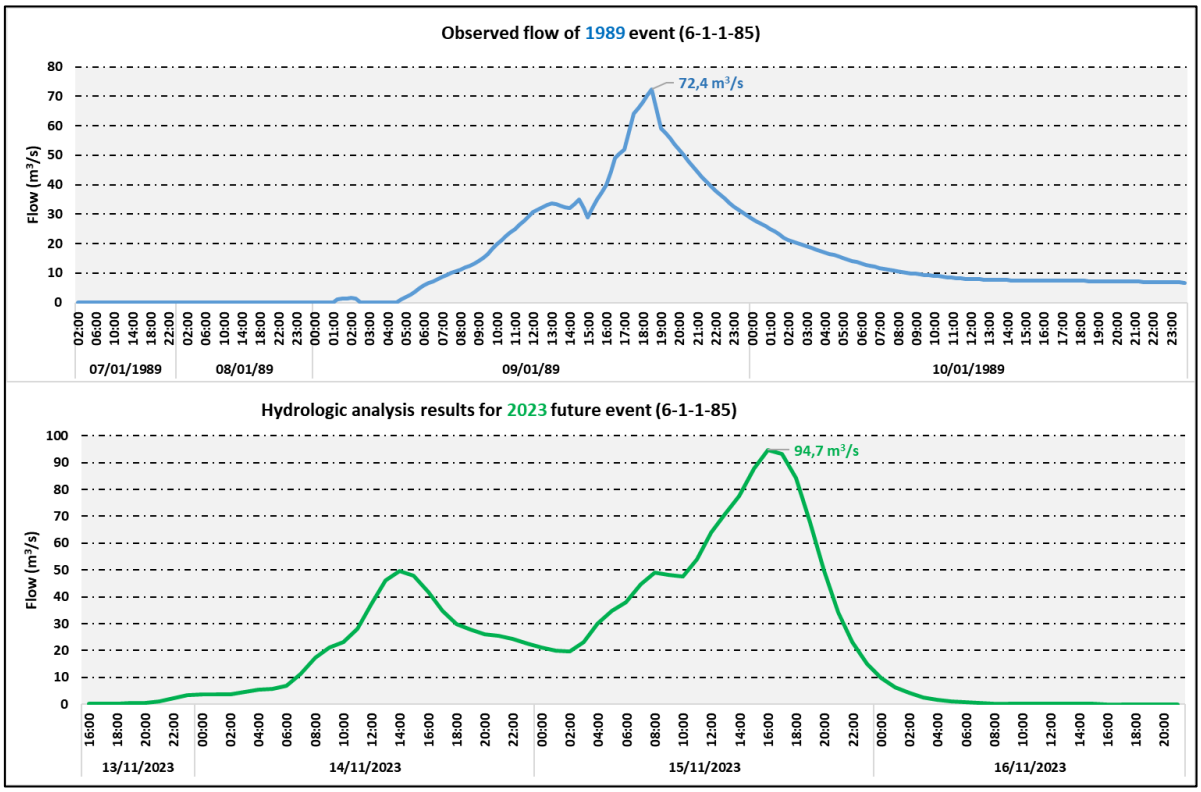

Figure 10: a) Observed flow (m³/s) of 1989 past extreme event (upper graph) and b) Derived hydrograph for "p16-2023" future extreme event at the location of the gauging station "6-1-1-85" (lower graph)

Table 3 summarizes the peak flow values for each examined precipitation member at the outlet of the model, for the three ensemble sets of 2018, 2022 and 2023. The most extreme event per year is highlighted.

Table 3: Peak Flow values (m^3/s) for each precipitation member

Precipitation Member	Peak flow (m^3/s)		
	2018	**2022**	**2023**
p16	76,3	13,4	**295,4**
p17	76,3	**48,0**	124,9
p18	54,5	1,5	80,9
p19	**91,8**	2,5	73,1
p20	70,9	30,1	251,5

As it is mentioned above, for better understanding of the effectiveness of the Tamassos Dam, the “p16-2018” precipitation member of the year 2018 was hydrologically simulated under two different initial dam conditions. It is noted that all the hydrologic simulations for the climate change and land-use change scenarios have been carried out considering full initial dam conditions.

The three initial conditions scenarios for the dam for which the results are presented in the following figures (Figure 11, Figure 12, and Figure 13) are as follow:

1. Dam is full (Initial Storage = 2.8 Mm^3)
2. Dam is half full (Initial Storage = 1.6 Mm^3)
3. Dam is almost empty (Initial Storage = 0.5 Mm^3)

As it can be seen here-below with the dam full, the inflow is equal to outflow, while with the dam being half full there is considerable attenuation. When the dam is almost empty, the achieved attenuation is even much greater.

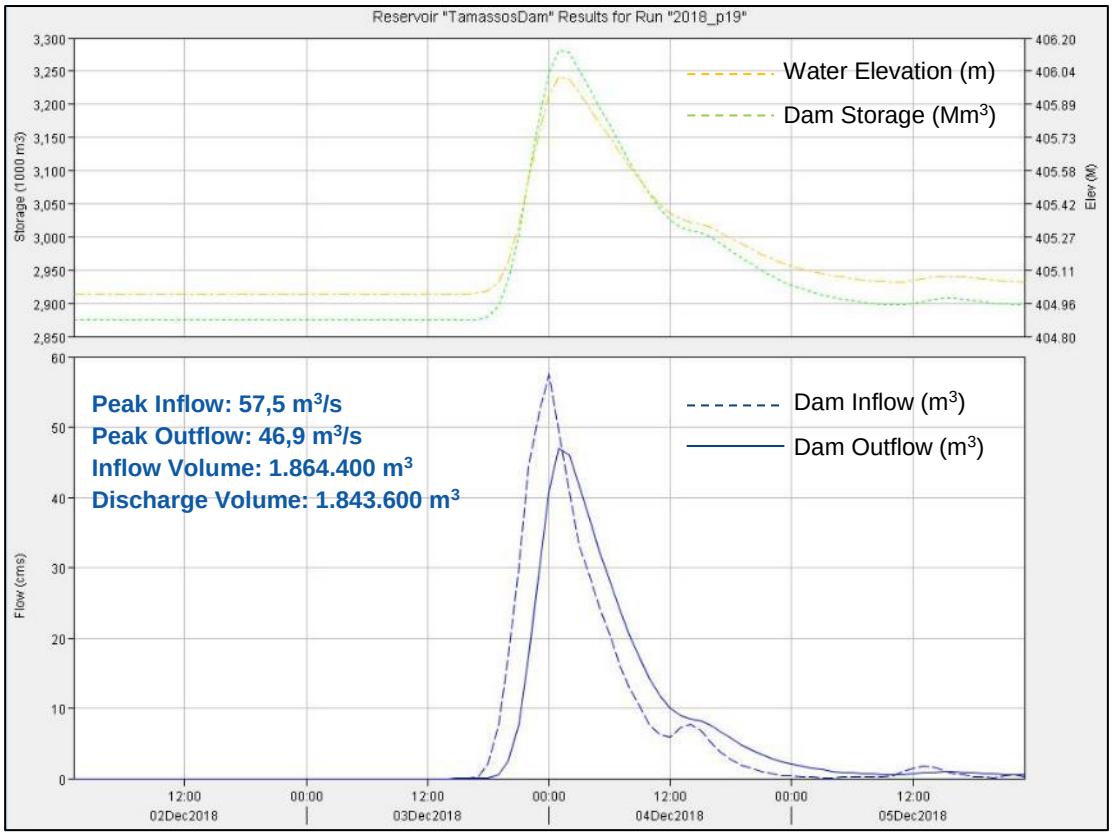

Figure 11: Hydrologic analysis results of the "p19 - 2018" rainfall event considering the Tamassos dam as full

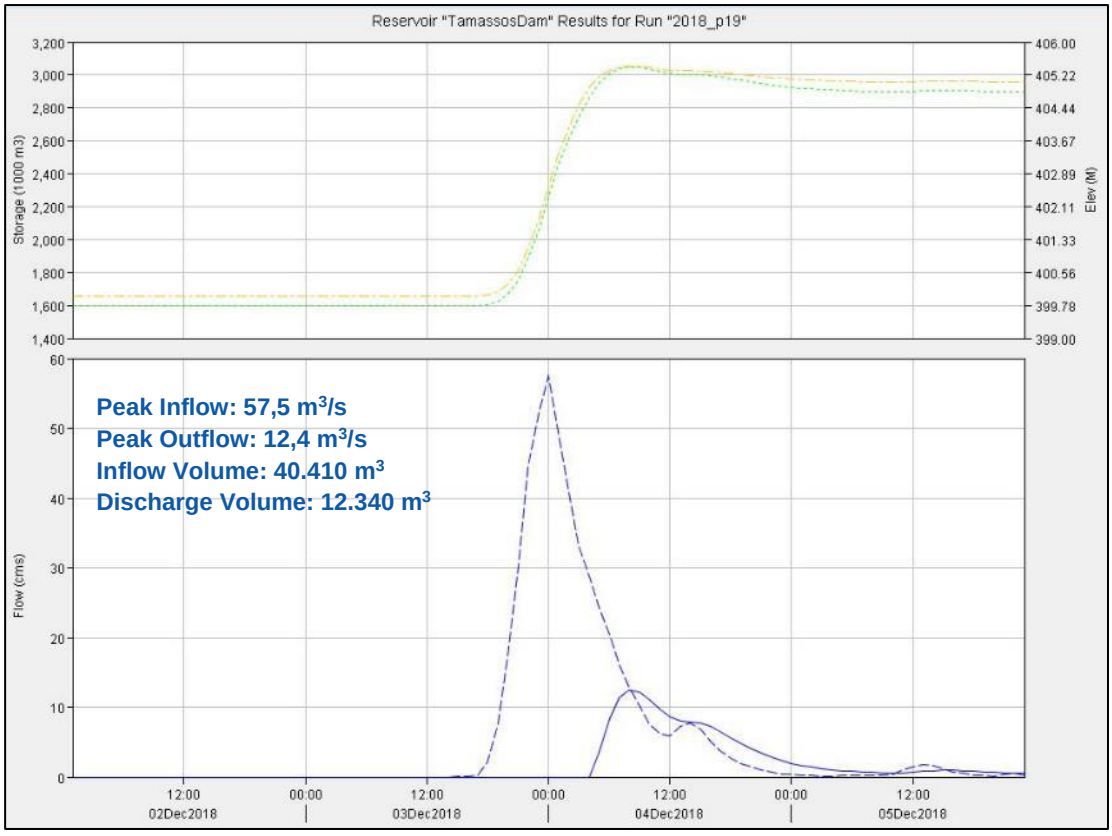

Figure 12: Hydrologic analysis of the "p19 - 2018" rainfall event considering the dam being half full

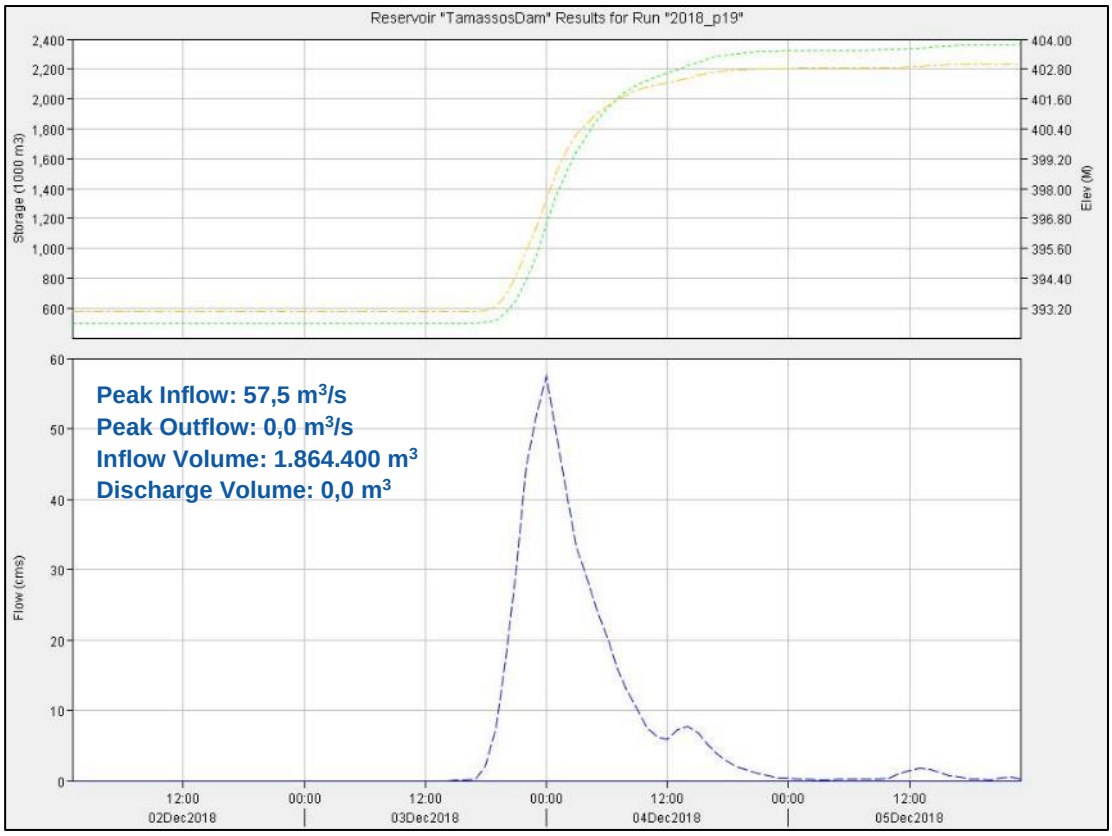

Figure 13: Hydrological analysis of the p19 - 2018 rainfall event considering the dam being almost empty

This analysis implies that the flood protection effectiveness of the dam is significant and the initial dam conditions, when a flood event occurs, determine the flood protection level to the downstream residential areas.

ii) Land use scenarios

The hydrologic simulations for the two land-use scenarios, were performed for the three most extreme rainfall events of each of the examined ensemble sets; a) “p19-2018” b) “p17-2022” and c) “p16-2023”, (highlighted in Table 3).

Figure 14 shows the derived hydrograph at the outlet of the model for the Economy and the Sustainable land-use scenarios during the “p19-2019” rainfall event. The analysis shows that the peak discharge at the Economy scenario (115.8 m^3/s) is slightly higher than that of the sustainable scenario (108.1 m^3/s). This is due to the slight increase of the Curve Number under the Economy scenario.

The derived hydrograph for the Sustainable and the Economy scenario for the “p17-2022” rainfall event is depicted in Figure 15. The peak flow at the Economy scenario is 60.0 m^3/s while in the Sustainable scenario is slightly lower, at about 56.0 m^3/s. Here again the same explanation as above holds true since at the Economy scenario the Curve Number is slightly increased due to increased sealed surface area.

Figure 16 depicts the hydrologic analysis for the both land-use scenarios for the rainfall event “p16-2023”. The derived hydrograph is quite similar for the two land-use scenarios, Economy and Sustainable, and the peak discharge is approximately 310 m^3/s and 304 m^3/s at the economy and the sustainable scenario respectively.

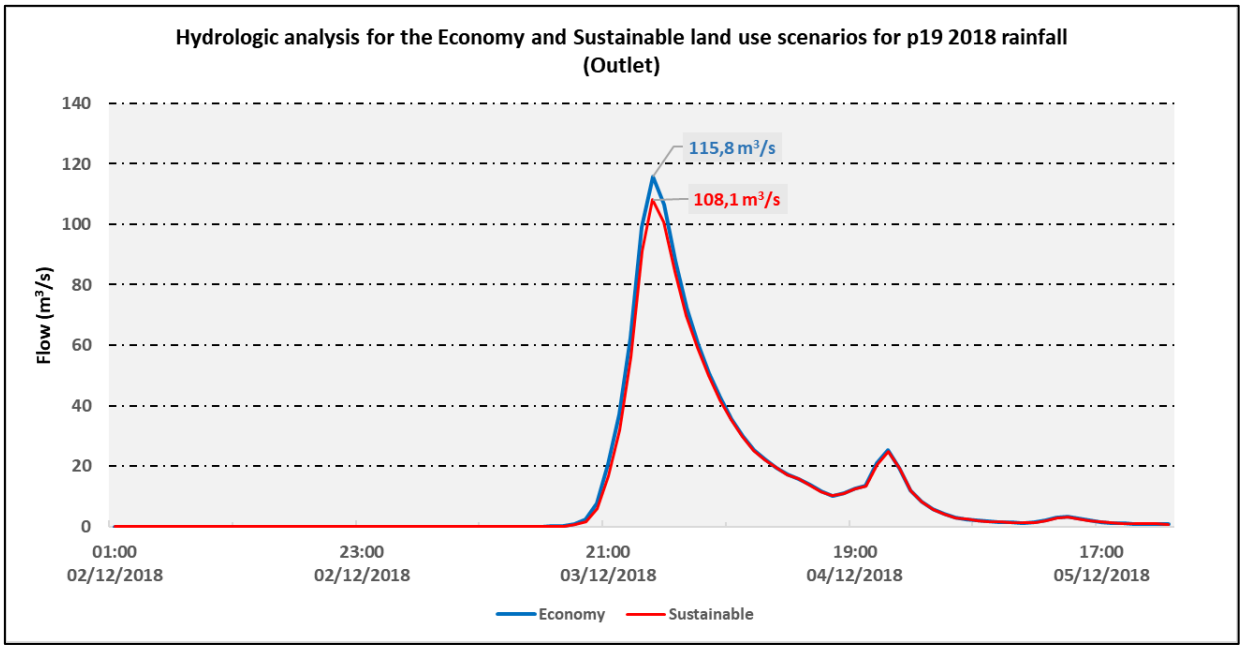

Figure 14: Hydrologic analysis for the Economy and Sustainable land use scenarios (2018 p19 rainfall event)

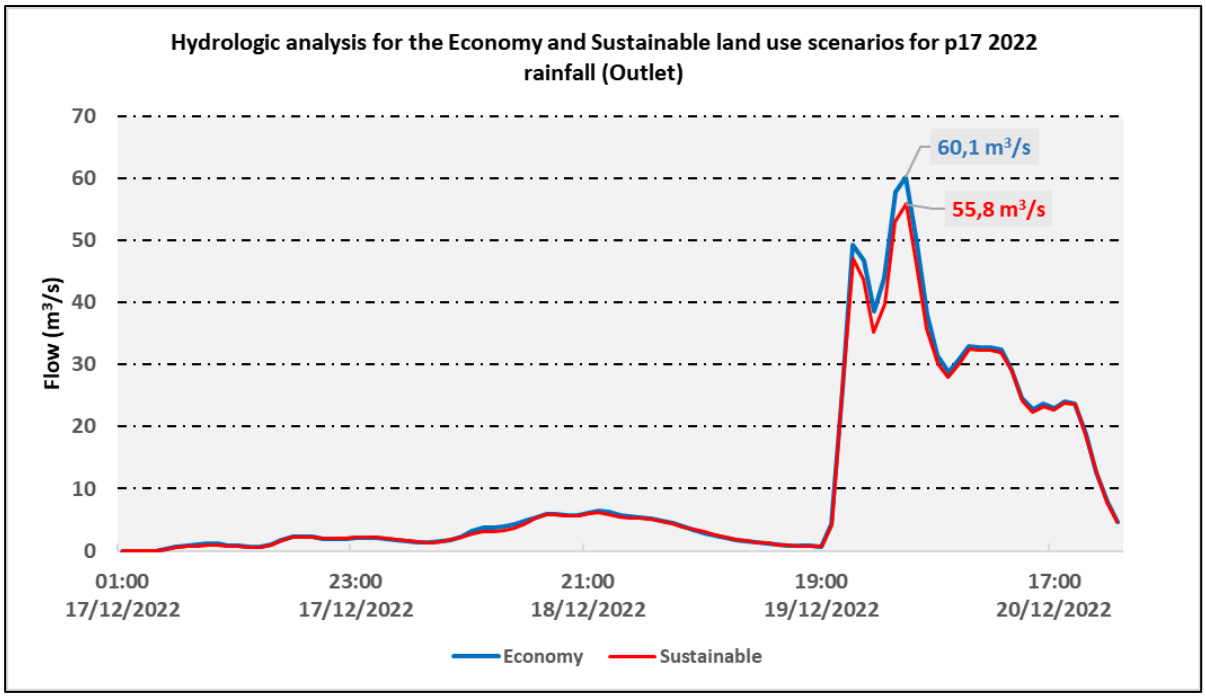

Figure 15: Hydrologic analysis for the Economy and Sustainable land use scenarios ("2022 - p17" rainfall event)

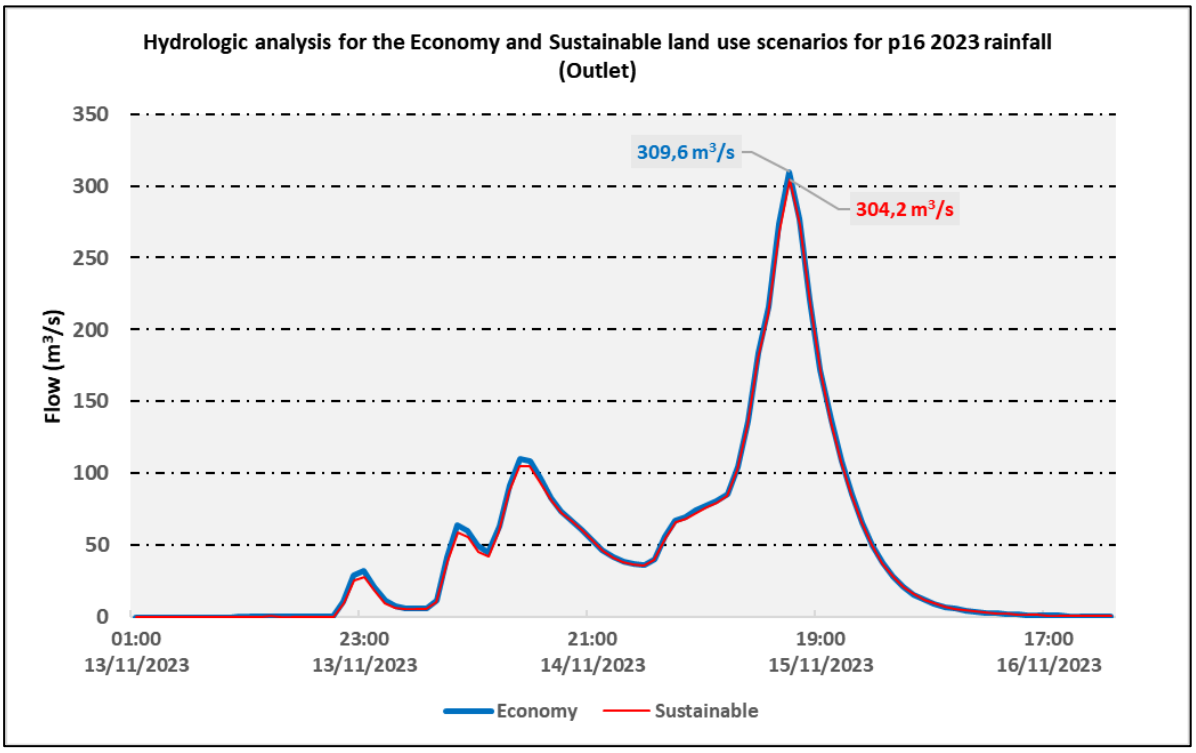

Figure 16: Hydrologic analysis for the Economy and Sustainable land use scenarios ("2023 - p16" rainfall event)

The following Table summarizes the calculated peak flow at the outlet of the model for the three most extreme rainfall scenarios, one for each ensemble set, in combination with the two land-use change scenarios; The maximum flow appears to be at the event p16-2023 at the economy scenario (309.6 m^3/s).

Table 4: Summary of the peak flow at the outlet for the most extreme rainfall events

Rainfall Event	Peak flow at the outlet of the model in m^3/s		
	Climate change + Current Land-Use	Climate change + Sustainable Scenario	Climate change + Economy Scenario
p19 - 2018	91,8	108,1	**115,8**
p17 - 2022	48,0	55,8	**60,1**
p16 - 2023	295,4	304,2	**309,6**

It should be noted that the peak flow at the outlet of the model as estimated within the WDD study (WDD 2015) for the 1:100-year flood event is 700 m3/s. This is more than twice the p16-2023 peak flow under current land use estimated under this study. This large difference is because the "WDD 1:100 - yr" flood event has been derived as reported (WDD 2015) based on the IDF curves for the various rain gauges that affect the catchment area which have been transformed to a "1:100yr "design storm event hyetograph" with the "alternating block method". This methodology tends to lead to an overestimation of the peak flow, since it is most unlikely that the extreme values of different gauges within the watershed would occur concurrently for the same event. Furthermore, the max 5-min, 10-min, 30-min, 1 hour etc. duration intensities are improbable to occur at the same event as well (occurrence of all maxima in one event). The occurrence of the combination of these assumptions is considered quite unrealistic.

- **Hydraulic model results**

The output hydrographs of the hydrologic analysis have been used as input flow data for the hydraulic analysis. As mentioned above the HEC-RAS software have been employed for the hydraulic simulations and the HECGeoRAS for the spatial analysis of the results and for the production of the pertinent flood maps.

The following Figures (Figure 17, Figure 18 and Figure 19) show on a satellite image the flood map of a selected indicative residential area as an example, located at the lower part of the Pedieos River, as generated by HEC-GeoRAS for the examined future extreme events. Furthermore, in the same Figures, two selected hydraulic cross sections, as produced by the hydraulic analysis, are shown as an example as well.

Figure 20, Figure 21, and Figure 22 illustrate on a satellite image the flood maps of the examined events for the various climate and land-use change scenarios. The inundation extent of each event and the affected residential infrastructure are clearly presented in these figures. In addition to this, in Figure 20 the flood extent of the "WDD 1:100 – yr" is indicated for comparison purposes bearing in mind the reservations expressed above regarding the magnitude of this event

2018 – Climate change

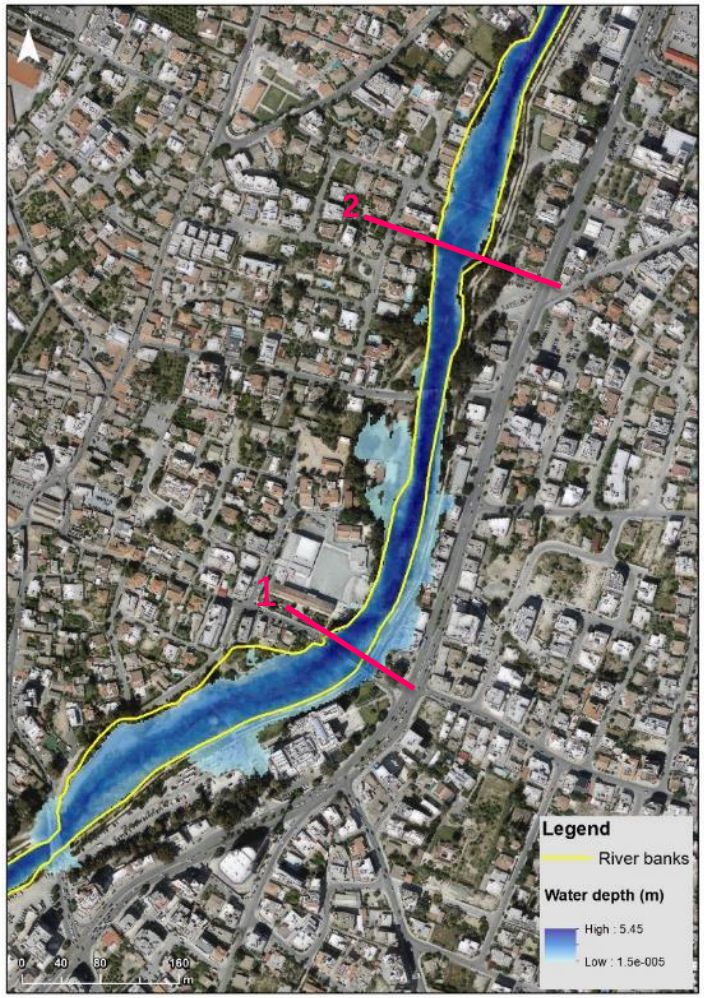

Cross Section 1 – Bridge

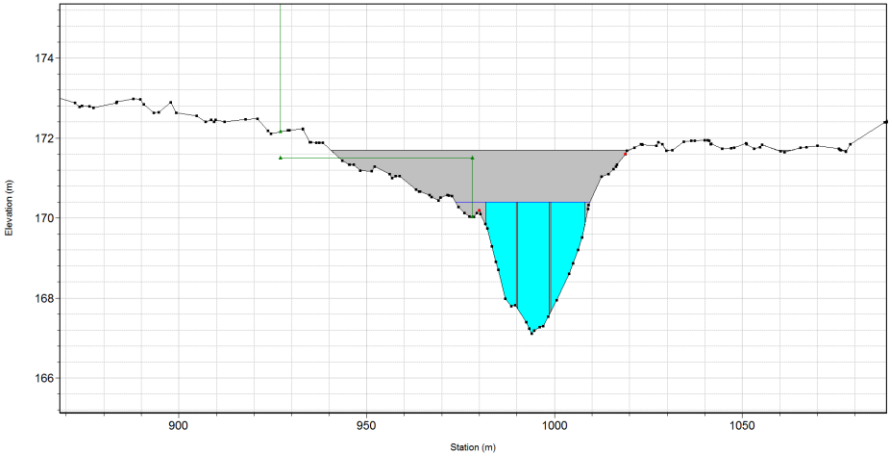

Cross Section 2

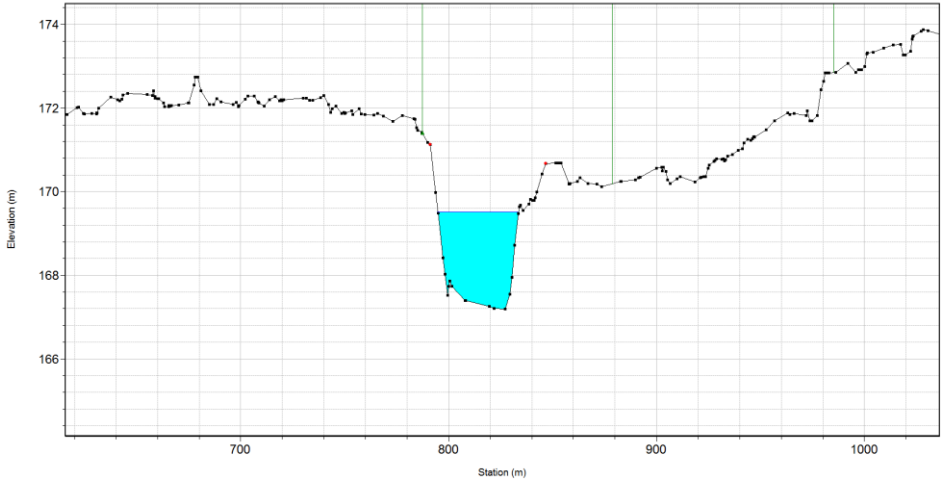

Figure 17: **Flood Map with water depth at a selected residential area (left) and two indicative hydraulic cross-sections, at a bridge (above) and river crossing (below), for the p19-2018 extreme event**

2022 – Climate change

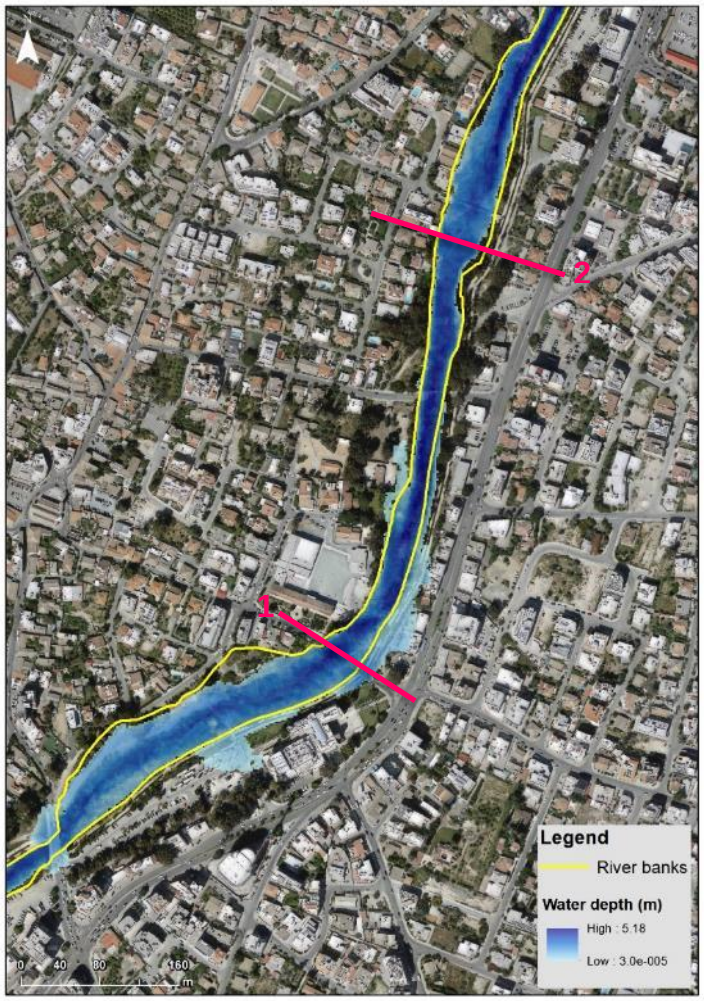

Cross Section 1 – Bridge

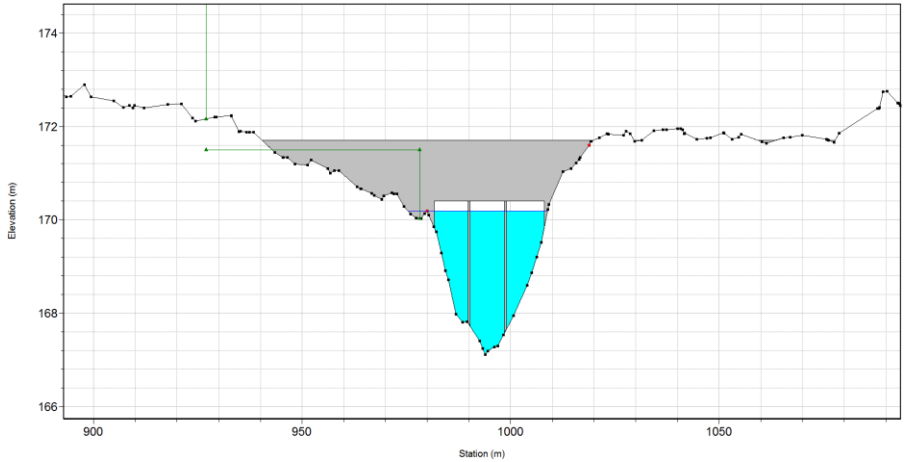

Cross Section 2

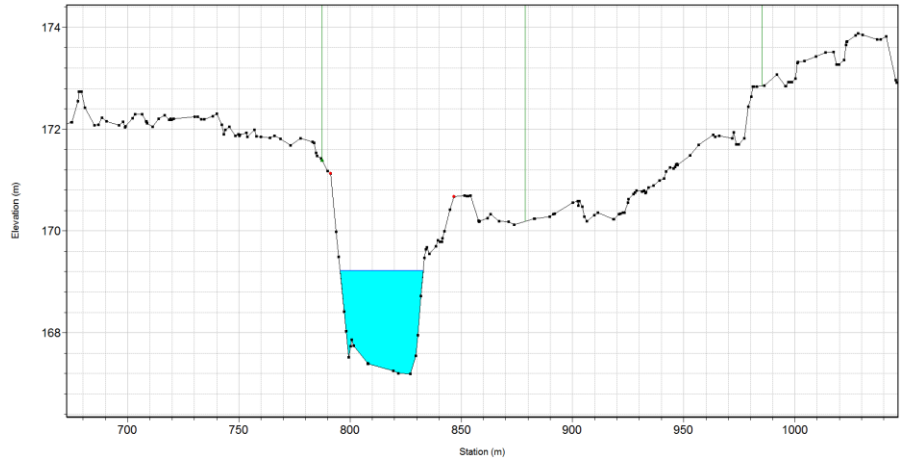

Figure 18: **Flood Map with water depth at a selected residential area (left) and two indicative hydraulic cross-sections, at a bridge (above) and river crossing (below), for the "p17-2022" extreme event**

2023 – Climate change

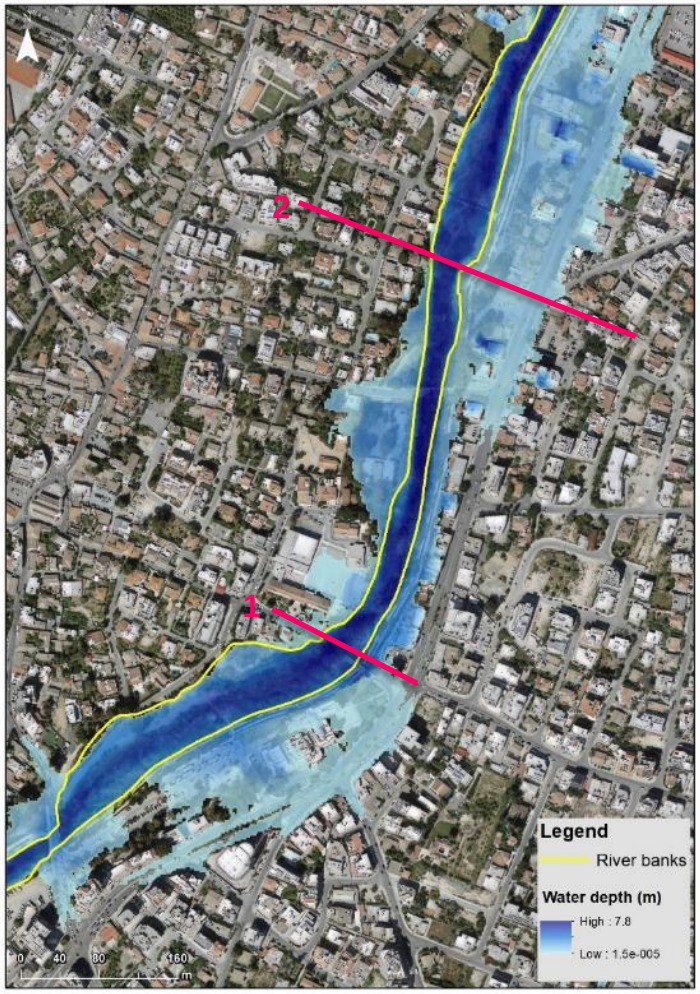

Cross Section 1 – Bridge

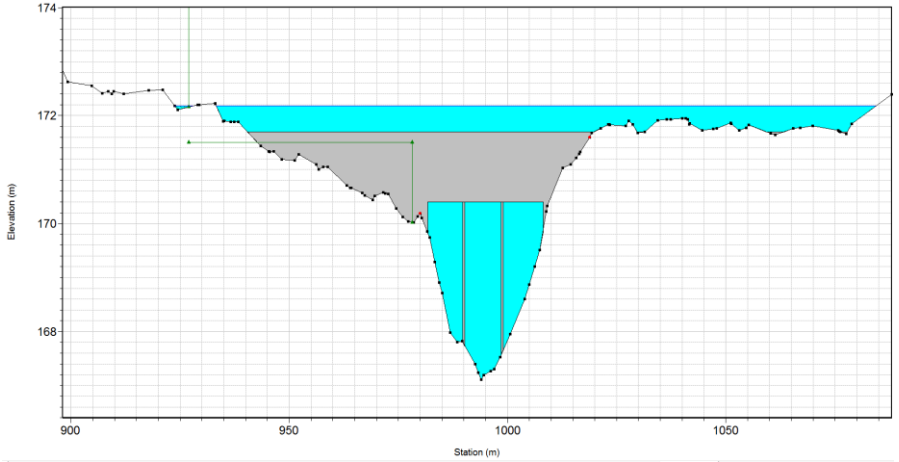

Cross Section 2

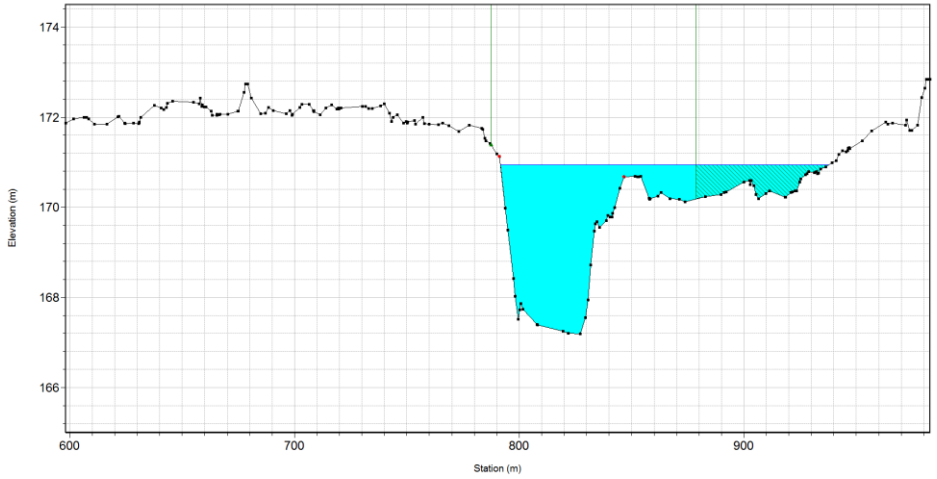

Figure 19: **Flood Map with water depth at a selected residential area (left) and two indicative hydraulic cross-sections at a bridge (above) and river crossing (below) for the "p16-2023" extreme event**

2018 –Climate change	2022 – Climate change	2023 – Climate change
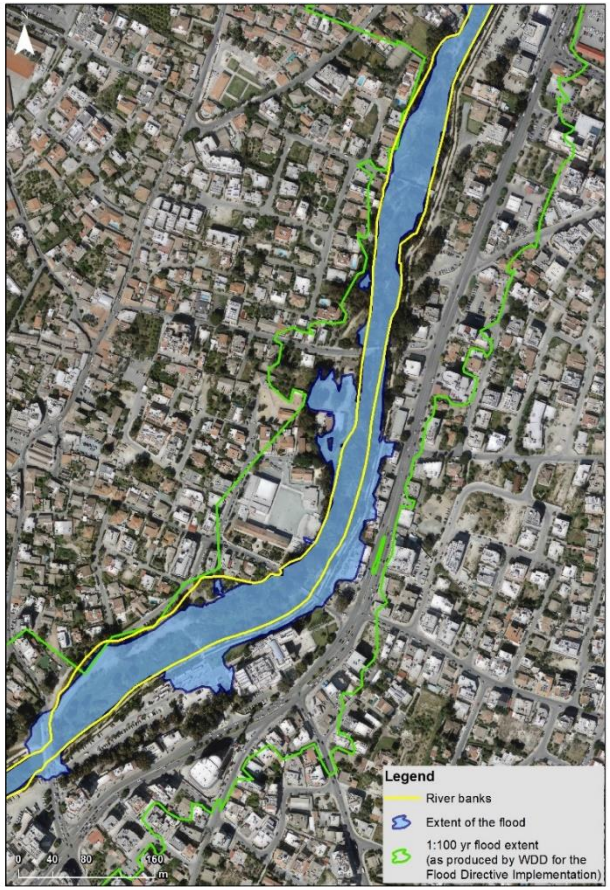	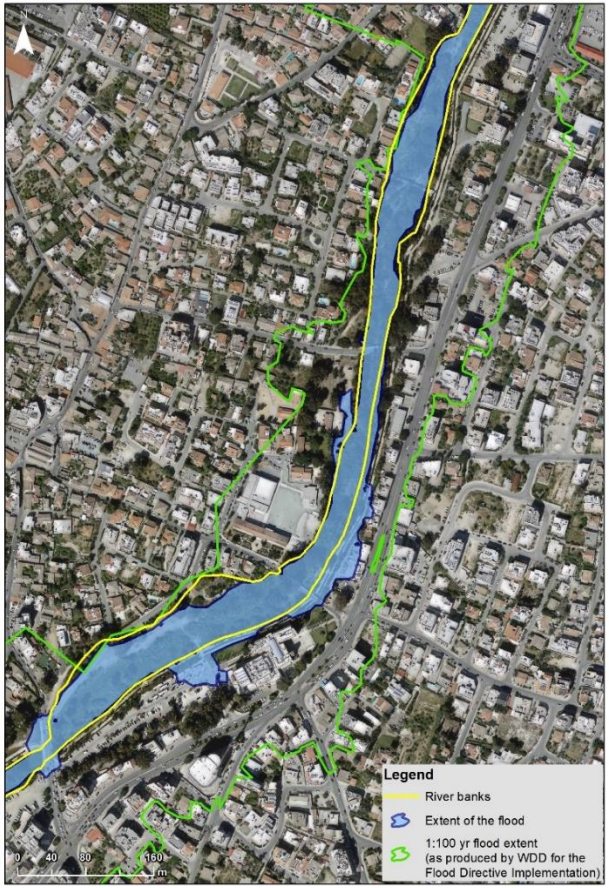	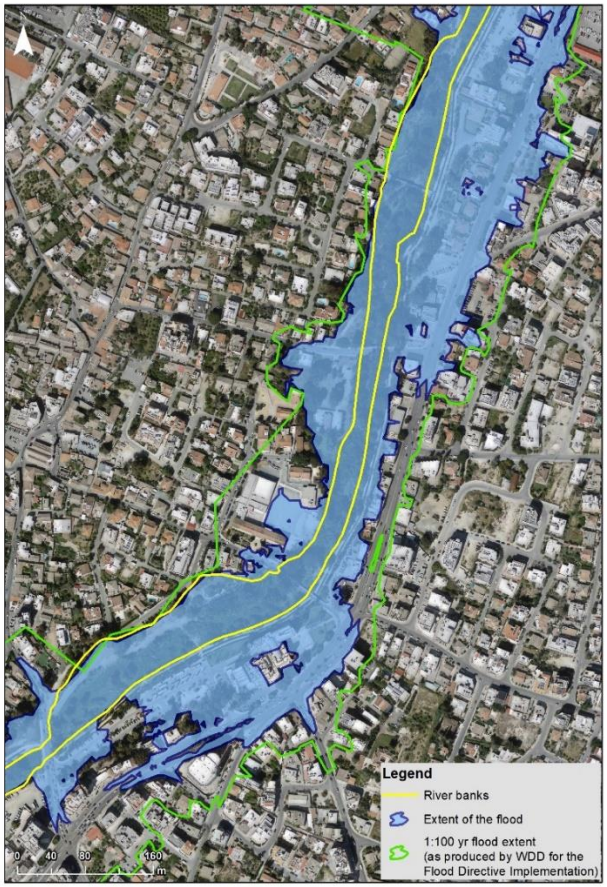
Limited extent of flooding. Few residential areas are affected.	Very limited extent of the flood. No residential areas are affected. The water is limited within the river banks.	The flood is well extended beyond the river bank. Adjacent Residential areas are inundated

Figure 20: **Flood Map at a selected indicative residential area of the examined flood events (most extreme ensemble member) under climate change scenarios**

2018 – Climate change + Sustainable Scenario	2022 - Climate change + Sustainable Scenario	2023 - Climate change + Sustainable Scenario
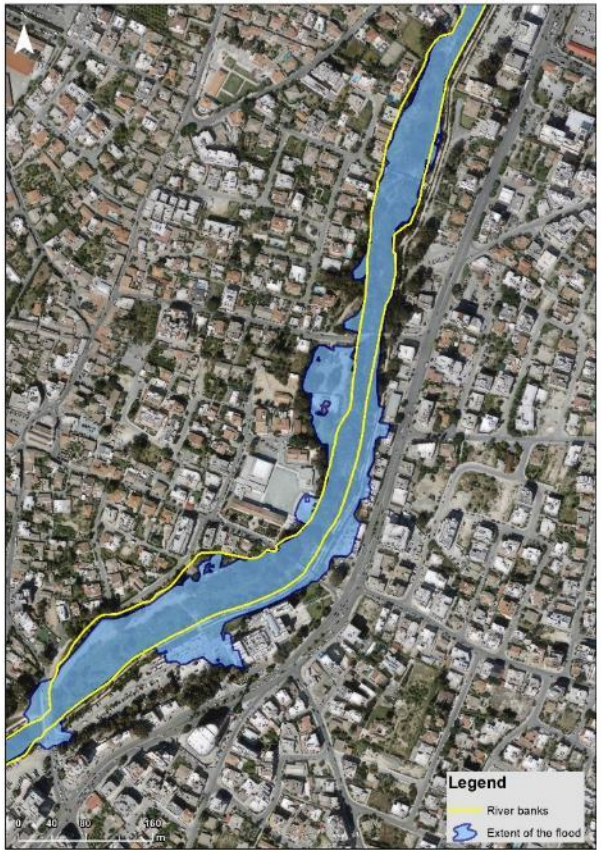		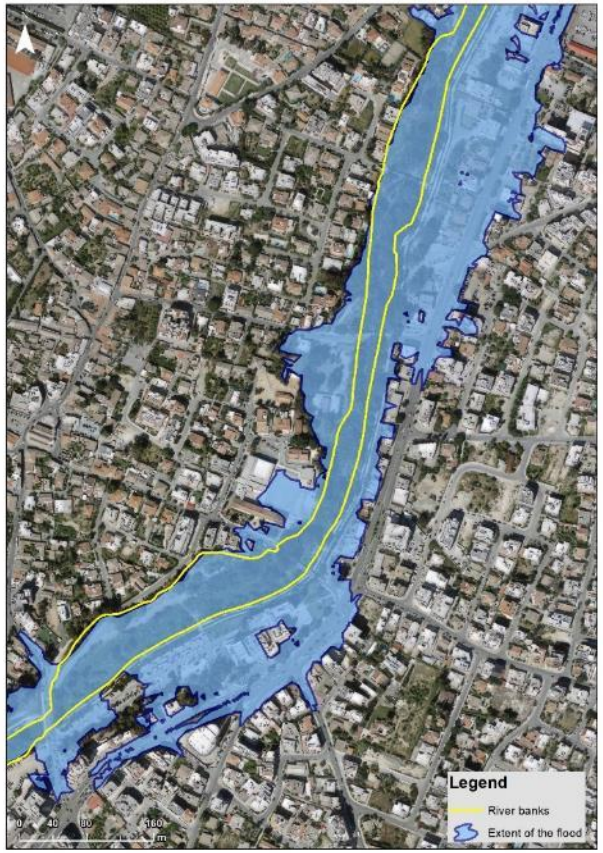
Limited extent of flooding. Few residential areas are affected.	Very limited extent of the flood. No residential areas are affected.	The flood is well extended beyond the river bank. Adjacent Residential areas and public roads are inundated.

Figure 21: **Flood Map at a selected indicative residential area of the examined flood events under climate and Sustainable land-use change scenarios**

2018 - Climate change + Economy Scenario	2022 - Climate change + Economy Scenario	2023 - Climate change + Economy Scenario
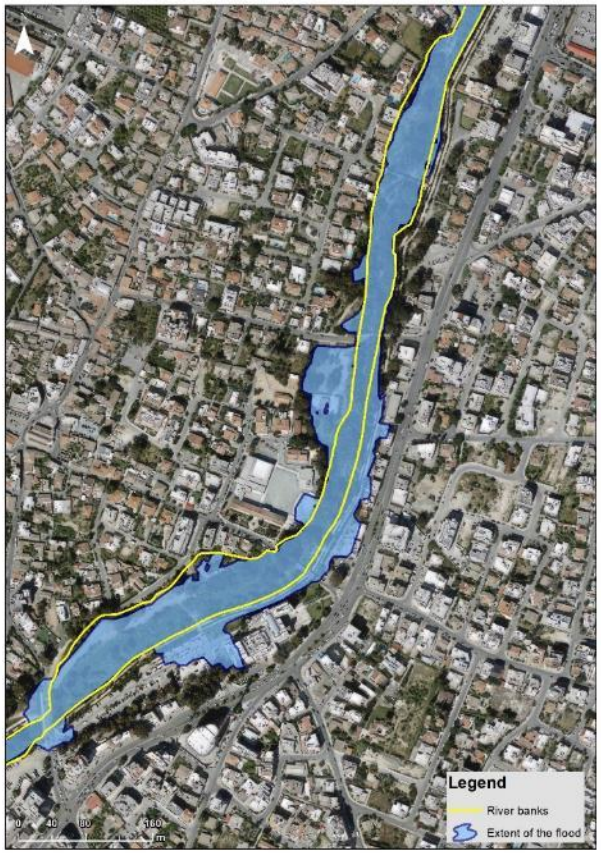		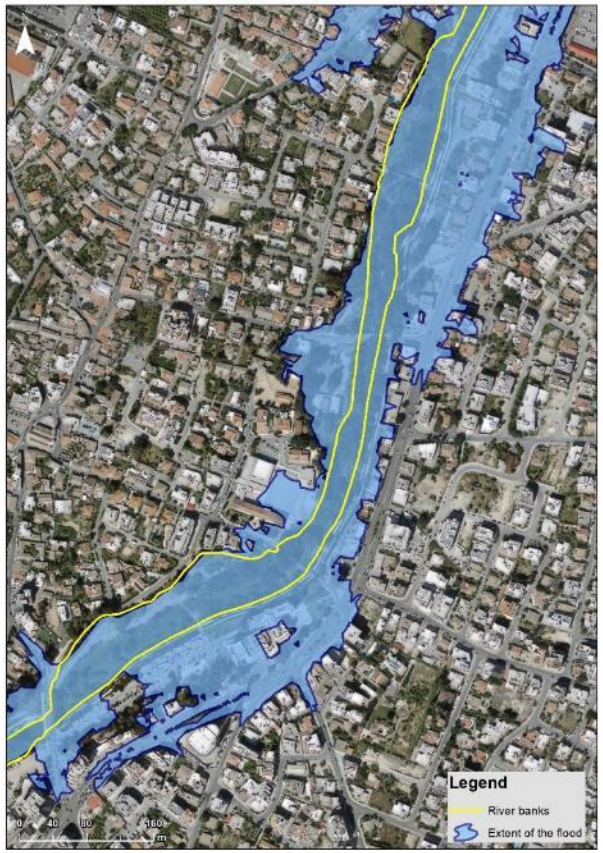
Limited extent of flooding. Few residential areas are affected.	Very limited extent of the flood. Few public spaces are affected.	The flood is well extended beyond the river bank. Adjacent Residential areas and public roads are inundated.

Figure 22: **Flood Map at a selected indicative residential area of the examined flood events under climate and Economy land-use change scenarios**

➢ **Synopsis and extent of the floods**

The following Table 5 summarizes the results of the hydrologic and hydraulic analyses for the examined future events under various climate and land-use change scenarios, considering the peak flow and the total volume as well as the overall extent of the flood area and the extent of the flood within residential town planning zones area.

The most extreme future flood event seems to take place in 2023 where the peak flow is at its maximum value (about 310 m^3/s) in the "Economy" scenario and the flood extends approximately over an area of 1.300.000 m^2 where 230.000 m^2 cover Residential Town Planning Zones (including public roads, residential, industrial and commercial town planning zones).

Table 5: Summary of the hydrologic and hydraulic analysis results for the examined flood future events under various climate and land-use scenarios

Various scenarios		Future Extreme Event	Peak Flow at outlet of the model (m^3/s)	Total Volume of the flood event (Mm^3)	Extent of the flood* (m^2)	Extent of the flood within the Residential Town Planning Zones** (m^2)
Climate change/Land use	**Dam Initial Condition**					
Climate change	Full	2018	91.8	3,457	241,775	28,700
		2022	48.0	3,025	29,600	13,560
		2023	**295.4**	**14,984**	**1,239,865**	**205,160**
Climate + Landuse change (Sustainable)	Full	2018	108.1	3,894	271,747	32,725
		2022	55.8	3,512	45,882	14,856
		2023	**304.2**	**15,700**	**1,282,949**	**220,725**
Climate + Landuse change (Economy)	Full	2018	115.8	4,086	298,185	34,710
		2022	60.1	3,665	73,413	16,500
		2023	**309.6**	**16,070**	**1,287,659**	**230,365**

** The area that extends beyond the river banks*

***These includes residential, industrial and commercial town planning zones (source: Town Planning and Housing Department)*

3.3. Discussion

All the future extreme events within decadal prediction, as derived by WP2, together with land-use change scenarios have been successfully simulated by employing an already calibrated hydrologic model. The choice of this calibrated model was made so as to have compatible results with the results of the competent authority when the Flood Directive study was implemented.

The results of the hydrological model have been used as input data to the hydraulic model for the production of the flood maps for the examined events. **It should be noted that no risk assessment is required to be conducted for the Pedieos watershed system (see Deliverable 4.1)**, as this will be executed only for the Peristerona watershed system, being the other case study for the Troodos mountains, in Cyprus.

As it is aforementioned, the segment of the river downstream the existing Tamassos dam, has been designated as one of the nineteen (19) areas of potential significant flood risk in Cyprus according to the Flood Directive implementation, so all the models and methodologies used, have been selected to be in line with the ones that were used by the competent authority, the Water Development Department, for the Flood Directive implementation. Therefore, all the derived modelling results of this task are comparable and compatible with the existing ones on past, real events.

It is believed that the modelling outcomes are policy-relevant, aiming to support the decision makers for the implementation of the EU Flood Directive through a comprehensive hydrological-hydraulic tool and a combination of various methodologies in order to enable the assessment and management of single flood events in coping with future climate and land use changes.

The main outcomes of this task that are considered to be important for the local competent authorities and stakeholders are the following:

- Within decadal prediction, flood events are expected to occur due to climate change, and some residential areas adjacent to the Pedieos River are prone to inundation. Furthermore, there are hydraulic structures (e.g bridges and culverts) that are incapable to safety route even events with high probability of occurrence (such as the 2022 examined event), resulting to significant flood hazards. Therefore, flood protection measures should be taken to specific areas of the River and some hydraulic structures need to be reconstructed in order to cope to, at least, these future flood events.
- The surface runoff is anticipated to increase slightly due to the expansion of the residential development within the Pedieos watershed. This, in combination with the climate change, will result to an increased peak flow of future flood events, and this should be taken into consideration by the competent authorities for any future flood protection studies and decisions on measures to be taken. It is noted that the residential areas are located downstream the Tamassos dam, so the anticipated increase of runoff will not be possible to be attenuated by the dam.
- The flood protection effectiveness of the dam is significant and the initial dam conditions, when a flood event occurs, determine the actual flood protection level to the downstream residential areas.

4. Germany

Acknowledgements

We would like to thank Mr. Alexander Löcke (Wupperverband) for his help with the preparation of the TALSIM model. Additionally, we would like to thank Prof. Dr.-Ing. Jackson Roehrig (Cologne University of Applied Sciences) for his help and support by the Python scripting. Finally, we would also like to thank Ms. Luisa Hoviele (Wupperverband) for her contribution in the preparation of annexes.

Abbreviations

GDT / TDHN	Große Dhünn-Talsperre (Große Dhünn Reservoir)
hurs	Air humidity
ist	Current state
MEZ	Mitteleuropäische Zeit (Central European Time)
PET	Potential evapotranspiration
Eta	Actual Evapotranspiration
ET	Evapotranspiration
pr	Precipitation
SBEV	Bever pluviometric station
SLEV	Leverkusen pluviometric station
SLIN	Lindscheid pluviometric station
SMAN	Manfort water gauge
SODT	Odenthal pluviometric station
SSLB	Schlebusch water gauge
SNEM	Neumühle water gauge
MHQ	Mean maximum discharge
MNQ	Mean low flow discharge
MQ	Mean annual discharge
NQ	Minimum low flow discharge
HQ100	100-year flood
SPEI	Standardised Precipitation-Evapotranspiration Index
SPI	Standardised Precipitation Index
SSU$	Sülzüberleitung (Sülz Diversion) pluviometric station

SVO$	Vorsperre Große Dhünn (Upstream Dhünn Reservoir) pluviometric station
tas	Near-surface air temperature
UGD	Upper Große Dhünn
UTC	Coordinated Universal Time
VGD	Vorsperre Große Dhünn (Upstream Dhünn Reservoir)

Units

T. m^3	Thousand cubic meters
Mm^3	Million cubic meters

Model frameworks

For this deliverable, the following three model frameworks were implemented:

Framework 1: TALSIM was used for the Dhünn catchment area (see D3.3) in order to simulate future climate scenarios (i.e., decadal predictions) in combination with land and water use scenarios ("economy first" and "sustainability eventually", see D3.2). This model addresses the case study "not enough water[1]", focusing on the problematic of dry periods at the GDT. The model was also run for past conditions (1937 - 2017) and different water use scenarios in order to identify past trends.

Framework 2: for UGD, the NASIM was forced with the realisations providing the largest span (max, min, and medium, namely, R1, R9, and R7) including land use scenarios ("economy first" and "sustainability eventually", see D3.2), for the sake of comparison with SWAT. This model does not consider water use changes.

For the whole Dhünn catchment area, the NASIM models calibrated and validated for past conditions (see D3.3) were forced with the ten members of the decadal predictions (not-bias and bias corrected) with current land and water use. These models were not used to simulate the combination of land and water use and climate scenarios due to GDT operational rules, which are better represented with TALSIM (a reservoir-oriented, water balance model). The results of the nine models runs are presented as annex.

Framework 3: NASIM was used for the simulation of extremal episodes for the case study "too much water[2]", specifically for the Mirke Creek in the city of Wuppertal (see D3.3), addressing the problematic of flash floods. The meteorological data used as input for all future conditions (i.e., the ten realisations not-bias and bias corrected as well as the extremal episodes) were provided by FU-Berlin in the frame of WP2.

Framework 4: The flood events of May-June 2018 were also analysed in this deliverable for the case study "too much water[3]". The Leimbach catchment area was simulated in NASIM and was driven with ground data from 1970 until June 2018. Additionally, the model was forced with the realisations providing the largest span

[1] The case study "not enough water" was defined in the frame of WP4 and WP5 together with relevant stakeholders.

[2] The case study "too much water" was defined in the frame of WP4 and WP5 together with relevant stakeholders.

[3] The case study "too much water" was defined in the frame of WP4 and WP5 together with relevant stakeholders.

(max and min, namely, R1 and R9) including land use scenarios ("economy first" and "sustainability eventually", see D3.2).

Table 6 shows a summary of all the simulations carried out for this deliverable.

Table 6: Simulations summary – Wupper research site

Catchment area	Model	Case study / objective	Land use scenarios	Water use scenarios	Decadal predictions	Extremal episodes	No. of simulations
Mirke Creek	NASIM	Too much water	Yes	No	R7 (no bias)	Yes	69
Upper Große Dhünn	NASIM	SWAT comparison	No	No	Ten members (no bias and bias corr.)	No	10
Upper Große Dhünn	NASIM	SWAT comparison	Yes	No	R1, R7, and R9 (no bias and bias corr.)	No	12
Dhünn	NASIM - 9 models	Not enough water	No	No	Ten members (no bias and bias corr.)	No	180
Dhünn	TALSIM	Not enough water	Yes	Yes	R1, R7, and R9 (no bias and bias corr.)	No	42
Dhünn	TALSIM	Not enough water	No	Yes	Past conditions - ground stations (1937 - 2017)	No	4
Leimbach Catchment Area	NASIM	Too much water	Yes	No	R1 and R9 (no bias and bias corr.) and ground stations (1970-2018)	No	14
						TOTAL	**331**

4.1. Model objectives in BINGO [TALSIM – Dhünn catchment area]

For dry periods at GDT (case study "not enough water" - Dhünn catchment area), the model objectives are:

- To establish how many times a threshold was exceeded / not exceeded at representative water gauges
- To determine duration of extreme dry events in terms of reservoir storage volume under a specified threshold
- To analyse the impacts of anthropogenic influences, such as land and water use on surface runoff and reservoir storage volume
- To analyse the impacts of future climate change scenarios on surface runoff and reservoir storage volume
- To analyse the impacts of future climate predictions in combination with land and water use scenarios

4.2. Model application

Future conditions

The TALSIM model was driven by the realisations providing the largest span (min, max, and medium, namely, R9, R1, and R7 - not-bias and bias-corrected) in combination with land and water use scenarios (current state, economy first, and sustainability eventually, see D3.2). For future conditions and under this model framework, 42 simulations were carried out (see Table 6), which implied expensive computing time. Thus, simulations with all ten decadal members was not carried out. The realisations providing the largest span are considered representative for future climate scenarios.

Simulations were carried out from 01.11.2015 to 01.11.2024, with a time step of 30 minutes.

Largest span

The decadal members providing the largest span (max and min) were determined based on resulting simulated discharge (total accumulated volume) at SNEM for the UGD model with NASIM (see Figure 23). Likewise, it was determined that R7 provided the medium span.

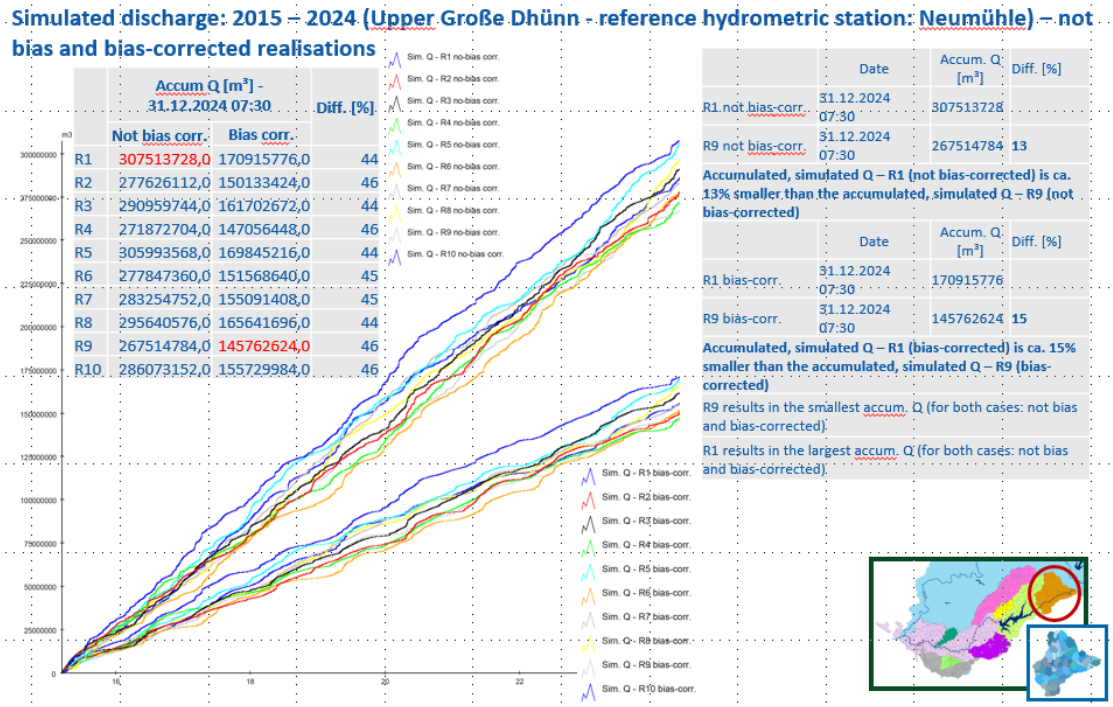

Figure 23: Decadal members with the largest span: R1 - max and R9 – min

Land use scenarios

Land use scenarios were already determined for D3.2, where the available information per administrative unit was regionalized for the Wupper catchment area and then combined with SCENES story lines.

As land use data for the next decade was generated based on past trends, future spatial distribution could not be established. However, it was possible to overcome this drawback on account of the properties of both hydrological models, namely, NASIM and TALSIM. For both models, sub-basin delineation must be carried out previously using GIS tools, based on topography and river network. In addition, with current available land use and soil type, different hydrological response units (HRUs) are determined per sub-basin. This data is then exported to the hydrological models.

Once exported, the available information per sub-basin on the computational domains of NASIM and TALSIM is the extent (i.e., the area) of each HRU, without considering each HRU geometry. Since the geometry of each HRU is neglected by the models, we were able to increase / decrease each land use unit of each HRU within the hydrological models with the determined factors accordingly.

Water use scenarios

Water use scenarios were also already established for D3.2. The main water use categories within the Wupper catchment area are summarized as follows: service water, domestic water, and process or industrial

water. Raw water is the sum of domestic water and process or industrial water. Please refer to D3.2 for detailed explanation of each category.

TALSIM allows the simulation of different operational rules taking into account raw water extraction and service water utilized for flood management and ecological flow regulation. Table 7 shows the operation rules established for the GDT.

Table 7: Operational rules in TALSIM for the GDT

Category	TALSIM denomination	TALSIM denomination (explanation)
Raw water	QW1	Water supply
Service water	QR1	Standard release (controlled at the GDT outlet - Loosenau water gauge)
	QN1	Low flow augmentation for ecological flow regulation (at Manfort water gauge)
	QS1	Flood control zone
	QH1	Flood relief spillway

Past conditions

Additionally, the TALSIM model was run for past conditions (from 1937 to 2017) with ground stations, current land use, and different operational rules (i.e., different water use scenarios) in order to identify past trends and number of occurrences where reservoir storage was under a pre-established threshold. The GDT was put in operation in 1988; however, the long-term past simulations for past conditions consider the GDT as existing reservoir.

4.2.1. Data

Future conditions

Meteorological input data

For future conditions, the TALSIM model was driven with meteorological input data from three realisations providing the largest span (min, max, and medium, namely, R9, R1, and R7 - not-bias and bias-corrected). Since both NASIM and TALSIM allow time steps lower than a day, the 3-hourly raster data was used (see Table 8).

Table 8: Parameter used from the 3-hourly raster provided by WP2

Parameter	Temporal resolution	Spatial resolution
pr (precipitation)	3-h	12 km
tas (near surface temperature)	3-h	12 km
hurs (air humidity)	3-h	12 km

Precipitation was accumulated for the whole time period (i.e., 2015 – 2024) according to the input requirements for TALSIM, keeping the 3-hourly temporal resolution. Mean daily temperature was estimated and entered also as input time series. Temperature and air humidity were linearly interpolated to generate

hourly data and shifted one hour in order to transform time zone UTC to MEZ[4]; then, PET was calculated after Haude method, which uses both parameters at 14:00. This process was carried out for the five raster points that cover the Dhünn catchment area, with a manual allocation of time series for all sub-basins (see Figure 24). Table 9 shows the post-processed input time series for the TALSIM model.

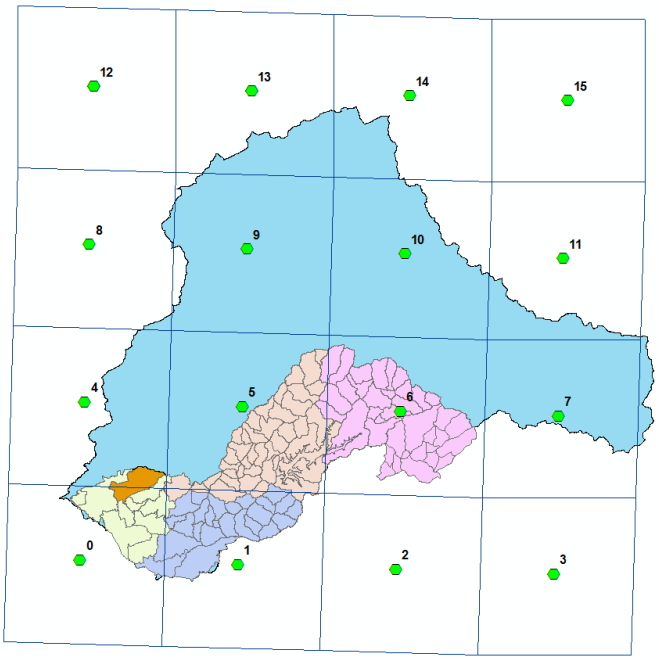

Figure 24: Dhünn catchment area and raster points from the realisations used for simulation of future conditions (five different colours correspond to the five raster points)

Table 9: Input time series for future conditions – GDT TALSIM model

Time Series	Temporal Resolution	Format	Raster point ID
pr (precipitation)	3-h	Accumulated sum	PID00; PID01; PID04; PID05; PID06
tas (temperature near the surface)	daily	daily mean	PID00; PID01; PID04; PID05; PID06
PET	daily	daily PET	PID00; PID01; PID04; PID05; PID06

Analysis of climate data

To analyse the climate data, precipitation from different WP2 data sets for past conditions was compared to ground stations (see Figure 25) by means of determination of the Standardised Precipitation Index (SPI) (Edwards und McKee, 1997) and Standardised Precipitation-Evapotranspiration Index (SPEI) (Beguería et al., 2016). SPEI is more suitable for climate change analysis than SPI since the former considers not only precipitation but also temperature.

Likewise, SPI for different bias correction methods was also compared; indices demonstrated to be more stable than one-to-one correspondence, where differences between raw WP2 (i.e., not bias corrected), CDFt bias corrected, and SeasGLM bias corrected data were negligible (see Annex 4.17.2).

Figure 26-a shows the resulting SPI for the month of June 2011 calculated with ground stations as example, where the results were interpolated using IDW (Inverse Distance Weighting). Figure 26-a shows a similar

[4] MEZ = UTC + 01:00 (winter time)

pattern with respect to Figure 26-b (calculated with WP2 data), indicating that for this particular month and year, the western part of the basin was dryer than normal. Similarly, there is barely a difference between Figure 26-c and Figure 26-d, where SPI was determined with different bias corrected data sets. Figure 26-e shows SPI calculated for June 2018 with R1 showing a drier pattern for the northern part of catchment area.

In conclusion, determination of representative indices serves to compensate spatial and temporal uncertainties. Annex 4.17.2 presents the estimated SPI and SPEI for various time scales and data sets.

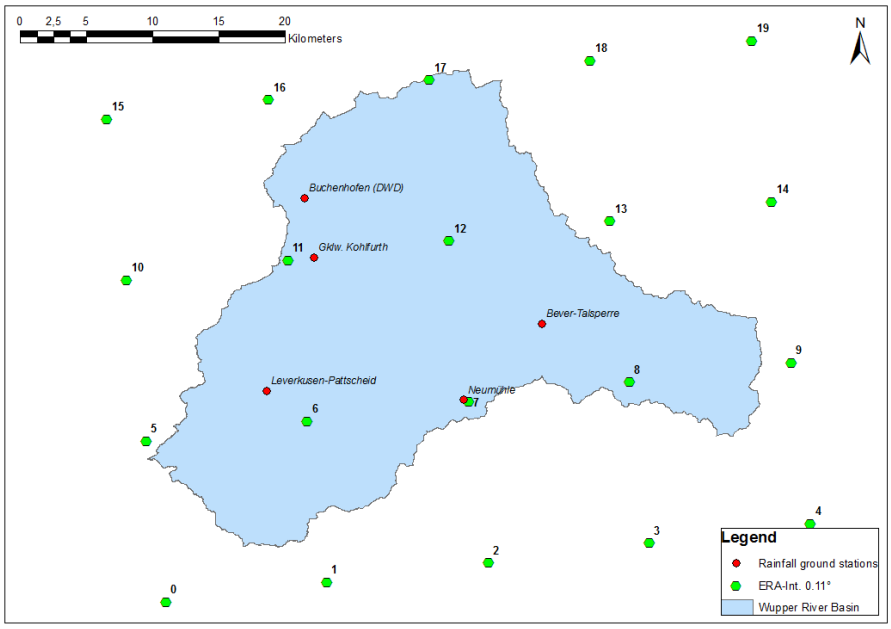

Figure 25: Ground stations used for the analysis of the climate data

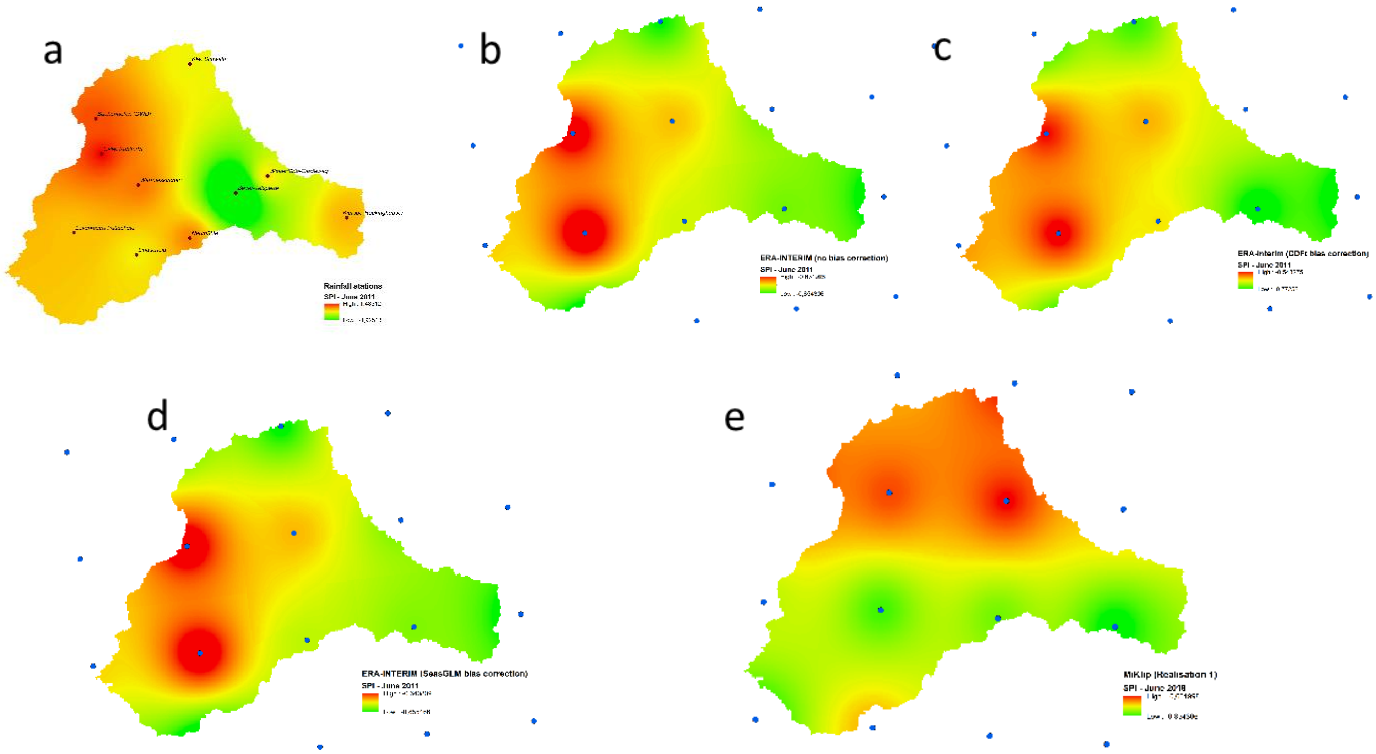

Figure 26: SPI for Wupper catchment area for June 2011

Land use

Future information was generated based on past trends for each administrative unit, as described in D3.2. In order to establish future land use scenarios for the Dhünn catchment area, the implementation of a procedure involving the regionalization of the available information per administrative unit using GIS tools was necessary, based on their surface within the Dhünn catchment (i.e., weight-by-area). Figure 27 shows the degree of sealing for economy first and sustainability eventually scenarios as well as the sub-basins corresponding to five 3-hourly raster points used for the simulations. For economy first, the degree of sealing at the Dhünn catchment area is expected to increase ca. 20 % within the next ten years, while for sustainability eventually, the degree of sealing is expected to increase ca. 2 % within the next ten years.

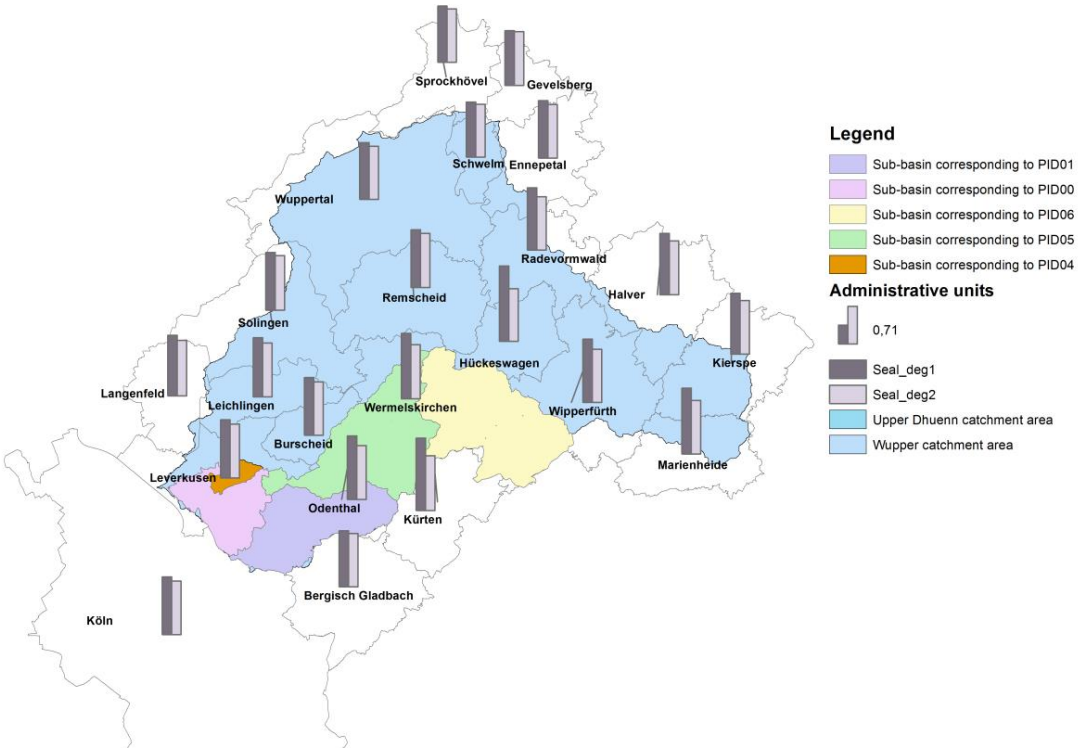

Figure 27: Degree of sealing per administrative unit and sub-basins corresponding to five 3-hourly raster points

Water use

For GDT, the following boundary conditions must be considered:

a) Objective of GDT: provision of raw and service water
b) Current contractual water delivery: 42 Mm³/year
c) Actual water delivery: 38 Mm³/year
d) Emergency water supply for the city of Düsseldorf: 10 Mm³
e) Ensuring of low flow augmentation of 1 m³/s at Manfort water gauge (ca. 8 Mm³/year)
f) Critical reservoir storage level: 35 Mm³ (defined threshold based on adequate limnological conditions)

Both future raw water scenarios (i.e., economy first and sustainability eventually) comprise water demand in terms of population growth and energy production; they were established with the available information per

administrative unit, regionalized for the Wupper catchment area, and then combined with SCENES story lines (see D3.2).

To obtain future water demand for the GDT for economy first and sustainability eventually, the following methodology was applied, based on Table 33 “Future water use in Wuppertal”, page 45, D3.2:

i) The change in percentage from the years 2015 to 2030 was calculated for both scenarios: a) for economy first, raw water supply is expected to increase ca. 20.8 % within the next 15 years; b) for sustainability eventually, raw water supply is expected to diminish ca. 10.6 % within the next 15 years.

ii) The current contractual water delivery was multiplied by both factors for both scenarios, respectively.

For economy first scenario, the obtained value of ca. 51 Mm³/year coincides with the sum of the current contractual water delivery (42 Mm³/year) and a theoretical constant water delivery for the city of Düsseldorf (10 Mm³). For sustainability eventually, the obtained value of ca. 37 Mm³/year coincides with the actual water delivery of 38 Mm³/year. The adopted values regarding future raw water demand for economy first and sustainability scenarios were rounded to 52 Mm³/year and 38 Mm³, respectively, in order to adapt them to current GDT conditions.

For service water, the low flow augmentation at Manfort water gauge was the only parameter from Table 6 taken into account for the establishment of both scenarios in the context of “not enough water” case study. The other parameters from Table 10 concerning service water are regarded as unmodifiable boundary conditions (flood control operational rules are established permanently based on the response to a flood wave considering the physical characteristics of the reservoir).

Low flow augmentation operational rules were established for both scenarios based on the current guaranteed ecological flow (i.e., 1 m³/s) and a newly proposed value of 0.7 m³/s (this subject is currently under discussion among various actors from Wupper research site). Table 10 shows a summary of the established water use scenarios for future conditions at GDT.

Table 10: Economy first and sustainability eventually water use scenarios for the Dhünn catchment area

Current state	**Economy first**	**Sustainability eventually**
Contractual raw water delivery = 42 Mm³/year	Raw water extraction = 52 Mm³/year (contractual raw water delivery + 10 Mm³/year of constant water delivery for the city of Düsseldorf)	Actual raw water delivery = 38 Mm³/year
Low flow augmentation: minimum downstream discharge at Manfort hydrometric station = 1 m³/s	Low flow augmentation: minimum downstream discharge at Manfort hydrometric station = 0.7 m³/s	Low flow augmentation: minimum downstream discharge at Manfort hydrometric station = 1 m³/s

Water gauges

Results were obtained at the following water gauges (see Figure 28): Neumühle (SNEM) – inflow; Manfort (SMAN) – outflow; Schlebusch (SSLB) – outflow; Große Dhünn Reservoir (GDT/TDHN) - storage volume.

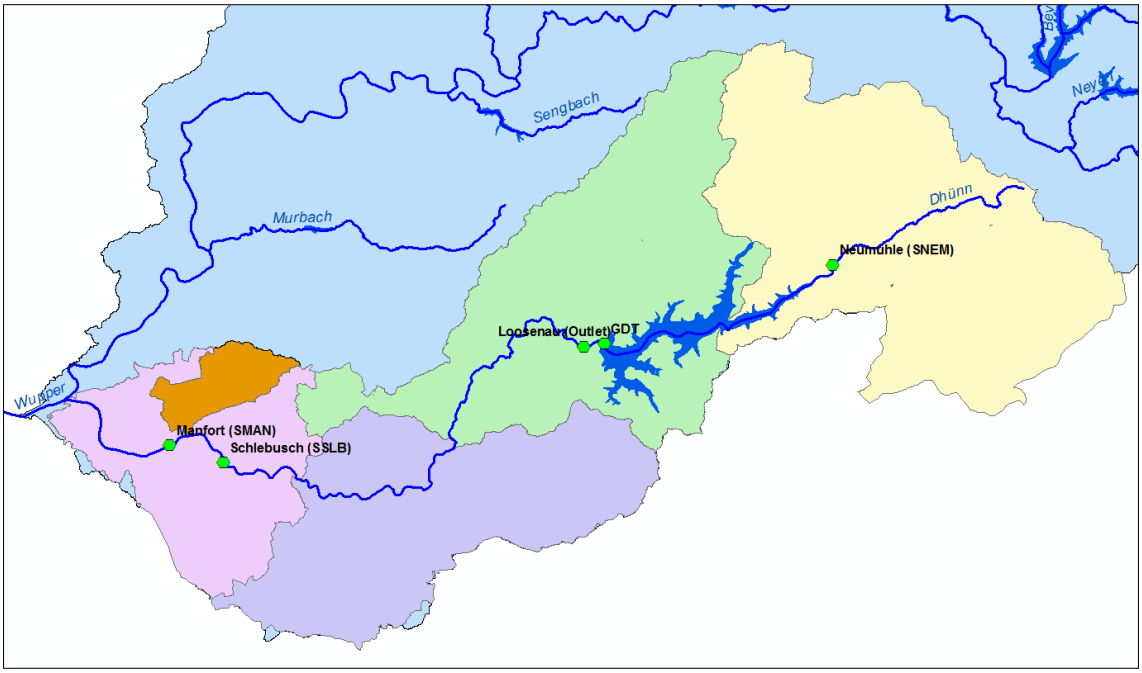

Figure 28: Water gauges where results were obtained

Past conditions

Meteorological input data

For past conditions (1937 – 2017), precipitation from the following six ground stations were used (see Figure 29): Lindscheid (SLIN), Upstream Dhünn Reservoir (SVO$), Leverkusen (SLEV), Bever (SBEV), Odenthal (SODT), and Sülz Diversion (SSU$).

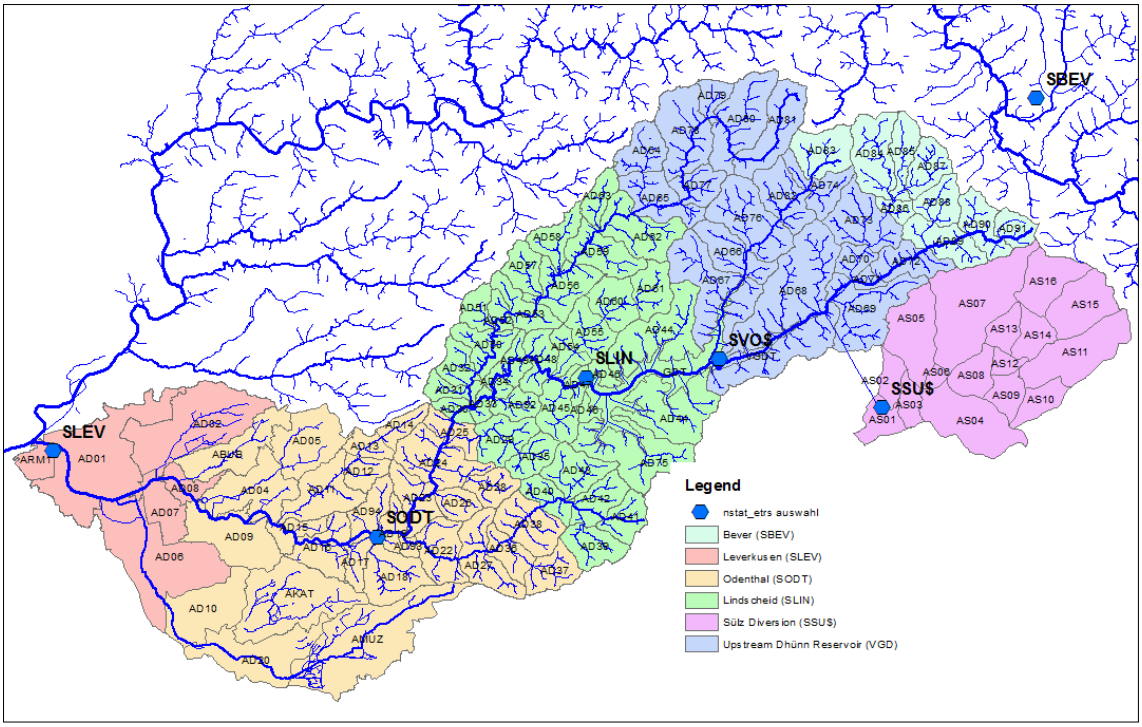

Figure 29: Ground stations with precipitation data used for the simulation for past conditions

Water use

Table 11 presents the set up scenarios based on different operational rules at GDT.

Table 11: Different water use scenarios used for simulation of past conditions

Variant 1	Variant 2	Variant 3	Variant 4
Actual raw water delivery = 38 Mm³/year	Contractual raw water delivery = 42 Mm³/year	Raw water extraction = 52 Mm³/year (contractual raw water delivery + 10 Mm³/year of constant water delivery for the city of Düsseldorf)	Contractual raw water delivery = 42 Mm³/year
Low flow augmentation: minimum downstream discharge at Manfort hydrometric station = 1 m³/s	Low flow augmentation: minimum downstream discharge at Manfort hydrometric station = 1 m³/s	Low flow augmentation: minimum downstream discharge at Manfort hydrometric station = 1 m³/s	Low flow augmentation: minimum downstream discharge at Manfort hydrometric station = 0.7 m³/s

Water gauges

Results were obtained at the following water gauges (see Figure 28): Neumühle (SNEM) – inflow; Manfort (SMAN) – outflow; Schlebusch (SSLB) – outflow; Große Dhünn Reservoir (GDT/TDHN) - storage volume.

4.2.2. Results

Future conditions:

The simulation results for the future conditions were analysed based on the model objectives for the case study “not enough water”. For this purpose, simulated discharge values (m³/s) were obtained from the following three water gauges (see Figure 28):

- Neumühle (SNEM) – located upstream of the Große Dhünn Reservoir
- Manfort (SMAN) – located downstream of the Große Dhünn Reservoir
- Schlebusch (SSLB) – located downstream of the Große Dhünn Reservoir

Additionally, the results of the simulated storage volume (T. m³) of the Große Dhünn Reservoir (TDHN) were also considered for the future conditions analysis (see Figure 28).

The analysis of the model results for future conditions was performed in three steps:

- The determination of threshold values for the discharge at each water gauge under study and the storage volume for the GDT
- The selection of scenarios that apply to different schemes of land and water use within the future conditions representing the selected realisations (see 4.2)
- The comparison between the selected scenario combinations based on the number of occurrences exceeding and/or laying below the established threshold value

Two thresholds were determined for the analysis of results of the discharges at the three water gauges, one upper and one lower threshold value. The thresholds applied to the discharge values were defined based on two characteristic indicators of the water gauges, previously established through historical data: the mean maximum discharge (MHQ) was set as the upper threshold value and the mean low flow discharge (MNQ) as the lower threshold value. The minimum reservoir storage volume, which corresponds to the critical

volume fulfilling the limnological conditions of the reservoir, was defined as the lower threshold value for the GDT.

The simulated discharge values of the three water gauges obtained in each combination were correlated to the upper and lower threshold. As a result, the frequency of threshold exceedance and lower deviation could provide significant insights regarding the effect of change in climate conditions, land use, and water use on the water quantity within the study area. Regarding the GDT, the simulated volume values were compared to the reservoir storage volume threshold. Thereby, not only the frequency of the threshold lower deviation could be determined, but also the duration of extreme events in terms of reservoir storage volume with respect to alteration in the climate, land use, and water use circumstances.

Seven scenario combinations were selected in order to approach all the aspects of the main model objectives. As a result, seven comparisons were carried out and provided the main input for the result analysis. The first two scenario combinations focused on the differences among the results of the three selected decadal members (not-bias and bias-corrected) within the current state of land and water use. The third comparison aimed at investigating the significance of the impacts due to land use change during one climate scenario, while comparison four focused on the impacts due to different water use conditions. Within the fifth combination, the results of the current state in land and water use was compared to the future scenarios “economy first” and “sustainability eventually”.

Table 12: Summary of the comparisons of future scenarios

Comparison	Future realisations (decadal members)	Land use scenarios	Water use scenarios	Compared scenarios
Comparison 1	R1, R7, R9 (not bias corrected)	Current State (LU ist)	Current State (WU ist)	R1 LU ist – WU ist R7 LU ist – WU ist R9 LU ist – WU ist
Comparison 2	R1, R7, R9 (bias corrected)	Current State (LU ist)	Current State (WU ist)	R1 LU ist – WU ist R7 LU ist – WU ist R9 LU ist – WU ist
Comparison 3	R1 (bias corrected)	Current State (LU ist) Econ. First (LU 1) Sust. Eventually (LU 2)	Current State (WU ist) Econ. First (WU ist) Sust. Eventually (WU ist)	R1 LU ist – WU ist R1 LU 1 – WU ist R1 LU 2 – WU ist
Comparison 4	R1 (bias corrected)	Current State (LU ist) Econ. First (LU ist) Sust. Eventually (LU ist)	Current State (ist) Econ. First (WU 1) Sust. Eventually (WU 2)	R1 LU ist – WU ist R1 LU ist – WU 1 R1 LU ist – WU 2
Comparison 5	R1 (bias corrected)	Current State (LU ist) Econ. First (LU 1) Sust. Eventually (LU 2)	Current State (WU ist) Econ. First (WU 1) Sust. Eventually (WU 2)	R1 LU ist – WU ist R1 LU 1 – WU 1 R1 LU 2 – WU 2
Comparison 6	R1, R7, R9 (bias corrected)	Econ. First (LU 1)	Econ. First (WU 1)	R1 LU 1– WU 1 R7 LU 1 – WU 1 R9 LU 1 – WU 1
Comparison 7	R1, R7, R9 (bias corrected)	Sust. Eventually (LU 2)	Sust. Eventually (WU 2)	R1 LU 2 – WU 2 R7 LU 2 – WU 2 R9 LU 2 – WU 2

The last two combinations aimed at illustrating the impact of the future scenarios for land and water use "economy first" and "sustainability eventually", respectively, derived from the three future selected climates scenarios. Table 12 summarises the comparisons of future scenarios that were carried out for the analysis of results:

Analysis of results

Comparison 1

In the first scenario combination, it is observed that simulated discharge at the hydrometric station SNEM, upstream of the GDT, is higher within the climate scenario R1 (see Figure 30-b). At the same time, the highest frequency of low discharge values is observed during the climate scenario R9 (see Figure 30-a). Furthermore, the simulated discharge levels derived from the three climate scenarios do not exceed the flood flow threshold on a high frequency, in contrast to their deviation below the mean low flow threshold.

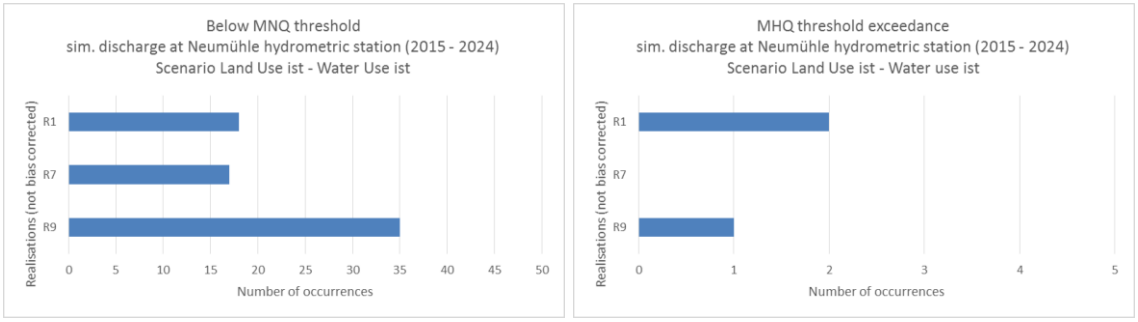

Figure 30: Comp. 1 SNEM (a) below threshold and (b) threshold exceedance

Downstream of the GDT, at the water gauges SMAN and SSLB, the simulated discharge is higher within the future condition R1 (see Figure 31-b and Figure 32-b), similar to the discharge performance at the water gauge SNEM. The lower frequency of threshold exceedance is observed within climate scenario R9 at the station SMAN (see Figure 31-b), while at the station SSLB it is detected during the scenario R7 (Figure 32-b). As far as the lower threshold is concerned, the discharge obtained from all three climate scenarios in both stations lays below the lower threshold only once during all the simulation period (see Figure 31-a and Figure 32-a).

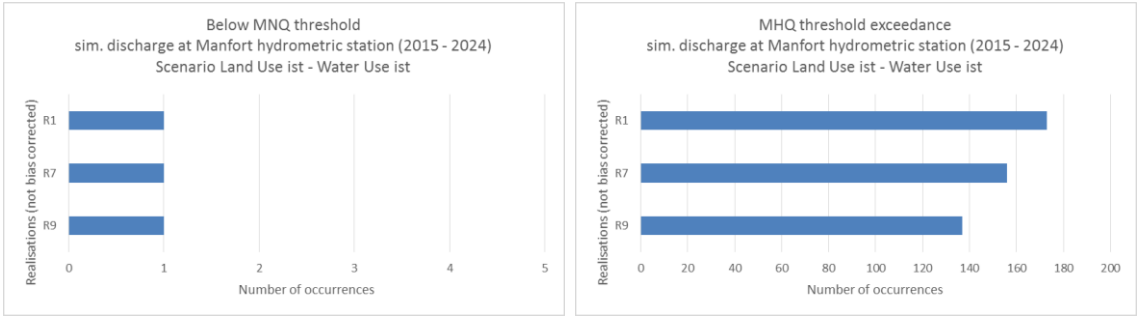

Figure 31: Comp. 1 SMAN (a) below threshold and (b) threshold exceedance

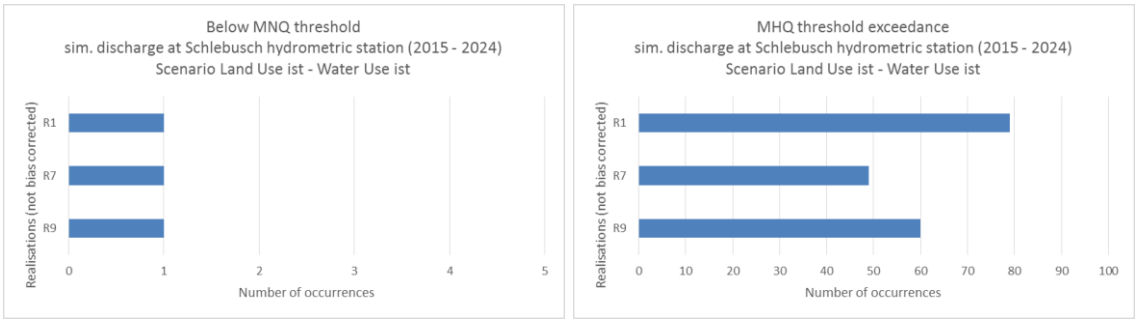

Figure 32: Comp. 1 SSLB (a) below threshold and (b) threshold exceedance

With respect to the simulated storage volume at the GDT reservoir, no occurrences of deviation below threshold are observed during the scenarios of the first combination.

Comparison 2

Similar to the scenarios of Comparison 1, the simulated discharge at all three hydrometric stations is observed to reach values below the lower threshold on a higher frequency within the climate scenario R9 (see Figure 33, Figure 34-a and Figure 35-a). However, compared to the results of the former combination, which are obtained by scenarios with no bias corrected decadal members, insights can be derived concerning the influence of the bias correction of the selected decadal members on the simulated discharge values. More specifically, it is observed that within the bias corrected R1 climate scenario, no discharge values at the hydrometric station SNEM exceed the higher threshold. At the same time, at the downstream stations SMAN and SSLB upper threshold exceedances appear to occur on a distinctly lower frequency (see Figure 34 and Figure 35). Moreover, the simulated discharge levels laying lower than the low flow threshold appear on a higher frequency at all three water gauges (see Figure 33, Figure 34 and Figure 35).

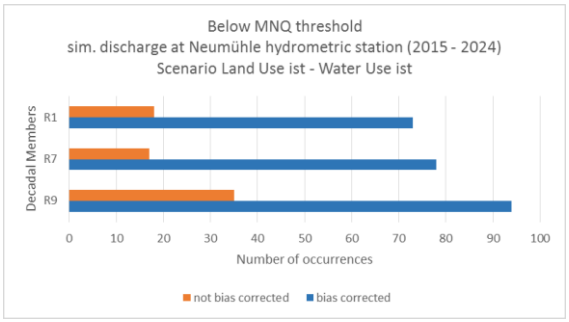

Figure 33: Comp. 2 SNEM below threshold

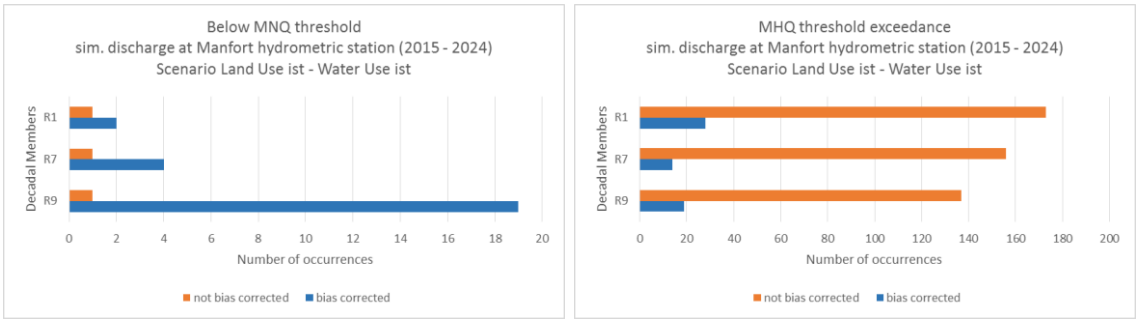

Figure 34: Comp. 2 SMAN (a) below threshold and (b) threshold exceedance

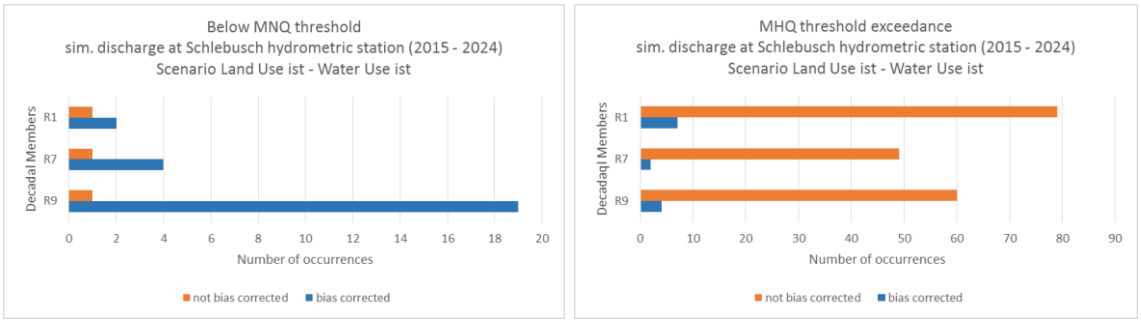

Figure 35: Comp. 2 SSLB (a) below threshold and (b) threshold exceedance

The same conclusion can be drawn regarding the results obtained by the bias corrected decadal members from the reservoir storage volume at TDHN, which lays under the critical reservoir storage volume more frequently within these scenarios (see Figure 36). In conclusion, a comparison between the first and second scenario combination leads to the assumption that the climate scenarios derived from bias corrected decadal members tend to present lower discharge and volume values.

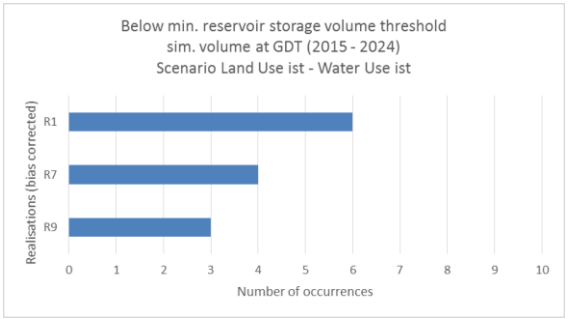

Figure 36: Comp. 2 TDHN below threshold

Comparison 3

The comparison results derived from the third scenario combination provide insights regarding the impact of the changes in land use on the water quantity. More specifically, the focus was placed on the influence of

land use changes on water quantity with respect to the upper threshold more than the lower threshold, since land use changes affect directly the surface permeability leading to changes on the surface discharge. As illustrated in the following figures (See Figure 37, Figure 38-a, Figure 39-a and Figure 40), the frequency of deviation below threshold among the current state, the case study “economy first” and the case study “sustainability eventually” show no change. On the other hand, changes in the frequency of upper threshold exceedances is observed in the simulated discharge of the water gauges downstream the reservoir, however with no remarkable deviation (See Figure 38-b and Figure 39-b). In more detail, land use change corresponding to case study “economy first” leads to a higher frequency of exceedances, while results obtained by land use changes corresponding to case study “sustainability eventually” show the same performance as the results within the current state. As a result the assumption can be drawn that land use change alone does not lead to considerable changes in the water quantity.

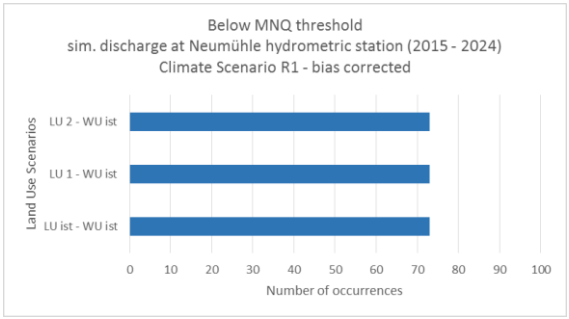

Figure 37: Comp. 3 SNEM below threshold

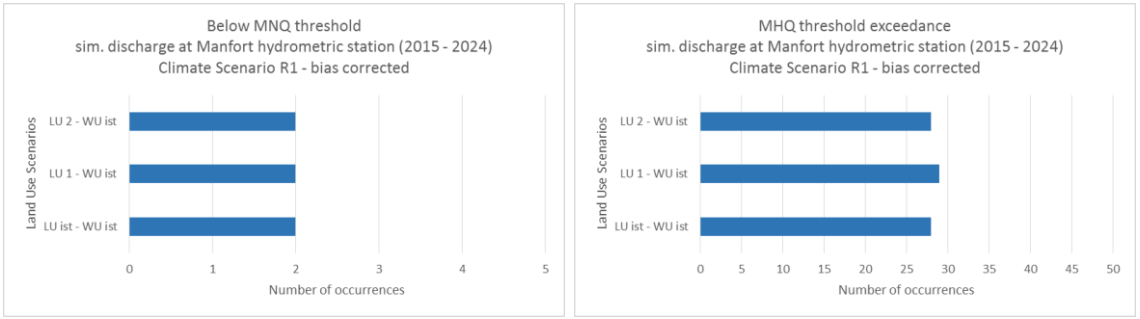

Figure 38: Comp. 3 SMAN (a) below threshold and (b) threshold exceedance

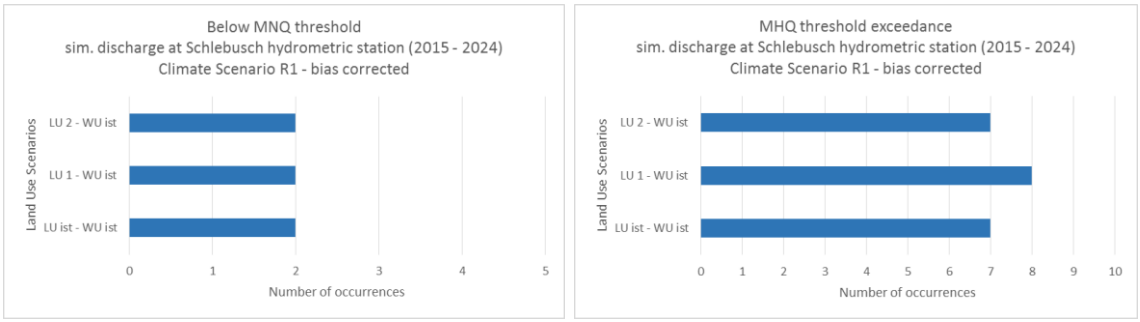

Figure 39: Comp. 3 SSLB (a) below threshold and (b) threshold exceedance

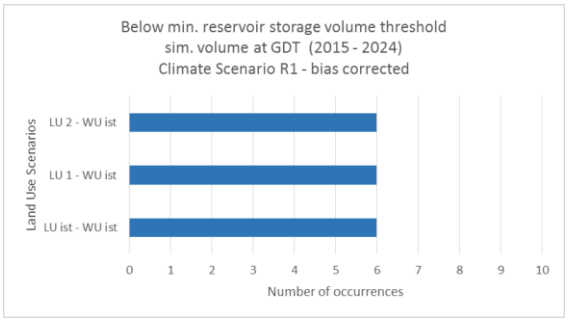

Figure 40: Comp. 3 TDHN below threshold

Comparison 4

In contrast to the former comparison, the results of the forth combination highlight the influence on water quantity due to changes in water use alone. Consequently, major focus in this comparison has been placed on the impact of water use changes with respect to the lower threshold value. Additionally, since the water use changes apply to the reservoir operational rules, possible impacts were expected and therefore observed in the simulated discharges at the two water gauges downstream of the reservoir (SMAN and SSLB) as well as the simulated reservoir volume at GDT. On the other hand, the results of the hydrometric located station upstream of the reservoir (SNEM), no changes on the discharge were neither expected nor observed (Figure 41).

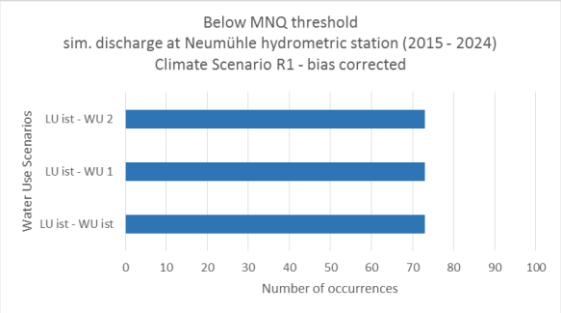

Figure 41: Comp. 4 SNEM below threshold

As illustrated in Figure 42-b and Figure 43-b, the number of threshold exceedances in the discharge of both water gauges downstream of GDT occurs more frequently in the case study “sustainability eventually”, followed by the current state in land and water use. Proportionally to the water use conditions of the three scenarios, case study “economy first” shows the lower frequency in over upper threshold discharge values (See Figure 42-b and Figure 43-b). On the contrary, the water use scenario that provides the highest frequency of discharge values laying below the low flow threshold is consequently “economy first” (See Figure 42-a and Figure 43-a).

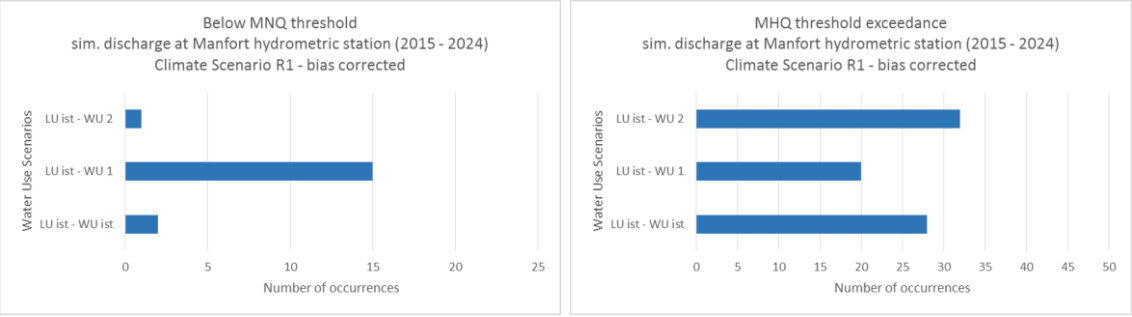

Figure 42: Comp. 4 SMAN (a) below threshold and (b) threshold exceedance

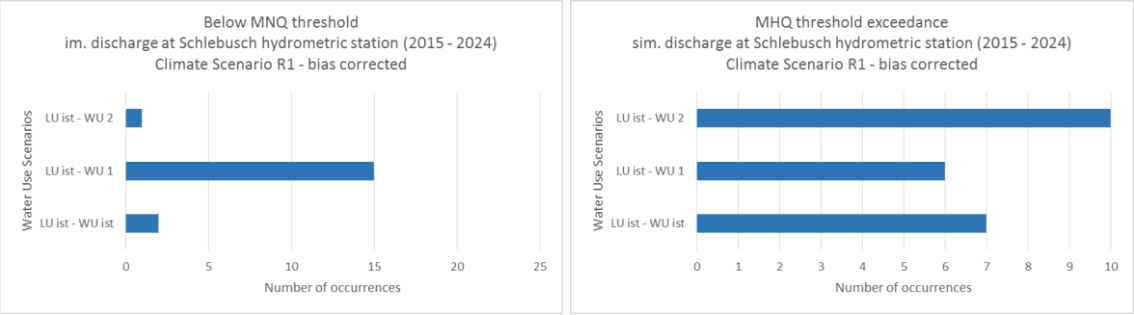

Figure 43: Comp. 4 SSLB (a) below threshold and (b) threshold exceedance

With respect to the simulated volume of GDT (See Figure 44-a), it is observed that the number of occurrences, where the simulated volume lays under the critical threshold, appear more often in the current state, followed by scenario “economy first”. Less frequency of occurrences below threshold are observed in

the “sustainability eventually” scenario. Nevertheless, the total duration of the occurrences illustrate a different image. During the scenario “economy first”, it has been observed that the total duration of events where the volume reached values below threshold is around two times more than in the current state. Additionally, the occurrences within the current state scenario have lasted in total eight times more than the occurrences within scenario “sustainability eventually” (See Figure 44-b).

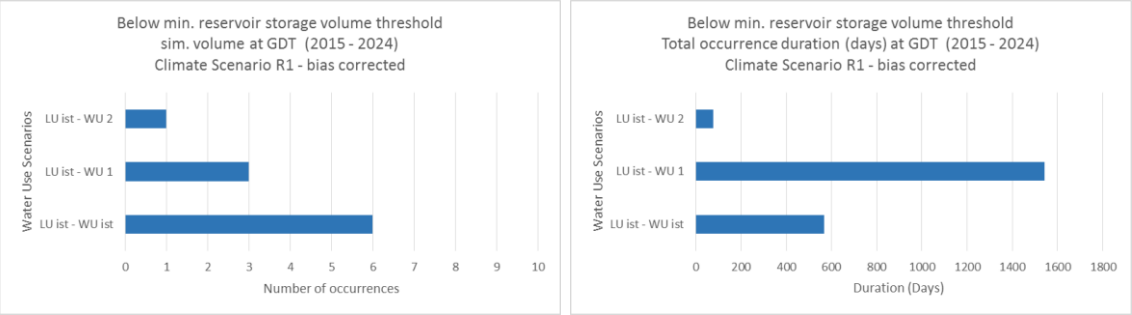

Figure 44: Comp. 4 TDHN (a) below threshold and (b) total occurrence duration

Comparison 5

The fifth comparison aims at analysing the differences among the scenarios “economy first”, “sustainability eventually”, and current state with respect to alterations on both land and water use. The results derived from this comparison, as illustrated in the following figures (See Figure 45, Figure 46, Figure 47 and Figure 48), show no difference compared to the results from the previous comparison, either on the behaviour regarding the simulated discharge and volume or on the total duration of occurrences below threshold in the case of GDT. Hence, the results of Comparison 5 support the conclusion drown in Comparison 3: land use changes do not cause any significant impact on the water quantity, within the time range from 2015 to 2024.

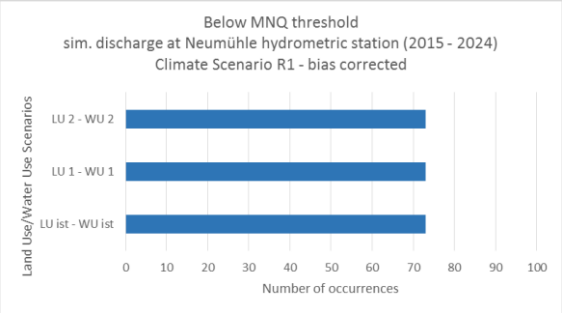

Figure 45: Comp. 5 SNEM below threshold

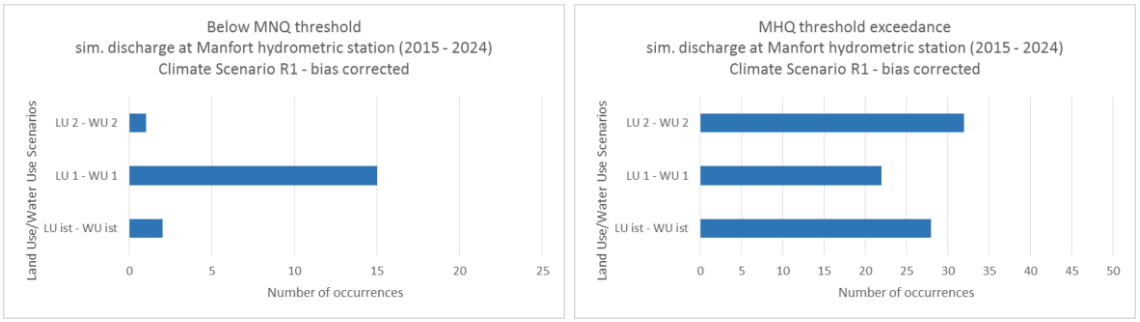

Figure 46: Comp. 5 SMAN (a) below threshold and (b) threshold exceedance

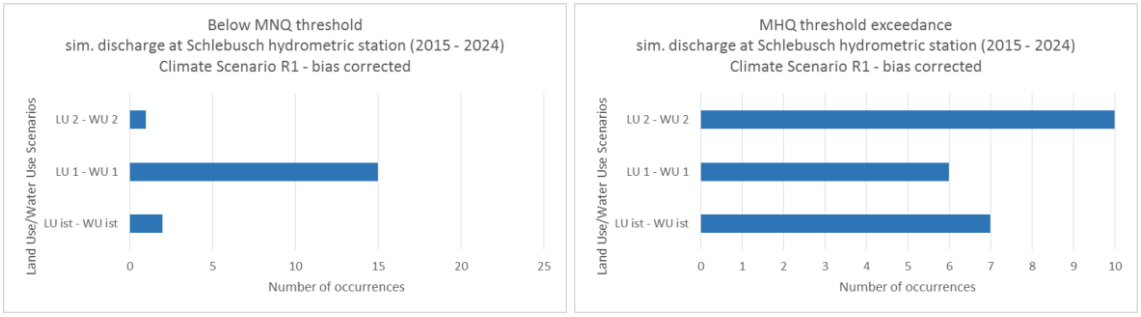

Figure 47: Comp. 5 SSLB (a) below threshold and (b) threshold exceedance

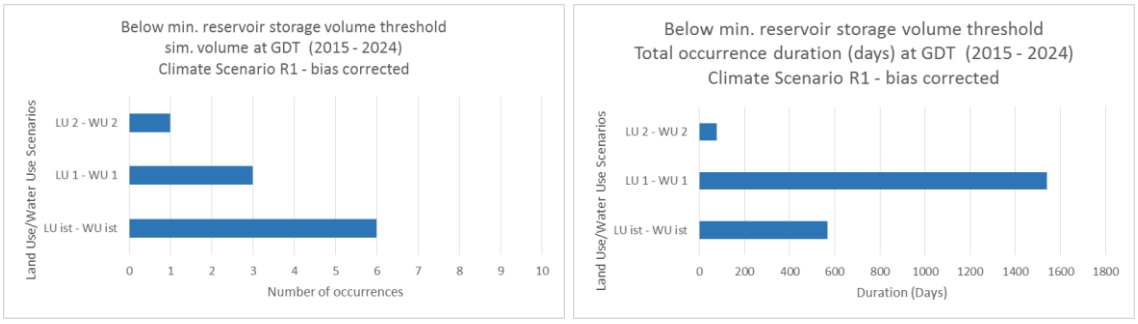

Figure 48: Comp. 5 TDHN (a) below threshold and (b) total occurrence duration

Comparison 6

The sixth combination of scenarios illustrates the behaviour of the simulated discharge and volume within the future scenario “economy first”, as a result of the three bias corrected decadal members R1, R7, and R9. As following figures show (See Figure 49, Figure 50, Figure 51 and Figure 52), the results show similarities to the results of the current state scenario forced by the bias corrected decadal members, although the value range is in a different scale.

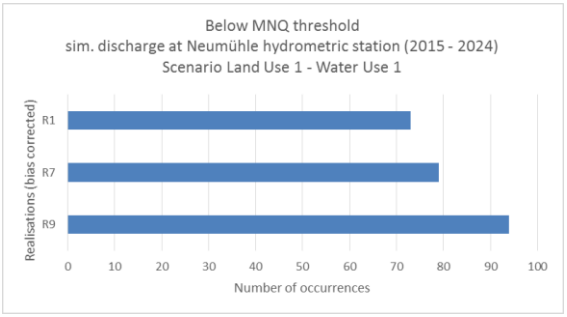

Figure 49: Comp. 6 SNEM below threshold

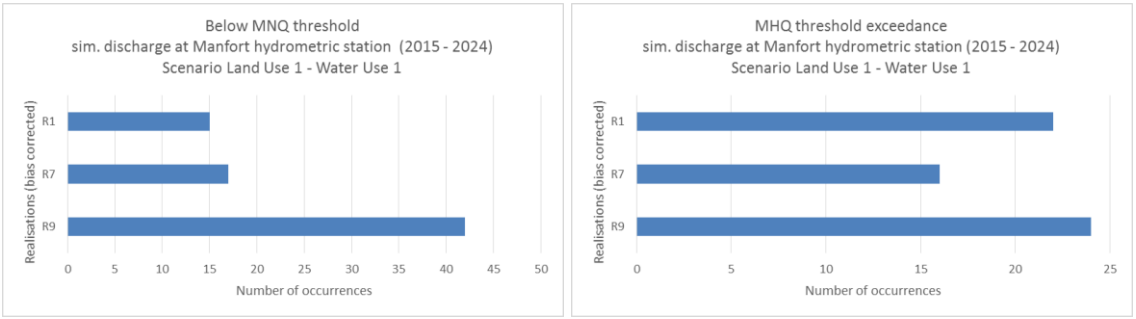

Figure 50: Comp. 6 SMAN (a) below threshold and (b) threshold exceedance

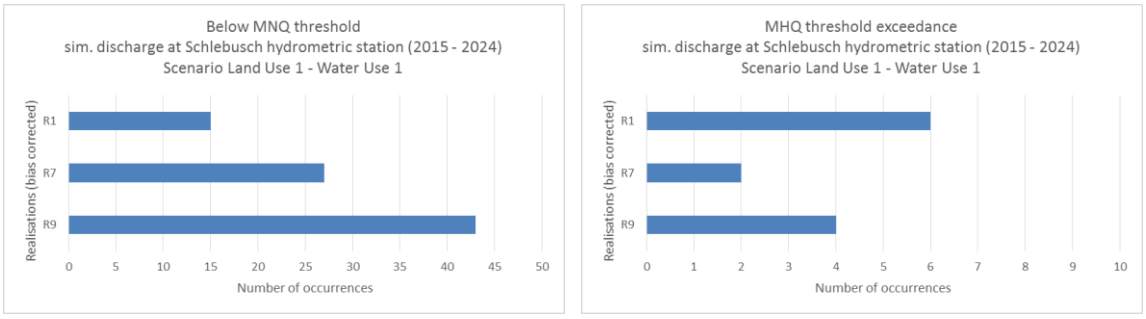

Figure 51: Comp. 6 SSLB (a) below threshold and (b) threshold exceedance

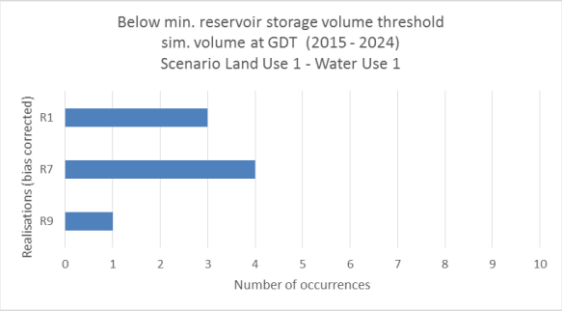

Figure 52: Comp. 6 TDHN below threshold

However, in order to obtain significant insights regarding the impact of all three factors (i.e., climate, water use, and land use) on the water quantity, it is essential to include the scenario “sustainability eventually” in the final combination.

Comparison 7

The last combination of this framework aimed at comparing the results of the current state with those of the scenario “sustainability eventually” within the three future conditions, similar to the previous comparison. However, as mentioned above, in order to obtain a comprehensive idea regarding the impacts of all three parameters, i.e., climate change, water use, and land use alterations, the results from all three scenarios forced by all three decadal members were compared together. As illustrated by the following figures (See Figure 53, Figure 55, Figure 54, and Figure 56), this comparison consists of summary of the conclusions drawn in the analysis above.

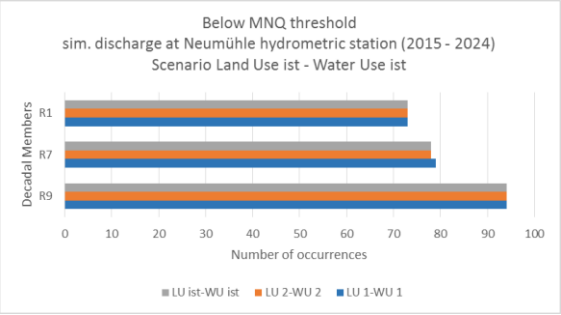

Figure 53: Comp. 7 SNEM below threshold

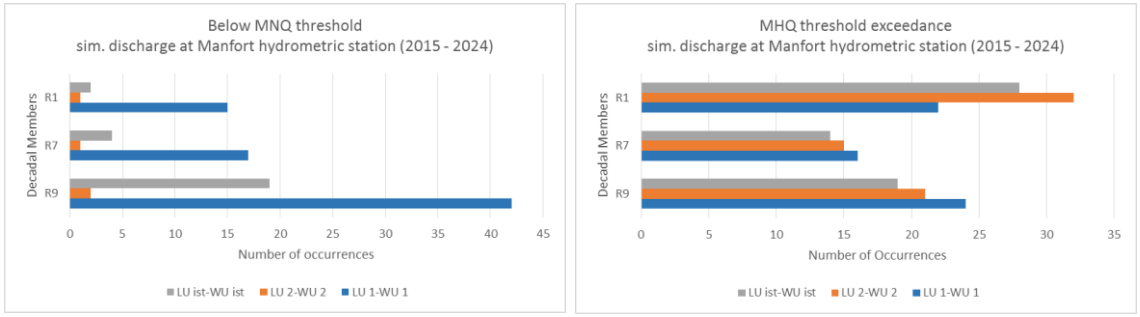

Figure 54: Comp. 7 SMAN (a) below threshold and (b) threshold exceedance

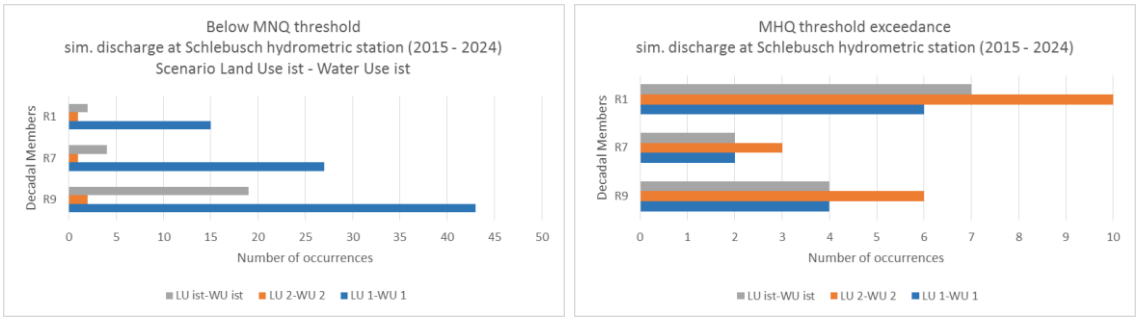

Figure 55: Comp. 7 SSLB (a) below threshold and (b) threshold exceedance

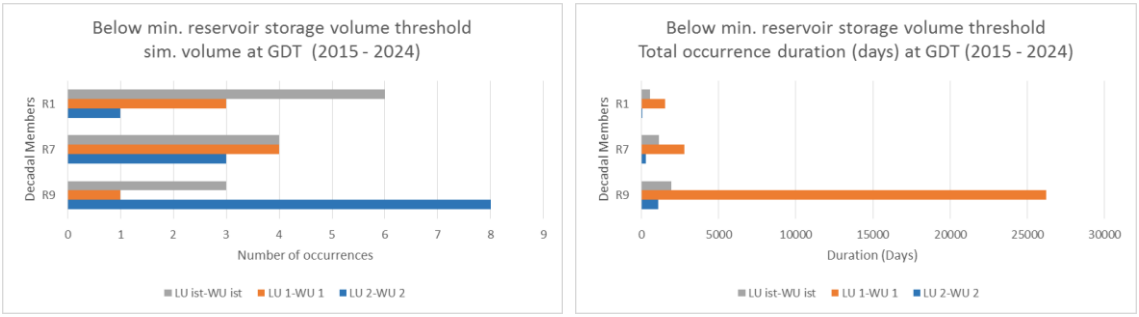

Figure 56: Comp. 7 TDHN (a) below threshold and (b) total occurrence duration

Annex 4.17.1 presents several hydrographs of the simulations carried out, illustrating the threshold exceedances / non-exceedances.

<u>Past conditions:</u>

Figure 57 to Figure 82 show the resulting simulated volume at GDT. Land use used for the time period from 1937 to 2017 was the current state. Variant 3, as expected, is the most critical one, being under the threshold almost a decade in the 40s. This is a very important result to present to relevant stakeholders.

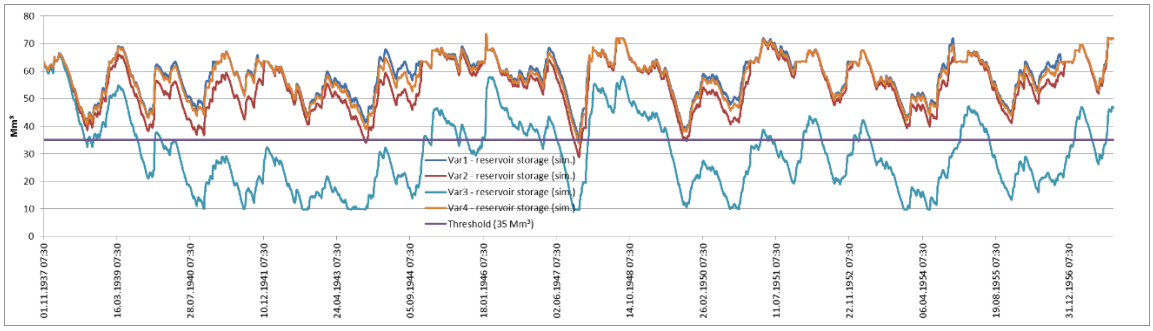

Figure 57: Simulated volume at GDT from 1937 – 1957 (dark blue – var 1; red – var 2; aqua – var 3; orange – var 4; purple – 35 Mm³ threshold)

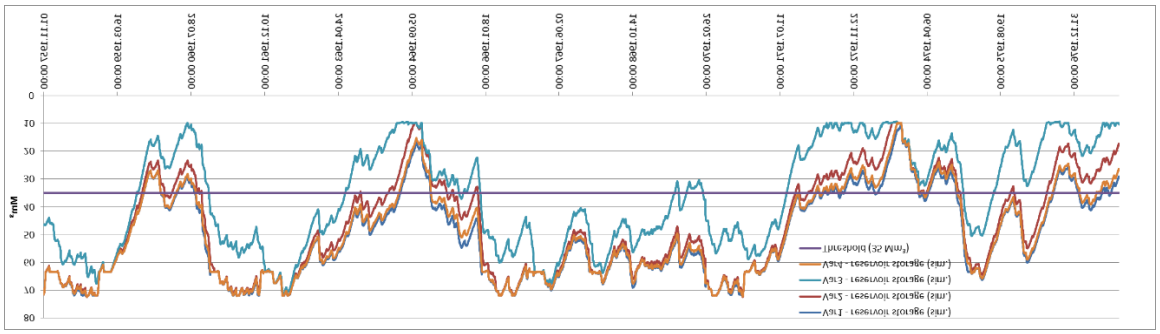

Figure 58: Simulated volume at GDT from 1957 – 1977 (dark blue – var 1; red – var 2; aqua – var 3; orange – var 4; purple – 35 Mm³ threshold)

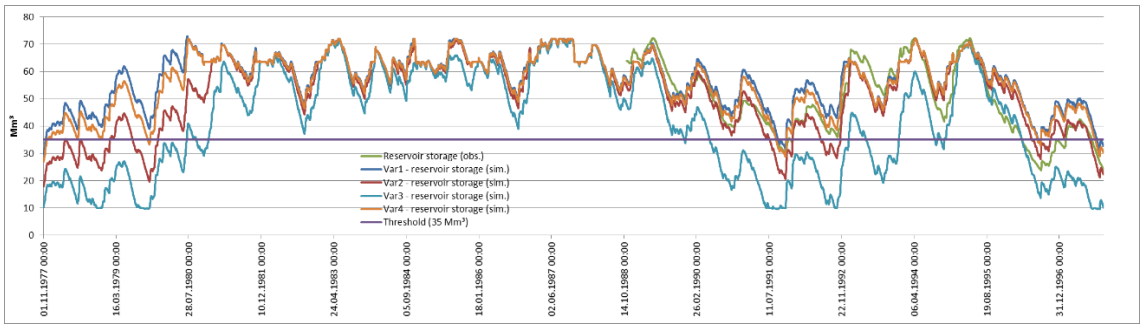

Figure 59: Simulated volume at GDT from 1977 – 1997 (green – observed volume as of 1988; dark blue – var 1; red – var 2; aqua – var 3; orange – var 4; purple – 35 Mm³ threshold)

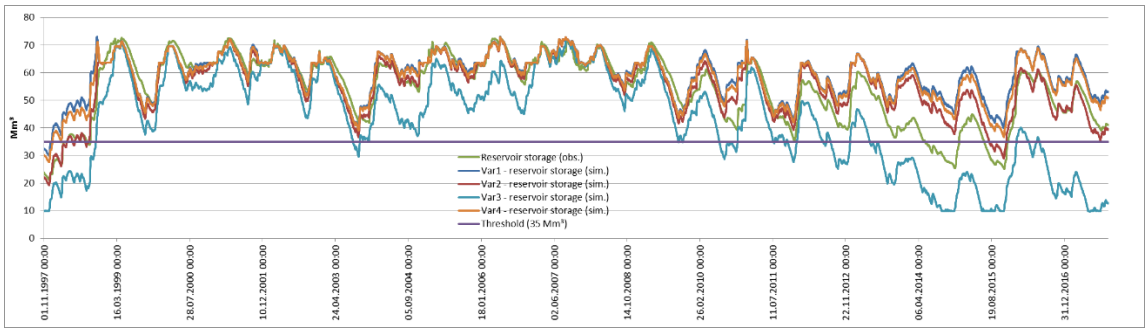

Figure 60: Simulated volume at GDT from 1997 – 2017 (green – observed volume as of 1988; dark blue – var 1; red – var 2; aqua – var 3; orange – var 4; purple – 35 Mm³ threshold)

4.3. Discussion

The following summarises the essential concluding points for future conditions:

- The future condition derived from the decadal member R9 consists of the most critical scenario as far as the case study “not enough water” is concerned.
- Changes on land use do not have any significant impacts on water quantity within the time range from 2015 to 2024. On the contrary, changes on water use have a significant impact both on reservoir storage and downstream runoff.
- No major impacts have been observed at the simulated discharge values at the upstream hydrometric station SNEM.
- The downstream water gauges SMAN and SSLB show similar behaviour regarding the simulated discharge values. More specifically, the scenario “economy first” within the future condition of the decadal member R9 appear to be the most challenging scenario.
- Same conclusion can be drawn with respect to the simulated volume values at the GDT, where the total duration of occurrences with volume below the critical conditions tends to be significantly longer within the scenario “economy first” forced by the decadal member R9.

For past conditions, similar conclusions can be drawn with respect to water use scenarios:

- By an assumed constant water delivery for the city of Düsseldorf (Variant 4) is simulated storage volume very often under the threshold

4.4. Bibliography

Begueria S., Latorre, B., Reig, F. und Vicente-Serrano, S.M., 2016. SPEI Global Drought Monitor. http://spei.csic.es/map/maps.html

D3.2 - Future Land and Water Use Scenarios

D3.3 – Calibrated water resources models for past conditions

Edwards D.C. and McKee, T.B., 1997. Characteristics of 20th century drought in the United States at multiple scales. Atmospheric Science, Paper No. 634, May; 1–30.

Rust, H.W., Richling, A., Meredith, E., Fischer, M., Vagenas, C., Kpogo-Nuwoklo, K.A., Kadow, C., Ulbrich, U. (2017). DECO - A plug-in for data extraction and conversion developed within and for BINGO. Freie Universität Berlin, Version from December 8, 2017

4.5. Model objectives in BINGO [NASIM – Dhünn catchment area]

For dry periods at GDT catchment area (case study "not enough water" - Dhünn catchment area), the general objective is:

- To analyse the impacts on simulated discharge with all decadal members (not bias-corrected and bias corrected data) at different water gauges of the Dhünn catchment area
- To carry out a comparison between NASIM and SWAT for the catchment area corresponding to GDT inflow (UGD)

This model framework is sub-divided as follows:

- NASIM – SWAT comparison for the UGD catchment area (climate and land use scenarios considered)
- NASIM nine sub-models for the whole Dhünn River Basin in accordance to D3.3 (only climate scenarios considered)

4.6. Model application

The NASIM models of the Dhünn catchment area (nine sub-models, see D3.3) were driven with the ten available decadal members and current land and water use. For the Wupper case, water use scenarios are directly related to the operational rules of the GDT (see D3.2). These operational rules are better simulated with TALSIM (reservoir oriented), while NASIM is more appropriate for detailed urban drainage. Thus, the combination of land and water use and climate scenarios was only simulated with TALSIM.

Figure 61 shows observed and simulated discharge at SNEM with different data sets. Observed discharge lies between not bias and bias corrected data sets, which could lead to the conclusion that not-bias corrected data is systematically overestimating discharge. However, after a closer look at simulated discharge at other water gauges, it was found out that this is not always the case. Sometimes, both not-bias corrected and bias corrected data sets underestimate observed discharge in terms of total volume (see Annex 4.17.4). Nevertheless, it can be concluded indeed that not-bias corrected data sets present wetter conditions compared to bias-corrected data set.

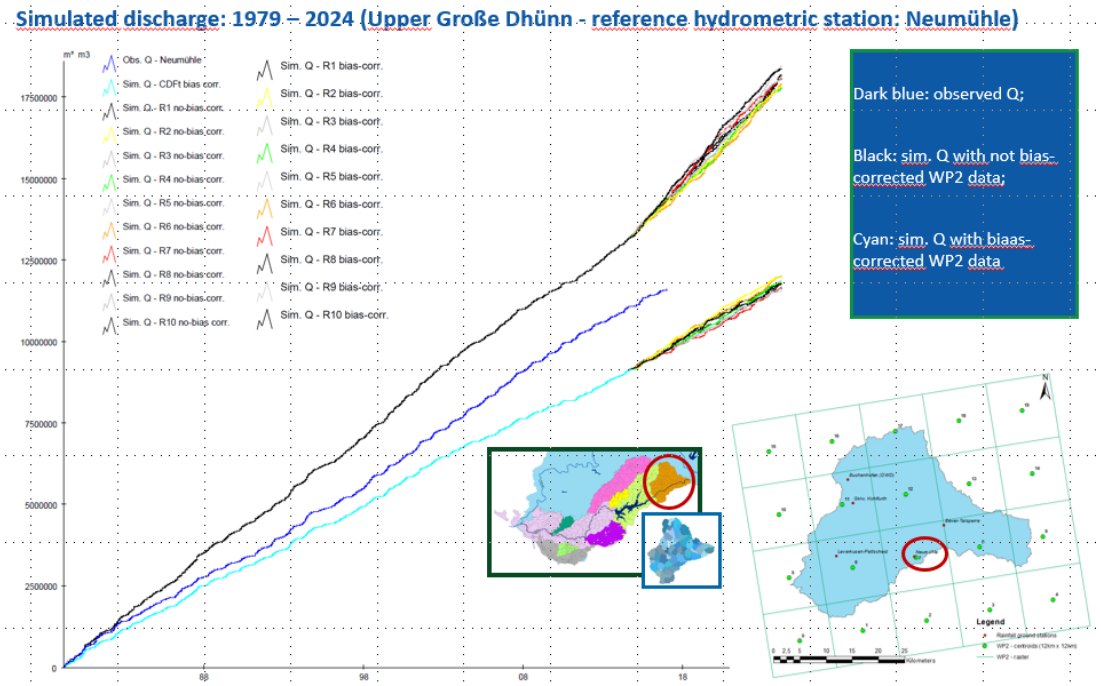

Figure 61: Observed and simulated discharge at SNEM with different data sets

The NASIM model of the Upper Große Dhünn was forced with R1, R9, and R7 in combination with land use scenarios (no water use are considered in this part of the basin).

Figure 62 shows simulated discharge at SNEM (R1 – not bias-corrected: land use - current state and vs. "economy first" scenario) as example.

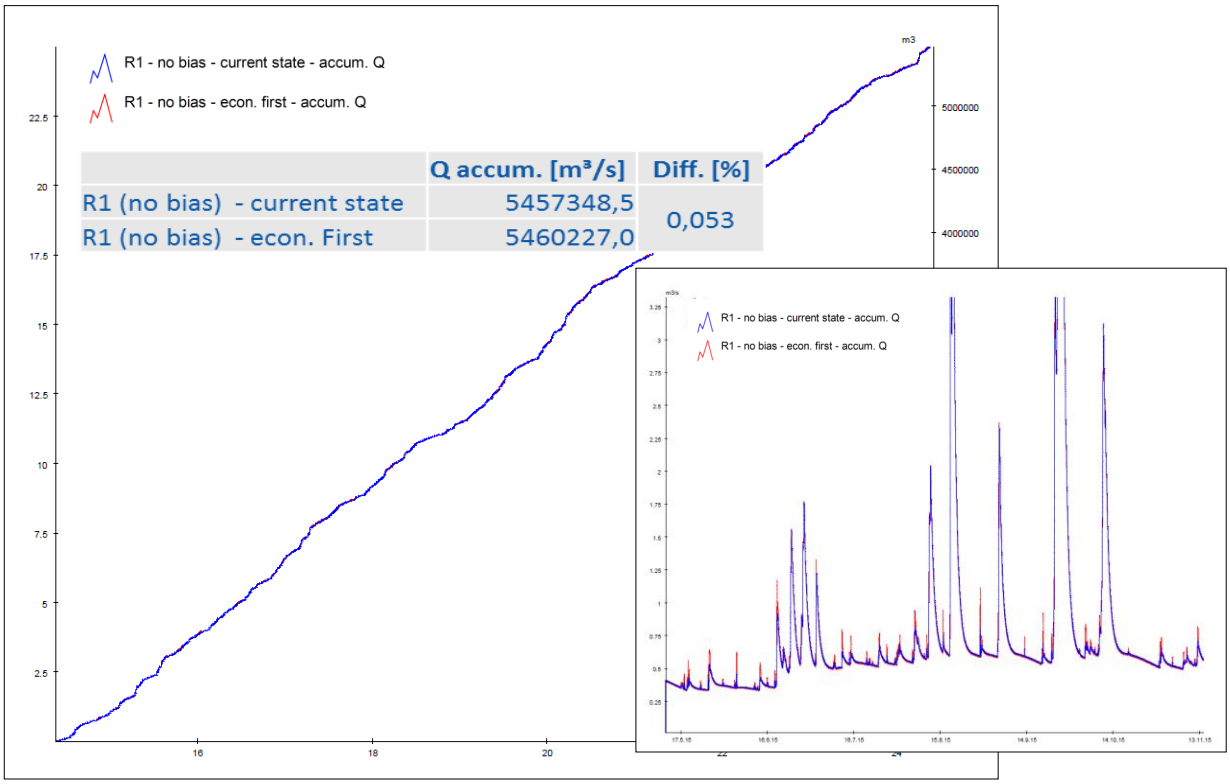

Figure 62: Simulated discharge at SNEM (R1 – not bias-corrected: land use - current state and vs. "economy first" scenario)

Figure 62 shows negligible differences in terms of overall discharge and only small differences by low discharge. Thus, it can be concluded that land use changes do not play a significant role for the water cycle.

In order to assess model uncertainty, i.e. to test if the model results are varying with the selected hydrological model type, a second model was set up for the Upper Große Dhünn Catchment. The Soil & Water Assessment Tool (SWAT) Model (Neitsch et al., 2011) was selected for this purpose. SWAT is a spatially distributed hydrological model, with detailed representation of soil water fluxes and it is mostly used to quantify the impact of land management practices in large, complex watersheds. The model includes more than 250 physically parameters based on land use, vegetation, topography, soil, climate and management aspects and can consider various land use and climate change scenarios and their effects on single water balance components. The main goal of the SWAT model application is to enable a comparative study of SWAT and NASIM to estimate potential model uncertainties regarding the future 10 decadal climate predictions (WP2).

4.6.2. Data

NASIM Model

Climate scenarios were derived from the ten decadal members, not-bias and bias-corrected. NASIM has the capability to assign automatically the corresponding time series on the sub-basins, based on their location. The influence of each raster cell is then determined within NASIM. Thus, all 16 raster points were used for the simulations. The input parameters are the same as TALSIM (see Table 8). Since both NASIM and TALSIM allow time steps lower than a day, the 3-hourly raster data was used.

SWAT Model

For the purpose of the model uncertainty assessment, the SWAT model was set up at a daily resolution, with detailed soil and land use information and 30 year historical weather station information (1983-2014). The station data was taken from the climate station “Neumühle”, located at the catchment outlet as well as from the former station “Westhofen” (see D3.3). A 17 year time span of station climate data (1983-1999) was used for a sensitivity analysis using the Latin Hypercube sampling strategy (LH-OAT) and for stochastic calibration using sequential uncertainty fitting (SUFI2). The remaining 15 years (2000-2014) were used for validation. Using the Nash-Sutcliffe efficiency criteria as calibration goal function, the calibration and validation yield the following statistics (see Table 13):

Table 13: SWAT Model - Calibration and Validation Results

Time period	Nash-Sutcliffe	R^2	Volume Error
Calibration (1983-2014)	0.76	0.76	- 1.4%
Validation (2000-2014)	0.79	0.80	- 10%

Hence, the model could be calibrated and validated successfully and was subsequently used for the prediction of future climate change scenarios in the Upper Große Dhünn Catchment using the 10 decadal predictions. Apart from changes in the climate parameter no further modifications (e.g. land use changes) were made. Thus changes of the hydrological variables (e.g. runoff) can be directly attributed to alterations caused by the climate change predictions.

4.6.3. Results

SWAT Model results

SWAT results indicate that in the next decade winter months will become drier and summer months will become slightly wetter. In winter discharge rates are projected to decrease by approx. 0.1 – 0.5 m3 s-1, whereas in summer discharge is slightly increasing by maximum 0.2 m3 s-1. With negligible variations, the same trend is projected for all 10 ensemble members (R1-R10). Figure 63 shows the projected changes in mean monthly discharge rates for all realizations compared to the mean monthly discharge rates of the 30 year historical data. November until March show clear decreasing trends while from April until October discharge rates are increasing.

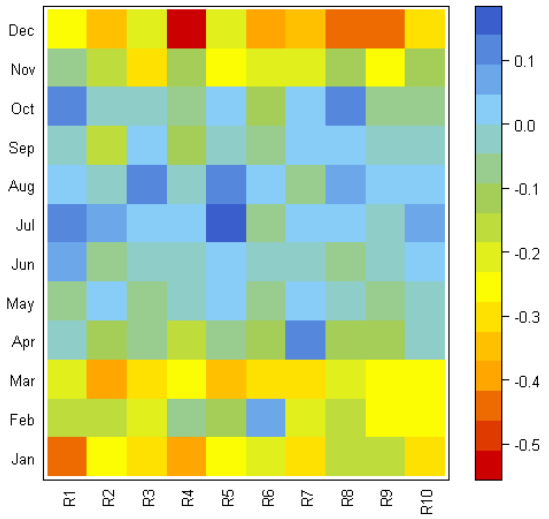

Figure 63: Changes in monthly discharge rates [m3/s] for each ensemble member compared to historical data.

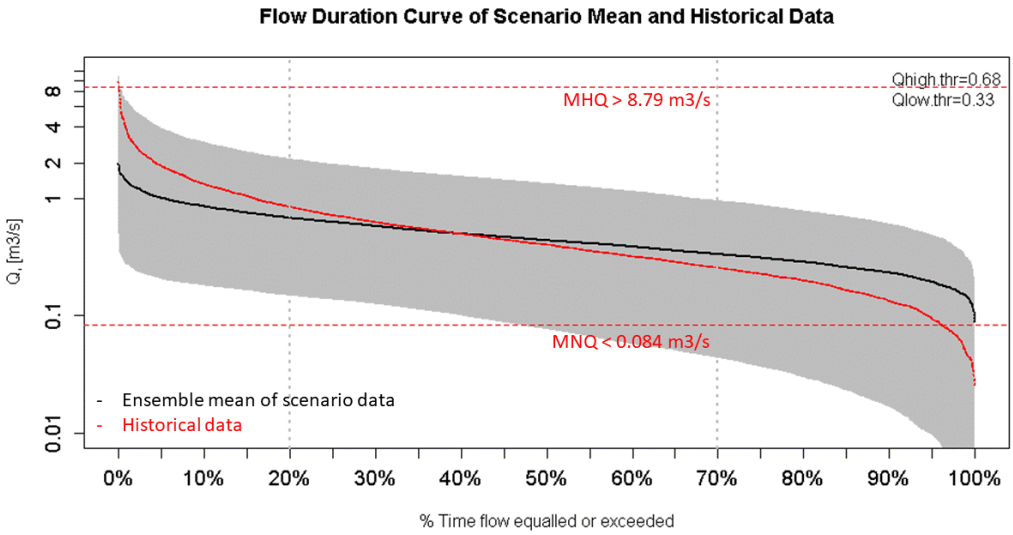

Figure 64: Flow duration curve of the ensemble mean (black) and the mean historical data (red)

The flow duration curve (Figure 64), shows the impact of these changes on the future flow regime. The figure displays the likelihood of exceedances of flow thresholds for the projected ensemble mean discharge rates (in black) as well as for the mean flow regime of the past 30 years (in red). According to the SWAT model estimations the probability of exceeding the current high flow threshold (MHQ =8.79 m^3 s^{-1}) will become smaller and the probability of low flows below the current low flow threshold (MNQ = 0.084 m^3 s^{-1}) will become close to 0%. Nevertheless uncertainty bounds (in grey) are large and should be considered when predicting future threshold exceedances.

The following plots show changes of precipitation rates (Figure 65), temperature (Figure 66) and actual evapotranspiration rates (Figure 67) with respect to historical data. Precipitation and temperature data is predicted by the decadal predictions whereas ETa data is estimated by the SWAT model. The data indicate that the main reason for the decreasing winter discharge rates lays in the decreasing precipitation rates during the respective winter months. While the fall season will experience negligible precipitation changes compared to the past, winter and spring will face decreasing precipitation rates. In addition, temperature and concurrently also ET rates will increase during winter, which will intensify the decrease in discharge rates. Summer months will experience a similar increase in temperature and ET but their effect on discharge reduction will be offset by increasing precipitation rates, hence resulting in the slight increase in summer discharge rates which are estimated by the model simulations.

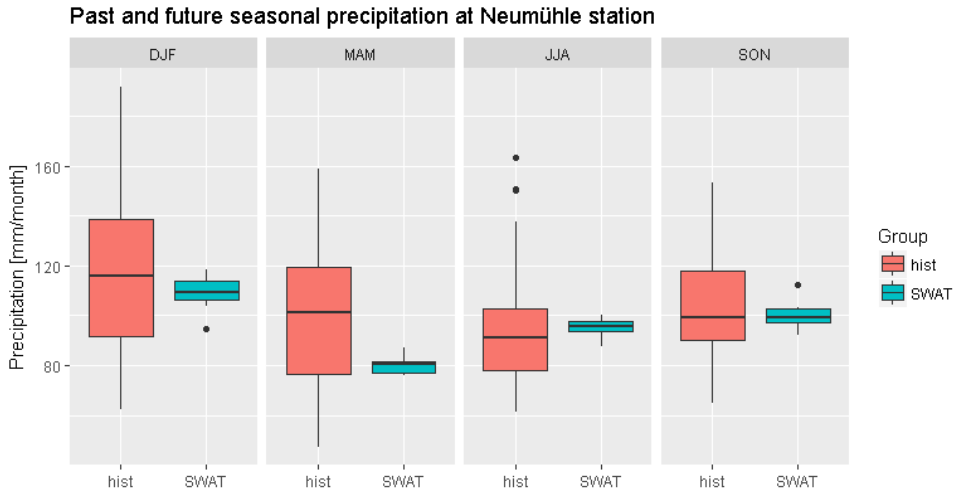

Figure 65: Changes in Precipitation Rates

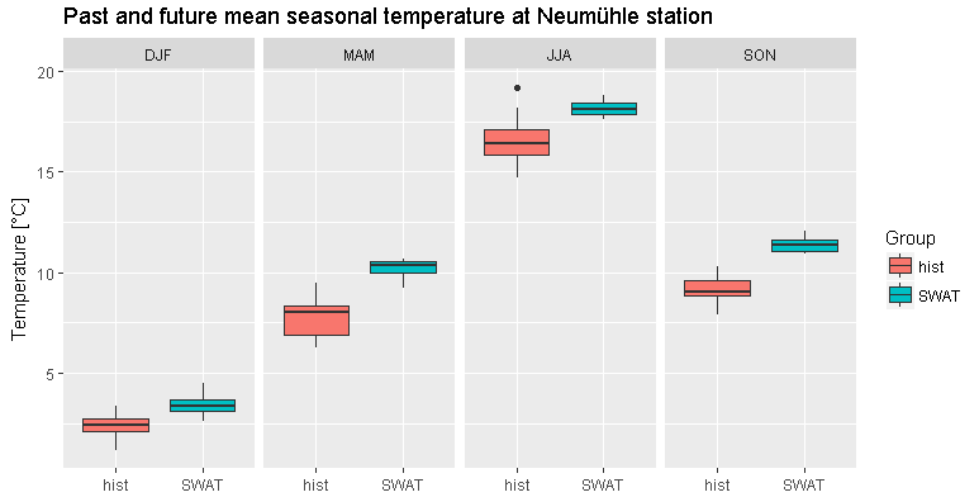

Figure 66: Changes in Temperature

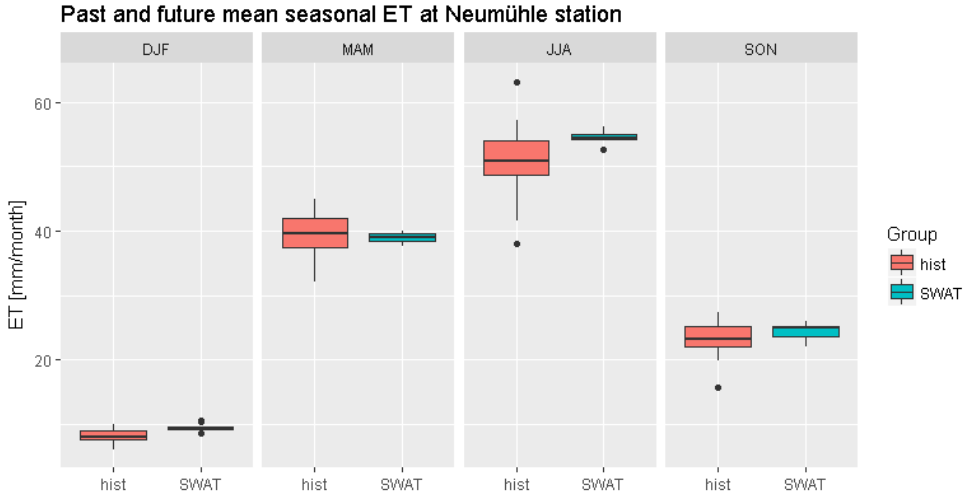

Figure 67: Changes in Evapotranspiration

Comparison of SWAT and NASIM

As mentioned above, the principal aim of the application of two different hydrological models is the estimation of model errors which occur due to the selected model type (e.g. different physical equations used by the model leading to different results of important hydrological parameter estimates). Therefore model results from the SWAT and NASIM Model are compared and their similarity is tested.

Figure 68 shows the estimated discharge rates of both models (NASIM in green and SWAT in blue) for all ensemble members as well as the 30 year historical data (in red). Both models show similar trends with respect to increasing or decreasing future discharge rates, i.e., decreasing discharge in winter and spring and increasing discharge in summer. Only for fall months (SON), NASIM predicts a slight increase of mean runoff whereas SWAT estimates a slight decrease of mean runoff rates. However, both fall model prediction lay within the interquartile range of the historical data, and a significant increase or decrease compared to past conditions cannot be stated for either model (see Table 14).

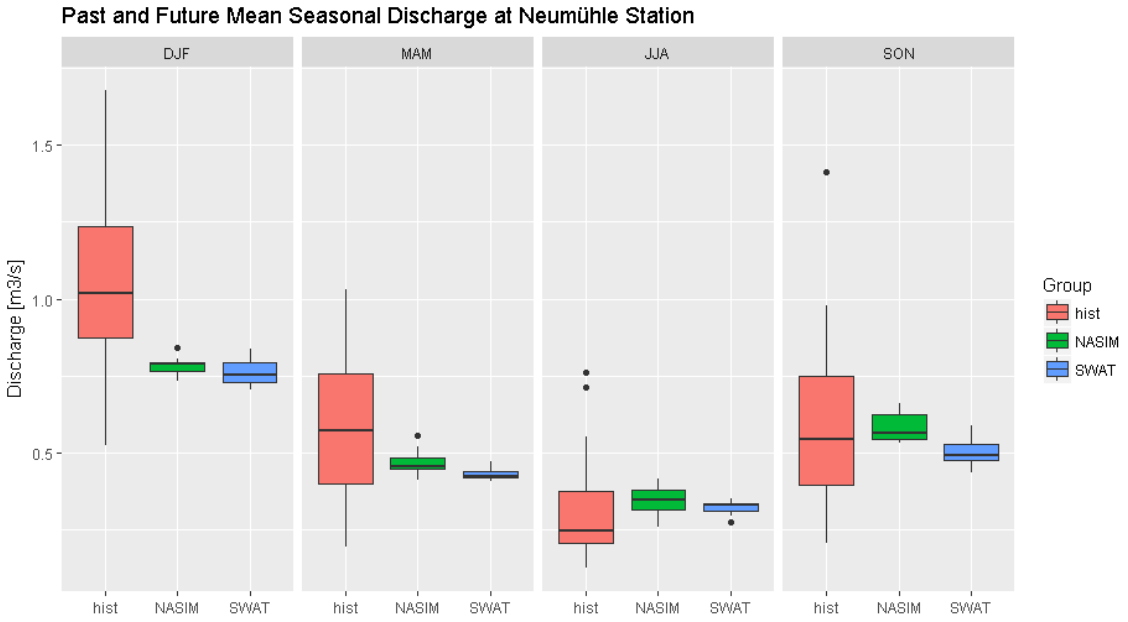

Figure 68: Comparison of historical data, NASIM and SWAT – Seasonal discharge rates

Table 14: Mean seasonal discharge rates (in m3 s^{-1}) and results from a t-test testing differences in model means

Season	Historical Data [m3 s^{-1}]	NASIM [m3 s^{-1}]	SWAT [m3 s^{-1}]	NASIM vs. SWAT Significantly different?	Historical Data vs. Models Significantly different?
DJF	1.03	0.79	0.76	no	yes
MAM	0.58	0.47	0.43	no	yes
JJA	0.3	0.34	0.32	no	no
SON	0.59	0.58	0.5	yes	no

Table 14 shows the seasonal mean values for both model as well as for the historical data. In addition it shows the results of a student t-test, indicating if the model means are significantly different from each other as well as significantly different from the historical mean (yes = model means are significantly different with a p-value < 0.05; no = models means are not significantly different at a 5 % confidence interval).

The test statistic confirms the previous observations that the results from both hydrological models show similar outcomes and only the estimations for fall discharge rates deviate from each other. But as mentioned above, fall discharge cannot be distinguished from the historical mean (mean of historical data and model means are not significantly different), hence no significant future trend can be stated for this season. Similarly future changes in summer months are too small to detect a significant deviation from the historical mean. Winter and spring seasons however show a significant difference of the model results compared to the historical data and confirm the decreasing trend of discharge rates during these two seasons.

Figure 69, shows the same analysis at monthly resolution. The good model agreement between SWAT and NASIM shows again that model uncertainty is small in this Framework 2 setup. Decreasing trends in runoff rates during winter months are captured by both models and likewise both models show equally low differences to past runoff values during the summer months.

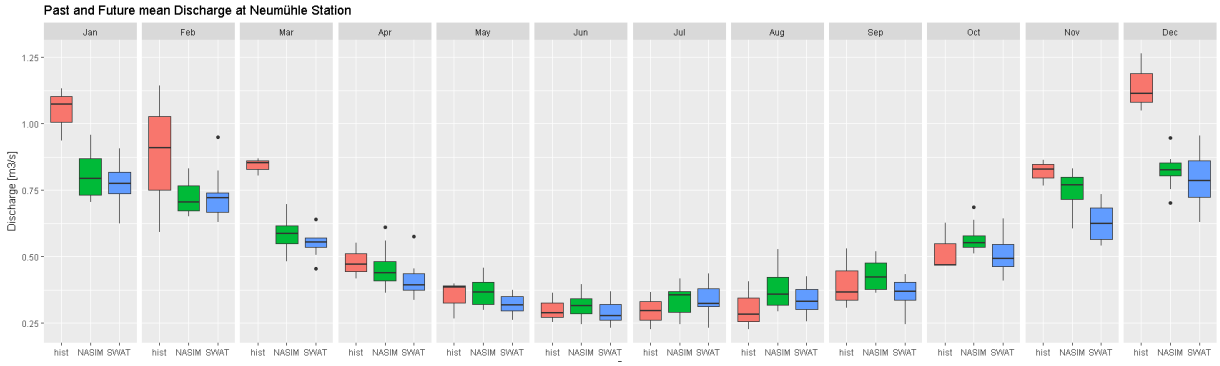

Figure 69: Comparison of historical data, NASIM and SWAT - Mean monthly discharge rates

4.7. Discussion

In conclusion the following can be summarized:

- The comparison of both model showed a good agreement of their outputs and indicates that NASIM is able to capture the hydrological processes and future changes accurately. Hence model uncertainty can be considered as small.
- Changes of runoff values (decreasing) are strongest during Winter and Spring months in both model estimations and show significant differences from past runoff rates
- Trends of increasing runoff rates during summer months are too small to be detected as a significant change with respect to historical data. This is true for both models.

4.8. Bibliography

D3.2 - Future Land and Water Use Scenarios

D3.3 – Calibrated water resources models for past conditions

Neitsch, S. L., Arnold, J. G., Kiniry, J. R., and Williams, J. R.:Soil andWater Assessment Tool Theoretical Documentation Version 2009, Grassland, Soil andWater Research Laboratory, Agricultural Research Service and Blackland Research Center, Texas Agricultural Experiment Station, College Station, Texas, 2011.

Rust, H.W., Richling, A., Meredith, E., Fischer, M., Vagenas, C., Kpogo-Nuwoklo, K.A., Kadow, C., Ulbrich, U. (2017). DECO - A plug-in for data extraction and conversion developed within and for BINGO. Freie Universität Berlin, Version from December 8, 2017

4.10. Model objectives in BINGO [NASIM – Mirke Creek]

For extreme precipitation events and consequent flash floods (case study “too much water” – Mirke Creek in the city of Wuppertal), the model objectives are:

- To simulate 20 future extremal episodes in order determine if obtained discharge exceeds the 100-year flood (HQ100) at the downstream area of Mirke Creek, i.e., at the confluence with the Wupper River
- To determine the impacts of anthropogenic influences such as land use on a dense sealed catchment area

On 29.05.2018, there was an extreme event caused by torrential rains of short duration, which led to the highest flood recorded at the city of Wuppertal of the last 100 years. This took place during a heavy thunderstorm season. This episode was followed by further intense precipitation, causing two more flood events (on 07.06.2018 and on 10.06.2018) on the cities of Wuppertal, Leverkusen, and Solingen.

4.11. Model application

For the Mirke Creek, the NASIM model described on D3.3 was driven by 20 extremal episodes for different land use scenarios (water use scenarios are not considered). Figure 70 shows the Mirke Creek catchment area.

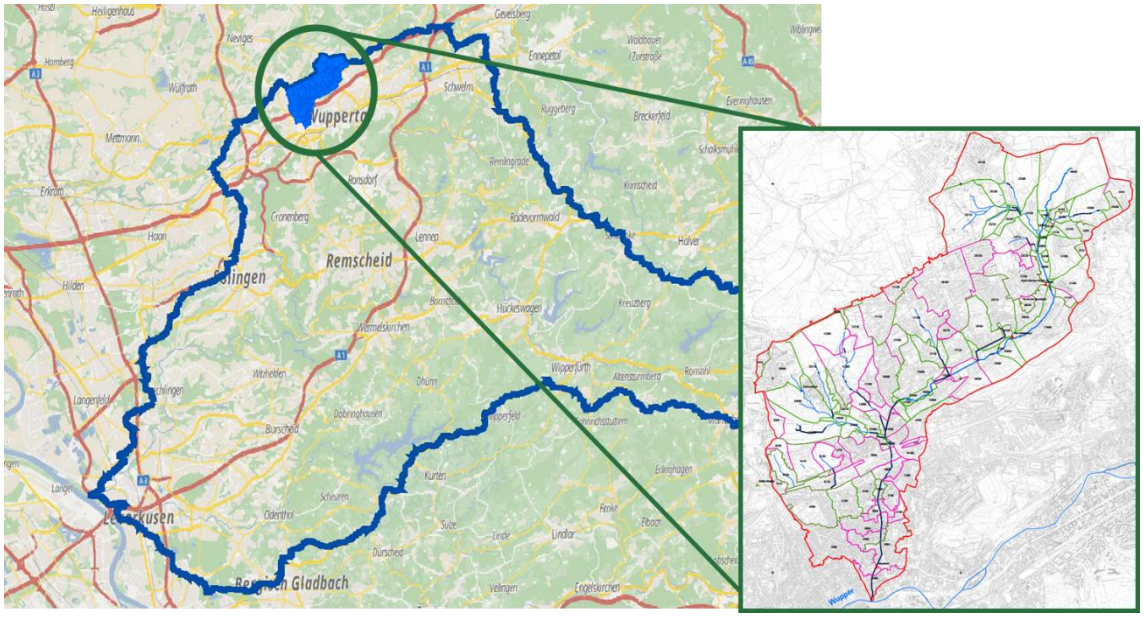

Figure 70: Mirke Creek catchment area – city of Wuppertal

The Mirke Creek has a length of ca. 6 km and disembogues into the Wupper River, in the city of Wuppertal. This model was developed by Hydrotec, using ground stations and radar data. The 100-year flood (HQ100) was calculated for the last element of the computational domain (element number 1000, see Figure 71), that is, for the element corresponding to the inflow to the Wupper River (HQ100 at element 1000 = ca. 25 m³/s).

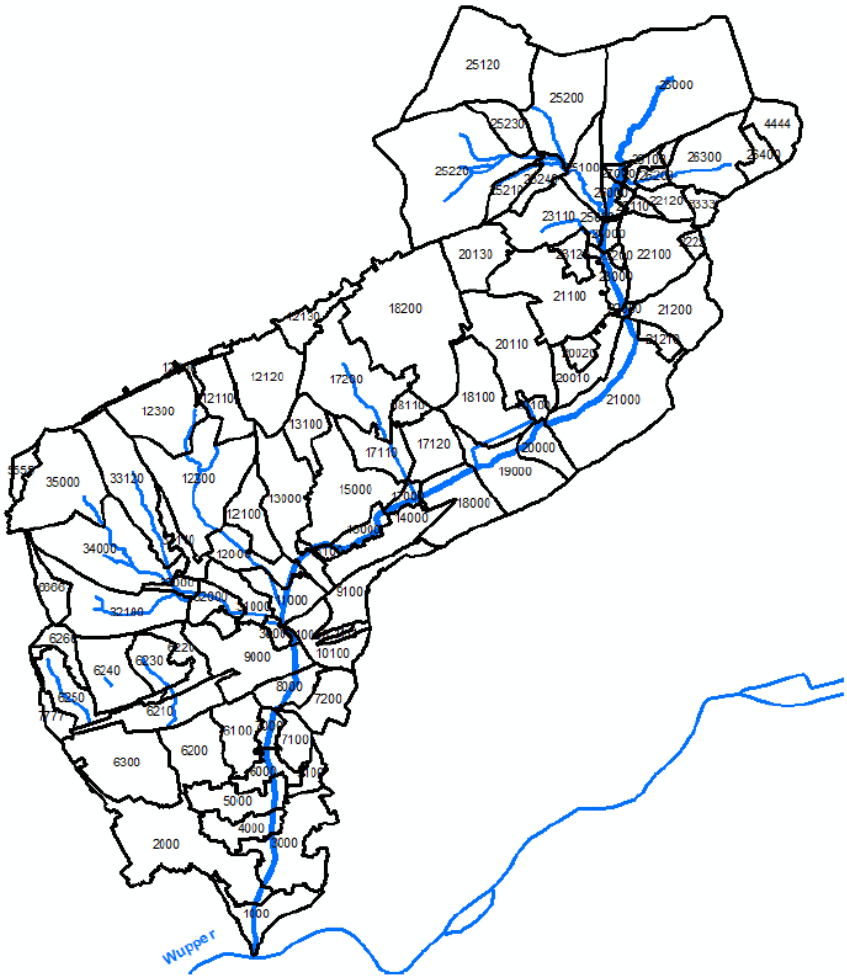

Figure 71: Computational domain – Mirke Creek NASIM model (source: Hydrotec)

4.11.1. Data

Twenty extremal episodes were selected by FU-Berlin based on precipitation severity. The ranking was performed by Edmund Meredith. After the extreme events of 29.05.2018, 01.06.2018, and 10.06.2018 at the Wupper catchment area, three additional episodes around these days were also selected. Table 15 shows the simulated extremal episodes (in total, 23 extremal episodes). All extremal episodes were simulated for: a) land use - current state; b) land use – economy first; and c) land use - sustainability eventually. For economy first and sustainability scenarios, the methodology described in D3.2 was applied.

Figure 72 shows the raster points of the extremal episodes that lay over and close to the Mirke Creek catchment area (in total, 16 raster points).

The following land use scenarios were simulated and compared to the current state:

- Scenario 1 – economy first: 7,75% increase of the sealed areas by 2025
- Scenario 2 – sustainability eventually: 0,7% increase of the sealed areas by 2025

Table 15: Simulated extremal episodes (blue highlighted correspond to the extreme flood events of May – June 2018)

No.	No. realisation	No. episode	From	To
1	r1	eps. 1	22.07.2024 12:00	29.07.2024 12:00
2	r1	eps. 2	08.06.2023 12:00	10.06.2023 12:00
3	r2	eps. 1	25.07.2016 12:00	28.07.2016 12:00
4	r2	eps. 2	12.08.2017 12:00	14.08.2017 12:00
5	r2	eps. 3	20.06.2018 12:00	23.06.2018 12:00
6	r3	eps. 1	07.07.2020 12:00	09.07.2020 12:00
7	r3	eps. 2	25.08.2018 12:00	27.08.2018 12:00
8	r4	eps. 1	31.08.2020 12:00	02.09.2020 12:00
9	r4	eps. 2	30.06.2020 12:00	02.07.2020 12:00
10	r5	eps. 1	12.07.2015 12:00	30.07.2015 12:00
11	r5	eps. 2	13.08.2021 12:00	18.08.2021 12:00
12	r6	eps. 1	03.07.2018 12:00	07.07.2018 12:00
13	r6	eps. 2	13.08.2018 12:00	15.08.2018 12:00
14	r6	eps. 3	10.06.2018 12:00	13.06.2018 12:00
15	r7	eps. 1	13.07.2023 12:00	16.07.2023 12:00
16	r7	eps. 2	21.06.2017 12:00	25.06.2017 12:00
17	r8	eps. 1	19.06.2017 12:00	25.06.2017 12:00
18	r8	eps. 2	07.07.2019 12:00	16.07.2019 12:00
19	r9	eps. 1	13.07.2018 12:00	15.07.2018 12:00
20	r9	eps. 2	04.08.2017 12:00	06.08.2017 12:00
21	r10	eps. 1	24.06.2023 12:00	28.06.2023 12:00
22	r10	eps. 2	21.07.2017 12:00	23.07.2017 12:00
23	r10	eps. 3	20.06.2018 12:00	27.06.2018 12:00

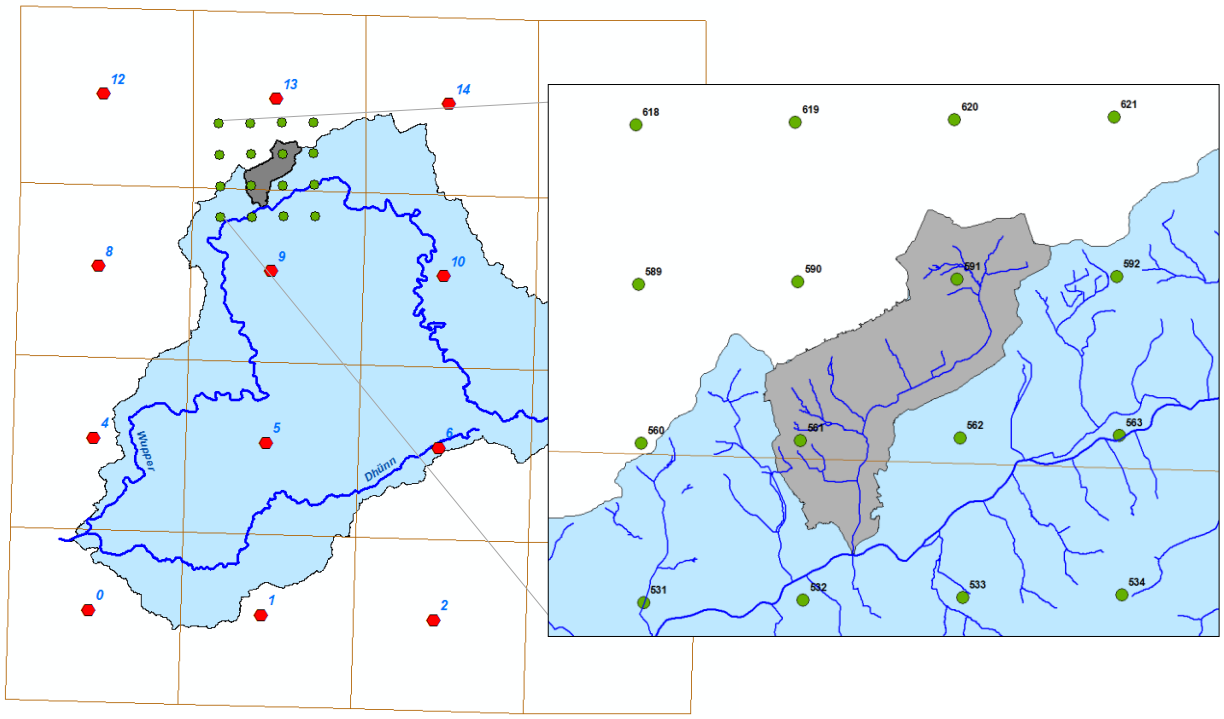

Figure 72: Raster points of the extremal episodes over and close to the Mirke Creek catchment area

4.11.2. Results

As there are no hydrometric stations operated by the Wupper Association in this area, the results are presented for the last element of the computational domain - element number 1000 (i.e., inflow to the Wupper River). Figure 73 illustrates an example of a simulated extremal episode. Annex 4.17.5 presents the resulting hydrographs for the 23 extremal episodes.

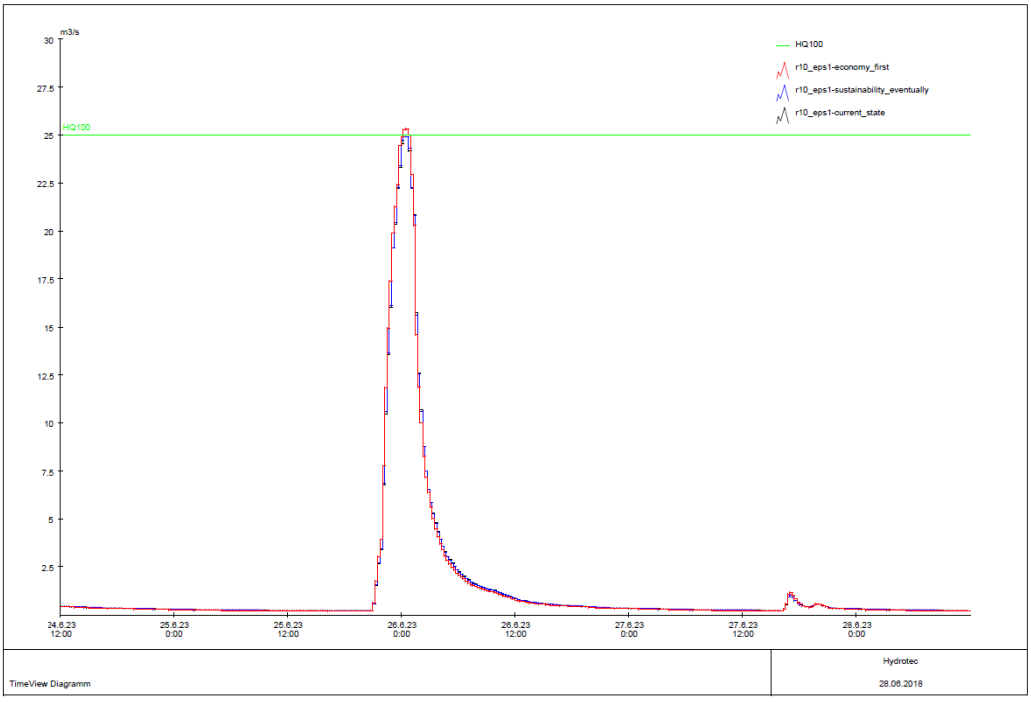

Figure 73: R10 – eps 1 – HQ100 threshold exceedance

4.12. Discussion

Land use changes – particularly changes in the degree of sealing expected for the next decade based on the available data - do not have a significant impact on surface runoff generation for the Mirke Creek catchment area. Furthermore, the simulated episodes seem to produce too low discharge: only the episode 1 - realisation 10 reached the HQ100 value. The rest of the episodes fall below this threshold. Additionally, it is considered that the episode of May – June 2018 was not well captured (peak discharge seems too low), which is not very realistic. This issue should be further investigated.

4.13. Bibliography

Rust, H.W., Richling, A., Meredith, E., Fischer, M., Vagenas, C., Kpogo-Nuwoklo, K.A., Kadow, C., Ulbrich, U. (2017). DECO - A plug-in for data extraction and conversion developed within and for BINGO. Freie Universität Berlin, Version from December 8, 2017

4.14. Model objectives in BINGO [FRAMEWORK 4 – NASIM –Leimbach Catchment Area]

After the extreme events of May – June 2018, an additional model was implemented in the frame of BINGO for the case study “too much water”. The model objectives are:

- To determine whether the simulation with ground precipitation captured the flood events, caused by convective rains
- To determine the impacts of anthropogenic influences such as land use on a dense sealed catchment area for two decadal members (maximum and minimum)

Figure 74 shows the urban catchment of Leimbach in Wuppertal. Leimbach is a tributary of the Wupper in the district Barmen of the city of Wuppertal. It originates in Barmen-Hatzfeld and takes its course as a surface fixed channel. Downstream of the Schützenstraße starts a channelized section of the Leimbach. The catchment area of Leimbach is in total ca. 2.7 km², and since it is an urban area, 51.7 % of the surface is sealed. Furthermore, about 14.2 % of the catchment is cover by forests, mainly around Nordpark, and around 33.3 % is covered by grassland, for the most part private gardens and allotments. An elevation difference of ca. 155 m characterizes the area of observation.

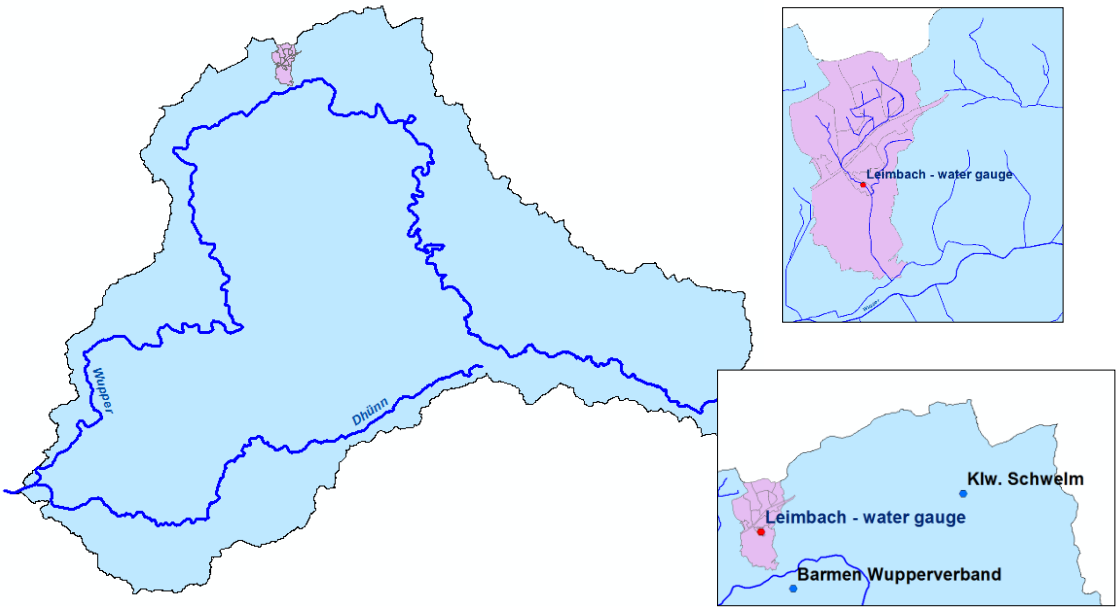

Figure 74: Leimbach catchment area

4.15. Model application

The catchment area of Leimbach was simulated in NASIM. The model was originally developed by the engineering office Ingenieurbüro Reinhard Beck GmbH & Co. KG and was recalibrated with ground precipitation data. The model calibration followed a simulation based on ground data from two pluviometric stations. Additionally, land use scenarios were integrated to the current state model. The combination of land use changes with climate change predictions aimed at investigating their impacts on the discharge.

Economy first and sustainability eventually land use scenarios were simulated and compared to the current state model, applying the methodology presented in D3.2.

4.15.1. Data

The model was driven with ground data from two pluviometric stations: Klw. Schwelm and Barmen (see Figure 74). The simulation of climate change impacts was based on the realisations providing the largest span (max and min), i.e., R1 and R9, respectively.

4.15.2. Results

Simulation with ground data

The calibrated model was driven with rainfall data from the pluviometric stations Barmen for the period 2011-2018 and Schwelm for the period 1970-2018. Focus was placed on the simulated discharge of several single events. Following figures (Figure 75, Figure 76) illustrate the flood events observed in the years 2013, 2016, and 2018.

The simulated with ground data from the rainfall station Schwelm flood event on the 20.06.2013 was overestimated. As illustrated in Figure 75, the simulated discharge reaches values almost two times higher than the observed discharge in Leimbach water gauge. The obtained results from the simulation with ground data from Barmen station tend also to overestimate the discharge during the same flood event, however in a smaller scale.

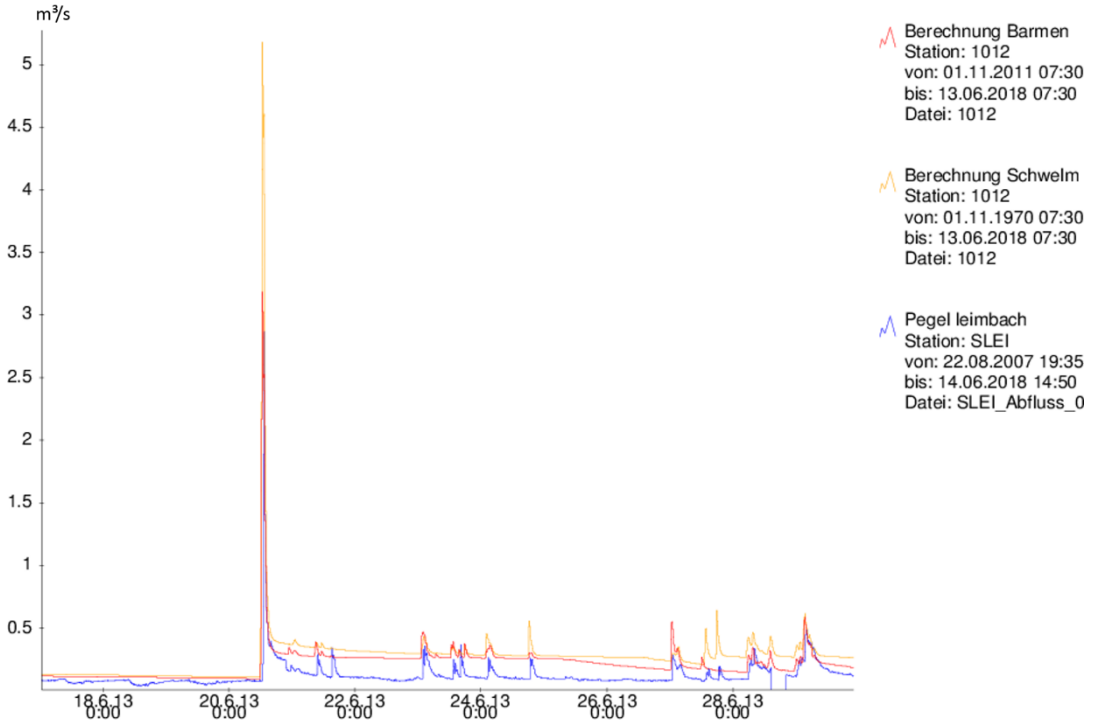

Figure 75: Flood event 20.06.2013

Figure 76 illustrates the flood event of the 07.06.2016. In this case, the event is not accurately represented by the model. The obtained results from the simulation with data from Barmen station present a strong overestimation, while the second simulation with data from Schwelm underestimate the discharge during the flood event. In conclusion, none of the two ground data time series are representative for the simulation of these events. The reason for this is the convective nature of the extreme precipitation that took place.

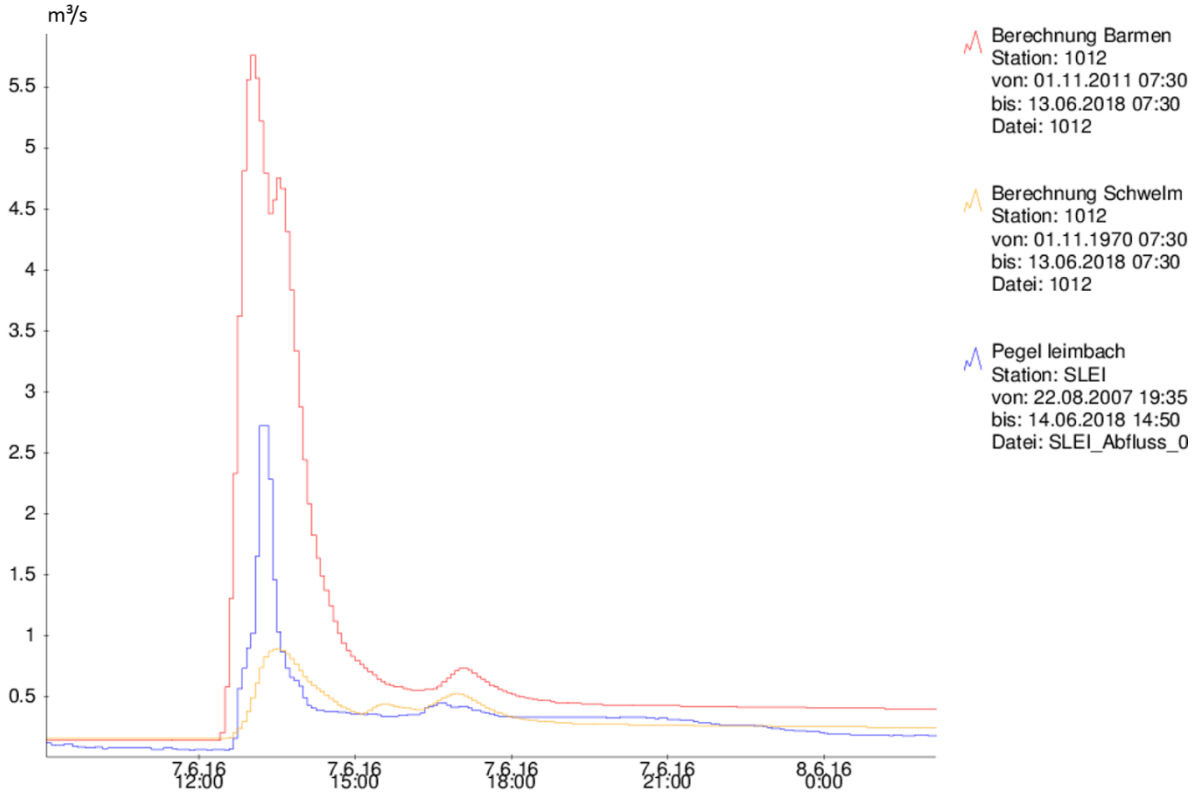

Figure 76: Flood event 07.06.2016

The flood events from the 29.05.2018, 01.06.2018 und 10.06.2018 are shown in Figure 77. The results obtained from the model with data from Barmen present an overestimation of the 29.05.2018 event, while the simulated events in June 2016 are underestimated. On the other hand, the simulated model with data from Schwelm underestimate all three flood events. The analysis of the radar data demonstrated the local nature of the three events. As a result, the simulation with ground data of the two pluviometric stations are not appropriate for the simulation of those specific events. Therefore, the determination of the spatial distribution of precipitation is crucial as far as convective extreme precipitation events are concerned.

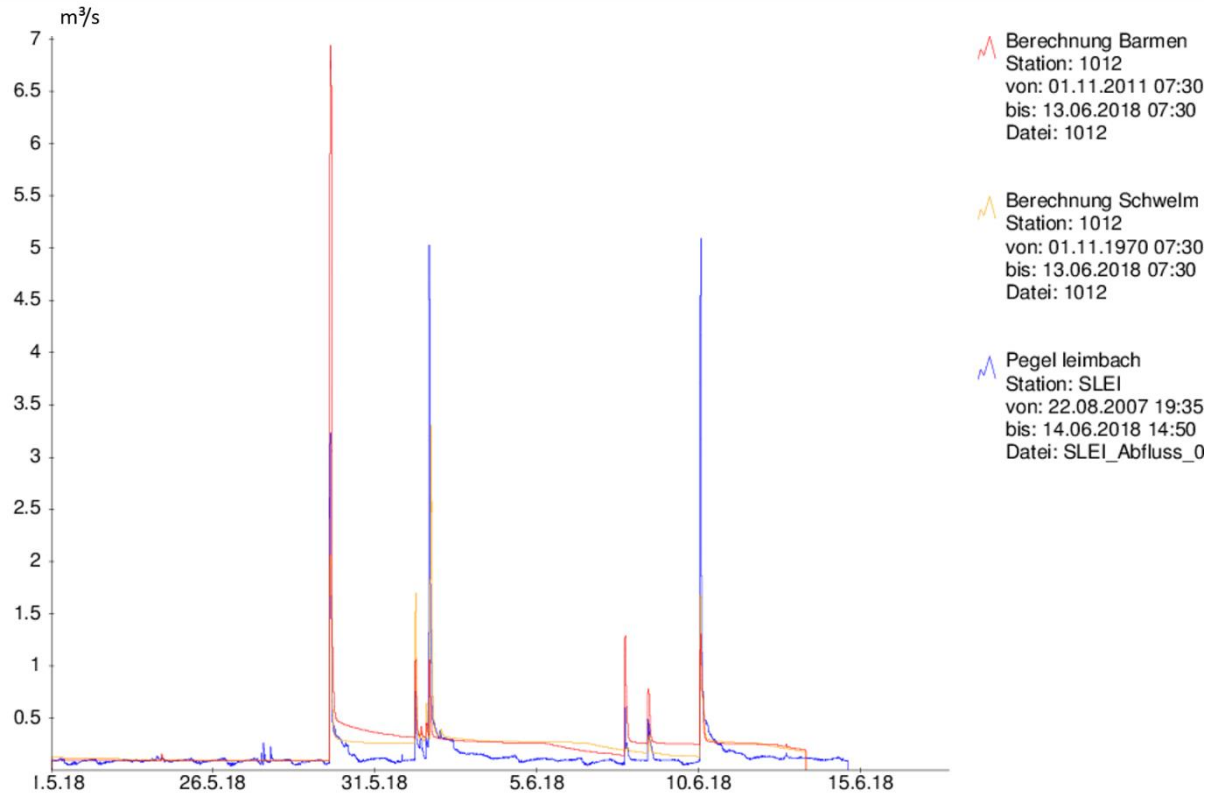

Figure 77: Flood event.05.2018, 01.06.2018 and 10.06.2018

Simulations with decadal members

The future change on the land use in urban catchment areas is affected by the further increase of sealed areas. In order to determine the impacts on the discharge due to higher degrees of sealed areas, the following two scenarios were simulated:

- Scenario 1 – economy first: 7,75% increase of the sealed areas by 2025
- Scenario 2 – sustainability eventually: 0,7% increase of the sealed areas by 2025

The two future scenario results were compared with the current state of the catchment area as well as with each other. The three land use scenarios current state, economy first, and sustainability eventually were forced by the decadal members R1 and R9, the realisations providing the largest span (max and min).

Table 16 presents the accumulated volume obtained by the different scenarios as well as its deviation among the different land use and climate change scenarios. As expected, the higher accumulated volume as well as the highest deviation with respect to the current state corresponds to economy first. Figure 78 to Figure 80 present the current state and the two land use scenarios forced by the bias corrected decadal members. Figure 81 to Figure 82 illustrate the results of the three land use cases forced by the not bias corrected decadal members. The difference in the magnitude of discharge peaks between the three land use states can be observed.

Table 16: Influence of land use change and future climate scenarios on the accumulated volume

Land Use Scenario	Decadal Member	Accumulated Volume [m³]	Bias Corrected	Deviation from Current State [%]
Current State	R1	170.780	yes	-
		250.975	no	-
	R9	146.428	yes	-
		227.979	no	-
Economy First	R1	171.748	yes	0,56
		252.246	no	0,50
	R9	147.319	yes	0,61
		229.153	no	0,51
Sustainability Eventually	R1	170.867	yes	0,05
		251.090	no	0,05
	R9	146.508	yes	0,06
		228.085	no	0,05

The analysis shows that although R1 displays the highest accumulated volume, peak discharges have been observed more often in the future scenarios forced by R9. In order to verify this assumption, a discharge threshold of Q=1m³/s was chosen and the occurrences of exceedance above that threshold were calculated for all scenarios (see Table 17).

Table 17: Number of occurrences of peak discharges over the chosen threshold Q= 1m³/s

Land Use Scenario	Decadal Member	Bias corrected	Count peaks Q>1m³/s
Current State	R1	yes	1
	R9		6
	R1	no	1
	R9		12
Economy First	R1	yes	2
	R9		6
	R1	no	9
	R9		16
Sustainability Eventually	R1	yes	1
	R9		6
	R1	no	6
	R9		12

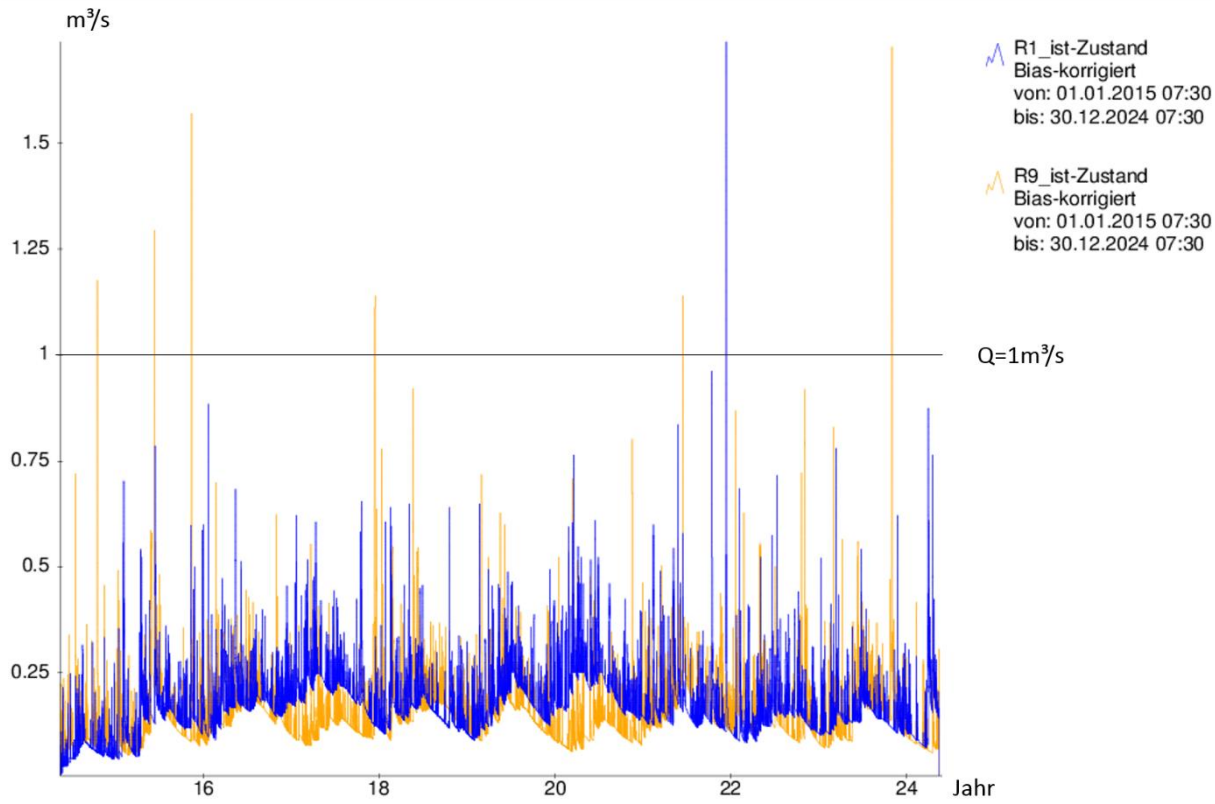

Figure 78: Future scenarios R1 und R9 (bias corrected); land use: current state

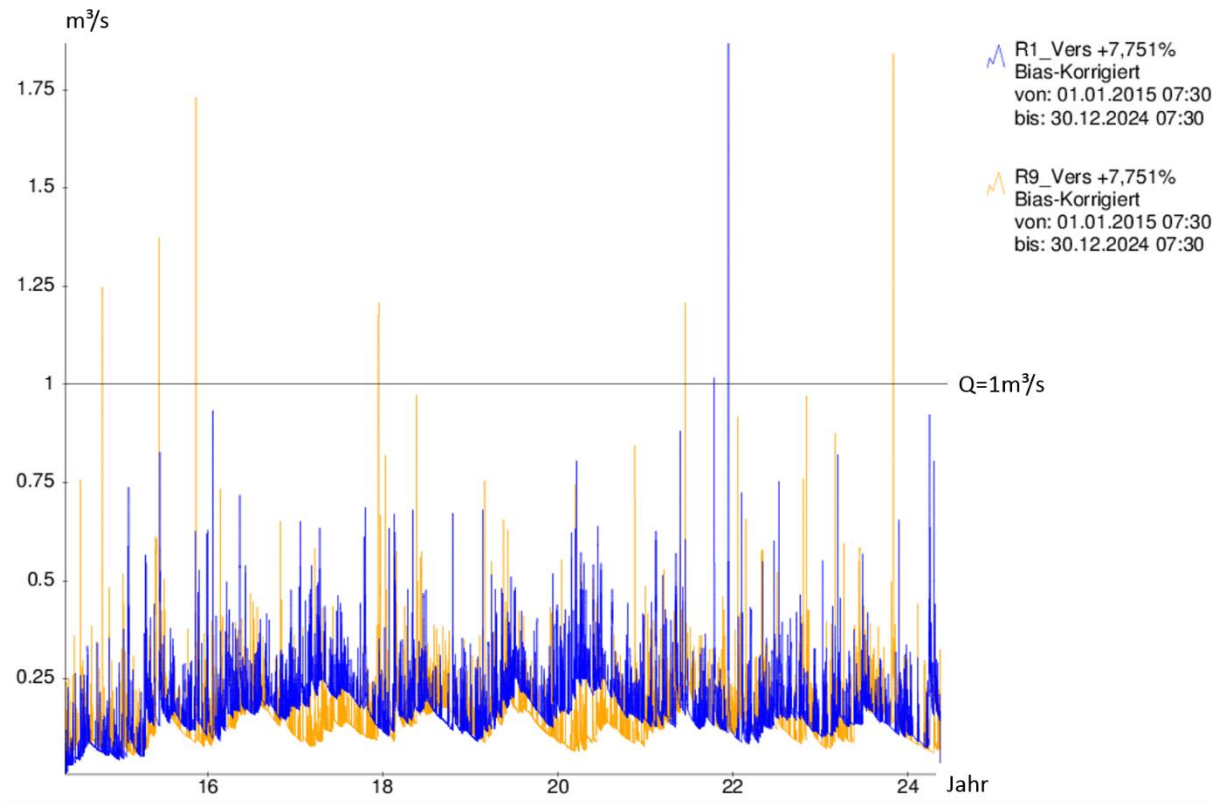

Figure 79: Future scenarios R1 und R9 (bias corrected); land use: economy first

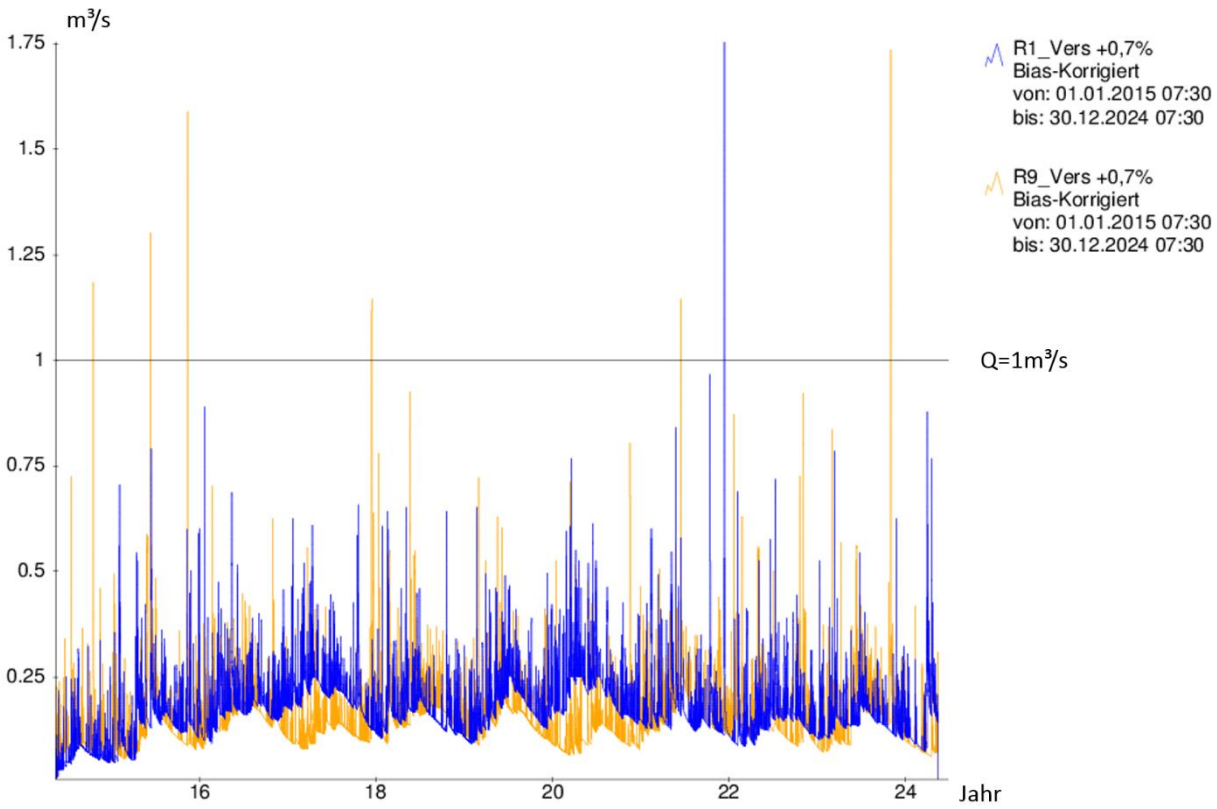

Figure 80: Future scenarios R1 und R9 (bias corrected); land use: sustainability eventually

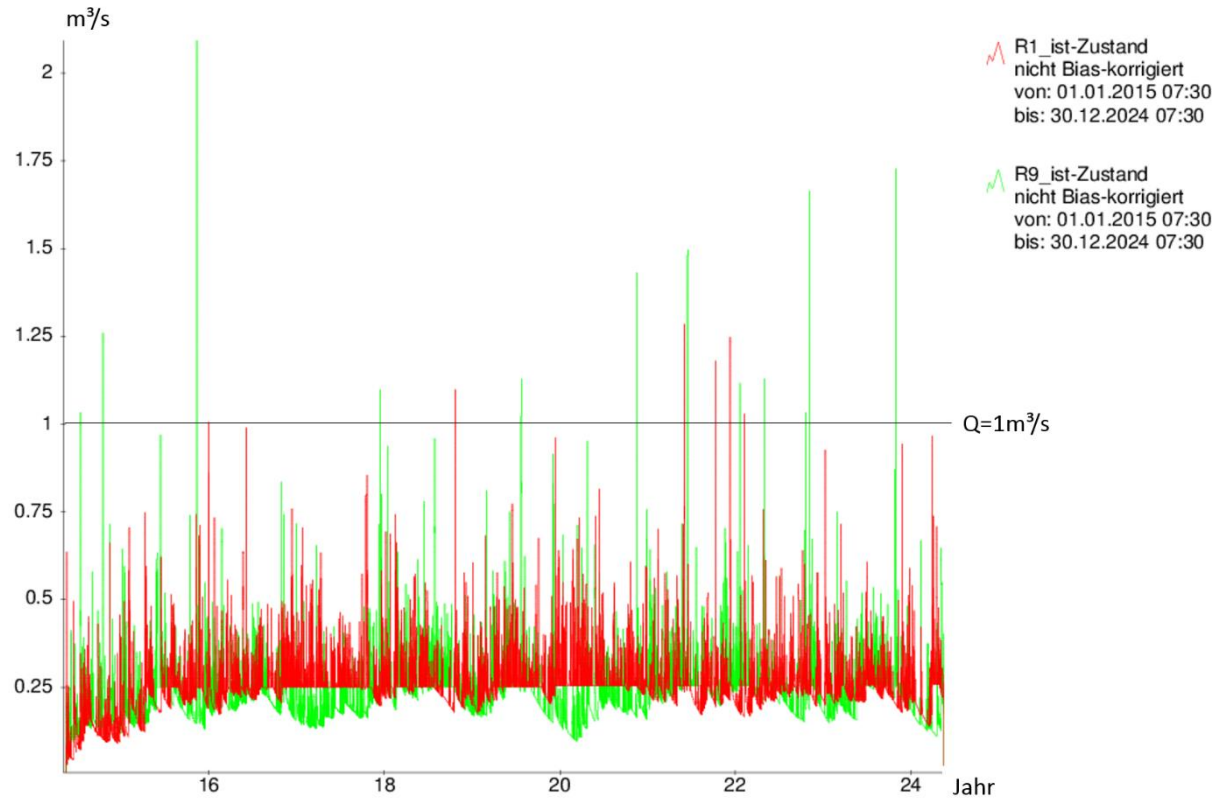

Figure 81: Future scenarios R1 und R9 (not bias corrected); land use: current state

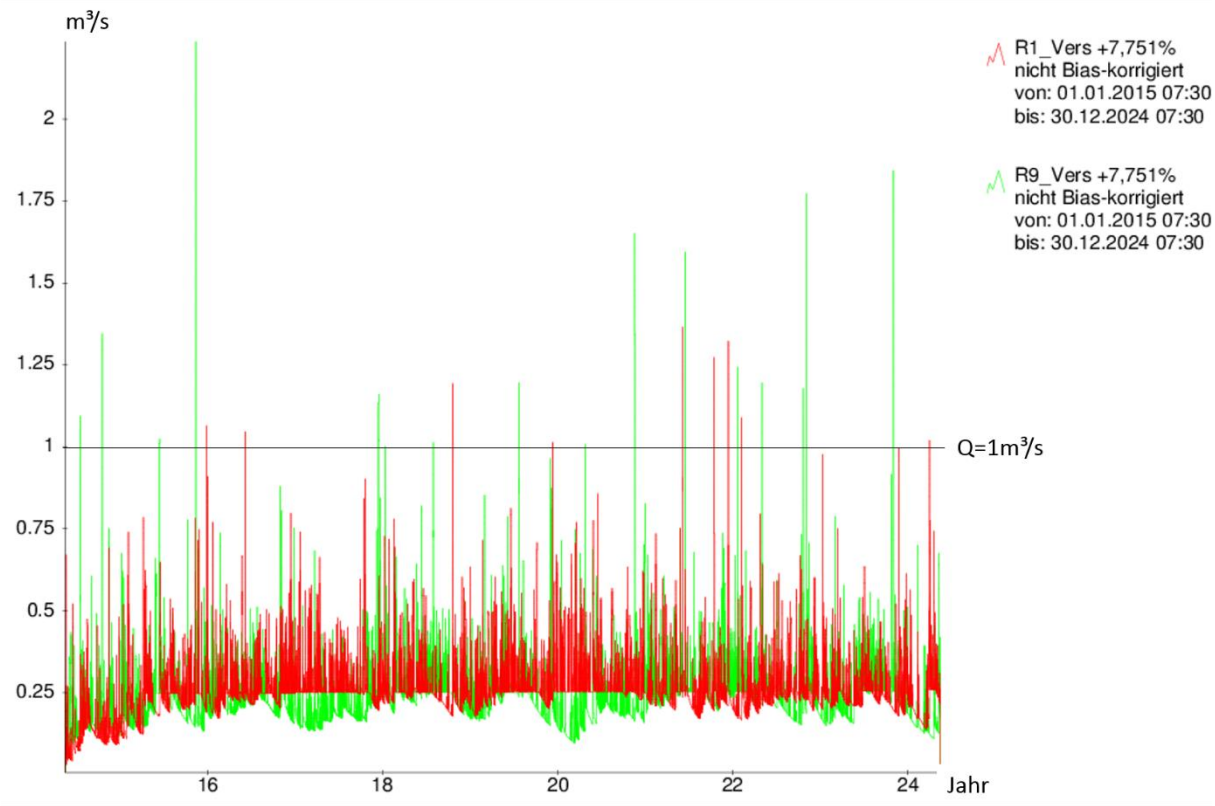

Figure 82: Future scenarios R1 und R9 (not bias corrected); land use: economy first

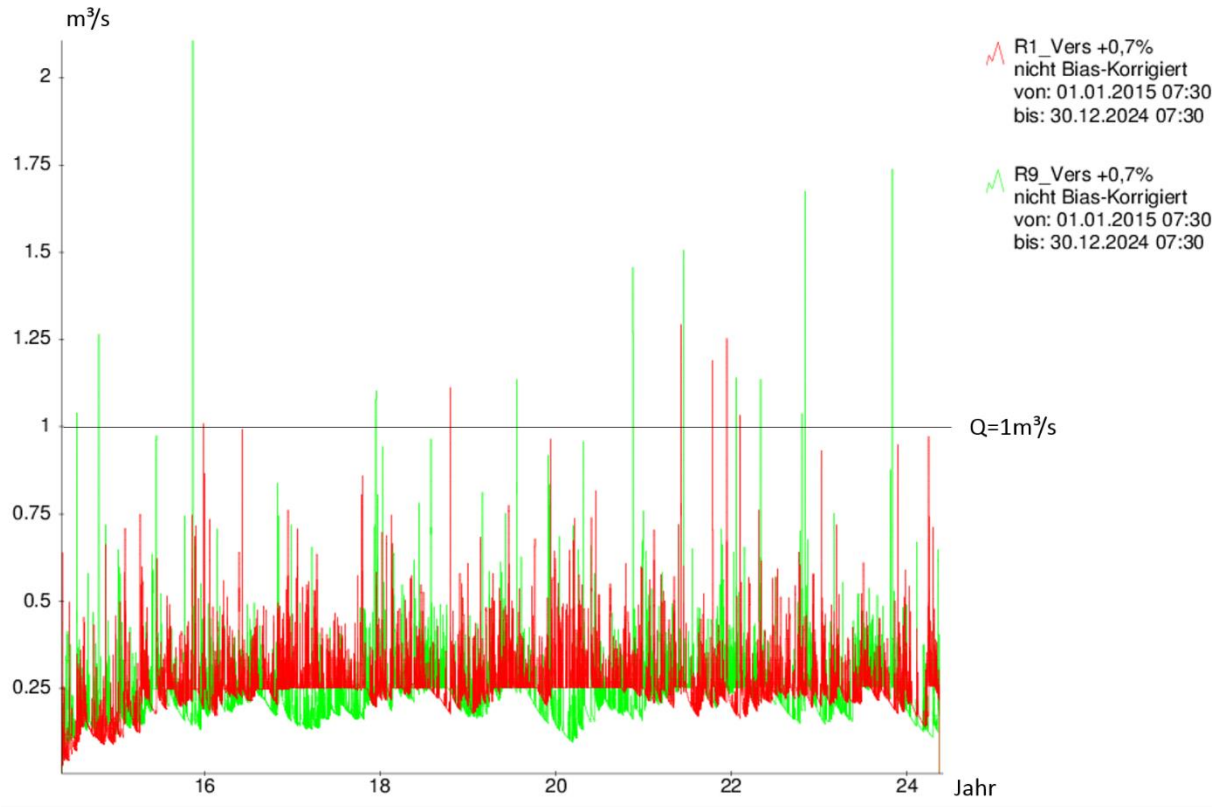

Figure 83: Future scenarios R1 und R9 (not bias corrected); land use: sustainability eventually

4.16. Interaction between sites

Synergies between research sites have been identified based on the following topics:

- Soil moisture measurements and their applications in hydrological modelling (Cyprus)
- Modelling of interception, e.g., leaf area index – LAI (Netherlands)
- Evapotranspiration – interpretation of the results and application on hydrological modelling, including a comparison of measured and simulated actual evapotranspiration ETa (Netherlands)
- Information exchange regarding HBV (model used by Bergen research site) and TALSIM (reservoir-oriented hydrological model used by the Wupper Association); comparison of snow depth calculation by the models (Norway)
- Exchange on the behavior of the sewer network regarding overflow (Norway)
- Strategic approaches for using streets as overflow paths (Norway)

4.17. Annexes

4.17.1. Framework 1 – TALSIM – Dhünn catchment area

Comparison 1

SMAN

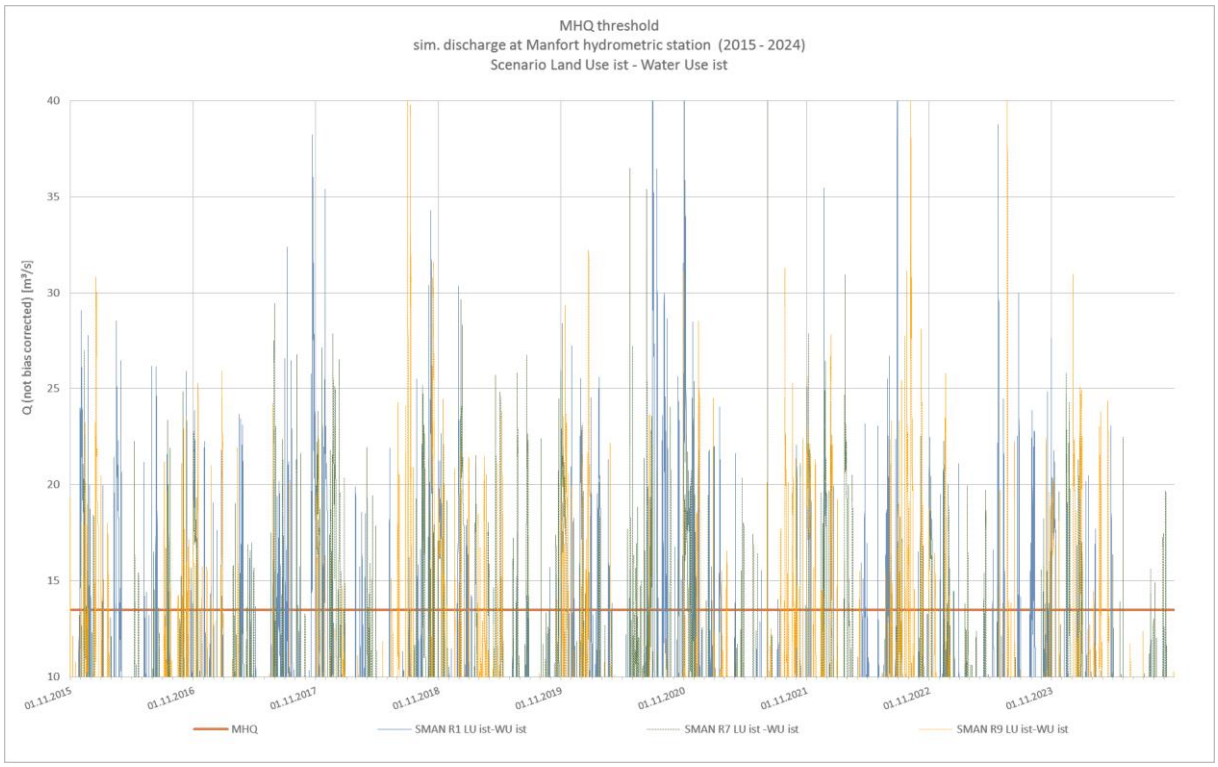

SNEM

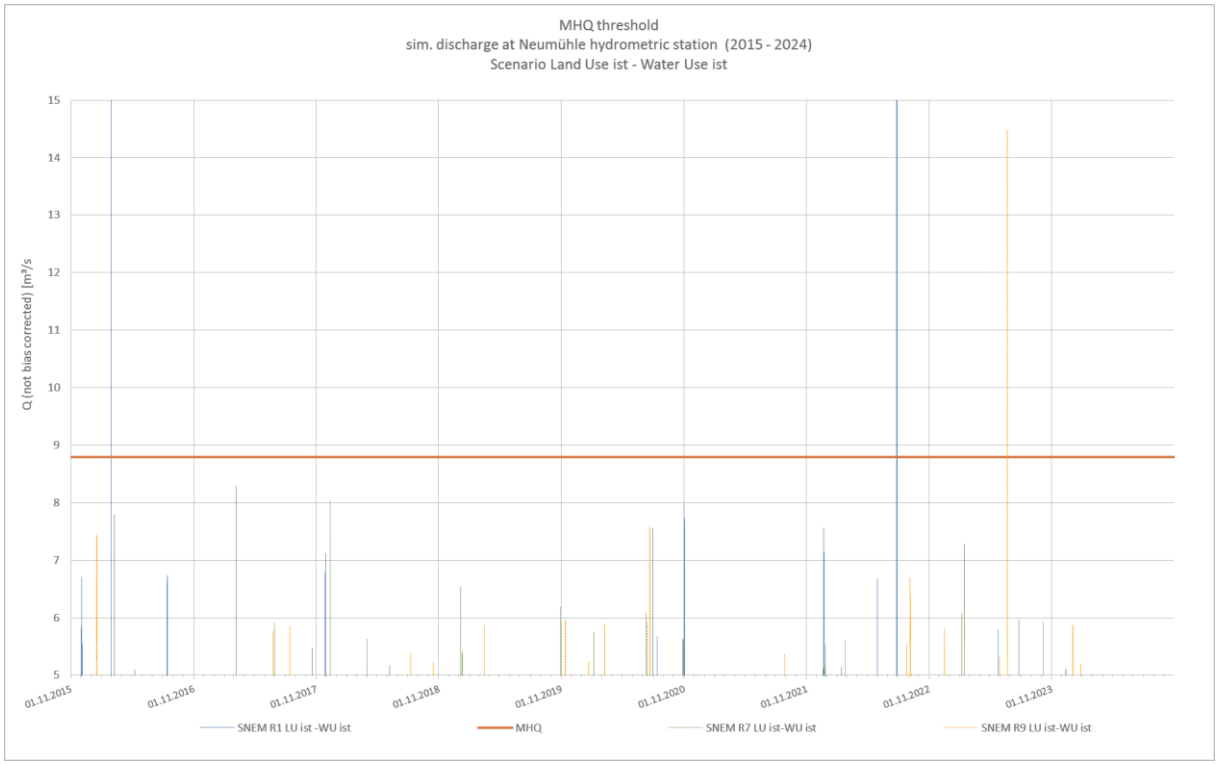

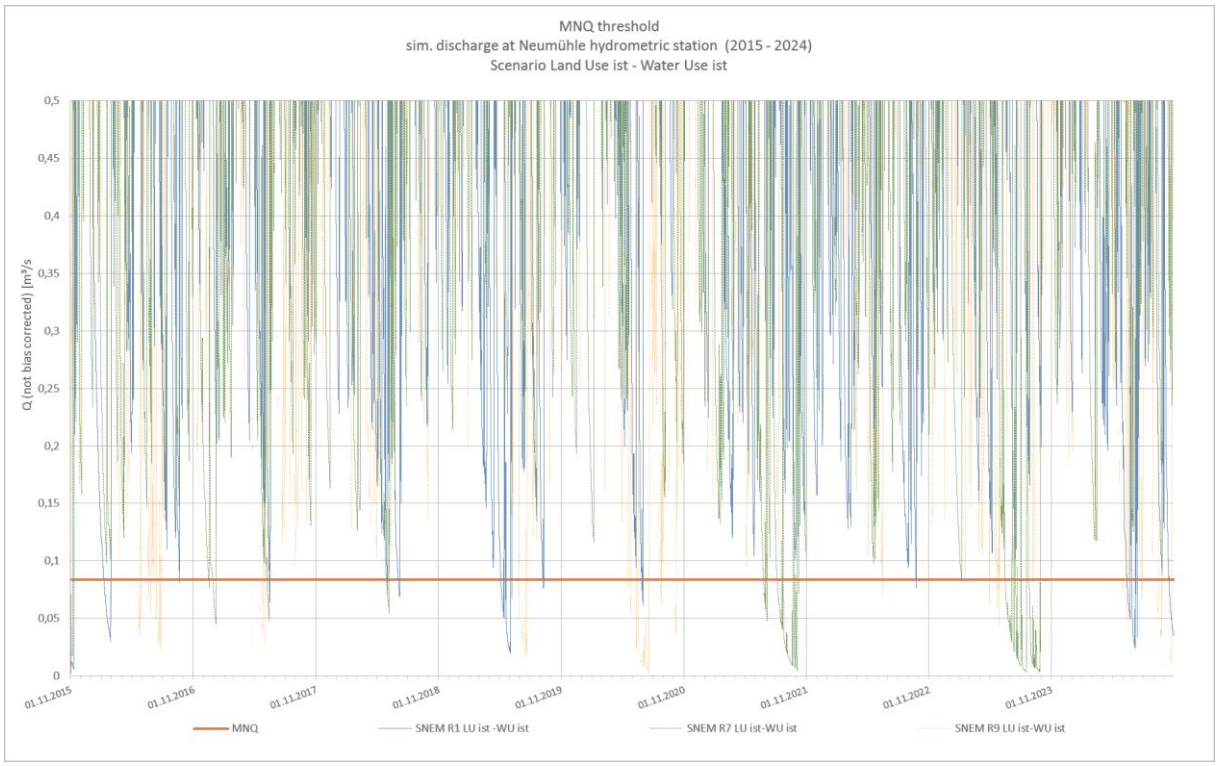
MNQ threshold
sim. discharge at Neumühle hydrometric station (2015 - 2024)
Scenario Land Use ist - Water Use ist
Q (not bias corrected) [m³/s]
0,5
0,45
0,4
0,35
0,3
0,25
0,2
0,15
0,1
0,05
0
01.11.2015
01.11.2016
01.11.2017
01.11.2018
01.11.2019
01.11.2020
01.11.2021
01.11.2022
01.11.2023
MNQ
SNEM R1 LU ist -WU ist
SNEM R7 LU ist-WU ist
SNEM R9 LU ist-WU ist

SSLB

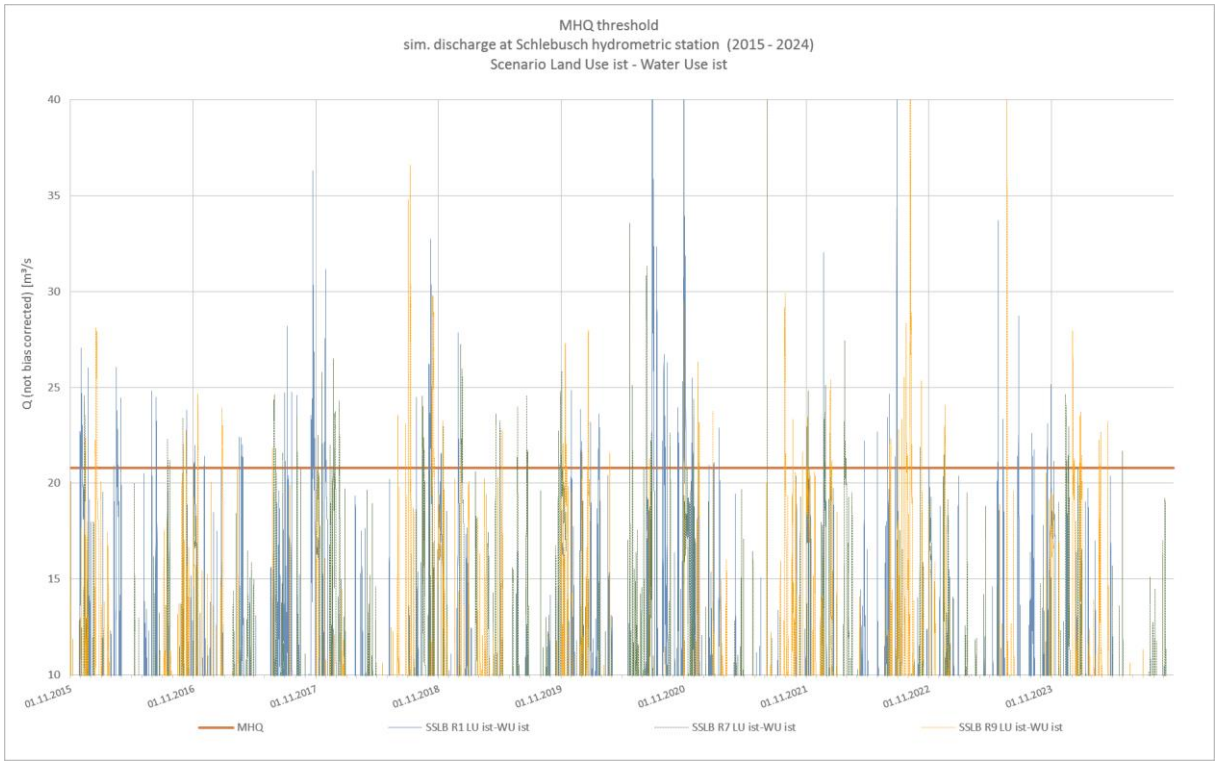
MHQ threshold
sim. discharge at Schlebusch hydrometric station (2015 - 2024)
Scenario Land Use ist - Water Use ist
Q (not bias corrected) [m³/s]
40
35
30
25
20
15
10
01.11.2015
01.11.2016
01.11.2017
01.11.2018
01.11.2019
01.11.2020
01.11.2021
01.11.2022
01.11.2023
MHQ
SSLB R1 LU ist-WU ist
SSLB R7 LU ist-WU ist
SSLB R9 LU ist-WU ist

Comparison 2

SMAN

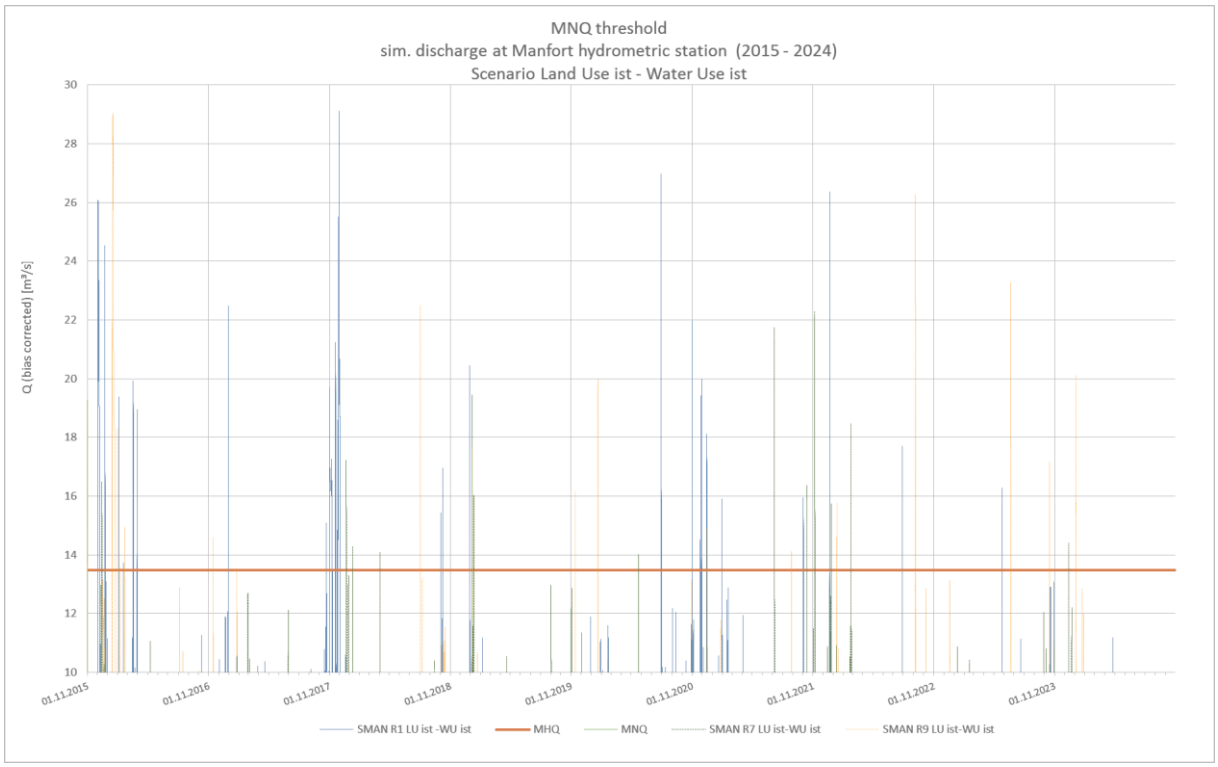

SNEM

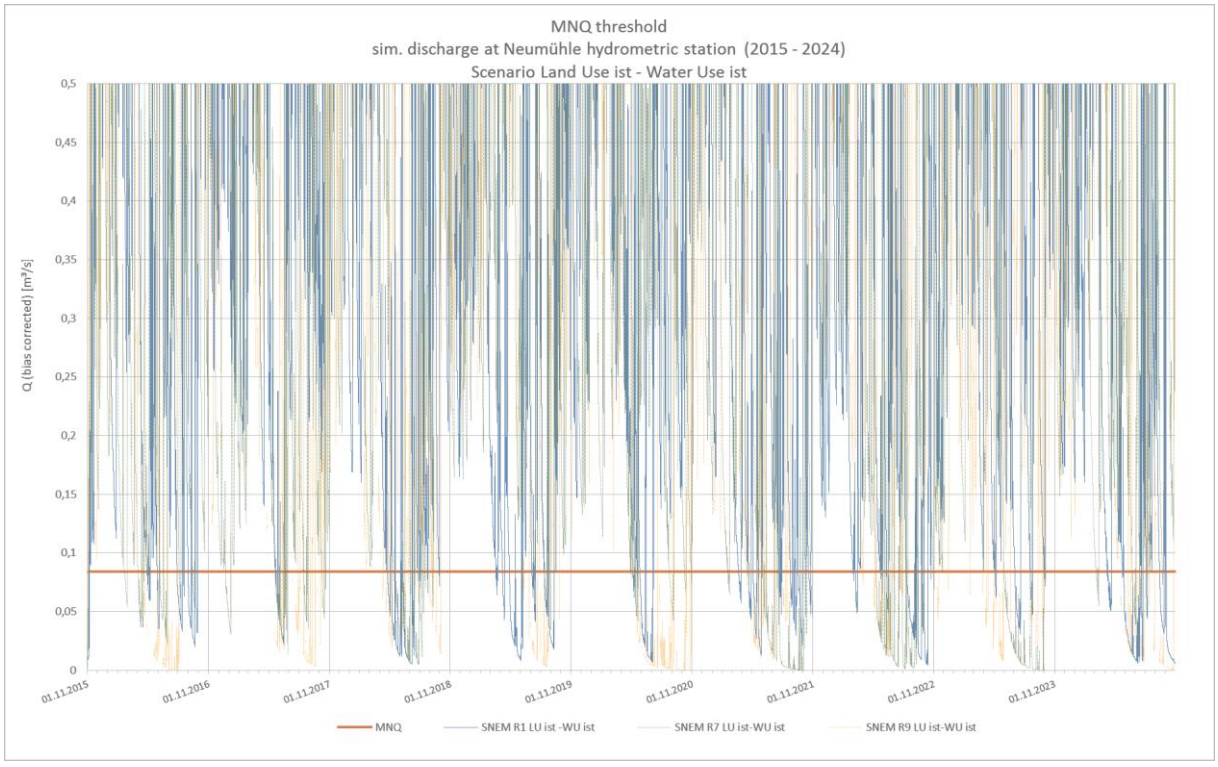

SSLB

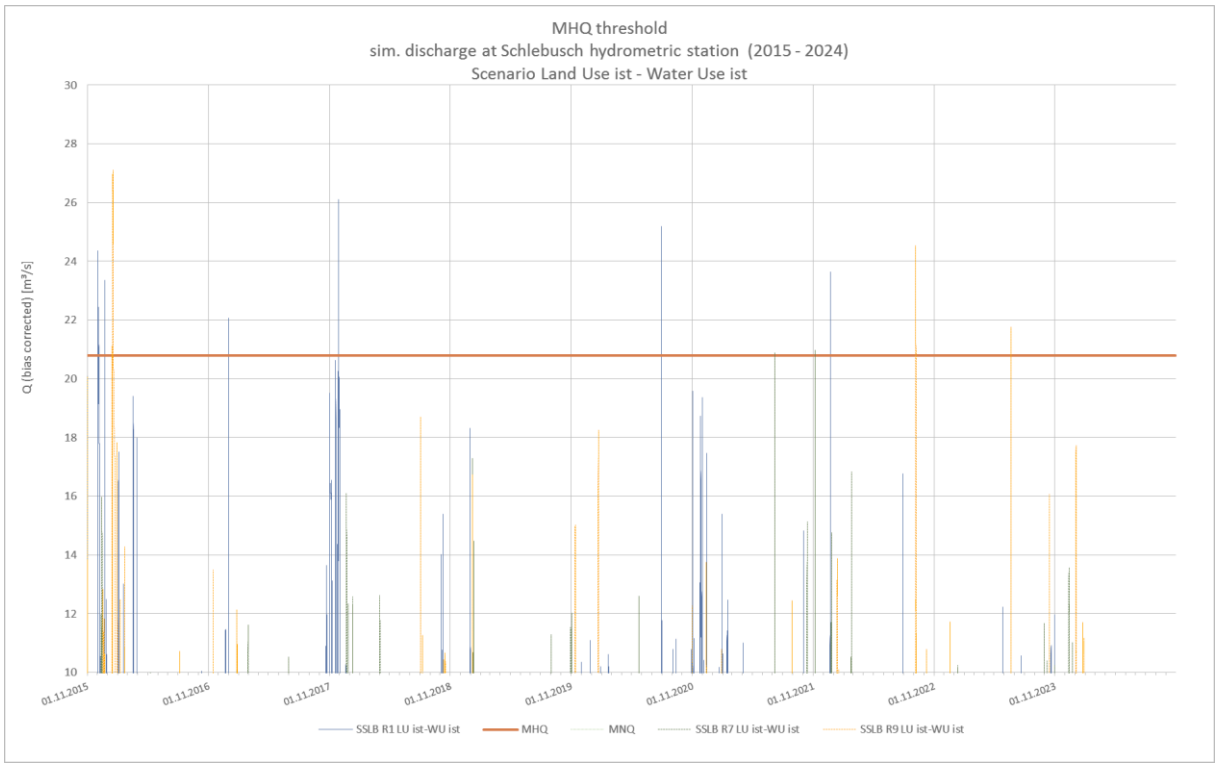
MHQ threshold
sim. discharge at Schlebusch hydrometric station (2015 - 2024)
Scenario Land Use ist - Water Use ist
Q (bias corrected) [m³/s]
30
28
26
24
22
20
18
16
14
12
10
01.11.2015
01.11.2016
01.11.2017
01.11.2018
01.11.2019
01.11.2020
01.11.2021
01.11.2022
01.11.2023
SSLB R1 LU ist-WU ist
MHQ
MNQ
SSLB R7 LU ist-WU ist
SSLB R9 LU ist-WU ist

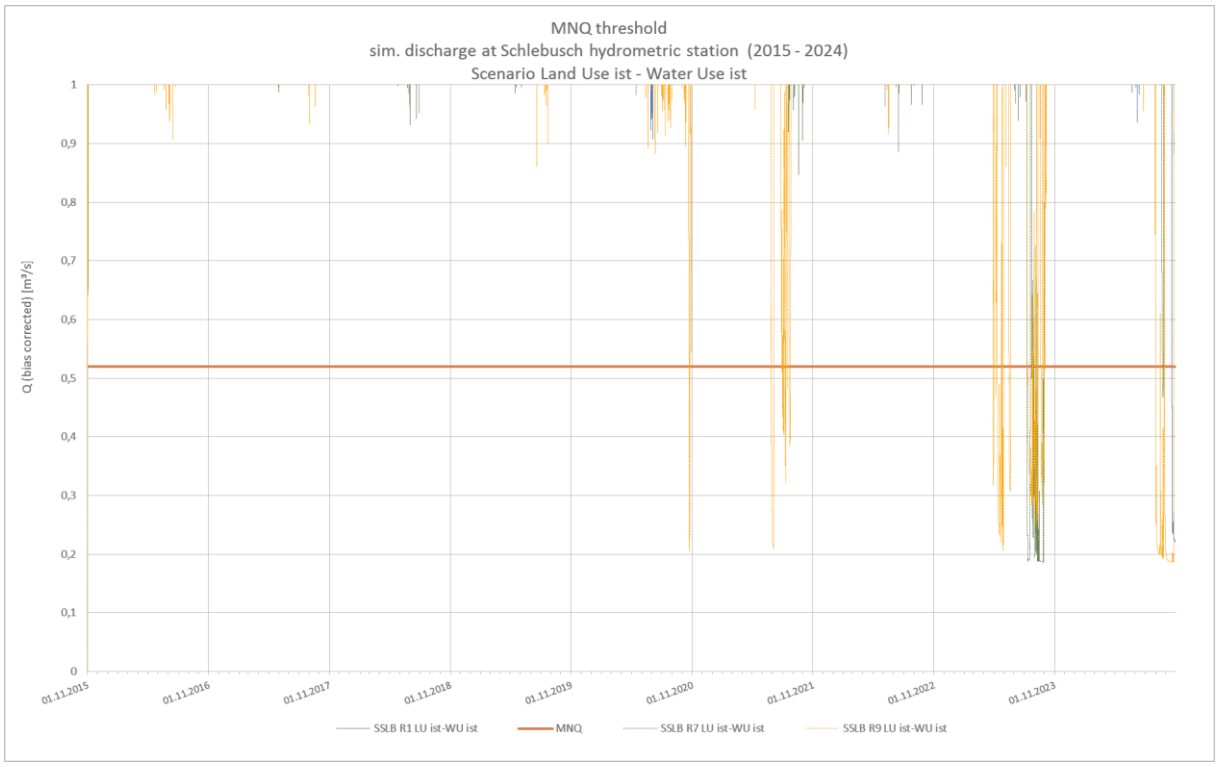
MNQ threshold
sim. discharge at Schlebusch hydrometric station (2015 - 2024)
Scenario Land Use ist - Water Use ist
Q (bias corrected) [m³/s]
1
0,9
0,8
0,7
0,6
0,5
0,4
0,3
0,2
0,1
0
01.11.2015
01.11.2016
01.11.2017
01.11.2018
01.11.2019
01.11.2020
01.11.2021
01.11.2022
01.11.2023
SSLB R1 LU ist-WU ist
MNQ
SSLB R7 LU ist-WU ist
SSLB R9 LU ist-WU ist

TDHN

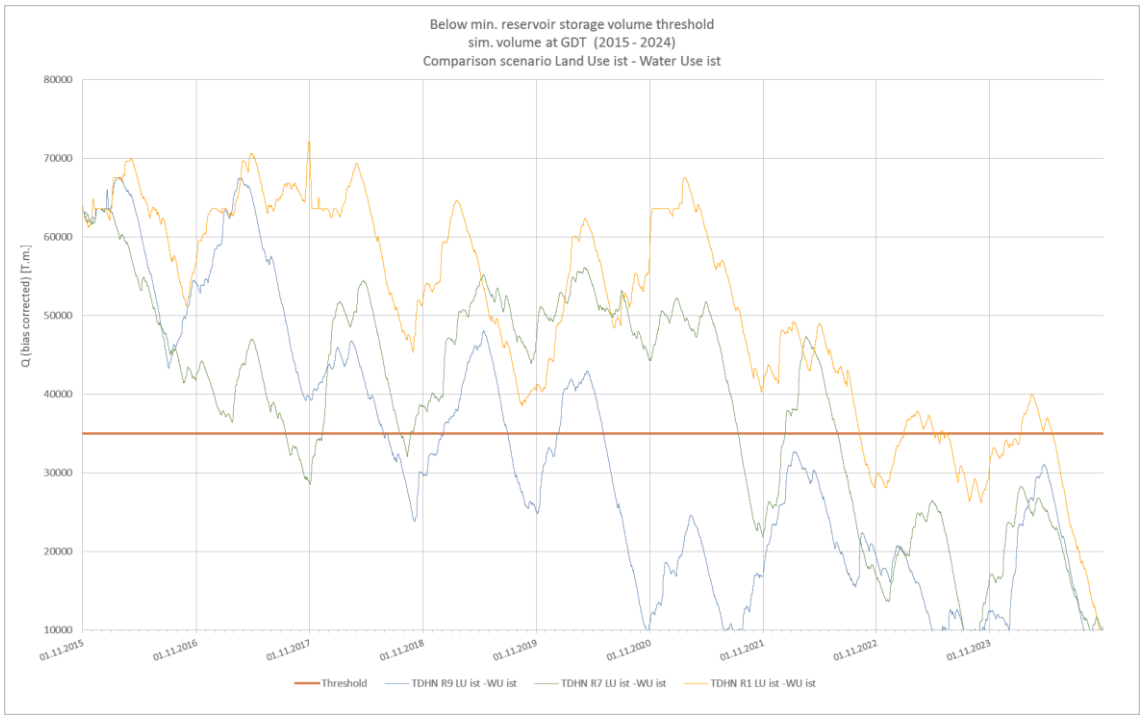

Comparison 4

SMAN

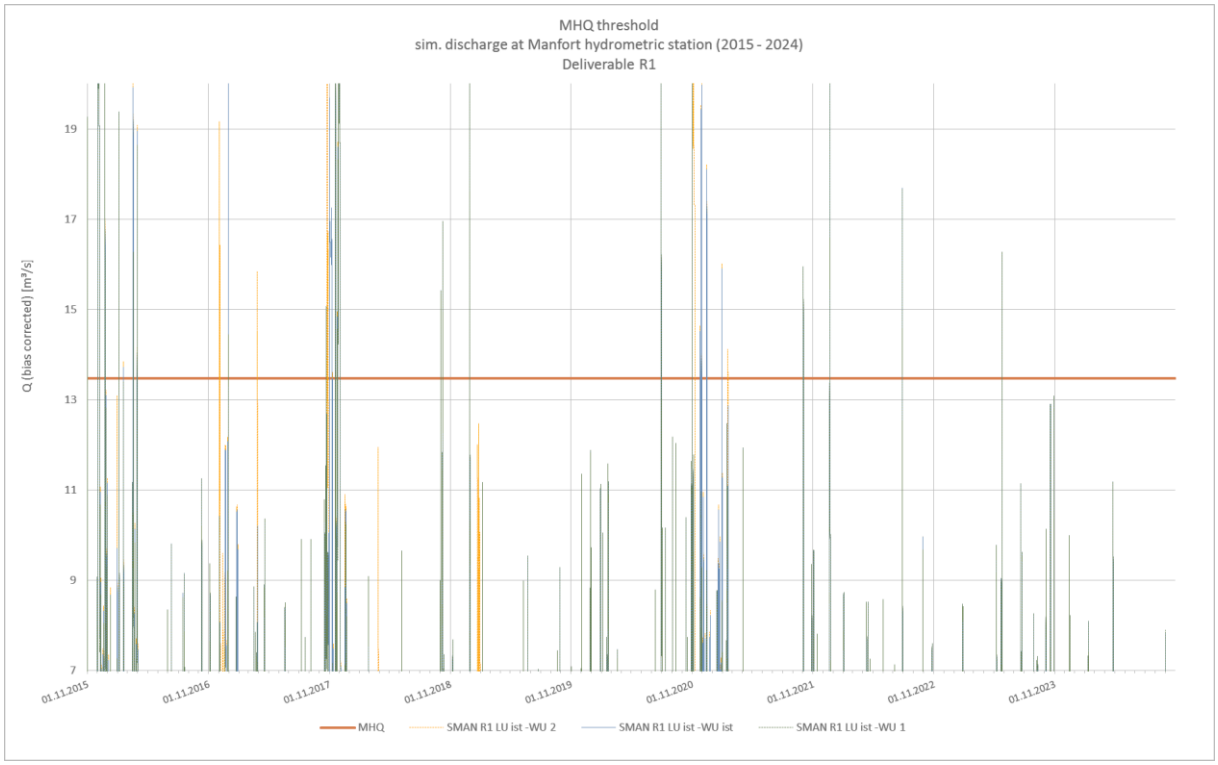

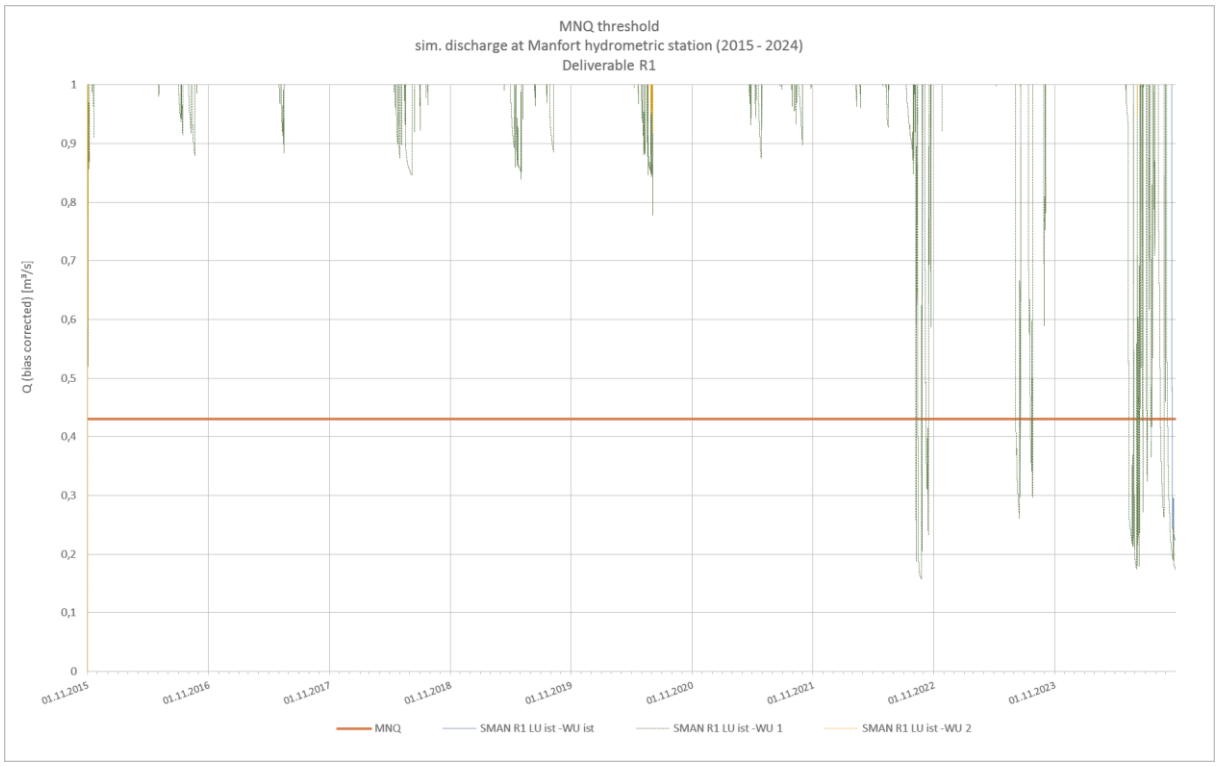
MNQ threshold
sim. discharge at Manfort hydrometric station (2015 - 2024)
Deliverable R1
Q (bias corrected) [m³/s]
1
0,9
0,8
0,7
0,6
0,5
0,4
0,3
0,2
0,1
0
01.11.2015
01.11.2016
01.11.2017
01.11.2018
01.11.2019
01.11.2020
01.11.2021
01.11.2022
01.11.2023
MNQ
SMAN R1 LU ist -WU ist
SMAN R1 LU ist -WU 1
SMAN R1 LU ist -WU 2

SSLB

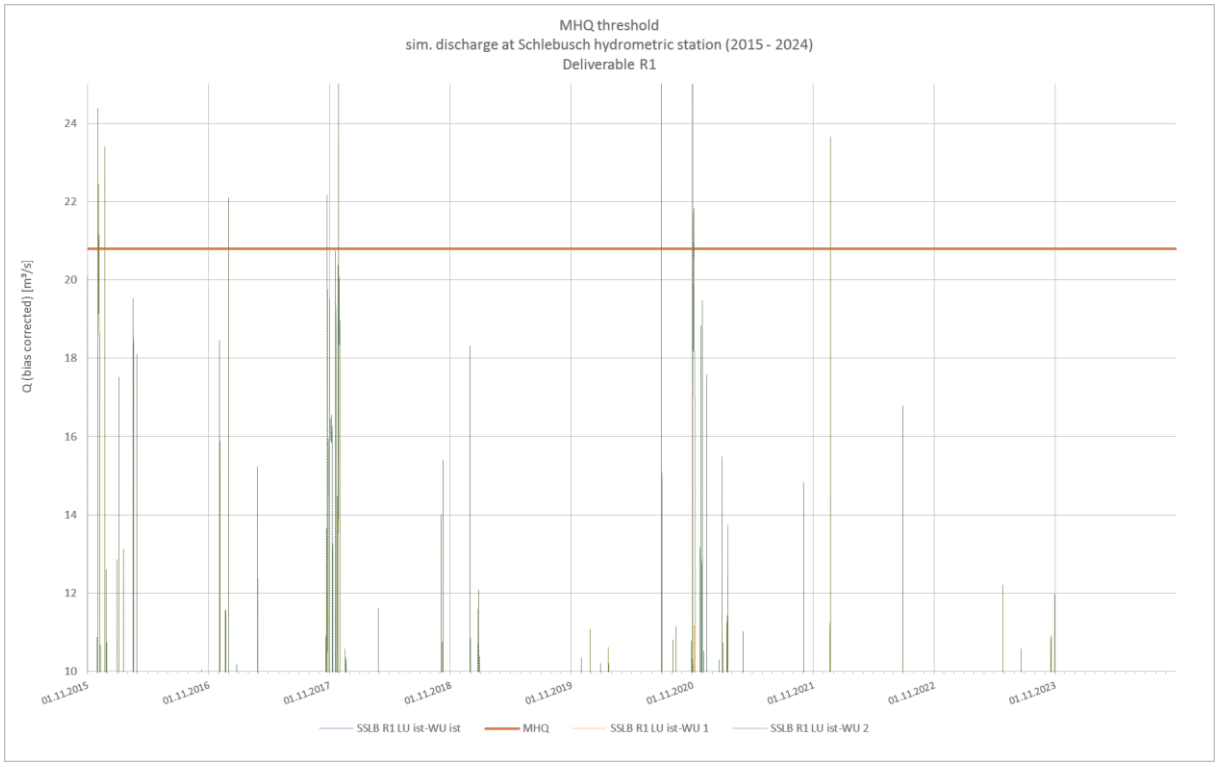
MHQ threshold
sim. discharge at Schlebusch hydrometric station (2015 - 2024)
Deliverable R1
Q (bias corrected) [m³/s]
24
22
20
18
16
14
12
10
01.11.2015
01.11.2016
01.11.2017
01.11.2018
01.11.2019
01.11.2020
01.11.2021
01.11.2022
01.11.2023
SSLB R1 LU ist-WU ist
MHQ
SSLB R1 LU ist-WU 1
SSLB R1 LU ist-WU 2

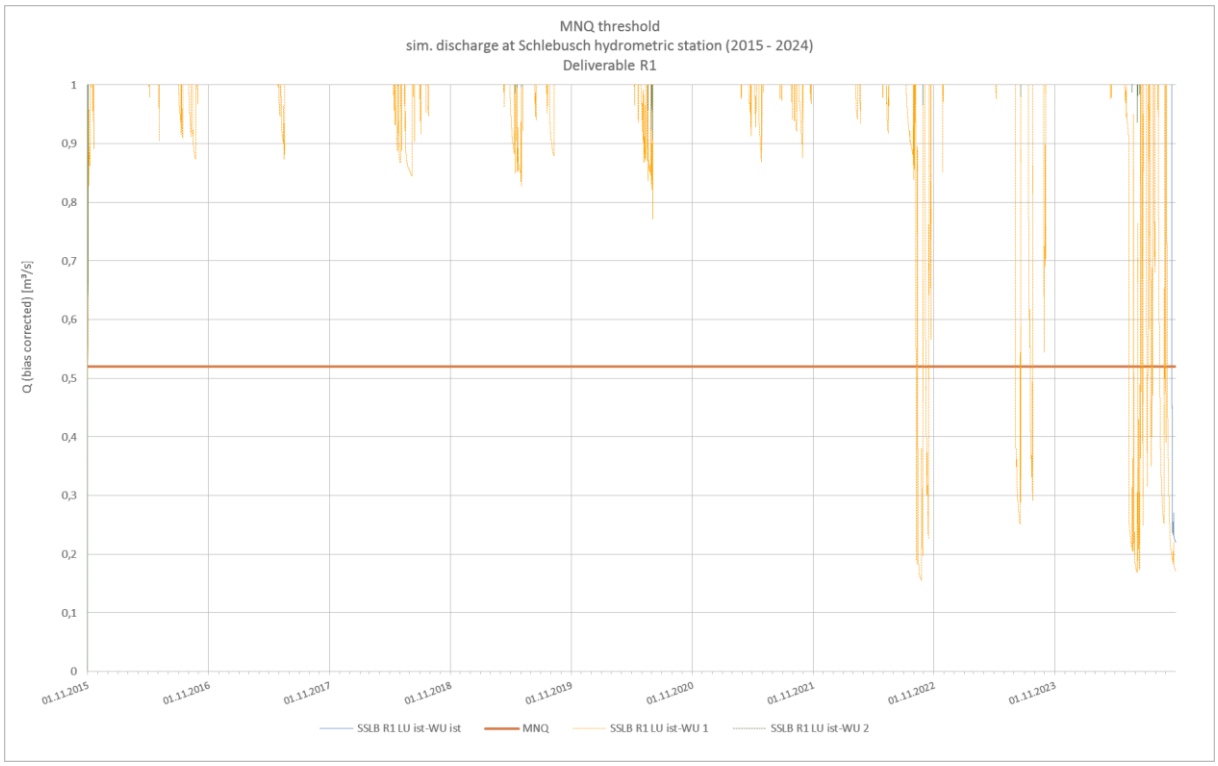
MNQ threshold
sim. discharge at Schlebusch hydrometric station (2015 - 2024)
Deliverable R1
Q (bias corrected) [m³/s]
1
0,9
0,8
0,7
0,6
0,5
0,4
0,3
0,2
0,1
0
01.11.2015
01.11.2016
01.11.2017
01.11.2018
01.11.2019
01.11.2020
01.11.2021
01.11.2022
01.11.2023
SSLB R1 LU ist-WU ist
MNQ
SSLB R1 LU ist-WU 1
SSLB R1 LU ist-WU 2

TDHN

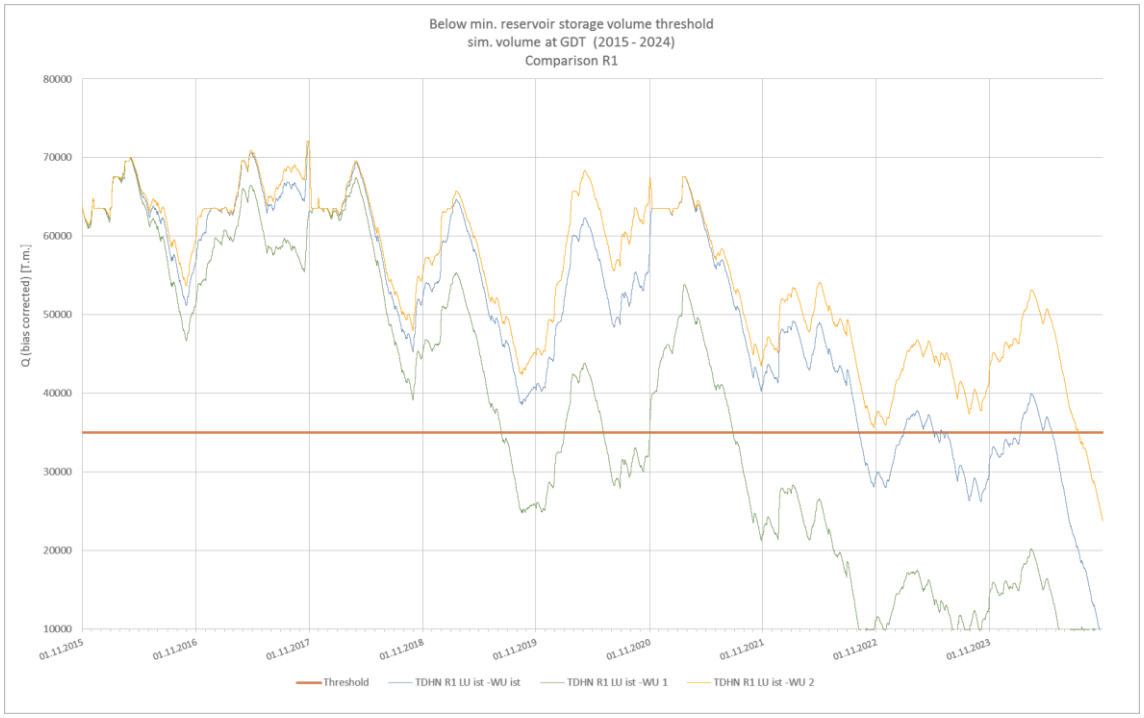
Below min. reservoir storage volume threshold
sim. volume at GDT (2015 - 2024)
Comparison R1
Q (bias corrected) [T.m.]
80000
70000
60000
50000
40000
30000
20000
10000
01.11.2015
01.11.2016
01.11.2017
01.11.2018
01.11.2019
01.11.2020
01.11.2021
01.11.2022
01.11.2023
Threshold
TDHN R1 LU ist -WU ist
TDHN R1 LU ist -WU 1
TDHN R1 LU ist -WU 2

Comparison 5

SMAN

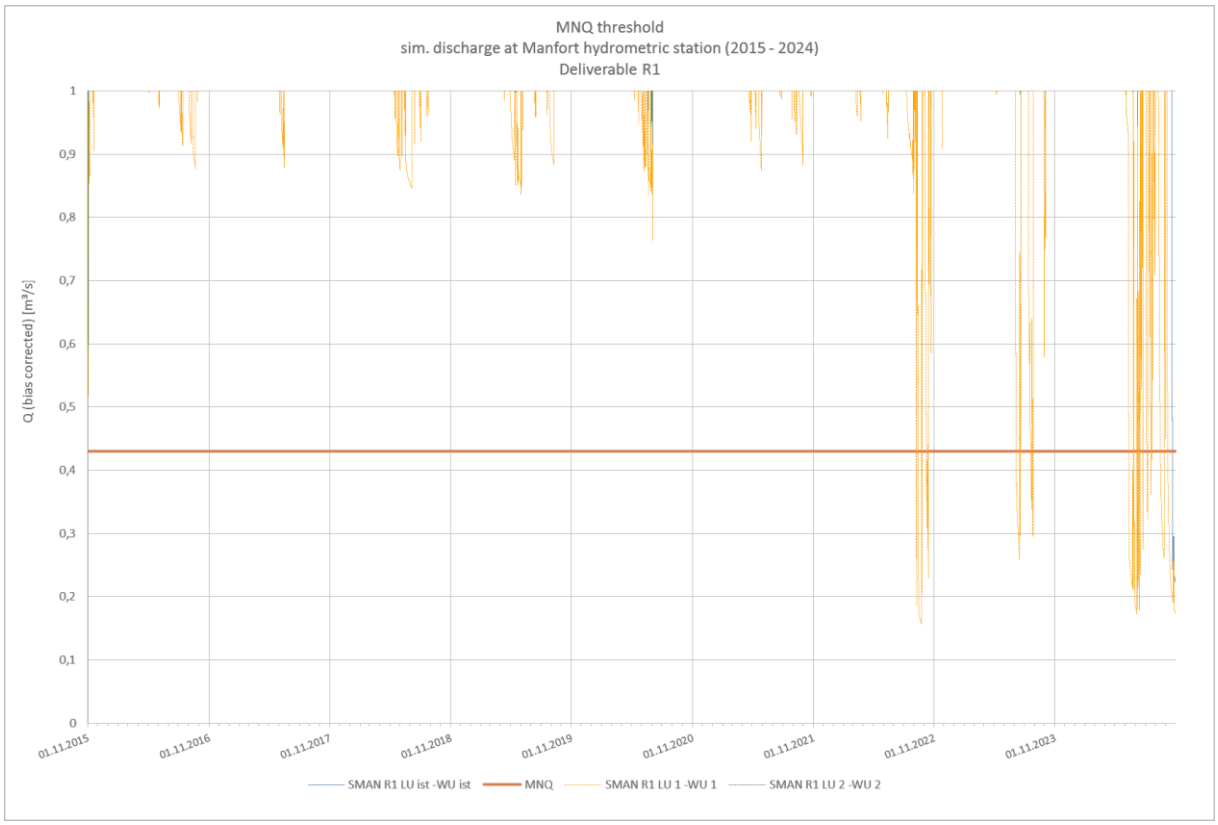

Comparison 6

SMAN

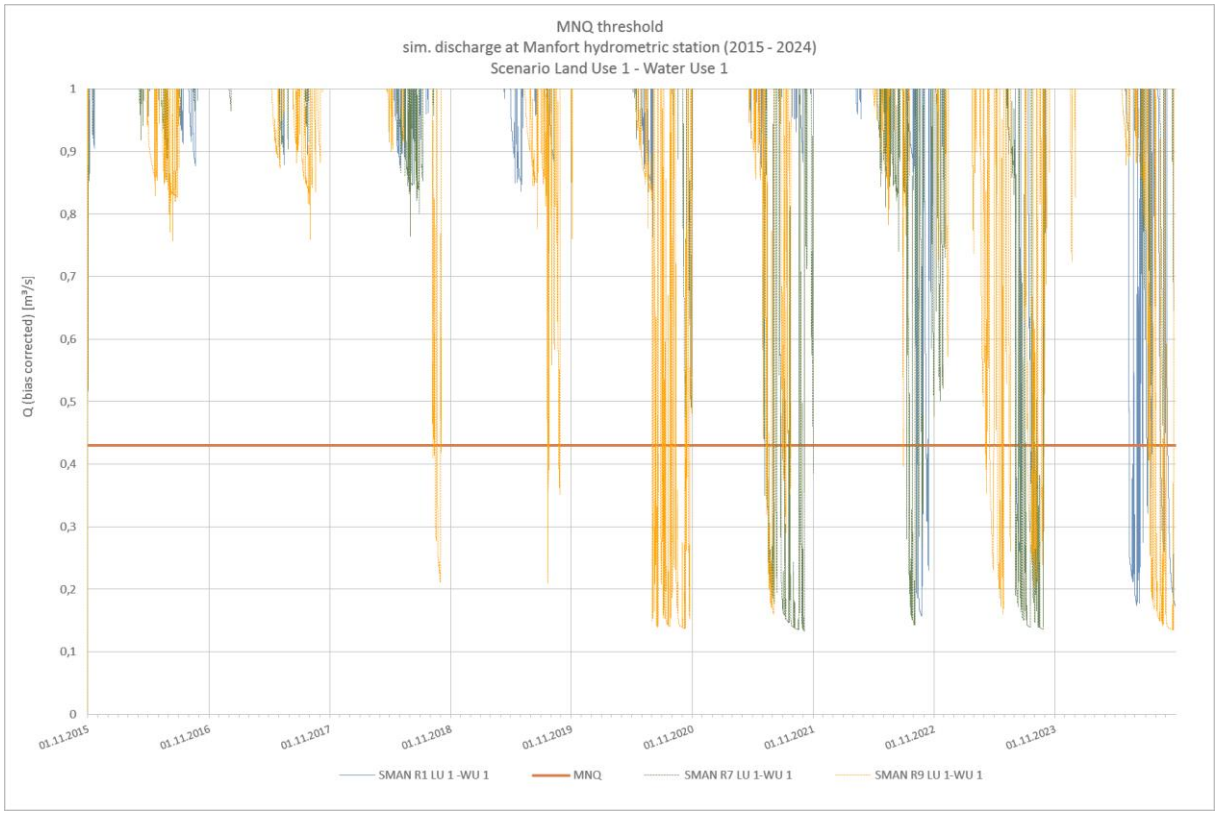

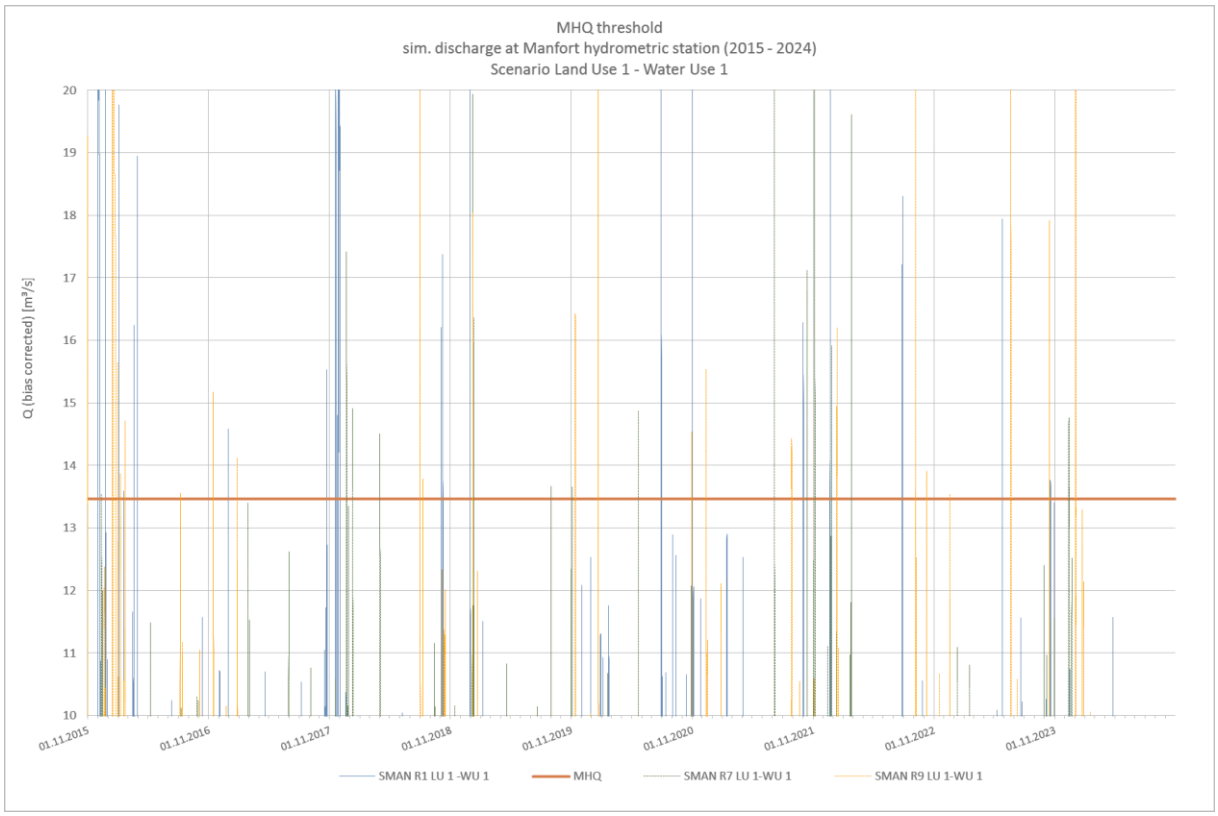
MHQ threshold
sim. discharge at Manfort hydrometric station (2015 - 2024)
Scenario Land Use 1 - Water Use 1
Q (bias corrected) [m³/s]
20
19
18
17
16
15
14
13
12
11
10
01.11.2015
01.11.2016
01.11.2017
01.11.2018
01.11.2019
01.11.2020
01.11.2021
01.11.2022
01.11.2023
SMAN R1 LU 1 -WU 1
MHQ
SMAN R7 LU 1-WU 1
SMAN R9 LU 1-WU 1

SSLB

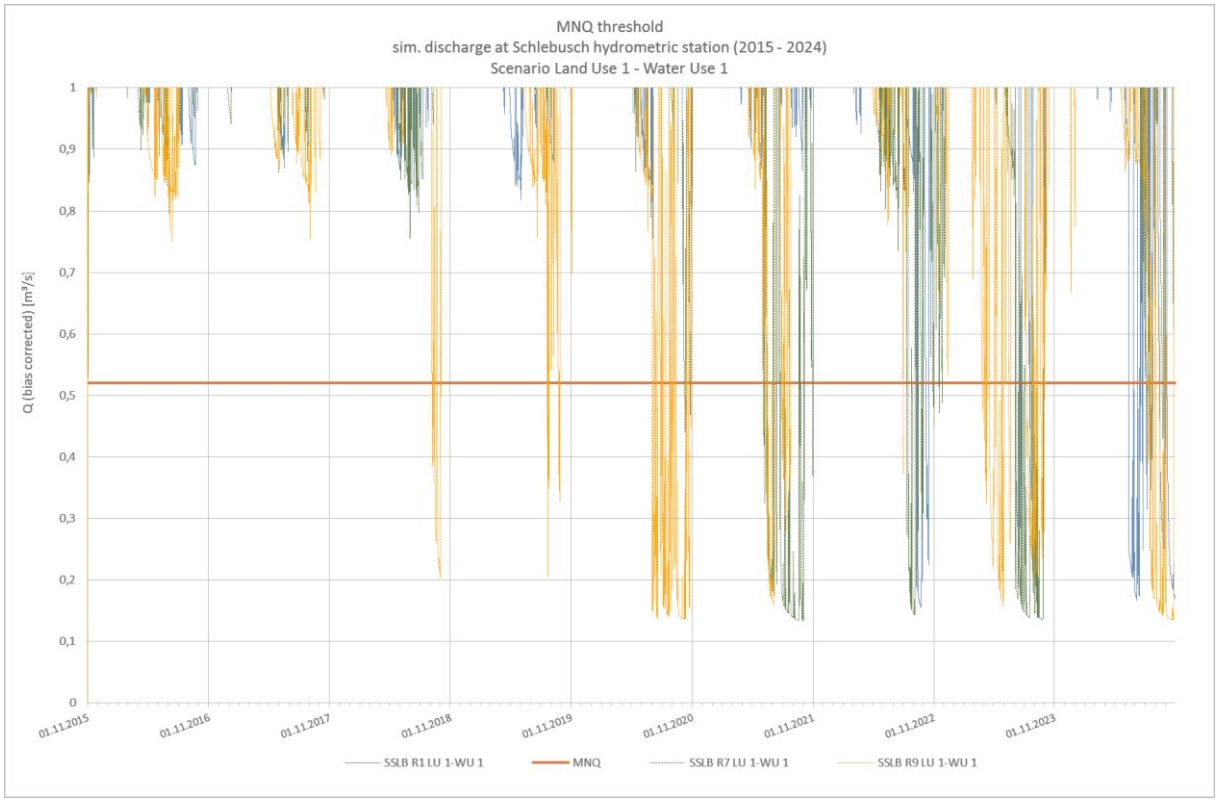
MNQ threshold
sim. discharge at Schlebusch hydrometric station (2015 - 2024)
Scenario Land Use 1 - Water Use 1
Q (bias corrected) [m³/s]
1
0,9
0,8
0,7
0,6
0,5
0,4
0,3
0,2
0,1
0
01.11.2015
01.11.2016
01.11.2017
01.11.2018
01.11.2019
01.11.2020
01.11.2021
01.11.2022
01.11.2023
SSLB R1 LU 1-WU 1
MNQ
SSLB R7 LU 1-WU 1
SSLB R9 LU 1-WU 1

TDHN

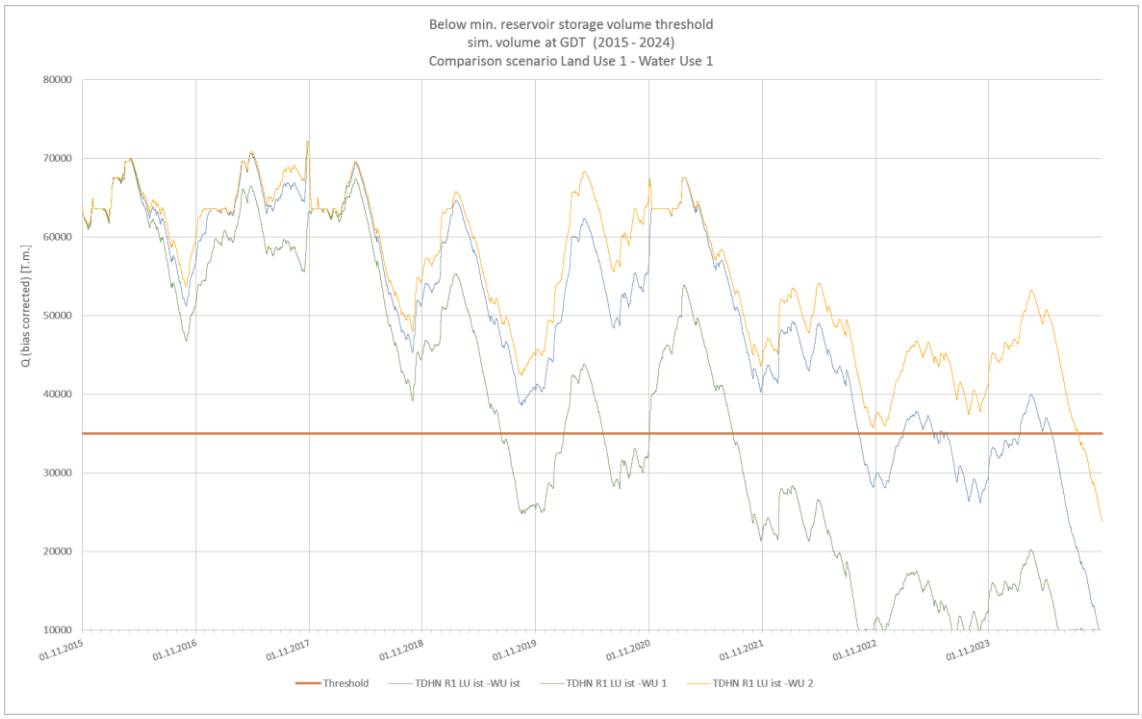

Comparison 7

SMAN

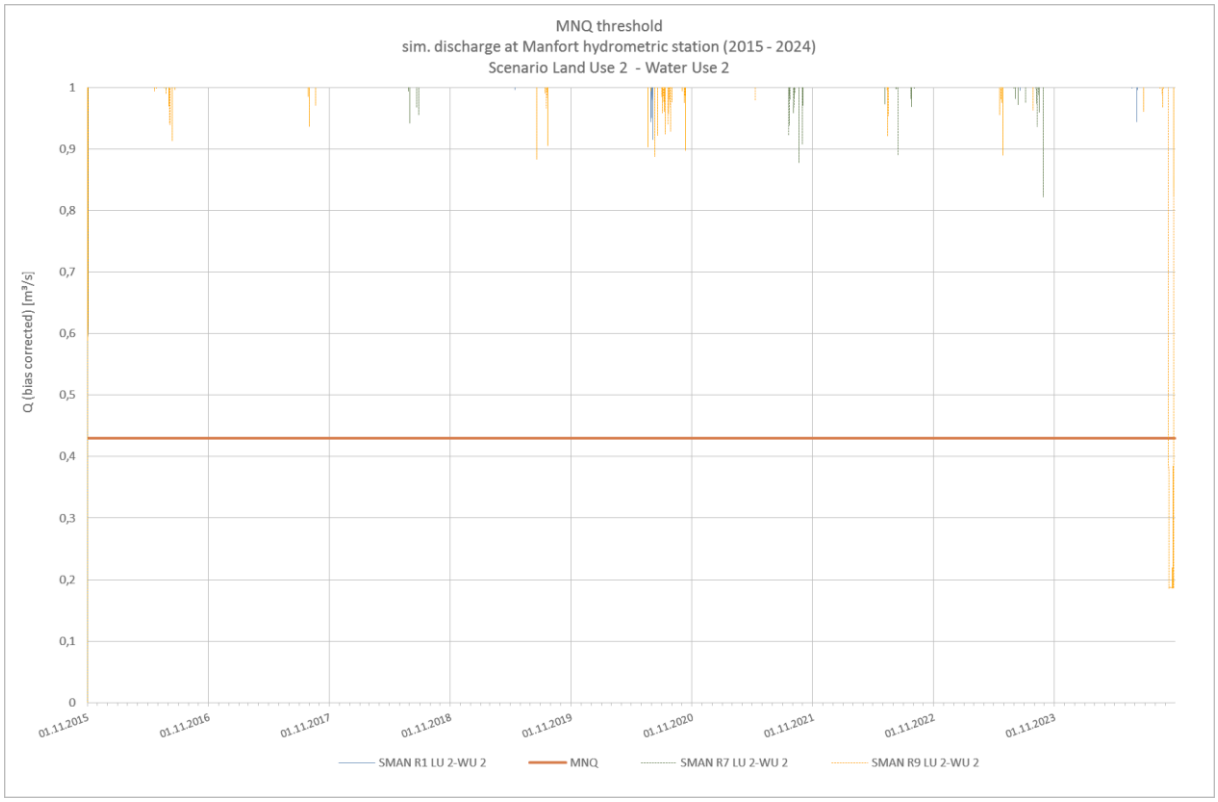

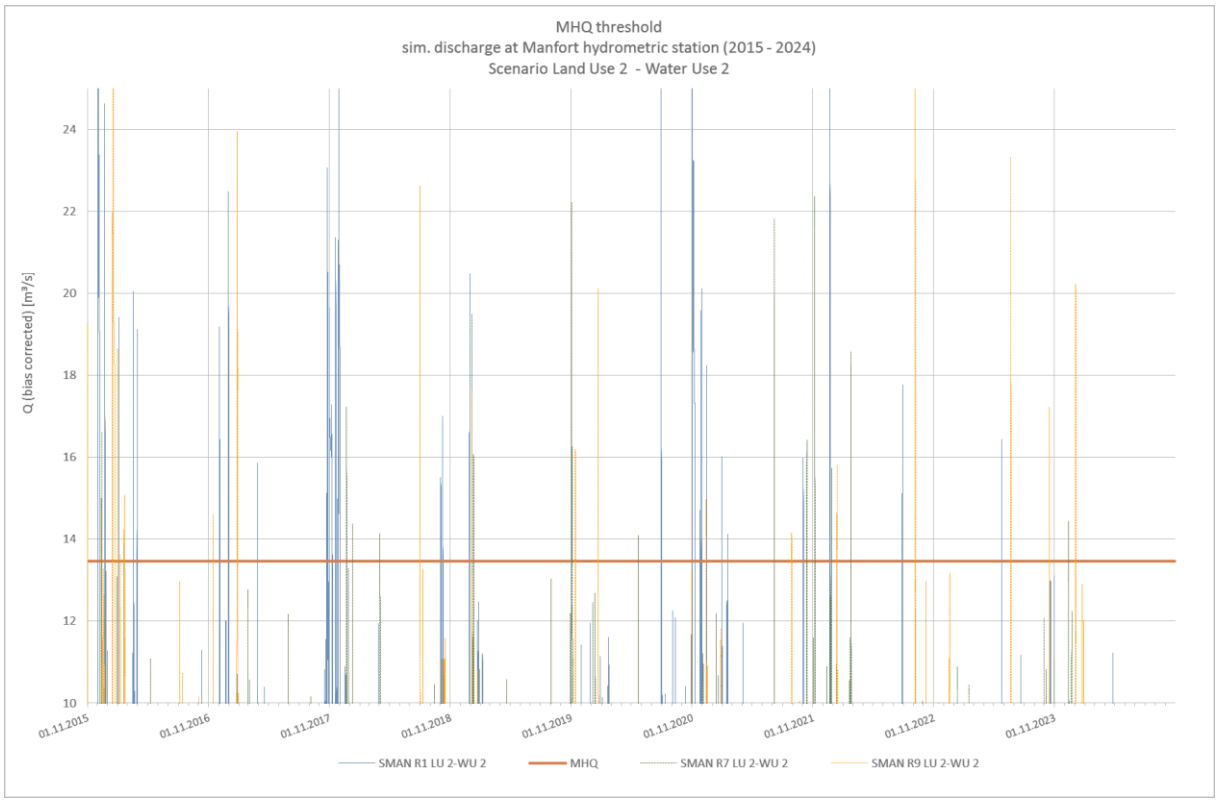
MHQ threshold
sim. discharge at Manfort hydrometric station (2015 - 2024)
Scenario Land Use 2 - Water Use 2
Q (bias corrected) [m³/s]
24
22
20
18
16
14
12
10
01.11.2015
01.11.2016
01.11.2017
01.11.2018
01.11.2019
01.11.2020
01.11.2021
01.11.2022
01.11.2023
SMAN R1 LU 2-WU 2
MHQ
SMAN R7 LU 2-WU 2
SMAN R9 LU 2-WU 2

SSLB

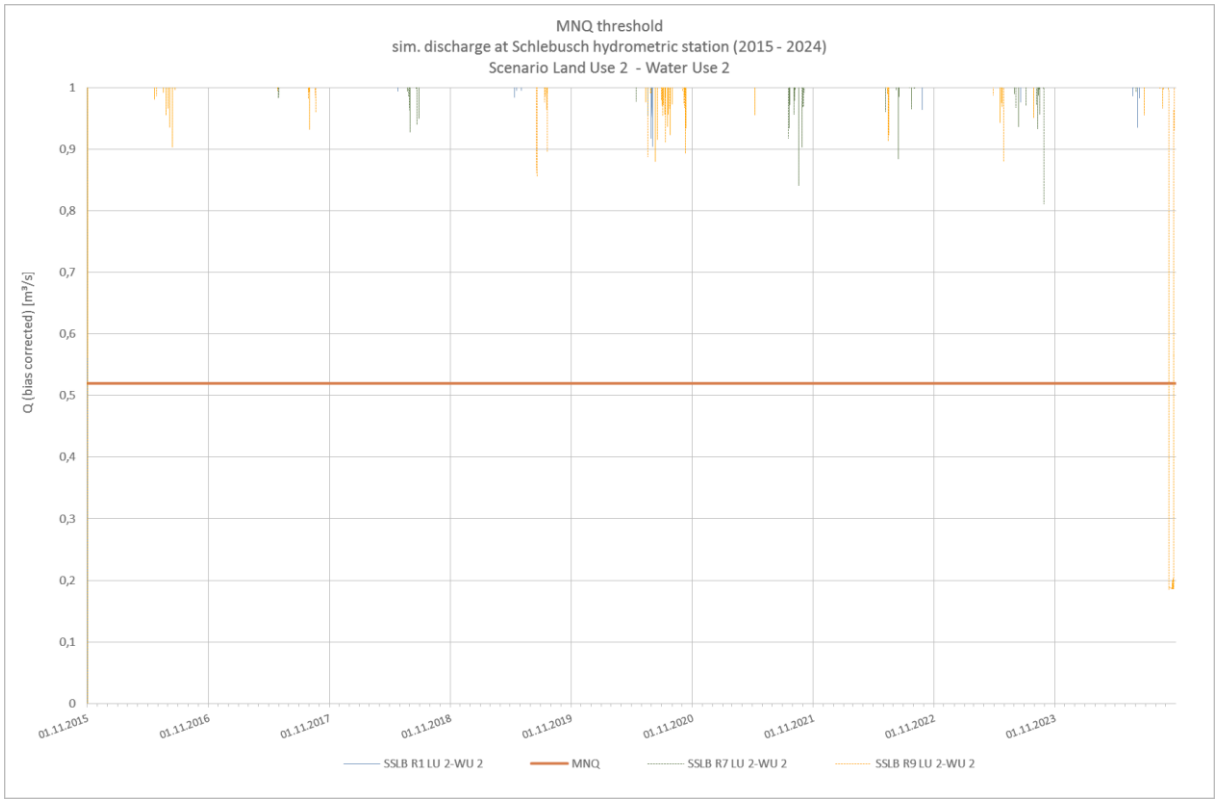
MNQ threshold
sim. discharge at Schlebusch hydrometric station (2015 - 2024)
Scenario Land Use 2 - Water Use 2
Q (bias corrected) [m³/s]
1
0,9
0,8
0,7
0,6
0,5
0,4
0,3
0,2
0,1
0
01.11.2015
01.11.2016
01.11.2017
01.11.2018
01.11.2019
01.11.2020
01.11.2021
01.11.2022
01.11.2023
SSLB R1 LU 2-WU 2
MNQ
SSLB R7 LU 2-WU 2
SSLB R9 LU 2-WU 2

TDHN

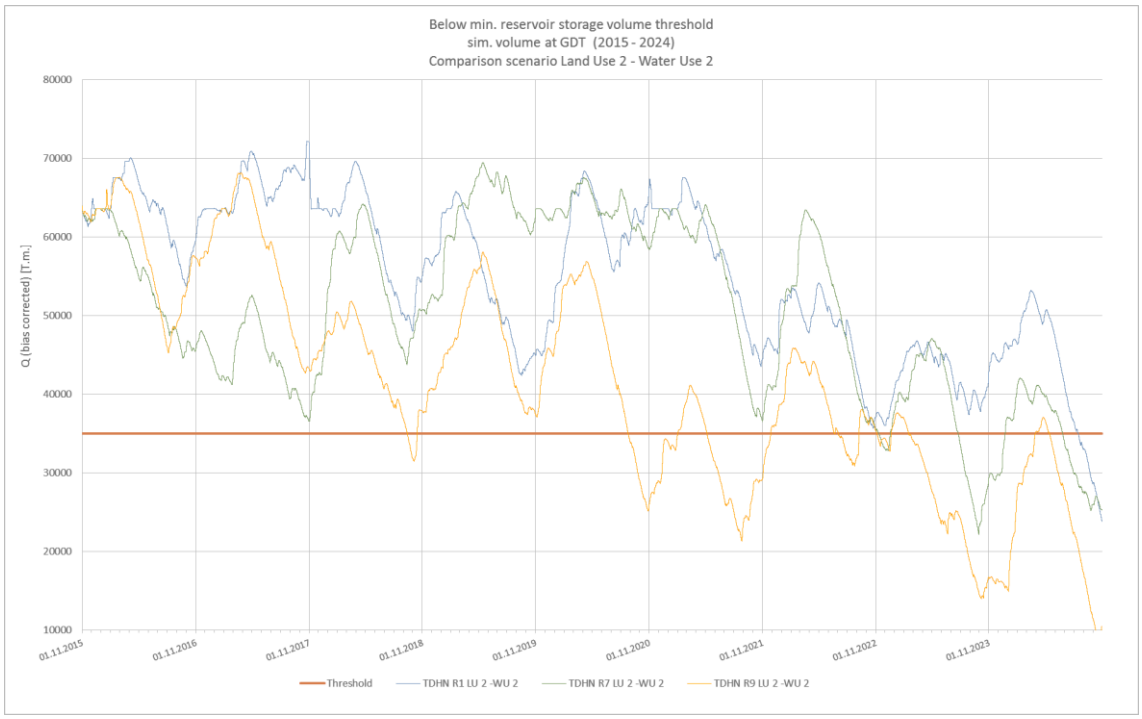
Below min. reservoir storage volume threshold
sim. volume at GDT (2015 - 2024)
Comparison scenario Land Use 2 - Water Use 2
Q (bias corrected) [T.m.]
80000
70000
60000
50000
40000
30000
20000
10000
01.11.2015
01.11.2016
01.11.2017
01.11.2018
01.11.2019
01.11.2020
01.11.2021
01.11.2022
01.11.2023
Threshold
TDHN R1 LU 2 -WU 2
TDHN R7 LU 2 -WU 2
TDHN R9 LU 2 -WU 2

4.17.2. Framework 1 – Analysis of climate data

1-month SPI calculated with WP2 data for past conditions and ground stations - June

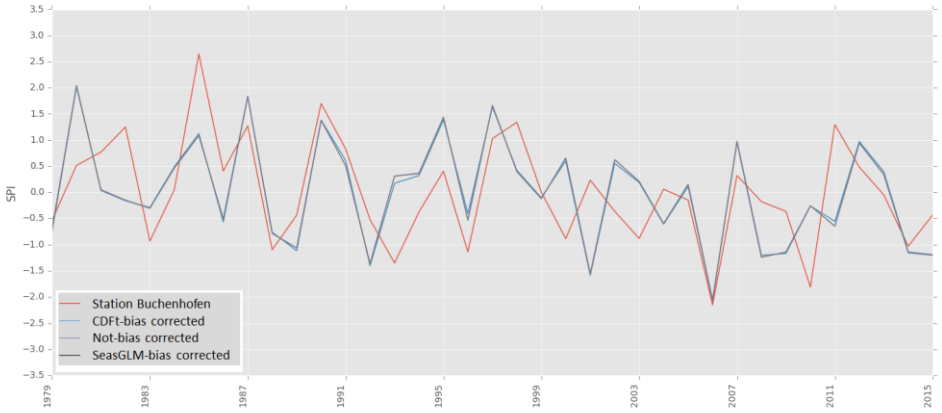

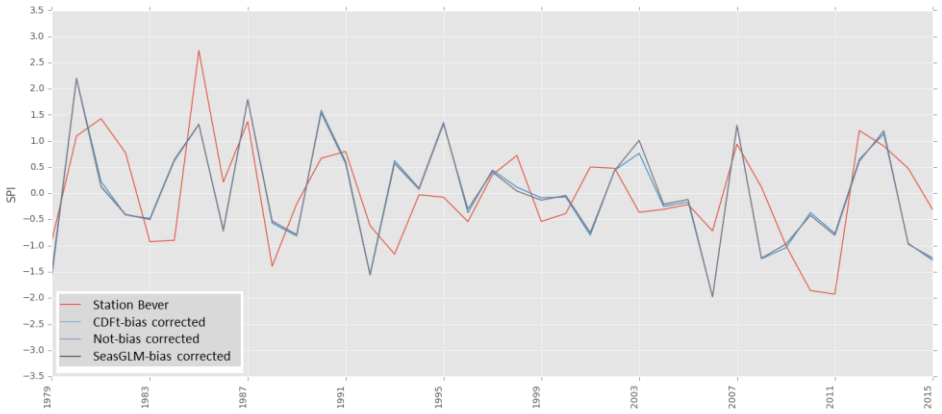

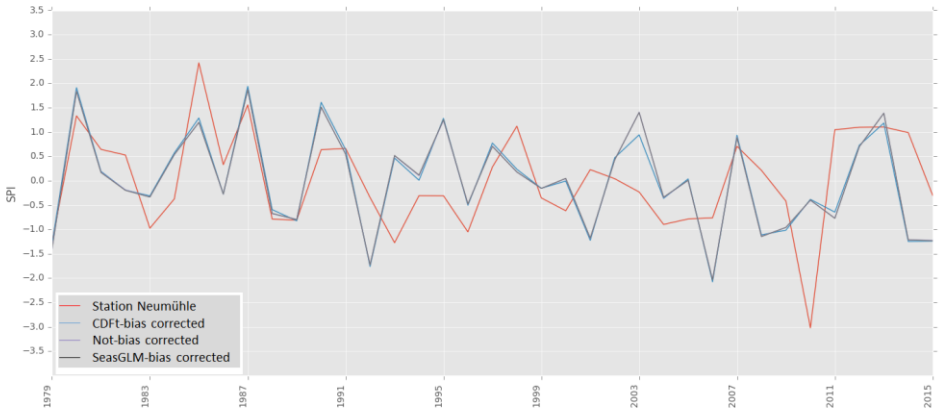

1-month SPI calculated with WP2 data (corresponding grid points) for past conditions – June

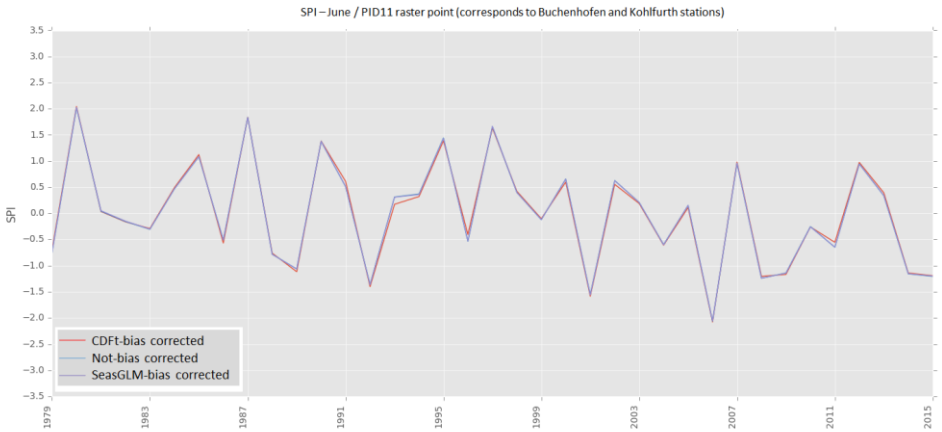

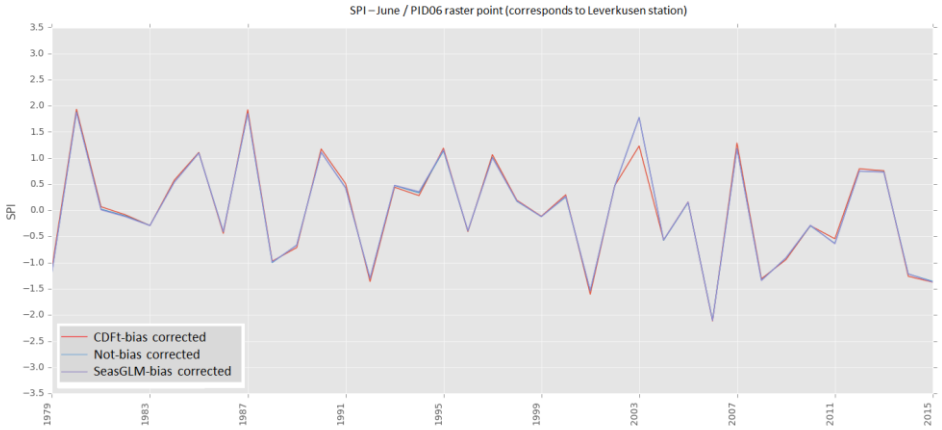

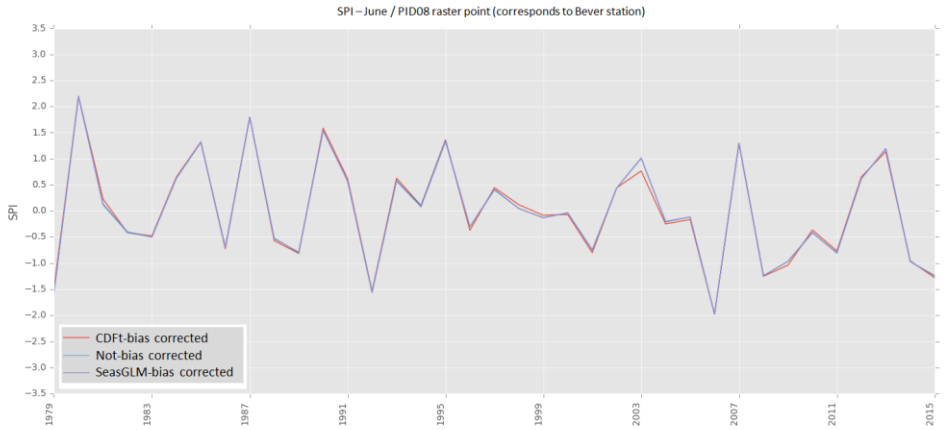

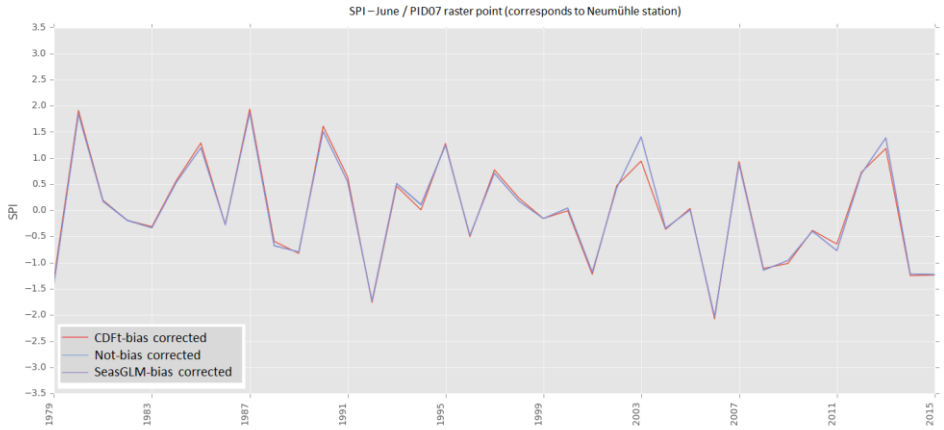

1-month SPI calculated with ground stations (past conditions) - June

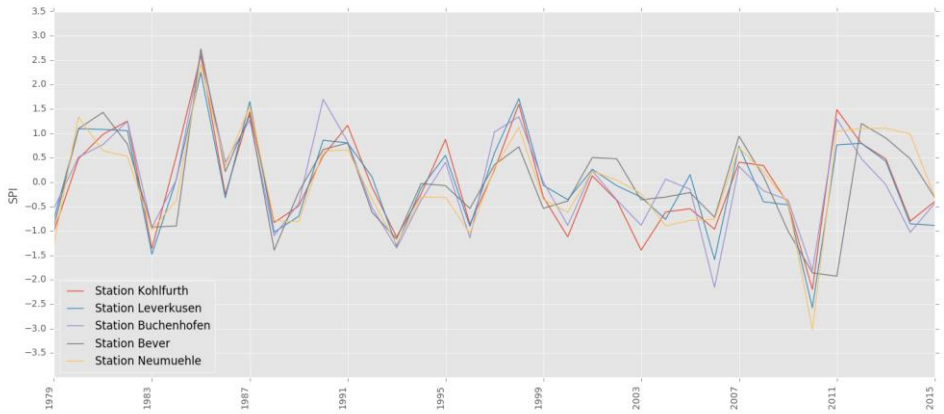

1-month SPI calculated with WP2 data (past conditions) for all grid points together - June

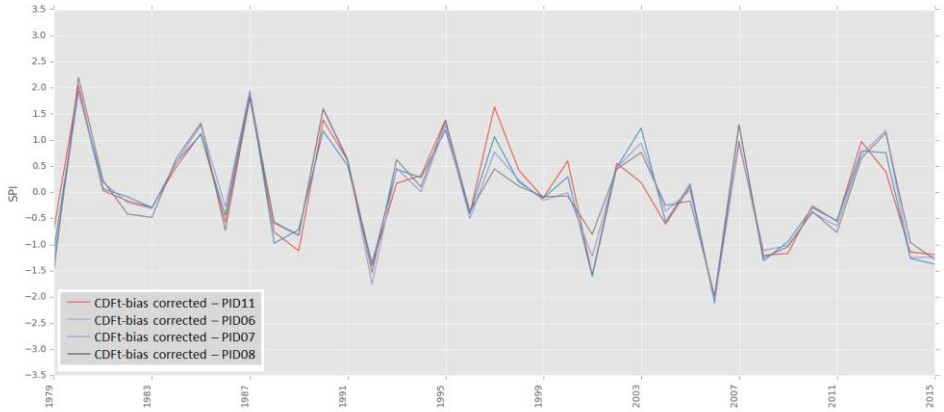

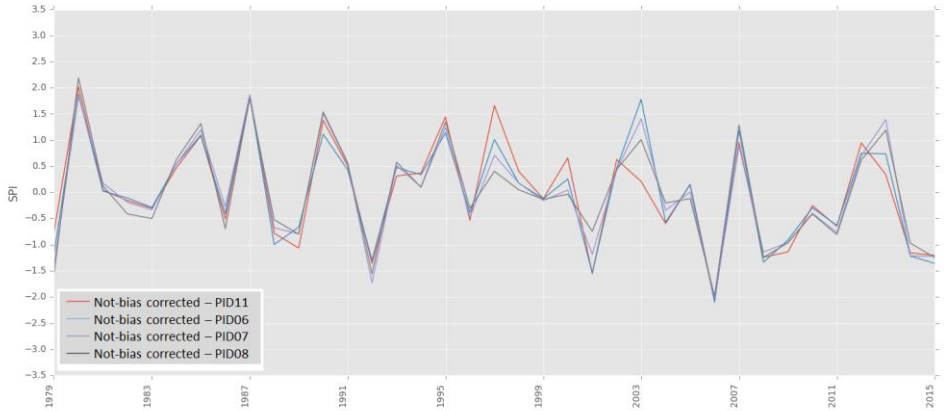

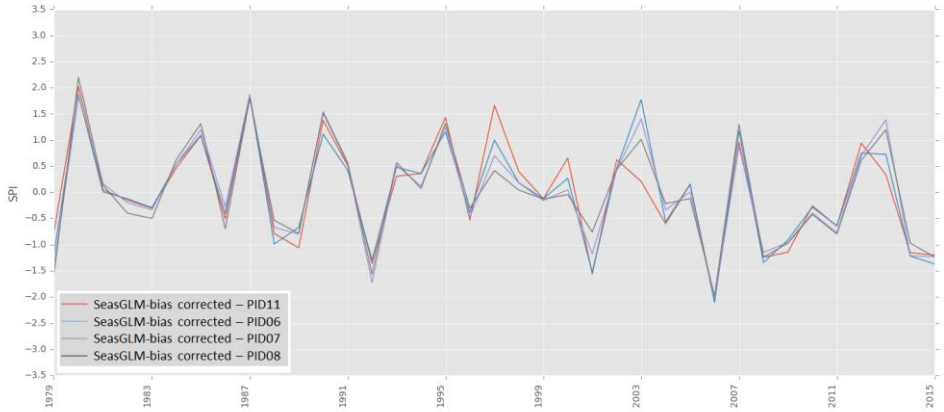

SPI calculated with WP2 data for past conditions and different time scales

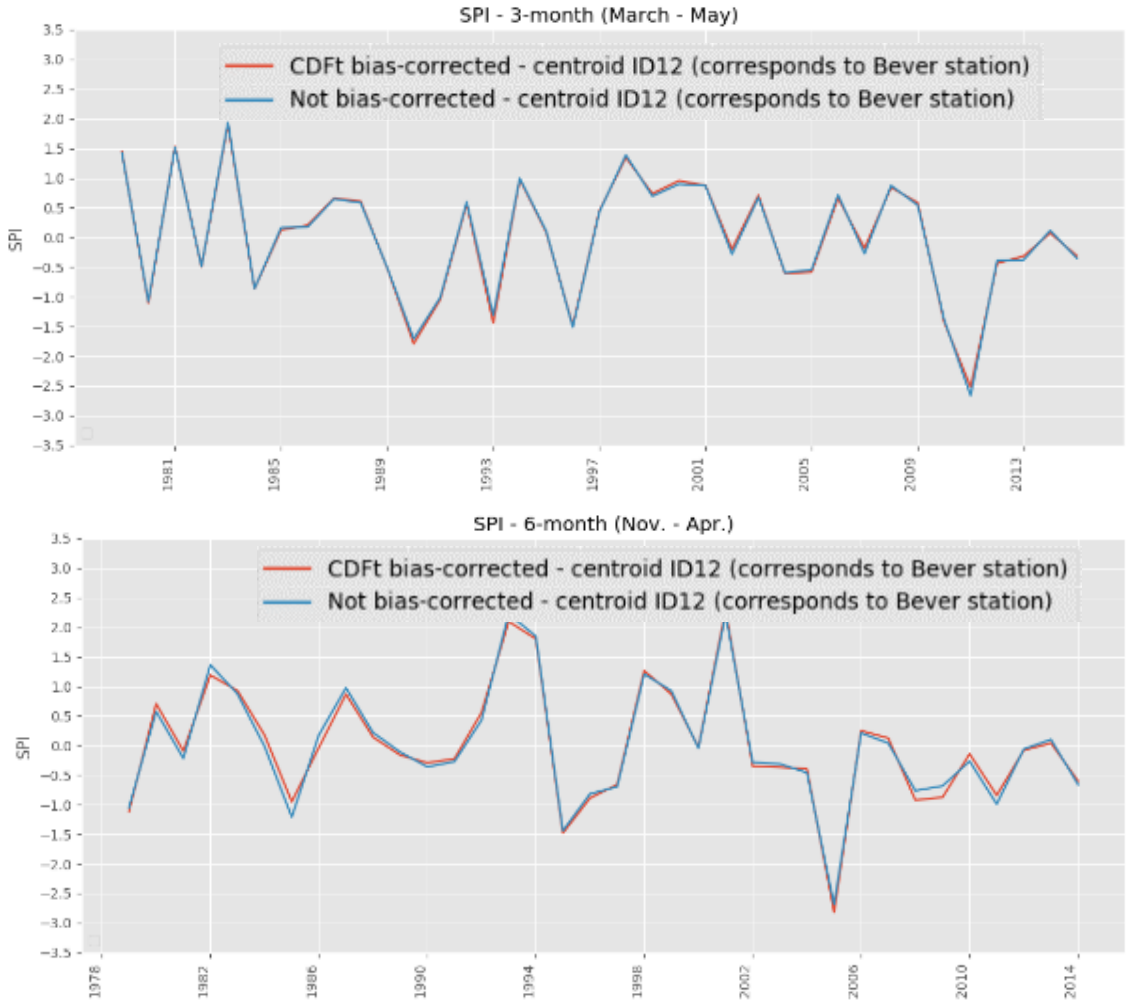

SPEI calculated with WP2 data for past conditions

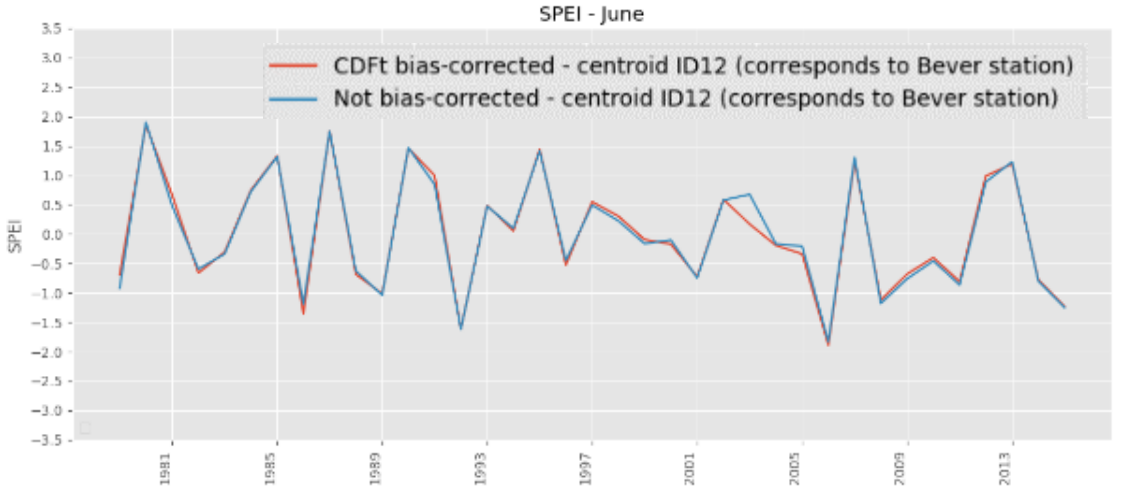

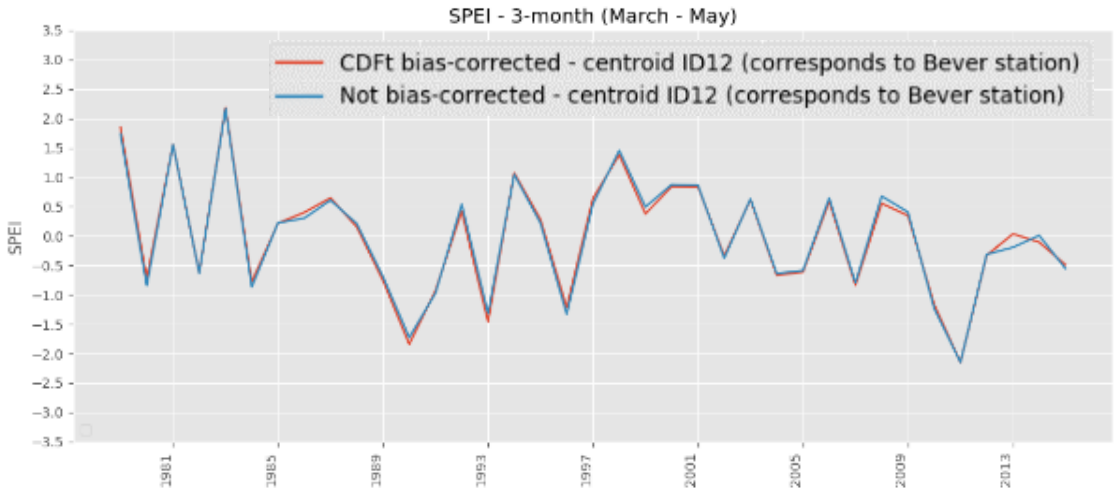

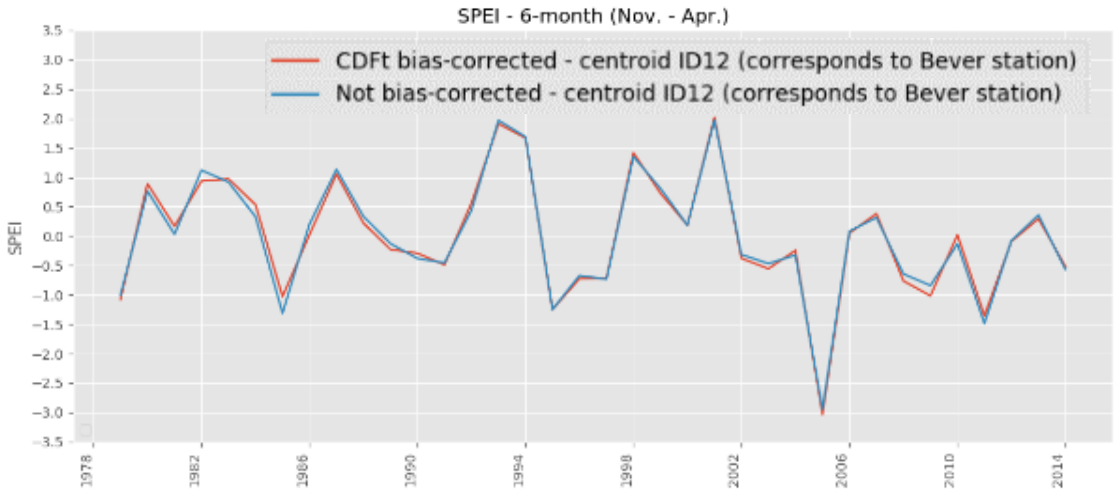

SPI with WP2 data for past and future conditions

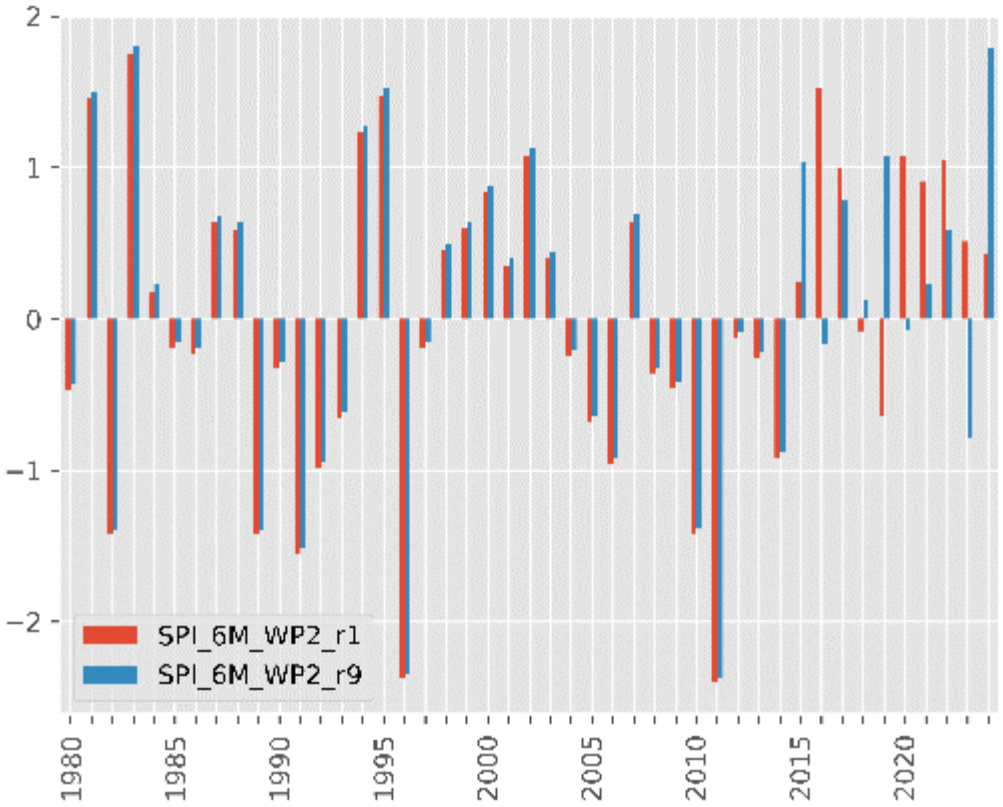

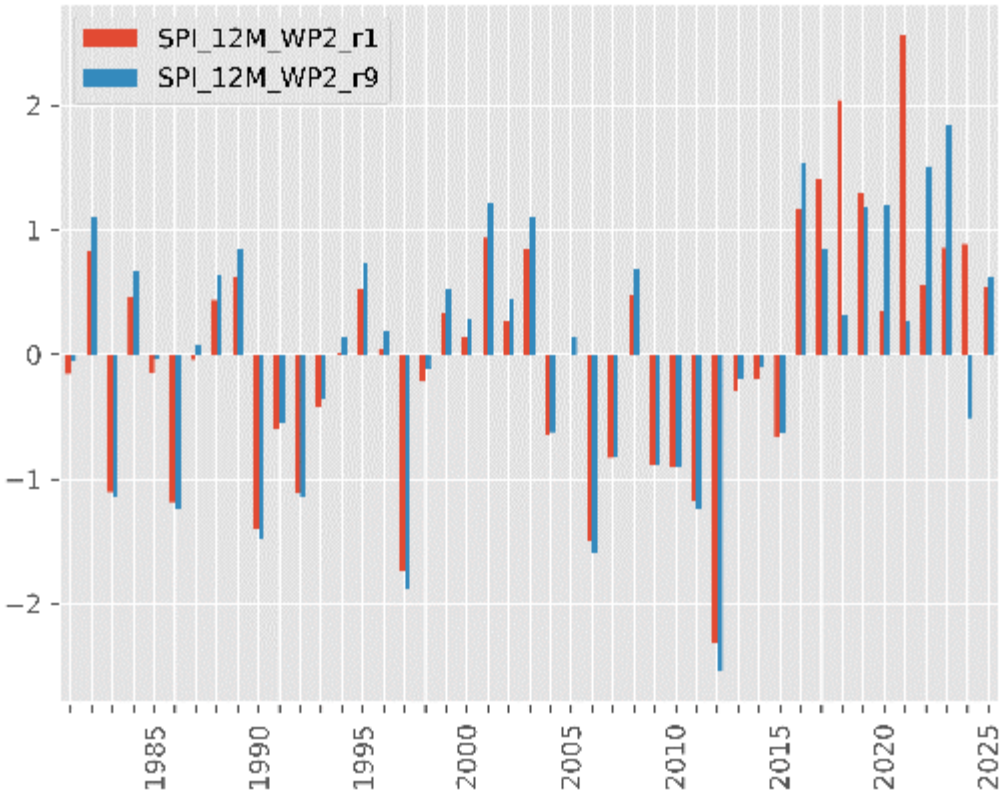

SPEI with WP2 data for past and future conditions

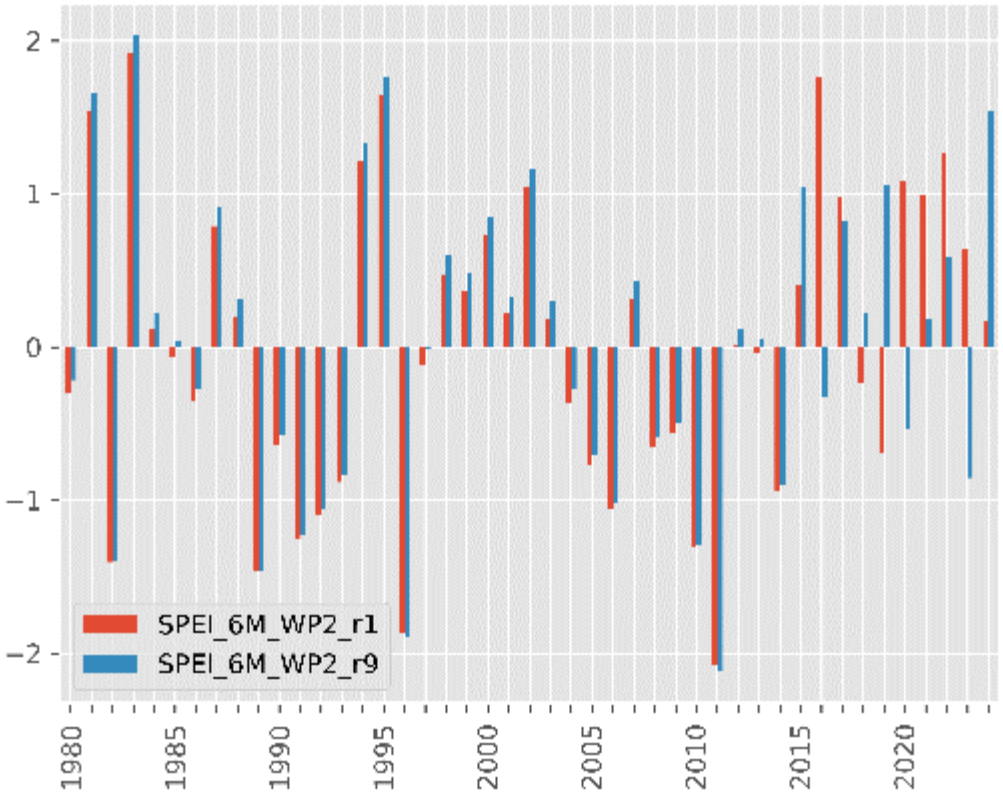

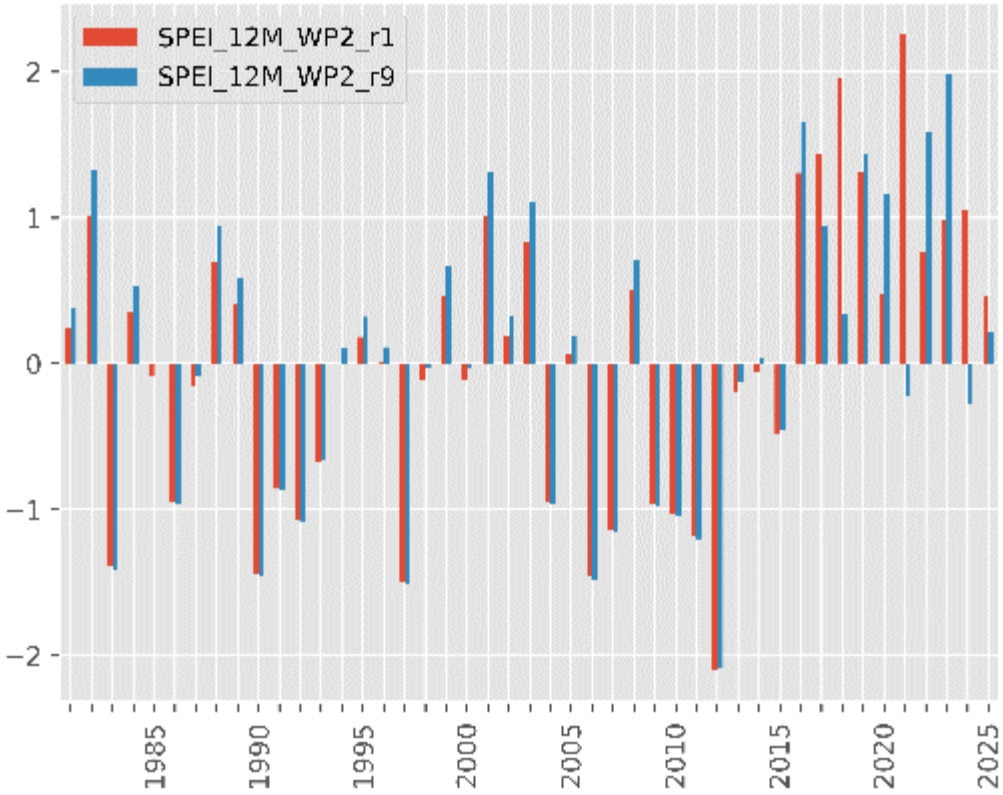

4.17.3. Framework 2 – NASIM – Dhünn catchment area (typical flow rates and trend analysis)

Typical flow rates – comparison between observed Q at SNEM and realisations (not bias corrected)

	MNQ [m³/s]	NQ [m³/s]	MHQ [m³/s]	MQ [m³/s]
Neumühle station (1965 - 2017)	0.084	0.020	8.773	0.580
Neumühle station (1980 - 2017)	0.097	0.031	9.037	0.582
Sim. Q - no-bias corr. (1980 - 2015)	0.197	0.066	10.435	0.702
Sim. Q - CDFt-bias corr. (1980 - 2015)	0.096	0.010	5.695	0.488
Realisation 1 (1980 - 2024)	0.235	0.066	10.786	0.779
Realisation 2 (1980 - 2024)	0.227	0.066	10.442	0.757
Realisation 3 (1980 - 2024)	0.234	0.066	10.742	0.768
Realisation 4 (1980 - 2024)	0.223	0.066	10.256	0.754
Realisation 5 (1980 - 2024)	0.232	0.066	10.721	0.783
Realisation 6 (1980 - 2024)	0.214	0.066	10.293	0.760
Realisation 7 (1980 - 2024)	0.219	0.066	10.415	0.768
Realisation 8 (1980 - 2024)	0.223	0.066	10.367	0.772
Realisation 9 (1980 - 2024)	0.218	0.066	10.667	0.755
Realisation 10 (1980 - 2024)	0.226	0.066	10.776	0.765
Realisation 1 (2016 - 2024)	0.380	0.229	11.827	1.057
Realisation 2 (2016 - 2024)	0.343	0.144	10.466	0.955
Realisation 3 (2016 - 2024)	0.377	0.197	10.699	1.000
Realisation 4 (2016 - 2024)	0.325	0.186	9.402	0.929
Realisation 5 (2016 - 2024)	0.370	0.249	10.141	1.048
Realisation 6 (2016 - 2024)	0.289	0.121	9.723	0.962
Realisation 7 (2016 - 2024)	0.306	0.071	9.444	0.976
Realisation 8 (2016 - 2024)	0.322	0.149	9.184	1.014
Realisation 9 (2016 - 2024)	0.300	0.078	11.159	0.933
Realisation 10 (2016 - 2024)	0.340	0.145	11.634	0.983

Typical flow rates – comparison between observed Q at SNEM and realisations (bias corrected)

	MNQ [m³/s]	NQ [m³/s]	MHQ [m³/s]	MQ [m³/s]
Neumühle station (1965 - 2017)	0.084	0.020	8.773	0.580
Neumühle station (1980 - 2017)	0.097	0.031	9.037	0.582
Sim. Q - no-bias corr. (1980 - 2015)	0.197	0.066	10.435	0.702
Sim. Q - CDFt-bias corr. (1980 - 2015)	0.096	0.010	5.695	0.488
Realisation 1 (1980 - 2024)	0.110	0.010	5.932	0.509
Realisation 2 (1980 - 2024)	0.103	0.010	5.837	0.495
Realisation 3 (1980 - 2024)	0.113	0.010	5.747	0.502
Realisation 4 (1980 - 2024)	0.103	0.010	5.432	0.491
Realisation 5 (1980 - 2024)	0.112	0.010	5.897	0.510
Realisation 6 (1980 - 2024)	0.097	0.010	5.722	0.496
Realisation 7 (1980 - 2024)	0.108	0.010	5.535	0.502

	MNQ [m³/s]	NQ [m³/s]	MHQ [m³/s]	MQ [m³/s]
Realisation 8 (1980 - 2024)	0.097	0.010	5.785	0.505
Realisation 9 (1980 - 2024)	0.099	0.009	5.772	0.494
Realisation 10 (1980 - 2024)	0.112	0.010	5.728	0.500
Realisation 1 (2016 - 2024)	0.165	0.075	6.882	0.588
Realisation 2 (2016 - 2024)	0.130	0.035	6.405	0.515
Realisation 3 (2016 - 2024)	0.181	0.040	5.934	0.554
Realisation 4 (2016 - 2024)	0.132	0.046	4.381	0.500
Realisation 5 (2016 - 2024)	0.177	0.031	6.320	0.579
Realisation 6 (2016 - 2024)	0.105	0.046	5.828	0.522
Realisation 7 (2016 - 2024)	0.158	0.017	4.358	0.535
Realisation 8 (2016 - 2024)	0.103	0.043	6.145	0.564
Realisation 9 (2016 - 2024)	0.111	0.009	6.081	0.513
Realisation 10 (2016 - 2024)	0.176	0.058	5.859	0.537

Trend analysis - comparison between observed Q at SNEM and realisations (not bias corrected) – Q annual maxima

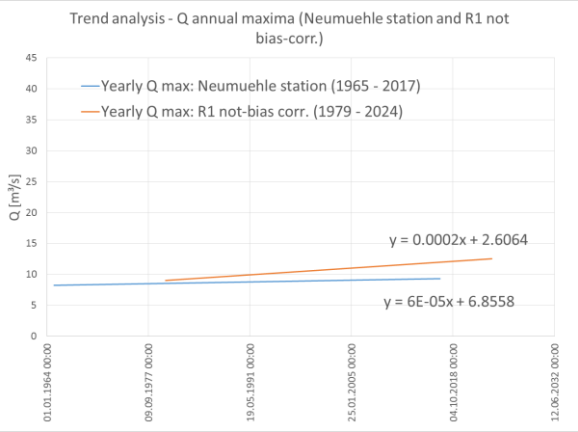

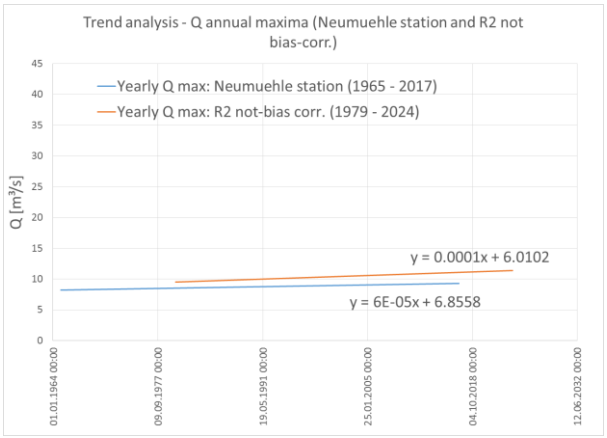

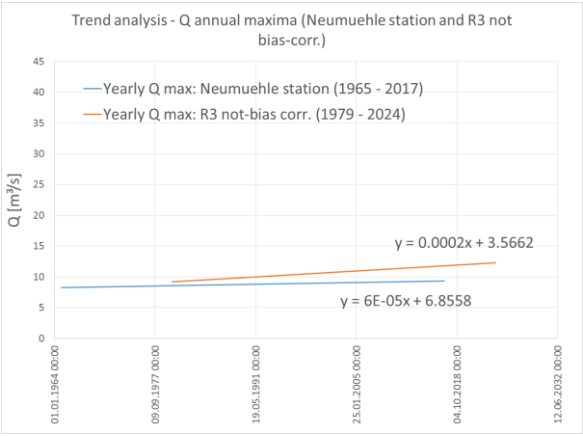

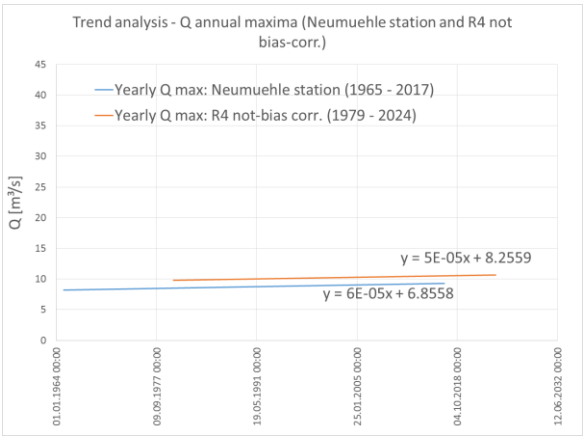

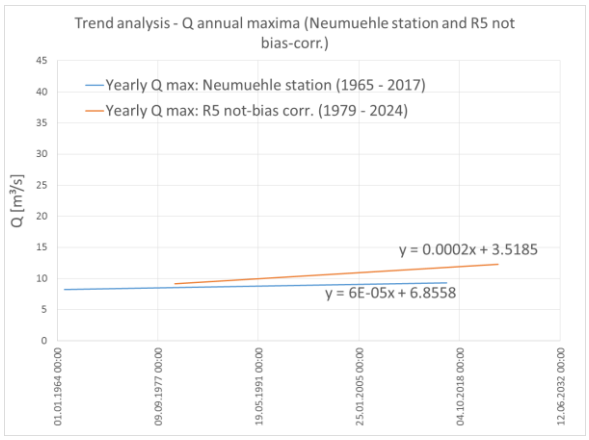
Trend analysis - Q annual maxima (Neumuehle station and R5 not bias-corr.)
Yearly Q max: Neumuehle station (1965 - 2017)
Yearly Q max: R5 not-bias corr. (1979 - 2024)
Q [m³/s]
y = 0.0002x + 3.5185
y = 6E-05x + 6.8558
01.01.1964 00:00
09.09.1977 00:00
19.05.1991 00:00
25.01.2005 00:00
04.10.2018 00:00
12.06.2032 00:00

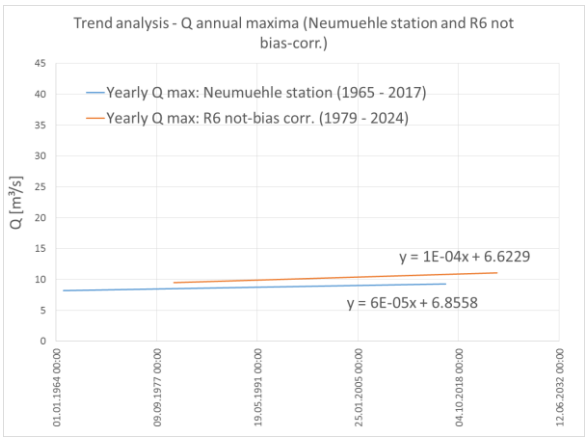
Trend analysis - Q annual maxima (Neumuehle station and R6 not bias-corr.)
Yearly Q max: Neumuehle station (1965 - 2017)
Yearly Q max: R6 not-bias corr. (1979 - 2024)
Q [m³/s]
y = 1E-04x + 6.6229
y = 6E-05x + 6.8558
01.01.1964 00:00
09.09.1977 00:00
19.05.1991 00:00
25.01.2005 00:00
04.10.2018 00:00
12.06.2032 00:00

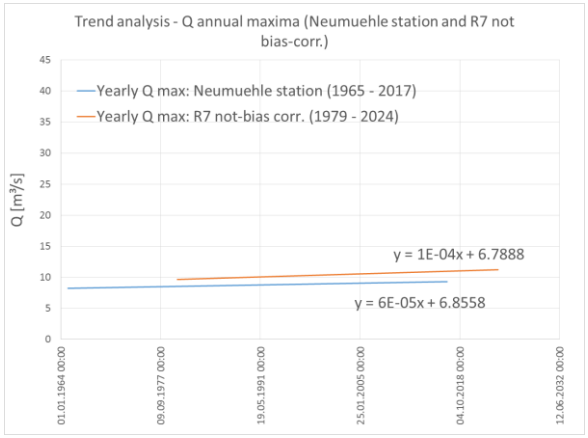
Trend analysis - Q annual maxima (Neumuehle station and R7 not bias-corr.)
Yearly Q max: Neumuehle station (1965 - 2017)
Yearly Q max: R7 not-bias corr. (1979 - 2024)
Q [m³/s]
y = 1E-04x + 6.7888
y = 6E-05x + 6.8558
01.01.1964 00:00
09.09.1977 00:00
19.05.1991 00:00
25.01.2005 00:00
04.10.2018 00:00
12.06.2032 00:00

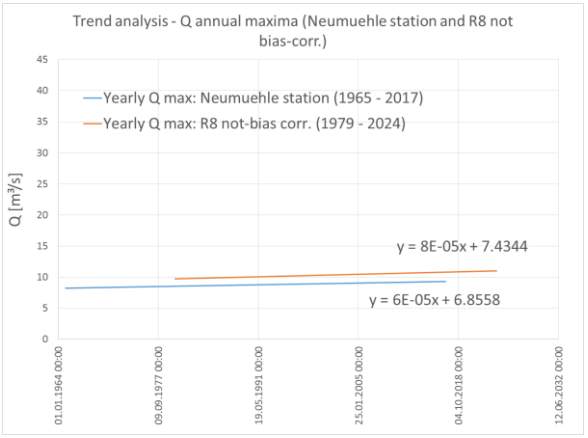
Trend analysis - Q annual maxima (Neumuehle station and R8 not bias-corr.)
Yearly Q max: Neumuehle station (1965 - 2017)
Yearly Q max: R8 not-bias corr. (1979 - 2024)
Q [m³/s]
y = 8E-05x + 7.4344
y = 6E-05x + 6.8558
01.01.1964 00:00
09.09.1977 00:00
19.05.1991 00:00
25.01.2005 00:00
04.10.2018 00:00
12.06.2032 00:00

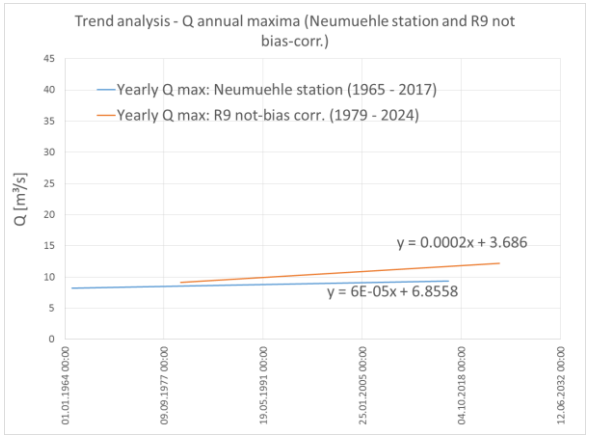
Trend analysis - Q annual maxima (Neumuehle station and R9 not bias-corr.)
Yearly Q max: Neumuehle station (1965 - 2017)
Yearly Q max: R9 not-bias corr. (1979 - 2024)
Q [m³/s]
y = 0.0002x + 3.686
y = 6E-05x + 6.8558
01.01.1964 00:00
09.09.1977 00:00
19.05.1991 00:00
25.01.2005 00:00
04.10.2018 00:00
12.06.2032 00:00

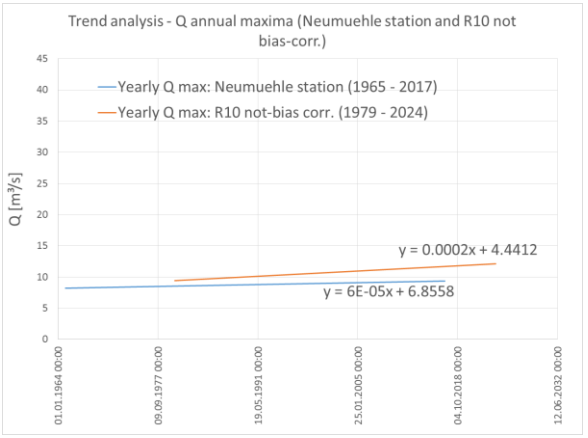
Trend analysis - Q annual maxima (Neumuehle station and R10 not bias-corr.)
Yearly Q max: Neumuehle station (1965 - 2017)
Yearly Q max: R10 not-bias corr. (1979 - 2024)
Q [m³/s]
y = 0.0002x + 4.4412
y = 6E-05x + 6.8558
01.01.1964 00:00
09.09.1977 00:00
19.05.1991 00:00
25.01.2005 00:00
04.10.2018 00:00
12.06.2032 00:00

Trend analysis - comparison between observed Q at SNEM and realisations (bias corrected) – Q annual maxima

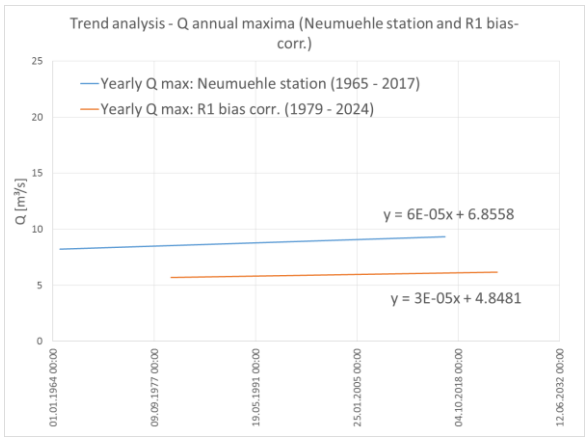

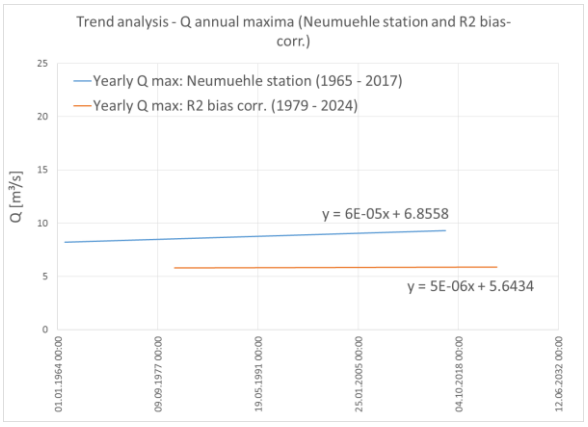

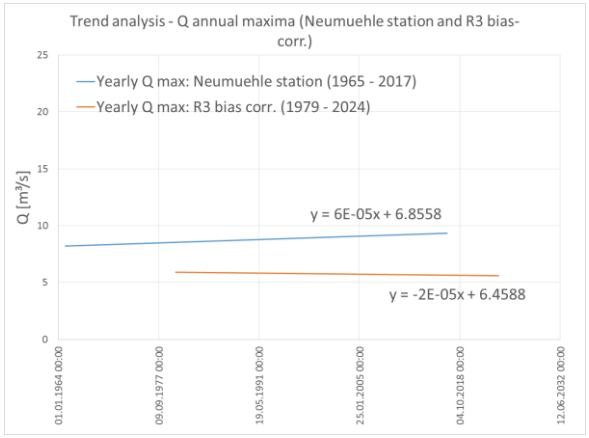

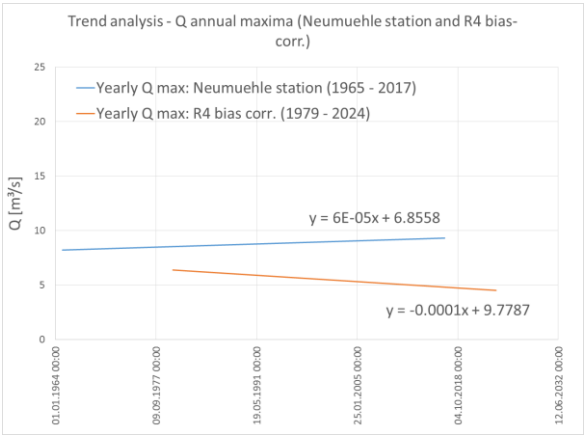

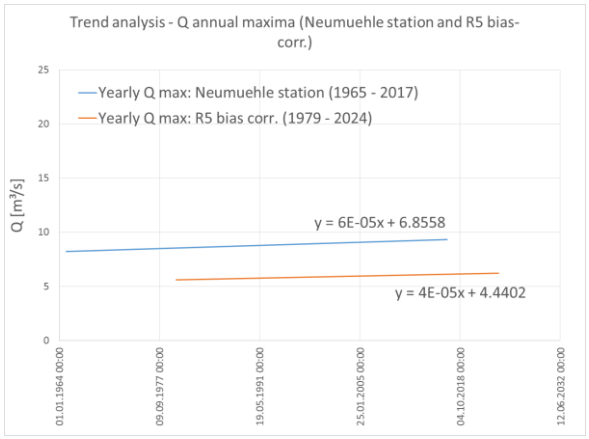

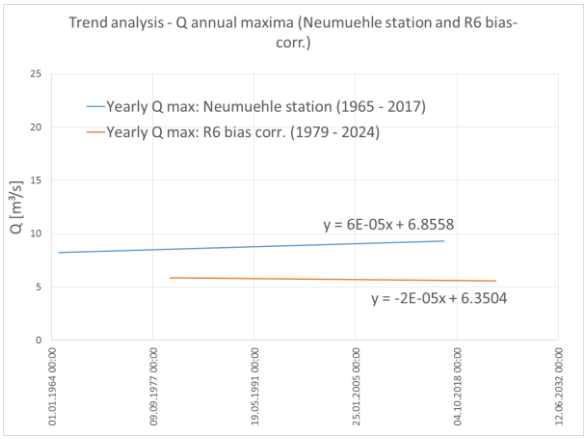

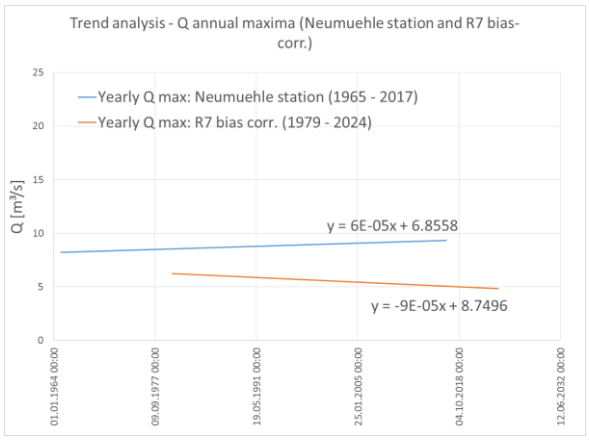

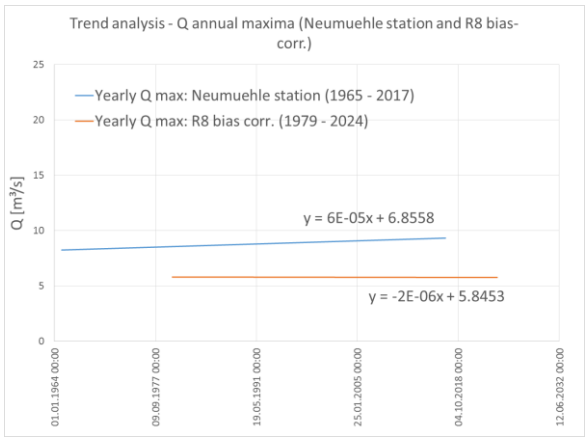

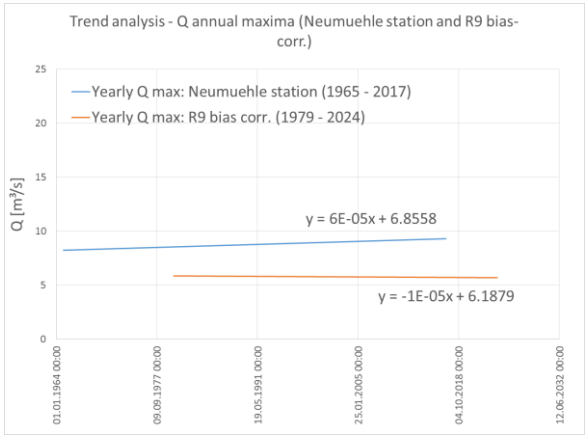

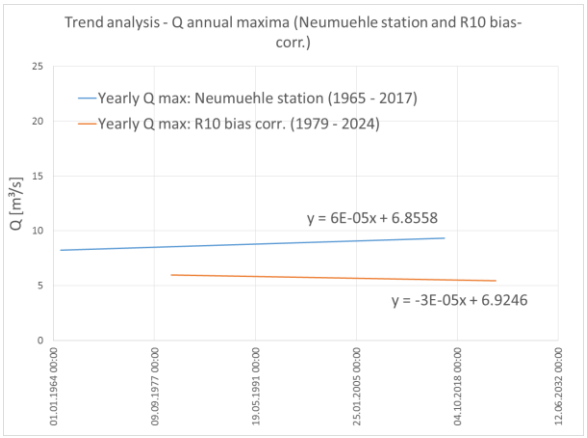

Trend analysis - comparison between observed Q at SNEM and realisations (not bias corrected) – Q mean

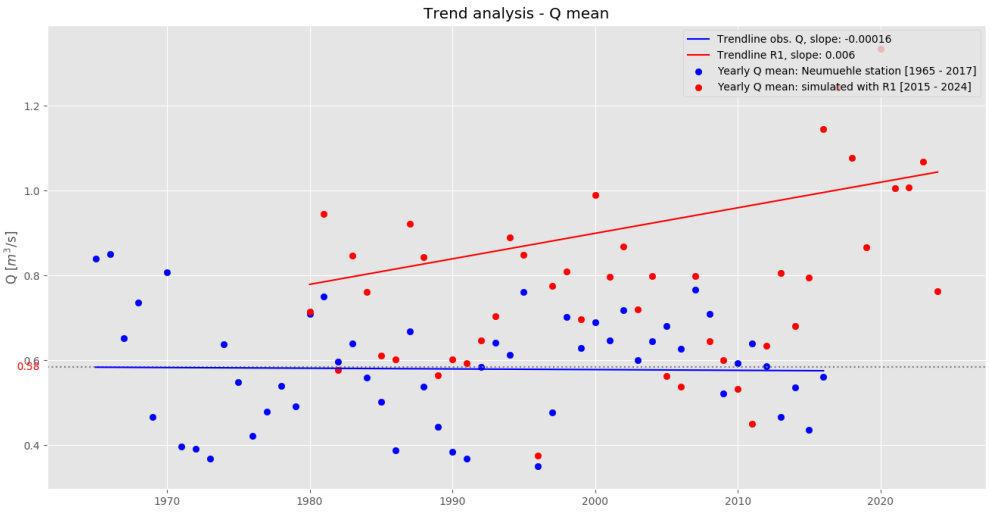

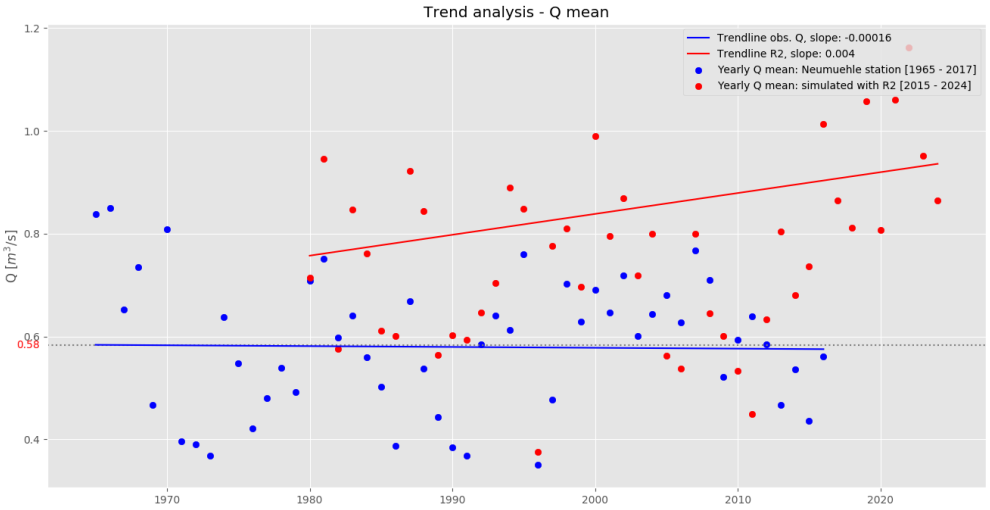
Trend analysis - Q mean
Trendline obs. Q, slope: -0.00016
Trendline R2, slope: 0.004
Yearly Q mean: Neumuehle station [1965 - 2017]
Yearly Q mean: simulated with R2 [2015 - 2024]
Q [m³/s]
0.58
1970
1980
1990
2000
2010
2020

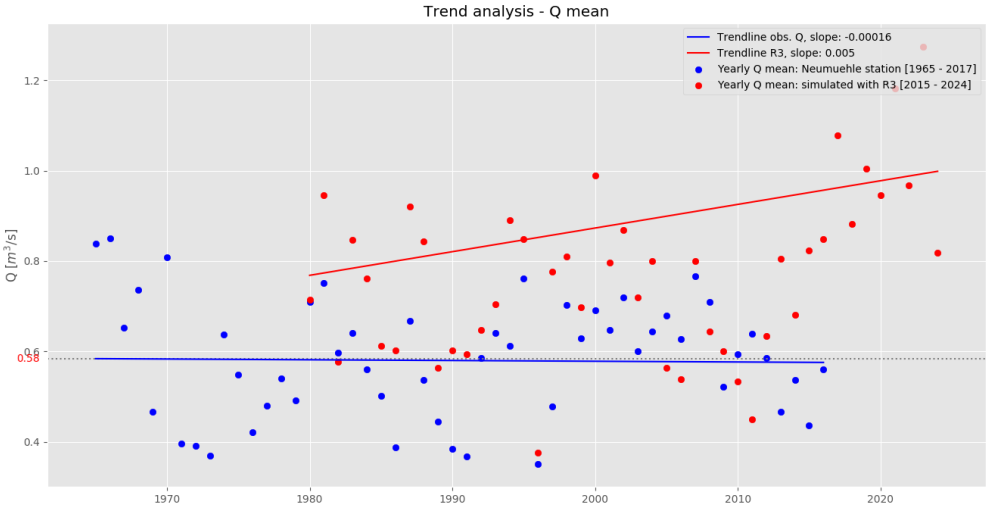
Trend analysis - Q mean
Trendline obs. Q, slope: -0.00016
Trendline R3, slope: 0.005
Yearly Q mean: Neumuehle station [1965 - 2017]
Yearly Q mean: simulated with R3 [2015 - 2024]
Q [m³/s]
0.58
1970
1980
1990
2000
2010
2020

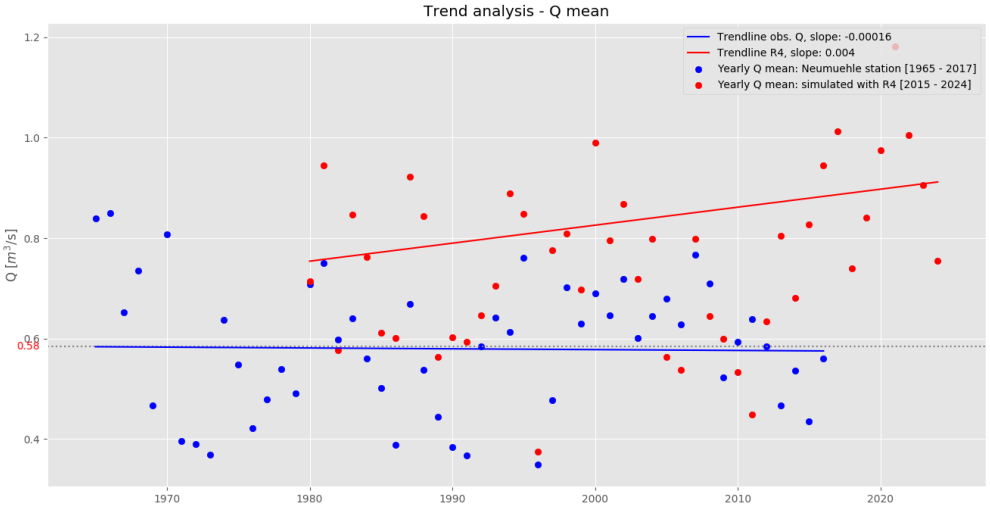
Trend analysis - Q mean
Trendline obs. Q, slope: -0.00016
Trendline R4, slope: 0.004
Yearly Q mean: Neumuehle station [1965 - 2017]
Yearly Q mean: simulated with R4 [2015 - 2024]
Q [m³/s]
0.58
1970
1980
1990
2000
2010
2020

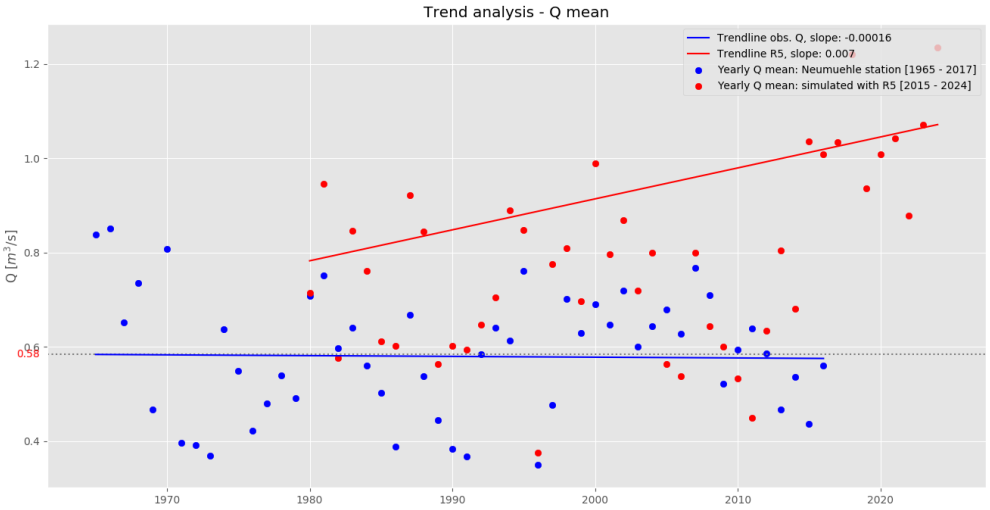
Trend analysis - Q mean
Trendline obs. Q, slope: -0.00016
Trendline R5, slope: 0.007
Yearly Q mean: Neumuehle station [1965 - 2017]
Yearly Q mean: simulated with R5 [2015 - 2024]
Q [m³/s]
0.58

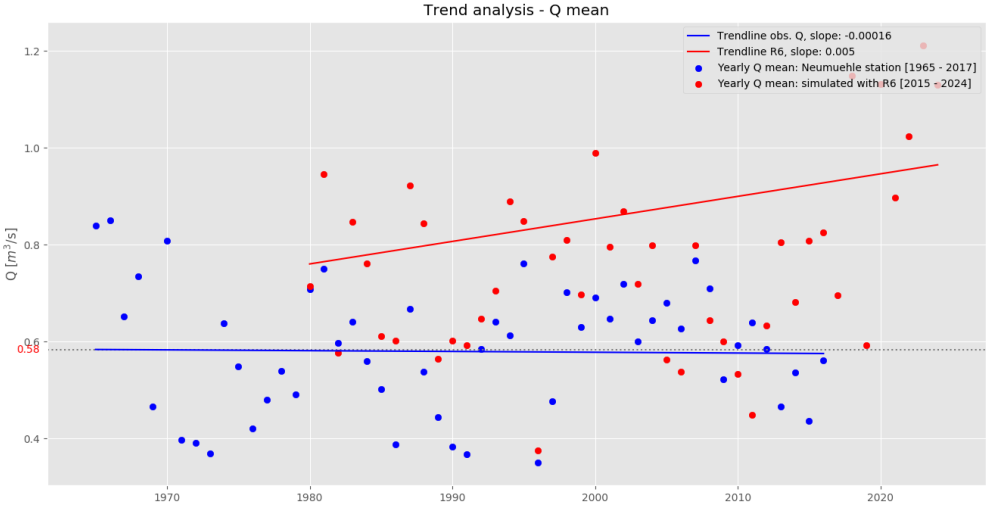
Trend analysis - Q mean
Trendline obs. Q, slope: -0.00016
Trendline R6, slope: 0.005
Yearly Q mean: Neumuehle station [1965 - 2017]
Yearly Q mean: simulated with R6 [2015 - 2024]
Q [m³/s]
0.58

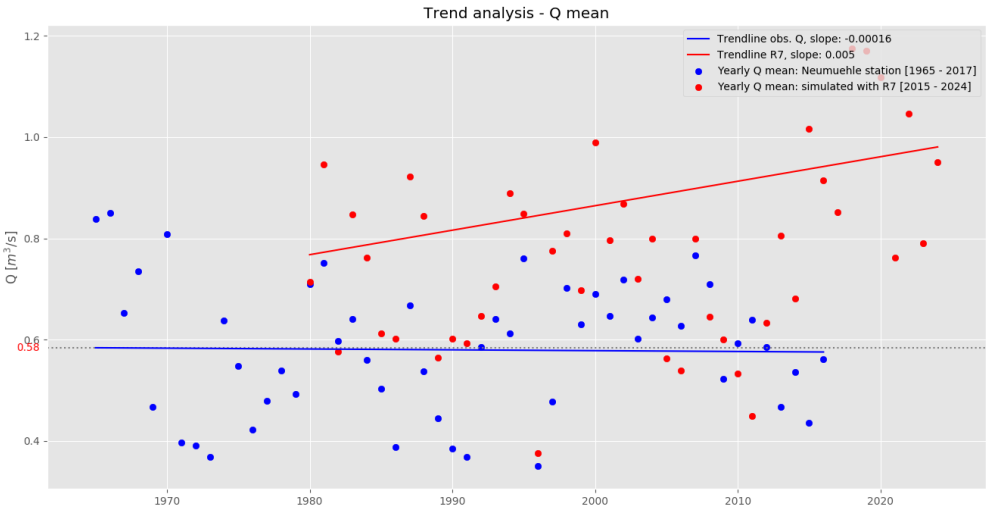
Trend analysis - Q mean
Trendline obs. Q, slope: -0.00016
Trendline R7, slope: 0.005
Yearly Q mean: Neumuehle station [1965 - 2017]
Yearly Q mean: simulated with R7 [2015 - 2024]
Q [m³/s]
0.58

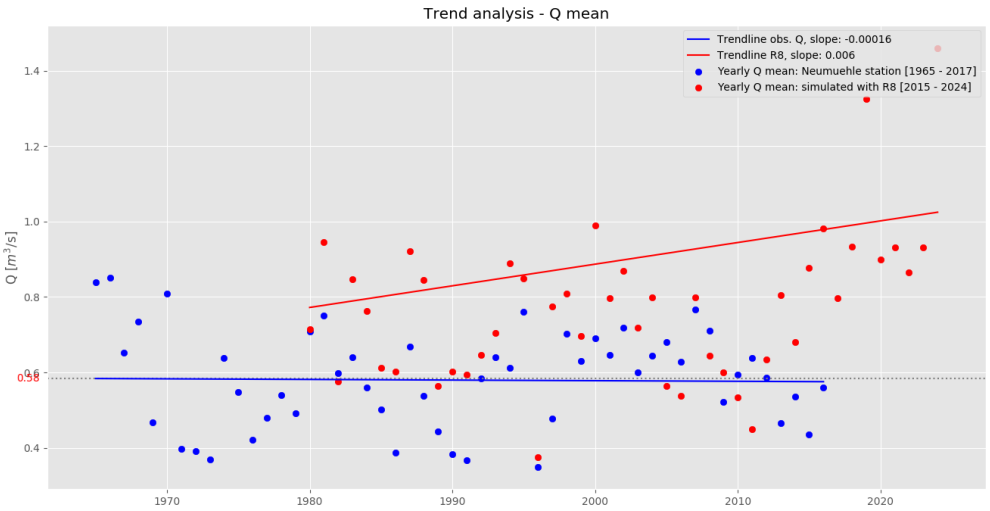
Trend analysis - Q mean
Trendline obs. Q, slope: -0.00016
Trendline R8, slope: 0.006
Yearly Q mean: Neumuehle station [1965 - 2017]
Yearly Q mean: simulated with R8 [2015 - 2024]
Q [m³/s]
0.58
1970
1980
1990
2000
2010
2020

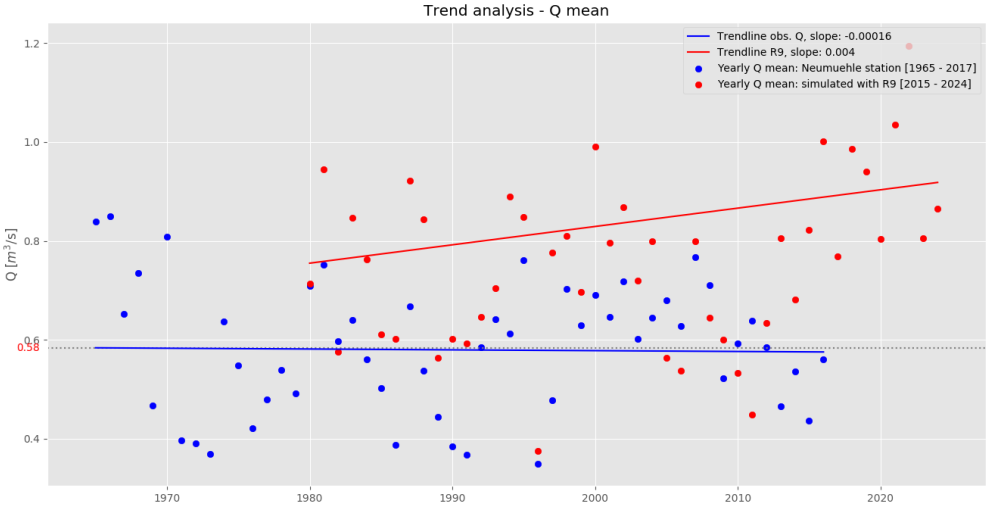
Trend analysis - Q mean
Trendline obs. Q, slope: -0.00016
Trendline R9, slope: 0.004
Yearly Q mean: Neumuehle station [1965 - 2017]
Yearly Q mean: simulated with R9 [2015 - 2024]
Q [m³/s]
0.58
1970
1980
1990
2000
2010
2020

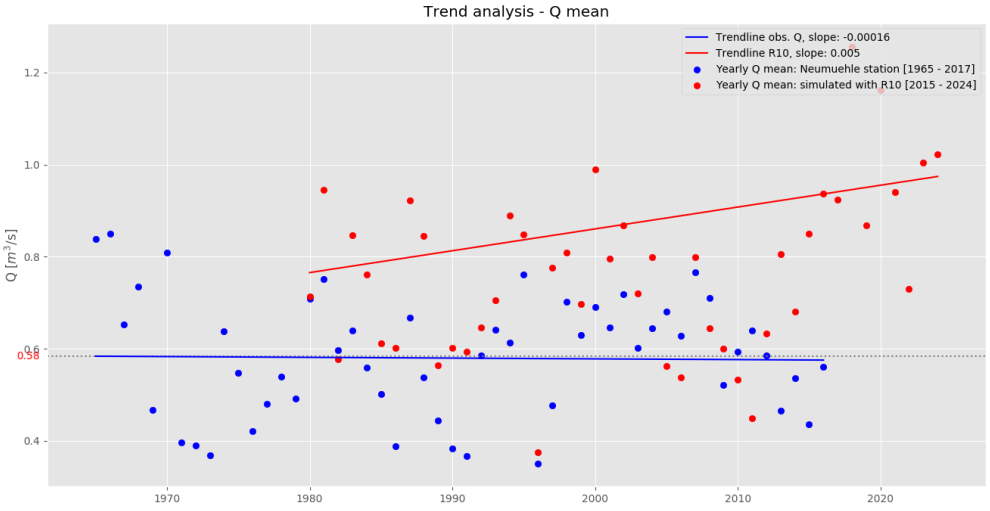
Trend analysis - Q mean
Trendline obs. Q, slope: -0.00016
Trendline R10, slope: 0.005
Yearly Q mean: Neumuehle station [1965 - 2017]
Yearly Q mean: simulated with R10 [2015 - 2024]
Q [m³/s]
0.58
1970
1980
1990
2000
2010
2020

4.17.4. Framework 2 – Dhünn catchment area (simulations results)

Unterpilghausen

Comparison bias corrected and not bias corrected (R1 – R10) (1988 – 2024)

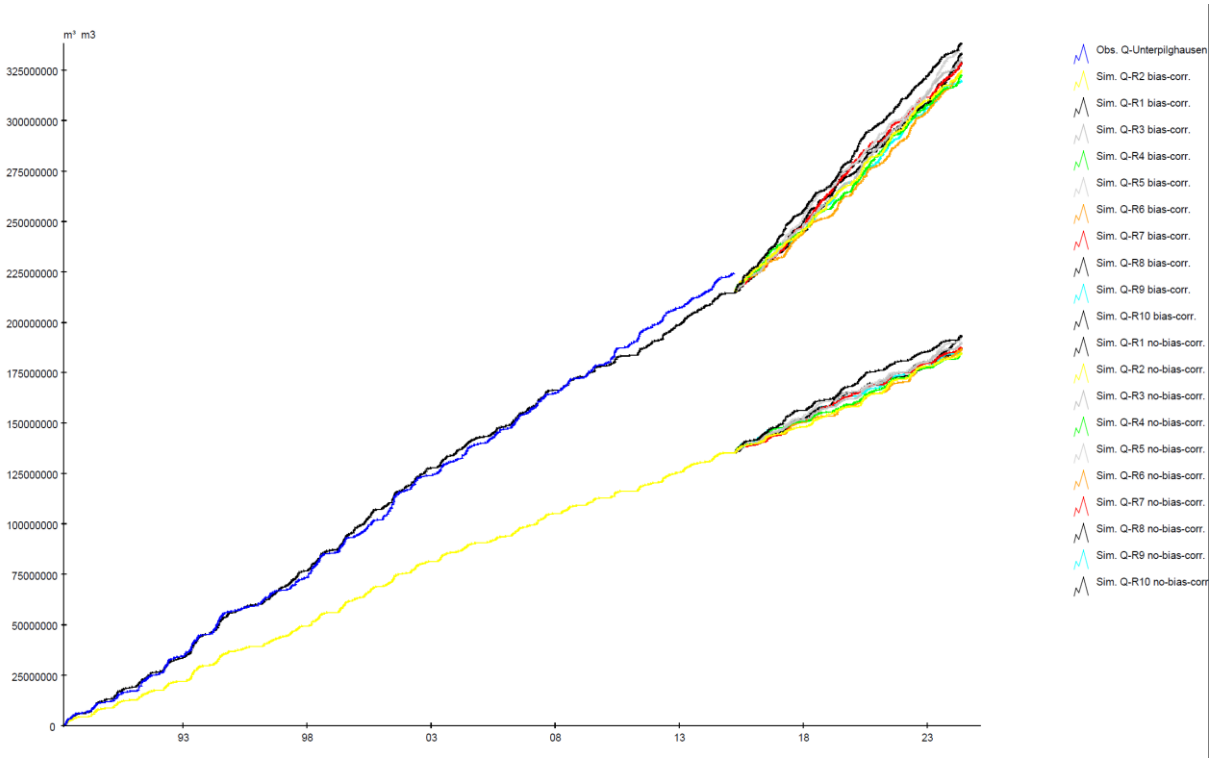

Comparison bias corrected and not bias corrected (R1 – R10) (future scenarios 2015 – 2024)

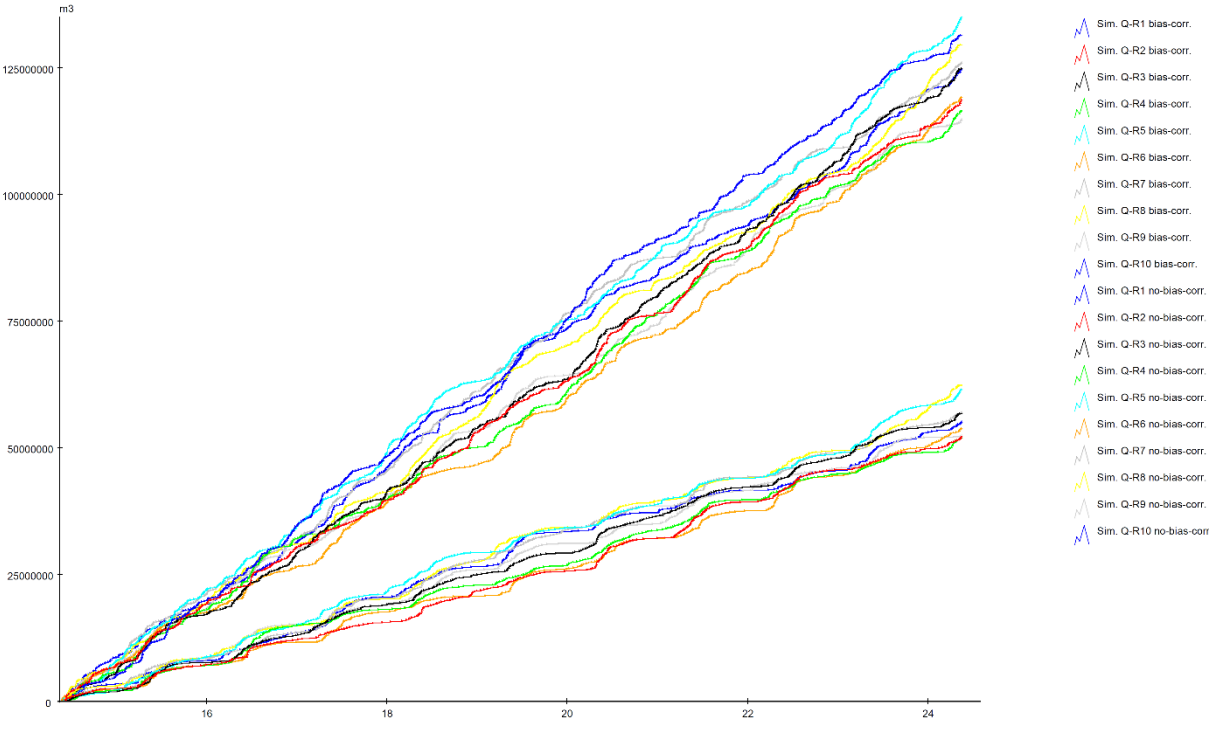

Eifgenbach

Comparison bias corrected and not bias corrected (R1 – R10) (2003 – 2024)

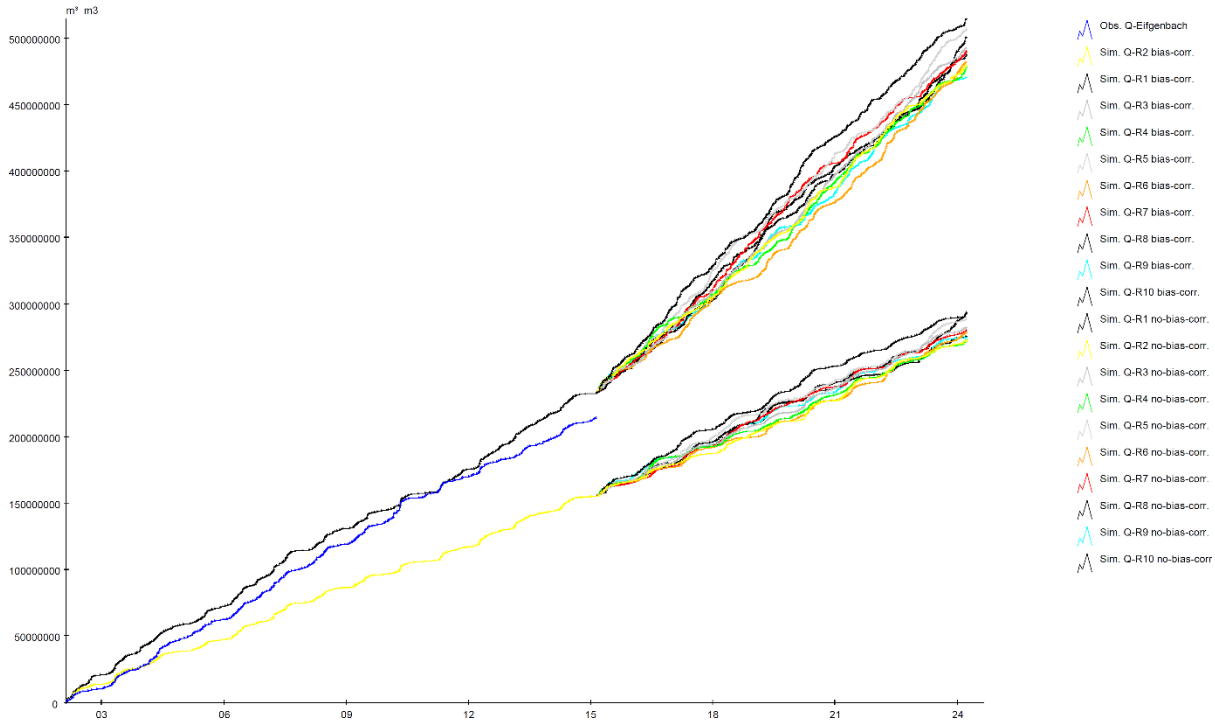

Comparison bias corrected and not bias corrected (R1 – R10) (future scenarios 2015 – 2024)

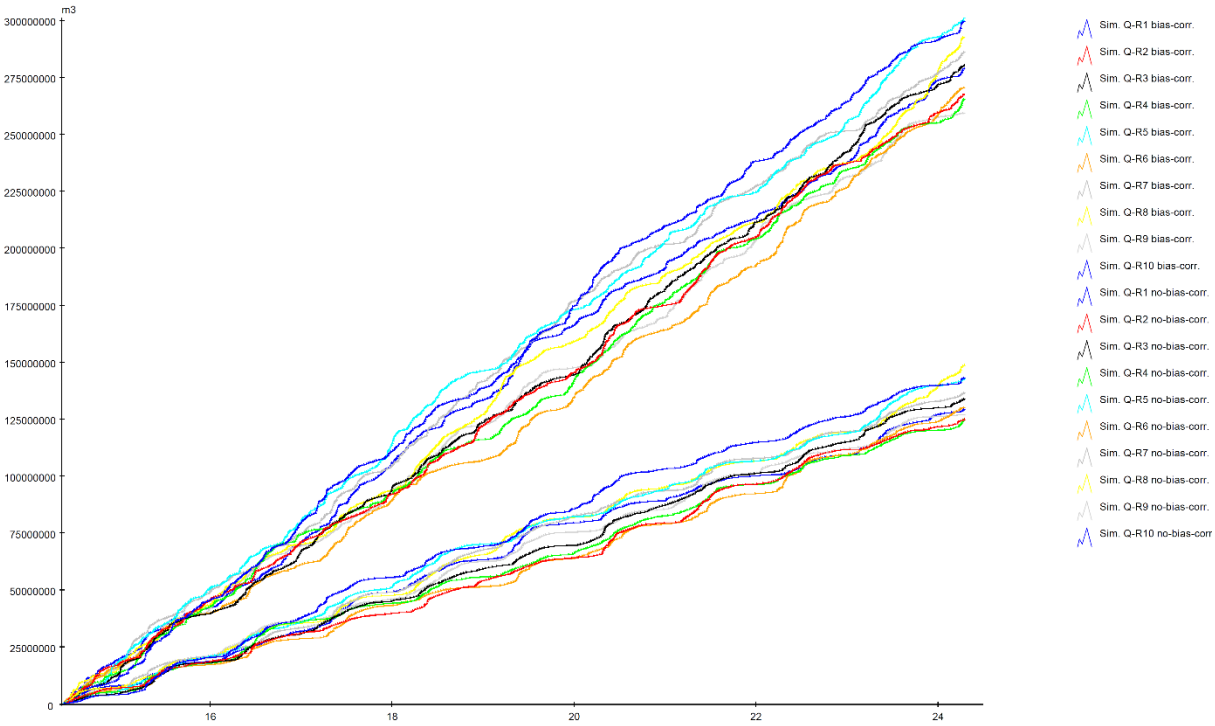

Hummelsheim

Comparison bias corrected and not bias corrected (R1 – R10) (1989 – 2024)

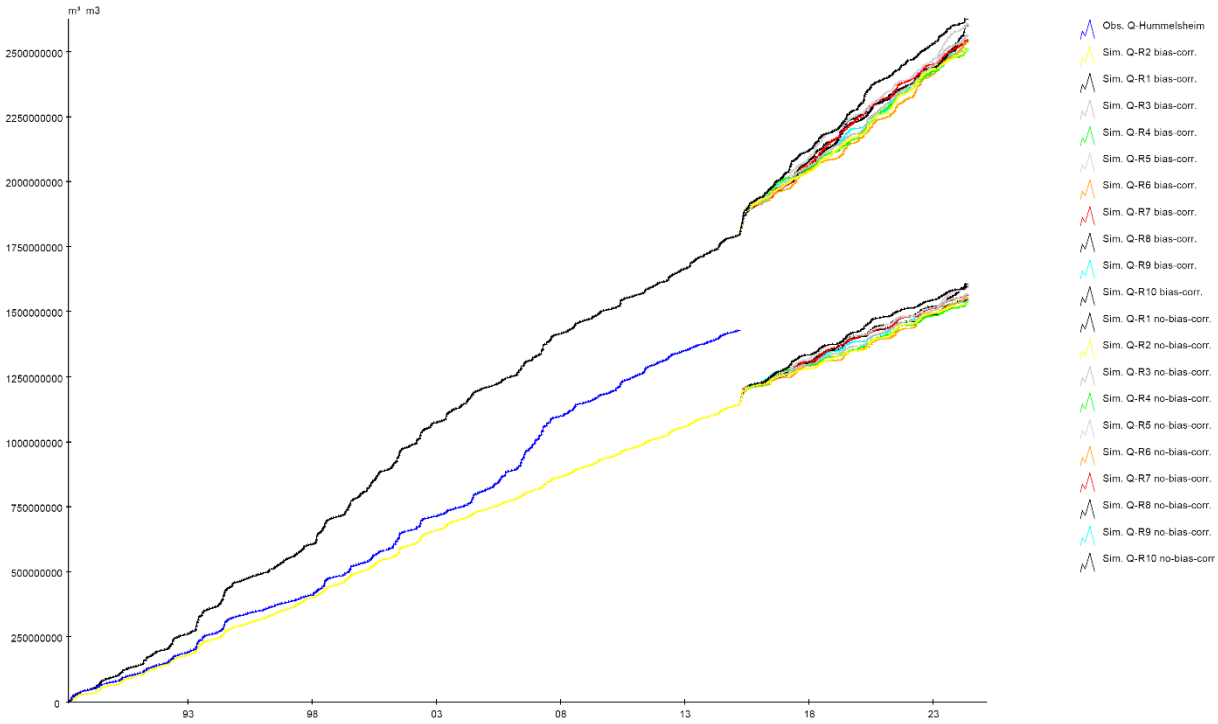

Comparison bias corrected and not bias corrected (R1 – R10) (2015 – 2024)

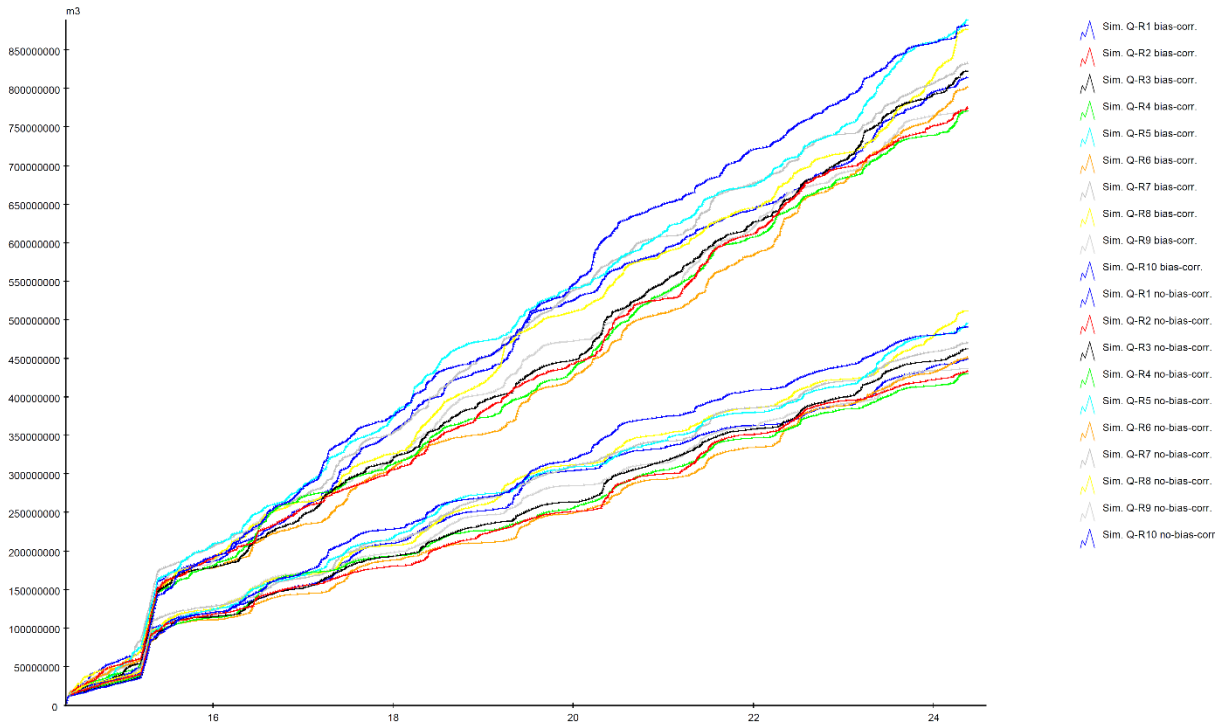

Manfort

Comparison bias corrected and not bias corrected (R1 – R10) (1989-2024)

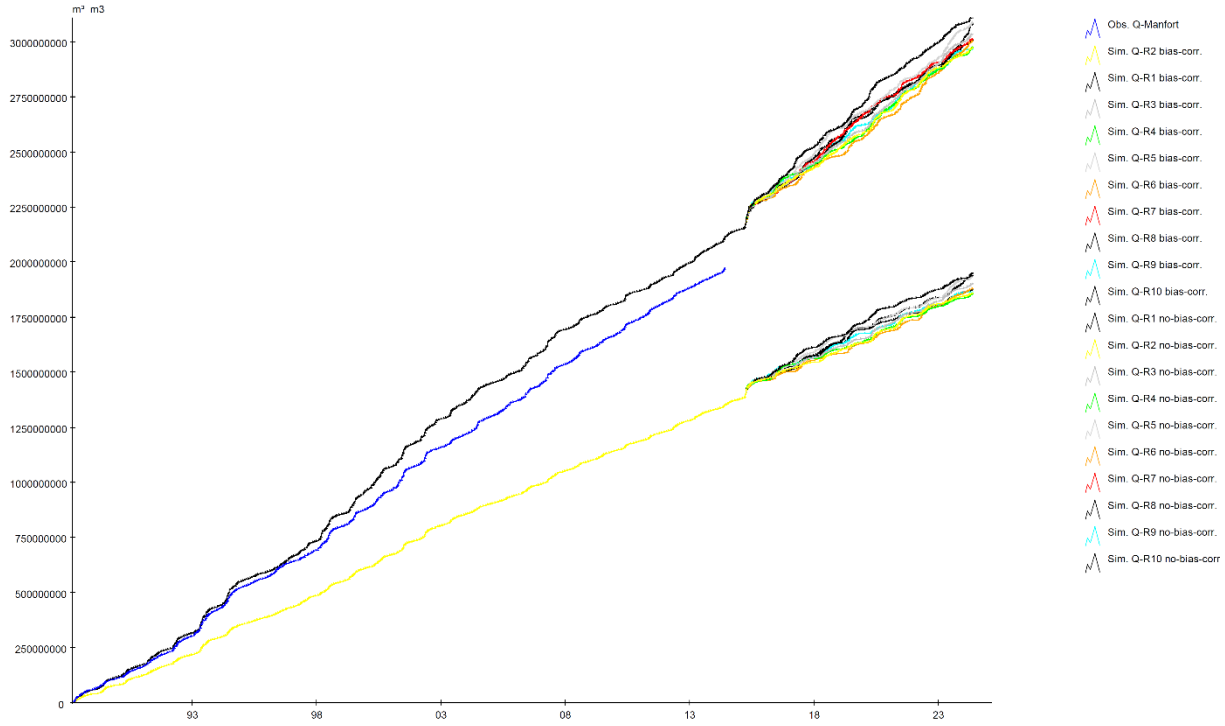

Comparison bias corrected and not bias corrected (R1 – R10) (2015 – 2024)

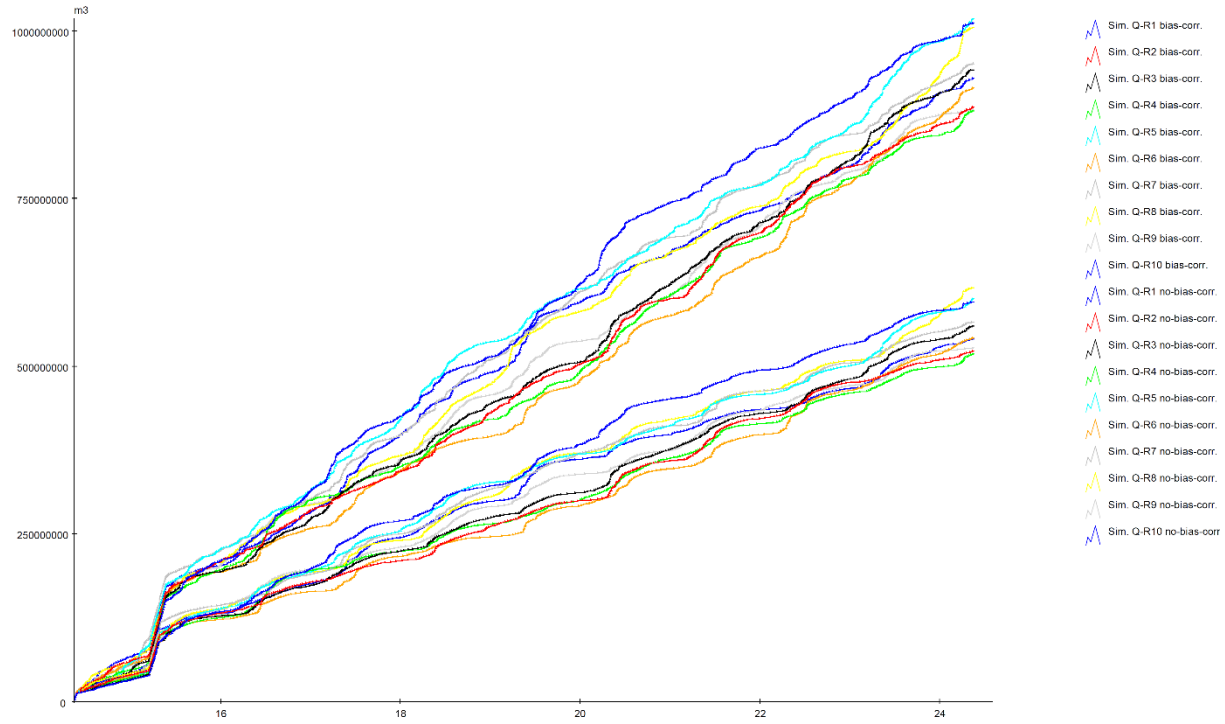

Schlebusch

Comparison bias corrected and not bias corrected (R1 – R10) (2007-2024)

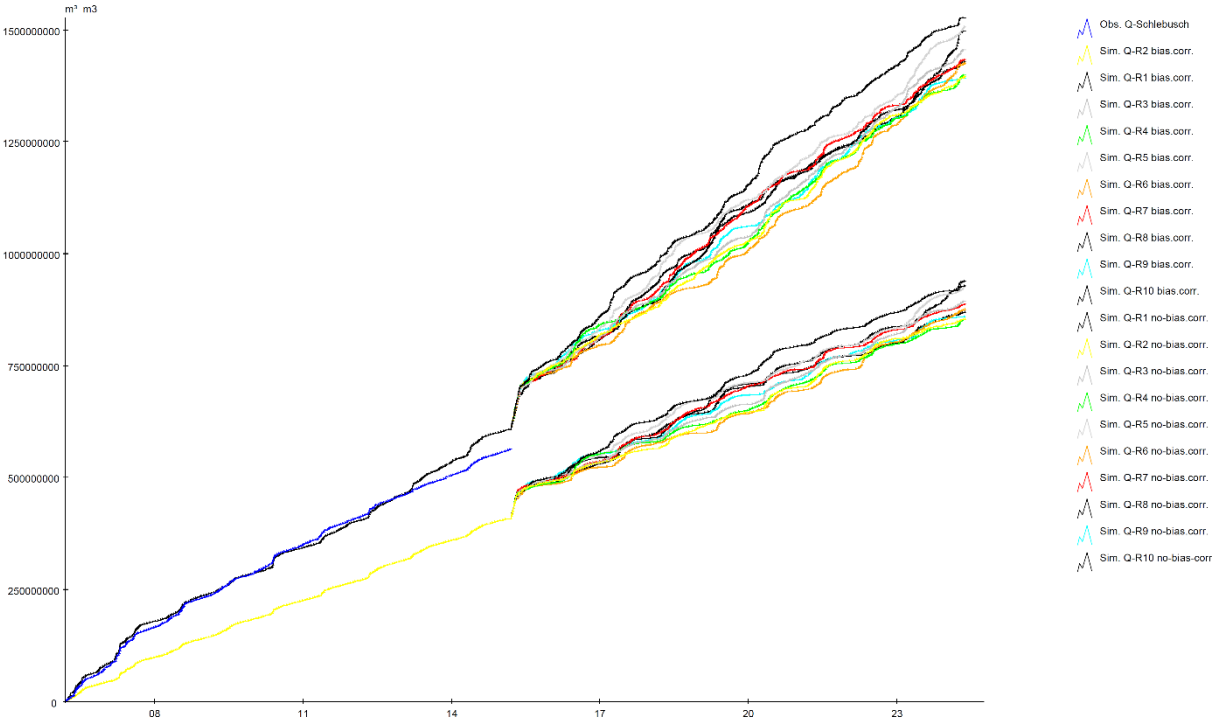

Comparison bias corrected and not bias corrected (R1 – R10) (2015 – 2024)

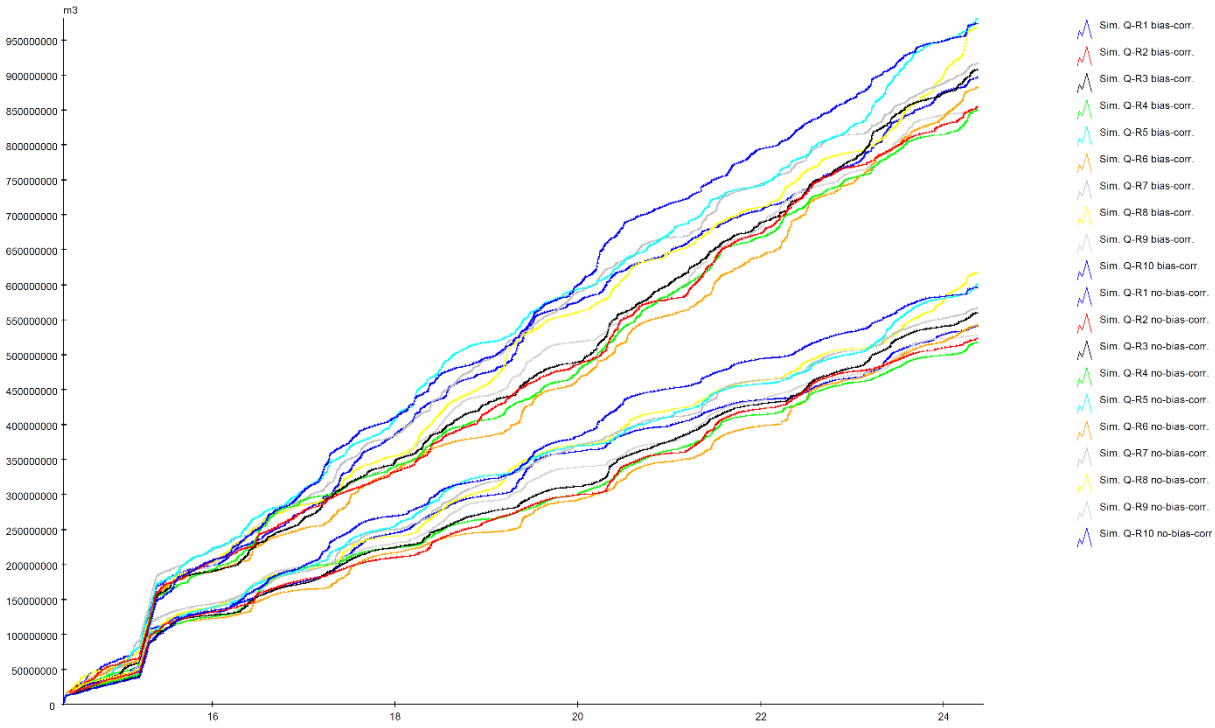

4.17.5. Framework 3 – NASIM – Mirke Creek catchment area

r1_xeps_eps1

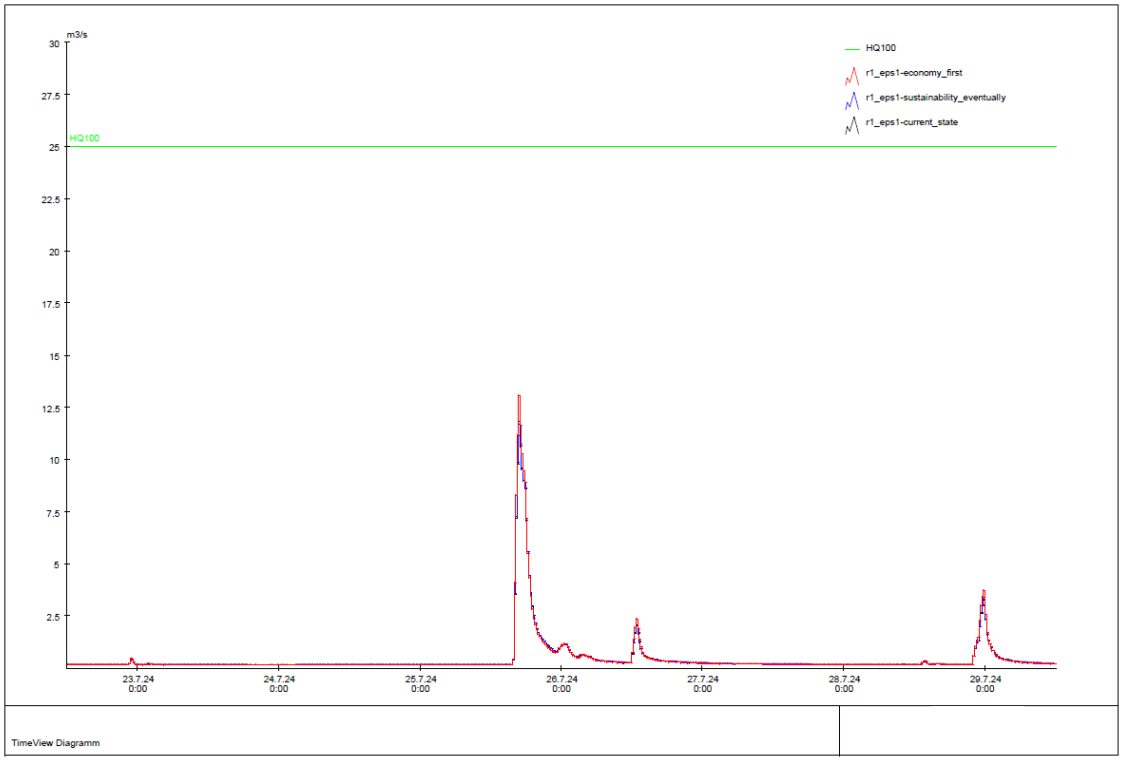

r1_xeps_eps2

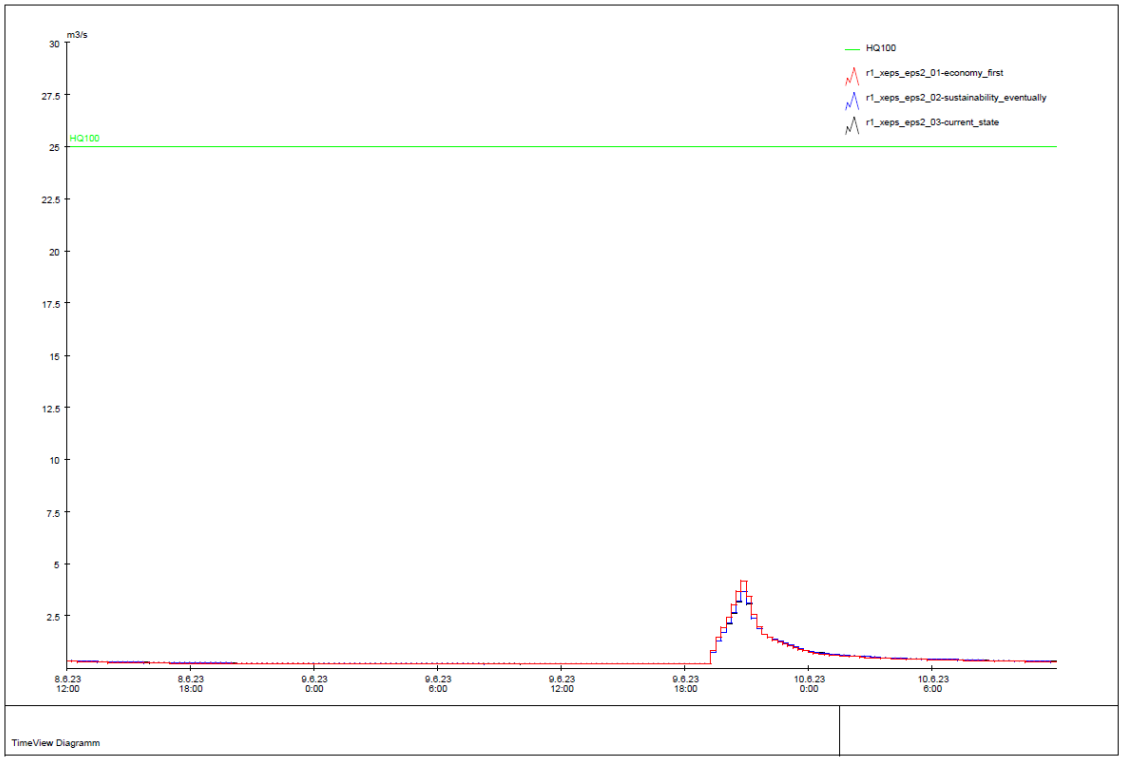

r2_xeps_eps1

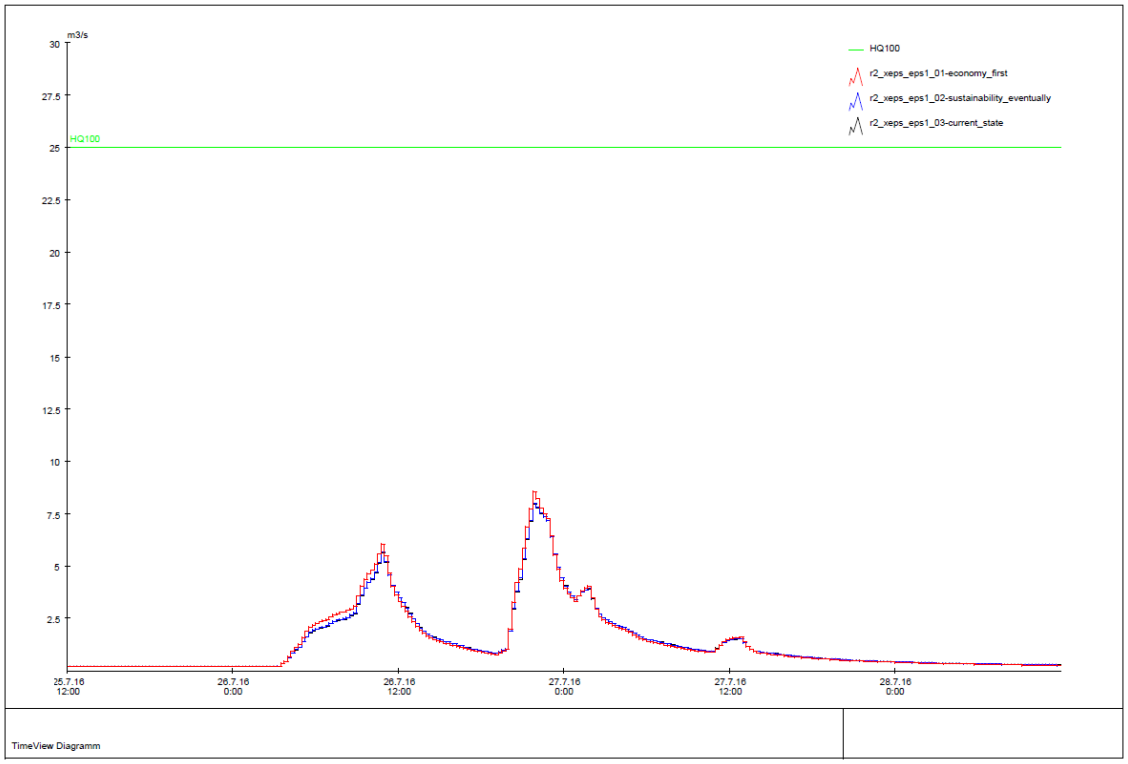

r2_xeps_eps2

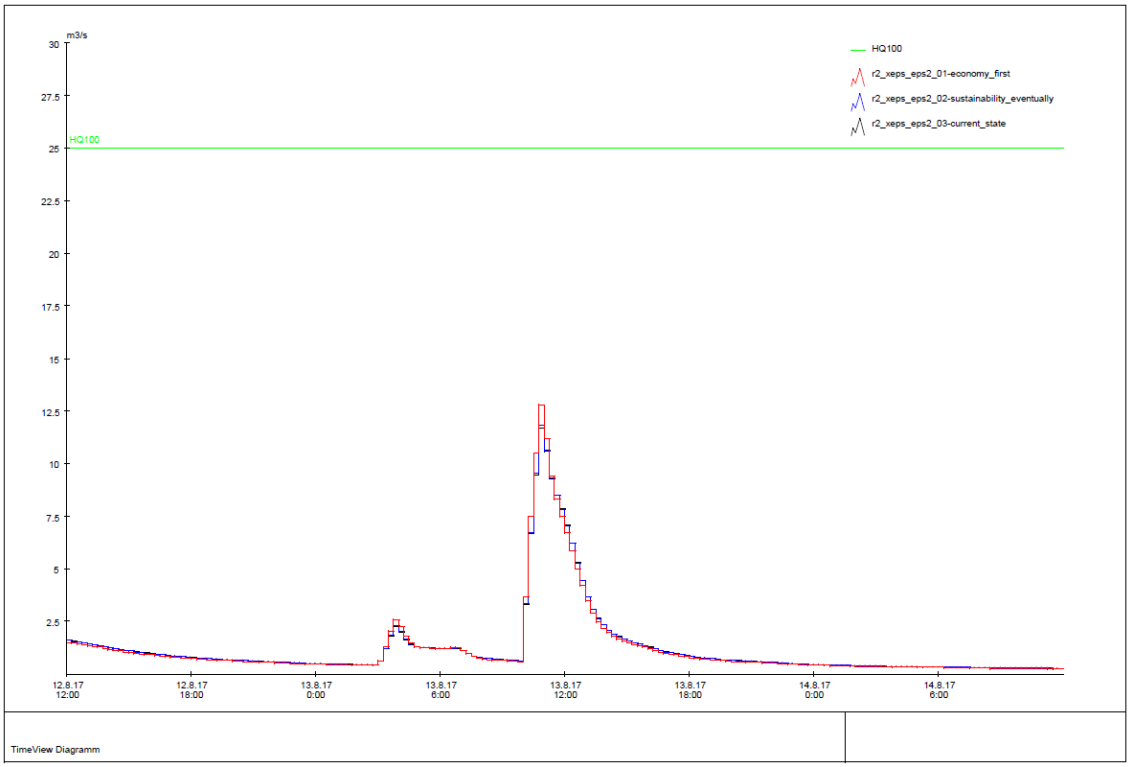

r2_xeps_eps3

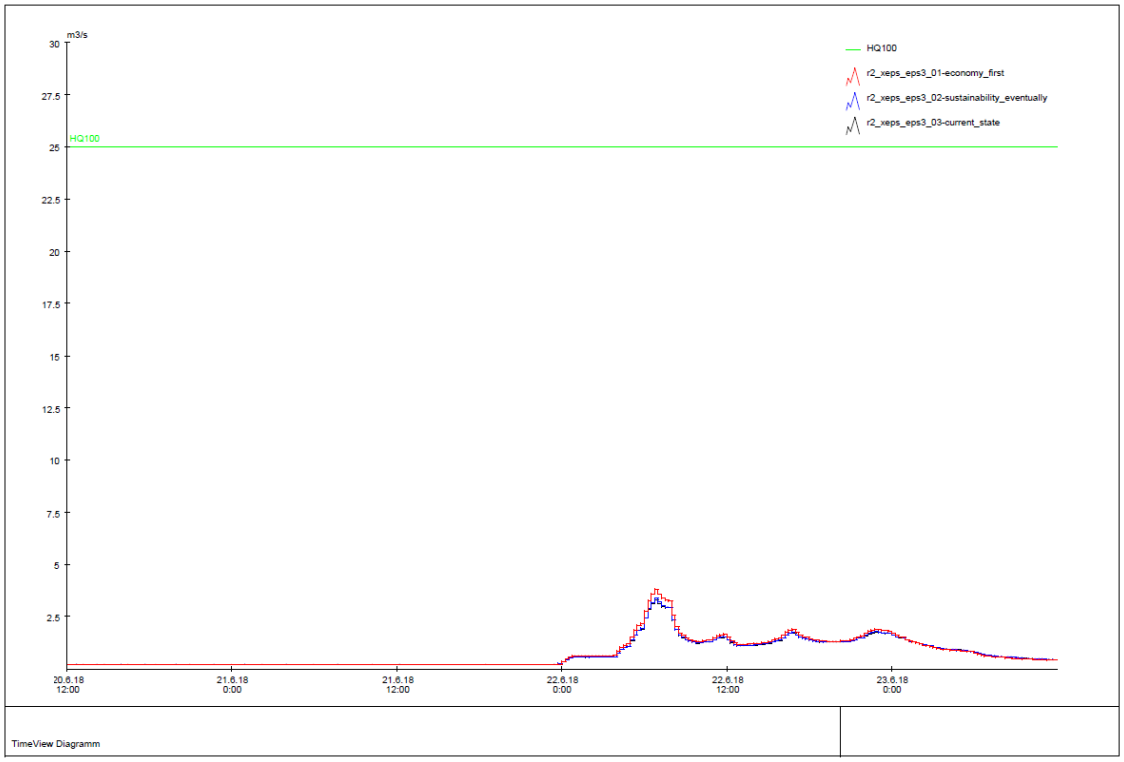

r3_xeps_eps1

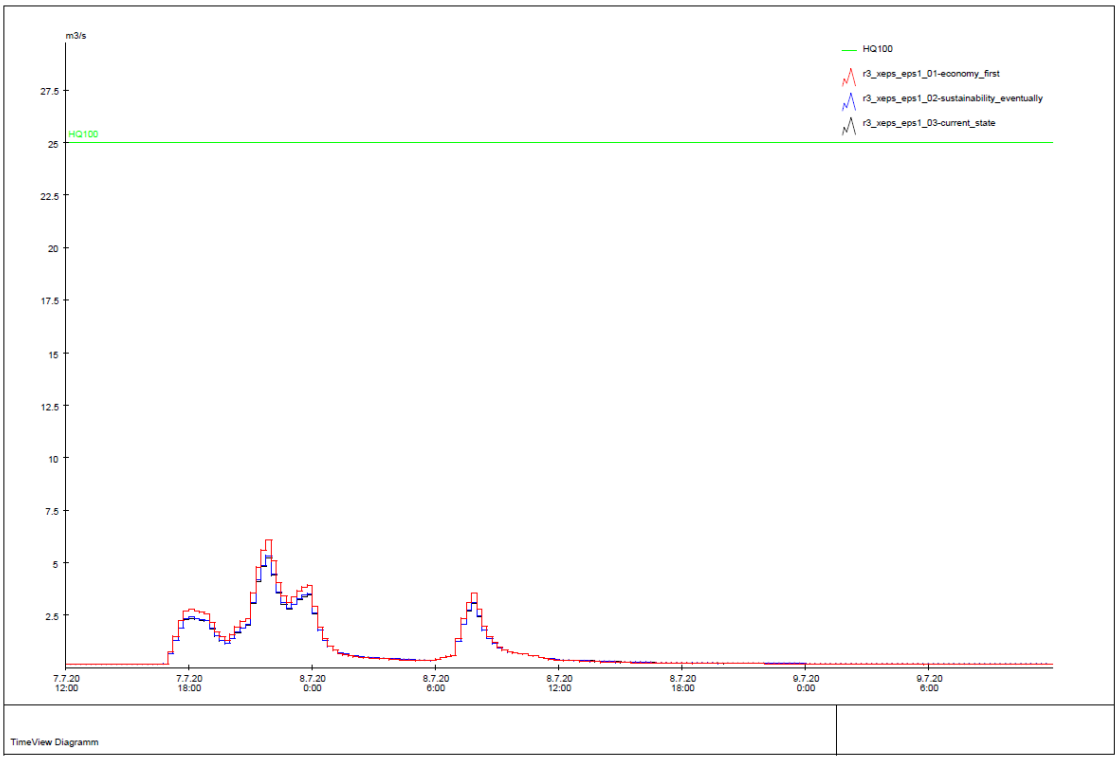

r3_xeps_eps2

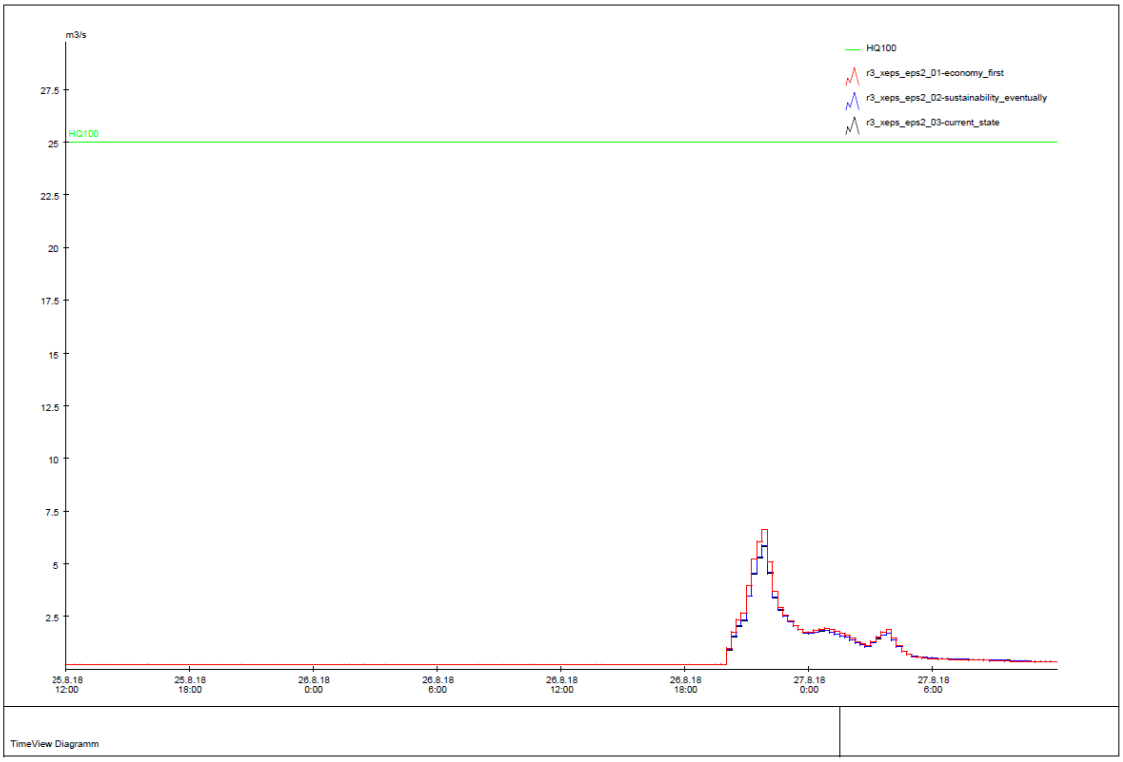

r4_xeps_eps1

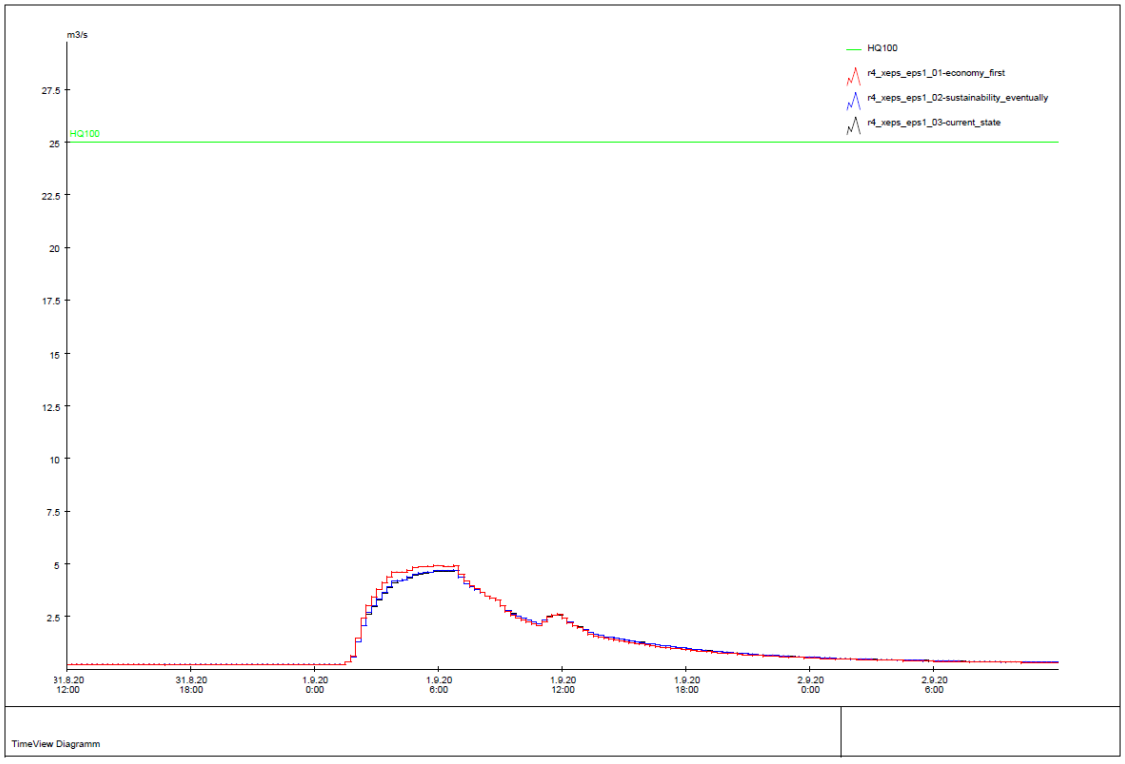

r4_xeps_eps2

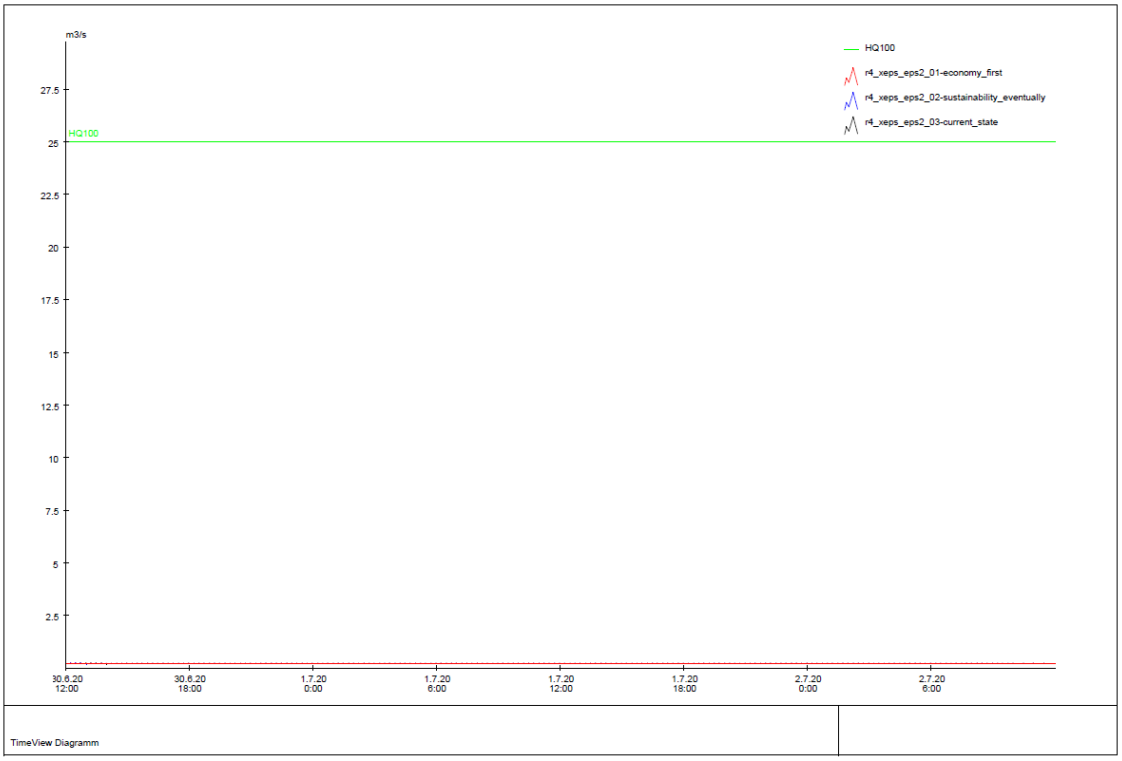

r5_xeps_eps1

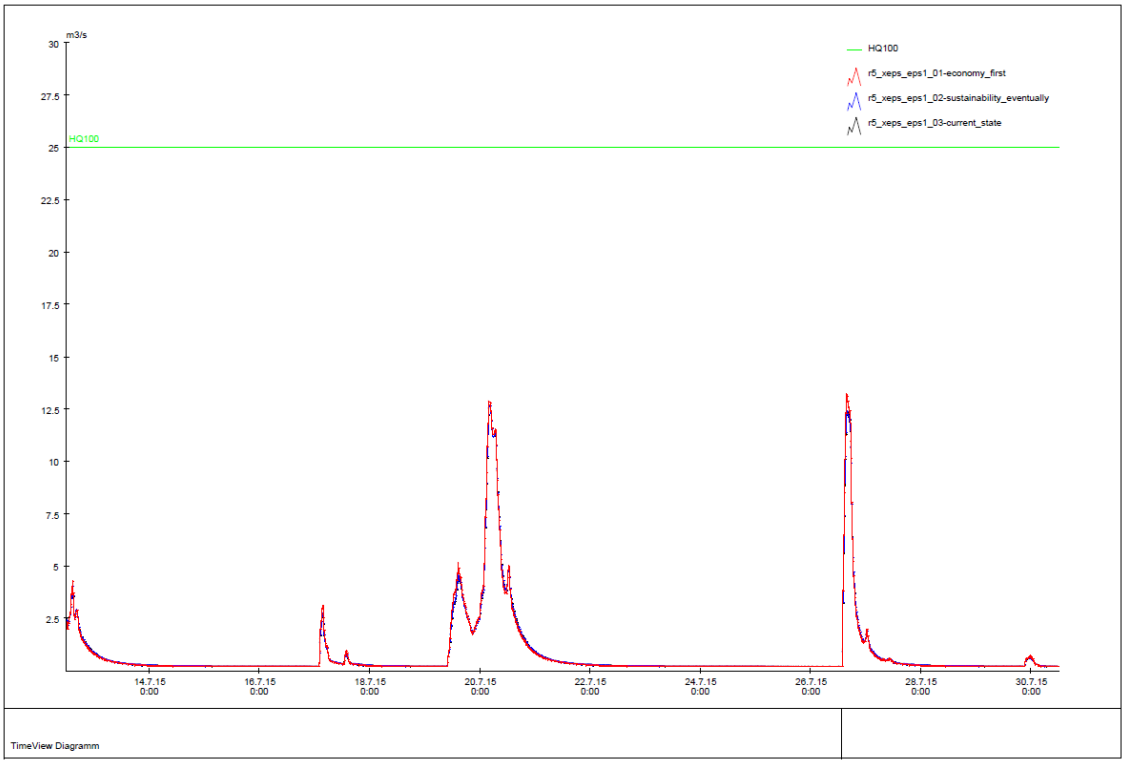

r5_xeps_eps2

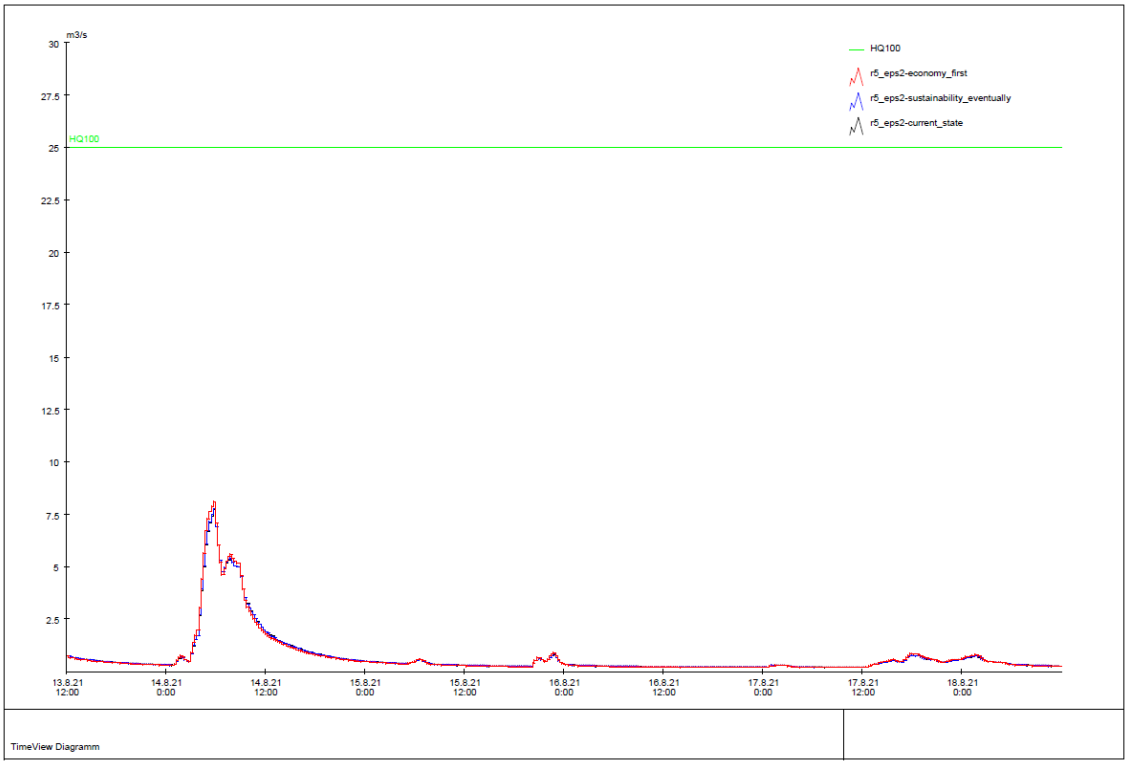

r6_xeps_eps1

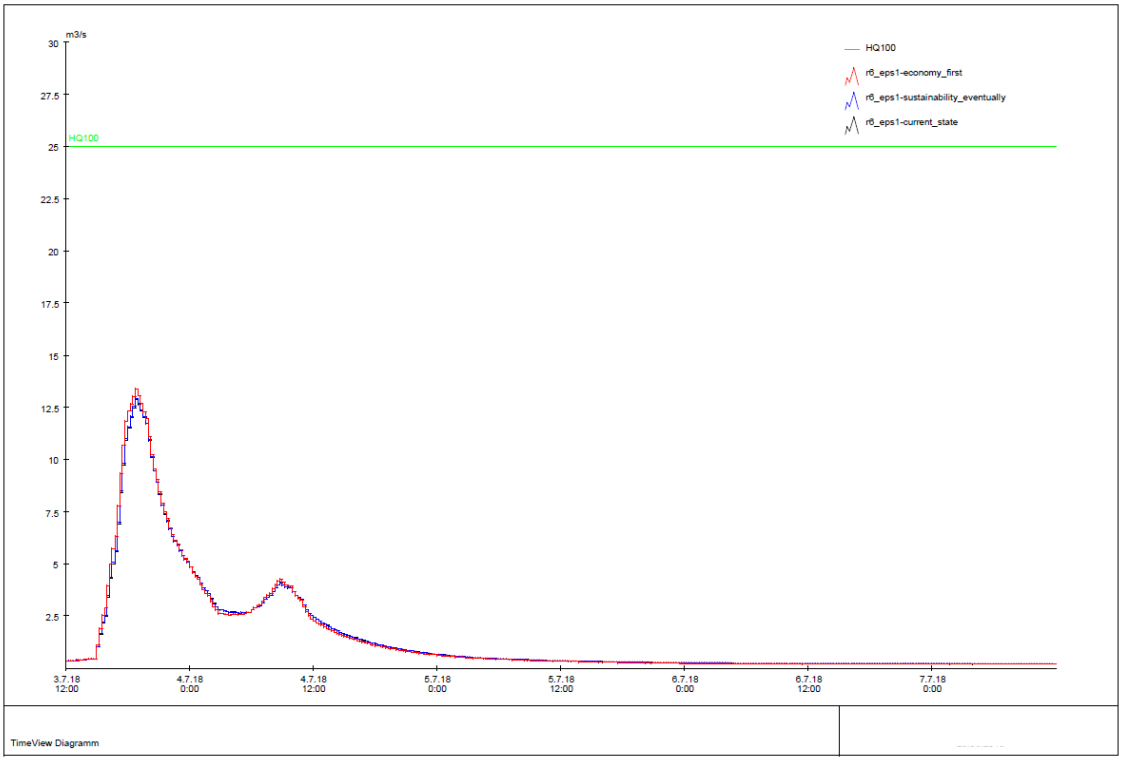

r6_xeps_eps2

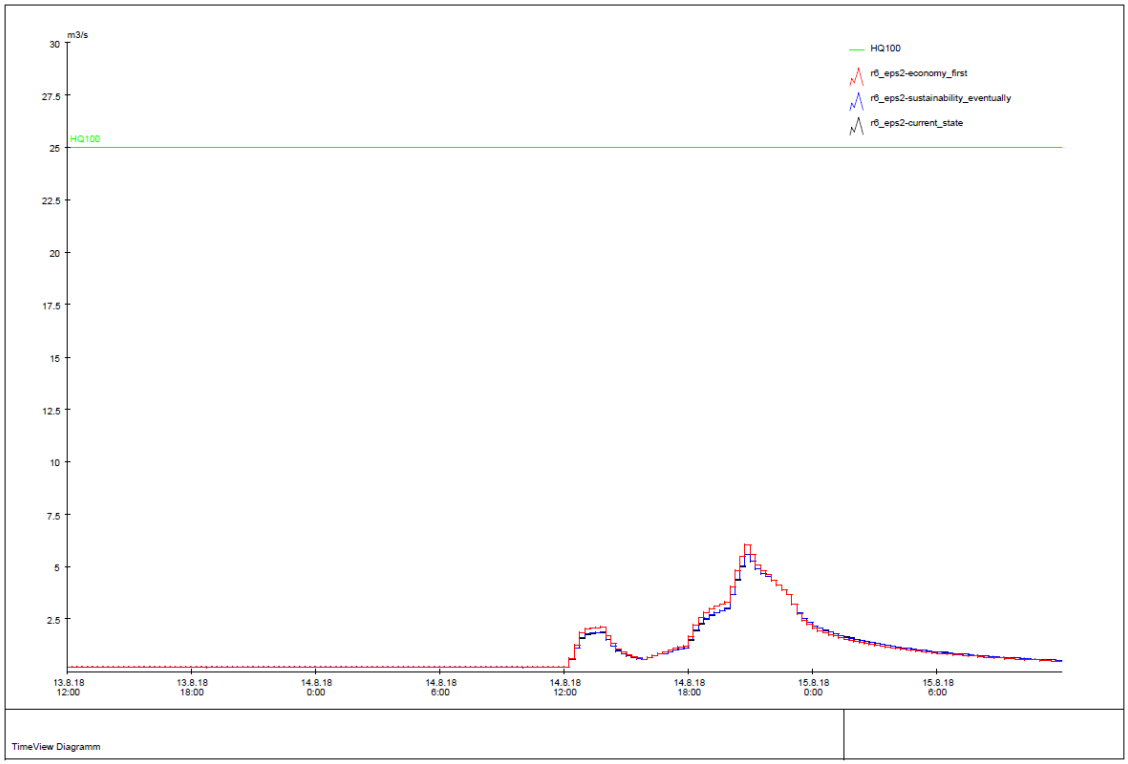

r6_xeps_eps3

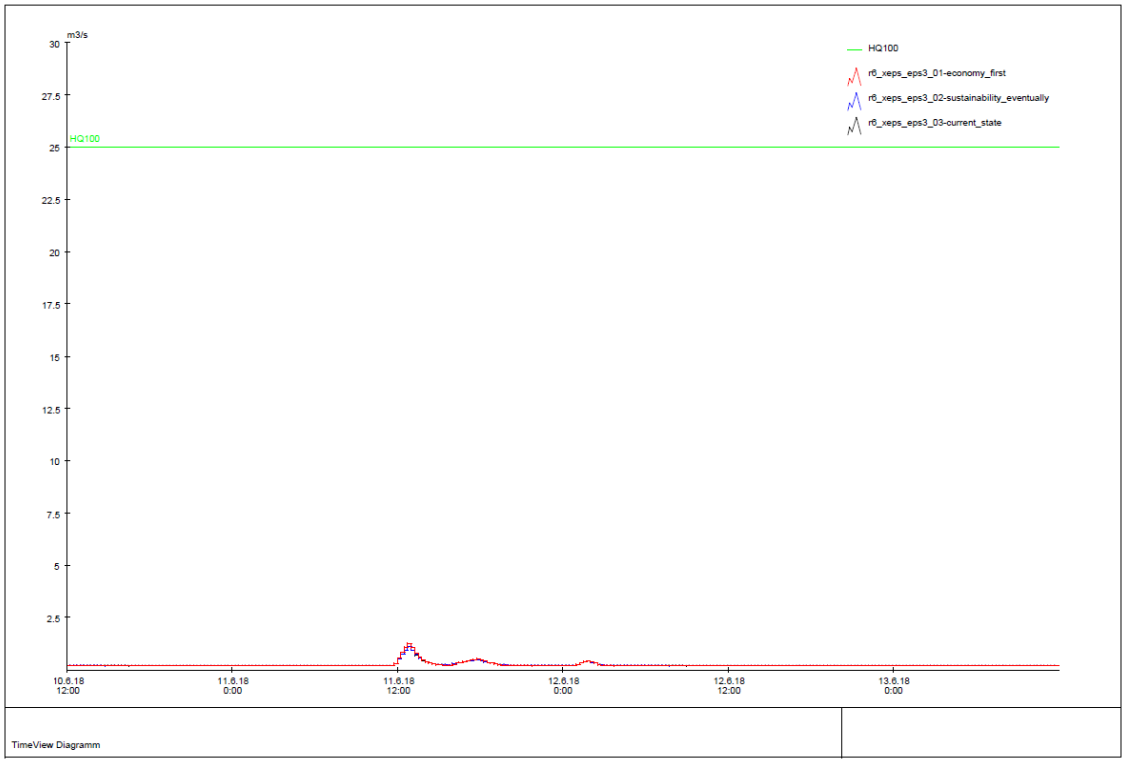

r7_xeps_eps1

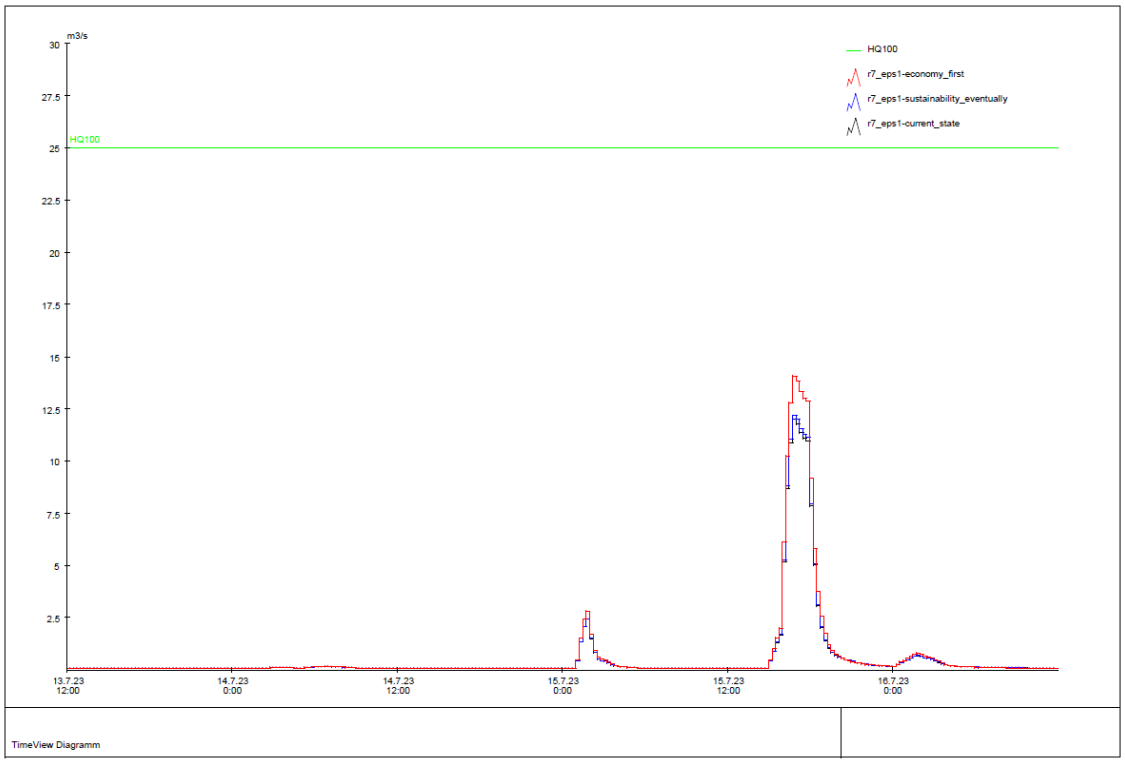

r7_xeps_eps2

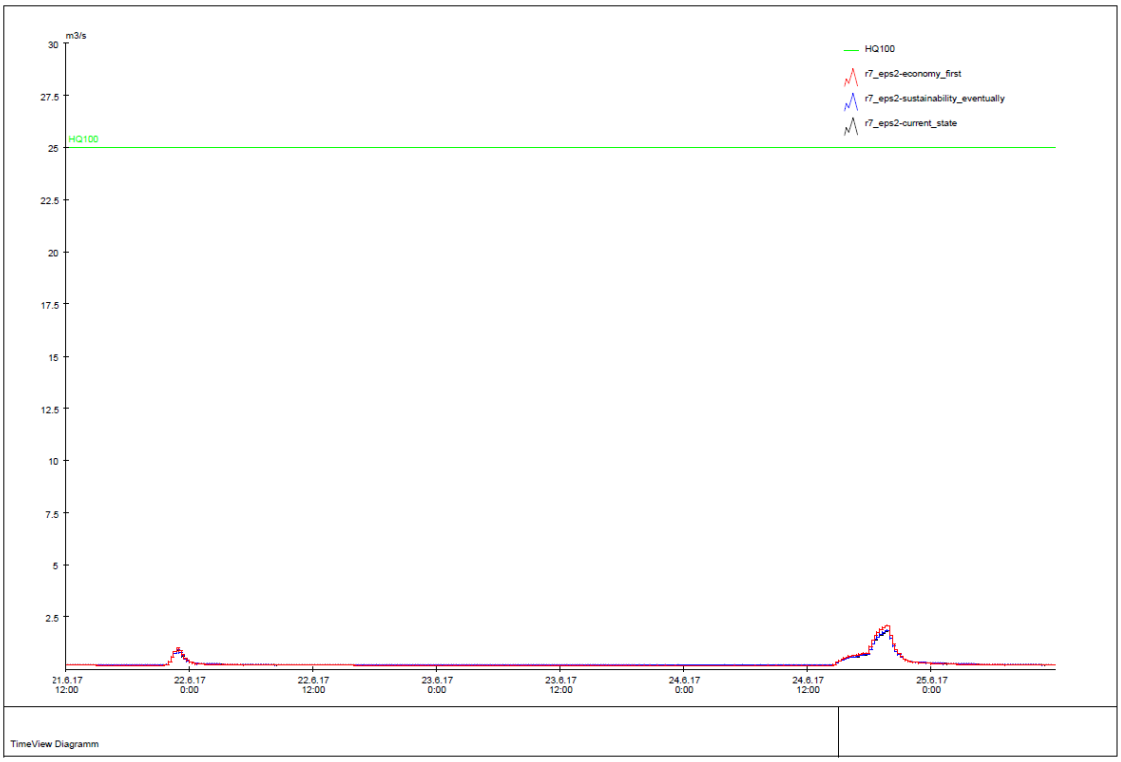

r8_xeps_eps1

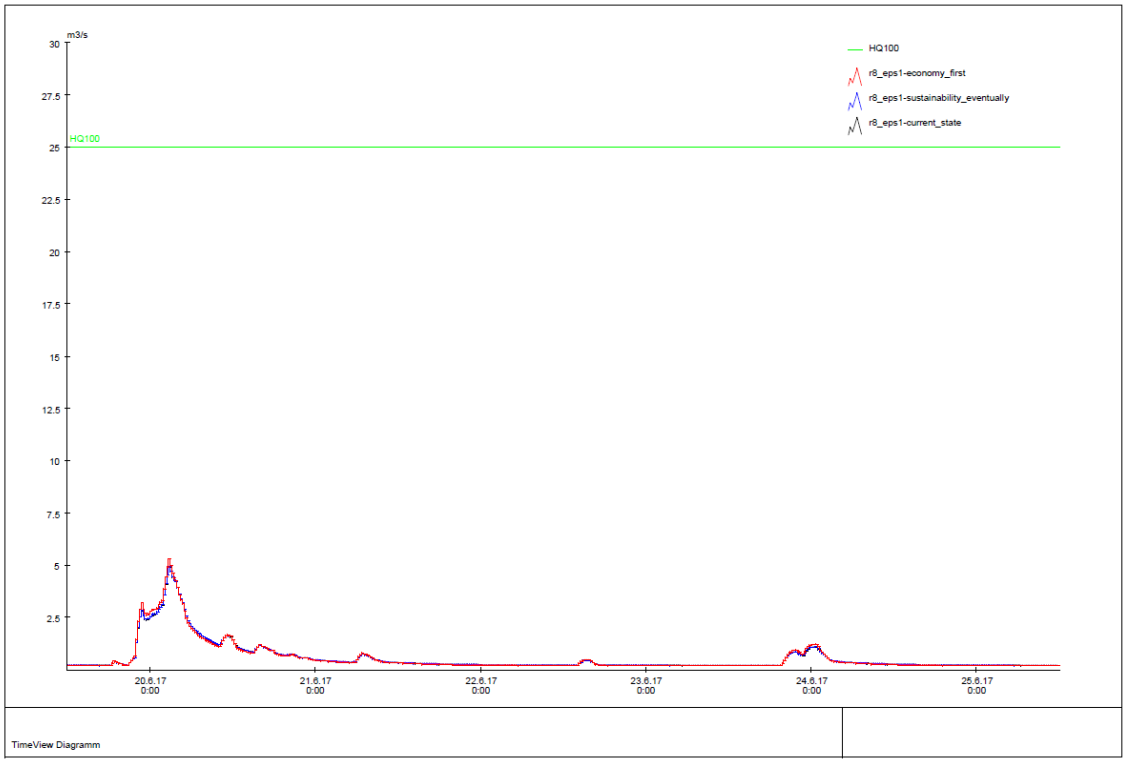

r8_xeps_eps2

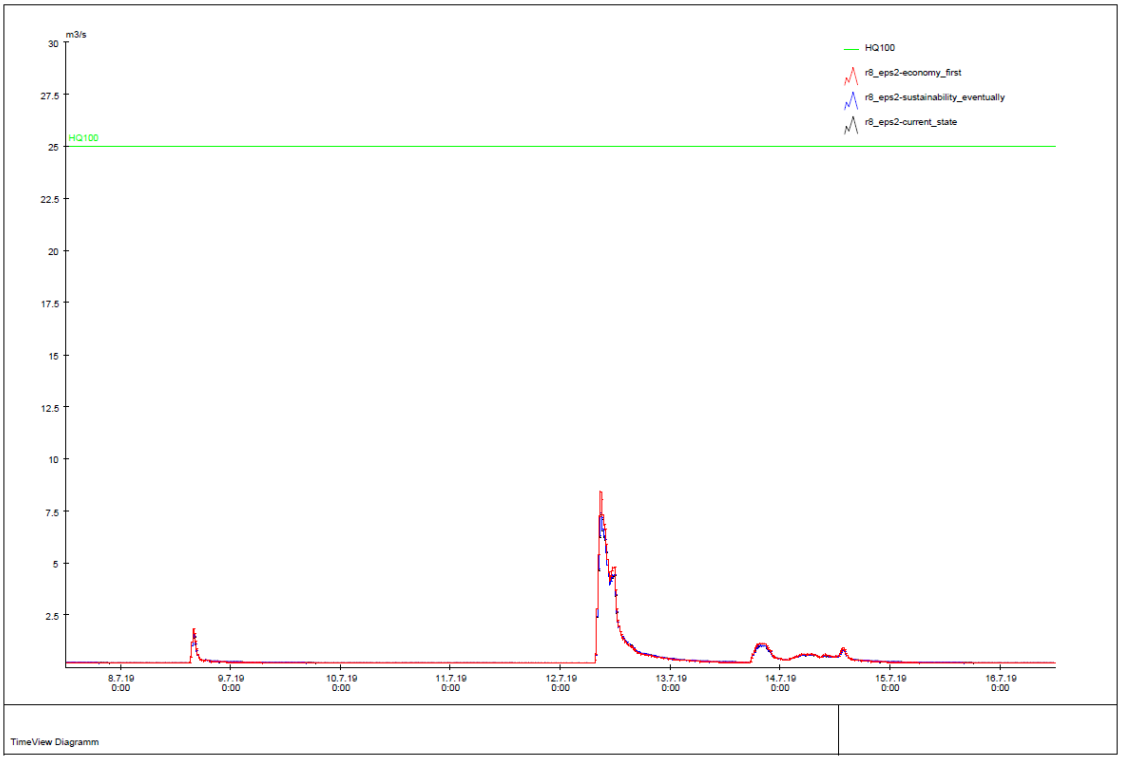

r9_xeps_eps1

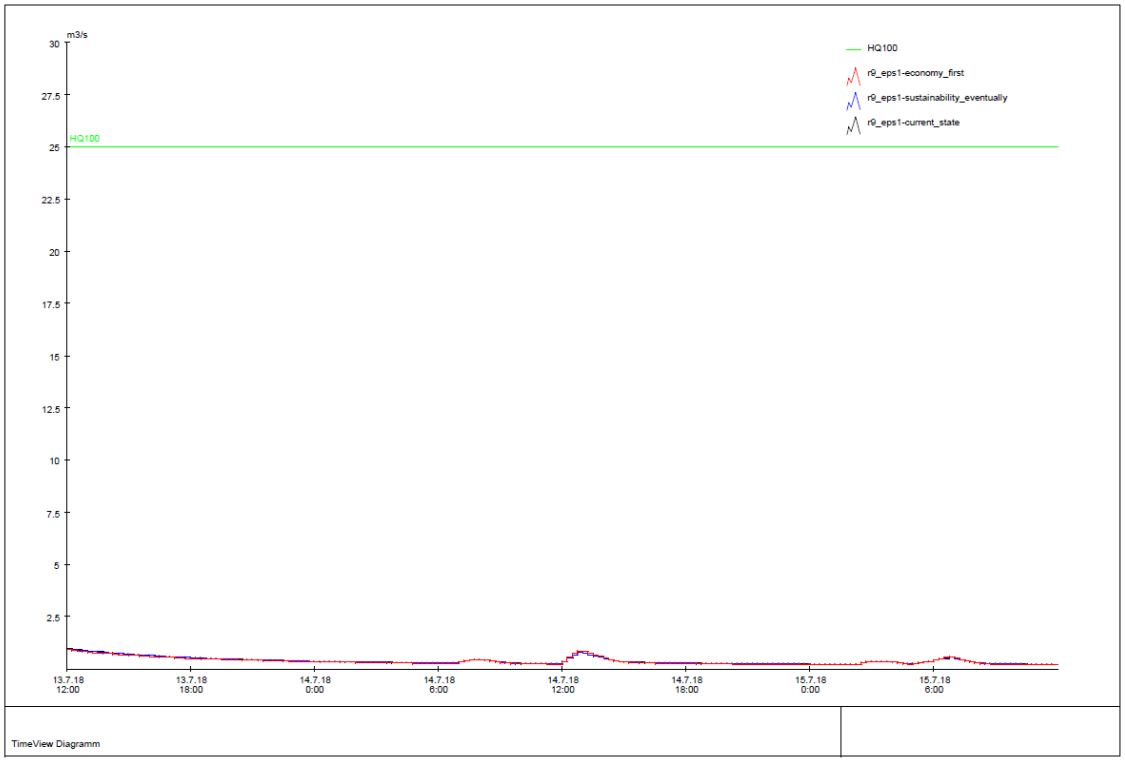

r9_xeps_eps2

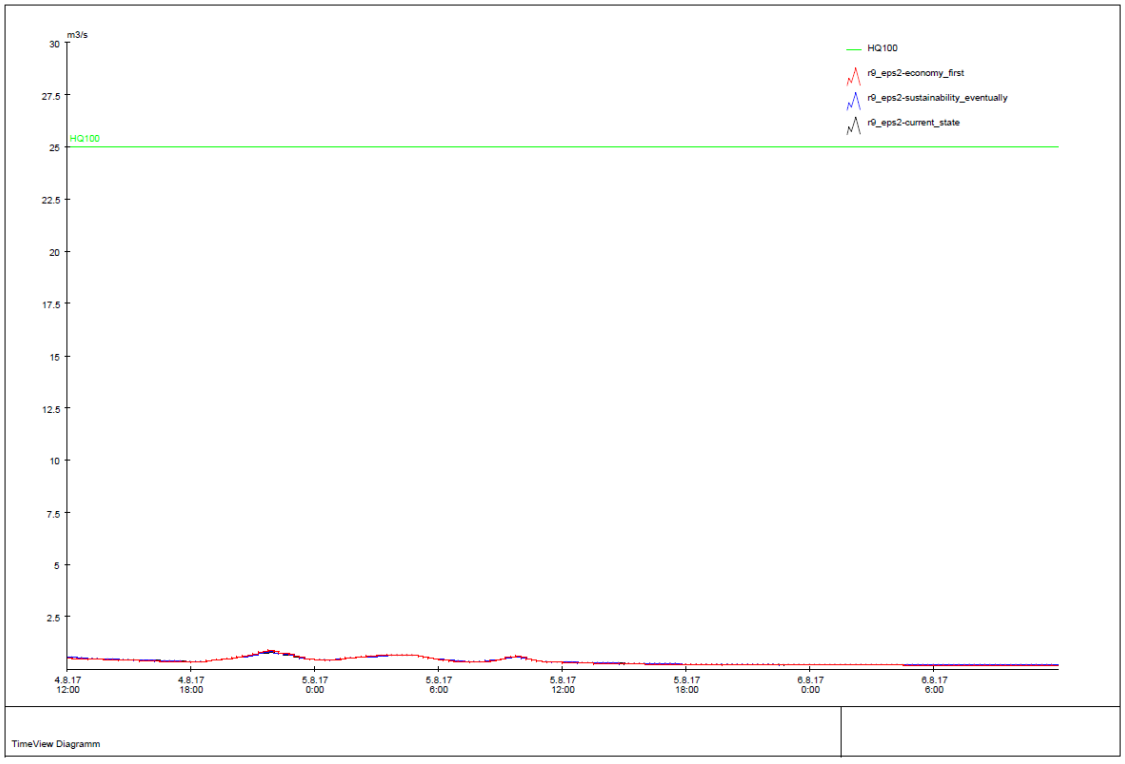

r10_xeps_eps1

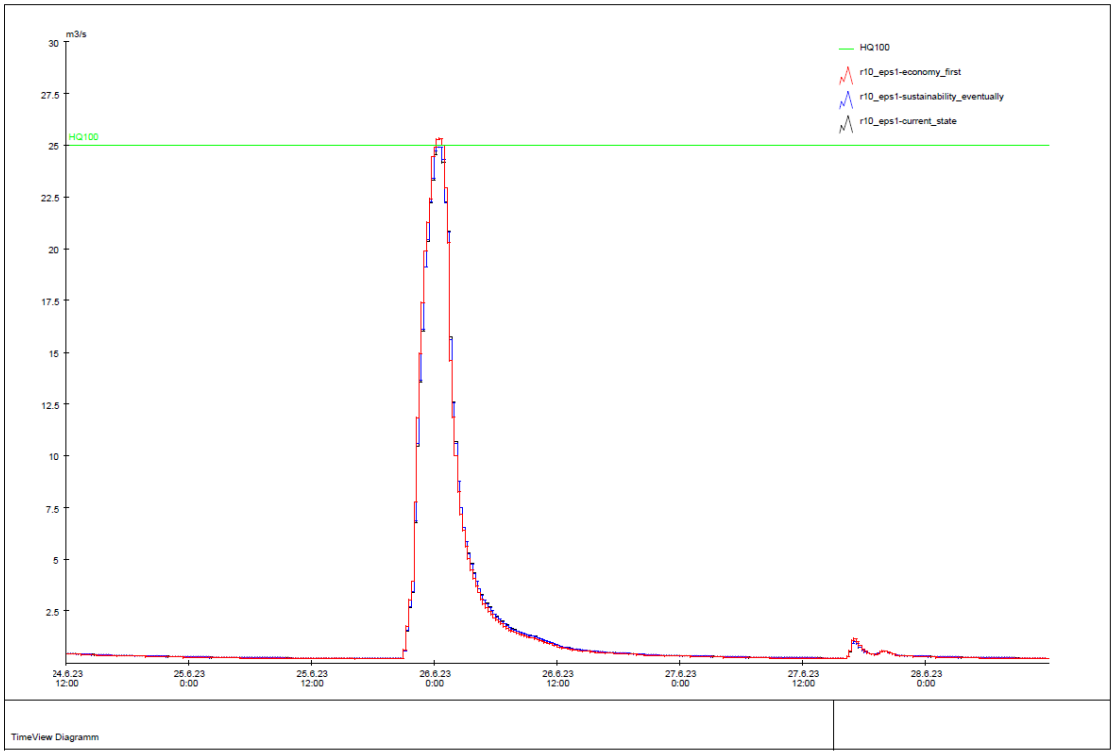

r10_xeps_eps2

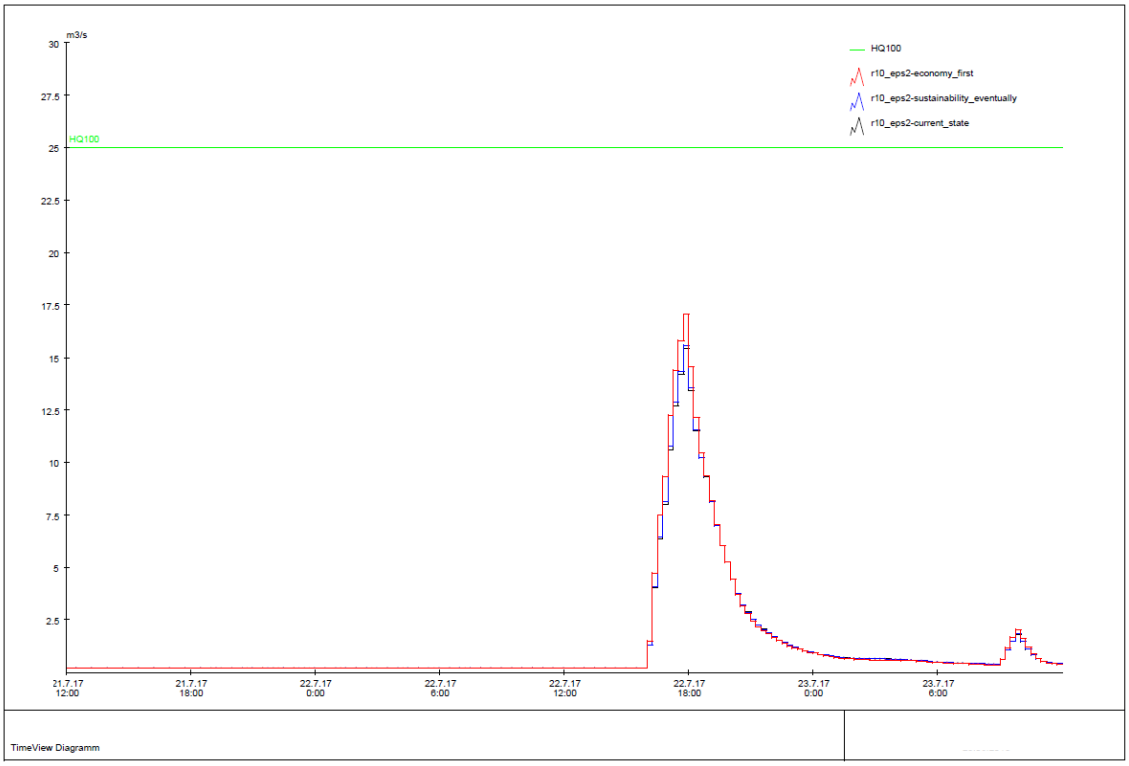

r10_xeps_eps3

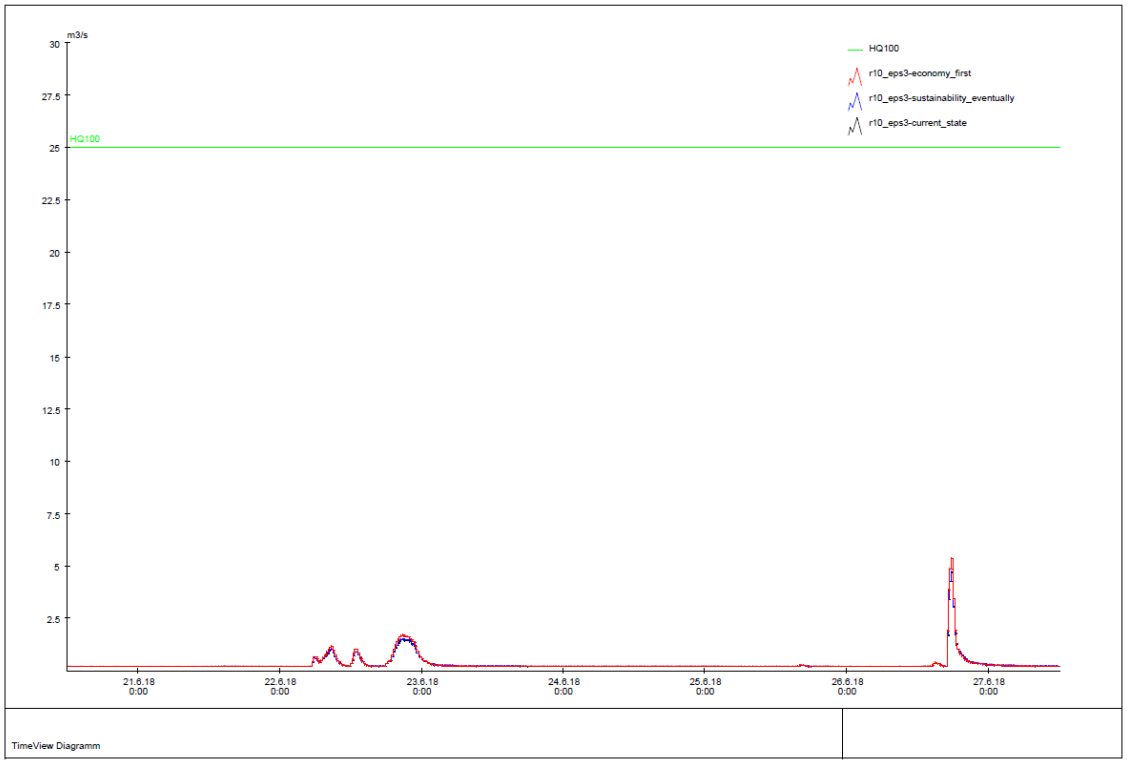

5. The Netherlands

5.1. Model objectives in BINGO

The Veluwe area is important for the drinking water supply in the Netherlands. It is an elevated sandy area which contains a large aquifer of fresh groundwater. Most of the area is designated nature reserve and land use mainly consists of forests (predominantly pine), heather and drift-sand. Due to the expanse of the area and its large unsaturated zone, the groundwater system responds slowly to changes in meteorological conditions. Brooks and streams are found at the fringe of the sandy area, where water exfiltrates. Upward seepage also occurs in surrounding lower lying agricultural areas. No large drainage systems or surface water bodies exist in the central part of the area. A complete description of the site including historical information can be found in Deliverable 3.1.

Precipitation shifts from summer to winter are expected in the future, combined with increased evapotranspiration demands in summer due to higher temperatures (KNMI 2014). This can lead to longer and more intense dry spells occurring more often across the Netherlands (KNMI 2014). These dry spells can pose a threat to the drinking water supply as well as to other land use functions, in particular agriculture and nature. In these circumstances the large groundwater body of the Veluwe becomes even more important. Groundwater abstractions from this area would then be increased. It is important to manage the groundwater system in a sustainable way to ensure enough water for the drinking water supply, and groundwater dependent nature and agriculture at the fringe of the Veluwe. To accomplish this, the amount of groundwater available for drinking water, agriculture and nature should not decrease. This amount is mainly determined by the groundwater recharge. In absence of surface water, the recharge on average equals the precipitation minus the actual evapotranspiration. By managing the land use, the actual evapotranspiration can be influenced, because, for example, pine forest has a much higher evapotranspiration (transpiration and interception losses) than drift sands. Because of the expanse of the groundwater body, any change to the water abstractions or land use will also affect the surrounding areas that depend on the drainage and seepage from the Veluwe. It is, therefore, essential to study the effect of these changes in an integrated approach. Within the BINGO project the model objective for the Veluwe is to quantify the effect of climate, land use changes and changes in water use over multiple time periods. Here we will present the results of the model simulations for the near future (2015-2024). A more detailed description of the model objectives was given in Deliverable 3.3.

5.2. Model application

For the Veluwe, the AZURE model (De Lange and Borren 2014) was used to simulate the impact of the climate, land use and water use changes on the water resources. The groundwater part of AZURE is based on MODFLOW (Harbaugh 2005) and it is coupled to MetaSWAP (van Walsum and Groenendijk 2008, van Walsum et al. 2010) for the simulation of the unsaturated zone. MetaSWAP simulates the actual evapotranspiration and groundwater recharge based on water availability, soil properties and land use. The potential evapotranspiration has been determined by multiplying the Makkink reference crop evapotranspiration (Makkink 1957) with land use specific crop factors. The land use classes of MetaSWAP were adjusted to include heather. The model simulations were done on a 250 by 250 m resolution for the Veluwe area and surroundings, in total an area of about 6 500 km^2. A detailed description of the model can be found in Deliverable 3.3.

To estimate the impact of future changes, the following model simulations were done:

- 3 decadal members (2015-2024) with current land and water use
- 3 decadal members (2015-2024) with 2 future land use scenarios and current water use
- 3 decadal members (2015-2024) with 2 future water use scenarios and current land use
- 3 decadal members (2015-2024) with 2 future land and water use scenarios

Because of the computation time of the model, only the most extreme decadal members (minimum and maximum) and an intermediate ensemble member were chosen (see 5.2.1).

To analyse the effect of the changes in climate, land use and water use, model results will be shown as spatial maps and as time series for five selected locations, indicated by the characters A-E (Figure 93a). These locations roughly form a transect across the southern part of the Veluwe area, including different land use types. The exact locations are based on the areas where land use will be changed in the scenarios and situated in proximity of drinking water abstractions where changes will be applied. This way, the effects and area of influence of the different scenarios can be determined.

5.2.1. Data

Hydrogeology

The AZURE model has nine hydrogeological layers with a horizontal and vertical conductivity. The initial conductivities were based on the national Dutch hydrogeological database REGIS 2.1 (Vernes and Van Doorn 2005). These values were adjusted after the calibration with historical data (Deliverable 3.3). Major soil textures are ‘sandy gravel’, ‘sand’ and ‘clay’. The complex features of the Veluwe from its geological setting are accounted for by using different horizontal anisotropy factors (Deliverable 3.3). Ice pushed ridges received a low anisotropy value in the direction perpendicular to the ridge.

The model boundaries of AZURE are defined as constant head boundaries. The extent of the model is chosen in such a way that a constant head boundary coincides with large rivers (‘IJssel’ and ‘Rijn’) or lake ‘IJsselmeer’. Large lakes, as the ‘IJsselmeer’, are simulated as constant head boundaries as well. For terrestrial parts, the upper boundary is controlled by recharge estimated by MetaSWAP.

Meteorological data

The AZURE model was run with daily meteorological data for the historical period (1980-2014) and the near future (2015-2024). The meteorological data used as input are the simulated climate data generated by WP2. These data are described in Deliverable 2.2. The data consisted of a bias-corrected dataset for the period 1980-2015 and an ensemble of ten decadal predictions for the near future (Figure 84). For the bias correction the WATCH forcing data ERA-interim (Weedon et al. 2014) were used, except for radiation. Bias correction for radiation was based on a gridded product of interpolated station data from the Royal Netherlands Meteorological Institute.

From the ten ensemble members that were provided, the most extreme members and an intermediate member were selected for the model simulations. The selection of the minimum and maximum ensemble members was based on the cumulative value of the potential precipitation surplus (i.e. precipitation - Makkink reference crop evapotranspiration, Makkink 1957) for each member (Figure 85a). The intermediate ensemble member was determined based on the cumulative value of the precipitation surplus and an additional ranking of all the members. The member that most frequently had a ranking between the maximum and minimum members was chosen as the intermediate ensemble member. Since the selection is based on the cumulative precipitation surpluses over the whole decadal prediction, the precipitation surplus of the dry

ensemble member is not the lowest in all separate years (Figure 85b) and the wet ensemble member does not have the highest precipitation surplus in all years. The ensemble members show a similar range in potential recharge as the historical period (Figure 84). The mean yearly potential precipitation surplus was 247 mm/year for the dry member, 306 mm/year for the intermediate member and 353 mm/year for the wet member over the near future period (2015-2024). In the reference period (1985-2014) the mean yearly potential precipitation surplus was 283 mm/year.

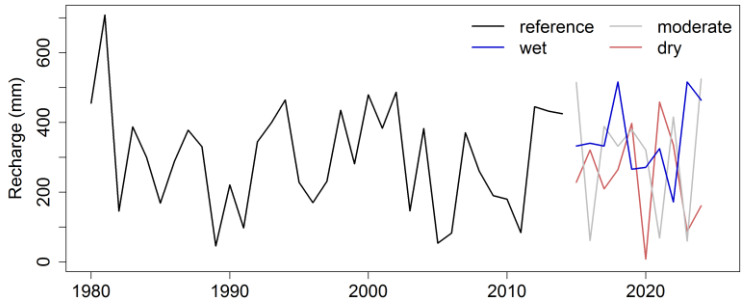

Figure 84 Yearly potential precipitation surplus for the reference period and three ensemble members.

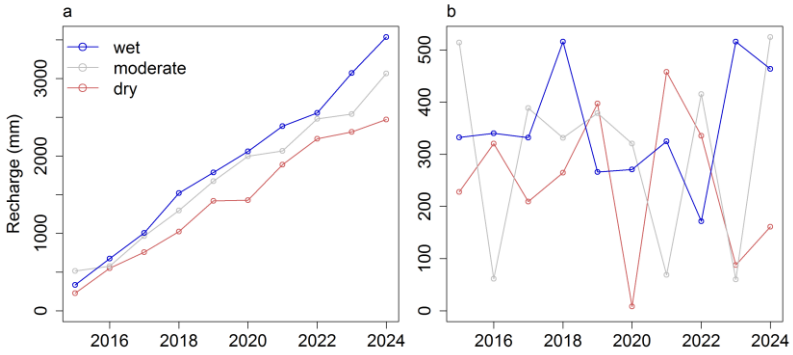

Figure 85 a) Cumulative yearly potential precipitation surplus (mm) for the three ensemble members, b) Yearly potential precipitation surplus (mm) for the three ensemble members.

Changes in the meteorological variables are determined between the near future (2015-2024) and a 30-year reference period (1985-2014). The differences in mean yearly potential evapotranspiration and mean yearly precipitation between the three ensemble members and the reference period are shown in Figure 86 and Figure 87 respectively. The potential evapotranspiration was determined by multiplying the Makkink reference crop evapotranspiration (Makkink 1957) with separate crop factors for transpiration, soil evaporation and interception evaporation. For all ensemble members the Makkink evapotranspiration increases compared to the reference period (Figure 86) due to an increase in temperature. The dry ensemble member shows the largest increase of up to 86 mm/y (Figure 86b), whereas the maximum increase for the wet ensemble member is 53 mm/y (Figure 86d). For precipitation, the spatial pattern is more diverse, but in general precipitation increases in the wet and intermediate ensemble member (Figure 87). The dry ensemble member shows a decrease in large areas up to 26 mm/y and the smallest increase in precipitation over part of the model domain with a maximum increase of 49 mm/y (Figure 87b). For the intermediate ensemble member, precipitation shows a slightly higher increase over the model domain of up to 69 mm/y (Figure 87c). Precipitation increases most in the wet ensemble member with a maximum increase of 121 mm/y (Figure 87d).

The mean monthly values for the reference period and the ensemble members for the potential evapotranspiration and precipitation are given in Figure 88. The increase in potential evapotranspiration for the three ensemble members occurs in spring and summer (Figure 88a). The difference in precipitation does not show a clear pattern throughout the year (Figure 88b). The main difference is found in the dry ensemble member in spring and summer, when precipitation for the dry ensemble member is mainly lower than the reference period, especially in May. The difference between the dry ensemble member and the reference period is less clear in the mean annual values because of the increase in precipitation in January in the dry ensemble member and the low precipitation values in April in the reference period. The main increases in precipitation occur in April, August, September and October for all members (Figure 88b). In the dry ensemble member, the precipitation decreases and potential evapotranspiration increases coincide, which could lead to longer and more intense dry spells.

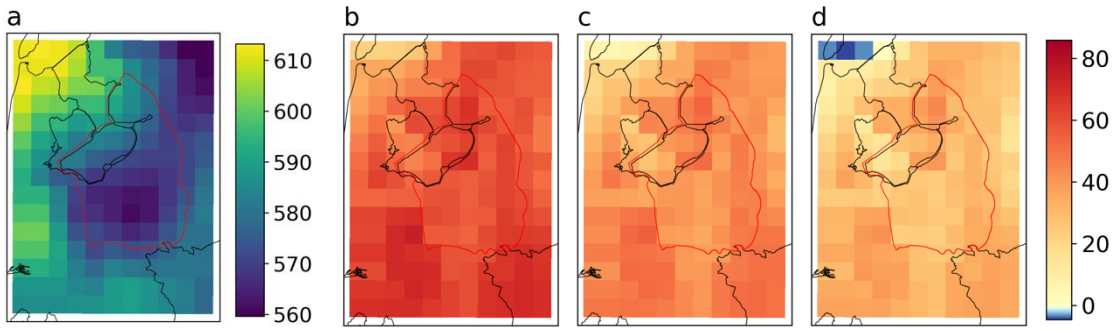

Figure 86 Mean yearly potential evapotranspiration (mm/y) for the reference period (1985-2014, a), and difference in mean yearly potential evapotranspiration (mm/y) between the three ensemble members (2015-2024): b) dry, c) moderate, and d) wet and the reference period. Red line indicates the model domain, the resolution of the meteorological data is 12 by 12 km.

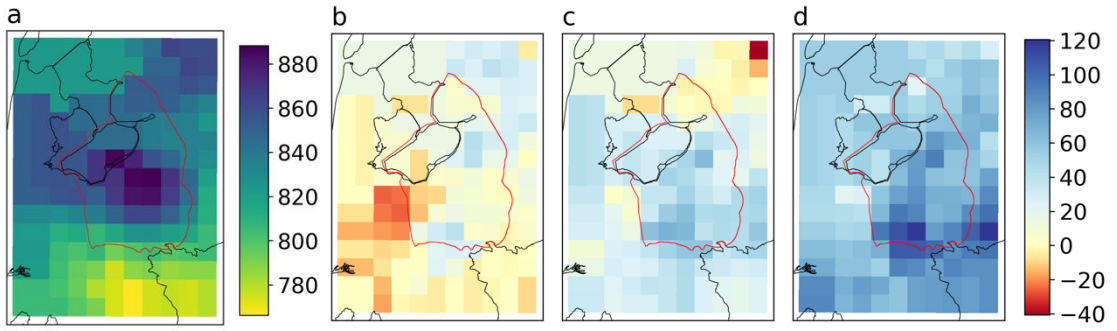

Figure 87 Mean yearly precipitation (mm/y) for the reference period (1985-2014, a), and difference in mean yearly precipitation between the three ensemble members (2015-2024): b) dry, c) moderate, and d) wet and the reference period. Red line indicates the model domain.

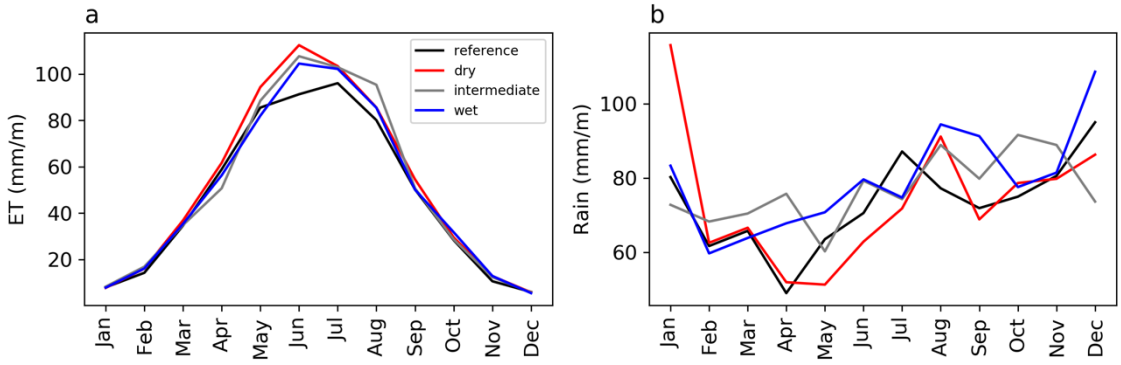

Figure 88 Mean monthly a) potential evapotranspiration (mm) and b) precipitation (mm) of the reference period (1985-2014) and of the three ensemble members (2015-2024) averaged over the Veluwe area.

Land use

The land use classes at the Veluwe for the AZURE model for the reference period (Figure 89) are based on the LGN6 Dutch land use database (LGN6, Hazeu et al. 2011). This database combines information from satellites images, topographical maps and older land use databases. For the AZURE model, the land use database was converted to a 250 by 250 m grid (Figure 89).

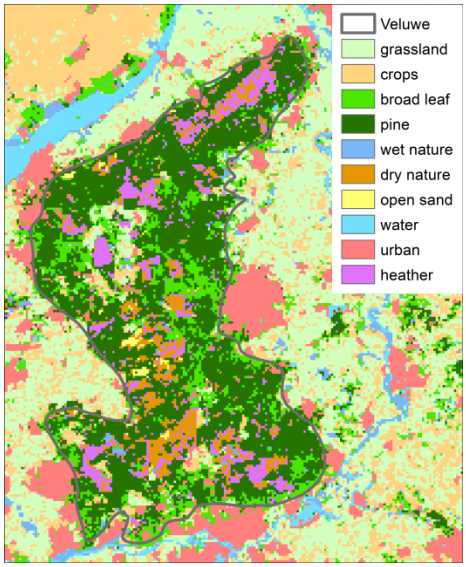

Figure 89 Land use classes at the Veluwe area for the AZURE model in the reference period.

The land use scenarios have been derived from the scenarios described in Deliverable 3.2. Both scenarios, Economy First and Sustainability Eventually, have been used in the model simulations. The applied land use changes are based on the given scenarios, but were adjusted for the AZURE model. The most extreme land use changes were the conversions of 'pine forest' into 'deciduous forest' and 'woody savannah' (D3.2). These changes have been applied in the scenarios. For practical use in MetaSWAP, the land use class 'woody savannah' has been interpreted as a mixture of 'open sand' and 'dry nature'. Since the other land use changes were negligibly small (e.g. changes in grass and heather only cover 2 km^2) or in protected land use classes (where land use change is not likely), they were not included. The changes in the areas of the land use classes for the different scenarios are given in Table 18. The exact locations of the land use

changes were based on interviews with the province of Gelderland and the location of protected regions, where land use change is not likely. The locations of the changes in land use for each scenario are shown in Figure 90.

Other studies have simulated the actual evapotranspiration values and corresponding recharge of the different types of land use (Verhagen et al. 2014, Table 19). These values show an increase in recharge for all conversions from pine forest. The change from pine forest to open sand will increase the recharge value almost three times.

Table 18: Changes in land use (km2) for the two scenarios between 2015 and 2024

Scenarios	Pine forest	Broadleaf	Dry nature	Open sand
Sustainability eventually	-20	+20	-	-
Economy first	-100	+20	+60	+20

Table 19: Modelled actual evapotranspiration and recharge for the Veluwe (Verhagen et al. 2014)

Land use	ETa (mm/y)	Recharge (mm/y)
Pine forest	681	152
Broadleaf forest	609	224
Heather	494	339
Open sands	261	569

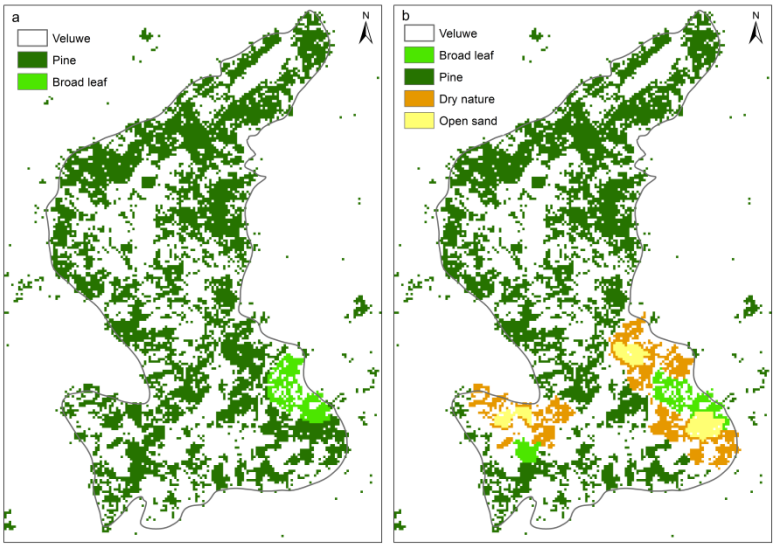

Figure 90 Land use changes for the Veluwe, a) Change in pine forest for the Sustainability Eventually scenario, b) Change in pine forest for the Economy First scenario. Currently all coloured areas are pine forest.

Water use

The water use scenarios have also been derived from the scenarios described in Deliverable 3.2. For the model application, the water use scenarios only include the increase of groundwater abstractions for drinking water supply (Figure 91). The increases in groundwater abstractions are derived from the values given in Deliverable 3.2 for the two scenarios for the domestic water use for 2025. For the Sustainability Eventually scenario this means an increase of 1.4% compared to domestic water use in 2015. In the Economy First

scenario, domestic water use increases with 6.9%. To meet the increased water demand in the scenarios, the groundwater abstractions were expanded with these percentages at the following drinking water stations: Amersfoortseweg, La Cabine, Schalterberg, De Haere, Ede, Eerbeek, Ellecom, Epe, Harderwijk, Hoenderloo, Oosterbeek, Putten, Pinkenberg, Wageningen and Boele.

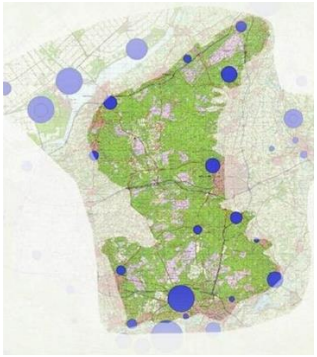

Figure 91 Locations of groundwater abstractions at the Veluwe. The size of the circles represents the abstracted amount of groundwater.

5.2.2. Results

Historical situation

The elevation and simulated mean groundwater heads (m +NAP, Normaal Amsterdams Peil or Amsterdam Ordnance Datum) for the Veluwe area over the reference period (1985-2014) are shown in Figure 92. As expected, the highest parts of the Veluwe have higher absolute groundwater levels and clearly stand out. The difference between the elevation and groundwater heads also gives an estimate of the large unsaturated zone in this area. At the borders, a steep gradient in the groundwater levels exists.

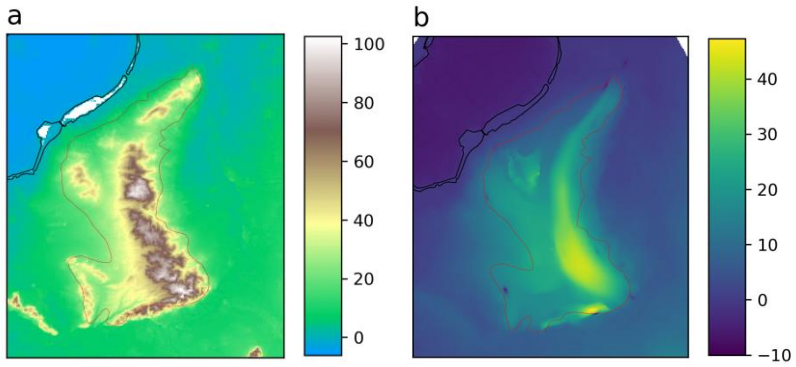

Figure 92 a) Elevation (m +NAP) of the Veluwe area, b) Mean groundwater head (m +NAP) over the Veluwe for the period 1985-2014. The red line indicates the area of the Veluwe.

To get an estimate of the reliability of the model results, observed groundwater levels from two monitoring wells close to locations C and D are shown (Figure 93). The slow response of the Veluwe due to the deep groundwater levels is clearly visible in the observed groundwater levels from the highest parts of the Veluwe (Figure 93b). As a result of the slow response, the groundwater shows no intra-annual variability.

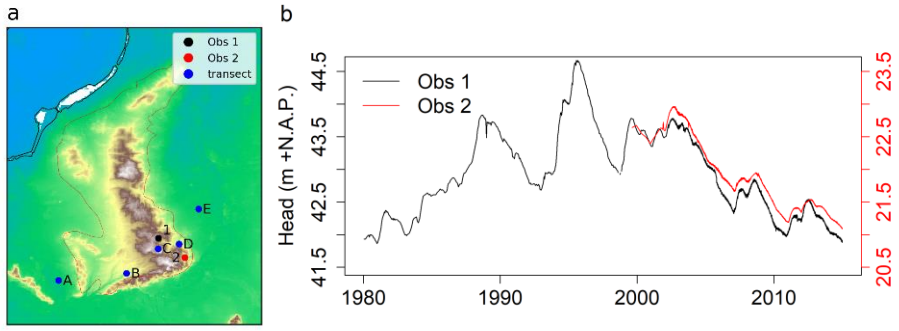

Figure 93 a) Selected locations within the transect and locations of observed groundwater levels, b) Observed groundwater heads in locations 1 and 2 (m +NAP).

In order to compare the model results with the observations, the groundwater heads were normalized by dividing each time series of groundwater levels by its mean value (Figure 94). Comparison between the observed levels and simulated levels is only meant as a rough indication of model reliability, because the transect locations are not the same as the locations of the monitoring wells. Also, the bias-corrected forcing data of the historical period is not completely similar as the actual situation (Figure 94a).

In general, the simulated groundwater levels show a very similar behaviour as the observed groundwater, although the response seems to be slightly underestimated by the model (Figure 94b). In the period 2003-2014 a strong decline occurred in the observed groundwater levels, this decline is delayed in the simulated groundwater levels. The observed data show a slight recovery during this period (2008 and 2012) that is not visible in the model results, however, this could be explained by the differences in precipitation. The precipitation used as model input is lower in the years preceding these recoveries (e.g. 2005, 2006, 2007 and 2010, 2011) than the observed precipitation (Figure 94a). Therefore, the sharp decline in the period 2005-2014 in the simulated time series can be considered as realistic behaviour over this period.

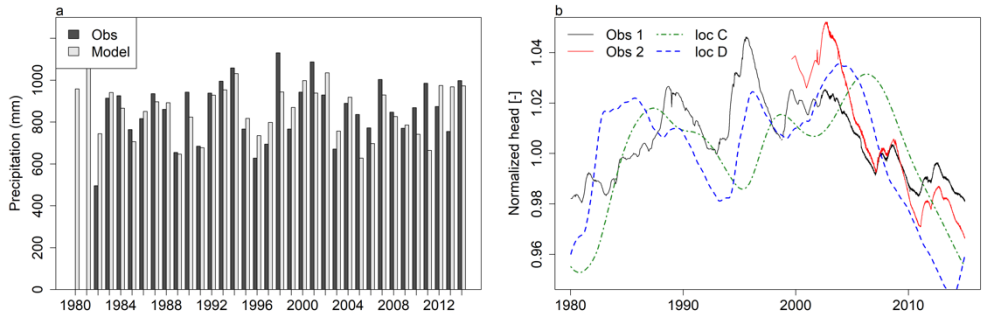

Figure 94 a) Observed and modelled yearly precipitation (mm) over the Veluwe, b) normalized groundwater heads for the groundwater wells and at 2 locations across the transect (see Figure 93a for locations).

Effect of climate

The model was run for the near future with different scenarios and different forcing datasets. In the reference situation no changes have been made to the current land use and water use. The differences in simulated mean groundwater head between the near future and the reference period for the different forcing datasets over the whole Veluwe area are shown in Figure 95a-c. The highest parts of the Veluwe show the largest decrease in the mean groundwater head, whereas in the rest of the elevated area there is a smaller decrease in groundwater head and an increase in some parts.

The opposite reactions in the different parts of the elevated area are explained by the slow reaction of the Veluwe over time. There is a large difference in the response time between the highest middle parts and areas at the borders (Figure 96). The recharge in the last part of the reference period (2005-2014) was relatively low compared to the historical record. Therefore, the locations in the natural area of the Veluwe (location B, C and D, Figure 96) show a strong decline in groundwater head in that period. Location C is located in the middle of the highest part of the Veluwe and shows the largest decrease and slowest response. Location B and D start to recover again at the end of 2013, whereas location C does not show an increase until the beginning of 2015. During the near future, locations B, C and D show an increase in groundwater head. The mean head in the reference period, however, is higher for locations in the higher parts of the Veluwe (location C) leading to a decrease in the mean groundwater head when comparing with the near future (Figure 95a-c). The locations in the agricultural surrounding areas (A and E) show completely different behaviour with much more variation and a faster response to precipitation (Figure 96).

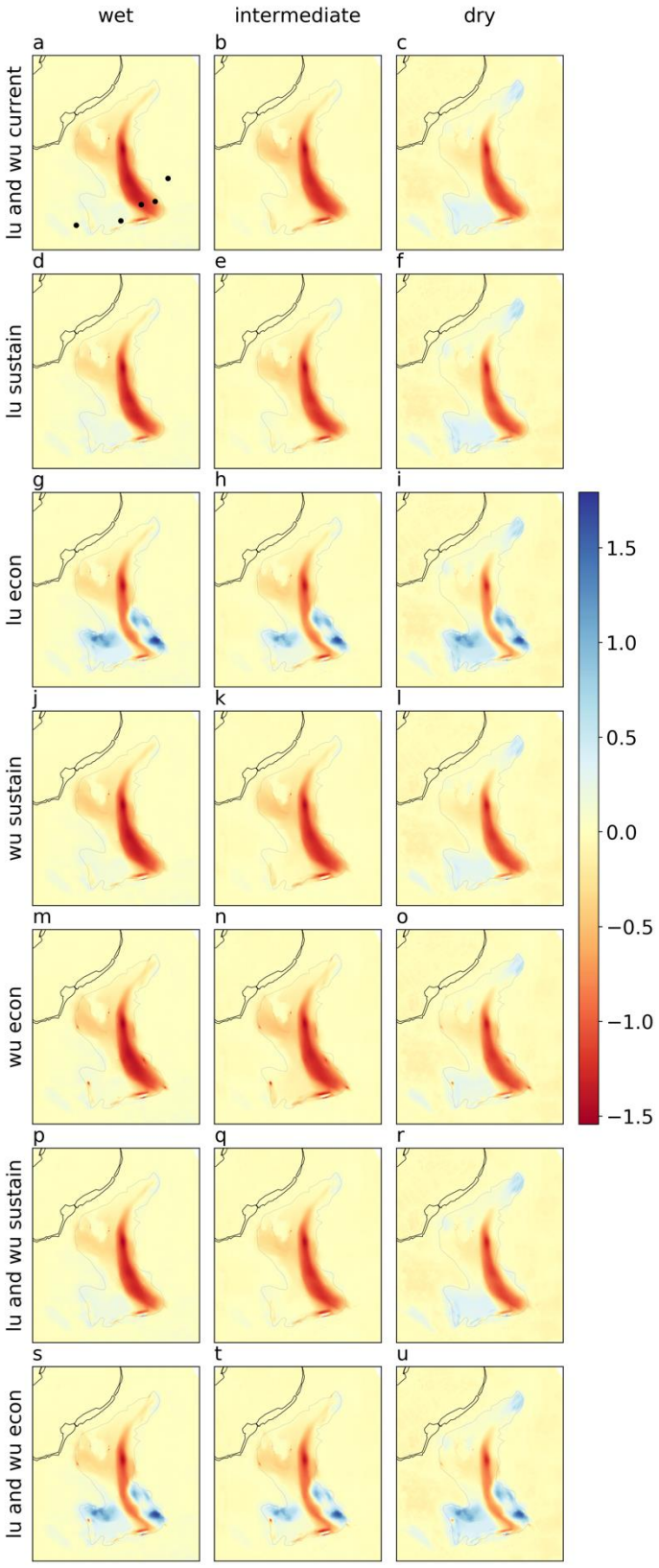

Figure 95 Changes in mean groundwater head (m) between the near future (2015-2024) and the reference period (1984-2014) for all the model runs with the three ensemble members, a-c) no changes in land use and water use, d-f) land use change following the Sustainability Eventually (sustain) scenario, g-i) land use change following the Economy First (econ) scenario, j-l) water use change with sustain scenario, m-o) water use change with econ scenario, p-r) change in land use and water use with sustain scenario, s-u) change in land use and water use with econ scenario. The grey line indicates the area of the Veluwe, black dots show the five selected locations.

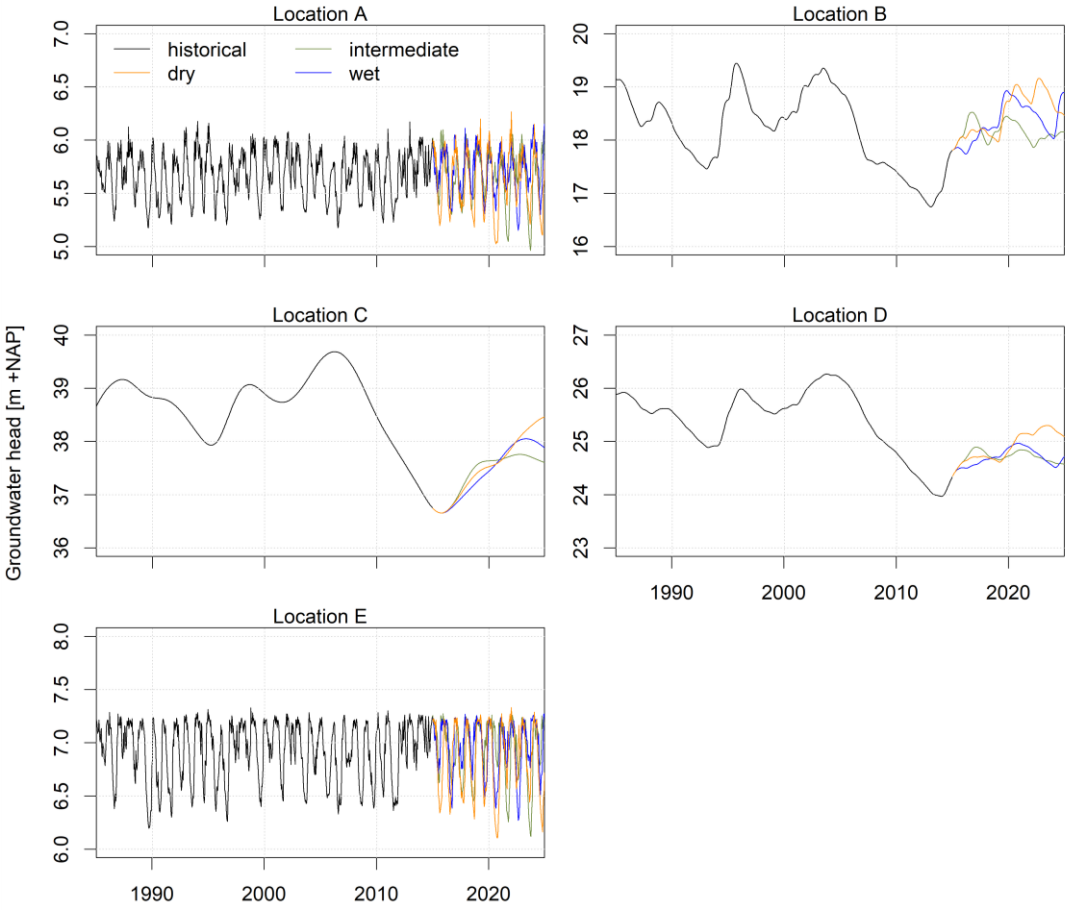

Figure 96 Groundwater heads (m +NAP) at five locations along a transect over the Veluwe area for the reference situation (no changes in land use and water use)

The differences between the three ensemble members are relatively small. The wet ensemble member (Figure 95a) indicates a slightly larger decrease in groundwater heads in the highest parts than the other members. The dry ensemble member (Figure 95c) shows a lower decrease in groundwater heads on the highest parts and an increase in part of the elevated area, but a higher decrease in the surrounding low-lying agricultural areas. For the intermediate ensemble member almost the entire model domain shows a decrease in groundwater heads. The selected locations also give an indication of the differences between the climate ensemble members (Figure 96). The groundwater levels increase during the near future for the slow responding locations B, C and D, whereas for locations A and E mainly differences in variation are found. The dry ensemble member leads to higher groundwater levels at the end of the near future period in the locations B, C and D. This could be linked to the higher precipitation values in winter in the dry ensemble member, especially in January. The timing of these higher precipitation amounts would lead to more recharge, because evapotranspiration is low in winter. In spite of the higher potential evapotranspiration values in the dry ensemble member, the actual evapotranspiration could have been reduced substantially by a lack of available water in the sandy soil (Witte et al. 2012). Recharge could therefore increase more in the dry ensemble member compared to the other ensemble members.

At locations A and E a fast response to precipitation can be seen, leading to lower groundwater heads in summer for the dry ensemble member in most years of the near future. This is especially clear in the summer of 2020, when the low recharge in the dry ensemble member leads to very low groundwater heads (Figure 96). The lower recharge values in the years 2021 and 2023 in the intermediate member also stand out, especially at location A.

Effect of land use changes

To investigate the effect of land use change, two scenarios are used (paragraph 5.2.1), Sustainability eventually (sustain) and Economy first (econ). The locations of the land use change are given in Figure 90. The change in mean groundwater head over the whole model domain is shown in Figure 95d-f for the sustain scenario and in Figure 95g-i for the econ scenario. The differences between the climate ensembles are again relatively small. The changes over time at the five selected locations are given in Figure 97 and Figure 98. The locations A and E are situated in the agricultural areas surrounding the Veluwe and are further away from the areas where land use change was simulated. These locations, therefore, did not show any differences between the reference situation and the scenarios for any ensemble member (Figure 97). They are outside the area of influence from the land use changes; groundwater levels are primarily influenced by surface water levels and irrigation in these agricultural regions.

From the spatial maps, the differences between the reference situation (Figure 95a-c) and the sustain scenario seem relatively small. This was expected, because the changes applied in the sustain scenario (Table 18) are not extensive. However, at the individual locations closer to the areas where land use was changed, a difference in groundwater heads is found, e.g. approximately 0.45 m at location D (Figure 98a). The change from pine forest to broadleaf forest leads to a reduction in evapotranspiration and therefore an increase in groundwater heads.

The land use changes applied in the econ scenario are more extensive (Table 18), which leads to larger differences with the reference situation. A large part of the southern Veluwe is affected in this scenario (Figure 95g-i), where the groundwater heads are higher, e.g. show an increase instead of a decrease. The changes from pine forest to broadleaf forest, dry nature and drift sands lead to a reduction in evapotranspiration and as a result groundwater heads increase compared to the situation without land use change. The difference between the scenarios is especially visible in the locations where land use changes have been applied (Figure 98a). At location D, the increase in groundwater heads for the econ scenario is 3.85 m compared to the current land use scenario in the intermediate ensemble member at the end of the time series. Further away from the changed areas (location B) the difference is smaller, but the increase under the intermediate ensemble member is still 0.38 m.

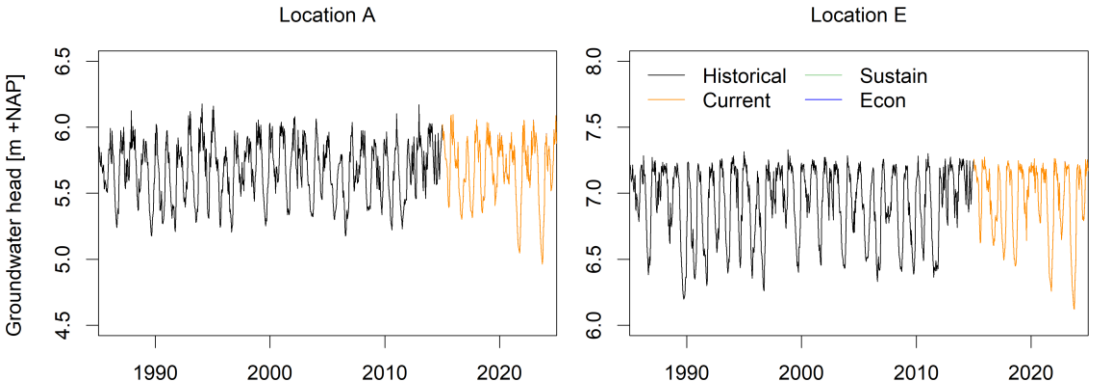

Figure 97 Groundwater heads for locations A (left) and E (right) for the reference period and intermediate ensemble member with different land use scenarios (current, Sustainability eventually, Economy first). Heads from the land use change scenarios coincide with heads from the current land use scenario.

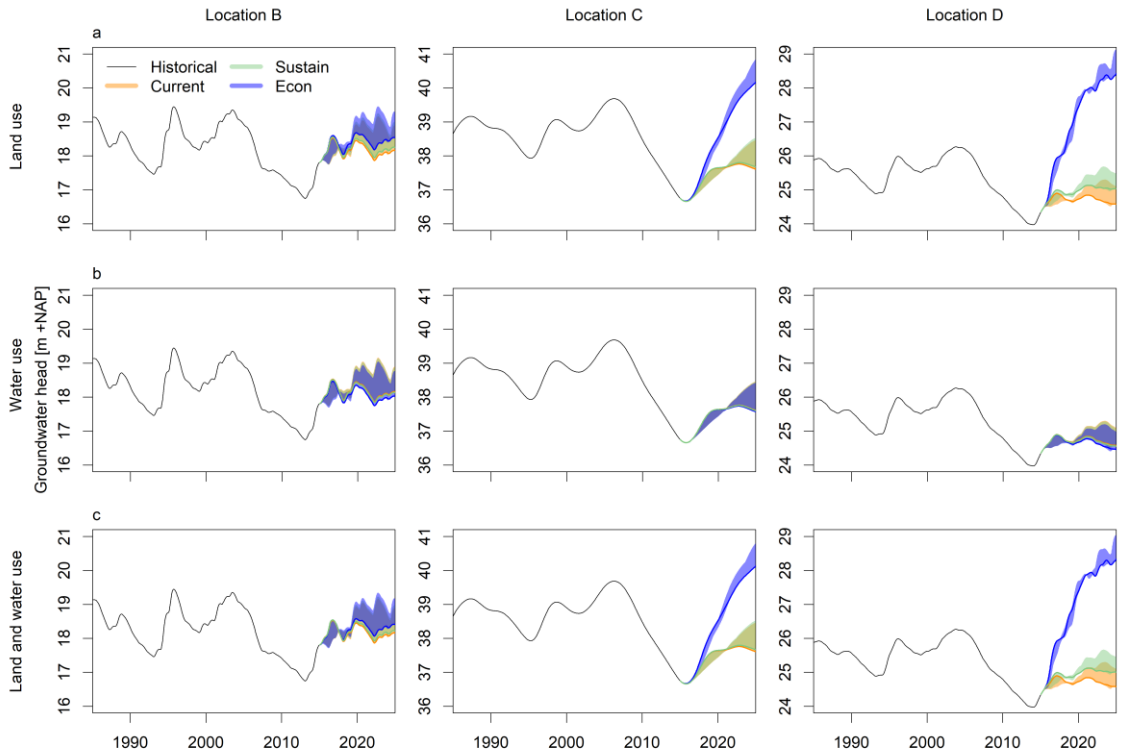

Figure 98 Groundwater heads for locations B, C and D for, a) land use scenarios (current land use, Sustainability eventually, Economy first), b) water use scenarios, and c) land and water use combined scenarios. 'Historical' refers to the reference period. The colour range indicates the range resulting from the different climate ensemble members, the lines show groundwater levels from the intermediate ensemble member.

Effect of water use changes

The applied increases to the groundwater abstractions for the sustain scenario have limited effect on the groundwater levels (Figure 95j-l). The changes in groundwater head are comparable to the changes of the reference situation. In the econ scenario, decreases in groundwater levels at the locations of the abstractions (Figure 91) are found (Figure 95m-o). Especially at the borders of the Veluwe the decrease in groundwater level due to the increase in abstractions is clear.

Compared to the effect of the changes in climate and land use, the changes in water use have a small effect on the groundwater heads at the selected locations (Figure 98b). Location B and D are close to groundwater abstraction wells and have the largest decrease. The groundwater heads decrease about 0.12 m for the econ scenario compared to the reference situation at the end of the near future period for all ensemble members. At location C, situated further away from abstractions, this difference is about 0.04 m at the end of the near future period. No influence of the changes in water use is found at locations A and E.

Effect of combined land use and water use changes

For the combined changes in land use and water use following the sustain scenario, differences in groundwater heads across the Veluwe (Figure 95p-r) are very similar to the differences from land use change only. The differences in groundwater heads for the econ scenario (Figure 95s-u) show a similar pattern as well, however, the effect of the increased abstractions is also visible, especially further away from regions where land use change are applied. Land use changes and water use changes had a contrasting influence

on the groundwater heads, leading to a smaller decrease in groundwater heads near abstractions that are close to regions where land use change occurred (e.g. southeastern part of the Veluwe).

The combined effects of the changes are dependent on the location within the Veluwe. No influence was found for the land use and water use changes at locations A and E, hence, the combined scenarios also do not affect these locations. At the remaining locations the influence of land use changes dominates the effect of water use changes. The increases in groundwater heads caused by land use change become smaller due to the increased abstractions (Figure 98c). At location D groundwater head increases 3.76 m by the end of the near future period for the combined econ scenario; for the econ scenario with land use change only the increase was 3.85 m. The increase in groundwater head at location B is 0.26 m for the combined econ scenario compared to 0.38 m for land use change only.

To compare the effects of changes in climate, land use and water use, we calculated the variance in simulated groundwater levels across different ensembles (Figure 99), e.g. only changes in climate, only land use changes, only water use changes and the influence on the total variance of all combined (total). The variance in groundwater head was calculated separately for the different combinations. For climate only this means the dry, intermediate and wet members with the reference situation, for land use only this means the current, sustain and econ land use scenarios with current water use for the intermediate climate member and for water use only this means the current, sustain and econ water use scenario with current land use for the intermediate climate member. The resulting variances in groundwater head give an indication of the changes with the most impact at the five selected locations. The interaction between the effects is reflected by the influence on the total variance (total). At all locations the total variance is smaller than the variance for the ensembles, therefore, the influence on the total variance (total) is negative (Figure 99).

At locations further away from the regions with applied changes in land use the effect of climate is larger than the land use and water use changes (Figure 99, location A, B and E). The range in groundwater heads between the different climate ensemble members is larger than the differences between the land use and water use scenarios. The low-lying agricultural areas surrounding the Veluwe reacted differently to the climate ensemble members (Figure 96, location A and E), but groundwater heads were identical for the land use and water use scenarios. For all locations, the influence of changes in water use was smaller than the other influences. Only at location B, the effect of water use changes is visible. In the regions where land use changes were applied, these changes dominated the effects on the groundwater heads (Figure 99, location C and D).

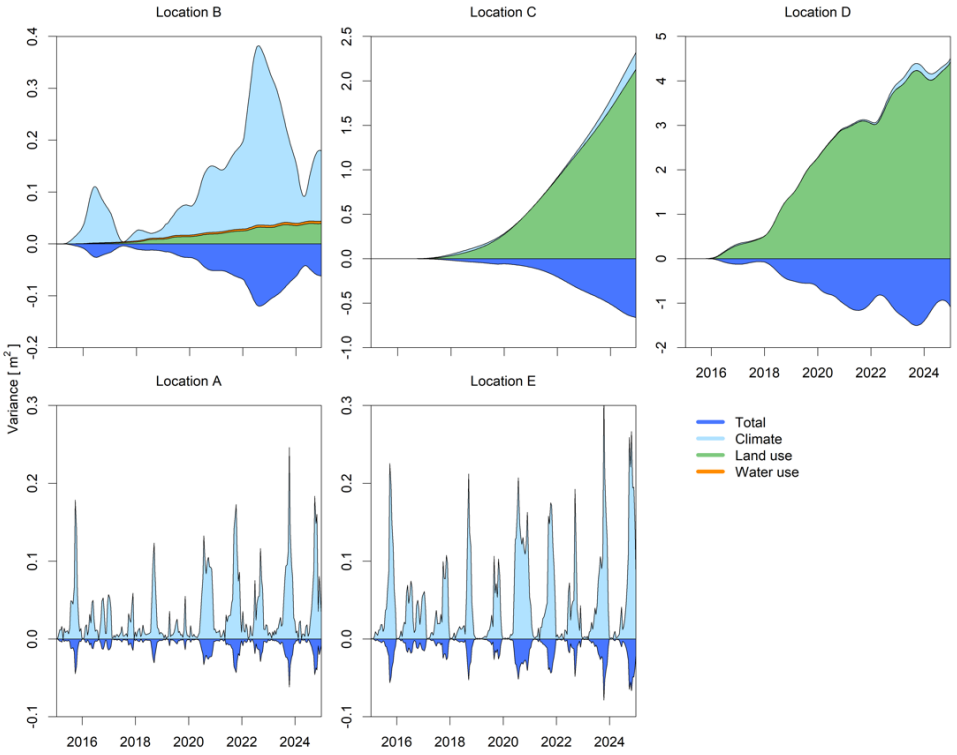

Figure 99 Relative importance of the future changes expressed in variance of the simulated groundwater heads for different combinations of model simulations (Climate: changes in climate only, Land use: land use scenarios only with intermediate climate member, Water use: water use scenarios only with intermediate climate member). Total reflects the influence on the total variance of all model simulations (total variance is smaller than the sum of the separate variances, which leads to negative values for the influence).

5.3. Discussion

The centre of the Veluwe area has a large unsaturated zone and a large drainage resistance due to the large distance to low lying drainage areas. This leads to a slow response of the system and the groundwater levels do not show any intra-annual variability. Here the effects of climate, land use and water use changes for the near future (2015-2024) on water resources were studied with a groundwater model.

Most parts of the Veluwe showed a decrease in mean groundwater level for all three ensemble members. The last part of the reference period (2005-2014) was relatively dry and caused a sharp decline in groundwater levels. The groundwater levels did not recover completely during the near future period, especially in the highest parts of the Veluwe. Therefore, mean groundwater levels in those areas decreased in the near future, even though groundwater levels at specific locations increased during the near future period.

The response of the elevated parts of the Veluwe to the three ensemble members (dry, intermediate, wet) was fairly similar, except for an increase in groundwater levels in some regions in the dry ensemble member. All ensemble members showed a similar interannual variability, whereby wet and dry years alternated between the ensemble members. In order to see the long-term effect of climate change on the Veluwe, the model simulations have to be expanded towards the far future. The low-lying agricultural regions next to the Veluwe did show a difference in response between the ensemble members with decreases in groundwater levels for the dry ensemble member that did not occur for the wet ensemble member. In contrast to the elevated areas, these low-lying regions are thus prone to water shortages, especially in summer. The different response to climate change of the low-lying regions is presumably mainly caused by the effect of

shallow groundwater levels, which enables capillary supply of groundwater to the root zone in dry periods. Next, differences in soil type (usually a higher water holding capacity in the discharge area) may play an important role.

At some of the five selected locations (located at higher elevations) and parts of the elevated areas, the dry ensemble member gave higher groundwater levels by the end of the near future than the other ensemble members. The uncertainty in potential and actual evapotranspiration and the distribution of the precipitation over the year could be an explanation for these results. When soil moisture is limited, the soil will not be able to deliver enough water to meet the demands of the higher potential evapotranspiration in the dry ensemble member. This phenomenon especially occurs in the elevated sandy regions. In combination with higher winter precipitation, this reduction in evapotranspiration will lead to higher recharge compared to the other ensemble members.

In contrast to changes in climate, the changes in land use in the Economy First scenario had a large effect on the groundwater heads across the southern part of the Veluwe. Groundwater levels increased due to reduced evapotranspiration and the associated increase in recharge. This increase in recharge could be almost three times the original amount (Verhagen et al. 2014). This large increase could partly explain why the change in land use was already visible in the groundwater levels after one year in spite of the deep groundwater levels. Another reason is the change in response time due to the change in land use. Recharge water will reach the groundwater earlier under open sands than forests. The groundwater system has to be considered in a two-dimensional way and lateral flow has to be included to understand the effect of the land use changes. The groundwater will not only be replenished through transport in the unsaturated zone, but will also be affected by lateral water transport through the saturated zone (Verhagen et al. 2014). When fast-responding areas (e.g. thin unsaturated zone, heather or open sands) exist in the proximity, the groundwater levels under the thick unsaturated zone can reflect the signal from these areas through the lateral flow. So by creating more fast responding areas (i.e. more recharge), the groundwater shows a faster response across the system. However, the role of the thick unsaturated zone in the Veluwe area and the response time of the measured groundwater levels are still not completely understood and uncertainties remain.

Over a large region of the Veluwe and the surrounding low-lying agricultural areas, the impact of changes in climate dominates the response of the groundwater level. These regions could therefore be vulnerable for water shortages. In regions closer to areas where land use changes were applied, the effect of the land use changes determines the future changes. Groundwater levels increased over these regions, which could alleviate the effects of dry spells on groundwater dependent nature. On the other hand, though, these increased groundwater levels could lead to inundation in the urban areas at the fringe of the Veluwe. Redistribution of groundwater abstractions, both in space and time, could potentially prevent this inundation. The impact of water use changes was limited compared to the land use changes and mainly concentrated to regions around the groundwater abstraction wells. However, in these regions groundwater levels decreased, especially when no land use changes were applied. Therefore, increasing abstractions could damage nature areas at the fringe of the Veluwe and reduce agricultural productivity in surrounding agricultural areas. The possible contrasting impacts of the changes show the complexity of the groundwater system at the Veluwe.

5.4. Bibliography

De Lange, W. and W. Borren (2014). Grondwatermodel AZURE versie 1.0. Actueel instrumentarium voor de Zuiderzee Regio, Deltares.

Harbaugh, A. W. (2005). MODFLOW-2005, the U.S. Geological Survey modular ground-water model -- the Ground-Water Flow Process. U.S. Geological Survey Techniques and Methods 6-A16.

Hazeu, G. W., A. K. Bregt, A. J. W. de Wit and J. G. P. W. Clevers (2011). "A Dutch multi-date land use database: Identification of real and methodological changes." International Journal of Applied Earth Observation and Geoinformation **13**(4): 682-689.

KNMI (2014). KNMI'14 climate scenarios for the Netherlands; A guide for professionals in climate adaption. De Bilt, The Netherlands, KNMI.

Makkink, G. F. (1957). "Testing the Penman formula by means of lysimeters." J. Inst. of Water Eng. **11**: 277-288.

van Walsum, P. E. V. and P. Groenendijk (2008). "Quasi steady-state simulation of the unsaturated zone in groundwater modeling of lowland regions." Vadose Zone Journal **7**(2): 769-781.

van Walsum, P. E. V., A. A. Veldhuizen and P. Groenendijk (2010). SIMGRO 7.1. 0, Theory and model implementation. Wageningen, Alterra. **913**.

Verhagen, F., T. Spek, F. Witte, B. Voortman, E. J. Moors, E. P. Querner and G. A. P. H. van den Eertwegh (2014). "Expertdialoog de Veluwe. Begrijpen we het watersysteem?" Stromingen: vakblad voor hydrologen **20**(3): 5-19.

Vernes, R. W. and T. H. M. Van Doorn (2005). Van Gidslaag naar Hydrogeologische Eenheid TNO. Utrecht, TNO.

Weedon, G. P., G. Balsamo, N. Bellouin, S. Gomes, M. J. Best and P. Viterbo (2014). "The WFDEI meteorological forcing data set: WATCH Forcing Data methodology applied to ERA-Interim reanalysis data." Water Resources Research **50**(9): 7505-7514.

Witte, J. P. M., J. Runhaar, R. van Ek, D. C. J. Van Der Hoek, R. P. Bartholomeus, O. Batelaan, P. M. Van Bodegom, M. J. Wassen and S. E. A. T. M. van der Zee (2012). "An ecohydrological sketch of climate change impacts on water and natural ecosystems for the Netherlands: bridging the gap between science and society." Hydrology and Earth System Sciences **16**(11): 3945-3957.

6. Norway

Model frameworks

The objectives of BINGO for the city of Bergen, Norway, are twofold. These are: 1) assessing future water availability for drinking water supply, and 2) assessing future changes in stormwater and impacts on receiving water bodies. For this reason, two modeling frameworks are used.

- Framework 1: The HBV-model for modelling of inflow to the main water reservoirs providing drinking water in Bergen (sections 6.1 – 6.4)
- Framework 2: The SWMM-model for modelling of the hydrology and urban stormwater system in the Damsgård area of Bergen (sections 6.5 – 6.8)

6.1. Model objectives in BINGO [Reservoirs]

The city of Bergen is supplied with drinking water from an interconnected network of surface reservoirs located within, and close to, the city. Due to high annual rainfall amounts, water scarcity is rarely a concern. However, the awareness of supply capacity problems was raised during a drought incident during the winter of 2009/2010. Supply capacity problems occur when water availability does not correspond with the city's water demand. Over the past years, the city's water consumption has been heavily reduced due to reduction of leakages in the distribution system (Bergen Kommune, 2015), but the risk of lowered water availability remains to be further investigated in light of climate change induced shifts in temperature and precipitation patterns.

To pursue this, an HBV-model (**H**ydrologiska **B**yråns **V**attenavdelning; Bergström (1976)) for each catchment contributing to the drinking water reservoirs of Bergen is set-up and calibrated (Kristvik and Riisnes, 2015). The HBV-model is a conceptual-based, deterministic rainfall-runoff model. Within the BINGO project, the model is used to simulate the hydrological response, in terms of inflow to the drinking water reservoirs in Bergen, to scenarios of temperature, precipitation and evapotranspiration. Inflow estimation is further used in a reservoir storage balance in order to assess total water availability for the city.

For further information on catchment descriptions, specific modelling objectives within the HBV-framework and detailed model description, the reader is referred to BINGO Deliverable 3.1 'Characterization of the catchments and water systems and BINGO Deliverable 3.3 'Calibrated water resources models for past conditions', respectively.

6.2. Model application

The HBV-model used in this study is a dynamic excel-model, consisting of several linked files and pre-programmed macros for running analyses. The user adds inputs in designated input files, makes sure all links are updated and run the analyses from the main model file. Computational time for a 10-year period is <10 minutes. Therefore, all decadal members (FUB1-FUB10) for the period 2015-2024 have been applied.

Water availability is further investigated in a simple storage balance:

$$S_t = \begin{cases} (S_{t-1} + \frac{Q_t + Q_{t-1}}{2} - W & if\ S_t < S_{max} \\ S_{max} & if\ S_t \geq S_{max} \end{cases}$$

Where S is storage, Q is inflow and W is withdrawal. The balance is set up as a one-reservoir balance because the reservoirs are interconnected trough transfer tunnels. The total storage capacity, S_{max}, in Bergen is 26480246 m3.

Scenarios for future water use are incorporated in the withdrawal part, W, of the water balance. Withdrawal is estimated based on the equation:

$$W = (1 + a)C_{sp}P$$

Where a is the leakage rate of the distribution network, C_{sp} is specific consumption related to the real consumption (domestic, industrial and other) and P is the number of supplied people (Kristvik et al. 2018).

6.2.1. Data

Decadal predictions

Required input data to the HBV-model is temperature, precipitation and potential evapotranspiration (PET) at a daily time step. Figure 100 displays the projected monthly precipitation for Bergen by FUB. The projections are compared to climatology of two normal periods: 1) the official normal period 1961-1990 provided by the Norwegian Meteorological Institute, and 2) computed normals for the 30-year period that is closest to the starting point of projections. There is a clear increase in monthly normals, which is also reflected the projections. The projections are in agreement with seasonal patterns of both normal periods, but in closer fit with the 1985-2015 precipitation amounts.

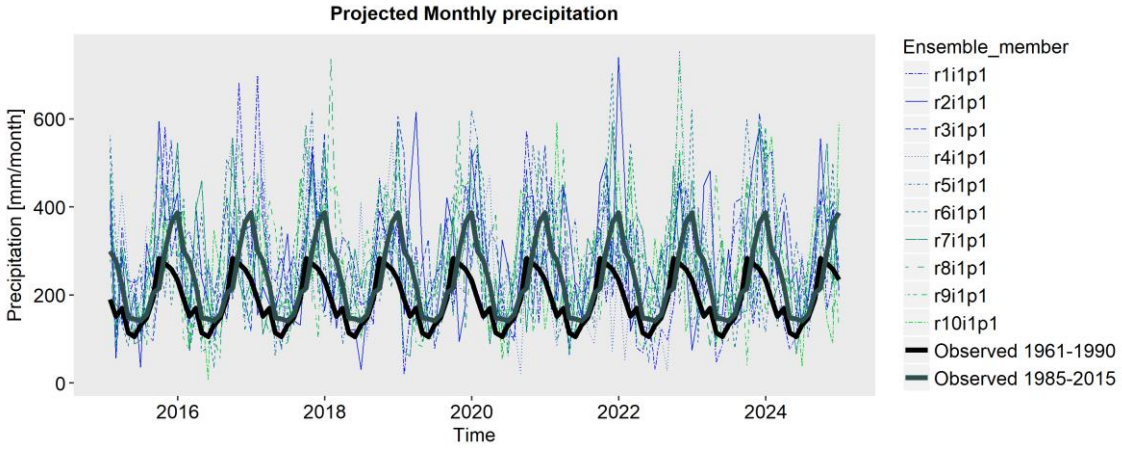

Figure 100: Visualization of the 10 ensemble members (r1i1p1 – r10i1p1) compared to observed climatology (mean monthly precipitation for period 1961-1990 ans 1985-2015).

Monthly change factors for all 10 decadal members are shown in Figure 101. The change factors indicate steady conditions the next ten years for months April-October (change factors ~1). For some months, however, a wide range is projected. In January change factors between 4 and 6 can be seen for several scenarios, as well as negative change factors indicating decreased temperatures.

The temperature projections are further used to estimate the last input variable required by the HBV-model, PET. In this study, PET has been estimated by the Thornthwaite method where only temperature is required as input (Thornthwaite, 1948).

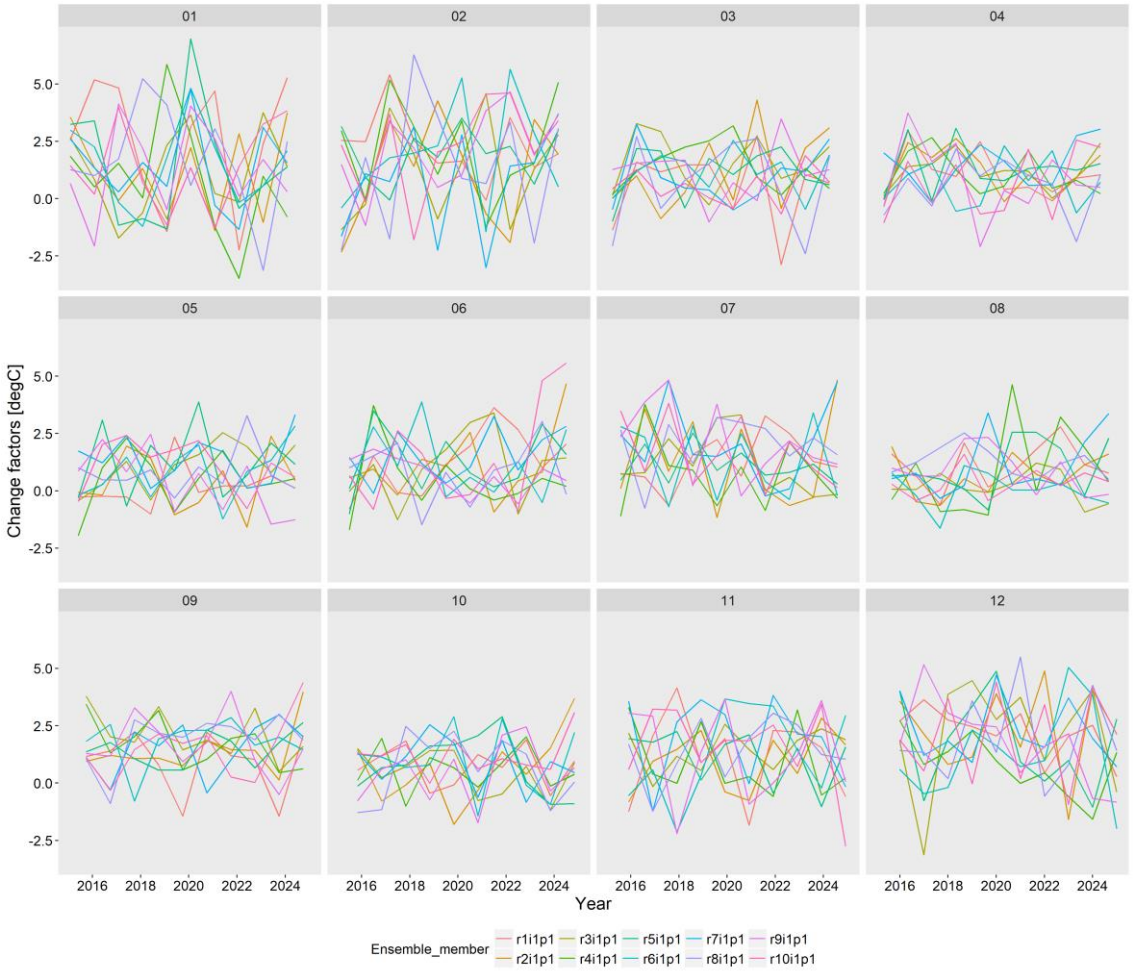

Figure 101: Monthly temperature change factors based on FUB1-FUB10 ensemble members and adjusted for temperature normals from observational period 1961-1990.

Water use scenarios

Two water use scenarios were developed in BINGO deliverable D3.2 "Future Land and Water Use Scenarios". For the Bergen case, these are trends of population growth that will lead to higher water consumptions in a moderate scenario (sustainability eventually) and a high scenario (Economy first).

Furthermore, the leakages of the distribution network in Bergen have historically been high (31 % of total production in 2014). The municipality has a goal to reduce this to 20 % by 2024. This is included in the water use scenarios along with the case where no leakage reduction is obtained by 2024. To summarize, this results in two main water use scenarios:

- Best case: Moderate population growth and 20 % leakages in 2024
- Worst case: High population growth and 31 % leakages in 2024

6.2.2. Results

The results of the inflow projections are summarized in Figure 102 and Figure 103. On average, a general increase in inflow is found, with a few exceptions. Figure 103, in particular, shows this. E.g. for months July-

September it can be seen that the minimum mean monthly inflow is for some ensemble members negative, but the high mean and max of ensemble members indicate that a general increase.

Figure 104 renders the final results of the analyses by showing the behavior of the storage volume to the worst case water use scenario. Overall, the storage stays steady on its maximum level, with occasional drops. The minimum storage volume found in the time series is 24444639 m3 (FUB7). This amounts ~92% of the maximum capacity. The municipality has a policy of always have available a reserve volume corresponding to 50 days of consumption, i.e., never to withdraw an amount of water that causes the storage level to fall below this limit. The 50 days of consumption limit correspond to approximately 5.5 mill. m^3 with the present population size. The minimum storage volume found in the timeseries is approximately 4.5 times higher than this lower storage reserves limit.

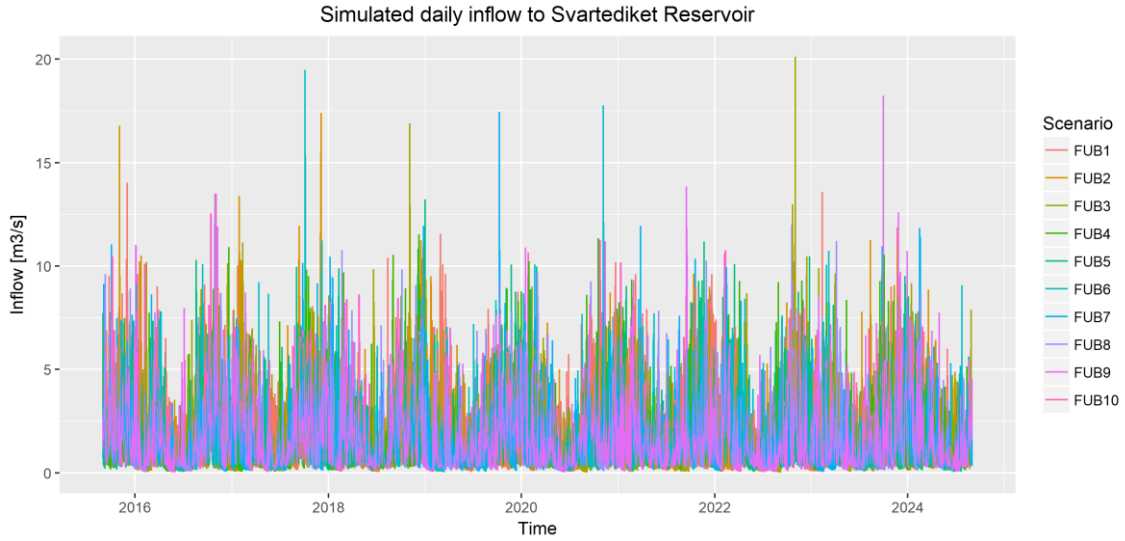

Figure 102: Simulated daily inflow to Svartediket reservoir

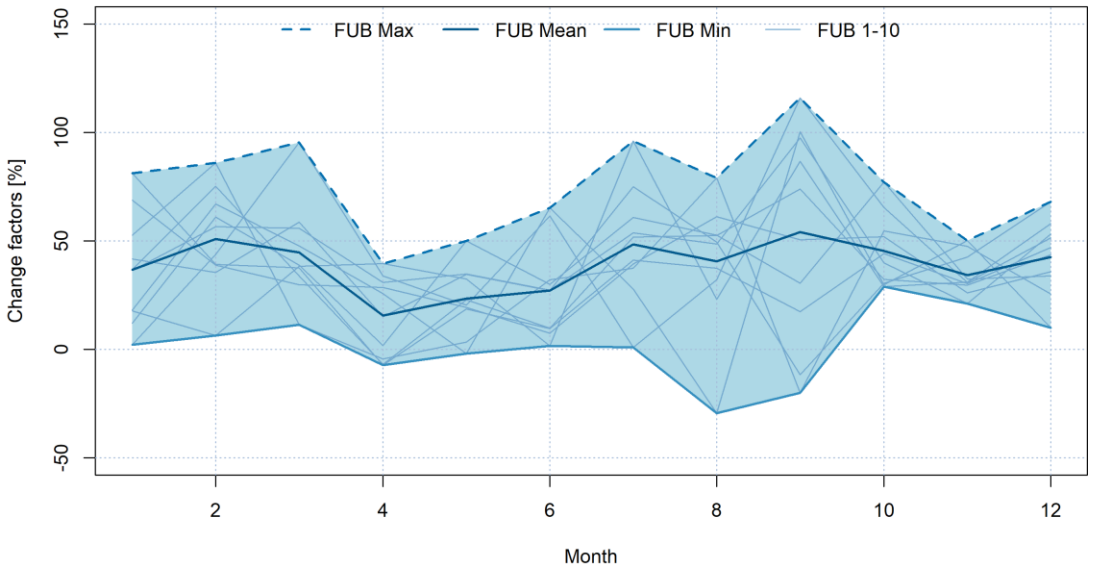

Figure 103: Computed change factors for monthly mean inflow to Svartediket reservoir based on observed inflow 1980-2009 (Kristvik et al. 2018) and FUB1-FUB10 scenarios for period 2015-2024.

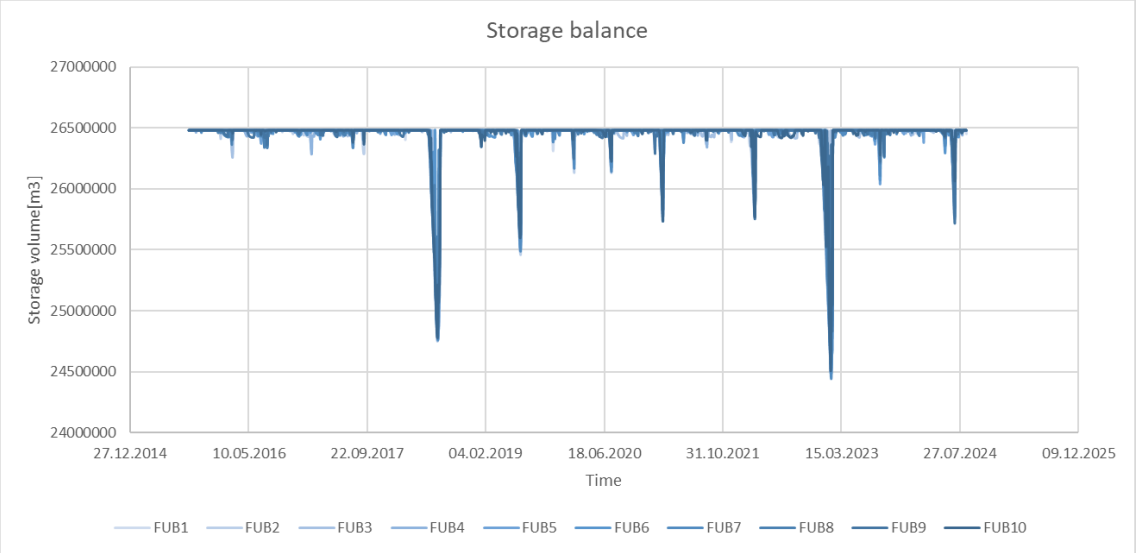

Figure 104: Computed storage levels for 'worst case' scenario with high population growth (Economy first) and no leakage reduction.

6.3. Discussion

The results of these analyses suggest that water supply in Bergen is well covered in the municipality´s current planning period (2015-2024), as the projected increase in inflow compensate for the explored scenarios with increases in water consumptions. Water availability studies in Bergen was initiated due to the winter drought 2009/2010. Since then, one of the reservoirs have been upgraded resulting in a larger storage capacity. This measure itself has provided the municipality with a much more reliable water supply.

6.4. Bibliography

Bergen Municipality 2015 Hovedplan for vannforsyning 2015-2024 (Strategic plan for water supply 2015-2024), Bergen. Available at: https://www.bergen.kommune.no/omkommunen/avdelinger/vannog-avlopsetaten/9081/article-129478.

Bergström, S. (1976) Development and application of a conceptual runoff model for Scandinavian catchments, SMHI Report RHO 7, Norrköping, 134 pp.

Kristvik, E., Muthanna, T.M. and Alfredsen, K., 2018. Assessment of future water availability under climate change, considering scenarios for population growth and ageing infrastructure. *Journal of Water and Climate Change*, p.jwc2018096.

Thornthwaite, C.W., 1948. An approach toward a rational classification of climate. *Geographical review*, *38*(1), pp.55-94.

6.5. Model objectives in BINGO [Stormwater]

Stormwater in the Damsgård area of Bergen is collected and transported with a combined sewer system causing frequent floodings and combined sewer overflows (CSOs) to the subjacent fjord, Puddefjorden. The area has previously been dominated by industrial activities along the water front, but is undergoing a large scale transformation where the industrial areas are being rezoned to urban residential purposes. As part of the large-scale transformation the sewer system will be upgraded in order to protect the environment and improve and facilitate conditions suitable for leisure activities along the water.

The modeling objectives in BINGO are to support the planning of an upgraded sewer system in the Damsgård area and find sustainable measures for storm water management that reduce the risks posed by a changing climate. . Problems caused by flooding are few in the Damsgård area, compared to risks posed by frequent CSOs. Thus, the main objective of the municipality in Bergen is to reduce CSOs. Consequently, this report focuses on the impacts of climate change scenarios on CSOs in the area.

For this, a SWMM model has been set up and calibrated for the respective area. Detailed descriptions of the Damsgård area and development of the model framework can be found in BINGO Deliverable 3.1 'Characterization of the catchments and water systems and BINGO Deliverable 3.3 'Calibrated water resources models for past conditions', respectively.

6.6. Model application

Auto-calibration

Auto-calibration of the combined sewer system's model has been one of the tasks D3.3 outlined in order to improve the performance of the model presented previously. Accordingly, the Shuffled Complex Evolution (SCE-UA) algorithm (Duan et al. 1992) was employed with the Nash-Sutcliffe efficiency (Nash and Sutcliffe 1970) set as objective function. The auto-calibration procedure further incorporated a parameter-regionalization procedure such that the parameters: (i) exhibit a physiography-based variability among the sub catchments, and (ii) be easily transferrable to ungauged sub catchments. The implemented procedure calibrated a transfer-function for selected parameters, which Choi and Ball (2002) categorize as inferred parameters, instead of direct calibration. Table 1 highlights the regionalized parameters and the associated physiographic variables. For detailed description of the regionalization approach, please refer Mittet (2017).

Model execution

In order to automate the calibration and execution of the model, scripts written in the R language (R Core Team 2013) were used and SWMM was run as a console application from the command line. Table 20 provides overview of the materials and tools used. There were some difficulties to carry out continuous high-temporal-resolution simulation of the system due to the size of the combined system (please refer to Table 21 for summary of the system). In order to overcome the challenges, the flow-generation-processes and the hydraulics were simulated independently. First, the runoff or sewer generated from each watershed/sewer shed was computed. Subsequently, the computed flows were specified as inflows at the corresponding receiving node and the time series were provided as external files. These enabled overcoming two main challenges: (i) the limit on the output file size that stores the results (<2GB), and (ii) the computation time. However, the limit on the number of external files that could be opened at a time was the challenge that arose from providing the time series as external file. Overcoming this challenge necessitated recompiling

the SWMM source code by setting a number higher than 512 to the number of files that could be opened at a time.

Scenarios

The simulations covered the period from 2004 to the end of the decadal prediction and was performed for all 10 decadal members. Thus, for comparison, the model was run with 10 years of observed climate and 10 years of projected climate (FUB). There is no evidence or indications towards a change in land use of the Damsgård area for the municipality´s current planning period (2015-2024) and the land use scenarios outlined in BINGO deliverable D3.2 "Future Land and Water Use Scenarios" are considered more unrealistic now than they were at the time they were developed. Due to this, and the high computation effort required to re-run all 10 decadal members for different land use scenarios, only current land use is simulated.

Table 20: Overview of the regionalised parameters and the associated physiographic variables

Parameters	Transfer functions
%Imperviousness	f(Fraction of impervious area)
Width	f(Total Area, Distance to the outlet)
Depression storage (Impervious)	f(Median slope – subcatchment cells)
Depression storage (Pervious)	f(Median slope – subcatchment cells)

Table 21: Summary of the system

Subcatchments (No.)	1705
Total Area (km^2)	13.4
Pipes length (km)	141.0
Pipes (No.)	5450
Manholes (No)	5450
Pumping stations (No.)	8
Weirs (No.)	29

6.6.1. Data

The SWMM model runs with continuous series of precipitation at a 5 minute interval as input. The decadal predictions are available at daily time step and has been disintegrated to the required interval using a K-nearest neighbor (KNN) approach as described in Sharif and Burn (2007).

6.6.2. Results

Running the SWMM model with all 10 decadal members resulted in a large dataset containing 10x10 (Ensemble members x years 2015-2024) years of data. In the following sections the discharge at outfall nodes (CSOs) are analyzed. Figure 105 presents the distribution of the 10x10 annual discharges simulated at 9 outlets. The figure shows a large spread in annual discharge from node to node. It is also visually clear which nodes that are discharging the highest amounts of polluted water to the fjord. Node #6 clearly stands out as the most contributing node, followed by node #7 and #3. Figure 105 is also accompanied by Table 22, which renders the a few statistics of the distributions for these nodes. In general, it is observed a high increase in average annual discharge (ranging from 34-49 %) and maximum discharge (29-57 %).

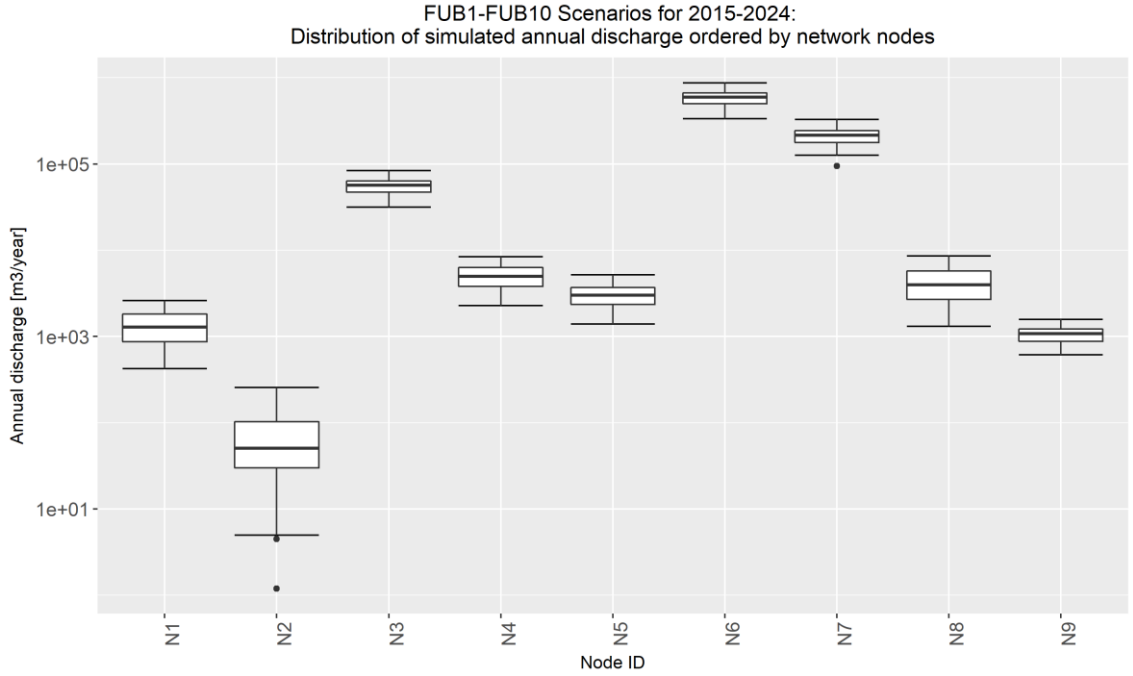

Figure 105: Distribution of simulated annual discharge to fjord for 9 outfall nodes of the network, represented in boxplots.

Table 22: Summary statistics for selected nodes.

	Observed (2004-2015)			Future FUB (2015-2024)				
Node	**Min [M3/y]**	**Average [M3/y]**	**Max [M3/y]**	**Min [M3/y]**	**Average [M3/y]**	**Max [M3/y]**	**ΔAvg [M3/y]**	**ΔMax [M3/y]**
#6	268804	438418	607822	333954	586055	869855	34 %	43 %
#7	79944	142695	218059	94284	213287	328505	49 %	51 %
#	24627	41486	58167	31540	56111	83938	35 %	44 %

Similar trends of the outfall nodes can be found in Figure 106, which shows the distribution of annual number of events. Node #6 and #7 are, in addition to discharging the most (Figure 105), also the nodes with the highest annual numbers of events. Interestingly, a higher number of events is simulated for Node #9, than Node #3 (the third most discharging node). The fact that the annual discharge of Node #9 is noticeably lower than Node #3, indicates that, in comparison of the two, Node #3 also discharges with a higher intensity (more discharge per event). For all nodes, an increase in number of events is detected in the FUB scenarios when compared to the control period.

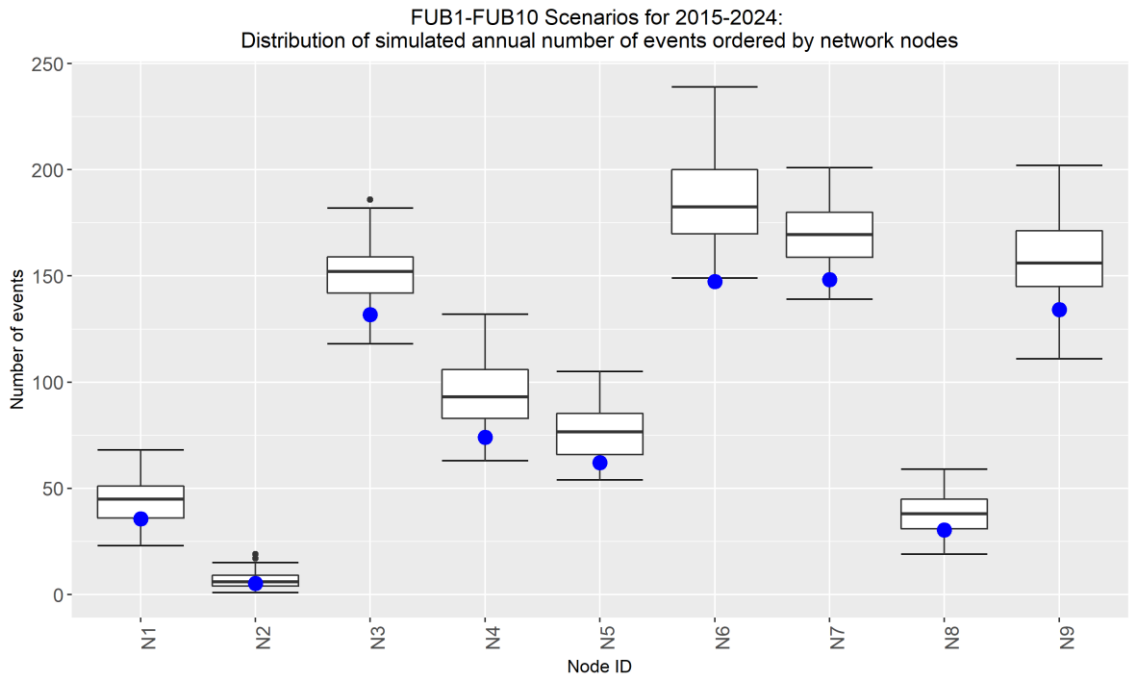

Figure 106: Distribution of annual number of events order by 9 outfall nodes of the network. The blue dots correspond to the 2004-2015 annual average for the respective nodes.

The cumulative discharge for nodes #3, #6 and #7 for all 10 ensemble members are plotted in Figure 107 along with the cumulative discharge in the reference period 2004-2015. There are large differences in the projected accumulated discharge over the ten year scenario period between the nodes, where the

cumulative discharge for node #6 is almost three times higher than the following node (#7). However, they all show the same trend: a large gap from discharge corresponding to FUB scenarios to simulated historic period. For all nodes ensemble member r2i1p1 (FUB2) results in the highest cumulative discharge and ensemble member r3i1p1 results in the lowest cumulative discharge (of the scenarios).

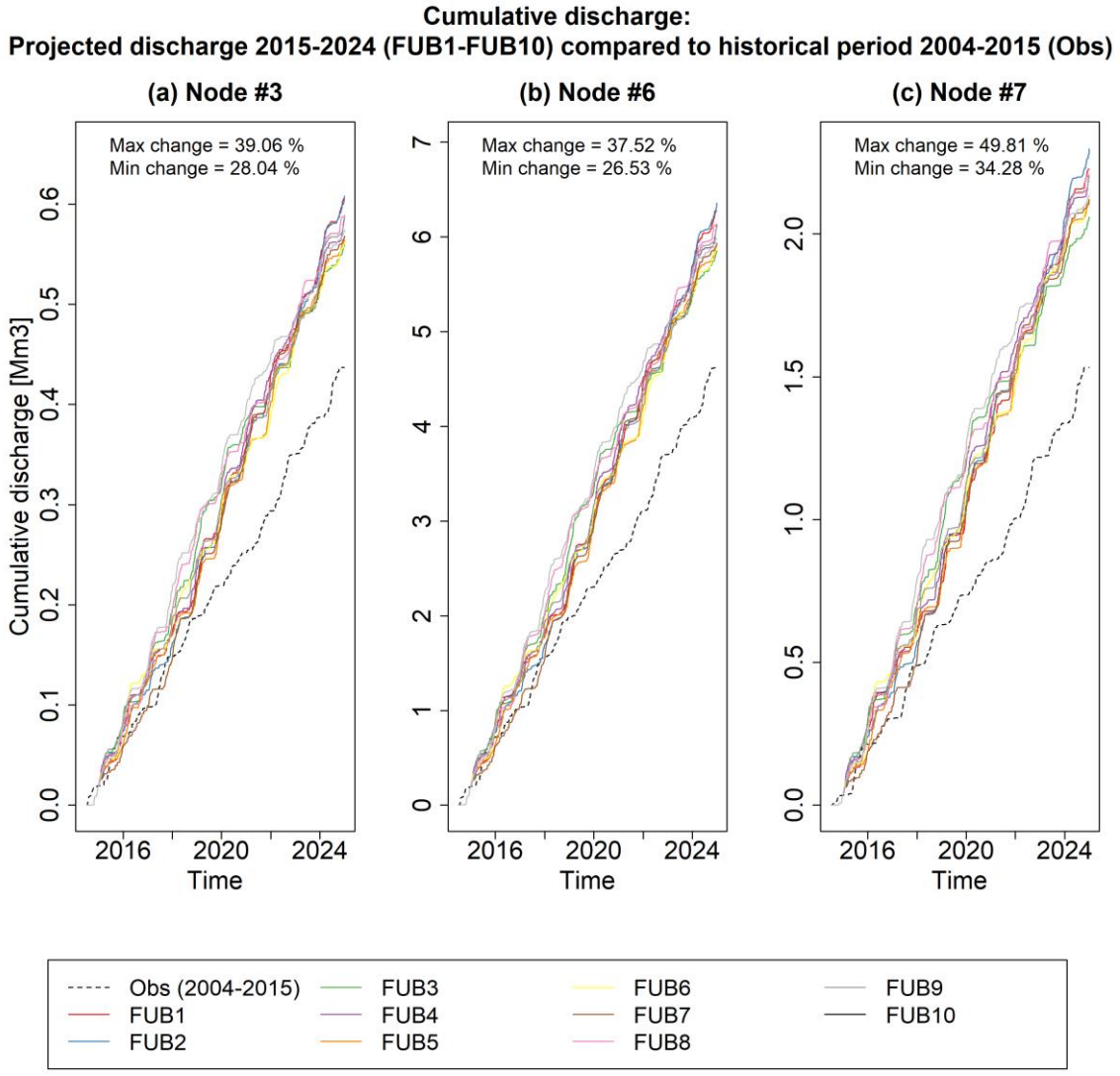

Figure 107: Simulated cumulative discharge for the period 2015-2024 (FUB1-FUB10 scenarios) compared to cumulative discharge for the period 2004-2015 (control period).

Besides the amounts of polluted water discharged to the fjord, the total time a CSO is active is a point of interest to the municipality. The distribution of active time for the 10 ensemble members is plotted on a seasonal basis in Figure 108 for the three most problematic nodes. It is observed that the nodes follow the same seasonal patterns and that these correspond to observed precipitation patterns, where fall and winter are the most intense. All nodes show an overall increase in active hours when comparing control and scenario period. Node #3, which also has the least discharge amount to the fjord, is shown to have less active hours than the other two nodes. Node #6 and #7 show more similar patterns. For a few months (e.g. January and February) Node #6 has less active hours than node #7, while more active hours during summer. Considering the similar characteristics of these two nodes' seasonal patterns of active hours, and the fact

that Node #6 causes substantially more discharge to the fjord, this indicate that the most polluting node in terms of discharge amounts also pollutes with the highest intensity.

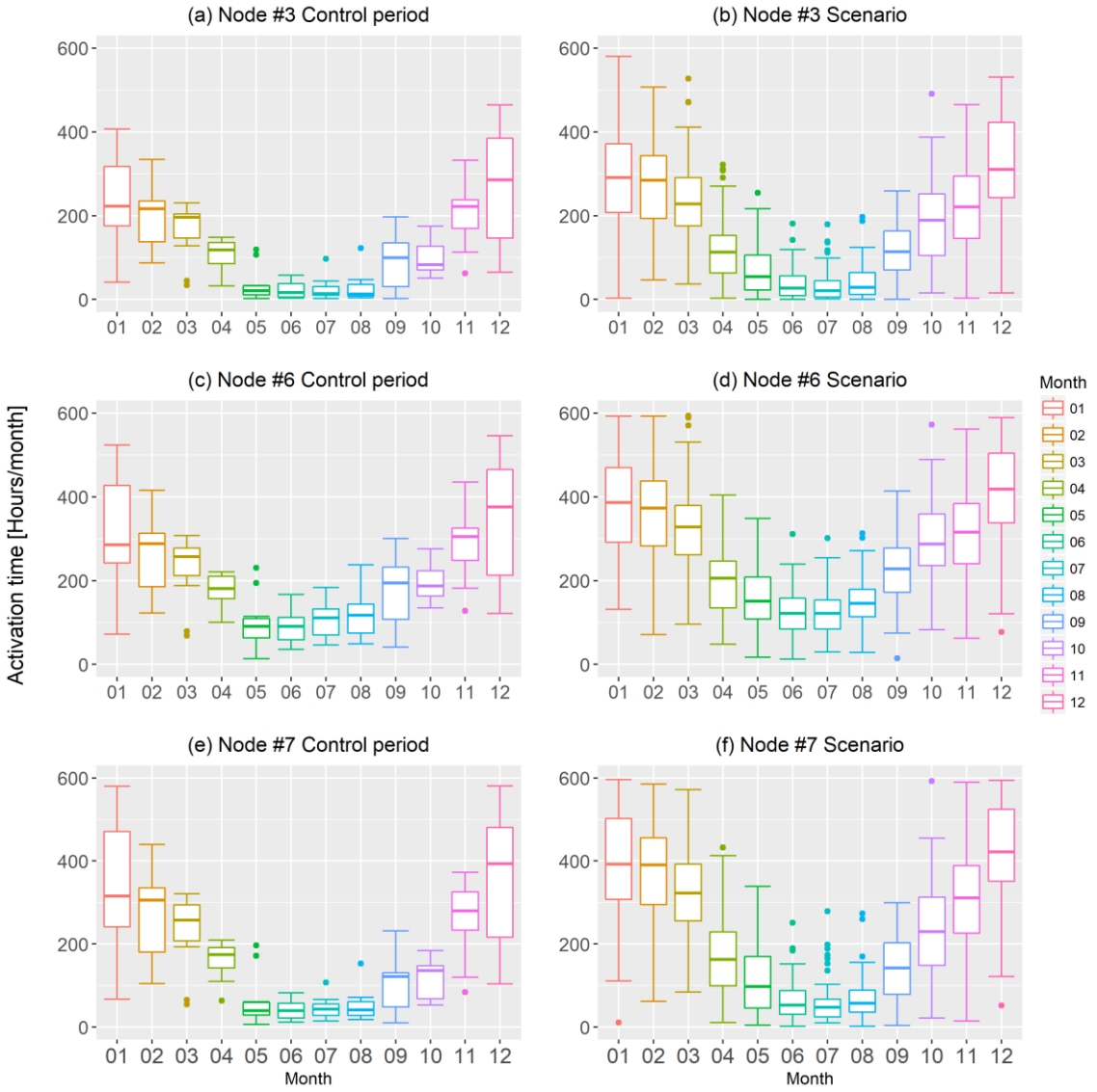

Figure 108: Distribution of monthly activation time for selected nodes, based on control period and FUB1-FUB10 scenarios for period 2015-2024.

6.7. Discussion

In general, these analyses have shown large potential impacts of climate change scenarios at the Damsgård area of Bergen. They have also shown how large-scale simulations with the SWMM network model can help locate problematic parts of the network. The results will be of high value for further work on selecting and prioritizing adaptive measures and for planning the upgraded storm water management. In this study, only CSOs have been investigated, but the framework could also be used to investigate bottlenecks and problematic areas further upstream in the system. In Bergen, however, there are few reports on such problems further upstream and has therefore not been prioritized in this study. Another reason is that in combined systems, the CSOs will activate before water starts ponding upstream, and the CSOs are thus a natural starting point of analyses. One drawback of the model framework is the high computational efforts needed to run the simulations. This is, however, difficult to avoid in such large and complex system requiring such high resolution input data and compensated for by the improved insights resulting from the analyses.

6.8. Bibliography

Choi, K., Ball, J.E. (2002) Parameter estimation for urban runoff modelling. Urban Water, 4(1), pp. 31-41. doi.org/10.1016/S1462-0758(01)00072-3

Duan, Q., Sorooshian, S., Gupta, V. (1992) Effective and efficient global optimization for conceptual rainfall-runoff models. Water Resources Research, 28 (4), pp. 1015-1031. doi: 10.1029/91WR02985

Mittet, J. (2017) A regionalisation technique for urban ungauged catchments. Master Thesis, Department of Civil and Environmental Engineering, NTNU.

Nash, J. E., Sutcliffe, J. V. (1970) River flow forecasting through conceptual models part I — A discussion of principles. Journal of Hydrology, 10 (3), pp. 282–290. doi:10.1016/0022-1694(70)90255-6

R Core Team (2013) R: A language and environment for statistical computing. R Foundation for Statistical Computing, Vienna, Austria. www.R-project.org.

Sharif, M. and Burn, D.H., 2007. Improved k-nearest neighbor weather generating model. Journal of Hydrologic Engineering, 12(1), pp.42-51.

7. Portugal

The Portuguese contribution to the BINGO objectives of testing different systems' vulnerabilities to climate change is fourfold:

1. Test climate change impacts in *estuary* bordering lands where expected sea level rise associated with more frequent storm surges and salt water intrusion are the driving forces;
2. Determine how potential reduction in aquifers recharge and, in coastal lowland areas, possible saltwater intrusion, may reduce the availability of *groundwater* to agricultural uses and water supply;
3. Estimate how vulnerable communities will become to increase *floods* frequency and magnitude in urban areas;
4. Assess how the potential changes in *surface water* flow regimes will jeopardize the current and future planned water uses.

Figure 109. locates geographically these issues and its associated systems.

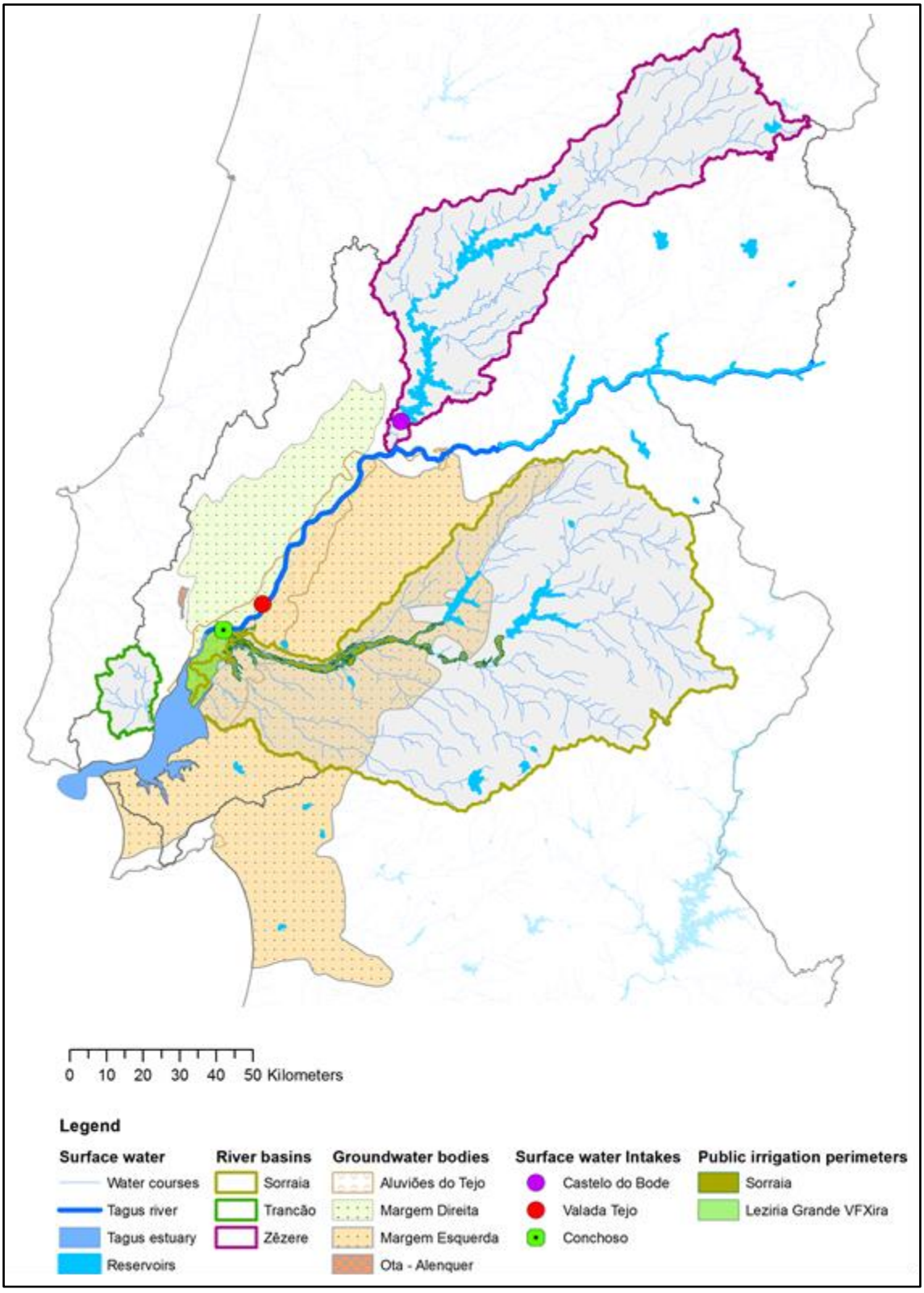

Figure 109. Different systems modeled in the Tagus basin

The developments already achieved in the modelling component of the scientific approach to these questions will be developed throughout the following sub-sections.

7.1. Transitional waters

7.1.1. Model objectives in BINGO [Tagus estuary]

Two main problems in the Tagus estuary are tackled in BINGO: i) the inundation of rich agricultural lands by the combined action of tides and storm surges; and ii) the salt water intrusion in the upper reaches of the estuary where a major water intake for irrigation is located. Both problems can have negative social, economic, and environmental implications, and can potentially be aggravated by climate change (e.g., through sea level rise or reduced river flow).

For each of these two problems, we aim to: i) implement, calibrate and validate appropriate process-based models; iii) use these models to characterize the present conditions, in particular extreme events; and iii) determine how the conditions will change in the near future. The implementation and validation of the models was described in detail in Deliverable 3.3 (Alves et al., 2016). The characterization of present and future conditions is presented below.

With a surface area of about 320 km^2, the Tagus estuary is one of Europe's largest estuaries (Figure 110). A detailed description of this estuary and its margins is presented in a previous report (Deliverable 3.1, Alphen et al., 2016) and will be omitted here for brevity. In order to properly represent all the relevant physical processes, the model domain includes the whole estuary, from the river to the ocean. The simulation of tides, surges and waves further requires regional models covering large parts of the Atlantic Ocean.

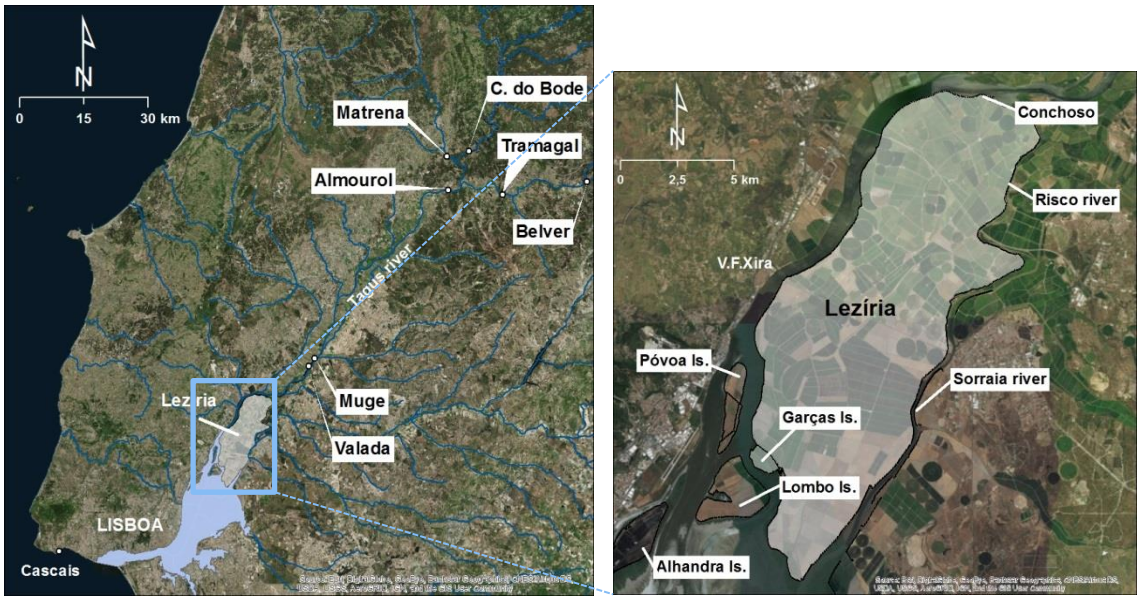

Figure 110. Tagus estuary: general perspective (left) and detail (right) of the study area in the upper estuary (source: background image from ESRI basemap).

7.1.2. Model application

This section describes the modeling approaches followed to analyze the inundation and salinity intrusion in the Tagus estuary. The modeling approaches are described separately for each problem.

Inundation by tides and storm surges

The inundation of the margins of the upper reaches of the Tagus estuary is due to several processes and forcing agents:

- from upstream: the river flow;
- from downstream: storm surges (forced by atmospheric pressure and wind), tides and surface waves.

BINGO focuses on the downstream agents, i.e., on inundations of marine origin. This choice is justified by the strong dependence of the river flow on decisions over the release of water from several Portuguese and Spanish dams. Transfers of water from the Tagus watershed to other watersheds also occur in Spain, thereby reducing the volume of freshwater that reaches the estuary. Hence, the impact of river flow is not assessed in detail, although a sensitivity analysis was performed and is presented in Fortunato et al. (2017).

The water-use and land-use scenarios can affect the water levels and the inundation by changing the river flow. However, since the impact of river flow is not considered, the water-use and land-use scenarios are irrelevant for the extent of the inundated areas and are ignored henceforth.

In order to characterize present extreme events, the major storm surge that hit the Portuguese coast during last century was identified. This storm surge occurred on February 15, 1941, causing extensive inundation and damage in the whole Iberian Peninsula, including in the Tagus estuary (Muir-Wood, 2011; Freitas and Dias, 2013; Freire et al., 2016). Tens of casualties were also reported along the Tagus estuary margins. Two alternative scenarios were considered. The first scenario (*extreme surge scenario*) is the occurrence of a similar storm nowadays, i.e., with the same ocean, atmospheric and meteorological conditions, but for the present bathymetry and mean sea level. A *worst case scenario* was also considered by combining the atmospheric conditions that occurred in February 1941 with an extreme spring tide. The extreme tide was selected as the one that had the highest tidal range in a 20 year period (2001-2020). It occurred on March 1st, 2006, and had a tidal range of 3.6 m at Cascais.

Determining the return period of the water levels associated to these scenarios is not a trivial task. In particular, the return period may vary in space. For instance, southerly winds will generate a set-up in the northern margins of the estuary and a set-down on the opposite margin. As a result, the return period of the water level for the same event may be higher at the northern margin than at the southern margin. In spite of these difficulties, Fortunato et al. (2017) estimated return periods for the two scenarios. The peak river flow had a return period of about 3 years. The storm had a return period probably higher than 65 years. The waves that hit the coast had a return period higher than 100 years. The maximum water levels at the coast had a return period of only 2-20 years because the tidal amplitude corresponded only to the percentile 91 of tidal amplitudes. Considering the extreme tidal amplitude in the *worst case scenario* leads to a return period of the water level at Cascais above 1000 years.

Because the atmospheric simulations available within BINGO do not cover 1941, an alternative source of atmospheric simulations was used: the 20CRv2 reanalysis database (Compo et al., 2011). This database has several members. Here we selected the member for which the atmospheric pressure better matches the observations in the vicinity of the Tagus estuary. Results from this member were then downscaled to the North Atlantic (Fortunato et al., 2017). Results from the atmospheric model were used to force two regional-scale ocean models: the model of Bertin et al. (2013) for waves, and the model of Fortunato et al. (2016) for storm surges. Finally, the atmospheric model and the two ocean models were used to force a model of the Tagus estuary (Figure 111). The Tagus estuary model simulates the water levels due to tides and surges, the waves, and the interactions between them. A detailed description of the model application and validation is given in Deliverable 3.3 (Alves et al., 2016).

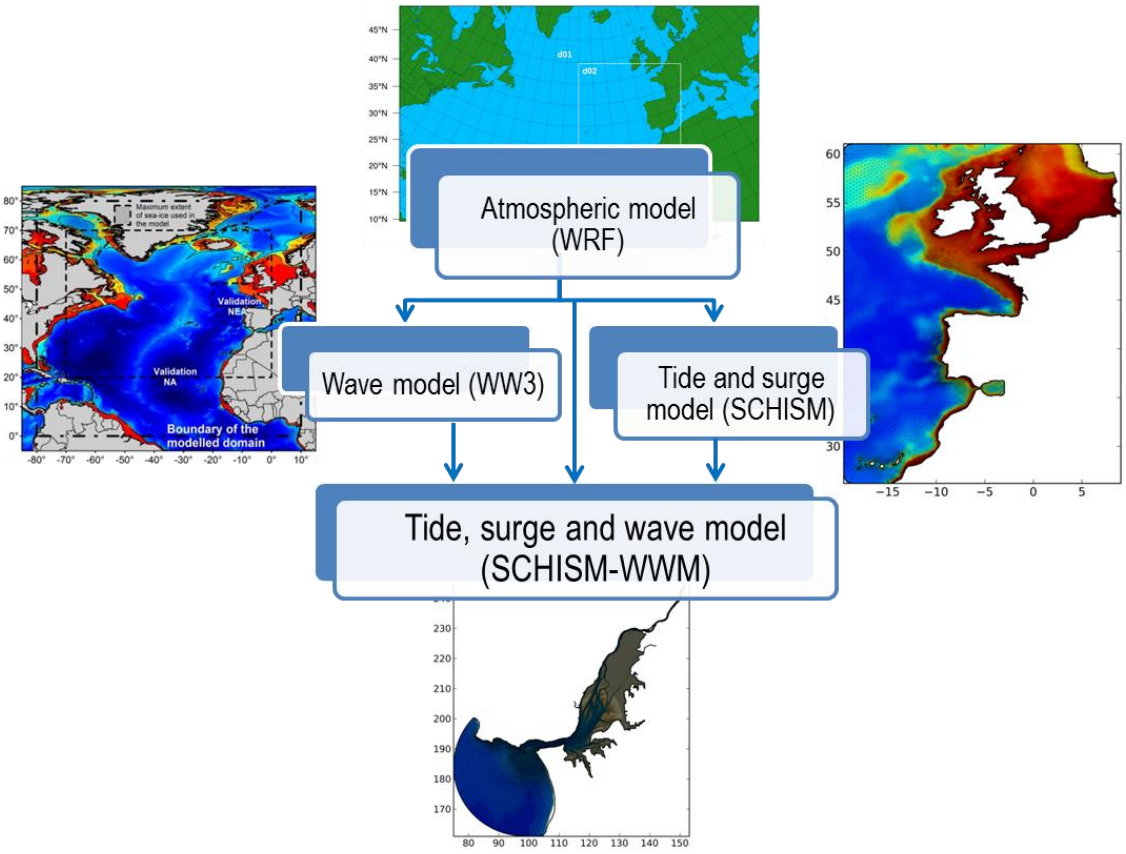

Figure 111. Modeling approach to simulate inundation in the Tagus estuary.

In order to study future conditions, and understand how extreme events can change from the present to the near-future, regional-scale simulations of tides and storm surges were performed. Statistical analyses were then carried out on the results to examine both storm surges alone and total water levels (i.e., due to tides and storm surges).

Two sets of about 40 years were simulated. The first represents “present” conditions (37 years: 1980-2016). The storm surge model is forced by atmospheric reanalyses from ERA-Interim (Dee et al., 2011). When the total sea level is required, tides from the model of Fortunato et al. (2016) are added to the storm surge signal. The second set of simulations represents “near-future” (2021-2024) conditions. In this case, the storm surge model is forced by results from the MiKlip atmospheric decadal predictions. Because there are 10 members in each prediction, there are 40 years of simulations for the 4 year period 2021-2024. Hence, 40 years of simulations were carried out for the near-future. Simulating more years would be computationally too expensive. Furthermore, this number is similar to the number of years of reanalyses available for “present” conditions. It is also sufficient to safely extrapolate extreme value statistics to 100 year return periods.

Given the conclusions of the analysis of the regional-scale sea levels and surges (discussed below), it was deemed unnecessary to pursue the analysis to the local (estuarine) level.

Salinity intrusion

The salinity propagation in the Tagus estuary is mainly controlled by the combined effect of tides and river flow (Rodrigues and Fortunato, 2017). A reduction of the freshwater discharge entering the Tagus estuary, in particular, may lead to a landward intrusion of saltwater that may impact negatively some of the uses and activities in the upstream area of the estuary (e.g. agriculture, water supply). A particular example is the

Lezíria Grande de Vila Franca de Xira Public Irrigation Perimeter (Lezíria Grande PIP), which main water supply is located close to the salinity propagation limit in the Tagus estuary. During the most recent droughts (2005 and 2012) the agricultural activities in this area were affected and several emergency measures to minimize the negative impacts were undertaken (Deliverable 4.2, Freitas et al., 2017). Moreover, some of these impacts may be aggravated by sea level rise. Thus, the scenarios established aimed to evaluate the influence of the freshwater discharge in the salinity propagation in the Tagus estuary during droughts. The effect of sea level rise will be analyzed in a future deliverable.

Several large Portuguese and Spanish dams were built in the Tagus River and its tributaries, to overcome the intrinsic flow seasonality in Tagus basin (Deliverable 3.1, Alphen et al., 2016) and, as mentioned in the previous section, there is a strong dependence of the river discharge on decisions over the release of water from these dams. Due to the highly modified hydrological regime in the Tagus river basin and the strong dependence of the freshwater discharge on human decisions in this basin, the river flow scenarios used as riverine boundary conditions in the Tagus estuary simulations were not established based on the precipitation decadal predictions. For the same reasons, although changes in the water-use and land-use scenarios can also affect the river flow, these changes were not considered in the establishment of the river flow scenarios.

Four scenarios were established including a reference scenario for the Tagus river discharge. Since the summer season is the most critical during droughts, and based on past events during which the most severe situations for agricultural activities begun around July, the river flow scenarios were established for this period. In order to establish similar initial conditions for all the scenarios, a warm-up simulation, between March 15 and June 30, was performed. The river flow scenarios simulated were the following:

- Scenario 0, *climatological scenario* – river flow of 132 m^3/s: scenario based on the climatological analysis of the mean daily discharge at the Almourol station (http://snirh.pt) between 1990 and 2017 during the month of July.
- Scenario 1, *worst recent drought* – river flow of 22 m^3/s: scenario that represents one of the worst recent droughts. The river flow was estimated based on Macedo (2006) using data from Matrena and Tramagal stations (http://snirh.pt) during July 2005.
- Scenario 2, *minimum river flow* – river flow of 16.5 m^3/s: scenario based on the revised Spanish-Portuguese Albufeira Convention and Additional Protocol (Parliament Resolution n. 62/2008, November 14). This river flow represents the minimum mean weekly flow that must be guaranteed between July 1st and September 30th near the upstream boundary of the Tagus estuary (Muge). However, it should be noted that the Convention considers the possibility of an exception during very dry years, and this weekly minimum value is not always achieved (Henriques, 2018). Also, the minimum weekly river flow at the Portuguese / Spanish border can be (and often is) achieved by discharging only a few hours per week (Henriques, 2018).
- Scenario 3, *worst case scenario* – river flow of 8 m^3/s. This value represents the minimum river flow that guarantees the operation of one of the main thermoelectric power plants in the Tagus River.

The river flow scenarios were simulated using the three-dimensional Tagus estuary model, which simulates water levels and the three-dimensional velocity, salinity and water temperature fields. A detailed description of the model application and validation is given in Deliverable 3.3 (Alves et al., 2016) and in Rodrigues and Fortunato (2017). The input data used in the river flow scenarios' simulations are described in the next section.

7.1.3. Data

Inundation by tides and storm surges

As outlined in the previous section, several sources of atmospheric model results were used to determine extreme sea levels. These sources are summarized in Table 23.

Table 23. Atmospheric model results used to determine extreme sea levels.

Purpose	Dataset name	Reference	Notes
Characterize present extreme events in the Tagus estuary	20CRv2 reanalysis database[5]	Compo et al. (2011)	Only one member of the ensemble was used
	Downscaling of the 20CRv2 for the region of interest	Fortunato et al. (2017)	Performed for the period 10/2/1941 to 16/2/1941
Characterize extreme statistics of present surges and water levels	ERA-Interim[6]	Dee et al. (2013)	
Characterize extreme statistics of near-future surges and water levels	MiKlip decadal predictions, downscaled to 0.44º resolution	Jacob et al. (2014)	10 members for 2021-2024 were used

Different validation exercises were performed to assess how the errors in the atmospheric models can affect subsequent simulations. Atmospheric pressure at mean sea level obtained with the downscaled 1941 model results was compared against field data (Figure 112). Results indicate that the model overestimates the low pressure peak by about 8-9 hPa. This overestimation should result in an underestimation of the peak surge of about 8-9 cm.

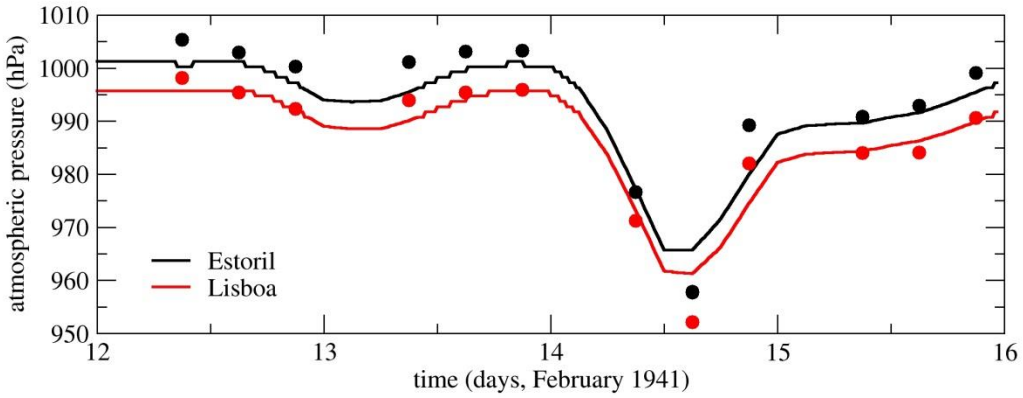

Figure 112. Validation of the atmospheric model for the 1941 event: comparison between the measured (circles) and modeled (lines) atmospheric pressures at two stations close to the Tagus estuary (from Fortunato et al., 2017).

The ability of the downscaled MiKlip predictions to reproduce extreme low pressures was assessed by comparing the statistics of low pressures obtained with MiKlip and ERA-Interim. The ERA-Interim reanalysis was used as "reality" since it combines model results with field data. It should therefore be more accurate

[5] https://www.esrl.noaa.gov/psd/data/gridded/data.20thC_ReanV2.html
[6] https://www.ecmwf.int/en/forecasts/datasets/reanalysis-datasets/era-interim

than the MiKlip predictions. Time series of atmospheric pressure at mean sea level were extracted from the ERA-Interim database at Cascais (a station close to the mouth of the Tagus estuary) for the period 1980-2014 (35 years). Generalized Extreme Value (GEV) statistical distributions were fitted to the surge annual maxima assuming stationarity in location, scale and shape parameters. The same procedure was applied to results from the downscaled MiKlip predictions for the same period and the same lead years. The differences (Figure 113) are smaller than 3 hPa, which translates into a difference of about 3 cm in storm surge. This result indicates that the downscaled MiKlip decadal predictions are appropriate to force storm surge models at Cascais.

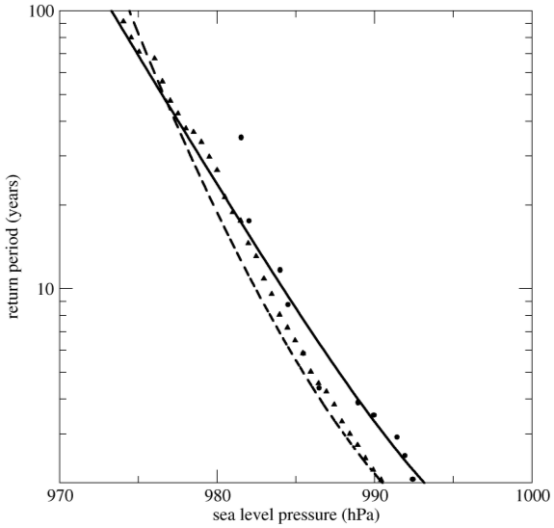

Figure 113. Verification of the ability of downscaled MiKlip decadal predictions (triangles, dashed line) to reproduce the statistics of extreme low pressures at Cascais, by comparison with ERA-Interim results (circles, solid line). The symbols represent the empirical distribution; the lines represent the fitted GEV distribution.

Salinity intrusion

The three-dimensional Tagus estuary model used for the salinity intrusion simulations was forced by tides at the oceanic boundary, river flows at the riverine boundaries and atmospheric data.

The river flow at the Tagus river boundary was established as described in the previous section. In the Sorraia river, the river flow is taken as 5% of the river flow in the Tagus River, based on the ratios between annual averages in the two rivers, following a similar approach to the one used for the calibration and validation of the model (Deliverable 3.3; Alves et al., 2016).

To allow the comparison between the river flow scenarios, the tidal and atmospheric forcing were similar in all the simulations and aimed to be representative of average conditions.

To setup the tide, the tidal amplitudes at Cascais (near the downstream boundary of the model) were determined between 1991 and 2010 using the tides from the regional model of Fortunato et al. (2016). For each year the mean and standard deviation were computed in the spring-summer season (between April and October), covering the period during which the simulations are performed. These values were then compared with the global mean and standard deviations, suggesting that the year 2001 is the most representative of average conditions (Figure 114).

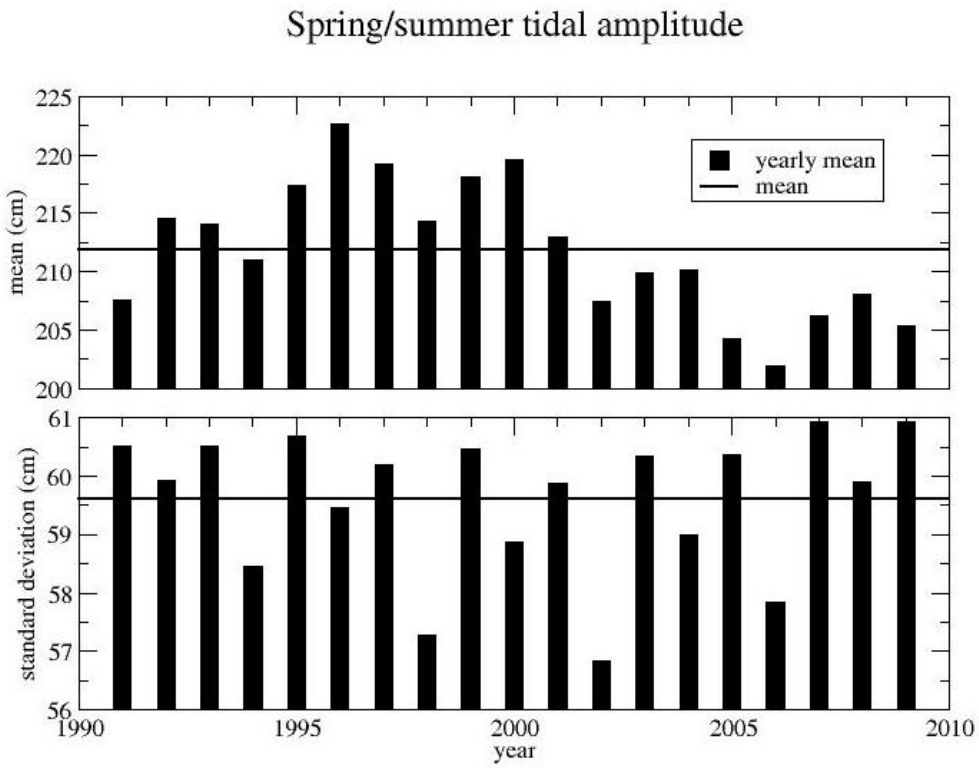

Figure 114. Spring/summer means and standard deviations of the tidal range at Cascais between 1991 and 2010.

A similar approach was used to define the atmospheric forcing for the scenarios simulations, using the decadal predictions (Deliverable 2.6, Kpogo-Nuwoklo et al., 2017). The analysis was performed at Cascais (downstream area of estuary) and Vila Franca de Xira (upstream area of the estuary). Mean values of air temperature, atmospheric pressure and wind intensity were computed for each pair of realization and year between 2018 and 2024. The yearly means were computed for the summer-spring period (between March and July), covering the period of the simulations. The yearly means were then compared with the global mean, suggesting that for both Cascais and Vila Franca de Xira the realization 3 for the year 2022 is the most representative of the average conditions.

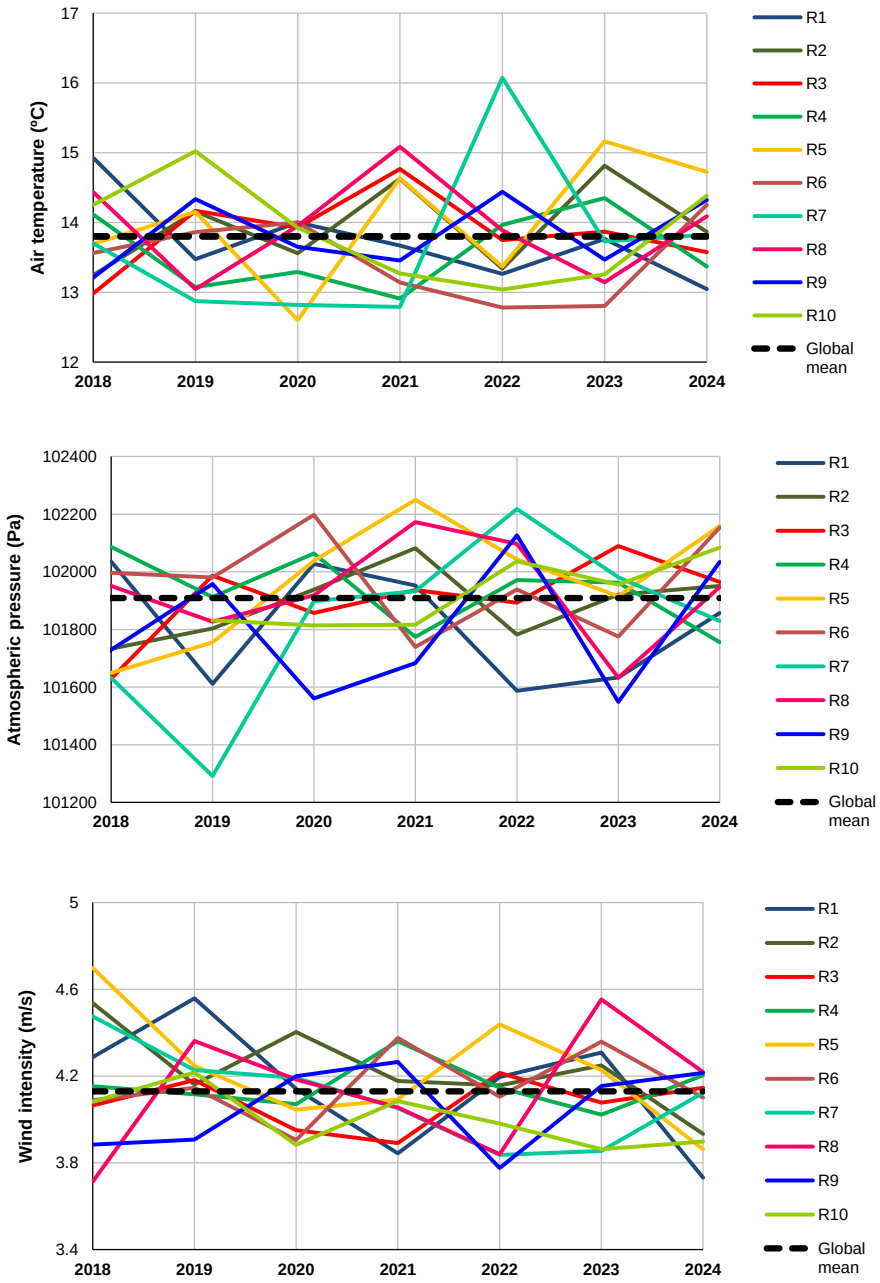

Figure 115. Yearly and global means of the air temperature, atmospheric pressure and wind intensity at Cascais between 2018 and 2024.

7.1.4. Results

Inundation by tides and storm surges

Extreme sea levels driven by tides and storm surges can lead to the inundation of agricultural lands in the upper reaches of the estuary. The extent of this inundation was simulated for two scenarios: the *extreme surge scenario* and the *worst case scenario*. The water depth for the two simulations is shown in Figure 116, and the extent of the inundated areas is shown in Table 24.

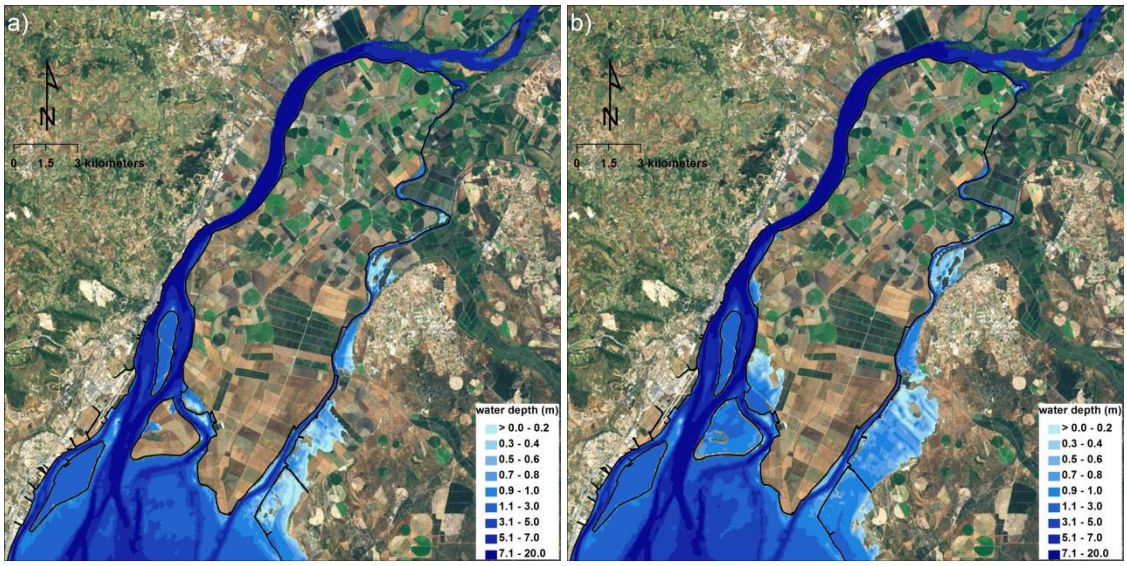

Figure 116. Inundation of the upper Tagus estuary for the 1941 storm: a) extreme surge scenario; b) worst case scenario, obtained by combining the 1941 storm with an extreme spring tide. Extracted from Fortunato et al. (2017). The maximum high water line (Rilo et al., 2014), where available, is represented in black.

Table 24. Inundated areas (km^2). Extracted from Fortunato et al. (2017)

Zone	Extreme surge scenario	Worst case scenario
Lezíria	1.6	2.5
Póvoa island	4.1	4.2
Lombo island	0.8	4.9
Alhandra island	2.4	2.5
Sorraia left margin	17.9	27.7

In order to assess the changes in storminess in the Portuguese coast between the present (1980-2016) and near-future (2021-2024), monthly means and standard deviations of storm surges were determined near the mouth of the Tagus estuary (Figure 117). Also, total water levels were computed by adding tides, surges and the expected sea level rise between present (taken as 1998) and near-future (taken as 2022). The sea level rise for this period was taken as 11 cm, following Nauels et al. (2017). Statistics of extreme sea levels for a return period of 100 years were computed along the Iberian Atlantic coast (Figure 118).

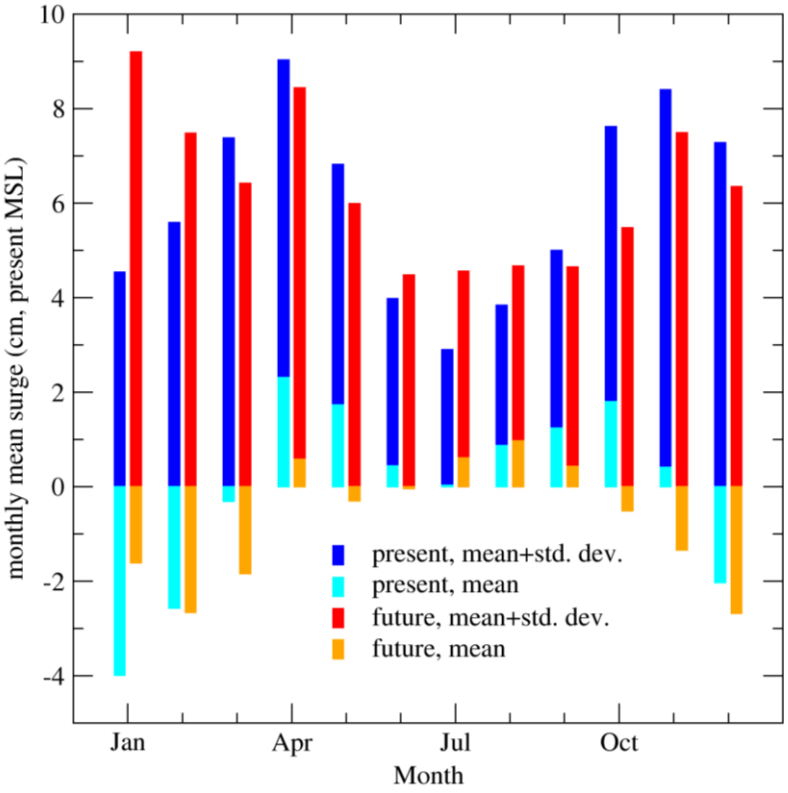

Figure 117. Monthly statistics of storm surges at the mouth of the Tagus estuary (Cascais) for present (1980-2016) and near-future (2021-2024) simulations. Adapted from Fortunato et al. (2018)

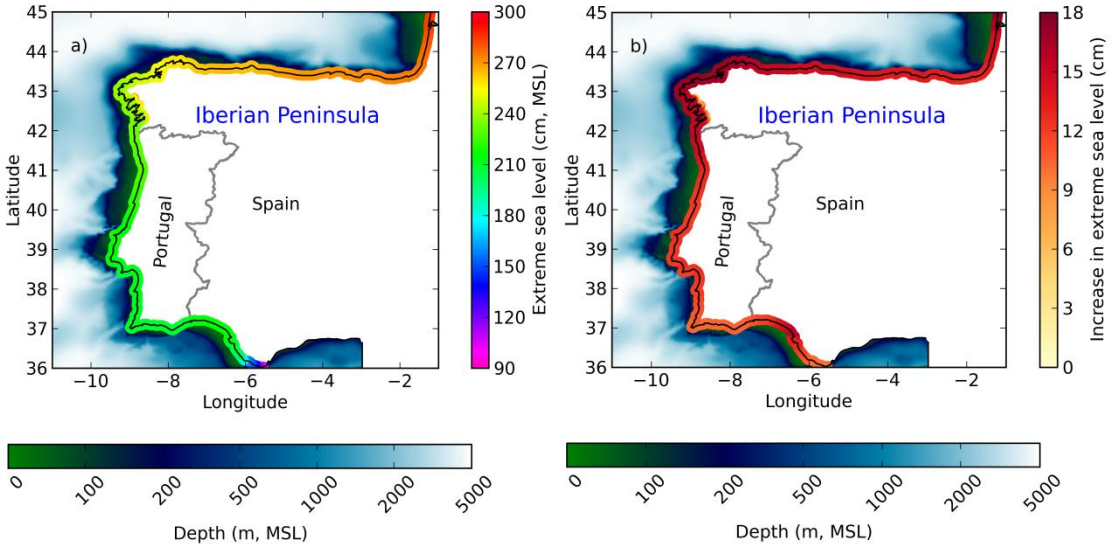

Figure 118. Evolution of extreme sea levels along the Iberian Atlantic coast for a return period of 100 years: a) present (1980-2016); b) increase from present to future (2021-2024). From Fortunato et al. (2018)

Salinity intrusion

Time series of surface salinities were extracted and analyzed at four locations (Figure 119): Vila Franca is usually considered the approximate location of the salinity intrusion limit in average conditions; Conchoso is the location of the major water intake of the Lezíria Grande PIP; Valada is a major water intake for drinking water; and Rio do Risco is the location of a possible alternative to Conchoso to extract water for irrigation.

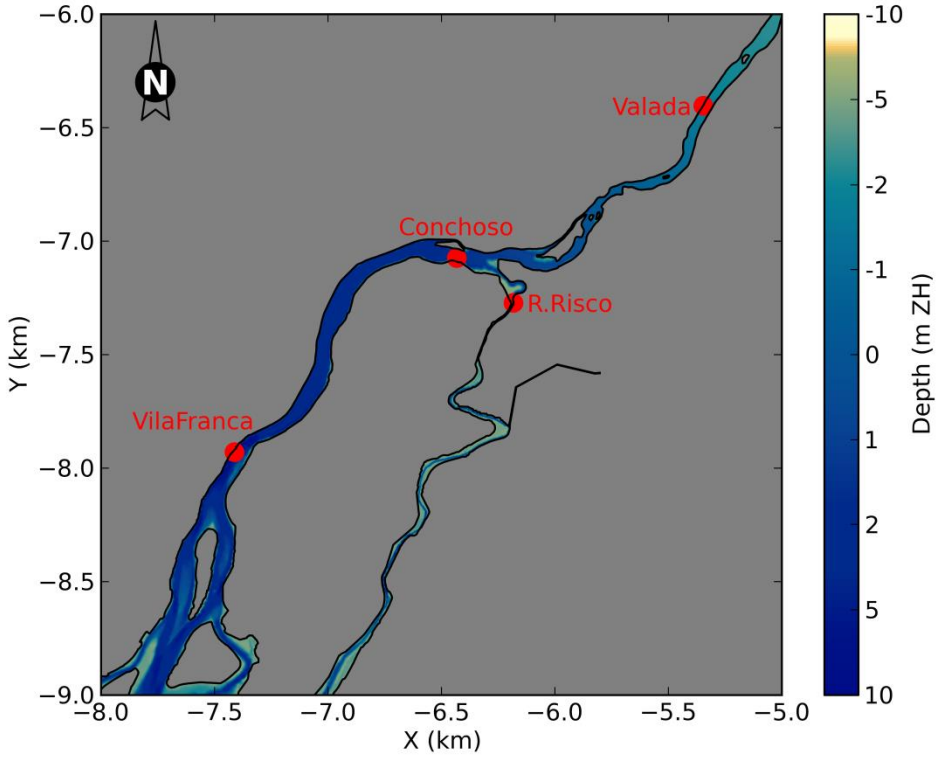

Figure 119. Virtual salinity stations where model results were analyzed

Time series of salinity at the surface are shown in Figure 120 for the month of July. Selected statistics of these time series are shown in Figure 121.

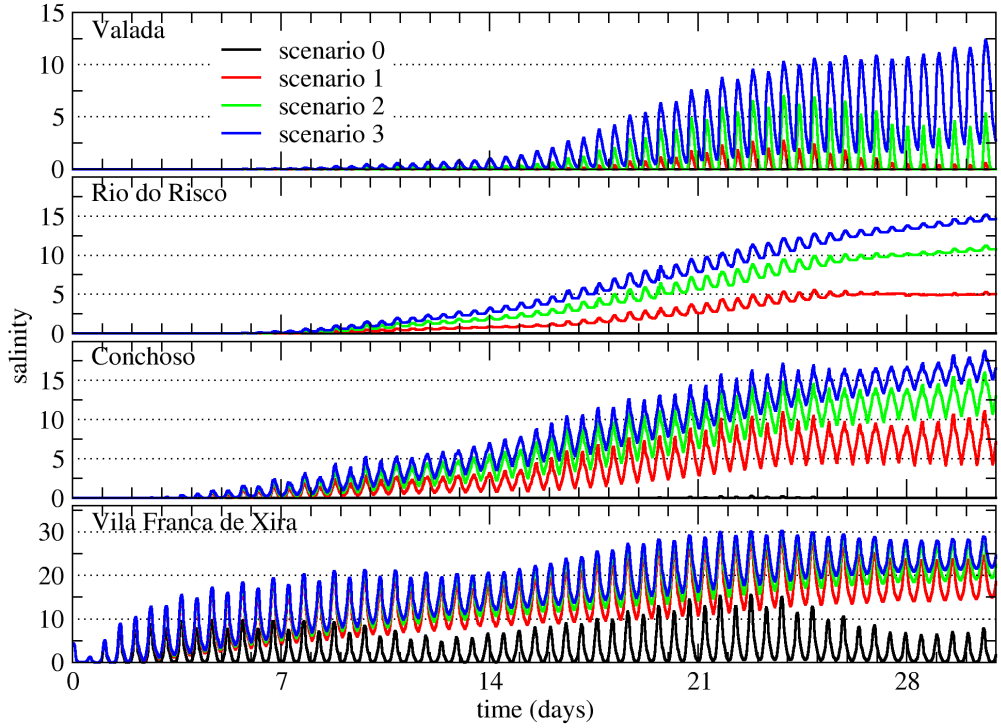

Figure 120. Time series of surface salinity at the four stations shown in Figure 119

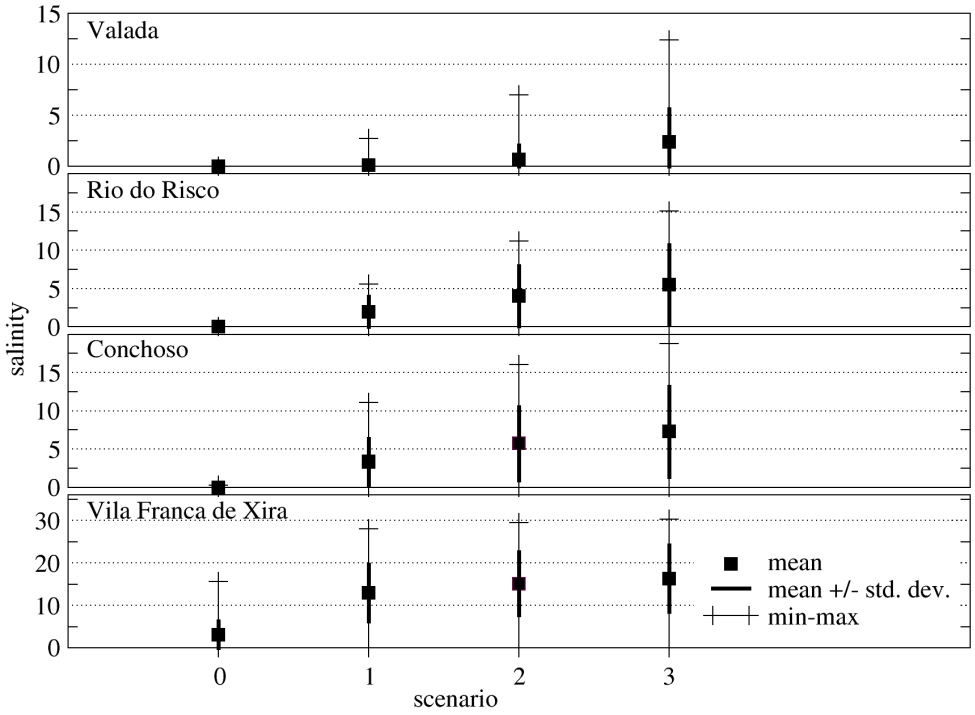

Figure 121. Statistics of surface salinity at the four stations shown in Figure 119

7.1.5. Discussion

Inundation by tides and storm surges

Results show that a storm similar to the 1941 event would cause today significant inundation of agricultural areas, in spite of the protective dikes (Figure 116a, Table 24).

The islands of Póvoa and Alhandra would be completely flooded. The Póvoa Island has little use presently. Actually, a part of the island is frequently flooded since May 2016, when one of the dikes was breached. To our knowledge, this breach remains to be repaired. Even though this breach is not present in the topography used in the model, which dates back to 2008, it is clear that the dikes are low and poorly maintained. In contrast, the Alhandra Island is used for cattle grazing and has two permanent inhabitants. Its flooding could therefore lead to dire consequences. The dikes of the Lezíria Grande PIP would be overflown at a former island (Garças Island), which was attached to the Lezíria sometime between 1973 and 1984. However, the volume of water that overflows the dike is small. A second dike, which protected the Leziria Grande PIP before it included the Garças Island, is sufficient to prevent that water to spread further. Note that this dike had already been overflown and damaged during the Xynthia storm in 2010. Although the dike was repaired and heightened after the storm, this particular spot appears to remain a weak link in the chain. Finally, on the left margin of the Sorraia River, an area of about 18 km^2 would be flooded due to the discontinuity and low height of some of the dikes.

Since the reliability of these results may be limited by the available topographic data, which may be particularly inaccurate around the dikes' crests, Fortunato et al. (2017) assessed the sensitivity of the results by repeating the simulation with the dikes' crests uniformly raised by 20 cm. Results indicated that, in most areas, the inundation extent is not very sensitive to errors of this magnitude, thereby providing further confidence in the estimated inundation areas. A related source of uncertainty is the dikes' erodibility, which

was not considered in the simulations. The dikes are fragile and require frequent repairs. In the case of an extreme event, it is likely that the dikes would give in at some places, further exacerbating the inundation.

The inundation extent would increase if the tidal amplitude was higher (Figure 116b, Table 24). The second dike in the Lezíria would be overflown, increasing the flooded area to 2.5 km^2, all three islands would be flooded, and the inundated area in the Sorraia left margin would increase by over 50%.

The regional-scale storm surge simulations aimed at understanding if the present inundation hazard, characterized above, can be affected in the near-future by changes in sea level or storminess. The monthly analysis of the storm surge at Cascais indicates a seasonal pattern. Storminess in the near-future (as measured by the mean plus the standard deviation of the surge) is predicted to increase in the early winter (January and February) and summer (June-August), and decrease in the other months (Figure 117). However, the tidal amplitudes are highest in mid-march and mid-September (Figure 122). Hence, the most extreme sea levels will seldom occur in January or February. This seasonality of tides and surges explains why the growth of surges in early winter does not affect the extreme sea levels at Cascais. Indeed, the extreme sea levels in this area grow by about 10 cm between 1998 and 2022 (Figure 118). This growth corresponds to the sea level rise considered in the analysis (11 cm).

In summary, predictions for the near future (2021-2024) indicate that there will be a small increase in storminess in January and February. However, there will actually be a small decrease in storminess in March and September, when tidal ranges reach their maximum. As a result, the changes in extreme sea levels will be mostly due to sea level rise. At the short time-scales considered herein, sea level rise is modest, and of the same order of magnitude as the uncertainty of the model results. Hence, we consider that the inundation hazard in the Tagus estuary will not change significantly.

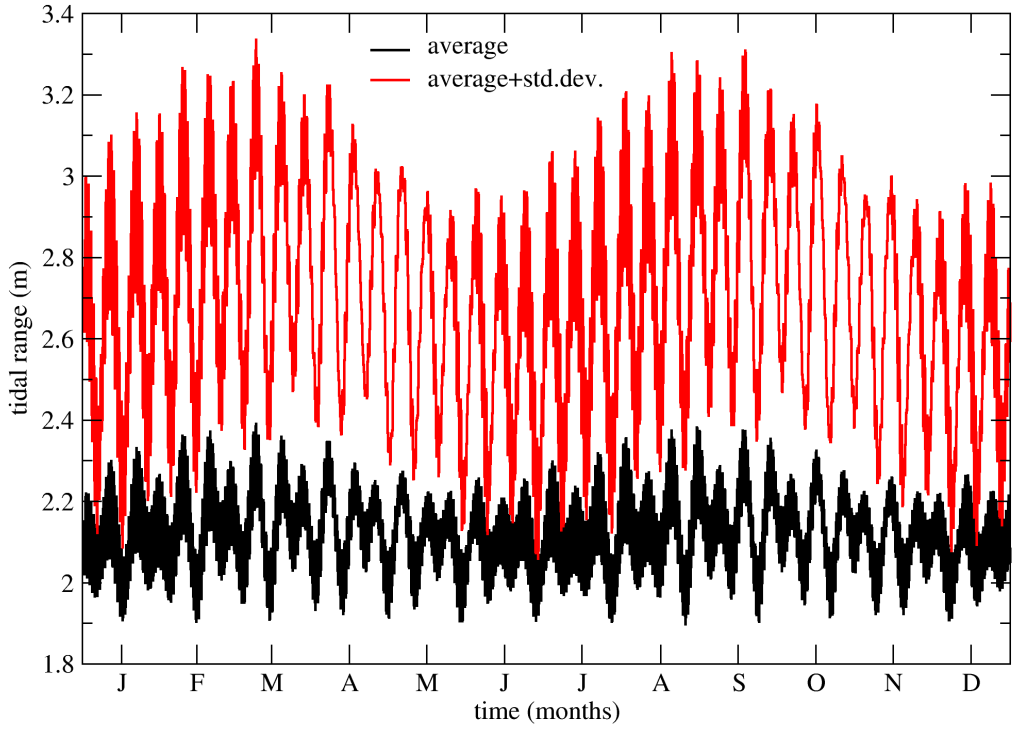

Figure 122. Seasonality of the tides at Cascais, highlighting the occurrence of equinoxial tides in mid-March and mid-September. The means and standard deviations were computed from a sample of 19 consecutive years (1991-2009). Extracted from Fortunato et al. (2018)

Salinity intrusion

Before the model results are analyzed, the accuracy of the salinity model must be discussed. First, because the model results are very sensitive to the river flow, in particular in the upper estuary (Figure 123), the accuracy of the model requires adequate estimates of the river flow. Therefore, the accuracy of the river flow data is assessed below. Secondly, the previous validation of the salinity model was done for high river flow conditions (Deliverable 3.3 – Alves et al., 2016), whereas the focus here is on droughts. Also, the validation was carried out for the mid and lower estuary, while we are now concerned with the upper estuary. Fortunately, data at the Conchoso station and for drought conditions became available in the summer 2017, after the previous validation was carried out. We thus examine the validity of the model where and when it matters the most in the context of BINGO: in the upper reaches of the estuary and during low river flow conditions.

Doubts about the quality of the river flow estimates led us to assess their quality. This assessment compared the river flow data from the Almourol station, upstream of the estuary, with the sum of the outflow from the two dams that drain into the lower Tagus river: Castelo de Bode, located in the Zêzere, an affluent to the Tagus River; and Belver, the dam in the Tagus River closest to the estuary. The comparison was restricted to the last decade (hydrological years 2008-2009 to 2016-2017). All these data are available at the Portuguese water resources information portal (www.snirh.pt). Since there are no significant inflows or water abstractions between the two dams and the Almourol station, the two time series should be very similar.

The comparison between the two time series reveals significant differences (Figure 124). The mean river flow is significantly smaller for the Almourol data than for the dams (219 and 261 m^3/s, respectively, considering only the days in which data are available for both time series). The discrepancy between the two time series was estimated as the difference between the Almorol and the dams data, scaled by the average of the two time series for each day. This discrepancy varies between -150% and 200%, and the mean of the absolute value of this discrepancy is 42%. Furthermore, the discrepancy is particularly large for small river flows (Figure 125), when salinity intrusion is high. The discrepancy can be both positive and negative, which excludes a systematic error associated to a source or abstraction of water between Almourol and the dams. The error could be partly due to an inadequate extrapolation of the relationship between the river flow and the water level measurements at Almourol, which would explain the concentration of points along a well-defined function in Figure 125. However, the spread around that function also suggests that there are other sources of errors. Hence, we have significant doubts about the accuracy of the river flow measurements.

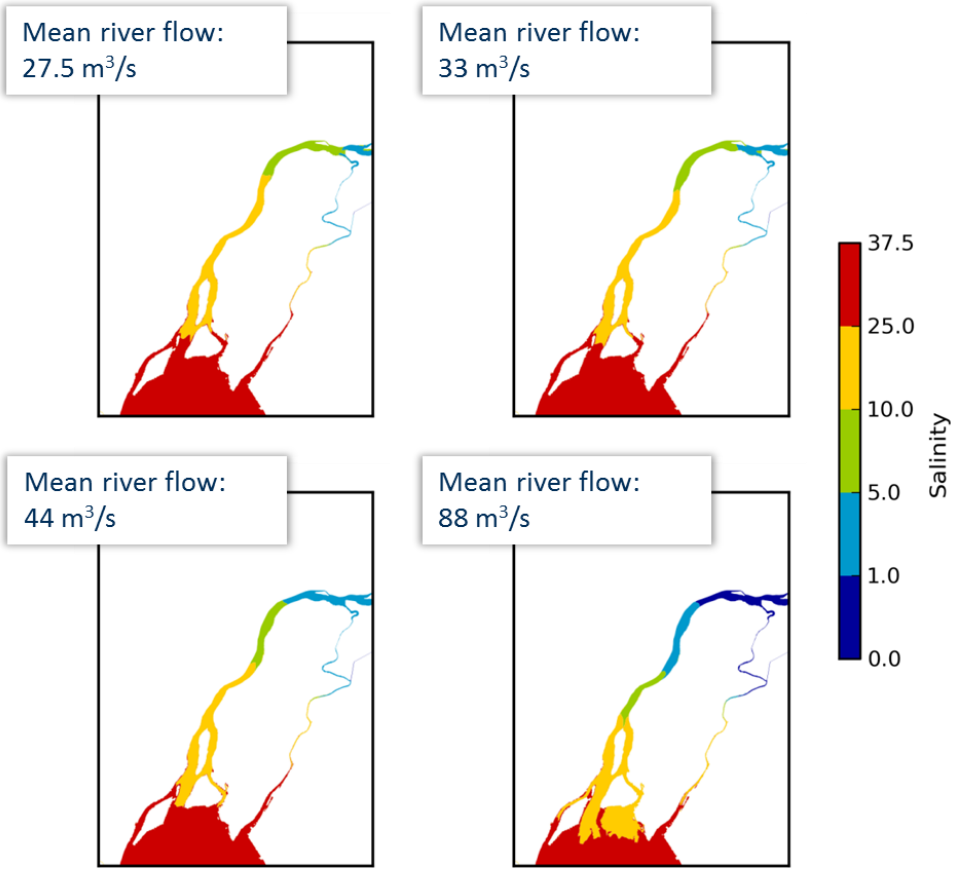

Figure 123. Illustration of the sensitivity of the salinity model results on the river flow:

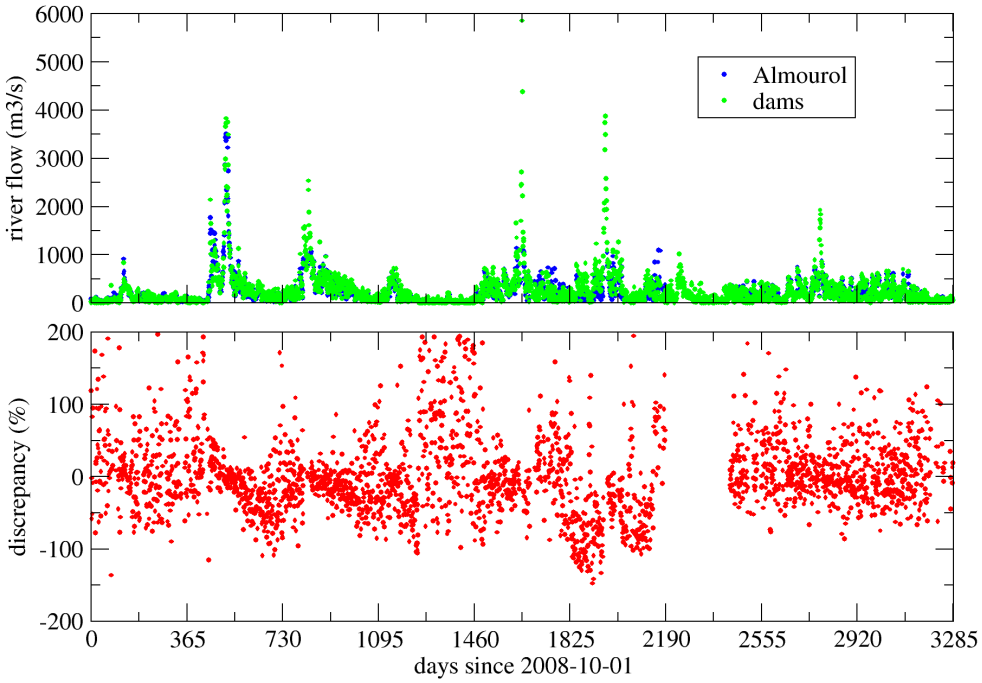

Figure 124. Comparison of two estimates of the daily river flow reaching the estuary for the hydrological years 2008-2009 through 2016-2017 at Almourol and sum of the outflow from the Castelo de Bode and Belver dams. The discrepancy is evaluated as the difference between the two time series scaled by their average

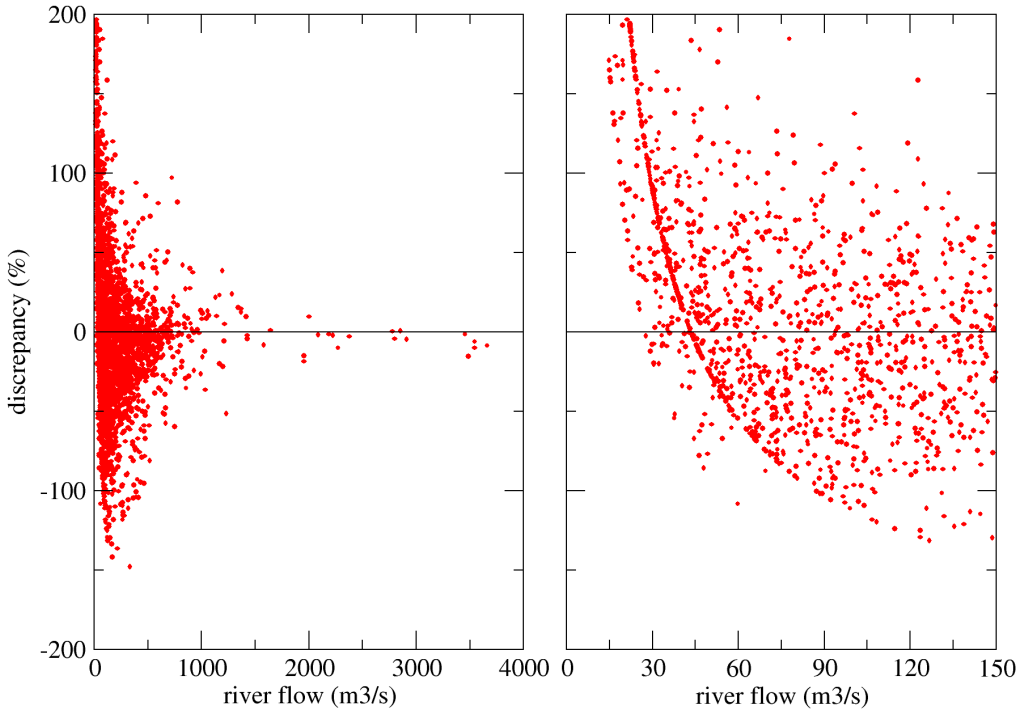

Figure 125. Comparison between the discrepancy and the river flow

The validation of the salinity model for drought conditions was done for July 2017. Given the uncertainty on the river flow data, two alternative input flows were used as the upstream boundary condition: data from Almourol and the sum of the outflows from the two dams. Results (Figure 126) indicate that the model correctly reproduces the phase of the signal, associated to the tide, but significantly overestimates the maximum salinity. Using river flow data from Almourol provides the best results. Still, the peak salinity is still overestimated by about 2. While the absolute error can actually be considered low for an estuarine model, the relative error (about a factor of 3) is very high because the salinity is very low. More importantly, the discrepancy between the two simulations (with the different river flows) largely exceeds the error between the best model result and the data. This behavior suggests that the uncertainty in the river flow data dominates the errors in the model results.

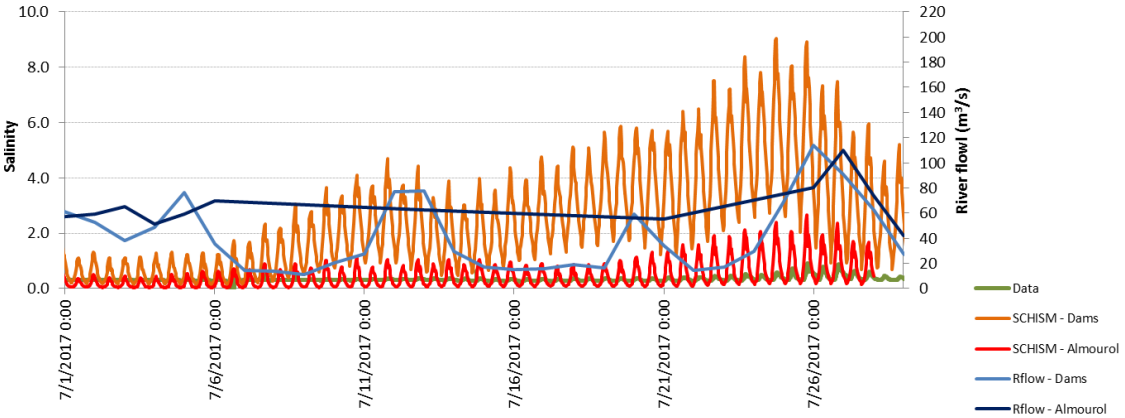

Figure 126. Validation of the salinity model in the upper reaches of the estuary (Conchoso station) and for low river flow conditions. Two alternative input river flows are considered: measured at Almourol, and the sum of the outflow from the two dams that discharge into the lower Tagus River

An additional potential source of model errors is the model bathymetry upstream of Vila Franca. Upstream of that point, only cross-sectional data of the river and estuary are available, with a longitudinal spacing of over 2 km. A sophisticated approach to transform the cross-sectional data into a 2D bathymetry was developed, loosely based on Cavides-Voullieme et al. (2014). However, it did not perform satisfactorily in this case due to the existence of islands in the riverine portion of the domain. As an alternative, rectangular cross-sections with varying width and depth were used. This simplification can potentially affect the proper reproduction of tidal propagation and salinity intrusion.

In summary, this validation exercise suggests that 1) the model overestimates the salinity intrusion in the upper reaches of the estuary, and 2) errors in the river flow data used to specify the boundary conditions constitute a major source of uncertainty in the model results. The simplified representation of the bathymetry upstream of Vila Franca de Xira, associated to the lack of detailed bathymetric data, is an additional source of errors.

The analysis of the salinity time series extracted from the model (Figure 120) provides detailed insight into the salinity intrusion in the Tagus River under drought conditions.

For climatological conditions (scenario 0), salinity does not reach the Conchoso station. This behavior is consistent with the empirical knowledge and provides confidence in the model.

For the worst recent drought (scenario 1), salinity reaches about 10 at Conchoso. The exceedance of the salinity thresholds acceptable for irrigation is consistent with testimonies from the stakeholders (see deliverable 3.1 – Alphen et al., 2016). For this same scenario, salinity at Valada reaches about 5. This value is probably too high to use this water for water supply. However, salinity only appears to be a problem at Valada for this scenario during spring tides: during neap tides, the salinity remains very low.

For the river flow agreed upon by the Portuguese and Spanish authorities (scenario 2), salinity makes the water not only inadequate for irrigation at Conchoso, but also inadequate for abstraction at Valada. Further reducing the river flow, as in scenario 3, obviously aggravates the consequences.

In general, tidally-averaged salinities display a rising trend even after one month of simulations with constant river flows. This behavior shows that salinity intrusion in the upper estuary depends not only on the river flow alone, but also on the duration of the droughts.

At Rio do Risco, the salinity exhibits very little tidal oscillations. Salinity is similar to the minima observed at Conchoso at each tidal cycle. The small oscillations suggest that the same water mass sloshes back and forth, with small exchanges with the Tagus River. Because this water mass is fairly small, creating an alternative source for water irrigation in this area would not solve the water shortage problem during a drought. Indeed, estimating the volume of the Risco River at 1-4 10^6 m^3 and considering a pumping rate of 0.7 10^6 m^3/day, this alternative pumping station would only provide water for less than a week.

The tidal signal present in the salinity time series suggests that, under drought conditions, water should only be abstracted from the river at low tide, in order to provide fresher water. A plot of the salinity versus water elevation (Figure 127) confirms that the highest salinities occur close to high tide. The exception is Rio do Risco where the salinity exhibits very little variations with the tide.

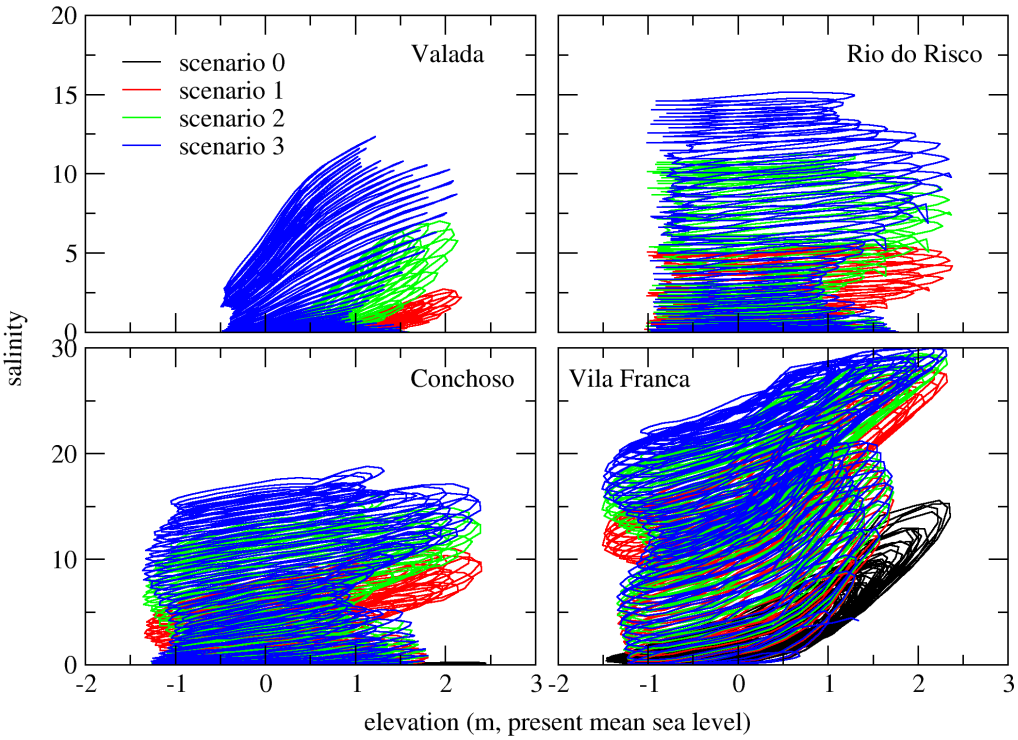

Figure 127. Relationship between the salinity and the tidal elevation

7.1.6. Bibliography

- Alphen, H-J., Alves, E., Beek, T., Bruggeman, A., Camera, C., Fohrmann, R., Fortunato, A., Freire, F., Iacovides, A., Iacovides, I., Kristvik, E., Kübeck, C., Lorza, P., Muthanna, T., Novo ,E., Rocha, F., Rodrigues, M., Rodrigues, R., Russo, B., Sánchez, P., Scheibel, M., Spek, T., Witte, F., Zoumides, C. (2016). Characterization of the catchments and the water systems, Deliverable 3.1, BINGO - Bringing innovation to ongoing water management – a better future under climate change assessment, 89 pp.
- Alves, E., aus der Beek, T., Bruggeman, A., Camera, C., Fortunato, A., Freire, P., Grange, A.S., Iacovides, A., Iacovides, I., Kristvik, E., Lorza, P., Montes, J., Mouskoundus, M., Muthanna, T.M., Nottebohm, M., Novo, E., Oliveira, M., Rijpkema, S., Rodrigues, M., Rodrigues, R., Russo, B., Sánchez, P., Scheibel, M., Sunyer, D., Viseu, T., Voortman, B., Witte, F., Zittis, G., 2016. Calibrated water resources models for past conditions, Deliverable 3.3, BINGO - Bringing innovation to ongoing water management – a better future under climate change assessment, 183 pp.
- Bertin, X., Prouteau, E., Letetrel, C., 2013. A significant increase in wave height in the North Atlantic Ocean over the 20th century, *Global and Planetary Change*, 106: 77-83. DOI:10.1016/j.gloplacha.2013.03.009.
- Caviedes-Voullieme, D., Morales-Hernandez, M., Lopez-Marijuan, I., Garcia-Navarro, P., 2014. Reconstruction of 2D river beds by appropriate interpolation of 1D cross-sectional information for flood simulation, *Environmental Modelling & Software*, 61: 206-228. DOI: 10.1016/j.envsoft.2014.07.016
- Compo, G.P., Whitaker, J.S., Sardeshmukh, P.D., Matsui, N., Allan, R.J., Yin, X., Gleason, B.E., Vose, R.S., Rutledge, G., Bessemoulin, P., Brönnimann, S., Brunet, M., Crouthamel, R.I., Grant, A.N., Groisman, P.Y., Jones, P.D., Kruk, M.C., Kruger, A.C., Marshall, G.J., Maugeri, M., Mok, H.Y., Nordli, Ø., Ross, T.F., Trigo, R.M., Wang, X.L., Woodruff, S.D., Worley, S.J., 2011. The

twentieth century reanalysis project, *Quarterly Journal of the Royal Meteorological Society*, 137: 1–28. DOI:10.1002/qj.77

- Dee, D.P., Uppala, S.M., Simmons, A.J., Berrisford, P., Poli, P., Kobayashi, S., Andrae, U., Balmaseda, M.A., Balsamo, G., Bauer, P., Bechtold, P., Beljaars, A.C.M., van de Berg, L., Bidlot, J., Bormann, N., Delsol, C., Dragani, R., Fuentes, M., Geer, A.J., Haimberger, L., Healy, S.B., Hersbach, H., Hólm, E.V., Isaksen, L., Kållberg, P., Köhler, M., Matricardi, M., McNally, A.P., Monge-Sanz, B.M., Morcrette, J.-J., Park, B.-K., Peubey, C., de Rosnay, P., Tavolato, C., Thépaut, J.-N., Vitart, F., 2011. The ERA-Interim reanalysis: configuration and performance of the data assimilation system. *Quarterly Journal of the Royal Meteorological Society,* 137, 553–597. DOI: 10.1002/qj.828.
- Fortunato, A.B., Li, K., Bertin, X., Rodrigues, M., Miguez, B.M., 2016. Determination of extreme sea levels along the Iberian Atlantic coast, *Ocean Engineering*, 111/1: 471-482. DOI: 10.1016/j.oceaneng.2015.11.031
- Fortunato, A.B.; Freire, P.; Bertin, X.; Rodrigues, M.; Ferreira, J.; Liberato, M.L. 2017. A numerical study of the February 15, 1941 storm in the Tagus estuary, *Continental Shelf Research* 144: 50 - 64. doi: 10.1016/j.csr.2017.06.023
- Fortunato, A.B., Meredith, E.P., Rodrigues, M., Freire, P., Feldmann, H., 2018. Near-future changes in storm surges along the Atlantic Iberian coast, *Natural Hazards*, DOI: 10.1007/s11069-018-3375-z.
- Freire, P., Tavares, A., Sá, L., Oliveira, A., Fortunato, A.B., Santos, P.P., Rilo, A., Gomes, J.L., Rogeiro, J., Pablo, R., Pinto, P.J., 2016. A local scale approach to estuarine flood risk management, *Natural Hazards*, doi:10.1007/s11069-016-2510-y
- Freitas, J.G., Dias J.A., 2013. 1941 windstorm effects on the Portuguese Coast. What lessons for the future? *Journal of Coastal Research*, Special Issue 65: 714-719. DOI : 10.2112/SI65-121.
- Freitas, A., Luis, A., Fortunato, A., Villanueva, A., Martins, B., Russo, B., Strehl, C., Martinez, E., Alves, E., Bergsma, E., Kristvik, E., Rocha, F., van Alphen, H.-J., Koti, J., Scheibel, M., Rodrigues, M., Sanchez, P., Freire, P., Lorza, P., Brito, P., Malgrat, P., Viseu, T., Munthanna, T., 2017. Risk identification: Relevant hazards, risk sources and factors, Deliverable 4.2, BINGO - Bringing innovation to ongoing water management – a better future under climate change assessment, 138 pp.
- Henriques, A.H., 2018. Reflexões sobre a monitorização dos recursos hídricos, a Convenção de Albufeira e o licenciamento de descargas nas massas de água, a propósito do incidente de poluição do rio Tejo de janeiro de 2018, *Revista Recursos Hídricos*, 39/1: 9-17 (in Portuguese).
- Jacob D, Petersen J, Eggert B, Alias A, Christensen OB, Bouwer LM, Braun A, Colette A, Déqué M, Georgievski G, Georgopoulou E, Gobiet A, Menut L, Nikulin G, Haensler A, Hempelmann N, Jones C, Keuler K, Kovats S, Kröner N, Kotlarski S, Kriegsmann A, Martin E, van Meijgaard E, Moseley C, Pfeifer S, Preuschmann S, Radermacher C, Radtke K, Rechid D, Rounsevell M, Samuelsson P, Somot S, Soussana J-F, Teichmann C, Valentini R, Vautard R, Weber B, Yiou P (2014) EURO-CORDEX: new high-resolution climate change projections for European impact research. *Regional Environmental Change*, **14**, 563–578. DOI: 10.1007/s10113-013-0499-2.
- Kpogo-Nuwoklo K., Meredith E., Vagenas C. (2017). Ensembles for decadal prediction extremal episodes downscaled to 3-1km/ 1h); Spatial stochastic precipitation generator for catchments, Deliverable 2.6, BINGO - Bringing innovation to ongoing water management – a better future under climate change assessment, 39 pp.

- Macedo, M.E.Z. (2006). Caracterização de Caudais, Rio Tejo. CCDR de Lisboa e Vale do Tejo, Lisboa, 30 pp.
- Muir-Wood, R., 2011. The 1941 February 15th Windstorm in the Iberian Peninsula. *Trébol*, 56: 4-13.
- Nauels A, Meinshausen M, Mengel M, Lorbacher K, Wigley TML (2017) Synthesizing long-term sea level rise projections – the MAGICC sea level model v2.0. *Geoscientific Model Development*, 10, 2495-2524. DOI: 10.5194/gmd-10-2495-2017
- Rilo, A, Freire, P, Mendes, RN, Ceia, R, Catalão, J, Taborda, R, Melo, R, Caçador, MI, Freitas, MC, Fortunato, AB, Alves, E, 2014. Methodological framework for the definition and demarcation of the highest astronomical tide line in estuaries: the case of Tagus Estuary (Portugal). *Revista de Gestão Costeira Integrada,* 14/1: 95‑107. http://dx.doi.org/10.5894/rgci450 (in Portuguese).
- Rodrigues, M, Fortunato AB 2017. Assessment of a three-dimensional baroclinic circulation model of the Tagus estuary (Portugal), *AIMS Environmental Science* 4, 6: 763 - 787. doi: 10.3934/environsci.2017.6.763

7.2. Groundwater

7.2.1. Model objectives in BINGO

Climate change impacts on groundwater levels are mainly due to the fact that changes in temperature and precipitation regimes will modify the amounts of water available for aquifer recharge and so the supply to these reservoirs is changed. A decrease in recharge, for instance, might lead to a lowering of the groundwater levels and lead to a dry out of some wells, compounding the problem of water supply for human activities. Modelling identifies such changes and critically impacted areas. This can then inform the risk analysis procedures.

The model objectives for groundwater are therefore to study the impact of possible climate changes in the recharge of four selected Lower Tagus aquifer systems and, for three of them, to study and analyse the corresponding impact in the groundwater levels.

The impact on groundwater recharge will be calculated by comparing the results obtained from the soil daily sequential water balance BALSEQ_MOD model with recharge values calculated for the Tagus river basin management plan that used time series spanning between 01-10-1979 and 30-09-2009 for the “Aluviões do Tejo” and “Margem Direita” aquifer systems, between 01-10-1980 and 30-09-2009 for the “Margem Esquerda” aquifer system, and between 01-10-1980 and 30-09-2002 for the “Ota-Alenquer” aquifer system.

For the groundwater flow modelling of the “Aluviões do Tejo”, “Margem Direita” and “Margem Esquerda” aquifer systems the impact of the modelled decadal recharge is verified by the change of the groundwater levels in relation to the past calibrated situation.

The results for the past conditions were briefly presented in Deliverable 3.3 and are described in more detail in Oliveira (2018) and in Novo (2018). A general aquifer system’s description was already presented in Deliverable 3.1.

7.2.2. Model application

As presented in Deliverable 3.2, and in accordance to the river basin management plan of Tagus River Basin operative until 2027, it is expected for the whole area an increase of 5 % of the irrigated land. This will have no sensible impact on the computation of aquifer recharge of the aquifer systems for the period 2015-2024 in relation to recent past usages. So the groundwater recharge model will be run only for the 10 decadal realizations (members) with current land use.

For the groundwater flow model, the minimum and maximum values of recharge will be selected to verify the impact of changing groundwater recharge in groundwater flow and levels.

7.2.3. Data

Decadal meteorological predictions were prepared for exactly the same locations of the 11 pluviometry stations and 5 meteorological stations used to compute groundwater recharge of the past period used in the Tagus river basin management plan (presented in Deliverable 3.3).

Data was prepared under WP2 and the final decadal time series passed through an iteration process where the decadal time series were analysed for their coherence. The daily values of precipitation and the monthly average of: daily maximum temperature, daily minimum temperature, daily maximum relative humidity, and daily minimum relative humidity; and monthly wind speed average, and monthly sunshine duration

(transformed into surface downwelling shortwave radiation) were used to bias correct the original values of decadal predictions.

The procedure to generate this data may be consulted in Rust et al. (2018, a text which is frequently updated at http://users.met.fu-berlin.de/~HenningRust/BINGO/DECO_docu.pdf). Data was withdrawn from BINGO_DECO plugin for FreVa (https://freva.met.fu-berlin.de/plugins/bingo_deco/detail/), selecting:

- Research site and hydrological model: RS5_Tagus-River_Feflow-BALSEQ
- Date range: 1979-03-01,2015-07-31
- Bias correction: CDFt
- Experiment of provided input data: decadal-predictions
- Data product providing input data: iberia-11
- Time frequency of provided input data: day
- Model providing input data: mpi-esm-lr-cclm4-8-19-v1

As explained earlier, land use scenario is the same used in Tagus river basin management plan for the past situation presented in Deliverable 3.3.

The decadal predictions were only accepted after a thorough process of validating the results for the historical time series, namely the comparison between the past hindcasts and the corresponding bias corrected time series and the observed values of the eleven precipitation stations and of the five meteorological stations. This was an iterative process between WP2 and WP3 and its results are reported separately (Oliveira, 2018).

For each precipitation station, with daily values, the comparison was made for the average annual value of the historical time series, for the annual values of the time series and for the cumulative distribution function of the values for each year. As a general result, for ten precipitation stations the average of the bias corrected precipitation decadal predictions is always just slightly higher than the corresponding historical average precipitation (between +2 % and +4 %); the only exception is *Ota* precipitation station with -10 % than the historical values.

For the other meteorological data, with monthly values, comparisons were made using plot charts of the observed and the bias corrected values.

Having accepted these past hindcasts the corresponding bias correction techniques were transferred for the decadal predictions. A new process was conducted here to check if the predictions were acceptable and a new iterative process between WP2 and WP3 took place. Again this is reported separately in Oliveira (2018).

The decadal predictions showed a somehow appreciable range of values. For each precipitation station the average of the 10 decadal average annual precipitations and the 10 decadal average annual precipitations were compared with the average observed past value. Besides as we are in the fourth year of the decadal predictions a comparison was made between the registered cumulative distribution function of the years 2015, 2016 and 2017 and the correspondent decadal predictions for these years in the four common precipitation stations that continue to operate. For the meteorological stations also the average of the 10 decadal average annual values of the meteorological variables and the 10 decadal average annual values of the meteorological variables were compared with the average observed past values. These results were finally accepted.

The mathematical flow model encompasses the 3 large aquifers of the case-study area assuming a 3 layered geological structure, which was discretized to 26 slices. The data used to build the model is:

1. **For model geometry**:
    - ***Coordinate System*** – used for all georeferenced data, the datum is ETRS89.
    - ***DTM, Horizontal limits of the model/aquifers, River network*** – they are shapefiles from 2011 Tagus Watershed Management Plan database, further corrected to eliminate errors.
    - ***Top and Bottom of aquifer layers*** – they result from the interpretation of boreholes data collected during the work for the 2011 Tagus Watershed Management Plan and partially presented in Lobo Ferreira et al. (2011).
2. **For hydraulic parameters**:
    - ***Hydraulic conductivity, Porosity, Specific storage*** – the initial shapefiles are from 2011 Tagus Watershed Management Plan (APA, 2012), having subsequently been changed during model calibration.
3. **For groundwater levels and recharge**:
    - ***Recharge*** – is given by the outputs of BALSEQ_MOD run for the 10 realizations of MiKlip. For the historical period, required for calibration, recharge is that of 2011 Tagus Watershed Management Plan, also computed by BALSEQ_MOD (Lobo Ferreira et al., 2011).
4. **For water abstraction and model calibration**:
    - ***Observation wells***, ***Heads for model calibration*** – the location of the wells and the observed heads are shapefiles from 2011 Tagus Watershed Management Plan database and data provided by ARH-Tejo (River Basin District Administration – Tagus). Heads per observation/calibration well refer to the period from 1980 to 2009.
    - ***Abstraction wells*** – the shapefile was built from the data in 2011 Tagus Watershed Management Plan (obtained from well reports in APA databases), INSAAR, EPAL, CCDR-LVT and Águas do Ribatejo databases.

7.2.4. Results

Groundwater recharge model

The groundwater recharge results are shown separately for each of the four studied aquifer systems.

The average recharge values obtained for the "**Margem Direita**" aquifer system for each one of the 10 realizations are shown in Figure 128 [series named Avg(r)]. The graph also plots the average recharge value calculated for the Tagus river basin management plan between 01-10-1979 and 30-09-2009 [series named Avg(1979/80-2008/9] and the average value of the 10 decadal realizations [series named Avg(r1-r10)]. The average recharge ranges between 110 or 111 mm/year (realizations 3 or 8, respectively) and 184 mm/year (realization 1). The average recharge of the ten realizations is 130 mm/year. This value is slightly larger than the past series value (123 mm/year).

The distribution of the annual recharge for each realization of the "**Margem Direita**" aquifer system is shown in Figure 129. It can be seen that the annual values may change significantly from year to year and predicted values can be as low as 16 mm/year and as high as 353 mm/year. Curiously these two extreme values occurred in the same realization (realization 4) and are related to the lowest (220 mm/year) and highest (1095 mm/year) predicted yearly precipitations.

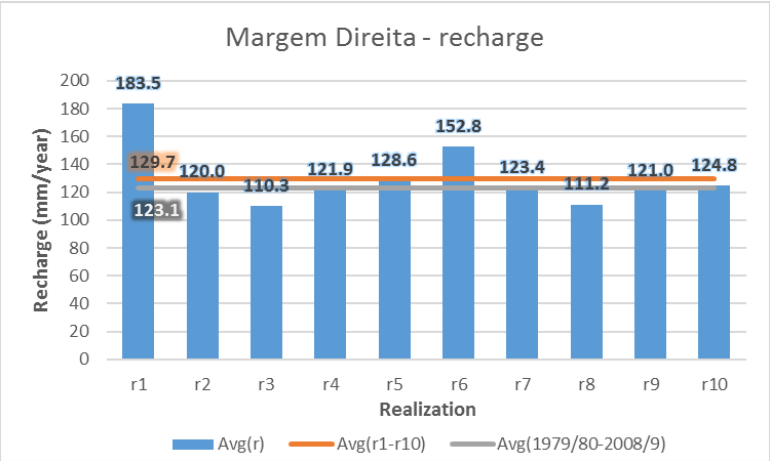

Figure 128: Average annual recharge for each realization for the whole "Margem Direita" aquifer system

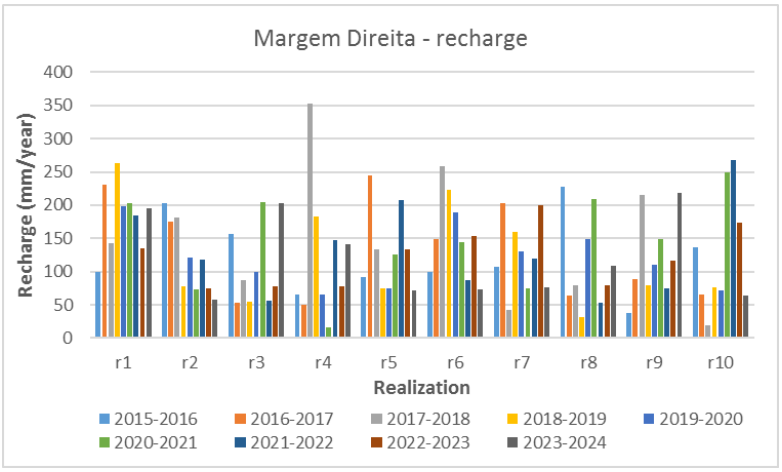

Figure 129: Distribution of the annual recharge for each realization for the whole "Margem Direita" aquifer system

The average recharge values obtained for the "**Margem Esquerda**" aquifer system for each one of the 10 realizations are shown in Figure 130 [series named Avg(r)]. The graph also plots the average recharge value calculated for the Tagus river basin management plan between 01-10-1980 and 30-09-2009 [series named Avg(1980/1-2008/9] and the average value of the 10 decadal realizations [series named Avg(r1-r10)]. The average recharge ranges between 132 mm/year (realization 3) and 229 mm/year (realization 1). The average recharge of the ten realizations is 174 mm/year. This value is slightly larger than the past series value (167 mm/year).

The distribution of the annual recharge for each realization of the "**Margem Esquerda**" aquifer system is shown in Figure 131. It can be seen that the annual values may change significantly from year to year and predicted values can be as low as 15 mm/year and as high as 474 mm/year. These two extreme values occurred in the same realization (realization 4) and are related to the lowest (219 mm/year) and highest (1115 mm/year) predicted yearly precipitations.

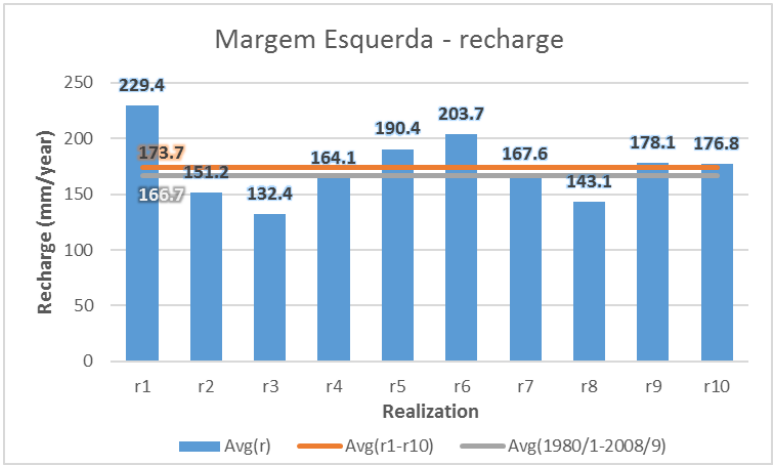

Figure 130: Average annual recharge for each realization for the whole "Margem Esquerda" aquifer system

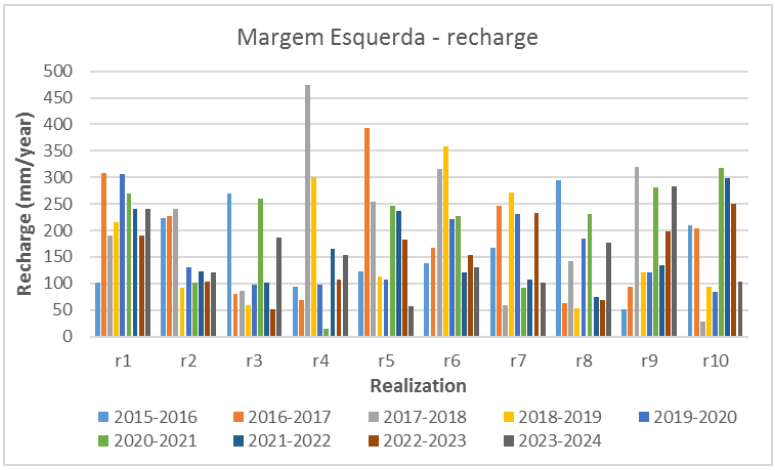

Figure 131: Distribution of the annual recharge for each realization for the whole "Margem Esquerda" aquifer system

The average recharge values obtained for the "**Aluviões do Tejo**" aquifer system for each one of the 10 realizations are shown in Figure 132 [series named Avg(r)]. The graph also plots the average recharge value calculated for the Tagus river basin management plan between 01-10-1979 and 30-09-2009 [series named Avg(1979/80-2008/9] and the average value of the 10 decadal realizations [series named Avg(r1-r10)]. The average recharge ranges between 182 mm/year (realization 3) and 267 mm/year (realization 1). The average recharge of the ten realizations is 207 mm/year. This value is equal to the past series value.

The distribution of the annual recharge for each realization of the "**Aluviões do Tejo**" aquifer system is shown in Figure 133. It can be seen that the annual values may change significantly from year to year and predicted values can be as low as 24 mm/year and as high as 519 mm/year. These two extreme values occurred in the same realization (realization 4) and are related to the lowest (213 mm/year) and highest (1069 mm/year) predicted yearly precipitations.

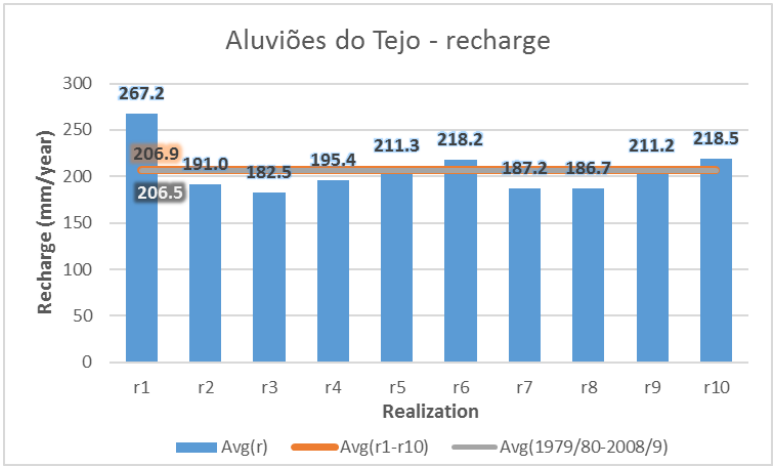

Figure 132: Average annual recharge for each realization for the whole "Aluviões do Tejo" aquifer system

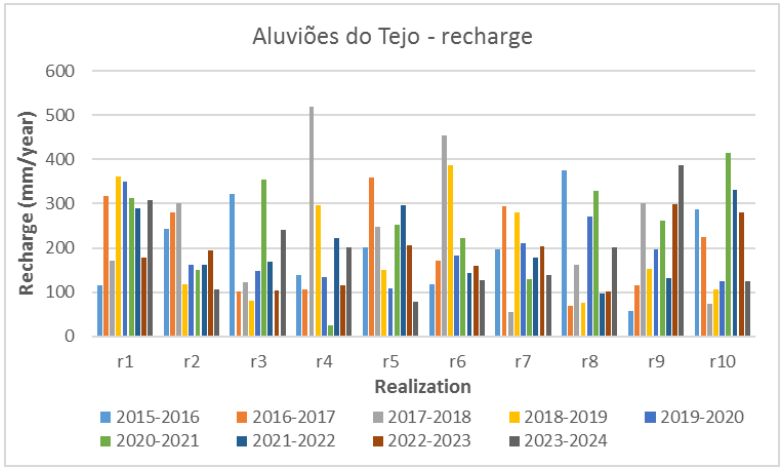

Figure 133: Distribution of the annual recharge for each realization for the whole "Aluviões do Tejo" aquifer system

The average recharge values obtained for the "**Ota-Alenquer**" aquifer system for each one of the 10 realizations are shown in Figure 134 [series named Avg(r)]. The graph also plots the average recharge value calculated for the Tagus river basin management plan between 01-10-1980 and 30-09-2002 [series named Avg(1980/1-2001/2] and the average value of the 10 decadal realizations [series named Avg(r1-r10)]. The average recharge ranges between 339 mm/year (realization 8) and 464 mm/year (realization 1). The average recharge of the ten realizations is 369 mm/year. This value is 11 % lower than the past series value (415 mm/year).

The distribution of the annual recharge for each realization of the "**Ota-Alenquer**" aquifer system is shown in Figure 135. It can be seen that the annual values may change significantly from year to year and predicted values can be as low as 86 mm/year and as high as 719 mm/year. These two extreme values occurred in the same realization (realization 4) and are related to the lowest (202 mm/year) and highest (1142 mm/year) predicted yearly precipitations.

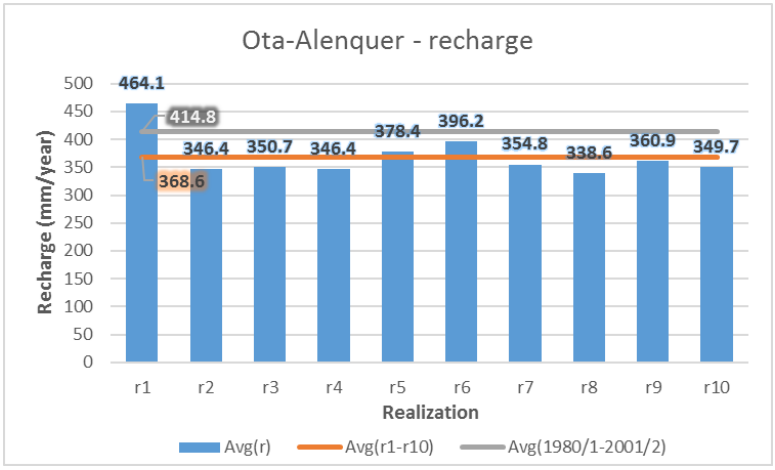

Figure 134: Average annual recharge for each realization for the whole "Ota-Alenquer" aquifer system

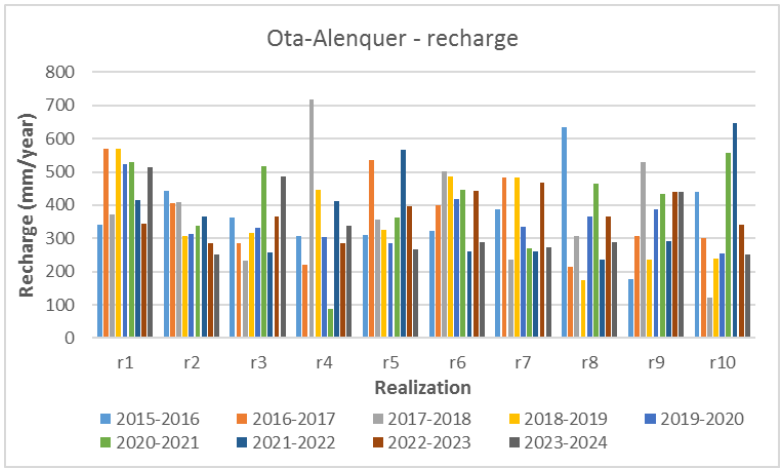

Figure 135: Distribution of the annual recharge for each realization for the whole "Ota-Alenquer" aquifer system

Table 25 summarises the minimum, maximum and average recharge variations for each aquifer system in relation to the historical period.

Table 25: Recharge variation from present day conditions

Aquifer system	Higher recharge		Lower recharge		Average recharge (Ensemble of realisations)
	Realisation	Variation	Realisation	Variation	
Margem Direita	R1	+49.1 %	R3	-10.4 %	+5.4 %
Margem Esquerda	R1	+37.6 %	R3	-20.6 %	+4.2 %
Aluviões do Tejo	R1	+29.4 %	R3	-11.6 %	+0.2 %
Ota-Alenquer	R1	+11.9 %	R8	-18.4 %	-11.1 %

The spatial distribution of the daily precipitation and potential plant/soil evapotranspiration distributions but also on the soil properties and land cover properties that influence the infiltration and percolation of water in the soil. In order to show how recharge varies in space Figure 136 shows **for all the aquifer systems** under study the distribution of the average recharge of the 10 realizations, Figure 137 the distribution of the average recharge of the lower average recharge realization (realization R3), and Figure 138 the distribution of the

average recharge of the higher average recharge realization (realization R1). The relation between the decadal recharge prediction and the past recharge average values is shown correspondingly in Figure 139, Figure 140 and Figure 141.

Tables and figures for all realizations are presented separately in Oliveira (2018).

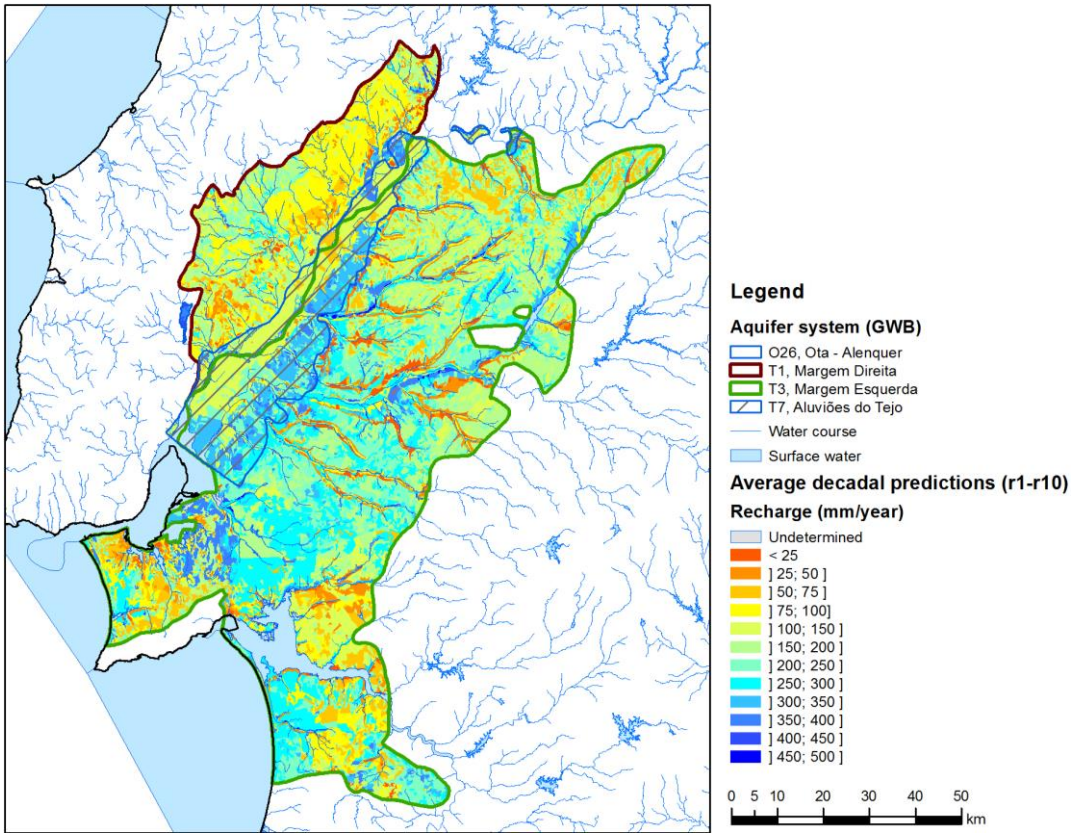

Figure 136: Distribution of the average annual recharge of the 10 decadal realizations (r1-r10)

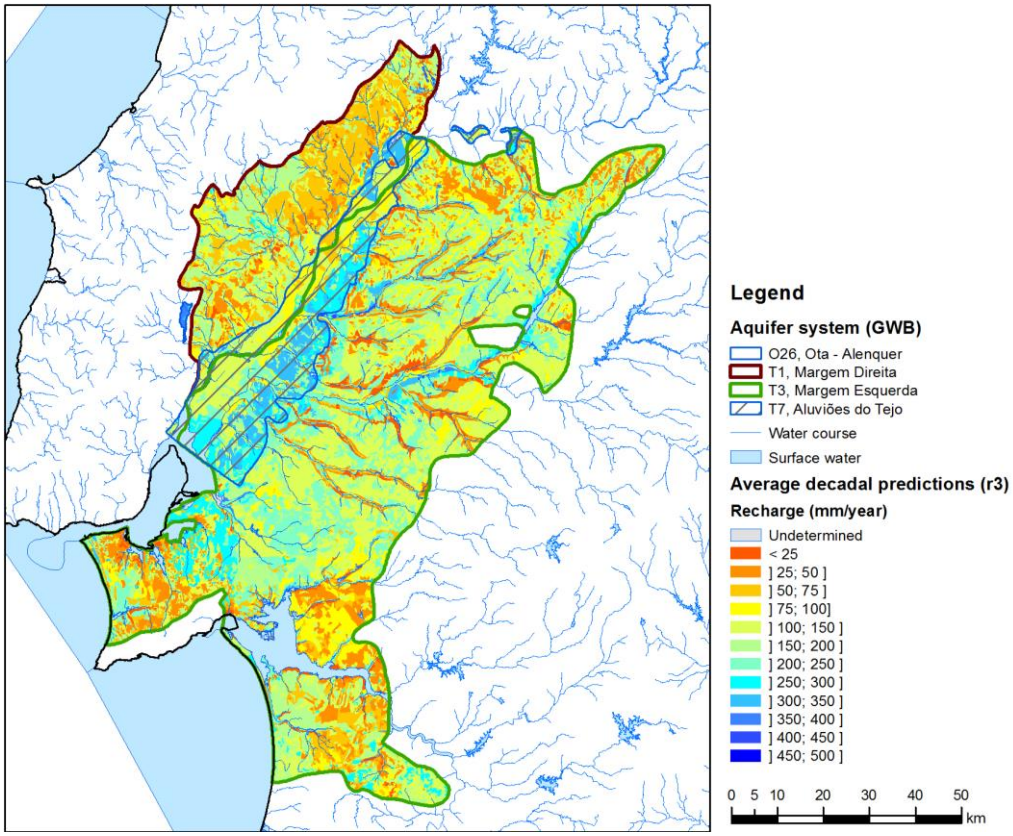

Figure 137: Distribution of the lowest average recharge decadal realization (r3)

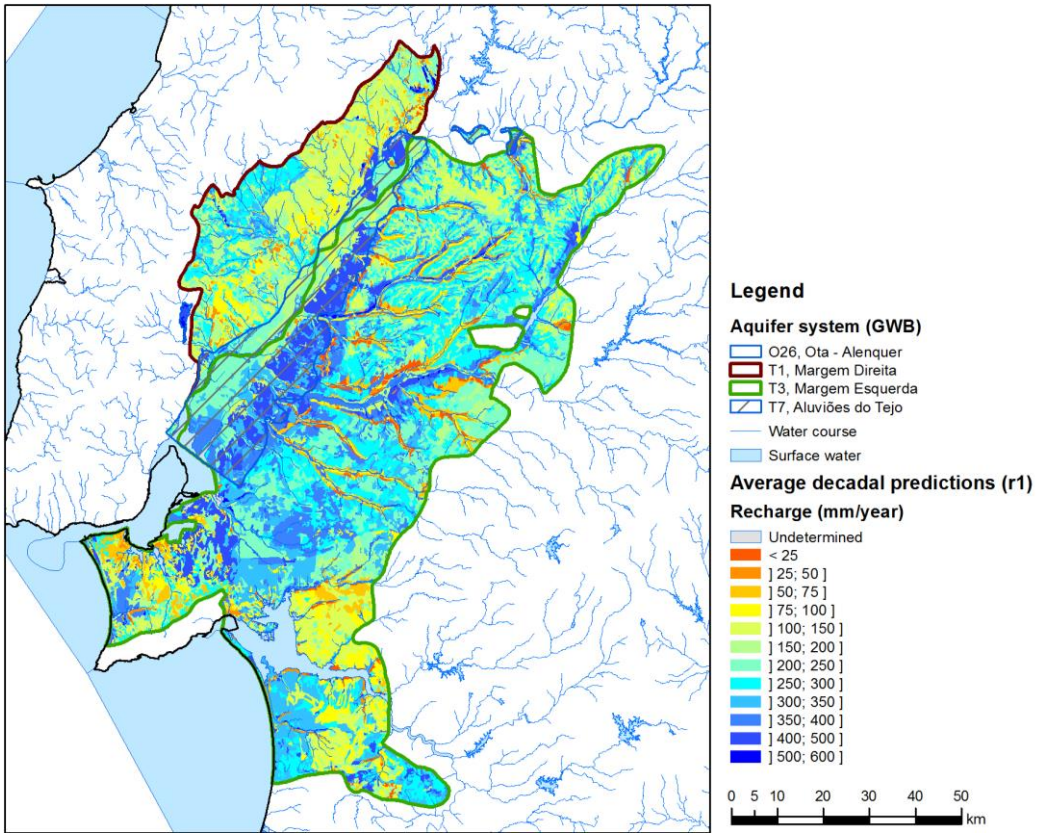

Figure 138: Distribution of the highest average recharge decadal realization (r1)

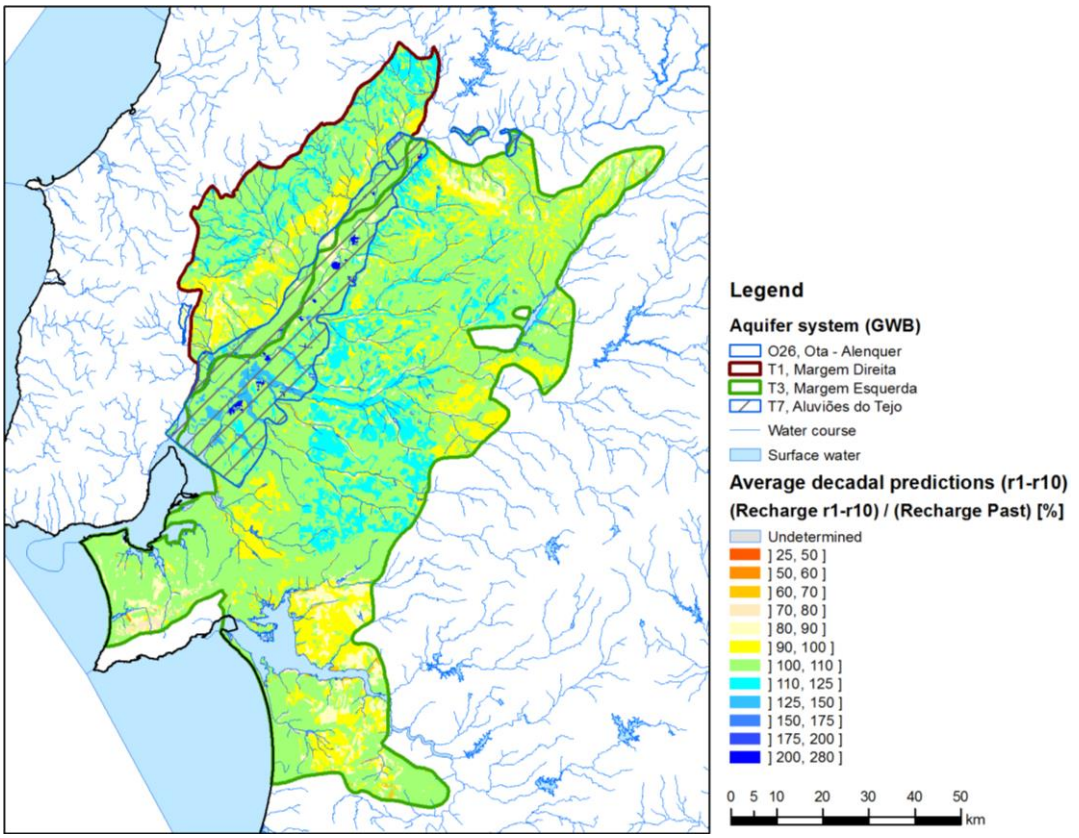

Figure 139: Distribution of the relation between average annual recharge of the 10 decadal realizations (r1-r10) and the past average recharge

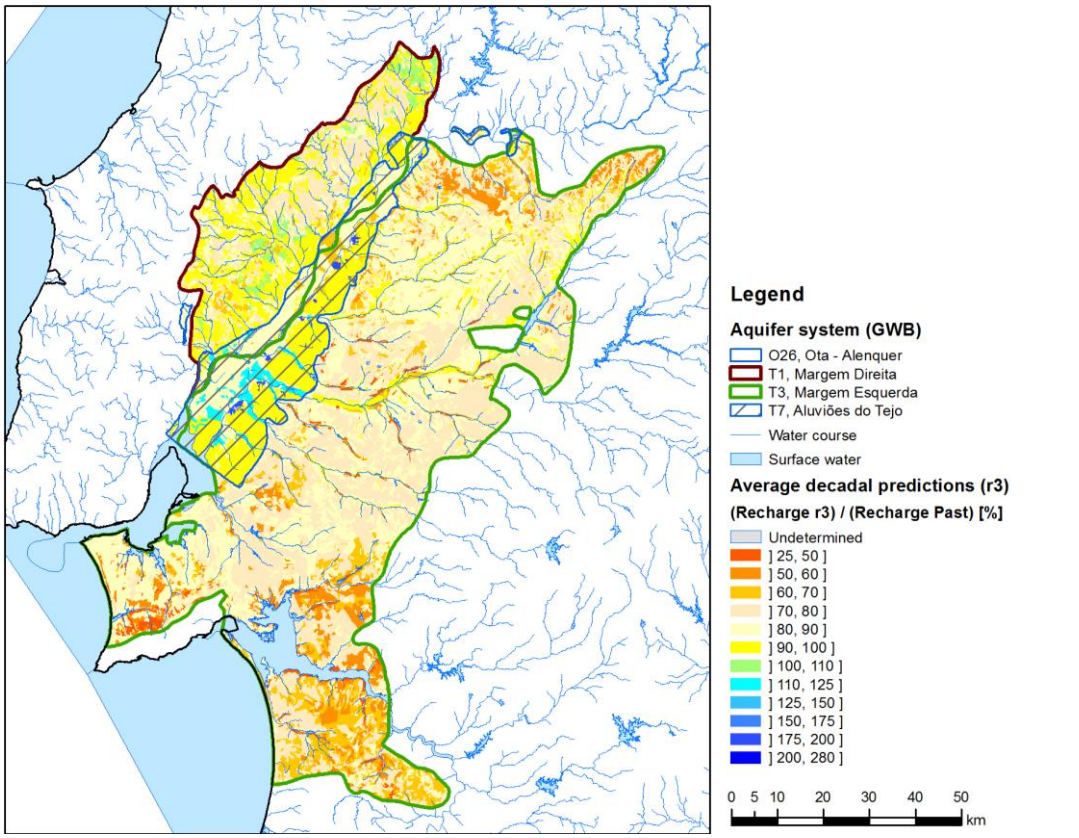

Figure 140: Distribution of the relation between lowest average recharge decadal realization (r3) and the past average recharge

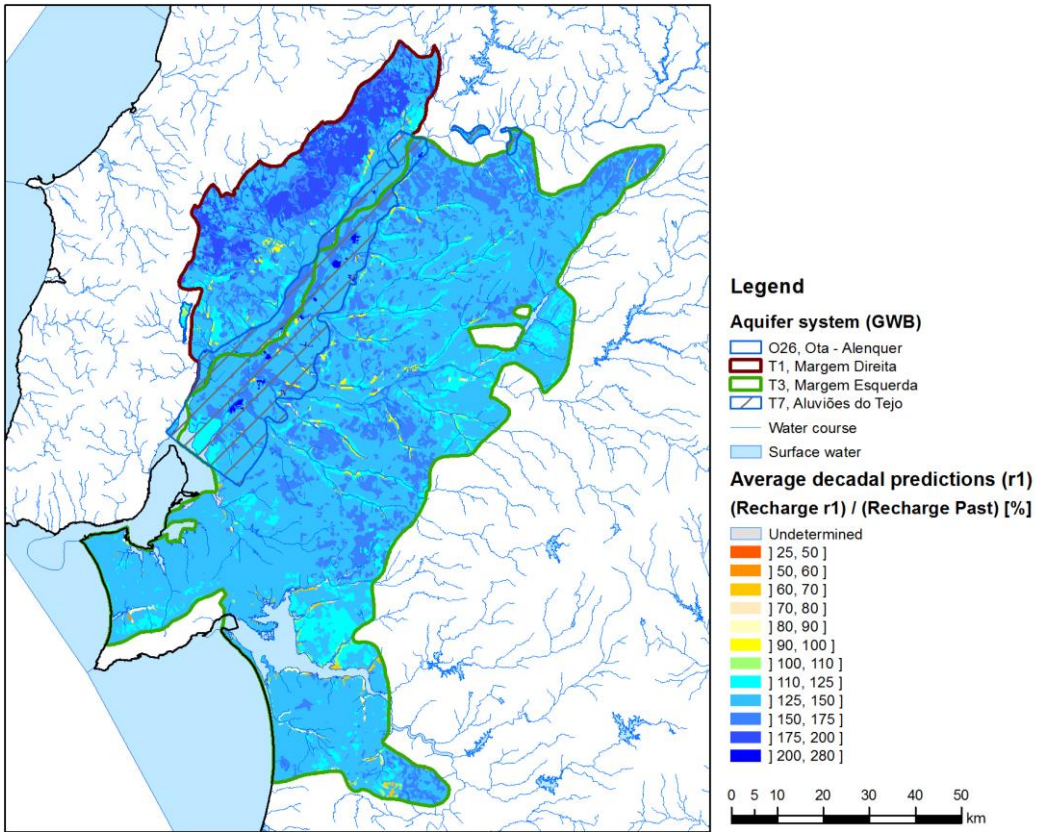

Figure 141: Distribution of the relation between highest average recharge decadal realization (r1) and the past average recharge

Groundwater flow model

The numerical flow model was first calibrated for the historical period (1979-2009). Calibration was performed for natural conditions (no pressures) and for pumping conditions in steady state in the whole area of the model.

After calibration, the recharge from the realisations R1 and R3 of MiKlip, which give rise to the maximum and the minimum recharge conditions respectively, was used to analyse the impacts of climate change in the groundwater levels and in this way identify the most sensitive areas to such changes and where, as a consequence, abstraction wells could be compromised and water supply be affected.

Besides these R1 and R3 realisations, a drought scenario was also used, in order to evaluate the impacts of this type of extreme events. This scenario used the recharge conditions of 2005, which was a year of severe drought, and the water abstraction volumes of the historical period since there is not enough reliable data concerning the water abstractions for this year.

As it was assumed no significant water use change (cf. Deliverable 3.2), pumping conditions are equal to those of the historical period, for all recharge realizations.

The results are presented below and, with more detail, in Novo (2018).

Climate change realizations steady state

As far as recharge is concerned present day conditions are similar to the average recharge of the ensemble of 10 realizations of MiKlip for Aluviões do Tejo and show a small increase of 4.2% and 5.4% for Margem Esquerda and Margem Direita aquifers, respectively. Since land cover will not change significantly from present day-conditions in 2025, this average recharge of the 10 realizations can be used to simulate the present day situation if present day exploitation rates are used, once the increases in recharge are too small to have a significant impact on the model behaviour and groundwater levels evolution. Once a refinement of the model for the present day conditions is on progress right now, it was decided then to use the average of the whole ensemble of realisations for comparing with the realisations giving the maximum and minimum recharge in order to compare for the same model conditions.

The results **for realisation R1**, to which a high recharge is associated (average recharge increases from between 29.4% and 41.5% for Aluviões do Tejo and Margem Direita, respectively), show that for the whole case-study area there is a general rise of the groundwater levels, usually of less than 2 m in the low lying areas (e.g. valleys) but away from the river network the rises become much higher, with large portions of the area showing rises of more than 5 m, with low permeability areas showing rises of up to 10 m (Figure 142). In Sorraia area the groundwater levels rise from less than 1 m up to 2 m in the downstream area, depending on the permeability of the terrain and the distance to river network, in particular the Tagus River; in upstream areas of low permeability the rises can be up to 10 m, although usually they range from 2 to 5 m and usually those higher rises occur away from the rivers (Figure 142). For the area N of Sorraia, groundwater level rise ranges from less than 1 m near the river network, to more than 5 m in an upstream low permeability area but the rises, on the whole range mostly from 1 to 2 m (Figure 142). In the area S of Sorraia region, the groundwater level rises are usually of little significance, being usually < 1 m, although areas with 2 m rise do occur; upstream these rises can reach up to 5 m and, locally, 10 m (Figure 142). For the region most downstream the Right Margin (Margem Direita Aquifer), nearing the estuary, groundwater level rises are in the range of < 1.5 m; the rise of the groundwater level increases as the location is further away from Tagus River (Figure 142). In this R1 scenario, due to the large recharge, several areas become inundated and typically they have very low permeability.

For realisation R3, to which the lowest recharge is associated, for the whole case-study area, low lying areas show a drawdown of less than 2 m while upstream areas show larger drawdowns, usually from 2 m to more than 10 m; low permeability areas show the largest drawdowns, usually on the range of 10 m of larger (Figure 143). In Sorraia area, the groundwater levels go down, in general from circa 0.5 m to 2 m in an area up to 12 km away from Tagus River, with the smallest groundwater level drawdowns near Tejo and Sorraia rivers; areas upstream from the main rivers (Tagus and Sorraia) show drawdowns of > 10 m, usually associated with low permeability zones (Figure 143). S of Sorraia, groundwater level drawdowns are < 0.5 m up 8 km away from the Tagus River, reaching up to a 2 m drawdown between 12 and 15 km away; the largest drawdowns (values above 5 m) are always linked to low permeability areas which usually are located upstream (Figure 143). N of Sorraia, groundwater level drawdowns range from less than 1 m to a bit above 2 m, with the highest drawdowns once again in the low permeability areas (Figure 143).

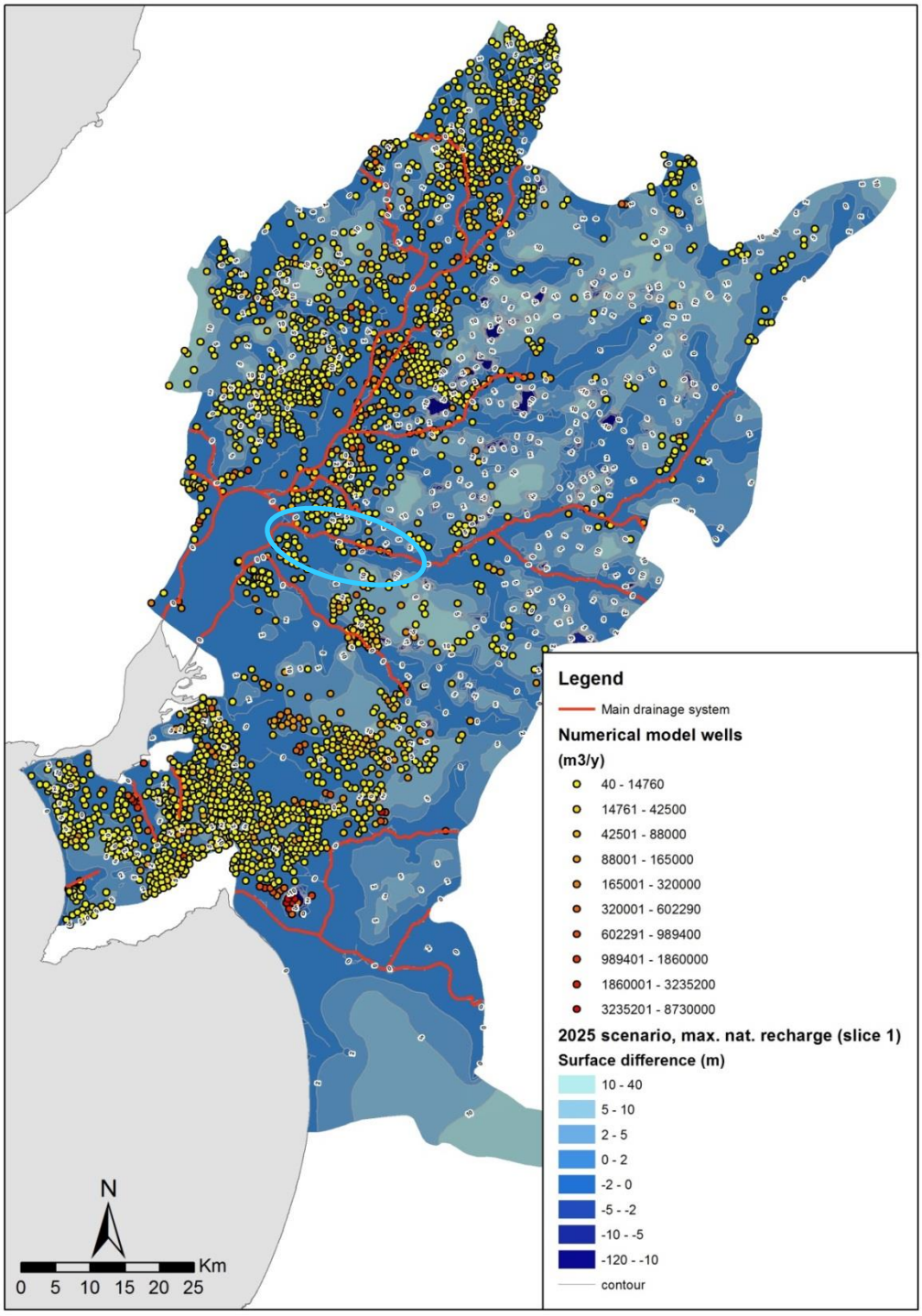

Figure 142: Groundwater level differences between the pumping conditions in the historical period (1979-2009) and the pumping conditions in Slice 1 and conditions under R1 realization (maximum recharge scenario)

For the area in the Right Margin (Margem Direita Aquifer) nearing the estuary, groundwater level drawdowns are small, with values never larger than 0.5 m, and the highest drops are further away from the Tagus River (Figure 143). Under R3 scenario flooded areas do not occur.

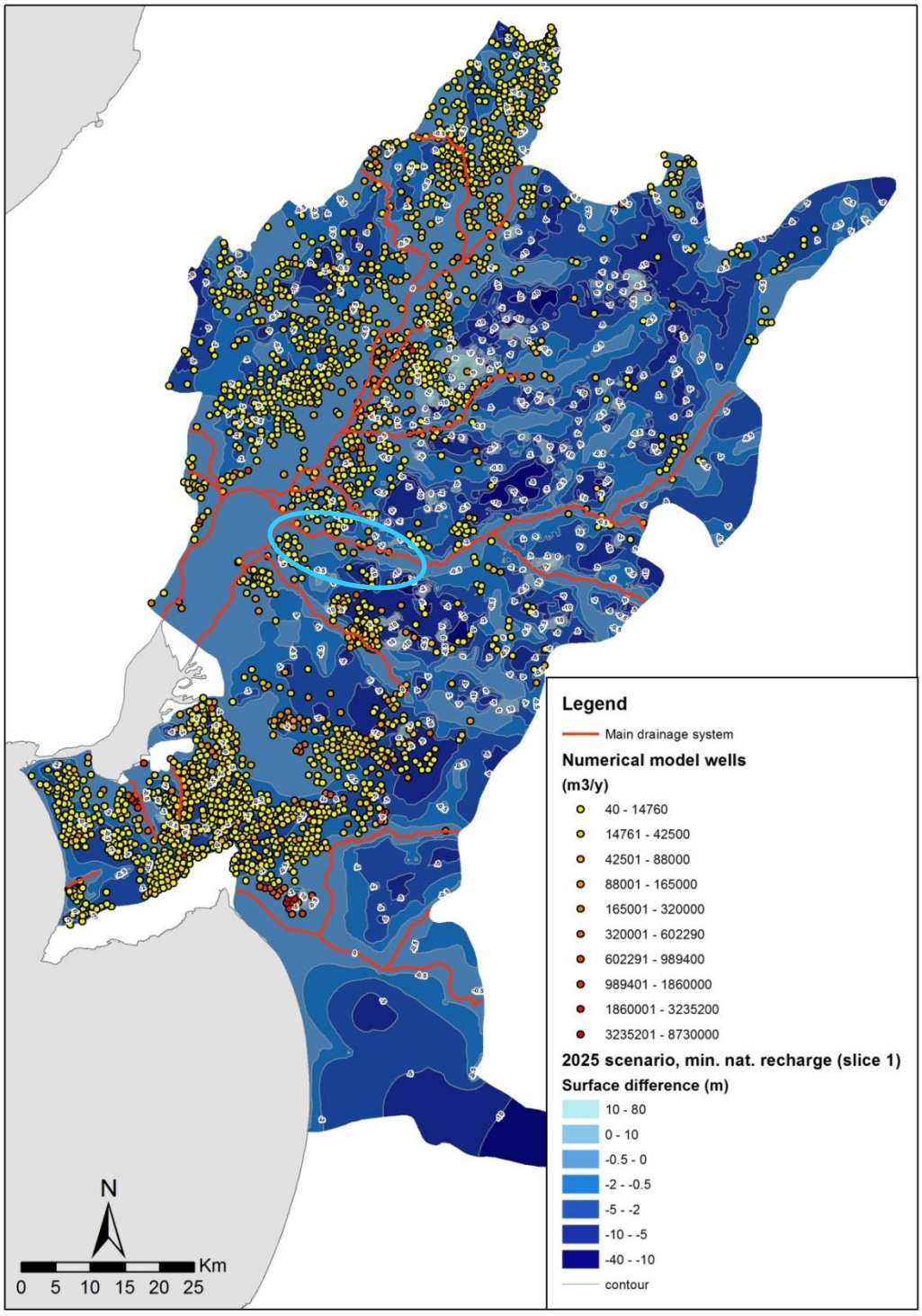

Figure 143: Groundwater level differences between the pumping conditions in the historical period (1979-2009) and the pumping conditions in Slice 1 and conditions under R3 realization (minimum recharge scenario)

Drought scenario steady state

The drought scenario was based in the conditions of the severe drought of 2005 and was used to set a worst-case scenario limit for the analysis of climate change impacts on aquifers. This scenario is not expected to become the new normal, once this would mean that the **future average recharge** would be equal to 2005 recharge (up to 50% less of the historical 1979-2009 average recharge). 2005 recharge was

estimated by BALSEQ_MOD (Oliveira, 2018) and pumping rates were assumed equal as those of the historical period.

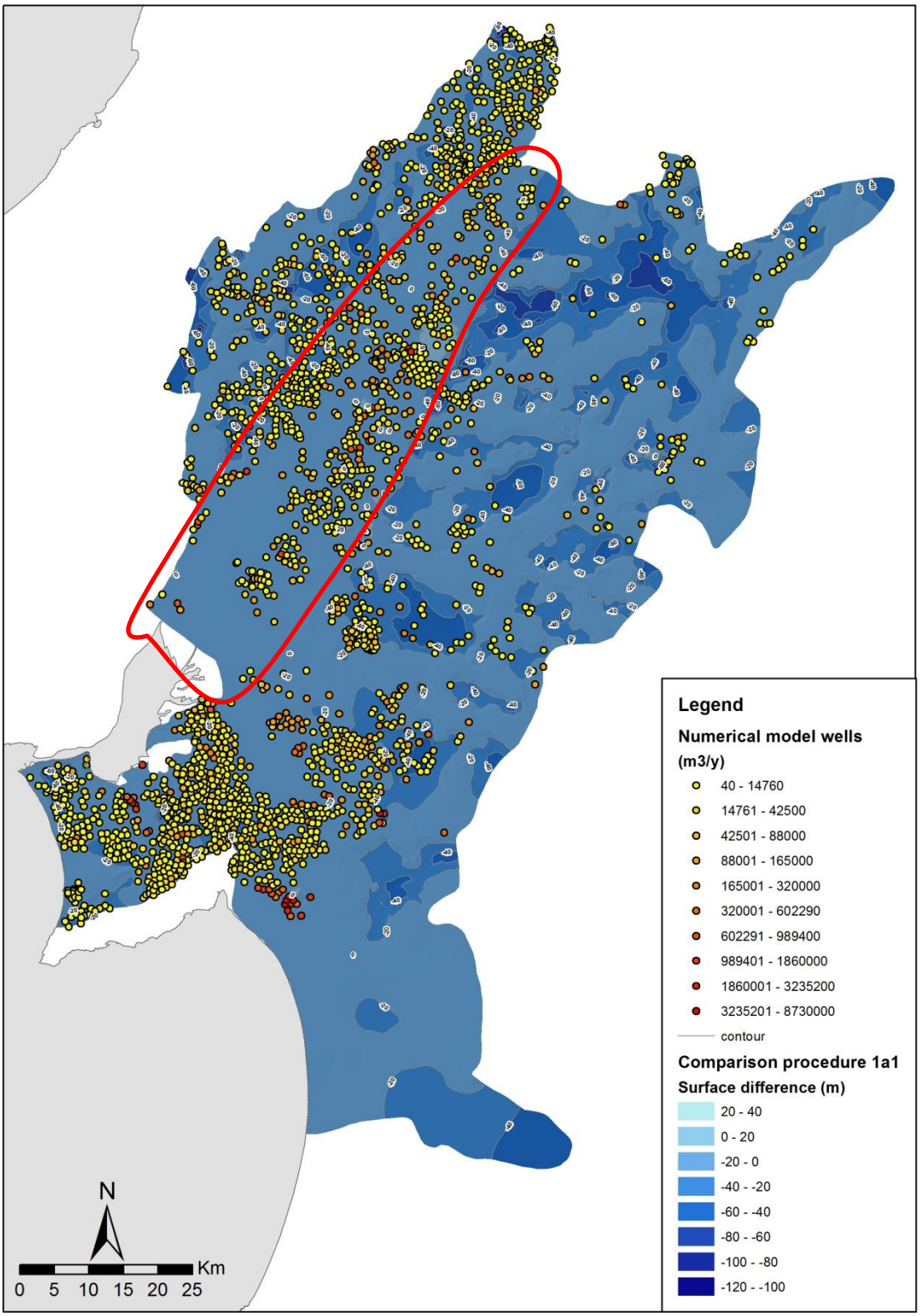

Figure 144: Groundwater level differences between the pumping conditions in the historical period (1979-2009) and the pumping conditions in Slice 1 in 2005 drought (annual mean values)

This drought-extreme scenario **shows a significant lowering of the groundwater levels** in the top layer, as can be seen from Figure 144. For the whole area of the model, groundwater level drawdowns are on the range of 20 m, with the Alluvial aquifer (central area of the model, red-fenced area) showing water level drawdowns of 10 up to 15 m. Areas with lower permeability have the larger drawdowns, as is the case of upstream Sorraia where drawdowns can be up to 20 or 40 m, and the Miocene deposits (Tejo/Sado-Margem Direita aquifer; NW zone of the model) where drawdowns can locally reach 60 m.

Drought scenario transient runs

In this scenario it is simulated the impact of a severe drought year, or a set of severe drought years (a multiannual drought). It starts at the end of a steady state run for the average historical conditions (period 1979-2009) and runs for several years in transient state. These years have recharge values similar to those evaluated with BALSEQ for 2005 (Oliveira, 2018). As such it can be seen how the groundwater levels evolve from the average conditions into a multi-year severe drought. This scenario is different from the drought scenario on steady state because here, what is under analysis is not where a groundwater surface would be if the average conditions for 20, 30 or more years would turn out as those of year 2005, but how a groundwater surface changes from the historical (1979-2009) average condition to a multiyear severe drought.

For the **1 year severe drought scenario** (Figure 145) the groundwater levels have decreased in general by less than 1 m, and in the low lying areas of the model by less than 0.5 m. This is partially due to the large volume of water stored in this aquifer system. Locally, as for instance in Sorraia region (blue circle), this can also be due to the type of boundary conditions used to simulate the river network. If reliable data were available to simulate water heights in rivers during the transient simulation period, then the results could give a larger groundwater level drawdown. However, some observation points show larger drawdowns – e.g. the -5 m area in Sorraia – typically if they are in lower permeability areas and away from the river network.

Figure 146 show the evolution of the groundwater levels from the average historical conditions after a **3 year severe drought** (2005 conditions). As can be seen, the drop in the groundwater surfaces is larger, with most part of the model suffering drawdowns of 1 to 2 m. Even in Sorraia area (blue circle), and in spite of the buffer effect of the boundary conditions simulating the river, drawdowns were dominated by drawdowns between 0.5 to 1 m. Locally drawdowns can be higher, typically in lower permeability areas and, for instance in Sorraia area, drawdowns of up to 3 or 5 m can occur in low permeability areas.

Figure 147 shows the evolution of the groundwater levels from the average historical conditions at the end of a **5 year severe drought** (assuming 2005 conditions). Drawdowns are now larger than in the former scenarios, with a wide area of the model showing drawdowns of ≥ 2 m and also large zones of 3 m (Figure 147). In Sorraia region drawdowns are dominantly from 0.5 to > 2 m, with the low permeability areas reaching values between 3 to > 5 m.

These results point to a continued deepening of the groundwater table as the drought period grows, as it happens in the real world. However, the groundwater level drawdown in the model tends to be smaller than the drawdowns in the real world under drought conditions. To simulate more realistic drawdowns, model compartmentation (and new calibrations) is required but present day knowledge of the system does not allow the adequate input of such compartmentation. As such, these results are an optimistic evaluation limit of the changes that might be expected under a protracted drought.

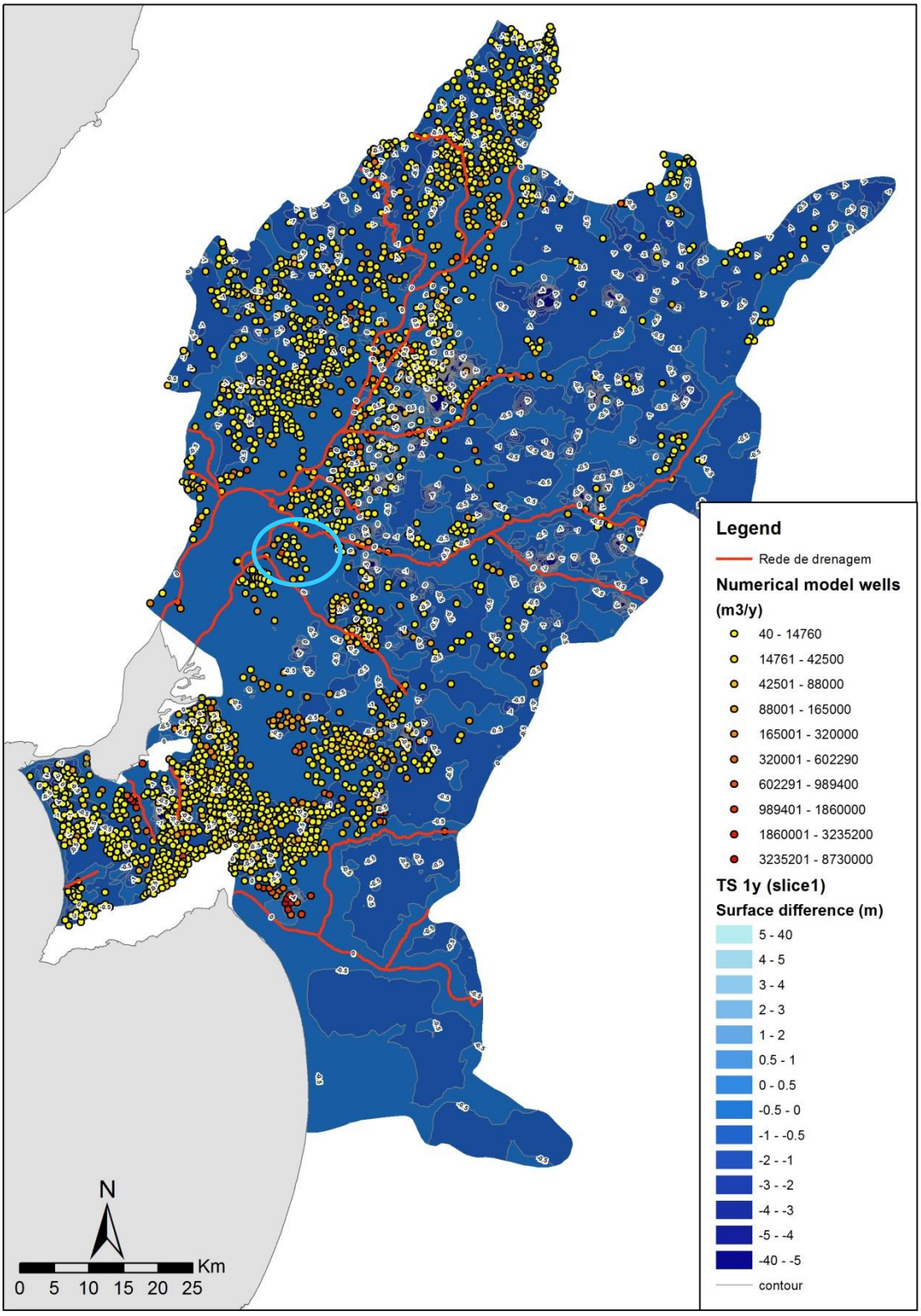

Figure 145: Groundwater level differences (Slice 1) between the average recharge of the historical period (1979-2009) and 1 year drought scenario (2005 conditions); pumping conditions = historical period

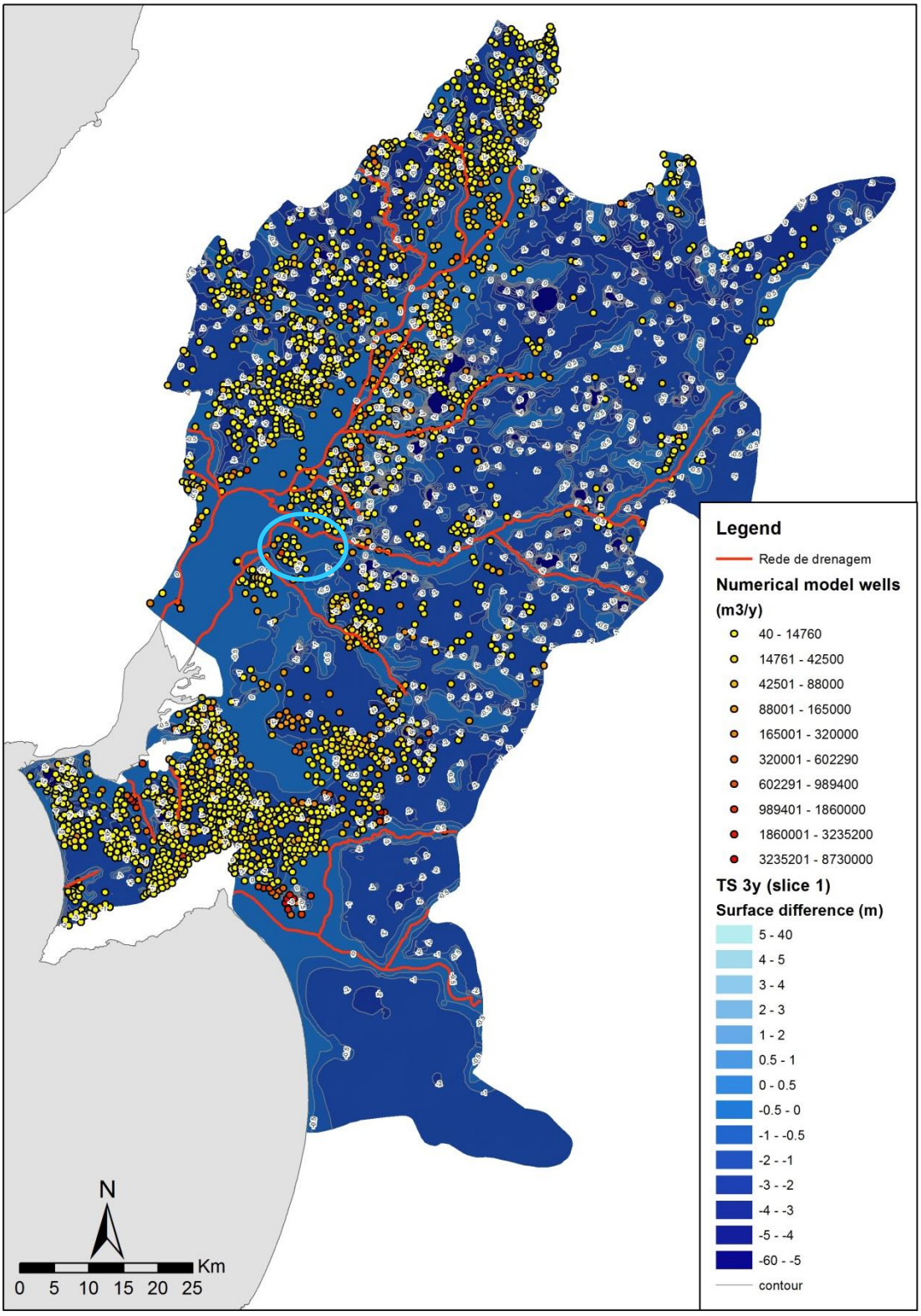

Figure 146: Groundwater level differences (Slice 1) between the average recharge of the historical period (1979-2009) and 3 year drought scenario (2005 conditions); pumping conditions = historical period

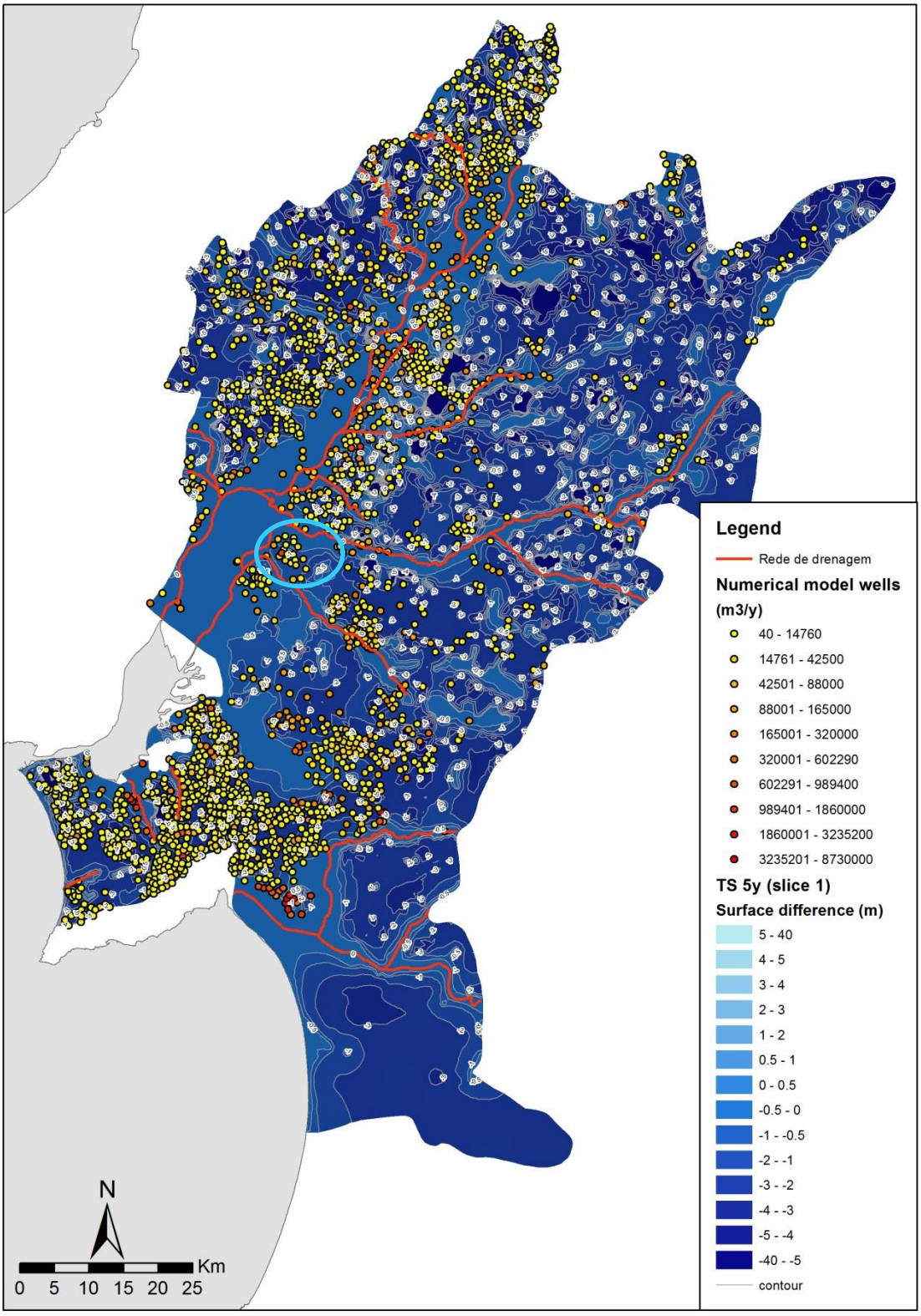

Figure 147: Groundwater level differences (Slice 1) between the average recharge of the historical period (1979-2009) and 5 year drought scenario (assuming 2005 conditions); pumping conditions = historical period

7.2.5. Discussion

Three lower Tagus aquifer systems (*Margem Direita*, *Margem Esquerda* and *Aluviões do Tejo*) are intergranular porosity reservoirs with large storage capacity able to regulate episodic events of low or large recharge, even if annual or wider. This means that for these aquifer systems in terms of the groundwater recharge (replenishment) the most important parameter would be the long term average recharge.

Ota-Alenquer is a smaller size aquifer system, karstic limestone and dolomitic, where secondary porosity (caves, fractures and fissures) plays an important role. Its storage capacity is much smaller and thus it has much less capacity to regulate episodic events and groundwater availability is more dependent on the rainfall events.

If the forecasted decadal climate change implies a change in the long term average recharge (regarded as the average of the nine hydrologic years under study from Oct/2015 to Sept/2024) in relation to the past (the average of the past series), then this change may represent an increase of the groundwater resources (in case of increasing) or a shortage of the groundwater resources (in case of decreasing), despite this is not a linear process.

Considering the average of the ten decadal predictions realizations, a small recharge increase of 6-7 mm/year was calculated for *Margem Direita* and *Margem Esquerda* aquifer systems, for *Aluviões do Tejo* the future recharge estimation is similar to the past one, while for *Ota-Alenquer* a recharge decrease of 46 mm/year is predicted.

As pointed out by the authors of the decadal predictions "The most accurate prediction will be found in the ensemble mean" (Rust et al., 2017), where the ensemble is the ten decadal realizations set. However, to account for inherent uncertainty in the initial conditions of the climate system used to run the climate model for decadal predictions each realization is thought to be as probable as the others and hence, based on these results, stakeholders and society in general should be prepared to any of these scenarios, either an increase of the groundwater recharge in this decade or either a decrease of 21 % of the recharge existing in the past.

Other sources of uncertainty of the model results are the bias correction methodology used to produce the decadal predictions, the soil and land cover properties needed to run the recharge model, the ability of the model to reproduce the process of the aquifer recharge and the difficulty in validating the model results.

The analysis of aquifer system's response to the possible futures in 2025 was done using the recharge of realisation R1 – which generated the highest recharge values for the whole area – the recharge of the ensemble of realisations and the recharge of realisation R3 (which generated the lowest recharge values for the whole area). In this way, the largest possible variation of groundwater level evolution can be simulated and give the uncertainty range of its evolution.

Variations in recharge between the present day conditions and realisations R1, R3 and the average of the ensembles, although can be quite large for some aquifers, are translated into relatively attenuated changes in the groundwater levels partly due to the large dimension of the aquifer system and as such, its high inertial response to changes. For large groundwater levels changes to occur, with wide spatial significance, recharge should shift dramatically. An example of such dramatic shifts is the case of the steady state drought scenario that was also simulated.

The model reacts accordingly to the recharge changes, showing a drawdown under realisation R3 and a rise under realisation R1, while for the ensemble of realisations the model shows a groundwater surface not much different from present day surface. Groundwater level changes tend to range from less than +1 m, near the rivers and low lying areas, to +10 m in upstream low permeability areas under R1 conditions and from less than -1 m to -5 m, with localized areas of up to -10 m under R3 conditions. However, the areas affected by the larger changes (namely those ≥ 10 m) are wider under R1 than under R3 realisations which mirrors the larger recharge variation versus the present day conditions in R1 scenario. Such large variations occur always in areas of low permeability, in particular if they are away from the river network, which functions as a discharge structure of the aquifer system. In fact, this level variation tends to amplify as further away a place is located from the river network.

The areas of lowest groundwater level variation are those near the river network and large permeability. Aluviões do Tejo show the lowest variations – typically less than 1 m – which might be due not only to the large permeability of this aquifer but also to the effect of the way the Tagus River was represented in the model.

Under R1 conditions (high recharge scenario) there are several areas that show flooding due to the rise of the groundwater levels. These flooded zones tend to cluster around low permeability zones.

Although the results display what should be expected, there are minor issues that might set the groundwater level evolution, at a local level, slightly off the reality. For instance, the real head changes along the Aluviões do Tejo might become larger in some areas than what is shown by the model due to two aspects: lack of detailed permeability data to simulate the variations in hydraulic behaviour of the aquifer and the way Tagus River and the river network is represented in the model. Lack of reliable data prevented modelling rivers as a fluid transfer boundary condition and forced its representation as a constant head boundary condition. This means that near the rivers, in the model, groundwater heads are strongly constrained – in spite of the fact that the rivers do act as discharge zones and so in fact control the groundwater level variations in the real world – and so, its variations might be too small. Locally there are some calibration issues not yet fully understood which generate too low groundwater levels (cf. Figure 142); these places are located in low permeability areas which had been quite difficult to calibrate during the calibration stage of the model.

Some low permeability areas also seem to amplify the variations of groundwater levels in a way that may not totally agree with what will be observed in the near future. For instance, groundwater level variations of 10 m between recharge scenarios corresponding to the realizations R1 and R3 and present day conditions in some locations, might be a bit extreme. However, permeability data were quite scarce and its spatial variation had to be achieved through model calibration, which relied on the availability and quality of observation data, and as a result, the model might be overshooting in those specific areas. On the whole, however, the model reacts as to be expected for the recharge conditions set up from the climate realizations of MiKlip. Once these recharges are not too different from the present day recharge, with the possible exception of R1, groundwater level changes, in a large system as this, have to be moderate.

Average annual recharges do not reproduce possible shifts in seasons and so, trying to simulate seasonal variations under each realization recharge scenario is not reliable. Besides, due to the relatively small changes between the present day conditions and the recharge scenarios, it is expected that significant seasonal shifts in recharge would not occur. The situation were such shifts would be more likely, is the scenario of higher recharge (R1 realization) and in this case the problem would be not the lack of water but, perhaps, an excess, which in general is not a problem for groundwater management.

However, and in spite of the fact that the annual recharge scenarios developed from MiKlip realizations are not able to represent how droughts can change up to 2025 – and due to the similitude of results with present day conditions, they might not change much – drought is a significant disruptive phenomena to demand an analysis of its own. To do this, it was assumed that multi-annual droughts can become more frequent and so 2 scenarios were used: 1) a transient scenario simulating a 5-year drought; 2) a steady state scenario simulating a climate that is permanently under severe drought (a case-limit scenario).

In the transient scenario, the drought can be followed from the 1st, to the 3rd until the 5th year, the consequences of which are expressed by a continuous drawdown of the groundwater levels. Although after the 1st year the drawdowns are small, in general, at the end of 5 years these are circa 2 m for the whole model area, with several areas with much larger drawdowns that may reach up to 10 m. This drawdown is what is to be expected as a drought grows but, nevertheless, the deepening of the groundwater levels seems a bit too small for what is to be expected, and so these results seem to be rather optimistic. The high inertia of this aquifer system, due to its large dimensions, can account for the results, coupled with the fact that the simulation of the river network had to use head constant boundary conditions due to the lack of reliable data, limiting the capacity of the model to simulate the discharge of the aquifer into the river network, as it happens in reality, preventing a more realistic simulation of aquifer behaviour and the interaction between surface and groundwater environments.

In the case of a radical change of climate towards a permanently severe drought condition, the steady state simulation of 2005 drought conditions show a large groundwater level drawdown of up to 20 m for most of the model area and values of 10 to 15 m drawdown for Aluviões do Tejo, on average, but locally it can reach drawdowns up to 60 m. This is what to be expected under such conditions and the picture emerging is one of significant water resources reduction and severe difficulties to access such resource, pointing to the dry-out of many wells. This is an extreme scenario and is not expected to occur in the near future. What might occur, if the evolution trend will be towards a drier climate, is a situation where, for long droughts, the conditions will be between those of the transient and steady state drought scenarios.

From the model results under these different scenarios it seems the present day conditions will not change significantly up to 2025, becasue the average of the realizations points to similar recharge values as those of present day conditions and this is reflected by the small change of the groundwater level surface under such average conditions when compared with present day' conditions. Nevertheless, higher wet or dry conditions are also made possible by the MiKlip realizations, with no clear trend towards one or the other, and as such we should be prepared for the impacts of either drier or wetter conditions. In fact, even if the climate trends towards higher dryness, it is as well likely that periods of very intense rain occur and so flooding conditions similar to those shown by the model for the R1 scenario (wet scenario) will occur. So the best is to be prepared for drier conditions but also to flooding conditions due to rise of groundwater levels after intense wet periods.

Droughts are a particularly relevant problem and regardless of a wetter or drier future, should be taken into account because it is expected a much wider variability of the climate. Even under realisations of wetter or similar to present day conditions (e.g. R4), wide variations can occur, with years of very low precipitation/recharge. This is the case, for instance, of R4 realization, with precipitation values less than 50 mm/year in 2020-2012. Under severe drought conditions local pumping volumes of groundwater increase sharply which, coupled with the local permeability conditions, lead to drawdowns that can be locally quite significant and pose a threat to the functioning of the abstraction wells.

7.2.6. Bibliography

APA, 2012 – Plano de Gestão da Bacia Hidrográfica do Tejo. Relatório Técnico. Versão Extensa. Parte 2 – Caracterização e Diagnóstico da Região Hidrográfica. APA, Lisboa, pp. 376. In https://sniambgeoviewer.apambiente.pt/Geodocs/geoportaldocs/Planos/PGRH5-TEJO/RB%5Cpgrhtejo_p2.pdf (accessed 4/12/2017).

Lobo Ferreira, J.P., Vaz Pinto, I., Monteiro, J.P., Oliveira, M.M., Leitão, T.E., Nunes, L., Novo, M.E., Salvador, N., Nunes, J.F., Pombo, S., Silva, M.F., Igreja, A., Henriques, M.J., Silva, D., Oliveira, L., Martins, T., Martins, J., Braceiro, A. Henriques, R.S., Monte, M., Quaresma, M., Martins, R. (2011). Plano de Gestão da Região Hidrográfica do Tejo. Lote 2: Recursos Hídricos Subterrâneos, 1.ª FASE, Segunda Versão dos Conteúdos do PGRH Tejo. Versão 2 Relatório Hidroprojecto-LNEC-ICCE, PGRH Tejo. Lisboa, Maio 2011, pp. 938.

Novo, M.E. (2018). BINGO project: Impacts of climate change on aquifer behaviour of the Lower Tagus area (Margem Direita, Margem Esquerda, Aluviões do Tejo aquifer systems). LNEC report under preparation.

Oliveira, M.M. (2018). BINGO project: Impact of climate change for the period 2015-2024 on the recharge of *Margem Direita*, *Margem Esquerda*, *Aluviões do Tejo* and *Ota-Alenquer* aquifer systems. LNEC report under preparation.

Rust, H.W., Richling, A., Meredith, E., Fischer, M., Vagenas, C., Kpogo-Nuwoklo, K.A., Kadow, C., Ulbrich, U. (2017). DECO - A plug-in for data extraction and conversion developed within and for BINGO. Freie Universität Berlin, Version from December 8, 2017.

7.3. Surface waters

7.3.1. Model objectives in BINGO

In order to study the impacts of climate change on water resources and detect vulnerabilities in the current water uses due to water scarcity induced by new rainfall regimes, two main case-studies were selected, both having high capacity reservoirs in the headwaters, and both described in BINGO Deliverable 3.1 (Alphen et al., 2016):

- The Zêzere River basin (a northern Tagus tributary), where the main water use is for power generation, which is not consumptive, with an added water supply component, not significant when considering the Zêzere natural flow, and;
- The Sorraia River basin (a northern Tagus tributary), with two main reservoirs in the headwaters, for irrigation purposes in the downstream valley.

The modelling objectives are to feed the previously calibrated model (in BINGO Deliverable 3.3 – Alves et al., 2016) with the climate estimates coming from WP2 in order to obtain the projected inflows to the reservoirs in the next decade, and evaluate the vulnerability of the water uses to the projected water inflows.

7.3.2. Model application

The use of pre-calibrated hydrological models to future climate scenarios is not straightforward if the simulations are to cover long time spans (from several decades to centuries) where the biological adaptation to climate and pedological evolution may change the non-linear SVAT relations (soil-vegetation-atmosphere transfer schemes).

In the present study the single decade climate predictions do not jeopardize the use of the same calibrations of the model.

As for the land-use scenarios, that can alter the evapotranspiration and soil moisture and infiltration amounts, the stability of the actual cover, with slight differences foreseen, did not justify any modification in the model's soil parameters. The higher expected changes can come from forest fires although there are no sound data to support numerical magnitude changes in soil parameters.

The water-use scenarios have no significant changes foreseen either, both from the water supply component as for the agricultural activities where most of water for new irrigated lands will be compensated by savings coming from irrigation efficiency.

7.3.3. Data

The meteorological predictions prepared under WP2 were generated for the same rainfall and climatological stations used in the model calibration phase for each case study (Alves et al., 2016). For each station 10 replicas for the same decadal period were generated (Rust et al., 2017).

The daily values of precipitation were integrated in monthly and annual totals and these latter's estimates were averaged in order to evaluate its ranking among the previous three decades of the historical calibration/validation period. Figure 148 shows the annual variability of the replicas both within the decade and along the two river basins and Figure 149 depicts the decadal variability of the climate predictions in the succession of historical decades.

As can be seen, the altitudinal factor is translated in decreasing rainfall amounts from headwaters to downstream valleys and the predictions for the 2015-2024 decade position it to be the second driest since the end of the seventies.

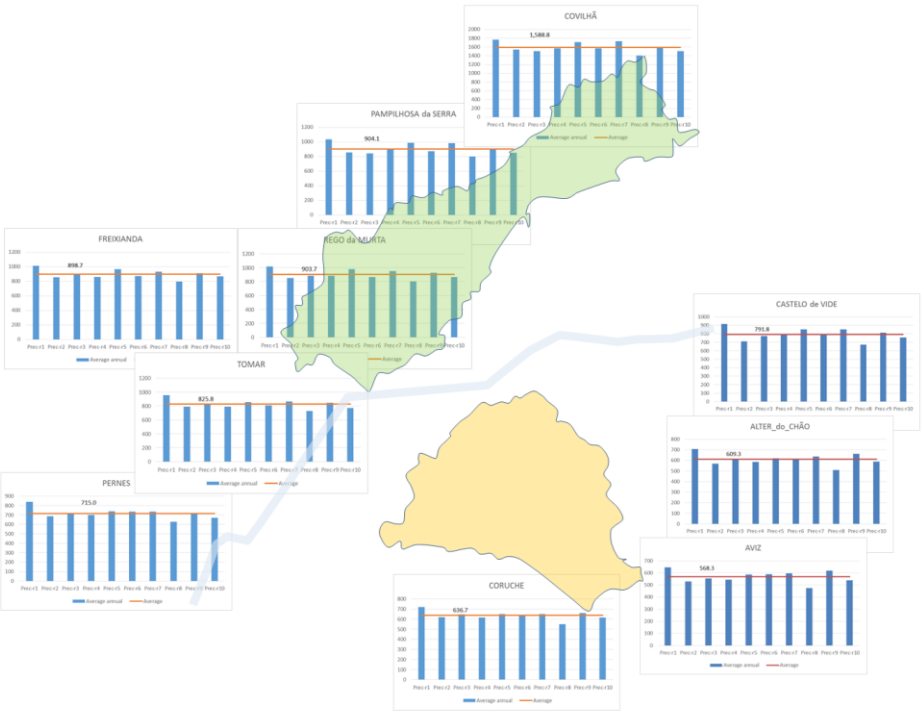

Figure 148: Variability of the annual replica's average within the decade and along the two river basins (Zêzere on green, Sorraia's headwaters on orange)

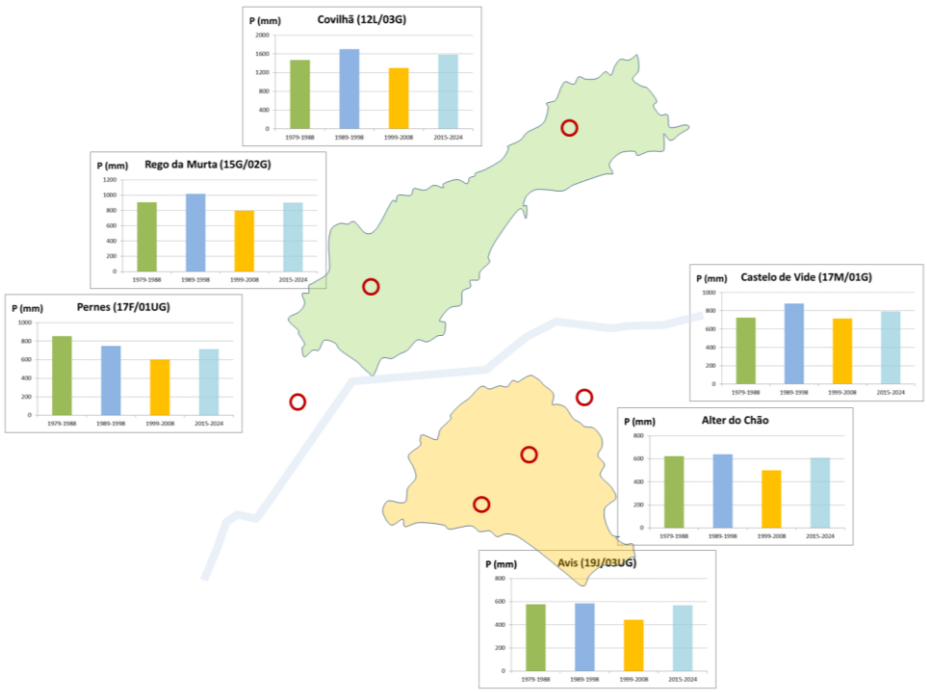

Figure 149: Decadal variability of the climate predictions in the succession of historical decades along the two river basins (Zêzere on green, Sorraia's headwaters on orange)

First the hindcast values generated from the atmospheric model for each rain gage site was tested against historical data and the projected data for the study decade of 2015-2024 were confronted with the data meanwhile being available during the course of the BINGO project (2015-2017). Figure 150 summarizes this activity for the monthly values (averaged through the replicas).

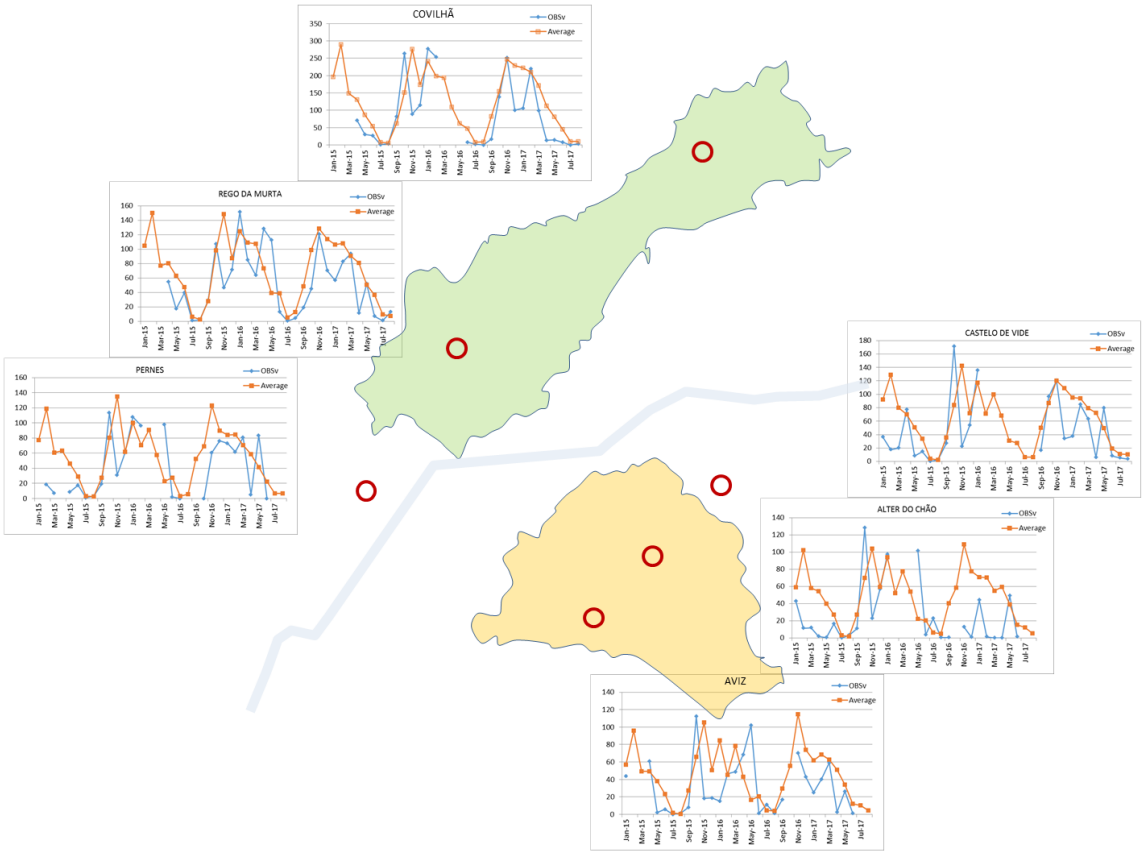

Figure 150: General fitting of the monthly rainfall predictions for decade 2015-2024 with the meanwhile monitored values (2015-2017) along the two river basins (Zêzere on green, Sorraia's headwaters on orange)

The climate modelling activity in WP2 proved very robust and helpful for the hydrological modelling in sub sequential phase.

7.3.4. Results

The model's results were analysed from two different viewpoints:

- Based on the duration curves, since what's must be evaluated from the new projections are changes in the flow regime;
- Based on runs of dry periods (mostly years) to evaluate vulnerability of current storage capacity to water stresses.

Figure 151 presents the duration curves for each rainfall-replica input, showing, by comparison with the 1999-2008 curves, less duration for the same magnitude of flows in 50 % of the replicas for the Sorraia basin headwaters.

These curves can be further analysed not only for the low flows but also for the higher flows: for instance, the duration of the flow equivalent to 20 mm can shift from being equalled or exceeded 30% in an average year to only 15% (Figure 151).

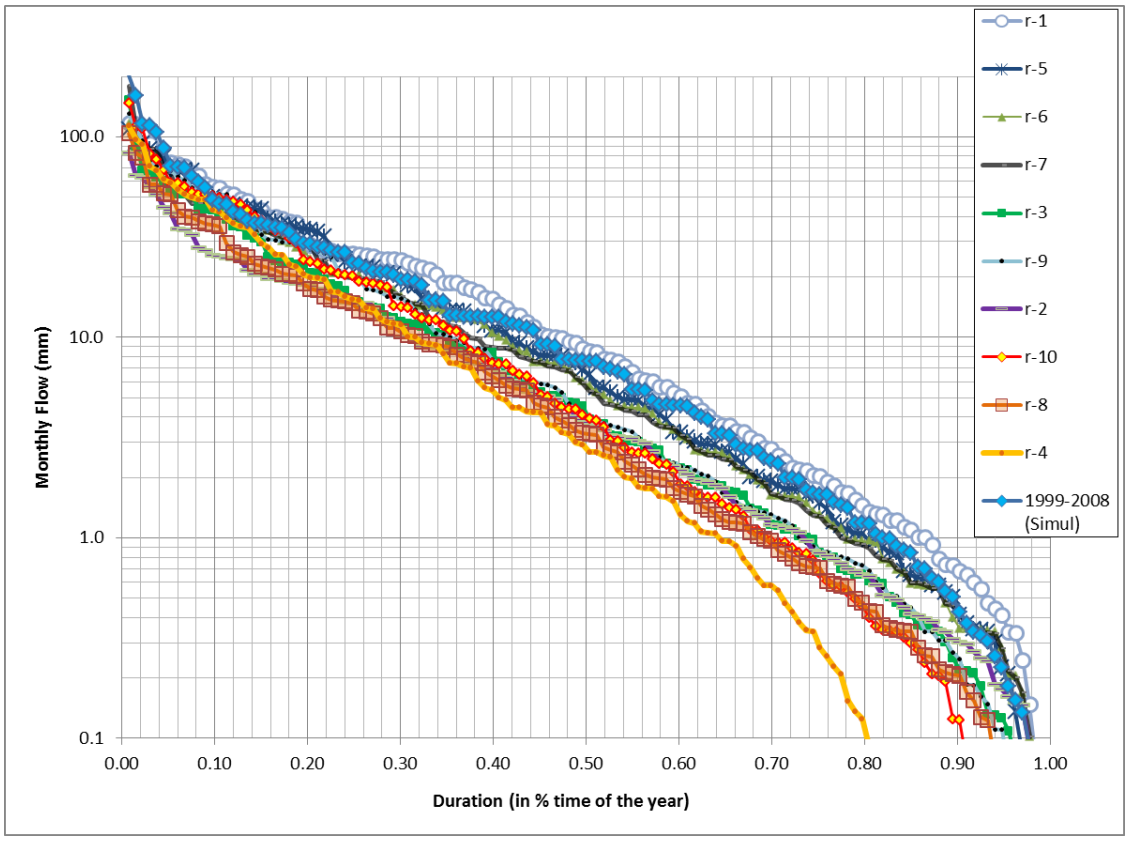

Figure 151: Duration curves for the 10 rainfall-replicas' input to the model and comparison with the last monitored decade data in the headwaters of the Sorraia basin

Figure 152 presents the duration curves for each rainfall-replica input for the Zêzere case study.

As opposed to the Zêzere case study, the gross majority of the rainfall-replicas' input projected for decade 2015-2024 generates flows that have higher durations (permanence) than the dryer decade of 1999-2008.

Only one of the rainfall-replica's input (replica 8) generates the same amounts of flow registered in the dryer decade of 1999-2008.

In what relates to the monthly runs of generated flow, two situations are depicted in Figure 153 and in Figure 154 that summarise the worst combination of storage for the reservoirs in the Sorraia and Zêzere, respectively.

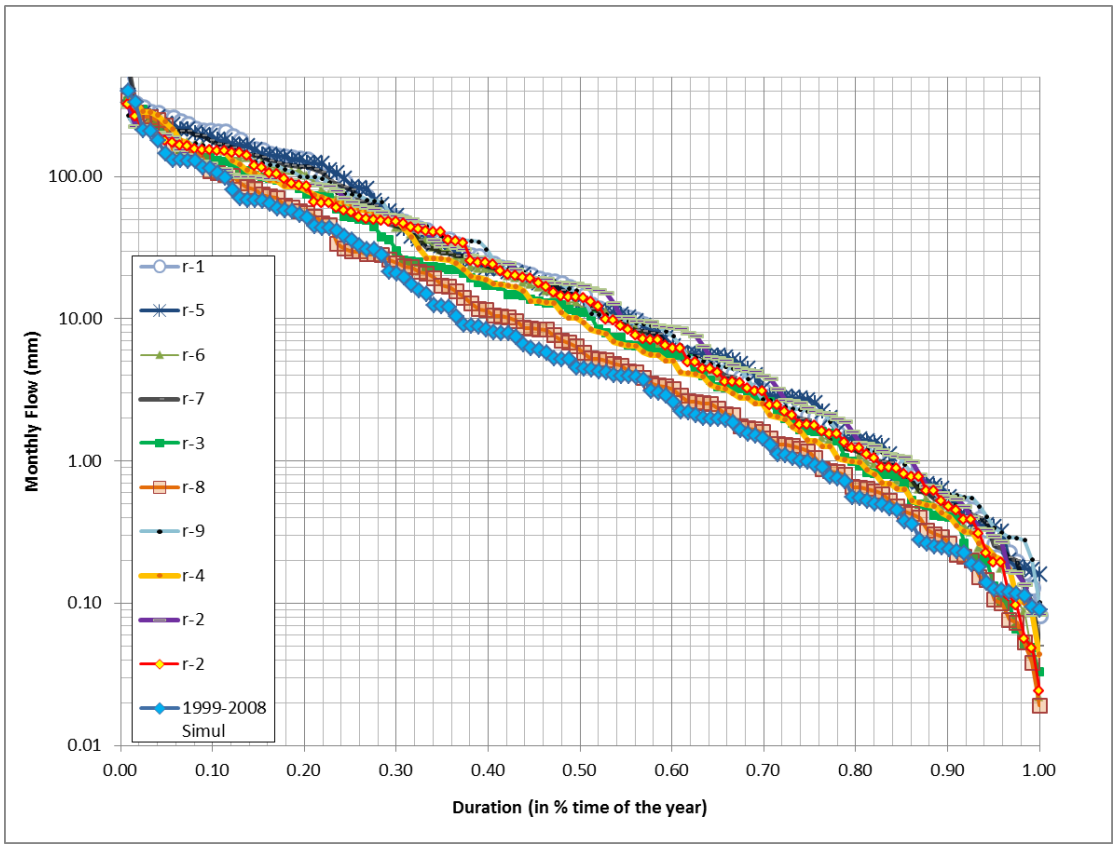

Figure 152: Duration curves for the 10 rainfall-replicas' input to the model and comparison with the last monitored decade data in the Zêzere basin

Other less severe situations can be retrieved from the same matrix created with model runs for other replicas.

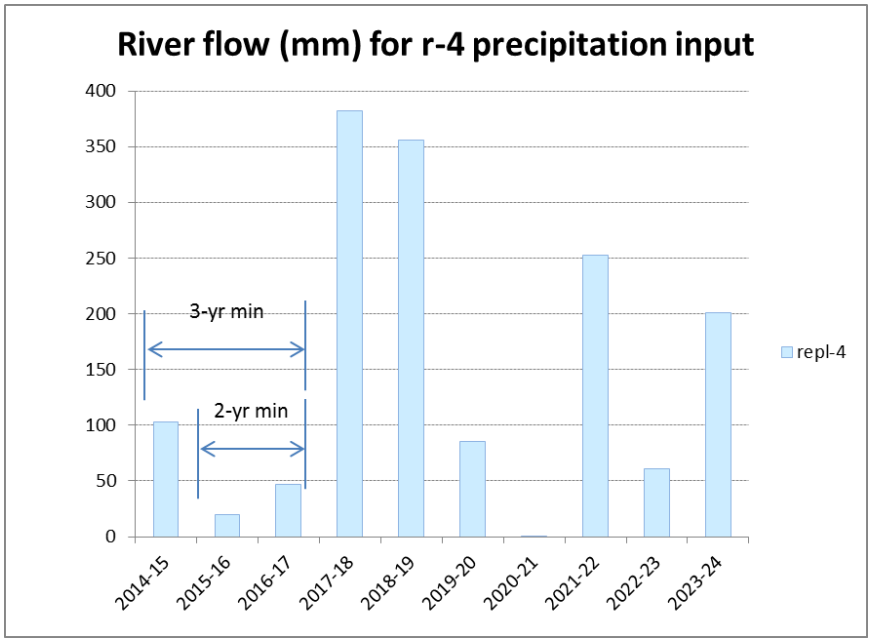

Figure 153: Results from replica-4 input to the model for the Sorraia basin with severest dry-run periods identified

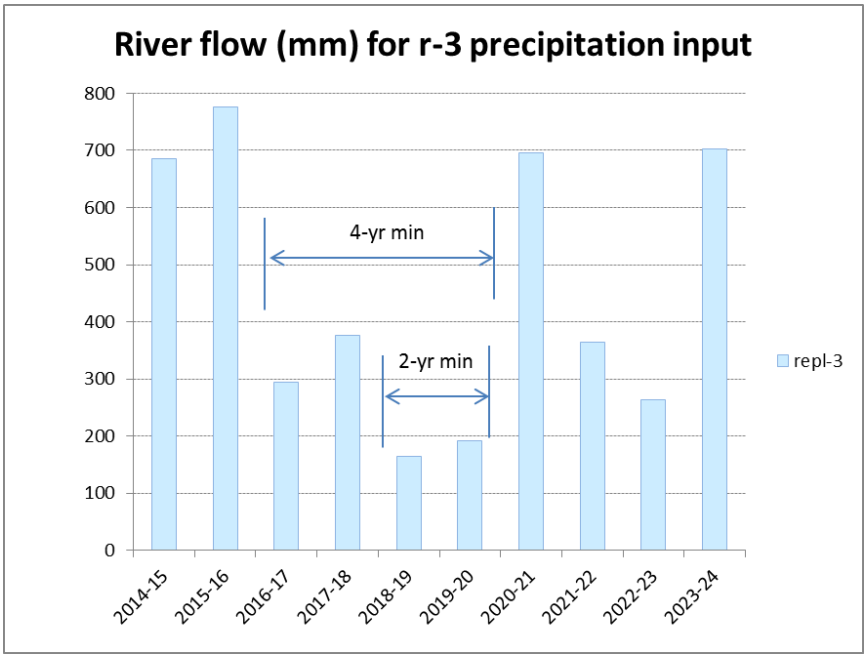

Figure 154: Results from replica-3 input to the model in the Zêzere basin with severest dry-run periods identified

7.3.5. Discussion

One vital information from the modelling activity for the Sorraia river basin was that the non-linear components of the water cycle are here very significant, probably due to the higher temperatures and less altitude of this area when compared with the Zezere (further north). Although the annual rainfall is on the average higher in the 2015-2024 decade than in the 1999-2008 decade, the monthly sequence of rainfall is very determinant.

7.3.6. Bibliography

- Alphen, H-J., Alves, E., Beek, T., Bruggeman, A., Camera, C., Fohrmann, R., Fortunato, A., Freire, F., Iacovides, A., Iacovides, I., Kristvik, E., Kübeck, C., Lorza, P., Muthanna, T., Novo ,E., Rocha, F., Rodrigues, M., Rodrigues, R., Russo, B., Sánchez, P., Scheibel, M., Spek, T., Witte, F., Zoumides, C. (2016). Characterization of the catchments and the water systems, Deliverable 3.1, BINGO - Bringing innovation to ongoing water management – a better future under climate change assessment, 89 pp.
- Alves, E., aus der Beek, T., Bruggeman, A., Camera, C., Fortunato, A., Freire, P., Grange, A.S., Iacovides, A., Iacovides, I., Kristvik, E., Lorza, P., Montes, J., Mouskoundus, M., Muthanna, T.M., Nottebohm, M., Novo, E., Oliveira, M., Rijpkema, S., Rodrigues, M., Rodrigues, R., Russo, B., Sánchez, P., Scheibel, M., Sunyer, D., Viseu, T., Voortman, B., Witte, F., Zittis, G., 2016. Calibrated water resources models for past conditions, Deliverable 3.3, BINGO - Bringing innovation to ongoing water management – a better future under climate change assessment, 183 pp.
- Rust, H.W., Richling, A., Meredith, E., Fischer, M., Vagenas, C., Kpogo-Nuwoklo, K.A., Kadow, C., Ulbrich, U. (2017). DECO - A plug-in for data extraction and conversion developed within and for BINGO. Freie Universität Berlin, Version from December 8, 2017.

7.4. Trancão basin – Floods

7.4.1. Model objectives in BINGO

The Trancão basin is located at the northern limits of Lisbon, covering an area of 292 km2. The Trancão River and its tributaries are prone to rapid floods due to intense rainfalls, strong slopes of the river basin headwaters and the existence of heavily urbanized areas. The overall aim of this BINGO research site is to evaluate flood discharges for current and future scenarios, which are necessary to obtain flood hazard maps of Trancão River. As referred in Deliverable D3.2 no land use changes are predicted in Trancão basin for the period 2015-2024, and since water uses do not have influence in flood events, the scenarios to be consider are changes in extreme precipitation events.

The hydrologic model used to simulate the Trancão basin runoff response to precipitation extreme events was the HEC-HMS (Hydrologic Engineering Center, Hydrologic Modeling System) developed by the US Army Corps of Engineers, described in Deliverable D3.3. The precipitation extreme events for different return periods were obtained using the IDF (Intensity-Duration-Curves) for current and future (2015-2024) scenarios. The later was provided by WP2 (Deliverable 2.9).

7.4.2. Model application

As described in Deliverable D3.3, the HEC-HMS model was designed to simulate the rainfall-runoff processes in a wide variety of basin types considering the soil and land use characteristics. The HEC-HMS model setup consists of four main components: the basin model, the meteorological model, control specifications, and input data (time series, paired data, and gridded data).

The HEC-HMS model was implemented in the Trancão River basin based on the digital terrain model, on the characteristics of the vegetation cover and land uses. The Trancão basin was divided into several subbasins to increase the modelling performance and to use HEC-HMS as semi-distributed model (Deliverable D3.3). The model was calibrated using historical flood events with observed hyetographs and hydrographs.

In this report the HEC-HMS model was used to simulate the flood events with return periods of 2, 20, 50 and 100 years for two precipitation scenarios: the evaluation period and the 2015-2024 period.

7.4.3. Data

To characterize extreme precipitations associated with the referred return periods the Intensity-Duration-Frequency (IDF) curves are required. The IDF curve for the evaluation period was provided for the meteorological station São Julião do Tojal located in Trancão basin in Brandão et al. (2001). The decadally adjusted IDF (2015-2024) for the same station (São Julião do Tojal) was provided by WP2 (Deliverable 2.9). Table 26 shows the intensities of precipitation for the two scenarios. The differences in precipitation intensities are not relevant for the 100-year return period, although for lower return periods it is observed a reduction of the intensity of precipitation in the 2015-2024 period.

In addition to the precipitation intensity, it is necessary to know its distribution during the rainfall event. In this study the methodology proposed by Huff (1967) for the precipitation distribution along the event was considered. According to Huff, the precipitation events are divided into four groups in which the peak rainfall intensity occurs in the first, second, third or fourth quarter of the rainfall duration. For each group the distribution of precipitation is determined for different probabilities of occurrence. In Brandão et al. (2001)

study, the distributions of precipitations during storm events were obtained for different stations based on Huff's methodology. Taking as reference the Lisbon station (near Trancão basin), around 31 % of the storm events belongs to the 1st quartile, 28% to the 2nd quartile, 20% to the 3rd quartile and 21% to the 4th quartile.

Table 26: Intensities of precipitation in São Julião do Tojal (Trancão basin)

Scenario	Intensity of precipitation (mm/h) for different return periods			
	2 years	20 years	50 years	100 years
Evaluation period	4.5	10.5	12.6	14.3
2015-2024	3.9	8.7	11.4	14.0

7.4.4. Results and Discussion

Based on HEC-HMS calibrated model, for each scenario (evaluation period and 2015-2024 period) a combination of a return period (2, 20, 50 and 100 years) with four different precipitation distributions (1st quartile, 2nd quartile, 3rd quartile and 4th quartile) were considered. This resulted in a total of 32 simulations of flood hydrographs. The range of discharges obtained are presented in Table 27.

To illustrate the results obtained, the distributions of precipitation (1st quartile, 2nd quartile, 3rd quartile and 4th quartile) associated to the return period of 2 years are presented in Figure 155 for the evaluation and 2015-2024 periods. The flood hydrographs produced by the HEC-HMS model for each of these precipitation distributions are shown in Figure 156.

For the same type of precipitation distribution (1st quartile, 2nd quartile, 3rd quartile and 4th quartile), the flood discharges during the period 2015-2024 are lower than those of the evaluation period for the 2year precipitation event. However, taken into account the influence of the precipitation distribution on the flood hydrograph and flood peaks (e.g. Figure 156), it is not possible to state that in the period 2015-2024 the flood peaks will be smaller. Indeed, they may be identical to the evaluation period flood peaks depending on the distribution of rainfall during the storm event. The same conclusions were obtained for the results for 20 and 50 years return peaks.

In the case of the flood with 100 year return period and for the same type of precipitation distribution, the range of peak discharges are identical in the evaluation and 2015-2024 periods.

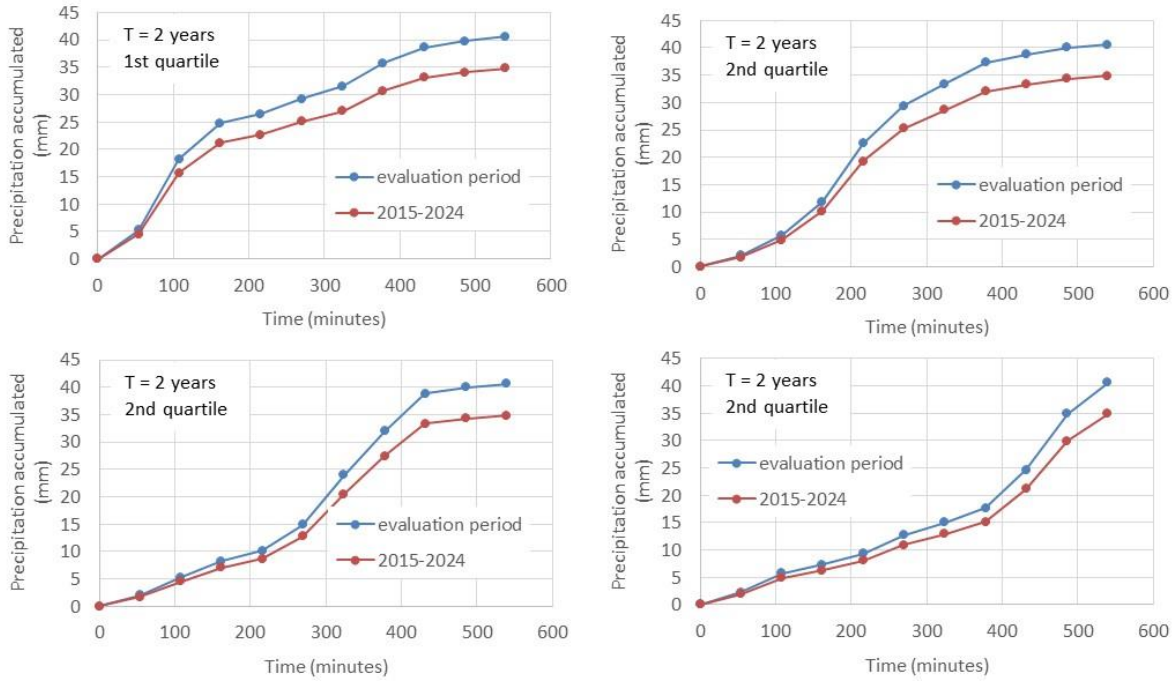

Figure 155: Precipitation distribution for the 2-year return period for the evaluation and the 2015-2024 scenarios

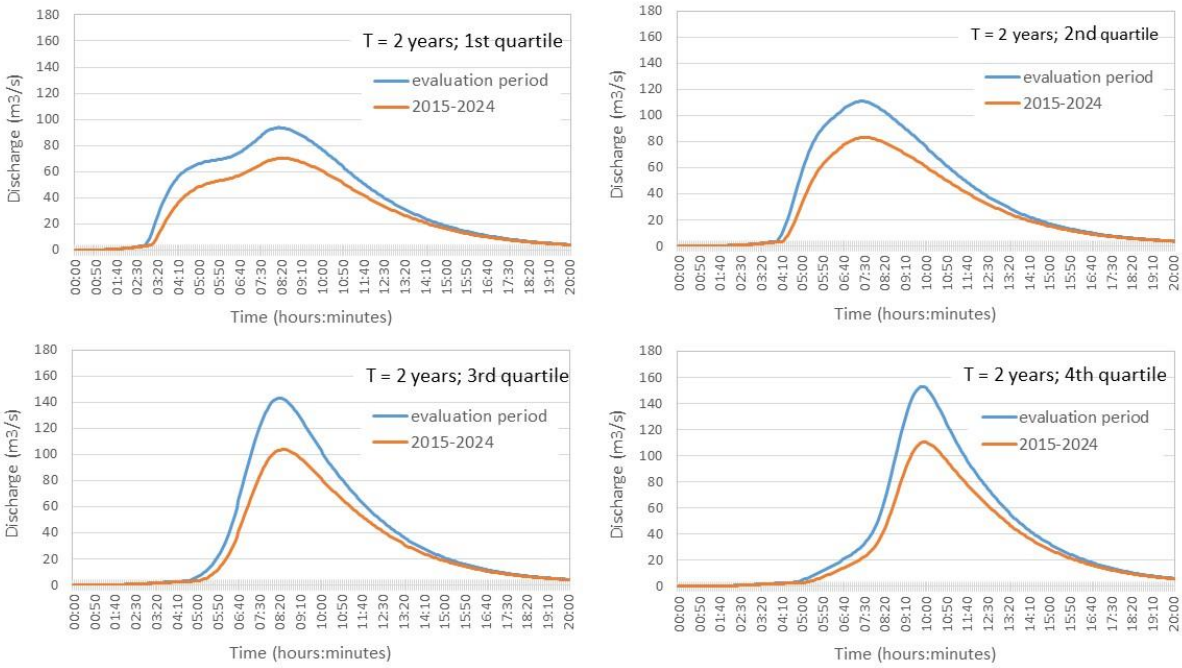

Figure 156: Flood hydrographs for the 2-year return period for the evaluation and the 2015-2024 scenarios

Table 27: Range of peak discharges (m3/s) for the evaluation and 2015-2024 scenarios

Scenario	Range of peak discharges (m^3/s)			
	2 years	20 years	50 years	100 years
Evaluation period	94 - 153	385 - 769	555 -1024	706 - 1233
2015-2024	70 - 110	289 - 555	454 - 877	678 - 1195

Finally, Table 28 presents the ratio between the peak discharge (m^3/s) for 2015-2024 decade and the peak discharge (m^3/s) for evaluation period. Considering the occurrence of the same type of precipitation distribution, the peak discharges are reduced for the 2, 20 and 50 return period floods considering the predictions of 2015-2024 decade. In the case of the 100 year return period flood the peak discharges are identical.

Table 28: Ratio between the peak discharge (m3/s) for 2015-2024 decade and the peak discharge (m3/s) for evaluation period

Distribution of precipitation	Peak discharge (m^3/s) for 2015-2024 decade / Peak discharge (m^3/s) for evaluation period			
	2 years	20 years	50 years	100 years
1st quartile	0.75	0.75	0.82	0.96
2nd quartile	0.75	0.69	0.84	1.13
3rd quartile	0.72	0.72	0.85	0.97
4th quartile	0.72	0.72	0.86	0.97

7.4.5. Bibliography

BRANDÃO, C.; RODRIGUES, R.; COSTA, J. P. (2001) - Análise de fenómenos extremos. Precipitações intensas em Portugal Continental. DSRH-INAG, Instituto da Água. Lisboa, Portugal.

HUFF, F. A. (1967) - Time distribution of rainfall in heavy storm, Water Resources Research, vol. 3, No. 4, pp. 1007-1019.

8. Spain

Model frameworks

Badalona (Spain) is part of the metropolitan area of Barcelona and has an area of 21.2 km^2 located between the coastal mountain range of 'Serralada de la Marina' and the Mediterranean Sea. The overall aim of this BINGO research site is to develop a full risk assessment related to flooding and Combined Sewer Overflows (CSOs). This deliverable D3.4 aims at developing hazard maps (as main outputs of the models developed within the project framework), which are an intermediate step toward the risk assessment (achieved in the context of WP4). Moreover, in this deliverable, several tasks to adapt WP2 outputs (extreme and continuous future time series) to the needs of the model concerning Badalona case study have been described in additional sections. Particularly high spatial and temporal resolutions are key requirements to carry out adequate and reliable hazard and risk assessments regarding flooding and CSOs in urban areas. The hydraulic, hydrological and marine models used in D3.4 for hazard assessment were fully described in D3.3.

Modelling activities regarding Badalona research site are presented through two different model frameworks/sections:

1) Flooding. This section aims to develop flood hazard maps of Badalona for current and future scenarios. Hazard maps for pedestrian and vehicles exposed to flooding are computed and the changes in terms of hazard from the past to the future scenarios are quantified.
2) Combined Sewer Overflows. This section aims to develop hazard maps for people swimming in the sea after CSO events and to quantify the future hazard of CSOs on the sea water quality of Badalona. The hazard regarding CSO has been assessed in terms of both number and volume of CSOs every bathing season.

8.1. Model objectives in BINGO [Flood analysis]

This sections aims to develop flood hazard maps of Badalona for current and future scenarios. Hazard for both pedestrians and vehicles exposed to flooding is considered. The changes of hazard between past and future scenarios are quantified in terms of differences in the extent of the different areas classified as high hazard maps. The rainfall inputs are used to simulate flood depth and surface runoff velocities using the 1D/2D model described in D3.3. Three different hazard criteria: low, medium and high are then defined as a function of simulated runoff velocities and water depth.

The decadal rainfall predictions from Work Package 2 were analyzed and treated applying a specific bias correction. Finally they did not show any increase of future rainfall intensities respect to the current IDF curves. Therefore, future rainfalls derived from climate change predictions of the period 2051-2100 were used. A detailed description of the rainfall data used is shown in the data section below.

8.2. Model application

The calibrated coupled 1D/2D (drainage network/surface runoff) model described in D3.3 is used to simulate flood depth and surface runoff velocities during single design rainfall events of different return periods. Decadal rainfall realizations were analyzed and did not show an increase of future rainfall intensities, therefore future rainfall derived from climate change predictions (2050-2100) were used. Future land use changes are minor in Badalona and only changes in adaptation measures for sediment reduction (erosion reduction in rural upstream catchments) are considered.

Flood hazard is analysed and assessed by comparing flood hazard maps obtained from simulated past and future scenarios. Flood hazard maps are computed for pedestrians and vehicles and are obtained by combining the simulated flood depth and surface water velocities obtained by the 1D/2D model with the specific hazard criteria for urban areas (Martínez et al., 2016 and 2017).

The coupled 1D/2D (combined sewer network/surface runoff) model was used to simulate the flooding depth and surface water velocities resulting from design storms of 2, 10, 100 and 500 years return-period. The design storm events have a 1-hour duration and were derived from the RIDF (Real IDF curves derived from the Fabra rain gauge presented in the data section) for the past scenario and from the CORDEX IDF curves for the future scenario. The design storm events were obtained from IDF curves according to the methodology of Raso et al. (1995).

Both the RCP 2.6 and the RCP 8.5 scenarios will be simulated. RCP 2.6 is the worst case scenario for rainfall intensities. However, RCP 2.6 is nowadays considered as an unrealistic scenario by the European commission (the latest year trends in global CO_2 emissions show that the emission assumptions of RCP 2.6 were too optimistic). Therefore, RCP 8.5 is the more realistic worst case scenario (if RCP 2.6 is excluded).

Hazard criteria are defined as ‘low’, ‘medium’ and ‘high’. Figure 157 shows the defined hazard criteria used for pedestrian and vehicles that are function of both the maximum simulated flood depth and water flow velocity. The criteria for the vehicle Seat Ibiza was chosen as it represents the most common type of vehicle. These criteria are applied to each computational cell of the 2D surface model in order to obtain the hazard. For each cell of the 2D domain (excluding buildings), the maximum flooded depth and the maximum water velocity during each simulated design storm event are computed.

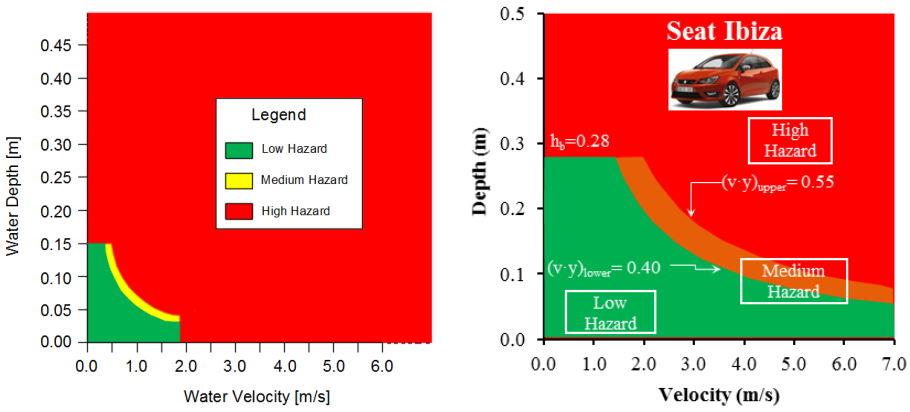

Figure 157. Hazard criteria for pedestrian (left) and for cars (right). From Martínez-Gomariz et al. (2016 and 2017). Water depth and velocity are the maximum simulated during the design storm.

8.2.1. Data

The rainfall realizations (time series) provided by Work Package 2 were analyzed and treated (bias correction was applied) and results showed that no increase of rainfall intensity is expected in the next 10 year period (decadal predictions). Therefore, a different data set was used for Badalona flood analysis. The rainfall data used was derived from the climate predictions of the EURO-CORDEX project. The next sub-sections show first the analysis of the rainfall realizations from WP2 and then the rainfall data that are used in flood analysis.

8.2.1.1. Analysis of the rainfall decadal predictions (2016-2024) data from WP2

In order to compute future design storms as inputs for the Badalona 1D/2D coupled model, rainfall time series data with high time resolution are required. Design storms for urban hydrology applications have commonly a one or a two hours duration due to the quick response (short time of concentration) of urban catchments. Based on this particular necessity for the Badalona research site, 5 minutes time resolution from both historic and future decadal predictions of extreme episodes were developed in WP2.

The historic (1951-2015) and decadal predictions (2015-2024) models of extreme episodes were based on the Miklip project (http://www.fona-miklip.de) funded by the German Ministry of Education and research aiming to develop a world class decadal prediction system. Moreover, within Miklip project the Max Planck Institute's GCM MPI-ESM was employed. These models provide a spatial and temporal downscaling down to 2.2 Km and 5 minutes respectively.

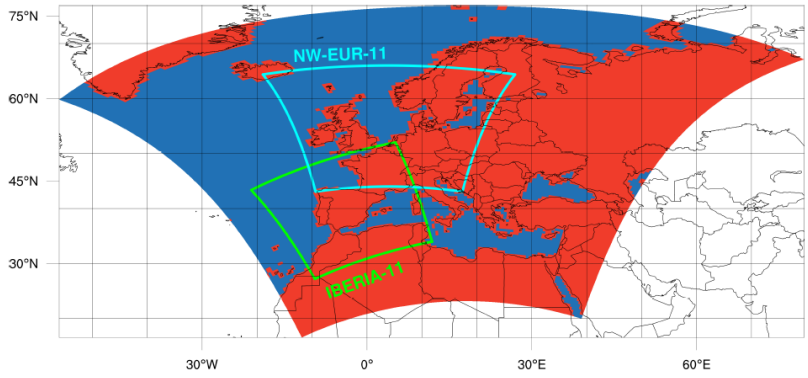

Figure 158. Iberia-11 domain where Badalona municipality is located (Miklip project)

Currently, IDF curves performed based on historic recorded time series data in the Fabra Observatory are freely available and, in fact, these are employed for urban hydrology studies not just in Barcelona but also across the surrounding municipalities. Therefore, these RIDF curves were employed for performing the current design storms as inputs for the 1D/2D hydrodynamic models of Badalona. Badalona is located just next to Barcelona, therefore IDF curves in Badalona are expected to be quite similar to Barcelona's in intensity values and also in RIDF shapes. For these reason, in order to analyse the appropriateness of the provided historic (1951-2015) rainfall time series data, their corresponding RIDF curves have been performed. The comparison of this performed "numerical" RIDF curves with the "real" ones obtained though observation data will allow us to establish the degree of adequateness for the numerical ones.

The provided rainfall time series data were stored within cells (~2.2 km) for a grid in the Iberia-11 domain (Figure 158). In Figure 159 a zoom of this grid for the Barcelona-Badalona area is shown, and the cell over Fabra Observatory is indicated. Therefore, the time series data stored within this cell has been employed to perform the RIDF curves for different return periods.

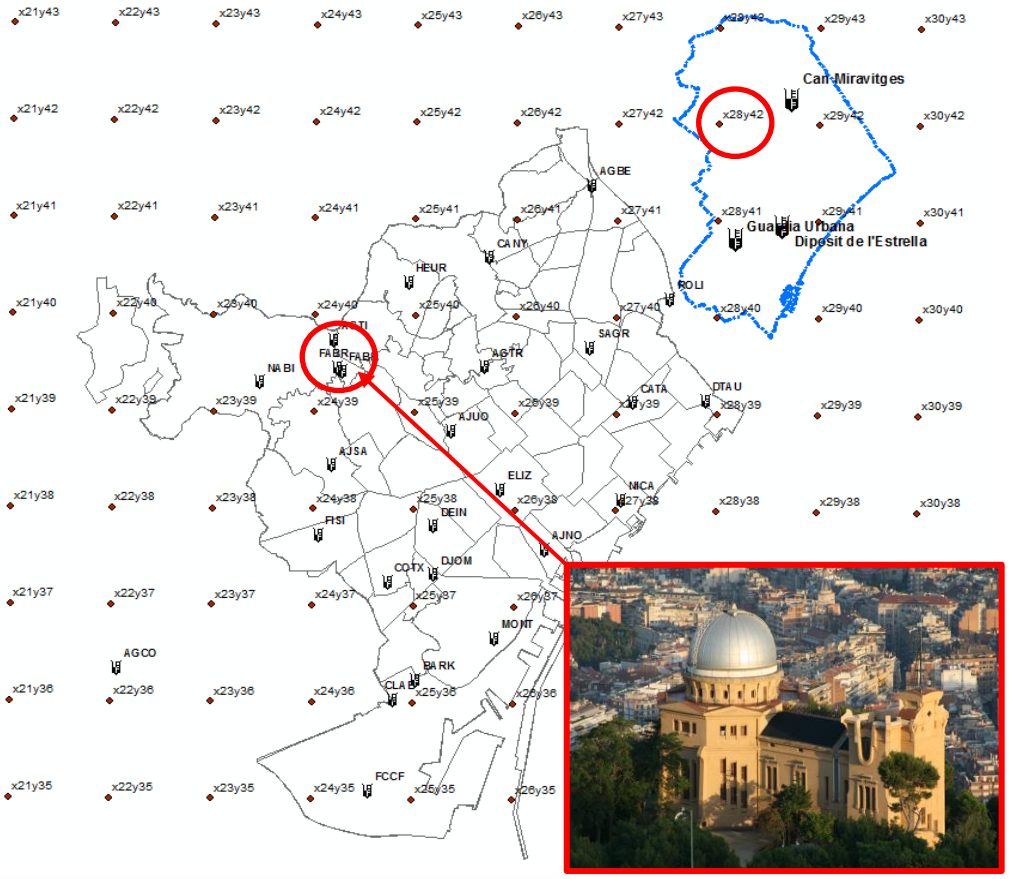

Figure 159. Grid (~2.2 km resolution) over Barcelona and Badalona (contour in blue). Fabra Observatory indicated.

The Gumbel distribution has been employed in order to analyse extreme annual values of intensities for each 5 minutes. Moreover, the rainfall time series data stored in the cell x28y42 (located over Badalona) (Figure 159) has been analysed and obtained its corresponding RIDF curves also. These curves for 5, 10 and 100 and 500 years return period, together with the real ones, are plotted in the graph that Figure 160 shows.

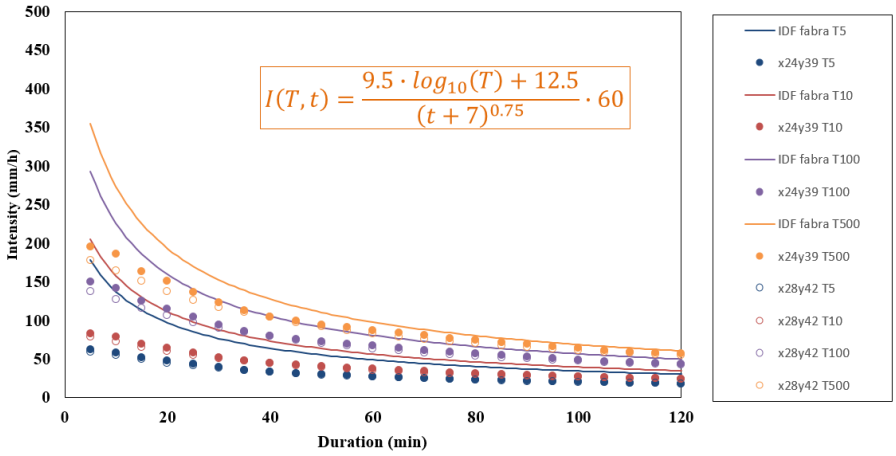

Figure 160. Historic real IDF curves for Barcelona (continuous lines) and numerical ones for Barcelona (dots) and Badalona (circles)

It can be observed that numerical values are quite lower than those from real RIDF curves, especially for short durations, which are actually the most important when it comes to impacts assessment in urban

hydrology. This underestimation is quite common for spatial downscaling developed using dynamic model that tend to smooth the extreme values provided for each cell (respect to punctual data provided by observation) and usually have some difficulties to represent convective and orographic causes of local storms events. On the other hand, it is proven that Barcelona (dots) and Badalona (circles) IDF curves are really similar, therefore the use of Barcelona real IDF curves in Badalona seems to be appropriate.

So, in order to apply properly the decadal predictions (2015-2024), a bias was proposed to fit numerical to observed extreme rainfall intensity values. Thus, a matrix bias (Table 29) was developed to fit intensities for each time and its corresponding return period. Figure 161 shows the position of each point on the real RIDF Barcelona curves after applying the matrix bias.

Table 29. Matrix BIAS proposed to fit numerical to real RIDF curves

T(years)/ t(min)	5	10	15	20	25	30	35	40	45	50	55	60
2	482%	402%	367%	344%	330%	324%	320%	316%	310%	305%	301%	299%
5	288%	236%	219%	204%	198%	196%	194%	192%	188%	184%	181%	178%
10	247%	201%	187%	174%	169%	168%	166%	164%	161%	158%	155%	152%
25	218%	177%	166%	154%	150%	149%	147%	146%	143%	140%	137%	134%
100	196%	159%	149%	138%	134%	134%	133%	131%	128%	126%	123%	121%
500	182%	147%	138%	128%	125%	124%	123%	122%	119%	117%	114%	112%

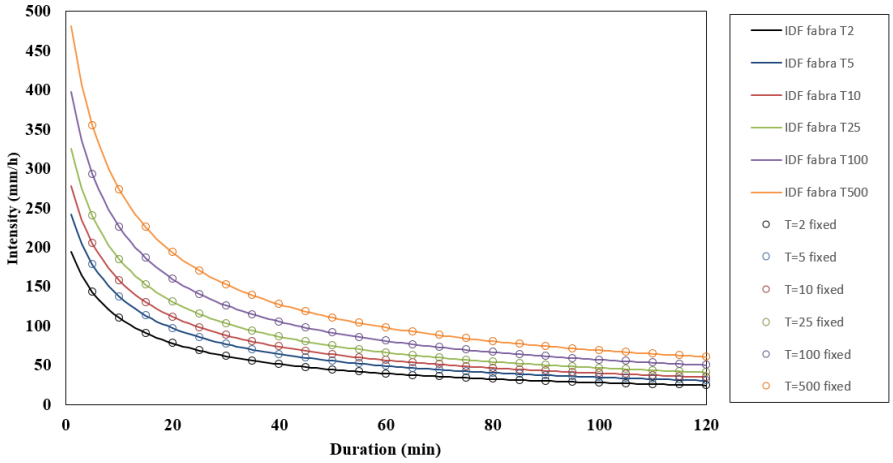

Figure 161. Fitted numerical RIDF curves into real RIDF curves for Barcelona

Decadal predictions provided 10 realizations (rainfall time series data) for each grid cell, therefore all ten time series have been analysed and their corresponding RIDF curves have been performed by following the same extreme analysis as for the historic data. Consequently, once all families of RIDF curves were developed, the bias matrix was applied in order to increase the intensities with the same proposition as it was done for the historic data. This procedure assumes that future RIDF curves will have the same shape as the historic real ones.

In Figure 162, it can be observed how all ten RIDF curves (for each realization) are located below the historic real one for 10 years return period. Therefore, according to this model, intensities will be as a maximum equal to the current ones for the next 10 years (2015-2024). This result was also confirmed by conducting the same analysis for the other return periods.

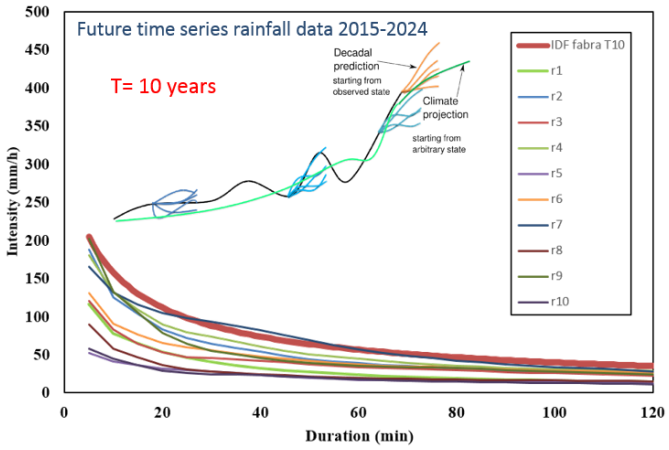

Figure 162. Historic real RIDF curve for 10 years return period

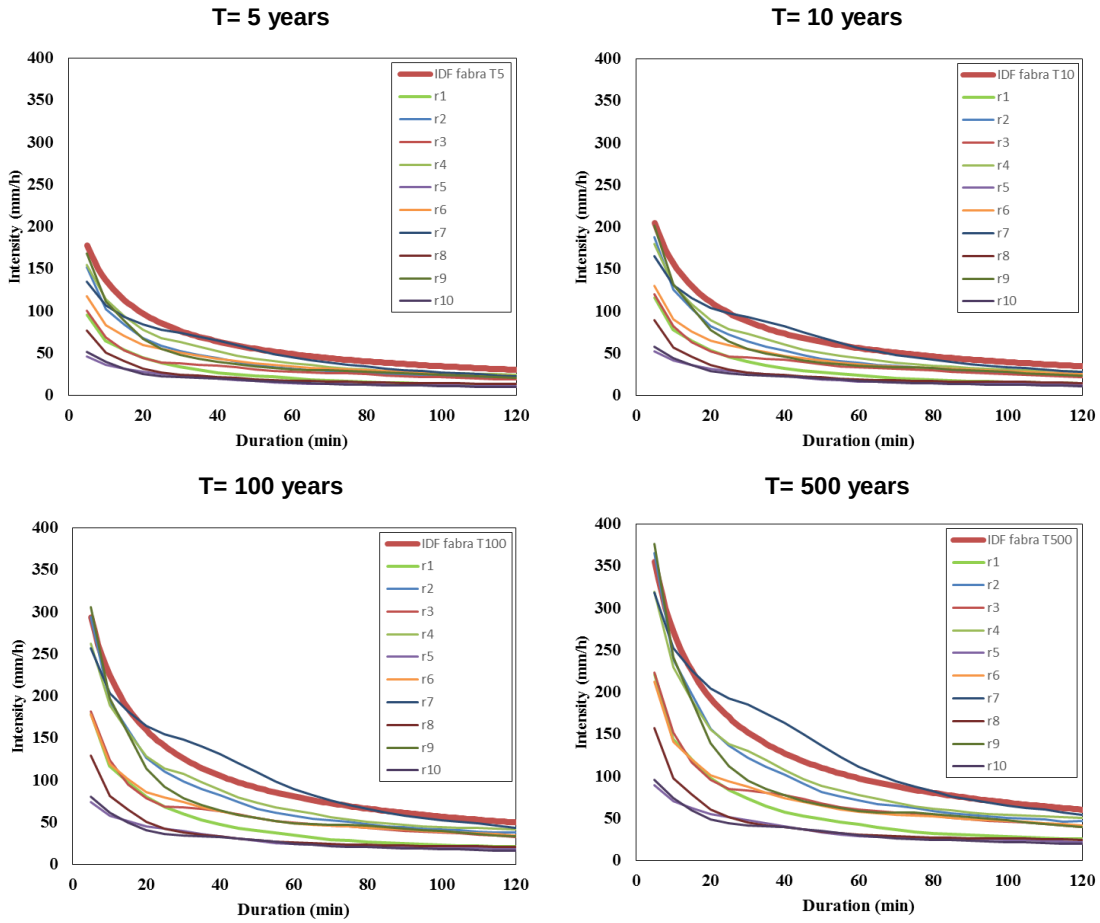

Figure 163. Comparison of historic real RIDF curves against future RIDF based on decadal predictions (2015-2024) for different return periods

In order to assess the reliability of these results, which indicate a great likelihood of lower extreme precipitations for the future short-term, the precipitation trend in the Fabra Observatory station has been analysed. Based on the observations in Fabra's station, the accumulated annual precipitation, the number of rainy days with accumulated volume precipitations higher than 0.1, 1, 10 and 50 mm has been plotted together with their respective trend (Figure 164, Figure 165, Figure 166 Figure 167 and Figure 168).

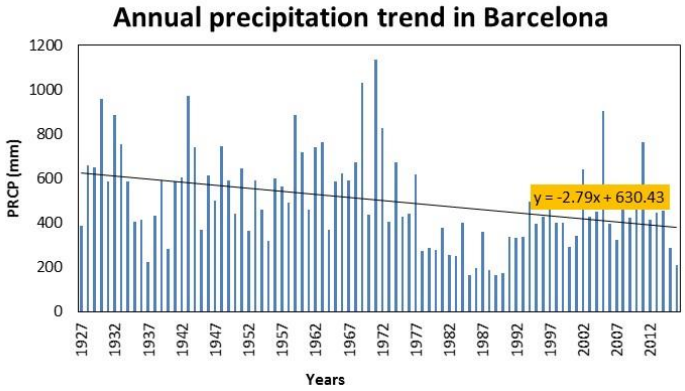

Figure 164. Annual accumulated precipitation trend in Barcelona

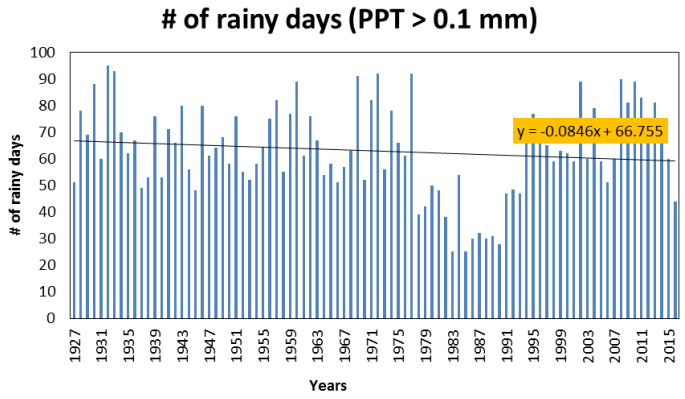

Figure 165. Number of rainy days with an accumulated precipitation higher than 0.1 mm

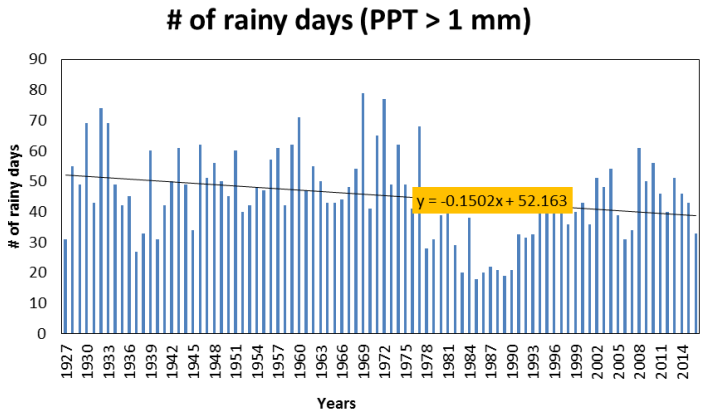

Figure 166. Number of rainy days with an accumulated precipitation higher than 1 mm

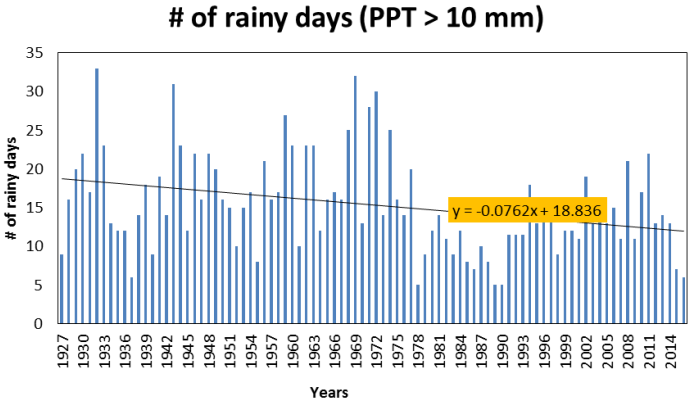

Figure 167. Number of rainy days with an accumulated precipitation higher than 10 mm

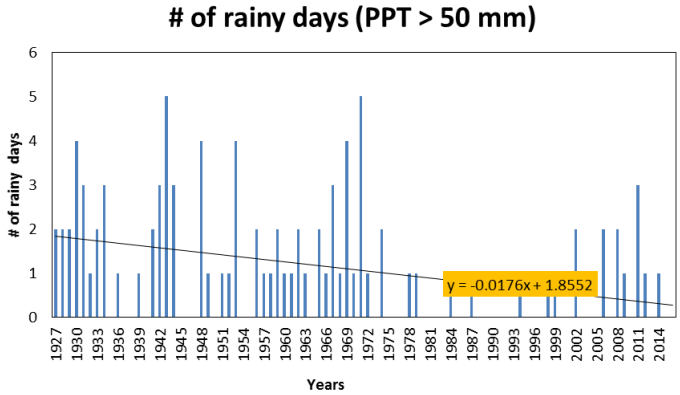

Figure 168. Number of rainy days with an accumulated precipitation higher than 50 mm

Moreover, the simple daily intensity index (1) (André Attogouinon *et al.*, 2017) has been calculated for all times series data available (i.e. from 1927 to 2016) in Fabra's station

$$SDII_j[mm/day] = \frac{\sum_{W=1}^{W} RR_{ij}}{W} \quad (1)$$

where,

RR_{ij} are the number of rainy days with an accumulated volume precipitation ≥1 mm

W is the annual accumulated volume precipitation for the corresponding year

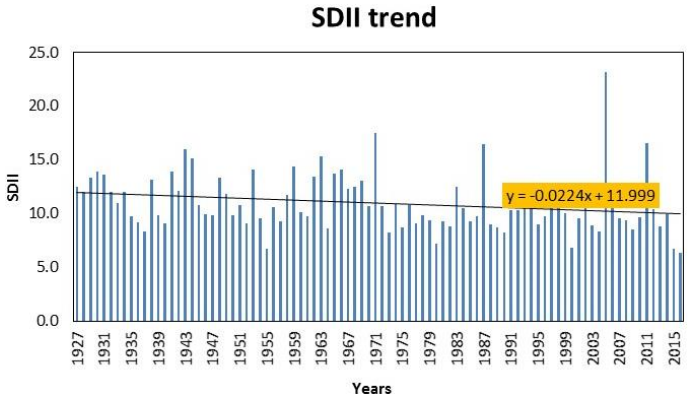

Figure 169. Simple daily intensity index trend from 1927 to 2015 based on Fabra Observatory observations

The intensity indices trends results are presented in Figure 169. All indicators show a descending trend. Above all, it should be paid a special attention when analysing number of days with accumulated precipitation higher than 50 mm, because it offers an idea about the trend of the extreme events.

On the other hand, it has to be taken into account that not only anthropogenic climate signal is affecting rainfall variations but also natural contribution (Redolat, 2018), which could justify the obtained rainfall reduction. The analysed decadal prediction could have been affected by a cycle of failing rainfall and it could vary when analysing long-term climate projections. For all these reasons, flooding analysis for Badalona research site has been finally focused on long term horizon (2051-2100) using RCPs scenarios.

8.1.2.2. Rainfall time series derived from long term climate projections (2051-2100)

As the rainfall realizations provided by WP2 and analysed in the previous section did not show an increase of the future rainfall intensities, a new dataset has been used to proceed with Badalona flood analysis. The new datased was derived from climate projections results of the EURO-CORDEX project.

A GCM MPI-ESM routine was employed and verified through the re-analysis of ERA-Interim. The downscaling process was carried out by employing the RCM COSMO-CLM model. The higher spatial resolution is 12 Km and the temporal is 24 hours. The historic period is 1951-2005 and the future period is 2051-2100. The EURO-CORDEX domain (Figure 170) is a standard reference domain for Europe defined as part of the CORDEX Experiment (http://www.cordex.org/).

Figure 170. EURO-CORDEX domain

In the same way as decadal predictions, rainfall time series data are stored in cells which form a grid that covers all the studied domain (Figure 170). If zooming in the Barcelona-Badalona area, cell centroids can be observed as Figure 171 indicates. Due to its spatial coarse resolution (~12 km) only four cells can be observed over Barcelona and Badalona cities. Moreover, in this case due to its time coarse resolution (24h) no RIDF performance is possible and, therefore, a real-numerical RIDF comparison neither.

Nonetheless, a Historic (1951-2005)-Projection (2051-2100) daily rainfall data comparison has been carried out in order to analyse differences between them. The aim of this study is just to find if any variation (i.e. either increase or decrease) exists in extreme values from past and future rainfall intensities for different return periods. Therefore another extreme values analysis has been conducted by using also Gumbel distribution for both samples, historic and projections. Thus, unlike decadal predictions, these samples were formed by the maximum values of 24h rainfall data per year, instead of 5 minutes as considered previously.

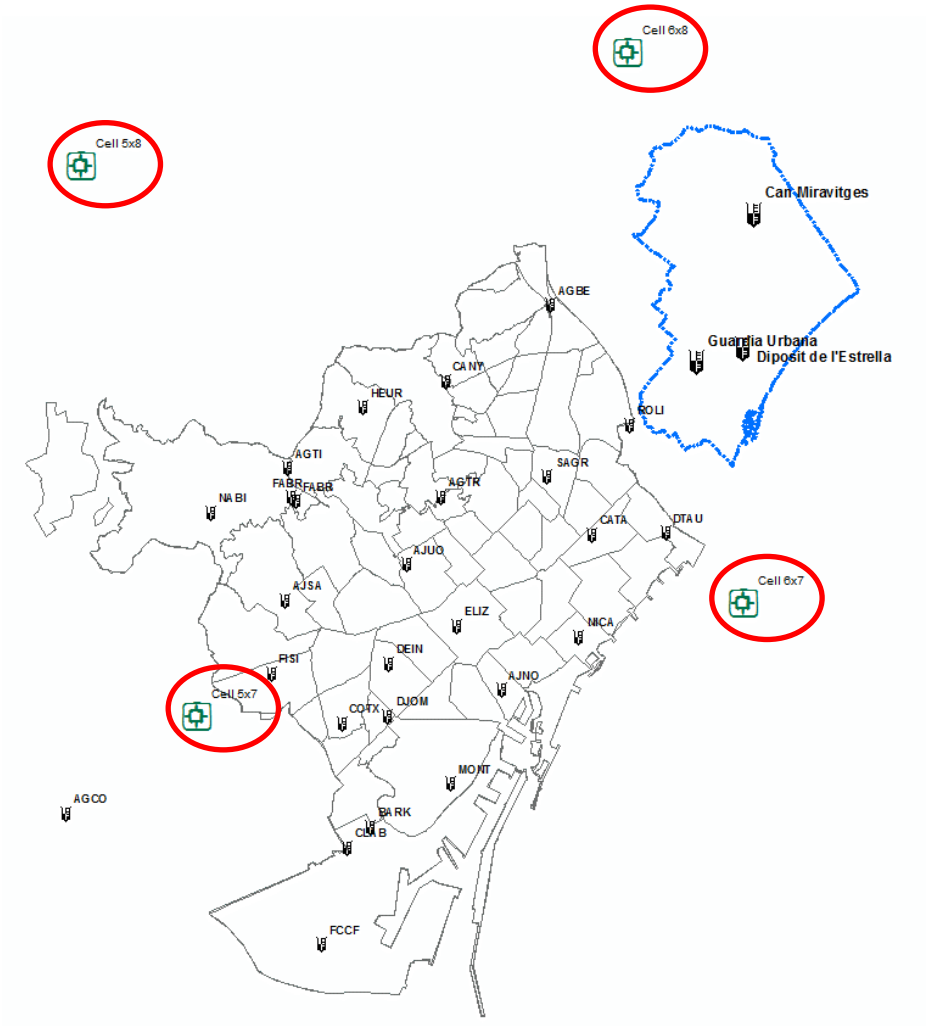

Figure 171. Grid (~12 km resolution) over Barcelona and Badalona (contour in blue)

If the total precipitation values are divided by 24 hours, the average hourly intensity is obtained. These intensity values have been compared from historic to future extreme values for each of the four cells over the Barcelona-Badalona area and for each CORDEX scenario (RCP 8.5, 4.5 and 2.6).

Figure 172 represents the variation values for each cell together with the average value of all of them. As observed the variation in three of them (x5y7; x5y8 and x6y7) indicate an overall increase in averaged intensities for RCP 8.5 and 2.6. However, a clear overall averaged-intensities decrease for almost all return period is observed when it comes to RCP 4.5 scenario. In this regard, the most unfavourable scenario in terms of extreme events is the RCP 2.6.

This historic-future variation percentages have been applied directly on the historic-real Barcelona RIDF curves in order to obtain the future ones and, therefore future design storms can be performed based on these new RIDF curves.

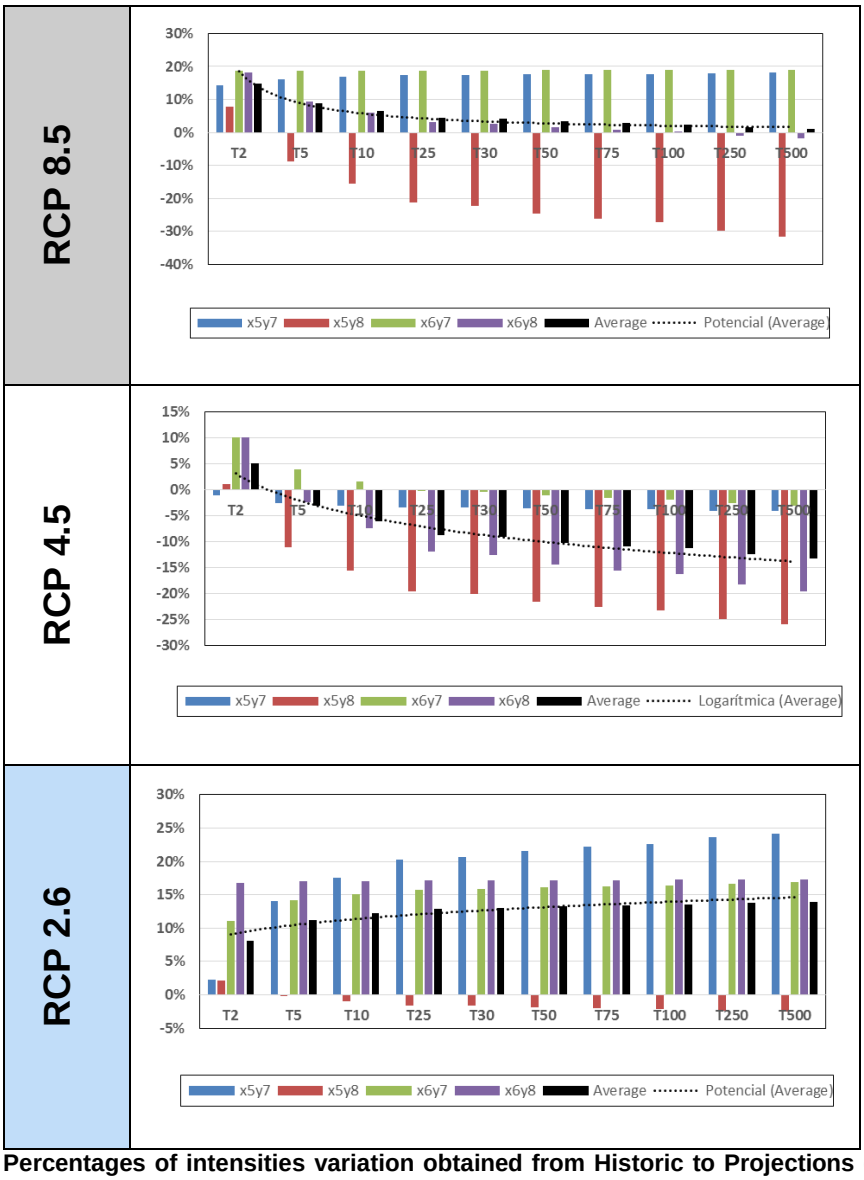

Figure 172. Percentages of intensities variation obtained from Historic to Projections data for the four cells over Barcelona-Badalona area

It has to be noted that there is not a linear relation between the considered scenario emissions with the amount of rainfall that will be obtained. That is to say, not necessarily a more restrictive RCP will offer higher rainfall increments, due to the climate models uncertainty, especially when it comes to rainfall (Figure 173). This fact can be observed in Figure 172, namely for RCP 4.5 that offers an overall rainfall decrease unlike the other two scenarios (i.e. RCP 8.5 and 2.6).

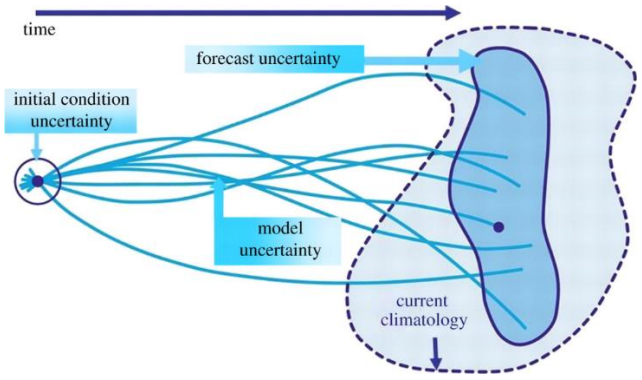

Figure 173. Climatic models uncertainty

		Return period [y]									
		2	5	10	25	30	50	75	100	250	500
Average climate factor [%]. Ratio between future and past rainfall intensities.	**RCP 2.6**	8	11	12	13	13	13	13	14	14	14
	RCP 4.5	5	-3	-6	-9	-9	-10	-11	-11	-12	-13
	RCP 8.5	15	9	7	4	4	3	3	2	2	1

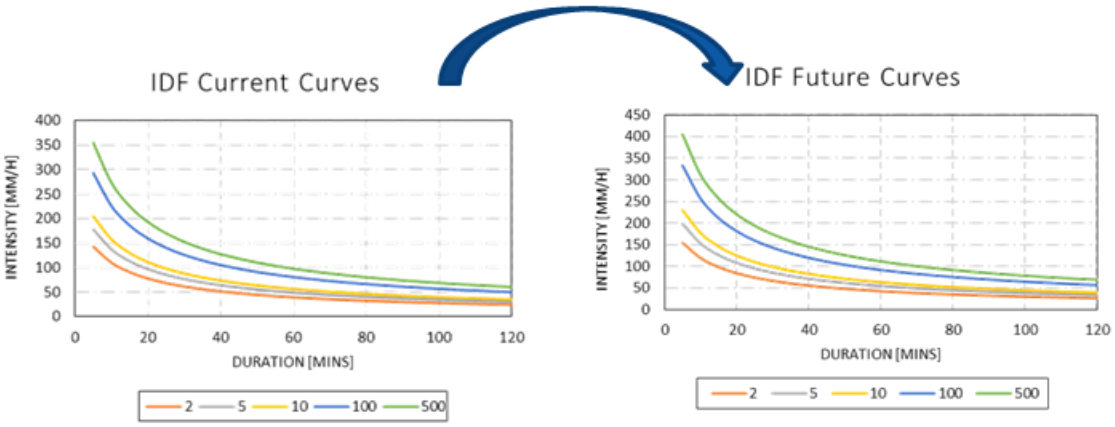

Figure 174. Example of the application of the intensity variation indexes on Historic-real Barcelona RIDF curves to obtain the future ones (example for the RCP 2.6)

Figure 174 summarizes the climate factors for different return periods and for each RCP. Moreover, it shows an example of how historical IDF curves are converted into future ones.

Overall, the average climate factors (Figure 174) significantly change as a function of both the return period and the different RCP scenarios (both positive and negative values are also observed). Moreover, RCP 8.5 that is the worst case emission scenario shows the highest rainfall intensity increase in the low return periods (see for instance T=2, 5 and 10 y of Figure 174).

8.2.2. Results

Figure 175 shows mostly low (green) hazard and some high (red) hazard spots in both some streets of the urban area and some drainage paths of the rural area in the rural part of Badalona. It is noted that hazard calculation is an intermediate step towards risk assessment. That is why some high hazard areas can actually be surface drains, i.e. areas where water is supposed to flow. The figure also show the percentage increase of high hazard areas (the ratio between future and past high hazard areas).

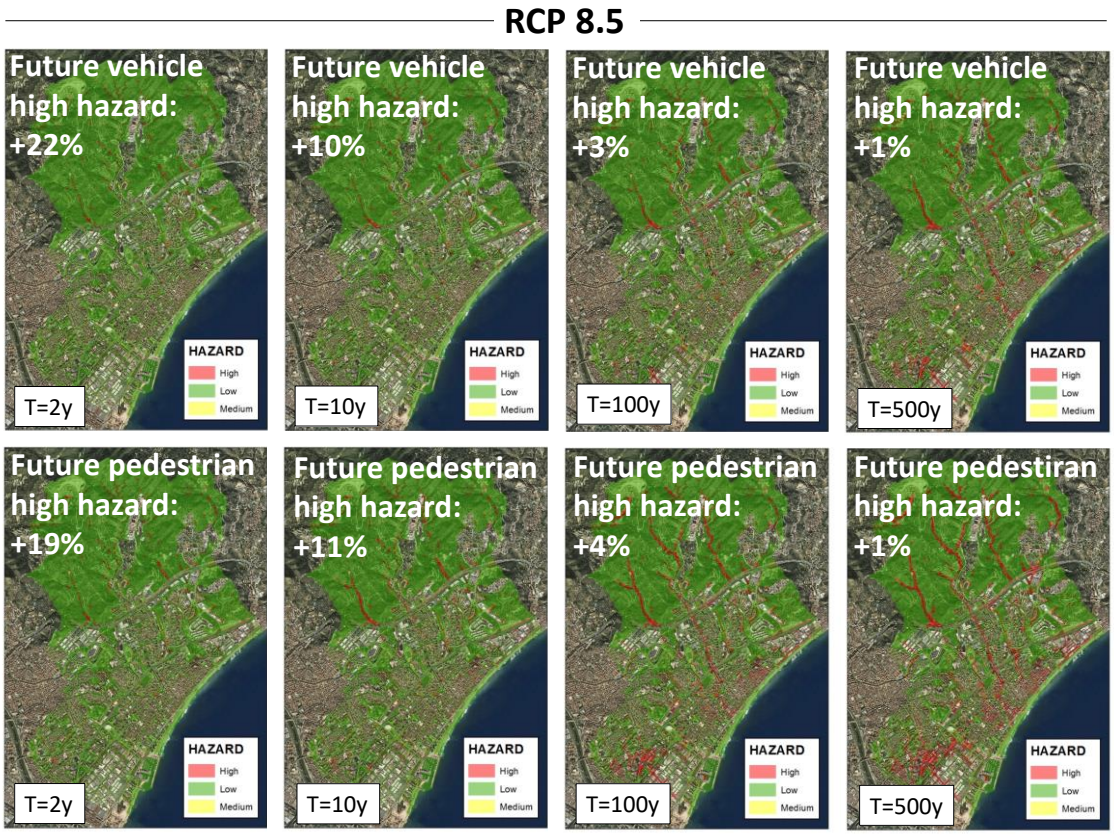

Figure 175. Vehicle and pedestrian hazard maps of Badalona obtained from simulation of future 2, 10, 100 and 500 year return-period events obtained from IDF curves resulting from CORDEX RCP 8.5. The results also show the percentage increase of the future scenario high hazard area compared to the past scenario.

Table 30 shows the high, medium and low hazard area both for pedestrian and vehicles and for different return periods. Overall, the low hazard areas are in the order of a thousand of hectares; medium hazard 0-4 hectares and high hazard 28-225 hectares; the higher the return period the larger the high hazard areas; future scenarios have larger high hazard areas compared to the baseline scenario.

Table 31 shows the comparison between the results obtained by the baseline and the future scenario. For each design storm (2, 10, 100 and 500 year return period) the low and high hazard areas are calculated. The medium hazard area is not shown as the percentage variations can be misleading because medium hazard areas are generally small (see Table 30). Overall, RCP 2.6 gives larger high risk areas compared to RCP 8.5 except for the case of 2 year return period, this is because the climate factor is the highest for the return period of 2 years. Furthermore, the high hazard area obtained from RCP 8.5 increases by 10-22% for the return periods of 2 and 10 years and 1-4% for the return periods of 10-100 years; this is because the climate factors are high for return periods of 2 and 10 years and low for 100 and 500 years.

Table 30. High, medium and low risk area obtained by the future and the baseline scenarios.

	Pedestrian hazard surface [ha]											
	T=2 years			T=10 years			T=100 years			T=500 years		
	Baseline	RCP 2.6	RCP 8.5	Baseline	RCP 2.6	RCP 8.5	Baseline	RCP 2.6	RCP 8.5	Baseline	RCP 2.6	RCP 8.5
High	44.0	48.7	52.6	70.7	85.5	78.6	134.8	171.4	140.1	191.1	224.9	193.8
Medium	0.0	0.1	0.1	0.4	1.0	0.8	2.2	2.3	2.2	2.4	3.2	2.6
Low	1542.8	1538.1	1534.2	1515.8	1500.4	1507.5	1449.9	1413.1	1444.5	1393.3	1358.8	1390.4

	Vehicle hazard surface [ha]											
	T=2 years			T=10 years			T=100 years			T=500 years		
	Baseline	RCP 2.6	RCP 8.5	Baseline	RCP 2.6	RCP 8.5	Baseline	RCP 2.6	RCP 8.5	Baseline	RCP 2.6	RCP 8.5
High	28.1	31.2	34.3	44.1	52.0	48.6	75.3	95.5	77.6	110.0	139.9	111.6
Medium	0.0	0.0	0.0	0.1	0.5	0.4	1.3	2.2	1.4	2.3	4.1	2.6
Low	1558.8	1555.7	1552.6	1542.6	1534.4	1537.9	1510.2	1489.2	1507.9	1474.5	1442.9	1472.6

Table 31. Comparison between the simulated hazard areas obtained by the future and the baseline scenarios. The topmost table summarizes the climate factors for the future scenarios RCP 2.6 and 8.5.

	Climate factor (ratio of future vs past rainfall intensity)			
	T=2y	T=10y	T=100y	T=500y
RCP 2.6	8	12	14	14
RCP 8.5	15	7	2	1

Pedestrian hazard area	Ratio of future vs past simulated hazard areas			
	T=2y	T=10y	T=100y	T=500y
High hazard area RCP 2.6	11%	21%	27%	18%
High hazard area RCP 8.5	19%	11%	4%	1%

Vehicle hazard area	Ratio of future vs past simulated hazard areas			
	T=2y	T=10y	T=100y	T=500y
High hazard area RCP 2.6	11%	18%	27%	27%
High hazard area RCP 8.5	22%	10%	3%	1%

On the other hand, Figure 176 shows an example of simulated pedestrian hazard resulting from a rainfall event that occurred the 16/10/2016 in (Vilassar de Mar), 15 km away from Badalona. This event (according to the Meteorological Catalan Service, SMC) had a total rainfall depth of 221 mm, a 30 minutes intensity of 170 mm/h and a 5 minutes intensity of 278 mm/h. The 30 minutes intensity has a return period larger than 500 years according to the IDF curves of the Barcelona rain gauge of Fabra (Figure 160). This event shows high hazard in 30% of the pedestrian urban areas.

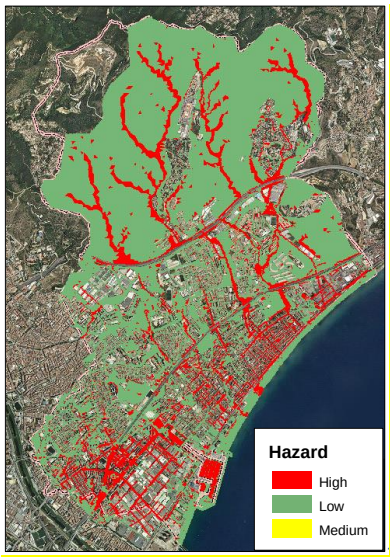

Figure 176. Pedestrian hazard map of Badalona obtained from simulation of an extreme rainfall event registered 15 km away from Badalona.

8.3. Discussion

The rainfall analysis results showed that rainfall intensities are likely not to increase within the next 10 years. As a consequence, flood hazard in Badalona is likely not to increase in the next 10 years. Nevertheless, rainfall intensities are likely to be higher than the actual ones in the future period 2050-2100 according to RCP 2.6 and 8.5 (RCP 4.5 showed a decrease in future rainfall intensities), producing an increase of the future flood hazard.

Simulations based on RCP 8.5 show a 10-22% increase of pedestrian and vehicle high hazard areas and an insignificant increase of high hazard areas for return periods of 100 and 500 years. It is noted that hazard maps are just an intermediate step toward the elaboration of risk maps, therefore an increase of high hazard might not result in a similar increase of risk. Overall, the drainage network of Badalona was designed to flood the streets of Badalona approximately once every 10 years; nevertheless, rainfall events of lower return periods were shown to produce flooding; moreover, the rainfall intensities associated with these events (the events with a return period of less than 10 years) are expected to increase more than events with high return periods such as 100 and 500 years (according to the selected climate predictions of the RCP 8.5).

8.4. Bibliography

André Attogouinon, A.; Lawin, A.E.; M'Po, Y.N.; Houngue, R. (2017) Extreme Precipitation Indices Trend Assessment over the Upper Oueme River Valley-(Benin). Hydrology. 4(3), 36.

Martínez-Gomariz, E., Gómez, M., Russo, B., 2016. Experimental study of the stability of pedestrians exposed to urban pluvial flooding. Nat Hazards (2016) 82:1259–1278.

Martínez-Gomariz, E., Gómez, M., Russo, B., Djordjevic, S., 2017. A new experiments-based methodology to define the stability threshold for any vehicle exposed to flooding. Urban Water Journal. 14, 2017.

Raso, J., Malgrat, P., Castillo, F., 1995. Improvement in the selection of design storms for the new master drainage plan of Barcelona. Water Science & Technology. Vol. 32, 1.

Redolat, D., Monjo, R., Lopez-Bustins, J.A., Martin-Vide, J. (2018) Upper-Level Mediterranean Oscillation index and seasonal variability of rainfall and temperature. Theoretical and Applied Climatology. p1-19. First Online.

8.5. Model objectives in BINGO [CSO analysis]

This section aims to develop hazard map for people swimming in the sea and to quantify the impact of future rainfall patterns on CSO. Hazard maps for bathing people are computed using hazard criteria applied to the simulated bacteria concentrations in sea waters. Moreover, the actual and future impacts of CSOs are evaluated in terms of average number and volume of CSOs per year. The models used in this sections were described in D3.3.

CSOs discharge water with high bacteria concentrations to the sea water of Badalona and this is considered a hazard for people health and safety. In fact people swimming in sea water with high bacteria (E. Coli or Enterococcus Intestinalis) concentrations can have health consequences. For this reason the municipality regulation (and also the current legislation REAL DECRETO 1341/2007 and the Bathing Water Directive) forbids bathing after CSO events and this also negatively affect local businesses. The produced hazard maps are an intermediate step towards the calculation of risk. High bacteria concentrations in sea water can persist during the 24-48 hours following a CSO event.

8.6. Model application

Future rainfall patterns could affect the impact of CSOs on receiving waters. The selected rainfall realization (see the following data section) was used to estimate the changes between the past and future number of CSOs and their total discharged volume to the sea of Badalona. The 1D/2D (sewer network/surface runoff) model of Badalona was used to simulate the CSOs number and volume and the marine model (implemented in MOHID Studio from Bentley Systems) was used to produce hazard maps for people swimming in the sea after CSO events.

First, the average seasonal number and volume of CSOs was computed using the coupled 1D/2D model (combined sewer network / surface runoff) of Badalona. Then results obtained from the past and future scenarios were compared and finally hazard maps for people swimming after CSOs events were developed. Hazard maps were developed using 3 different hazard criteria (low, medium and high hazard) that were applied to the simulated sea water concentrations after a CSO event (i.e., low concentration = low hazard and vice versa). The sea water concentrations are simulated using the marine model described in D3.3.

8.6.1.1. Application of the urban drainage model of Badalona

The coupled 1D/2D (sewer network/surface runoff) model of Badalona was used to simulate the average number and volume of CSOs per bathing season. Only the worst case rainfall realization (worst case scenario) was simulated together with observations from the Fabra rain gauge. The simulation with observed rainfall data was used to estimate the actual number and volume of CSOs. The rain gauge of Fabra is located 4 km away from Badalona, spatial rainfall variability in urban areas might be significant and rainfall can vary at distances of less than a km. Nevertheless, the rain gauge of Fabra is the only one having long term measurements (the Badalona rain gauge only had up to 4 years continuous measurements) and long term rainfall properties (volumes and intensities) are similar in Barcelona and Badalona.

Continuous simulations of 10 years of past (2005-2014) and 10 years of future (2015-2014) conditions were performed. Only the bathing season (from the 1st of June to the 1st of September) of each year was simulated. The number of CSO spills and the total volume per bathing seasons were simulated at the CSOs structures of Maria Auxiliadora and Riera Canyadò. A CSO event was defined as any overflow to the sea that had 6 hours of previous no-overflow. The 1D/2D model was run with a 60 s time step with distributed rainfall

according to Tyessen polygon (BA1, BA2 and BA3 rain gauges). Figure 177 shows the location of the rain gauges and the 2 catchments of Riera Canyadò and Maria Auxiliadora.

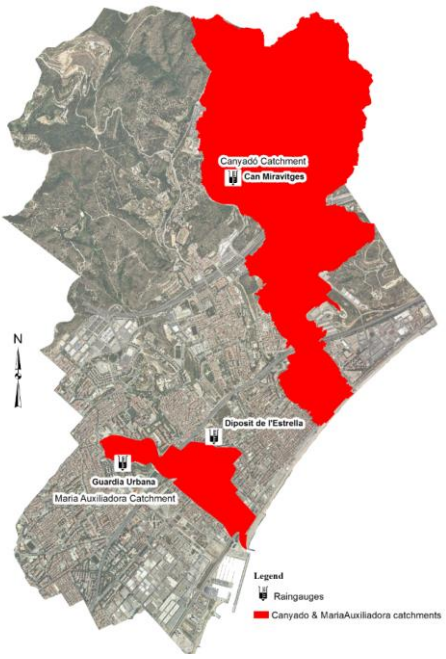

Figure 177. Location of the 3 rain gauges together with the location of the Riera Canyadò catchment (the northern red area) and Maria Auxiliadora (southern red area). Rain gauges: BA1=Deposit de l'Estrella; BA2=Guardia Urbana; BA3=Can Meravitges.

8.6.1.2. Application of the marine model of Badalona

The sea water quality of Badalona is affected by CSO events. The sea water concentration of bacteria (E. Coli and Enterococcus Intestinalis) can exceed the water quality standards for several hours up to few days after a CSO event. This is considered a people health risk by the Municipality of Badalona (amd by the current legislation REAL DECRETO 1341/2007) that closes down the beaches when there is insufficient water quality.

This section aims at developing hazard maps for people bathing in the sea of Badalona. The hazard map was obtained from the hazard criteria shown in Table 32. The hazard is low if concentrations are smaller than 250 ufc/100ml; is medium if concentrations are between 250 and 500 ufc/100ml and is high above 500 ufc/100ml. The threshold values shown in the table are similar to the municipality definitions of insufficient, good and excellent water quality (REAL DECRETO 1341/2007). The concentration of E. Coli were simulated for the few days following a CSO event and the hazard maps significantly change as a function of time after a CSO event, i.e. high hazard occurs immediately after the CSO event, whereas low hazard is likely to be re-established within 12-48 hours after the CSO event.

Table 32. Hazard criteria based on E. Coli concentration in sea water

Hazard criteria	E.Coli concentration [ufc/ 100 ml]
Low	<250
Medium	250<x<500
High	>500

8.6.2. Data

Historical and future rainfall realizations were provided from the project partners of FUB (Freie Universität Berlin). These rainfall data were not presented in the Work Package 2 deliverables because they were produced afterwards.

In the following the development and the analysis of the new rainfall realizations together with the selected worst case scenario are presented. Simulating all the different rainfall realizations with coupled 1D/2D model was considered unfeasible due to long computational times. Therefore a simple model was developed to simulate the number of CSO events from a continuous rainfall time series allowing us to select the worst case rainfall realization used to continue with CSO analysis.

8.6.2.1. Analysis of the past and future rainfall realizations

As said, past and future rainfall realizations were provided from FUB. These time series are compared and validated against observations in order to discuss their applicability.

FUB provided 10 rainfall realizations with a 5 minute time step for the location of the four rain gauges that were considered relevant for our analysis. Figure 178 shows the location of the four rain gauges (the red dots in the figure). Three of them (BA1, BA2 and BA3) are located in Badalona and registered data for less than four years and the other (FAB) is in Barcelona and have a much longer dataset.

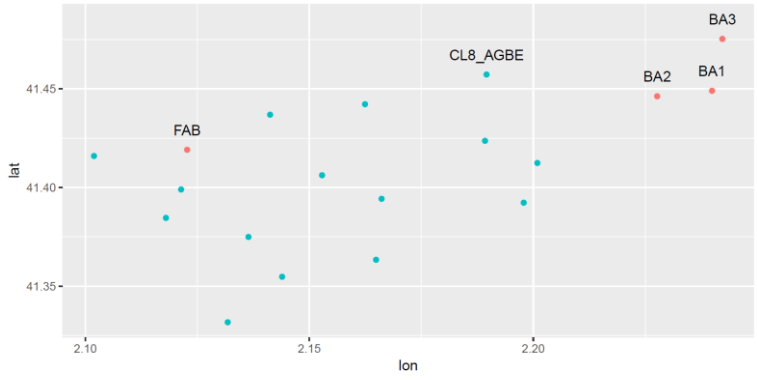

names	lon	lat	debut	end
FAB	2.123	41.419	2008	2016
BA1	2.240	41.449	2013	2017
BA2	2.228	41.446	2014	2017
BA3	2.242	41.475	2014	2017

Figure 178. Location of the rain gauges. Target stations are shown in red.

The FUB-provided rainfall time series have a duration of 29 years, from 1996 to 2024 (19 years of historical period from 1996 to 2015 and 10 years predictions from 2015 to 2004). The rainfall time series were generated in two steps:

1) Daily rainfall. Daily rainfall was simulated using the Daily Spatio-temporal Stochastic Precipitation Generator (see DECO documentation). The input model parameters for the target rain gauges were interpolated from all the stations represented in blue dots in Figure 178. Parameters obtained from the target rain gauges (red dots) were not considered accurate because their observation periods were too short.
2) Disaggregation of daily rainfall into 5-min values. A stochastic method that combines both the Bartlett-Lewis (Rodriguez-Iturbe et al. 1987) process to generate rainfall events and procedures to adjust the 5-min values to be consistent with the daily ones was used to disaggregate daily rainfall into 5-min values. The Bartlett-Lewis variant that introduces dependence between the cell intensity and duration was used. This variant is included in the R package 'HyetosMinute' and was shown in literature to outperform the other Bartlett-Lewis variants. The observed 5-min rainfall data are used to estimate the Barlett-Lewis model parameters for each month. The properties included in the fitting procedure of the Barlett-Lewis model are: the mean; variance; lag-1 auto-correlation and ratio of dry/wet periods at time scales of 5-min, 1-h, 6-h and 24-h.

In order to evaluate the disaggregation, different observed and simulated rainfall characteristics (annual rainfall; rainfall volume per single event; mean, variance and 99.99% quantile of the intensity; proportion of dry and wet spell length frequency) were compared. The comparison was made for the rain gauges CL8 AGBE, BA2 and FAB. Similar results were obtained for the different rain gauges, therefore only the FAB results are shown.

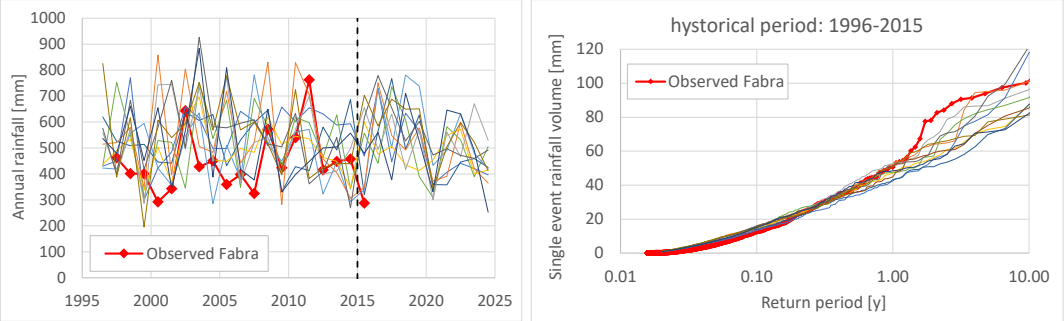

Figure 179. (Left) Annual rainfall from the 10 realizations and from the observed data at the rain gauge FAB. (Right) Rainfall volume for each single event as a function of the return period. The continuous colored thin lines represent the 10 realizations; the vertical black dashed line at 2015 is the boundary between historical and future realization.

Figure 179 (left) shows both the observed and the simulated annual rainfall from the 10 realizations. The results show that the observed annual rainfall falls mostly within the lower range given by the 10 realizations for the majority of the years. Nevertheless, for some years the observed rainfall is underestimated (below the range). Figure 179 (right) shows both the observed and the simulated single event rainfall volume from the 10 realizations as a function of the return period. The results show that the simulations well reproduce the observations up to 1-2 year return period and at higher return period the simulated single event rainfall volume is slightly underestimated.

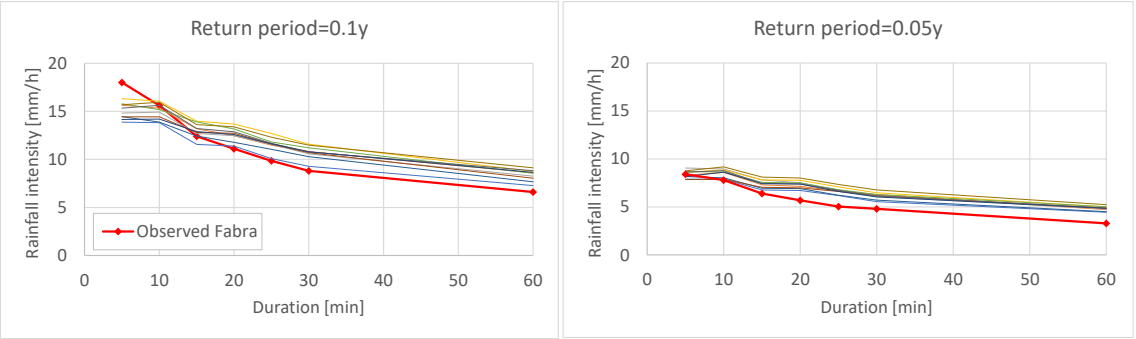

Figure 180. Observed and simulated rainfall intensity as a function of the duration for the historical period 1996-2015. . The continuous colored thin lines represent the 10 realizations. (Left) Return period of 0.1 years. (Right) Return period of 0.05 years.

Figure 180 shows both the observed and the simulated rainfall intensity as a function of the duration for the historical period 1996-2015. Low rainfall intensities with occurrence of 10 (0.1 year return period) and 20 (0.05 year return period) times per year were selected for our analysis because CSO events in Badalona are caused by even moderate intensity rainfall (for flooding analysis much higher return periods would be selected, i.e. > 5 years). Overall, observations and simulations show similar patterns and also some under/overestimation of the rainfall intensities.

Overall, the simulated rainfall patterns and values are in agreement with the observations and therefore the rainfall realizations are considered acceptable for this analysis. Moreover, an ensemble of 10 realizations

for each rain gauge location was considered appropriate to reproduce the rainfall characteristics of interest for this analysis.

8.6.2.2. Selection of the worst rainfall realization

The rainfall realizations are the main model input for this CSO analysis. Using all the realizations would give the most accurate results and uncertainty bounds (i.e. the annual CSO volume, the number of CSO events per year, etc…). Nevertheless, the computational time of drainage and marine models is significant and therefore it was decided to develop the analysis using only the worst case scenario and an average scenario.

In the following the analysis made to select the rainfall realization giving the worst case and the average scenarios are presented. The worst case realization is defined as the one that produces the highest increase of the number of CSO spills in the future. Similarly, the average case realization is the realization producing approximately the average increase of the number of CSO spills among all the 10 realizations. In order to compute the number of CSO spills, a simple model was developed (running the spatially distributed model was considered unfeasible due to the long computational time). This model aims at simulating whether a single rainfall event produces a CSO spill or not. The model was developed to simulate the number of CSO spills at the 2 most interesting (for our study) CSO structures of Badalona: Riera Canyado and Maria Auxiliadora.

The simple model is made of a rainfall intensity threshold, above which a single rainfall event is expected to produce an overflow. Table 33 shows the rainfall intensity thresholds of the simple model. If a rainfall event exceeds any of the intensity thresholds then this event is considered to produce a CSO spill. The threshold intensity values of M. Auxiliadora are higher than the ones of Riera Canayadò meaning that given the same rainfall events Riera Canyadò is expected to have a larger number of CSO spills.

The simple model thresholds were obtained by multiple running of the 1D/2D model. The 1D/2D model was run for several block rainfalls of different intensities until a CSO spill was observed. For example, a single event of 5 min duration was simulated several times for different intensities until a CSO spill was observed: i.e. a single event with an intensity > 10 mm/5min causes a CSO spill at Riera Canyadò but not at Maria Auxiliadora; similarly, a single event with an intensity > 26 mm/5min causes a CSO spill at both Riera Canyadò and Maria Auxiliadora. For each rainfall event in a time series all the different intensities at durations 5, 10, 15, 20, 25 and 30 min are compared with the Table 33 thresholds in order to compute the number of CSO spills.

Table 33. Threshold rainfall intensities of the simple model used to establish whether a single rainfall event produces a CSO spill.

	Riera Canyadò	Maria Auxiliadora
Duration (min)	Intensity (mm/h)	Intensity (mm/h)
5	10	26
10	6	14
15	4	10
20	4	8
25	4	6
30	2	6

The simple model was applied to all rainfall realizations and also to the observations from the 3 rain gauge of Badalona BA1, BA2 and BA3. Only the number of CSOs occurring during the bathing season was taken into account. The bathing season is assumed to start 1st of June and end 1st of September (similar to the

Badalona municipality definitions). Figure 181 shows the simulation results. The results show that the number of CSO spills obtained from the observations fall between the ranges obtained by the 10 realizations; further, at Riera Canyado there are more spills than at Maria Auziliadora due to the weir configurations; finally, no significant patterns are identifiable between past and future number of CSOs.

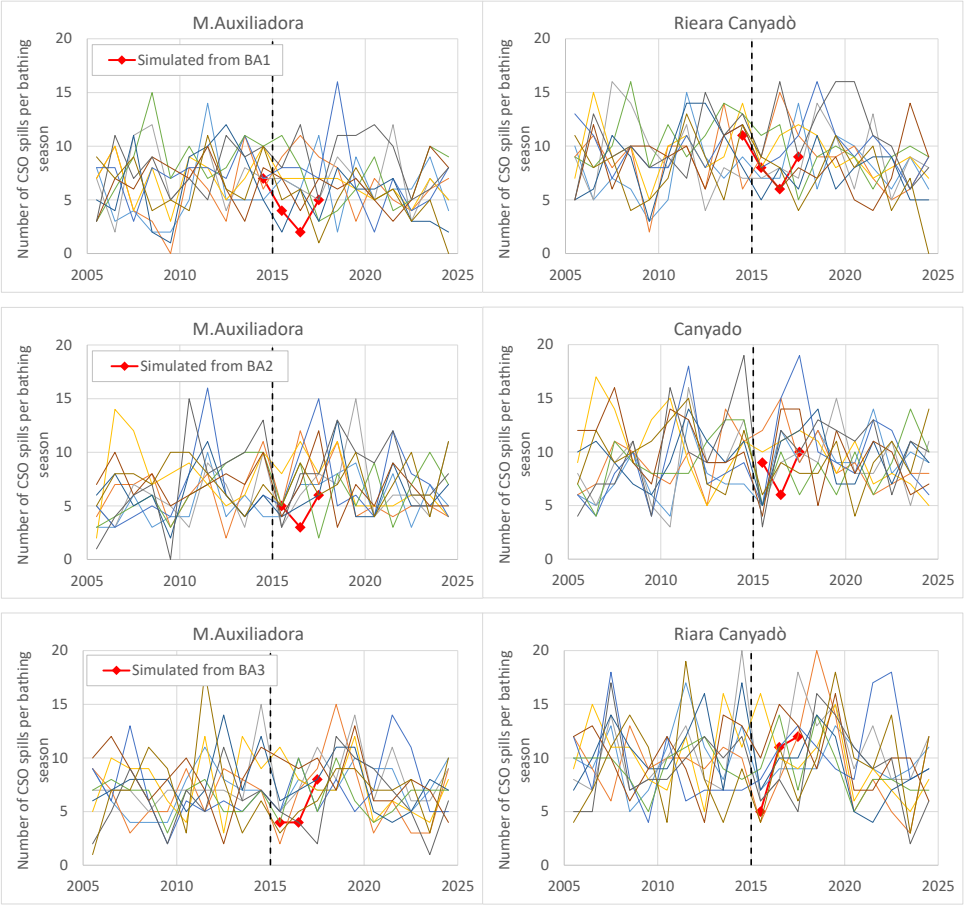

Figure 181. Simulated number of CSO spills at both M.Auxiliadora and Riera Canyado using the simple model. The continuous colored thin lines represent the 10 realizations; the vertical black dashed line at 2015 is the boundary between historical and future realization. The red line 'Observed BA' is the simulated number of CSOs based on the observed rainfall data.

The average number of CSOs for each realization was calculated for the past (1996-2015) and future period (2015-2024). Then for each realization the ratio of future CSO number versus past CSO number was calculated. The worst case realization gives that the future number of CSOs is 17 % higher compared to the past number. Each future realization is compared to its past in order to keep consistency since each realization is computed assuming the same climate model weather variables. The best case realization gives that the future number of CSOs decreases of 15 % compared to the past; the average realization gives approximately the same number of CSOs between the future and the past scenario.

8.6.3. Results

8.6.3.1. Number and volume of CSOs

Figure 182 shows the simulated number and volume of CSOs per bathing season for both the past and future scenarios; for both the worst case and average case scenarios and for the observed rainfall (from the rain gauge of Fabra). The results show that there is a significant variation from year to year due to different rainfalls during the 3 month bathing season (from 1st of June to 1st of September). The number of CSOs per

bathing season estimated from observed rainfall data inputs (the red line in the figure) varies between 3 and 9 with an average of 5-6 CSOs spills every bathing season. These results are similar at both the CSO structures of Maria Auxiliadora and Riera Canyadò. The CSO volume shows large variations from year to year and Maria Auxiliadora have an average of approximately 28000 m^3 per bathing season and Riera Canyado 85000 m^3.

The results based on the worst and average case scenarios are used to estimate the changes between future and past scenarios. Table 34 shows the average number and volume of CSOs per bathing season. The worst case results show an increase of 0-33% in the average number of CSOs per bathing season and a 22-53% increase of the average CSO volume per bathing season. Instead, the average case results show an increase of 12-14% in the average number of CSOs per bathing season and a 0-6% decrease of the average CSO volume per bathing season.

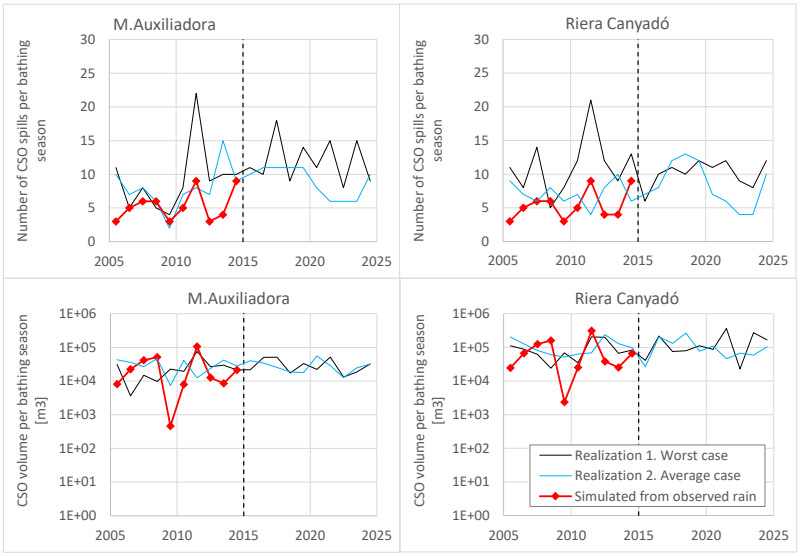

Figure 182. Simulation of past (2005-2014) and future (2015-2024) number and volume of CSO spills at both Maria Auxiliadora and Riera Canyado CSO structures.

Table 34. Future and past number and volume of CSOs. Simulated with the selected rainfall realization.

		Realization 1. Worst case			Realization 2. Average case		
		Past 2005-2014	Future 2015-2024	Future changes	Past 2005-2014	Future 2015-2024	Future changes
M. Auxiliadora	Average number of CSOs per bathing season	9	12	+33 %	8	9	12%
	Average CSO volume per bathing season [m^3]	25455	31117	+22 %	30667	28872	-6%
R. Canyado	Average number of CSOs per bathing season	10	10	0 %	7	8	14%
	Average CSO volume per bathing season [m^3]	94149	143689	+53 %	111871	109364	-0%

8.6.3.2. Hazard map for people safety

This section shows how the time varying hazard maps for people bathing were obtained together with an example of a time varying hazard map from a selected rainfall/CSO event. In the case of hazard mas for

people bathing it is not relevant to compute the maps for different design return period events (past and future) as it was done in the case of flooding. This is because CSO events are frequent and highly varying events and are generally not classified as extreme events (like flooding).

Figure 184 shows the hazard map for people swimming in the sea water of Badalona after and during a CSO event. A first rainfall event occurred between 0:00 and 2:00 of day 1 and the second CSO occurred between 19:00 and 20:00 of day 1; both of this events generated CSOs. Figure 183 shows the observed rainfall event used to simulate the hazard maps.

The hazard is based on simulated E.Coli concentrations in sea water. The results show that the hazard significantly changes as a function of time during and after CSOs. The hazard is high and close to the coastline during a CSO event (2:00 day1); subsequently, the high hazard area expands and becomes lager. Low hazard is re-established, after approximately 1 day (18:00 day2) from the second CSO event.

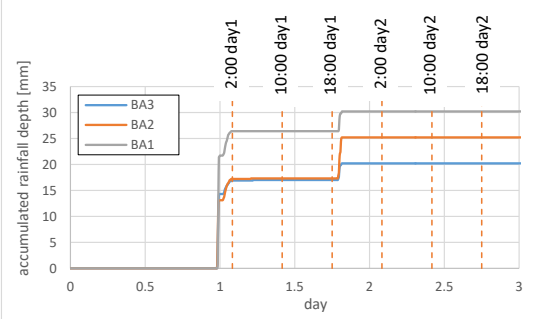

Figure 183. Rainfall event used to simulate hazard maps after CSOs. The vertical dashed orange lines show the timing at which the hazard maps are extracted.

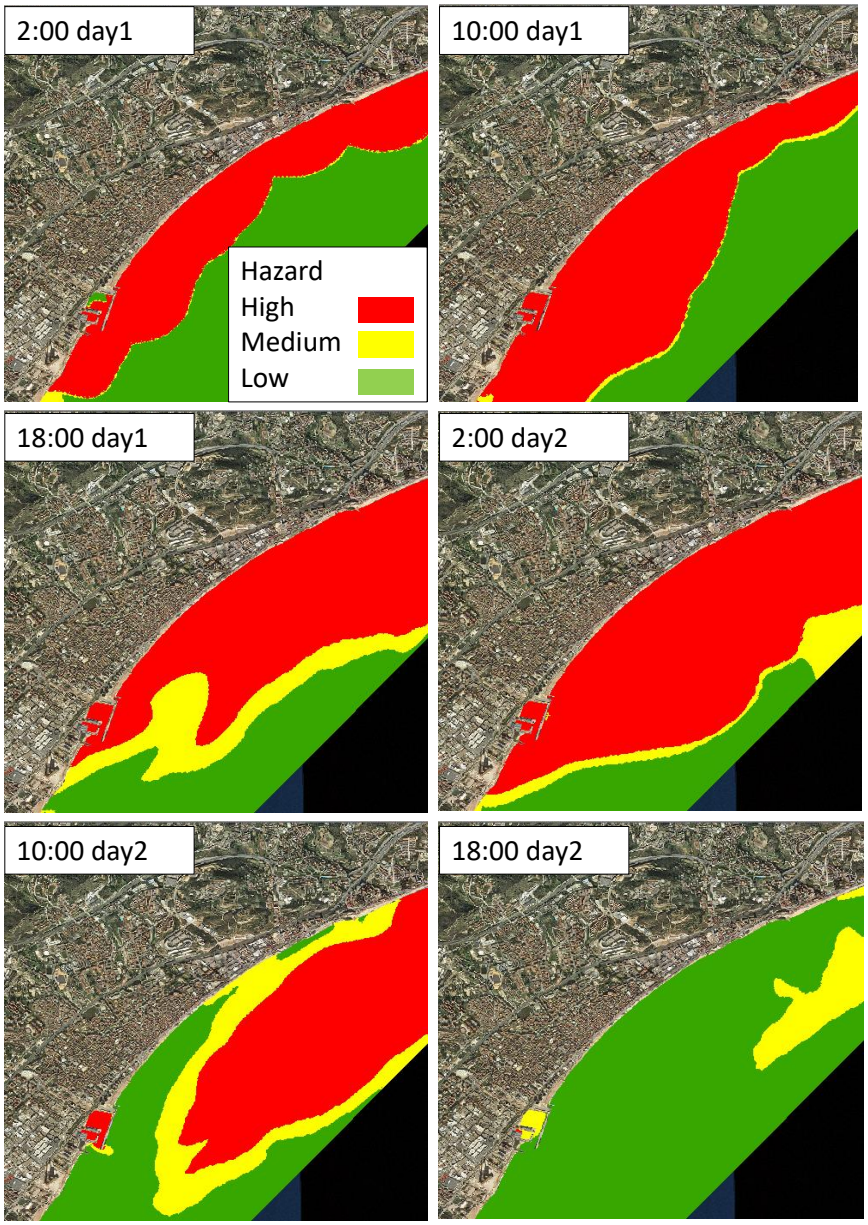

Figure 184. People hazard maps at different times during and following a CSO event.

8.6.4. Discussion

The rainfall analysis showed that no significant changes in both extreme rainfall intensities and annual precipitation volumes are expected for the period 2015-2024 compared to the past period 1996-2014. The actual number of CSO spills was estimated to be on average approximately 5 every bathing season (from the 1st of June to 1st of September).

The average case scenario based on the selected rainfall realization (the realization that would produce an average future increase of CSOs among the 10 rainfall realizations) showed that there would be an increase in the number (12-14 %) of CSOs and a decrease of CSO volumes (0-6 %) in Badalona. The worst case scenario based on the selected rainfall realization (the realization that would produce the highest future increase of CSOs among the 10 rainfall realizations) showed that there would be an increase in the number (0-33 %) of CSOs and an increase of CSO volumes (22-53 %) in Badalona.

The hazard maps for people swimming in the sea of Badalona showed high hazard up to 24 hours following the selected CSO event. This high hazard is due to simulated E.Coli concentrations exceeding the bathing water quality criteria of 500 ufc/100 ml. Low hazard (E.Coli concentrations <250 ufc/100 ml) is then re-established. The time it takes to re-establish low hazard after a CSO events depends on mainly on: discharged CSO volume, E.Coli concentration of the CSO water and wind conditions that generate coastal sew water currents. Generally, the higher the volume and concentrations of a CSO discharge, the longer the high hazard period, nevertheless volume and concentrations can be inversely correlated meaning that a higher CSO volume is likely to have a lower concentration and vice versa. Moreover, stronger winds are likely to generate faster coastal currents that would disperse the contaminant plumes faster. It is reminded that hazard maps are an intermediate step toward the final risk maps.

Bibliography

EU, 2006, Directive 2006/7/EC of the European Parliament and of the Council of 15 February 2006 concerning the management of bathing water quality and repealing Directive 76/160/EEC, (OJ L 64, 4.3.2006, p. 37)

REAL DECRETO 1341/2007, de 11 de octubre, sobre la gestión de la calidad de las aguas de baño. MINISTERIO DE LA PRESIDENCIA.

Rodriguez-Iturbe, I, Cox, DR, Isham, V, 1987. Some Models for Rainfall Based on Stochastic Point Processes. Proc R Soc Lond A Math Phys Sci;410:269–88.

9. Conclusions and outlook

This comprehensive Deliverable investigated climate change and socio-economic change at 15 sites (see Chapter 2) in six European countries. For the first time, decadal climatic predictions have been applied in a combined approach to tackle water related problems, such as floods and droughts.

The decadal predictions included 10 realizations for the time period 2015 to 2024, i.e. 100 modelling years, in order to account for climate variability. As the water related problems at the various sites are manifold, more than 20 different hydro models have been applied. However, as socio-economic changes can further decrease or increase climate change effects, their impacts have also been modelled at all relevant sites (see Chapter 2). Additionally, at a few sites extremal episodes have been modelled in high resolution, in order to analyze single flood events, which can cause massive damages in urban areas.

For decadal predictions the main impacts on the water cycle have been stated as follows:

- Decrease in river runoff in winter and spring (Wupper basin, Germany)
- In combination with socio-economic changes, reservoir levels will be below critical threshold more often (Wupper basin, Germany)
- Groundwater levels do not completely recover from dry period beforehand (Veluwe, Netherlands)
- Agricultural areas are prone to water shortages (Veluwe, Nethwelands)
- A redistribution of groundwater abstractions may be needed to prevent inundations at some areas, whereas an increase in groundwater abstractions may harm ecosystems (Veluwe, Netherlands)
- Increase in reservoir inflows (Bergen, Norway)
- Increase in CSOs (Bergen. Norway)
- Small increase in winter inundations by tides, but no hazard increase (Portugal)
- Water abstraction from rivers during droughts are recommended only at low tides due to increasing salinization problems (Portugal)
- Groundwater levels are predicted from small increases to medium decreases, depending on the aquifer (Portugal)
- No increase in precipitation intensities and thus no increase in urban floods (Badalona. Spain)
- Increase in CSOs indicating bathing hazards (Badalona, Spain)

For land-use and water use scenarios the main impacts on the water cycle have been stated as follows:

- Increase in peak flows of flood events by land-use changes (Pedieos, Cyprus)
- No significant change in river runoff by land-use changes (Wupper basin, Germany)
- Large impact of water use changes on reservoirs and river runoff (Wupper basin, Germany)
- Impact on evapotranspiration and groundwater recharge (Veluwe, Netherlands)

For extremal episodes the main impacts on the water cycle have been stated as follows:

- Flood hazards by inundations likely to increase (Pedieos, Cyprus)
- Flood protection by reservoir management necessary (Pedieos, Cyprus)
- Extremes below past events (Wupper basin, Germany)

These multiple model results, driven with homogeneous climate data, show that the impacts of climate and socio-economic change vary between geographical regions and water compartments affected (i.e. groundwater or surface water). For example, at the Norwegian reservoir an increase of inflow is predicted, while the German reservoir is predicted to remain stable or even decrease. The groundwater levels at the

Dutch and Portuguese site are both showing effects of not increasing to the same antecedent conditions (reference period) or even showing decreases. The combined sewer overflows at the Spanish and Norwegian sites both feature increasing trends.

The comparison of the impacts of land-use and water use changes as well as extremal episodes also provide an indifferent picture. For example, land-use changes are predicted to further increase flood peaks in Cyprus, while no changes in the hydrographs of the German sites have been observed.

For the first time, this Deliverable has managed to tackle the most relevant European water problems within one project framework and predict their potential development until 2024. The results, as summarized above, show that water problems in Europe cannot simply be harmonized by single parameters, as the reasons for those water problems are usually very complex. Thus, the combined bottom-up (stakeholder, water managers, local problems) and top-down (modelling framework, decadal predictions, socio-economic scenarios) approach has shown to be a very promising way ahead to tackle multiple water problems at multiple sites and countries at the same time.

Given the heterogeneity of the water problems, and thus of the applied methods, the BINGO team of WP3 has built on strong interactions among the sites. The figure below provides an overview of some of the interactions and linkages:

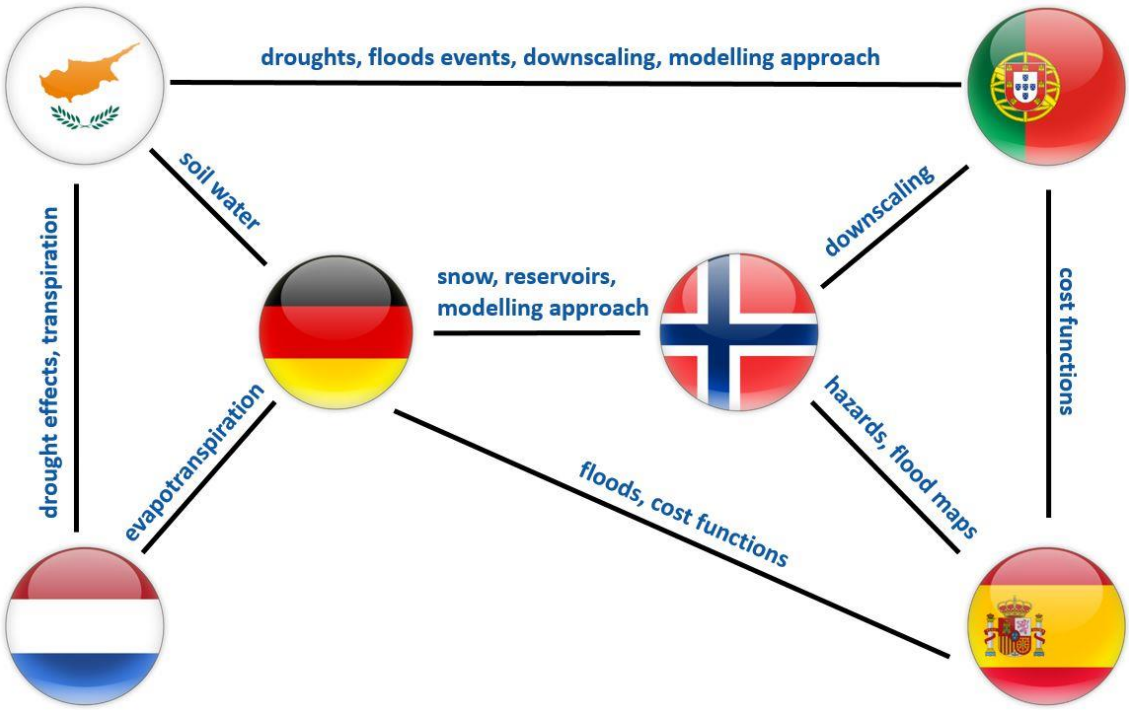

WP3 links and interactions between sites among the six BINGO countries

Some of the links have been obvious, such as CSO modelling in Spain and Norway, groundwater modelling in the Netherlands and Portugal, flood inundation modelling in Cyprus and Portugal, and reservoir modelling in Germany and Norway. Here, model results often were directly comparable, thus results and trends easily discussable. Other links have been established during often intense scientific exchanges, as for example, the German partners bought the same lysimeter as the Dutch partners, in order to compare

evapotranspiration data. Another example is the exchange of scientific staff between Spain and Norway for transfer of knowledge and methods. Generally, the transfer of knowledge and methods across nations and cultures has shown to be one of the auspicious messages of BINGO to tackle diverse water problems in Europe. This diversity can for example be depicted by the exchange on soil moisture between Cyprus and Germany and on snow modelling between Norway and Germany.

The interaction between the sites is also depicted in the internal review process of this Deliverable, which was based on topics:

- Bergen reservoir (chapter 6.1) vs Wupper reservoir (4.1 and 4.6)
- Bergen CSOs (6.5) vs Badalona CSOs (8.5)
- Badalona floods (8.1) vs Portugal salinity (7.1)
- Pedieos floods (3.1) vs Portugal floods (7.9)
- Portugal groundwater (7.5) and Peristerona vs Netherlands (5.1)

Following D3.4, the WP3 team will focus on long-term changes in the water cycle, which is not part of the BINGO description of work, but has been considered necessary and required by stakeholders and project partners (see Chapter 2). In addition, most sites are conducting ongoing field work, which aims at better understanding the processes driving the water cycle (D3.5). This data and improved process description will then be used to improve the models and/or make the predictions for the near-, mid- and long-term more reliable and to support water management strategies (D3.6).

Finally, the BINGO consortium will provide guidelines on water management based on the BINGO approach at the end of the current project phase. These guidelines aim at not only being applicable to the specific BINGO sites, but also to other European sites with similar settings and problems. This transfer of methods and results will include all knowledge and lessons learned from WP3. Thus, the results and discussions described in this Deliverable 3.4 are one of the key milestones in BINGO.